# Proceedings of the 4th International Brain-Computer Interface Workshop and Training Course 2008

September 18-21 2008
Graz University of Technology, Austria

G. R. Müller-Putz, C. Brunner, R. Leeb,
G. Pfurtscheller, C. Neuper

Verlag der Technischen Universität Graz 2008

Verlag der Technischen Universität Graz
http://www.ub.tugraz.at/Verlag

ISBN: 978-3-85125-004-6

Bibliografische Information der Deutschen Bibliothek:
Die Deutsche Bibliothek verzeichnet diese Publikation in der
Deutschen Nationalbibliografie; detaillierte bibliografische Daten sind im Internet über
http://dnb.ddb.de/ abrufbar.

Printed by TU Graz/Büroservice, Graz, Austria.

# PREFACE

This book contains the scientific contributions to the 4th International Brain-Computer Interface Workshop and Training Course 2008, held in Graz, Austria.

From the very beginning about 17 years ago, a growing number of research groups around the world started to develop and investigate Brain-Computer Interfaces (BCIs). To date, alternative approaches or prototypes, using different types of electrophysiological brain signals or metabolical changes in the brain, training/control paradigms or operating modes, are available and to be evaluated in practical use.

Exemplarily, the use of a self-paced BCI, which analyses the brain signals sample by sample and therefore, produces a decision sample by sample is mandatory for a real world application. The challenge here is to define a system which deals not only with the intentional control (e. g., motor imagery-related brain patterns), but also to handle the non-control state. With such a system users gain full control over timing and speed of communication.

Improvements in the emerging field of BCI research and development depend largely on cooperation between scientists and research groups of different fields. The interdisciplinary co-operation among neuroscientists, engineers, psychologists, and rehabilitation specialists is a necessary requisite. But also constructive collaboration and exchange of experiences and information between the involved research groups as well as creating the right community of young scientists are essential for a field like this. And finally, the work with user groups and clinics helps BCI researchers to refine and fine tune their systems for the "real" application to disabled persons.

After the positive responses to the previous BCI meetings, we were encouraged to organize a fourth meeting in Graz. In this 4th International Brain-Computer Interface Workshop and Training Course 2008 we offer a separate Training Course (especially dedicated to new researchers in the field), and the Workshop – the scientific part of the meeting.

This issue is devoted to the scientific contributions of the participants. The submitted papers were peer-reviewed with the help of external reviewers. We want to acknowledge the work of the following colleagues who contributed with their expertise and knowledge:

| | |
|---|---|
| Brendan Z. Allison | Benjamin Blankertz |
| Peter Desain | John Q. Gan |
| Rolando Grave | Kurtulus Izzetoglu |
| Andrea Kübler | Donatella Mattia |
| Dennis J. McFarland | Klaus-Robert Müller |
| Muhammad Naeem | Gerwin Schalk |
| Reinhold Scherer | Michael Tangermann |
| Carmen Vidaurre | Selina Wriessnegger |

The contributions cover a wide range of topics, including methods of signal processing and feature extraction, new methods of classification, different types of presenting feedback, and software/hardware development.

We are grateful that outstanding experts in the field, namely Fernando H. Lopes da Silva (University of Amsterdam), Andrea Kübler (University of Roehampton), and José del R. Millán (IDIAP, Switzerland) were able to accept our invitation to present keynote addresses at the Workshop.

We gratefully acknowledge the support of the Graz University of Technology for providing the facilities and thank the staff of the Institute of Knowledge Discovery, BCI Lab, for their dedicated assistance.

We hope that the content and scope of our program contributes to a successful and constructive 4th International Brain-Computer Interface Workshop and Training Course 2008!

The Editorial Board

Participants of the 3rd International Brain-Computer Interface Workshop and Training Course 2006.

# Contents

# Session-to-session P300 BCI performance correlation with baseline frequency spectra for a user with ALS

S. Halder[1], J. Hill[2], F. Nijboer[1], A. Furdea[1], A. Kübler[1,3]

[1]Institute of Medical Psychology and Behavioral Neurobiology,
University of Tübingen, Tübingen, Germany
[2]Max Planck Institute for Biological Cybernetics, Tübingen, Germany
[3]Clinical and Health Psychology Research Centre, School of Human and Life Sciences,
Roehampton University, London, UK

halder@informatik.uni-tuebingen.de

**Abstract**

Brain-computer interfaces (BCIs) provide a non-muscular communication channel for patients with late-stage motoneuron disease (e. g. amyotrophic lateral sclerosis (ALS)). The performance of BCI users, in particular of patients, can vary substantially from session to session. This could be due to technical problems caused by non-laboratory field conditions, but may also be due to fluctuations of physiological parameters that could be evident in the electroencephalogram (EEG) of the user. We analyzed visual P300 BCI sessions from one ALS patient over the course of two years to determine correlations between BCI performance and spectral components of the EEG. Classification performance in individual runs was compared to power in the base frequencies of the EEG, i. e. the Delta, Theta, Alpha and Beta bands. Our results show low to moderate but significant correlations of spectral power in the high alpha and low beta band, at parietal-occipital electrode positions during baseline recording before each training, and with performance in subsequent training. In order to confirm alpha and beta band power as predictors of P300-BCI performance more patient data will be analyzed in a future study. The ultimate goal of this endeavour is to find a set of physiological and psychological predictors of performance, possible explanations for variance in signal classification, and reasons for failure of classification. Moreover, physiological parameters may eventually serve as reliable predictors of BCI performance on a session to session basis.

## 1 Introduction

Brain-computer interface (BCI) systems provide a means of communication for locked-in state (LIS) patients or serve as an aid in motor restoration after paralysis [1]. Various BCI paradigms based on components of the electroencephalogram (EEG), such as slow cortical potentials (SCPs), sensorimotor rhythms (SMR) and event-related potentials (ERPs), have been used extensively with patients in the LIS [2]. In our laboratory, most of the patients using a BCI were diagnosed with amyotrophic lateral sclerosis (ALS). Three of these patients have been trained continuously on a weekly basis over the last two years with a BCI based on the P300 event-related potential (ERP) [3]. In this type of BCI, the user focuses on a single cell of a matrix on a computer screen usually containing $6 \times 6$ symbols. The rows and columns flash randomly. Whenever the cell the user is attending to lights up, due to one of the random flashes, a P300 is elicited. Depending on the application, this system is used for various tasks, such as surfing the internet, but is primarily used for spelling, i. e. communication [4, 5].

Despite the success of using a P300 BCI with patients, experience has shown that there is considerable variance in the performance on a session-to-session basis. If technical reasons for such a fluctuation can be ruled out, physiological factors may be the cause of such fluctuations. These can affect the latency and amplitude of the P300, which in turn have an impact on the performance of the classifier used in the BCI system. Previous studies, which analyzed the relationship between background EEG and P300 amplitude, have shown a positive correlation between the two [6, 7]. The strongest correlations were observed in the delta, theta and lower alpha bands.

In an effort to find predictors of performance in a P300-BCI, the current study investigates whether EEG spectra extracted from the baseline periods of each BCI session are correlated to performance in the subsequent training session. The ultimate goal is to find reliable physiological predictors of BCI performance, to explain the session-to-session variance in performance and reasons for classification failures.

# 2 Methods

We used data from one ALS patient who participated in previous BCI studies for this pilot analysis. Baseline periods were extracted from the recordings and transformed into frequency domain. A new classifier was trained on the epochs when the matrix was flashing and applied to the data to obtain hit-rates for individual runs. Correlation coefficients between the spectra and the classification rate were then calculated over all runs.

## 2.1 Dataset

Data from only one patient (female, age 39, ALS diagnosed 12 years ago, sporadic, spinal, not ventilated or tube-fed) was used in this pilot analysis. We chose this patient because she used the BCI system most regularly of all our patients. Training has started in May 2006 and is still continuing. All data were recorded using either a g.tec g.MOBIlab (8 channels) or g.USBamp (16 channels) amplifier. An 8 channel subset of the 16 channel sessions was used to render the electrode locations identical. The 8 electrodes were placed according to the international 10–20 system (Fz, Cz, Pz, P3, P4, Oz, Po7, Po8). Ground and reference were positioned at the mastoids (A1 and A2). The sampling frequency was set to 256 Hz. High and low pass filtering was applied offline during the analysis. EEG recording and stimulation was performed using the P300 speller modules contained in the BCI2000 software [8]. In total 197 runs were used in the analysis, in which 1200 letters were spelled (6.1 letters per run). Either $6 \times 6$ (15 runs) or $7 \times 7$ (182 runs) matrices were used. On average 6.5 flashes of each row and column were presented to the patient per selection of a single letter. This results in 92547 non-target epochs and 15600 target epochs. Mean duration of a flash was 67.3 ms, mean interstimulus interval 118.7 ms and mean intersequence interval 7.46 s. A sequence consisted of either 12 or 14 flashes (one flash per row and per column). The intersequence intervals result in a total of 149 min of baseline EEG which are on average 45.5 s per run.

## 2.2 Classification

Using stepwise linear discriminant analysis (SWLDA) data was classified on a run-by-run basis, with a run being a whole word spelled by the user. This analysis is based on Fisher's linear discriminant (FLD), but performs an additional feature reduction that progressively selects the most discriminant features and eliminates the least predictive ones. This method was also used in [3] and proved its feasibility for this type of analysis. Despite its simplicity this algorithm was shown to be competitive against more elaborate methods [9]. The classifier was retrained for the classification of each run on a leave-one-run-out basis. Meaning that the run to be classified was excluded from contributing to the classifier. Five stimulus repetitions (i. e. five flashes of each row and column of the matrix) were averaged to obtain the ERPs. The low number of flashes was chosen to avoid ceiling effects caused by the classification accuracy. Before classification the signals were high-pass filtered at 1 Hz and low-pass filtered at 20 Hz.

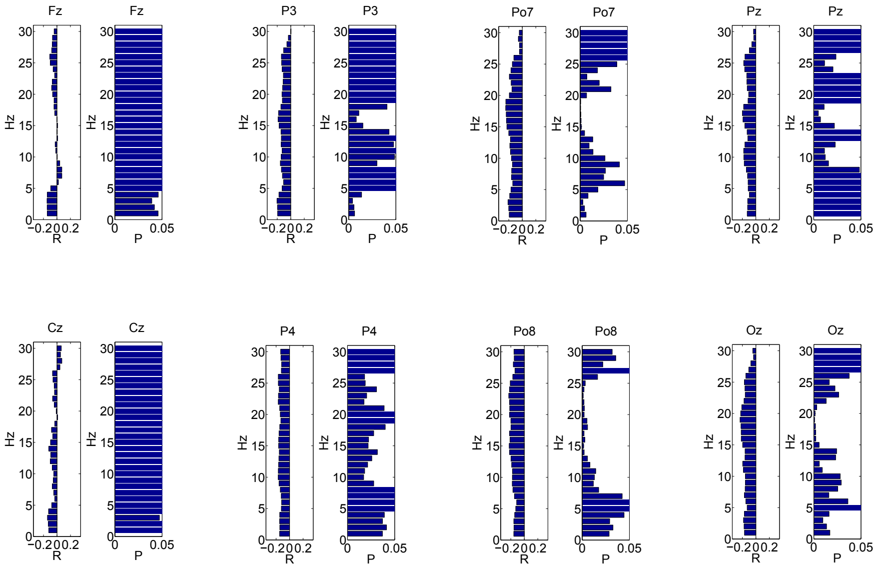


Figure 1: Overview of correlations between spectral power in dB at frequencies in Hz and classification accuracy of individual runs in %. All eight channels used for classification of the data are shown. All graphs showing $p$-values are scaled from 0 to 0.05 to allow a quick assessment of which frequency bands are significant. The graphs showing Spearman's $\rho$ are scaled from $-0.2$ to 0.2.

### 2.3 Analysis

Pre- and post-sequence intervals from the BCI training sessions were used to obtain EEG signals to calculate the baseline spectra. No additional filtering was applied. Power spectra were obtained in dB using Welch's method [10]. Spearman's $\rho$ was calculated between the spectra and the classification accuracies. $p$-values for Spearman's $\rho$ were calculated using permutation distributions. All calculations were carried out in Matlab 7.5.

## 3 Results

Figure 1 shows correlations of the power in frequencies from zero to 30 Hz and their significance for all eight channels that were analyzed. The analysis is restricted to the frequency bands delta (2–4 Hz), theta (4–8 Hz), alpha1 (8–10.5 Hz), alpha2 (10.5–13 Hz), beta1 (13–20 Hz), and beta2 (20–30 Hz). All significant correlations were negative.

The correlations increase from frontal to occipital channels. Correlations in central and frontal channels were weak with $p$-values close to or above 0.05. Po7, Po8 and Oz all show significant correlations from 15–20 Hz. Po7 is also the channel with the single highest correlation value ($\rho = -0.25$, $p = 0.00$ at 18 Hz). For an overview see Table 1.

In Figure 2 accuracy per run and spectral power for channel Po7 are plotted on a scale from zero to one. The inverse relationship between power and accuracy is clearly visible in the first 75 runs. In later runs the relationship becomes less clear. This might be due to the fluctuations in the 18 Hz band and classification accuracy.

To further illustrate the correlation of performance with the 18 Hz band, on channel Po7, we split the runs in two groups. The first group contained those runs with power in the 18 Hz band below the median value over all runs (5.25 dB), the second group those with 18 Hz power above the median. Figure 3 shows that the accuracy for those runs with 18 Hz power below the median

| Electrode/Band | delta | theta | alpha1 | alpha2 | beta1 | beta2 |
|---|---|---|---|---|---|---|
| Fz | * | | | | | |
| Cz | | | | | | |
| P3 | * | | | * | * | |
| P4 | * | | * | * | * | * |
| Po7 | * | * | * | * | ***** | * |
| Po8 | * | * | * | * | ***** | ***** |
| Pz | | | * | * | * | * |
| Oz | * | * | * | * | ***** | * |

Table 1: Overview of significant frequency bands for all electrodes ($p < 0.05$). The bands and electrodes with more significant correlations ($p < 0.005$) are emphasized by using bold print.

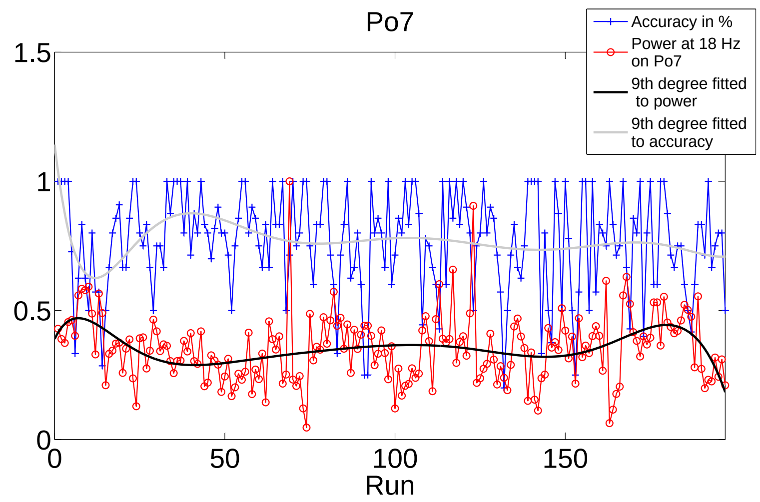


Figure 2: Mean power spectrum at 18 Hz versus accuracy in percent on channel Po7. The spectra are represented as power in dB (scaled from zero to one) per run. The accuracy is represented as classification result in % correct (also scaled from zero to one) per run. Two polynomials are fitted to the data to make the inverse relationship between power and accuracy clearer.

have a higher mean classification accuracy (80.0 % correct with 5 flashes) then those runs with high 18 Hz power (73.4 %).

# 4 Discussion

Our data show a negative correlation between performance with a P300 BCI and power in the baseline frequency spectra. This correlation is strongest on the parietal-occipital channels (Po7, Po8 and Oz) in the 15 to 20 Hz band. This is contradictory to the findings in [6, 7] where positive correlations between P300 amplitude (which should have a positive influence on classification) and baseline spectra were reported for an auditory oddball task. Bearing in mind that using a BCI comprises a cognitively more demanding task than an auditory oddball, the two results might not be directly comparable. Generally, large desynchronization of the EEG is associated with cognitive processing caused by frequency changes and phase shifts of the involved neural networks [11]. In contrast large scale synchronization of the EEG, in particular in the alpha band, reflects neural networks oscillating at the same phase and frequency. This is considered to be a sign of mental inactivity. Alpha and beta activity were also found to be connected to attention and cognitive

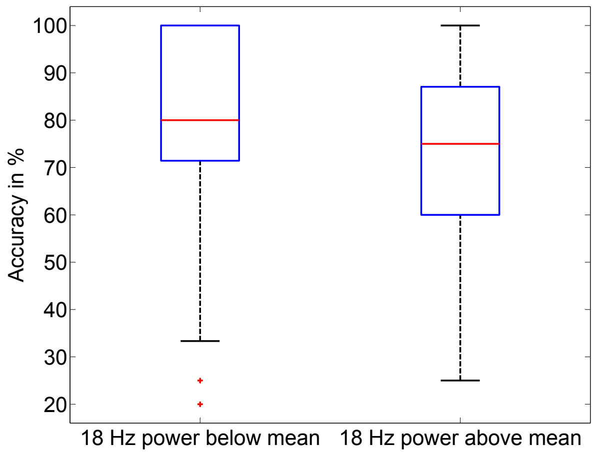


Figure 3: Distribution of classification accuracy above and below mean power at 18 Hz on electrode Po7. Mean accuracies for low power are at 80.0 %, for high power at 73.4 %. Each box has a line at the lower quartile (bottom line), median (middle line) and upper quartile values (top line). The whiskers extending from the boxes show the range of the rest of the data. If data lies beyond the reach of the whiskers (1.5 times interquartile range) it is marked with a plus symbol.

processing, respectively, though whether a synchronization or desynchronization could be observed was dependent on the task [12]. Beta suppression was found e. g. when subjects performed reading and arithmetic tasks [13]. Therefore, the negative correlation between power and accuracy could be an indicator of the cortical resources being recruited for the BCI task. This would indicate that the mental states, affecting the baseline spectra and BCI performance, are directly connected.

An alternative explanation would be that strong oscillations in the baseline frequencies have a negative influence on the classifier that we used without being directly related to the BCI task. If this were the case frequency filtering of the data with a low-pass at e. g. 8 Hz and above 1 Hz should remove the oscillations that interfere most with classification. Re-classification of the data showed, however, that the mean classification accuracy at 5 sequences decreases from 76.7 % to 71.0 %. This supports the hypothesis of a direct correlation between baseline spectral power and BCI performance. Nonetheless, further analysis with different classifiers and frequency bands is needed.

# 5 Conclusion

These findings could either be used to adapt a classifier to be invariant to base frequency changes or to recognize physiological states of the BCI user that cause bad performance. Both might reduce frustration of the user in subsequent sessions.

In the future, this should be repeated with more data from different patients. Additionally, a comparison with healthy subjects could reveal whether the effects found in this study were specific for ALS patients. Finally, the analysis method could be adapted to find non-linear relationships.

# References


[1] A. Kübler and N. Neumann. Brain-computer interfaces–the key for the conscious brain locked into a paralyzed body. *Prog. Brain Res.*, 150:513–525, 2005.

[2] A. Kübler, F. Nijboer, and N. Birbaumer. *Toward Brain-Computer Interfacing*, pages 373–391. MIT press, Cambridge, MA, 2007.

[3] L. A. Farwell and E. Donchin. Talking off the top of your head: toward a mental prosthesis utilizing even-related brain potentials. *Electroencephalogr. Clin. Neurophysiol.*, 70:510–523, 1988.

[4] E. Mugler, M. Bensch, S. Halder, W. Rosenstiel, M. Bogdan, N. Birbaumer, and A. Kübler. Brain-computer interface control of an internet browser. *Int. J. Bioelectromagnet*, 6(1), 2007.

[5] F. Nijboer, E. W. Sellers, J. Mellinger, M. A. Jordan, T. Matuz, A. Furdea, S. Halder, U. Mochty, D. J. Krusienski, T. M. Vaughan, J. R. Wolpaw, N. Birbaumer, and A. Kubler. A P300-based brain-computer interface for people with amyotrophic lateral sclerosis. *Clin. Neurophysiol.*, 2008.

[6] J. Intriligator and J. Polich. On the relationship between background EEG and the P300 event-related potential. *Biol. Psychol.*, 37(3):207–218, 1994.

[7] J. Polich. On the relationship between EEG and P300: individual differences, aging, and ultradian rhythms. *Int. J. Psychophysiol.*, 26(1-3):299–317, 1997.

[8] G. Schalk, D. J. McFarland, T. Hinterberger, N. Birbaumer, and J. R. Wolpaw. BCI2000: a general-purpose brain-computer interface (BCI) system. *IEEE Trans. Biomed. Eng.*, 51(6):1034–1043, 2004.

[9] D. J. Krusienski, E. W. Sellers, F. Cabestaing, S. Bayoudh, D. J. McFarland, T. Vaughan, and J. R. Wolpaw. A comparison of classification techniques for the P300 speller. *J. Neural Eng.*, 3(4):299–305, 2006.

[10] P. D. Welch. The use of fast Fourier transform for the estimation of power spectra: A method based on time averaging over short, modified periodograms. *IEEE Trans. Audio Electroacoust*, 15:70–73, 1967.

[11] W. Klimesch. EEG alpha and theta oscillations reflect cognitive and memory performance: a review and analysis. *Brain Res. Brain Res. Rev.*, 29(2-3):169–195, 1999.

[12] W. J. Ray and H. W. Cole. EEG alpha activity reflects attentional demands, and beta activity reflects emotional and cognitive processes. *Sci.*, (4700):750–752, 1985.

[13] T. Fernandez, T. Harmony, M. Rodriguez, J. Bernal, J. Silva, A. Reyes, and E. Marosi. EEG activation patterns during the performance of tasks involving different components of mental calculation. *Electroencephalogr. Clin. Neurophysiol.*, 94(3):175–182, 1995.

# Detection of foot motor imagery in a single Laplacian EEG derivation

T. Solis-Escalante, G. R. Müller-Putz, G. Pfurtscheller

Institute for Knowledge Discovery, BCI Lab, Graz University of Technology, Graz, Austria

teodoro.solisescalante@tugraz.at

**Abstract**

In this paper we report on the results of the validation of a general procedure for foot motor imagery classification. The proposed methods use a spatial filter in the form of a single Laplacian derivation at electrode position Cz. Ongoing electroencephalogram (EEG) is described with band power features from 6 to 36 Hz using time segments of one second. A pair of support vector machines (SVM) is trained to detect event-related desynchronization and the post-imagery beta synchronization individually from any other brain activity. A simulation of an asynchronous Brain-Computer Interface (BCI) is used to validate the method using the true positive rate (TPR) and false positive rate (FPR) as performance measurements. Both SVM are trained to predict the posterior probability of the motor imagery event-related patterns. With this information and the assumption of independence, both probabilities are combined. The results of three subjects show a maximum TPR of 0.53, 0.73 and 0.93 (for a fixed FPR $\leq 0.10$). Each performance is individually examined and analyzed.

## 1 Introduction

Execution of limb movement and the imagination of the same movement results not only in a desynchronization (event-related desynchronization, ERD) of the sensorimotor rhythms, but also in a beta rebound (beta event-related synchronization, beta ERS) after the termination of the motor task [1, 2, 3]. This means that two different physiological phenomena (ERD and beta ERS) are characteristic for a motor task. Both phenomena have a time span of 1.5 to 2 seconds when the motor task is short-lasting (e. g., brisk motor imagery). Of special interest is the midcentral region with the foot representation area and the supplementary motor area close to the vertex. It has been reported that not only foot movement but also hand movement involves the supplementary motor area and reveals a midcentral beta rebound [4].

Here we investigate whether foot motor imagery (MI) can be detected in the ongoing EEG with a simulation of an asynchronous Brain-Computer Interface (BCI) when both phenomena (ERD/ERS) are used for classification. Furthermore, a general procedure for the classifier setup (training and testing) is proposed and validated.

## 2 Methods

### 2.1 Data description

Recordings from three healthy subjects (S1, S2 and S3) were collected during cue-based MI. Each subject performed three runs of 30 trials each. All runs were conducted on the same day with several minutes in between. In the paradigm, a cross was presented at $t = 0\,\mathrm{s}$; then at $t = 2\,\mathrm{s}$, an arrow pointing downwards was displayed as a cue and the subject was asked to imagine a brisk movement (dorsiflexion) of both feet. The duration of MI was about one second. At $t = 3.25\,\mathrm{s}$ the cue and at $t = 6\,\mathrm{s}$ the cross disappeared. At the end of the trial ($t = 7.5\,\mathrm{s}$) a random

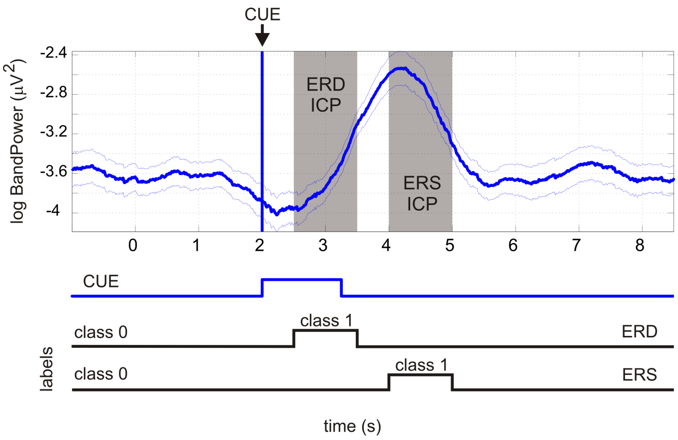


Figure 1: Labeling procedure and period definition. Event-related synchronization followed by an event-related desynchronization (average power from MI data from subject S3). The intentional control periods (ICP, shown at the bottom) are defined from the information related to the paradigm timing.

inter-trial interval between 0 and 1 s was presented. Sixteen Ag/AgCl electrodes placed over the sensorimotor area were used to record monopolar EEG signals (Guger Technologies, Graz, Austria) with a sampling frequency of 250 Hz. Reference and ground electrodes were located at the left and right mastoid, respectively. From this data one small Laplacian derivation [5] at the electrode position Cz was computed using orthogonal neighbor electrodes (anterior, posterior and both lateral). Further details about the data collection can be found in [6].

## 2.2 Feature extraction

Each trial was analyzed using time segments of 1 s in length with an overlap of 500 ms from $t = -1$ s to $t = 9$ s relative to the start of a trial (cue was presented at $t = 2$ s). The spectral description of each segment was computed by means of logarithmic band power: (i) band-pass filtering (62 order FIR), (ii) squaring the value of each sample, (iii) averaging all samples within the time segment and (iv) applying the logarithm. A feature vector of twenty nine features (frequency components from 6 to 36 Hz with a length of 2 Hz and an overlap of 1 Hz) was used for the full description of band power in EEG during MI.

Only the information related to MI (ERD or ERS) was labeled as class 1. All patterns were labeled twice for the classification of either ERD or ERS against all other brain activity. The ERD patterns during MI from $t = 2.5$ s to $t = 3.5$ s were labeled as class 1, all others patterns were labeled as class 0. In a similar way, ERS patterns after MI ($t = 4$ s to $t = 5$ s) were labeled as class 1. Figure 1 shows the labeling procedure for each trial.

The period where patterns are labeled as class 1 is from now on referred to as intentional control period (ICP). As a consequence, the rest of the time is referred to as non-intentional control period (NICP). Because ERD and post-movement ERS share slightly different frequency components [6] and only the latter coincides with the excitability level of motor cortex neurons, ERD and ERS can be described as mutually exclusive.

## 2.3 Pattern recognition

Two classifiers were trained for individual detection of ERD or ERS within their respective ICP. Support vector machines (SVM) with Gaussian kernels were used for this task. One (training) run was used to train a SVM with a specific combination of parameters (the performance of the SVM depends on the regularization parameter $C$ and the width of the kernel $\sigma$). The performance of this classifier was estimated using a 10-fold cross validation. A test was made with the patterns from a second (testing) run and the values of true positive rate (TPR) and false positive rate (FPR) were stored. Following this step, a new set of parameters $\{C, \sigma\}$ was tested with the same approach.

After testing several combinations, the parameters $C$ and $\sigma$, associated with the best performance (smallest FPR and highest TPR), were selected to train a new SVM with the data from the training run. The SVM model was also trained for posterior class probability estimation [7, 8]. The trained SVMs were used to compute the ERD and ERS posterior probability of the patterns obtained from a validation run (a third run not used to train/test the classifier). This run was described using the same number of logarithmic band power features for time segments of 1 s in a simulation of an online asynchronous system.

### 2.4 Evaluation

The output of each classifiers was additionally post-processed with three simple parameters: (i) a threshold, (ii) a dwell time dwell time and (iii) a refractory period refractory period [9]. The dwell time and refractory period values were set at 62 samples (248 ms) and 500 samples (2 s), respectively. The threshold was selected from a receiver-operator characteristics curve analysis. For evaluation the ICP was extended to two seconds, from $t = 2.5$ s to 4.5 s for ERD and from $t = 3.5$ s to 5.5 s for ERS. This was done since the ERD or ERS patterns may be presented at any time after the cue.

The values of TPR and FPR were computed by event detection. An event was detected every time that a consecutive number of samples equal to the number of samples during the dwell time exceed the threshold. After this, all events were suppressed during the refractory period. If the event was detected during the new ICP definition (relative to the cue) a true positive was counted in other case the event counted as a false positive.

#### 2.4.1 Combination of MI related information

Information about ERD and ERS were combined to enhance the accuracy and minimize false negatives, under the following assumptions:

1. ERD is present in all MI tasks
2. If an ERS is present, it is always after an ERD
3. Classifications of ERD and ERS are independent of each other

Following this the joint probability can be computed as the product of the independent event probabilities: $P(\text{ERD}, \text{ERS}) = P(\text{ERD}) \cdot P(\text{ERS})$, where $P(\text{ERD})$ and $P(\text{ERS})$ are the estimated probabilities for each event. This combination was called the $\prod$-rule. The physiological evidence behind the $\prod$-rule make it impossible that both events occur at the same time thus the $P(\text{ERD})$ is delayed by 1 s to match the ICP for ERS and then computing their product.

## 3 Results

Table 1 shows the performance from the three subjects. All results were obtained as the highest TPR value achieved for a FPR $\leq 0.10$.

In Figure 2 the time-frequency maps from all three MI runs are shown together with a few examples of single trial EEG and the average probability for each classifier.

Time-frequency maps were computed for each subject using the data from all three MI runs.

## 4 Discussion

All subjects presented an acceptable performance for at least one of the validation runs. Subject S1 attained a maximum TPR of 0.60 (FPR $\leq 0.08$) for runs #2 and #3. Subject S2 achieved

| ID | RUN | $P$(ERD) | | $P$(ERS) | | $\prod$-rule | |
|---|---|---|---|---|---|---|---|
| | | TPR | FPR | TPR | FPR | TPR | FPR |
| S1 | #1 | 0.33 | 0.09 | 0.40 | 0.06 | 0.37 | 0.07 |
| | #2 | 0.17 | 0.08 | 0.50 | 0.09 | **0.60** | 0.07 |
| | #3 | 0.07 | 0.05 | 0.57 | 0.09 | **0.60** | 0.08 |
| S2 | #1 | 0.43 | 0.06 | 0.20 | 0.07 | 0.27 | 0.07 |
| | #2 | 0.50 | 0.09 | 0.07 | 0.07 | **0.53** | 0.06 |
| | #3 | 0.17 | 0.08 | 0.23 | 0.09 | 0.27 | 0.08 |
| S3 | #1 | 0.10 | 0.08 | 0.43 | 0.05 | 0.53 | 0.07 |
| | #2 | 0.63 | 0.06 | 0.53 | 0.08 | **0.70** | 0.06 |
| | #3 | 0.60 | 0.09 | 0.70 | 0.08 | **0.70** | 0.06 |

Table 1: Performance for the different classification approaches based on $P$(ERD), $P$(ERS) and the $\prod$-rule. The highest individual performance (TPR $\geq$ 0.50) is highlighted with a bold face. RUN indicates the number of the run used for validation.

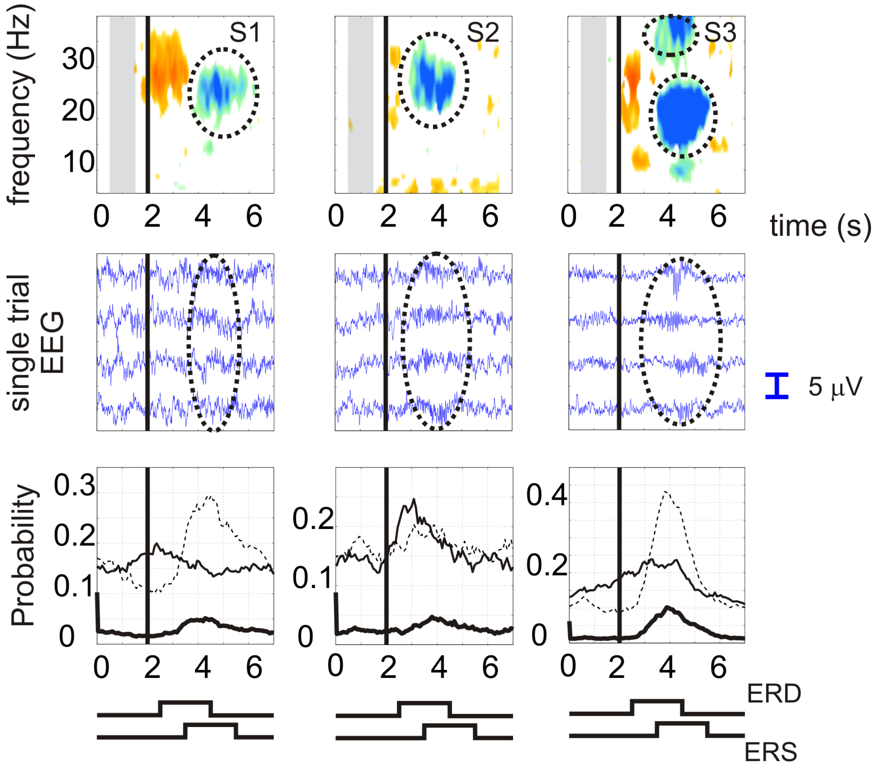


Figure 2: Visualization of ERD, ERS and their average probability. Top: ERD/ERS maps show the significant changes in power relative to a reference period (gray box from $t = 0.5\,\mathrm{s}$ to $t = 1.5\,\mathrm{s}$). Middle: Examples of single trial EEG. Bottom: The average posterior probability for class 1 is plotted for ERD (solid line), ERS (dotted line) and the $\prod$-rule (bold line). Their respective ICP for validation is shown at the very bottom. In all cases the cue appearance is presented with a vertical solid line (at $t = 2\,\mathrm{s}$) and ERS is marked with dotted lines/circles.

| ID | RUN | $P$(ERD) TPR | $P$(ERD) FPR | $P$(ERS) TPR | $P$(ERS) FPR | $\prod$-rule TPR | $\prod$-rule FPR |
|---|---|---|---|---|---|---|---|
| S1 | #1 | 0.33 | 0.09 | 0.37 | 0.07 | **0.50** | 0.08 |
| | #2 | 0.30 | 0.09 | **0.50** | 0.09 | **0.57** | 0.07 |
| | #3 | 0.13 | 0.00 | **0.50** | 0.09 | **0.73** | 0.09 |
| S2 | #1 | **0.57** | 0.05 | 0.23 | 0.04 | **0.50** | 0.05 |
| | #2 | **0.73** | 0.08 | 0.13 | 0.08 | **0.53** | 0.08 |
| | #3 | 0.23 | 0.09 | 0.33 | 0.09 | 0.43 | 0.09 |
| S3 | #1 | 0.13 | 0.09 | **0.93** | 0.07 | **0.93** | 0.05 |
| | #2 | **0.77** | 0.08 | **0.57** | 0.09 | **0.73** | 0.07 |
| | #3 | 0.47 | 0.10 | **0.90** | 0.09 | **0.83** | 0.06 |

Table 2: Performance measurements after adaptation of ICP. From the probability curves, the detection ICP values for $P$(ERD), $P$(ERS) and $\prod$-rule based classifiers were changed to: (S1) ERD from $t = 2$ s to $t = 4$ s, ERS from $t = 3$ s to $t = 5$ s; (S2) ERD from $t = 2$ s to $t = 5$ s, ERS from $t = 2$ s to $t = 5$ s and (S3) ERD from $t = 2.5$ s to $t = 5$ s, ERS from $t = 3$ s to $t = 5.5$ s. In all cases the ICP for $\prod$-rule and ERS have the same ICP.

a top performance of 0.53 (FPR = 0.06) just for run #2. The best subject was S3 achieving a maximum of 0.70 (in validations with run #2 and #3, FPR 0.06). In all cases the maximum performance was reached with the use of the $\prod$-rule. The difference between this rule and the best individual performance was between $-0.03$ and 0.10 (except S2 run#1).

The ERD/ERS patterns shown in Figure 2 are useful for understanding the differences in the individual performances. The best subject (S3) shows a large ERS pattern centered around 20 Hz after $t = 4$ s. The single trials show bursts related to power increase around the same time point. For the other subjects (S1 and S2), the ERS forms a smaller and more widespread pattern around 25 Hz at $t = 4$ s. Although the ERS is small for subject S1, the highest intensity is localized in a small area. Subject S2 shows an ERS pattern with several local maxima. Additionally, bursts in single trial EEG from the same subject are not easily identifiable. A closer look on the single trials revealed that not all of them presented neither ERD nor ERS, which is directly responsible for a bad training set and a small number of true intentional control events, e. g., S2 where runs #1 and #2 are similar while run #3.

ERD patterns are present in the maps from subjects S1 and S3; however, their localization just after the cue and outside the ICP for ERD makes their discrimination capabilities hard to express. If an ERD pattern is present between $t = 2$ s and $t = 2.5$ s, the feature vector that describes that pattern will be labeled as class 0. It can be seen that the ERD is very short lasting for S3, but it is present until $t = 3.5$ s for S1. The existence of patterns describing ERD (or perhaps ERS) inside and outside the ICP is misleading for the classifier (optimization of the SVM). In Figure 2 the average posterior probability estimation for each subject is shown. Noteworthily, both individual classifiers have almost the same output for subject S2, which indicates that both SVM are describing the same phenomenon, most likely ERS, since almost no ERD is present in subject S2's map.

Several points can be ascertained from the average probabilities: (i) ERD and ERS can be discriminated one from each other and both from any other brain-state, (ii) posterior probability value is changing shortly before and after the actual event definition (either ERD or ERS), (iii) the $\prod$-rule improves classification when both events are correctly described and detected; however, its classification value will be as good as the best individual event. Poor performance due to the definition of the ICP for validation was confirmed by changing its localization. New ICP intervals were selected from the probability averages in Figure 2. The results are presented in Table 2. All subjects and all runs (except S2 run #3) show TPR values over 0.5 for the classification based on the $\prod$-rule.

## 5 Conclusions

The methods described in this paper have shown to be appropriate to describe the ERD/ERS patterns and differentiate them from no MI patterns. All subjects showed acceptable performance when the detection interval was individually chosen. Generalization of the method was proven while all classifiers were trained in the same manner with predefined parameters from task-related and physiological knowledge. Combination of ERD and ERS by the $\prod$-rule succeed in preserving the classification accuracy of an ERD/ERS based asynchronous BCI. Tests were made with feature selection showing no difference with the use of the complete feature set.

**Acknowledgments:** This work was supported by EU project PRESENCCIA (IST-2006-27731), the "Steiermärkische Landesregierung" project GZ: A3-16 B 74-05/1 and the Austrian "Allgemeine Unfallversicherung AUVA".

## References

[1] R. Salmelin, M. Hämäläinen, M. Kajola, and R. Hari. Functional segregation of movement related rhythmic activity in the human brain. *Neuroimage*, 2:237–243, 1995.

[2] C. Neuper and G. Pfurtscheller. Evidence for distinct beta resonance frequencies in human EEG related to specific sensorimotor cortical areas. *Clin. Neurophysiol.*, 112:2084–2097, 2001.

[3] G. Pfurtscheller, C. Neuper, C. Brunner, and F. H. Lopes da Silva. Beta rebound after different types of motor imagery in man. *Neurosci. Lett.*, 378:156–159, 2005.

[4] G. Pfurtscheller, C. Neuper, K. Pichler-Zalaudek, G. Edlinger, and F. H. Lopes da Silva. Do brain oscillations of different frequencies indicate interaction between cortical areas in humans? *Neurosci. Lett.*, 286:66–68, 2000.

[5] B. Hjorth. An on-line transformation of EEG scalp potentials into orthogonal source derivations. *Electroencephalogr. Clin. Neurophysiol.*, 39:526–530, 1975.

[6] G. R. Müller-Putz, D. Zimmermann, B. Graimann, K. Nestinger, G. Korisek, and G. Pfurtscheller. Event-related beta EEG-changes during passive and attempted foot movements in paraplegic patients. *Brain Res.*, 1137:84–91, 2007.

[7] C.-C. Chang and C.-J. Lin. *LIBSVM: a library for support vector machines*, 2001. Software available at `http://www.csie.ntu.edu.tw/~cjlin/libsvm`.

[8] T. Wu, C. Lin, and R. Weng. Probability estimates for multi-class classification by pairwise coupling. *J. Mach. Learn. Res.*, 5:975–1005, 2004.

[9] G. Townsend, B. Graimann, and G. Pfurtscheller. Continuous EEG classification during motor imagery – simulation of an asynchronous BCI. *IEEE Trans. Neural Syst. Rehabil. Eng.*, 12:258–265, 2004.

# Multi-class independent common spatial patterns: exploiting energy variations of brain sources

C. Gouy-Pailler[1], M. Congedo[1], C. Brunner[2], C. Jutten[1] and G. Pfurtscheller[2]

[1]GIPSA-lab, CNRS/UJF-UPMF-Stendhal, Grenoble, France
[2]Institute for Knowledge Discovery, BCI Lab, Graz University of Technology, Graz, Austria

cedric.gouypailler@gipsa-lab.inpg.fr

**Abstract**

This paper presents a method to recover task-related sources from a multi-class Brain-Computer Interface (BCI) based on motor imagery. Our method gathers two common approaches to tackle the multi-class problem: 1) the supervised approach of Common Spatial Pattern (CSP) to discriminate between different tasks; 2) the criterion of statistical independence of non-stationary sources used in Independent Component Analysis (ICA). We show that the resulting spatial filters have to be adapted to each subject and that the combined use of intra-trial and inter-class energy variations of brain sources yield an increase of classification rates for four among eight subjects.

## 1 Introduction

The ultimate goal of Brain-Computer Interfaces (BCIs) is to provide disabled people suffering from severe motor diseases with a tool to restore communication and movement [1]. A typical example of a BCI is based on movement imagery, which results in somatotopic brain signal variations in specific frequency bands [2].

On the one hand, Independent Component Analysis (ICA) has been widely used for analyzing and cleaning brain signals in electroencephalography (EEG). This approach, initiated in the early 90's by Jutten and Hérault [3], aims at tackling the Blind Source Separation (BSS) problem (neither the mixing matrix nor the sources are known) by assuming mutual statistical independence between sources. Such models have proved useful to increase classification rates of BCIs [4, 5], but do not use a priori information about the tasks, namely the labels of tasks during the training step. Different separation principles can be used to tackle the BSS problem. They depend on the statistical properties of sources, and on how statistical independence is evaluated. When sources are assumed to be independent and identically distributed (iid), non-gaussianity of sources is required, which involves higher order statistics or mutual information. The non-gaussianity assumption case can be relaxed, yielding other families of algorithms based on second order statistics and requiring coloration or time-varying energy [6].

On the other hand, the goal-oriented approach of Common Spatial Pattern (CSP) has been introduced in [7]. The idea of CSP is to find the linear combination optimizing the ratio between within-class scatter and the mixture scatter matrices. From a methodological point of view, it is nothing but an exact joint diagonalization of two matrices, hence very similar to Approximate Joint Diagonalization (AJD). This approach proved useful to discriminate two motor imagery tasks but suffers from a lack of generalization to multi-class problems. A one-versus-rest (OVR) approach is often used to generalize the approach to multi-class discrimination problems. Following ideas from [8], an extension to multi-class problems has been proposed in [9, 10]. These approach were based on AJD of sample covariances matrices.

Extending the work of [9, 10], this paper presents an approach to use intra-trial energy variations of sources and inter-class diversity. Our method is compared to CSP and the approach proposed in [9]. The quality of separation is assessed by classification rates in a 8-subject 4-class motor imagery experiment (left hand, right hand, foot and tongue). The remainder of this paper is organized as follows: in Section 2, we present the experimental paradigm, Section 3 provides the reader with the detailed description of our method; finally we present and discuss results.

## 2 Subjects and experimental paradigm

In this study, the EEG data of eight subjects (three females and five males with a mean age of 23.8 years and a standard deviation of 2.5 years, [4, 5]), recorded during a cue-based four-class motor imagery task, was analyzed. Two sessions on different days were recorded for each subject, each session consisting of six runs separated by short (a couple of minutes) breaks. One run consisted of 48 trials (12 for each of the four possible classes), yielding a total of 288 trials per session.

As mentioned above, the paradigm consisted of four different tasks, namely the imagination of movement (motor imagery) of the left hand, right hand, foot, and tongue, respectively. At the beginning of each trial ($t = 0$ s), a fixation cross appeared on the black screen. In addition, a short acoustic warning tone was presented at this time instant. After two seconds (at $t = 2$ s), a cue in the form of an arrow pointing either to the left, right, down or up (corresponding to one of the four classes left hand, right hand, foot or tongue) appeared for 1.25 s, prompting the subjects to perform the target motor imagery task. No feedback (neither visual nor acoustic) was provided. The subjects were asked to carry out the mental imagination until the fixation cross disappeared from the screen at $t = 6$ s. A short break followed, lasting at least 1.5 s. After that, the next trial started. The paradigm is illustrated in Figure 1 (a).

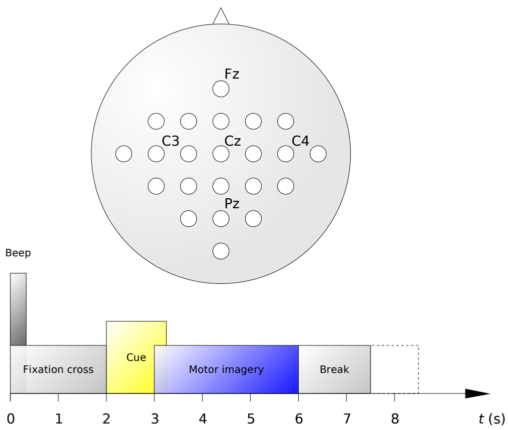


(a) Experimental paradigm

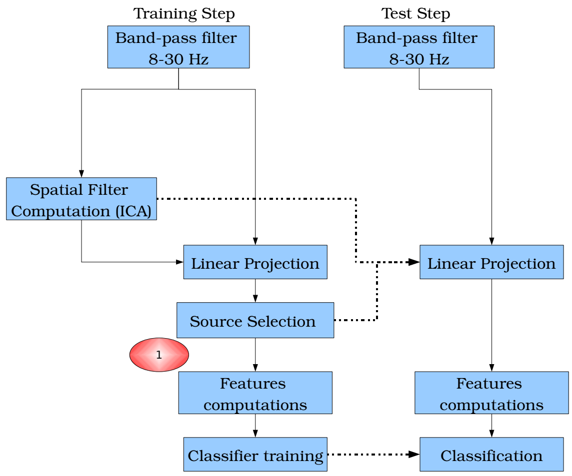


(b) Method Overview

Figure 1: (a): Timing scheme of the BCI paradigm and electrode setup of the 22 channels. (b) Method overview.

22 Ag/AgCl electrodes (with inter-electrode distances of 3.5 cm) were used to record the EEG, the setup is depicted in Figure 1. Monopolar derivations were used throughout all recordings, where the left mastoid served as reference and the right mastoid as ground. The signals were sampled at 250 Hz and bandpass-filtered between 0.5 and 100 Hz. An additional 50 Hz notch filter was enabled to suppress power line noise.

Although a visual inspection of the raw EEG data was performed by an expert, no trials were removed from the subsequent analysis in this study in order to evaluate the robustness and sensitivity to outliers and artifacts of each model. Three EOG channels and one ECG channel were also used to measure electrophysiological activity of the subjects.

# 3 Methods

We begin by stating the notations. $x \in \mathbb{R}^N$ represents EEG data, recorded at $N$ electrodes at each time $t$. In this work, we aim at finding a linear transformation of the data $s = W^T x$ to increase the classification rate. The following section presents different methods for finding $W$, based on different criteria. Intentions of the users are called classes and indexed $k \in [1 \dots 4]$.

Figure 1 (b) shows an overview of the whole processing stage during the training and the test step. The spatial filter computation is done according to the different methods described below. The training step is used to fix some of the parameters of the method whereas the test step consists in applying the procedure to unseen data with previously fixed parameters. The dashed lines represent information, which is shared between learning and test steps.

## 3.1 Method 1: Common Spatial Patterns

The idea of Common Spatial Patterns (CSP) [7] for two-class problems is to find the more discriminative spatial filters $v \in \mathbb{R}^N$, which optimizes the Rayleigh quotient

$$\{\min, \max\} \frac{v^T C_{xx|k=1} v}{v^T C_{xx|k=1,2} v}$$

where $C_{xx|k=i}$ is the covariance matrix of the data belonging to class $c_i$. This optimization problem can be solved by a generalized eigenvalue decomposition method. An advantage of this technique is that spatial filters are ranked according to their discriminative power, thus allowing to select specific features dimension $L$. Computations are also exact and fast. Although this method is optimal for two-class problems, extensions to multi-class paradigms is not straight-forward. We use in the following a One-Versus-Rest CSP to generalize to multi-class problems.

## 3.2 Multi-class independent common spatial patterns

Whereas some algorithms try to maximize independence, e. g. using non-gaussianity of the sources without considering time structure, another way to separate source components is to consider simple time structures within the data. The goal of our work is to study the performance of some simple time structures. We thus look for some kind of non-stationarity in the data.

The general framework is that we are trying to recover sources $s(t)$ related to each task by assuming the simplest source separation model for linear mixtures of sensor measurements $x(t)$:

$$x(t) = As(t) \tag{1}$$

where $A$ is the mixing matrix and $s$ are the sources. The separation principle given by Pham and Cardoso in [6] aiming at exploiting slow-varying variances of sources yields the joint diagonalization of covariance matrices.

The observation interval is partitioned into $Q$ parts: $\mathcal{T}_q$, with $q \in [1 \dots Q]$. For each time interval, we define the covariance matrix:

$$C_{xx}(\mathcal{T}_q) = \mathbb{E}_{t \in \mathcal{T}_q}(x(t)x(t)^T)$$

Then, the estimation of the separation matrix $B = A^{-1}$ is done by approximately jointly diagonalizing the set

$$\mathcal{S} = \{C_{xx}(\mathcal{T}_q) | q \in [1 \dots Q]\}.$$

This joint diagonalization may be performed for example by the Pham's algorithm [6]

A priori knowledge about the performed tasks during training is included by considering only task-specific covariance matrices. This makes our approach close to CSPs but with the advantage of inherently being a multi-class approach.

#### 3.2.1 Model-based source separation for spatial filtering

In the following, $\mathbb{E}_k(\cdot)$ will denote the average across all trials related to class $k$. $C_{xx}(t \in [t_1, t_2], k)$ will denote the set of covariance matrices for every trial of one session of a subject for task $k$ computed with EEG in the time domain between $t_1$ and $t_2$.

Different kinds of diversities are to be considered in the following models:

1. Inter-class diversity (ICD): sources related to motor imagery have a varying energy among classes. We exploit the fact that a source active for one mental task is active with a different energy (or not active at all) for another mental task. This kind of diversity is exploited by considering task-specific covariance structures, it is used by CSP to find discriminative linear transforms of sensors.

2. Time-varying energy (TVE): as motor tasks are known to be a succession of activations in different brain areas, it can be assumed that sources related to a mental task realization can be active with different energies across the task. Joint diagonalization covariance matrices computed using successive time windows will help recovering sources [6].

We want to stress the differences between these approach based on source-separation and the approach based on CSP. First of all, whereas CSP tries to find the quasi-optimal linear combination that optimizes the Rayleigh quotient given above, our methods try to incorporate the best physiological spatial diversity. These approaches not only estimates the most discriminating sources but also allow to recover some independent neurophysiological brain waves (according to the spatial diversity considered). Lastly we highlight the fact that the types of diversity mentioned here are sufficient conditions that can be provided to the joint diagonalization algorithm.

#### 3.2.2 Method 2: Exploiting inter-class diversity

This first model uses ICD and was shown to outperform the classical CSP [9]. We recall that this kind of diversity is exploited by considering task-specific covariance structures. For each trial of one specific task, we compute the covariance matrix of the EEG from $t = 2.5\,\mathrm{s}$ to $t = 7.5\,\mathrm{s}$. Then we average across every trials of one specific task. As this is done for every mental task, the procedure leads to a joint diagonalization of 4 covariance matrices (one for each task):

$$\mathcal{S} = \{\mathbb{E}_k(C_{xx}(t \in [2.5, 7.5], k)) \quad | \quad k \in [1 \ldots 4]\}$$

#### 3.2.3 Method 3: Exploiting inter-class diversity and time-varying energy

This second model aims at exploiting the idea that sources are active with different energies between different tasks and/or that the energy of a source is time-varying inside one task. This information is used by partitioning the previous interval to 4 subintervals, $[2.5, 7.5] = \cup_{i=1}^{4} \mathcal{T}_i$. Thus the diagonalization set consists of 16 covariance matrices:

$$\mathcal{S} = \{\mathbb{E}_k(C_{xx}(t \in \mathcal{T}_i, k)) \quad | \quad i \in [1..4], k \in [1 \ldots 4]\}$$

### 3.3 Global procedure

In order to test the generalization ability of each method, a cross-validation procedure is used. For each subject and each session, we have 72 trials for each of the four classes. We permute the 72 trials of each class to obtain four randomly ordered sets of labeled trials. We then select the first 7 trials of the four randomly ordered sets. They constitute the first test set of the cross-validation, the remaining trials constitute the first training set of the cross-validation. The second test set will be the 7 next trials of each class. One cross-validation is completed when the ten successive test sets and their associated training sets have been considered.

For each test and training sets, we apply the procedure as illustrated in Figure 1(b). We first consider the band-pass filtered signals corresponding to the training set to find the optimal spatial filters according to each methods. In the case of CSP, the best potential spatial filters are naturally ranked in the method, we only keep the first and last spatial filter of each of the one-versus-rest CSP, thus resulting in 8 spatial filters. In the case of method 2 and 3, the potential components are not ranked, we thus select relevant sources using the same method as [9], based on an approximation of the mutual information between the label and the sources. In order to achieve a fair comparison between the three methods, we also select the 8 best ranked sources and their associated spatial filters. Thus at the end of step one in Figure 1, we have 8 sources for each method. They correspond to the linear projections of the data onto the source space, depicting the same time courses as the EEG measurements.

The next step consists in computing the features related to each trial of the training set. In line with neurophysiological considerations, we computed the energy of each sources in the $\mu$ and $\beta$ band. This estimation is made by computing the Discrete Wavelet Transform of each sources. Thus the number of total features to be classified is 16 for each method. The features are gathered in a $65 \times 16$ matrix to train a LDA [5]. Parameters of the LDA are conserved for the test step.

Lastly, as depicted in Figure 1, the procedure is applied on the test set using the selected spatial filters to project the data, the same method to compute features for each trial. The LDA is used to classify features gathered in a $7 \times 16$ matrix.

This procedure is in fact applied 100 times, which corresponds to 10 cross-validations, a cross-validation consisting of 10 disjoint test sets.

# 4 Results

The mean classification accuracies across subjects and sessions are not significantly different: 70.7 %, 70.7 % and 70.6 % for respectively the CSP, ICD and ICD and TVE. Furthermore, we found a strong inter-subject variability. Overall, performances of our methods are satisfying considering the difficulty of the task. Our methods differ from the one employed in [5] because they did not select features according to some qualitative criterion. A slight increase of classification rates is thus not surprising. The best result was achieved with Infomax and was about 65 %. Moreover, Infomax was used in a completely blind manner and did not use any a priori information about the performed task to achieve the separation. Results obtained in [4] outperforms the results presented here (ranging from 65 to 75 %) but used a numerically demanding feature selection (sequential forward selection) to range about 1300 features from the feature extraction step.

High variability of classification rates across subjects (ranging from 40 to 80 %) leads us to consider subject-specific results. Table 1 presents results for each subject and each session. The classification rate (percentage and standard deviation) is considered in the second column of the table. All pairwise $t$-test comparing the three models for each subject separately using the cross-validations as observation units reveals that the best model outperforms the other two ($p < 0.5$) for five out of eight subjects (S2, S4, S5, S6, S7).

| | Correct (%) (Std Dev) | Best Model | | Correct (%) (Std Dev) | Best Model |
|---|---|---|---|---|---|
| S1 | 80.6 (0.9) | ICD, TVE | S5 | 82.1 (7.3) | CSP |
| S2 | 53.9 (2.2) | ICD, TVE | S6 | 62.8 (5.6) | CSP |
| S3 | 86.4 (1.5) | ICD | S7 | 43.3 (2.6) | ICD, TVE |
| S4 | 84.5 (2.2) | CSP | S8 | 86.0 (3.5) | ICD, TVE |

Table 1: Classification rates for each subject (S1 to S8) given by the best model.

## 4.1 Discussion

Different a priori information were considered in this paper, namely we used Inter-Class Diversity and Time-Varying Energy. First of all, we showed in Section 3 that finding multi-class spatial filters can benefit from the use of simple a priori knowledge. It was quite obvious that using a priori knowledge about the tasks performed would improve classification rates. But improvements due to a priori knowledge about time-varying energy was quite surprising. This result supports the hypothesis that different sources appears during the performance of the tasks and that their time course is not constant. Time interval partitioning was very simple and we think that some refined partitioning of intervals could result in significant improvements of the classification rates.

We pointed out a disadvantage of such a refined framework by showing that none of the presented methods could be considered as best for every subjects. Unsurprisingly, the design of optimal spatial filters have to cope with inherent difficulties of studying brains and real subjects: methods have to be subject-dependent to yield optimal results. This consideration has to be tackled to make such signal processing algorithm available for daily life use: an automatic procedure should be designed to select subject-specific methods.

## 5 Conclusion

In summary, we presented here an efficient framework for increasing classification rates of multi-class BCI paradigms. Our framework is well grounded on the Pham's theoretical work about joint approximate diagonalization and provides natural a priori knowledge that can be used to gather advantages of both Independent Component Analysis and Common Spatial Patterns.

## References

[1] N. Birbaumer and L. G. Cohen. Brain-computer-interfaces (BCI): Communication and restoration of movement in paralysis. *J. Physiol.*, 579:621–636, 2007.

[2] M. Congedo, F. Lotte, and A. Lécuyer. Classification of movement intention by spatially filtered electromagnetic inverse solutions. *Phys. Med. Biol.*, 51:1971–1989, 2006.

[3] C. Jutten and J. Hérault. Blind separation of sources, part 1: an adaptive algorithm based on neuromimetic architecture. *Signal Process.*, 24:1–10, 1991.

[4] C. Brunner, M. Naeem, R. Leeb, B. Graimann, and G. Pfurtscheller. Spatial filtering and selection of optimized components in four class motor imagery EEG data using independent components analysis. *Pattern Recognition Lett.*, 28:957–964, 2007.

[5] M. Naeem, C. Brunner, R. Leeb, B. Graimann, and G. Pfurtscheller. Seperability of four-class motor imagery data using independent components analysis. *J. Neural. Eng.*, 3:208–216, 2006.

[6] D.-T. Pham and J.-F. Cardoso. Blind separation of instantaneous mixtures of nonstationary sources. *IEEE Trans. Signal Process.*, 49:1837–1848, 2001.

[7] J. Müller-Gerking, G. Pfurtscheller, and H. Flyvbjerg. Designing optimal spatial filters for single-trial EEG classification in a movement task. *Clin. Neurophysiol.*, 110:787–798, 1999.

[8] G. Dornhege, B. Blankertz, G. Curio, and K.-R. Müller. Boosting bit rates in noninvasive EEG single-trial classifications by feature combination and multiclass paradigms. *IEEE Trans. Biomed. Eng.*, 51:993–1002, 2004.

[9] M. Grosse-Wentrup and M. Buss. Multi-class common spatial pattern and information theoretic feature extraction. *IEEE Trans. Biomed. Eng.*, 2008.

[10] C. Gouy-Pailler, M. Congedo, C. Jutten, C. Brunner, and G. Pfurtscheller. Model-based source separation for multi-class motor imagery. In *Proc. 16th European Signal Processing Conference (EUSIPCO-2008), EURASIP*, Lausanne, Switzerland, August 2008.

# Estimating noise and dimensionality in BCI data sets: towards illiteracy comprehension

C. Sannelli[1], M. Braun[1], M. Tangermann[1], K.-R. Müller[1,2]

[1]Machine Learning Laboratory, Dept. Computer Science, Berlin University of Technology, Berlin, Germany
[2]Intelligent Data Analysis Group, Fraunhofer FIRST, Berlin, Germany

claudia@cs.tu-berlin.de

**Abstract**

About one third of the BCI subjects cannot communicate via BCI, a phenomenon that is known as BCI illiteracy. New investigations aiming to an early prediction of illiteracy would be very helpful to understand this phenomenon and to avoid hard BCI training for many subjects. In this paper, the first application on to electroencephalogram (EEG) of a newly developed machine learning tool, Relevant Dimension Estimation (RDE), is presented. Detecting the label relevant information present in a data set, RDE estimates the intrinsic noise and the complexity of the learning problem. Applied to EEG data collected during motor imagery paradigms, RDE is able to deliver interesting insights into the illiteracy phenomenon. In particular RDE can demonstrate that illiteracy is mostly not due to the non-stationarity or high dimensionality present in the data, but rather due to a high intrinsic noise in the label related information. Moreover, in this paper is shown how to detect individual BCI-illiterate subjects in a very reliable way, based on a combination of the several features extracted by RDE.

## 1 Introduction

Rehabilitation and communication for amyotrophic lateral sclerosis (ALS) patients are the most important motivations and long term goals for Brain Computer Interfaces (BCI), a research area which has enjoyed a growing interest in the last decade. In contrast, most BCI studies are performed on healthy subjects and work on improving existing algorithms for the classification of mental states using electroencephalogram (EEG). Actually, about one third of the BCI-users is still not able to communicate with the machines. Even a healthy subject could become very frustrated during an experiment, when he realizes that he is a so called "BCI-illiterate", and very few patients are willing to experience this situation. BCI medical applications could find larger acceptance, if the ratio of BCI-illiterate users could be minimized to a very small percentage. A robust prediction of BCI illiteracy would also help to avoid false hopes and to reduce the efforts needed to train a patient for communication by BCI. For this purpose, new methods for EEG data set exploration and new features describing EEG data sets are needed in order to be used as predictors for BCI illiteracy.

Relevant Dimension Estimation (RDE) is an algorithm proposed in [1] which makes use of kernel PCA (Principal Component Analysis) in the feature space together with label information in order to assess the actual class related information contained in a data set. In particular, RDE estimates two properties: (1) the dimension of the subspace in kernel space containing the relevant information, and (2) the noise contained in the labels. Both numbers allow to measure the interaction between the data set and a chosen kernel, and in particular to give an accurate image of the problem complexity of the amount of noise contained in a learning problem.

| Setting Name | Band [Hz] | Time [ms] | Channels | Feature |
|---|---|---|---|---|
| calib-power-all | 0.5–45 | 750–4000 | all | band power |
| calib-power-sel | sel | sel | sel | band power |
| calib-power-cenCh | 0.5–45 | 750–4000 | C* | band power |
| calib-power-cenCh-alpha | 8–13 | 750–4000 | C* | band power |
| calib-CSP-feat | sel | sel | sel | CSP features |

Table 1: Preprocessing parameter settings.

In this study, a first application of RDE on EEG. Using Gaussian kernels of different widths, the dimensionality of the data set and the amount of noise is estimated at different scales. Our hypothesis is that a data set from an illiterate subject is intrinsically high dimensional and therefore not well classifiable with features generated by the Common Spatial Patterns (CSP) method. To test this hypothesis, features extracted by RDE are compared with the CSP features in terms of classification performance.

# 2 Experimental setup

A dataset of 48 BCI sessions from 40 healthy subjects has been investigated. Data was recording with the Berlin BCI (BBCI) during classical motor imagery BCI experiments (see e. g. [2, 3]). In the calibration session, the subjects were asked to perform 200–300 trials of motor imagery for the left or right hand and for the foot. Two classes were then chosen for the feedback session, depending on the offline classification performance of a linear classifier that processed CSP features [4]. In the feedback session, targets and feedback of the classifier output were given visually.

# 3 Methods

## 3.1 Preprocessing

Within this study, several preprocessing parameter settings have been used. The preprocessing steps for each setting are as follows: (1) low pass filtering at 100 Hz, (2) cutting continuous EEG in epochs in a specific time interval after the stimulus presentation, (3) optional channel selection, (4) rejecting bad trials and channels by variance based artifact rejection, (5) selecting trials belonging to the 2 classes already chosen for the online feedback, (6) filtering in a setting specific frequency band and (7) calculating band power.

Preprocessing settings differentiate in steps 2, 3, 6 and 7, see the overview in Table 1. In the Channel column, "all" means that all channels after step 2 are used in calculating the features, i. e. step 3 was ignored. On the contrary, "sel" means that a further channel selection has been applied. In particular, the channel subset was determined by a heuristic that at the day of the experiment in order to maximize CSP performance. The same convention for "sel" is valid for the second and third columns. Finally, C* means that all central channels (according to the 10–20 EEG system) were used.

## 3.2 RDE

RDE has been applied on each data set. A Gaussian RBF (radial basis function) kernel has been chosen. Two parameters had to be selected: the kernel width and the dimension, i. e. the number of leading kernel PCA components. The range for the kernel width $\gamma$ was between $10^{-2}$ and $10^{7}$. The range for the dimension $d$ was $[2, N/2]$ where $N$ is the number of trials available. For each kernel width $\gamma$, the kernel matrix $K(\gamma)$ and the sorted eigenvectors $E(\gamma)$ have been calculated. In order to estimate the kernel width and the dimension of each data set, both methods indicated in [1] have been used. The first method finds the kernel width $\gamma$ and the dimension $d$ which minimize the negative log-likelihood function $L(\gamma, d)$ defined as

$$L(\gamma, d) = \frac{d}{n} \log \sigma_1^2 + \frac{n-d}{n} \log \sigma_2^2 \tag{1}$$

$$\text{with} \qquad \sigma_1^2 = \frac{1}{d} \sum_{i=1}^{d} s_i^2 \qquad \text{and} \qquad \sigma_2^2 = \frac{1}{n-d} \sum_{i=d+1}^{n} s_i^2 \tag{2}$$

In the above equation, $s_i = u_i^T Y$ are the contributions to labels of the kernel PCA components and $u_i$ are the eigenvectors of $E(\gamma)$.

Within the second method, the label predictions are calculated for each parameter combination using the projections on the label of the kernel PCA components $S(d, \gamma) = \sum_{i=1}^{d} u_i u_i^T$. The best kernel width $\gamma$ and the dimension $d$ are then chosen minimizing the leave-one-out cross-validation error as computed in [5].

### 3.3 Noise estimation

The noise present in a data set is calculated by RDE as the mean squared error over the label predictions obtained using the estimated best number of kernel components and the best kernel width:

$$\text{Noise} = \frac{1}{N} \sum_{i=1}^{N} (SY_i - Y_i)^2 \tag{3}$$

The variance of the negative log-likelihoods over all kernel widths and kernel PCA dimensions has also been calculated as a feature, in order to capture the intrinsic noise. The smoothness of the log-likelihood function has also been calculated as the distance of the function from a smooth surface modelled by a fifth degree polynomial fitting the original function scaled between 0 and 1.

## 4 Results

### 4.1 Subject specific analysis

In Figure 1, the negative log-likelihood functions calculated as in Equation 1 for three different preprocessing settings (1, 2, and 3 described in Table 1) are shown. Results from a subject with very good BCI performance (calibration error = 3.20) are visualized in the top row, while results from a subject with bad BCI performance, probably illiterate (calibration error = 34.10) are visualized in the bottom row. An evident difference can be seen between the functions resulting for the two subjects, even with the first preprocessing, where no subject depending frequency band, channels and time interval selection has been applied.

Looking at the negative log-likelihood functions it can be hypothesized that the first method described in Section 3.2 will fail in searching the best kernel width and dimensionality, due to the extremely noisy function and many local minima. In fact, the results obtained looking at the minimum of the function 1 revealed to be not robust against small changing in preprocessing settings, especially for subjects with bad BCI performance. For this reason, the second method has been chosen to estimate robustly the best kernel width and the best dimension. Still, the negative log-likelihood function as shown in Figure 1 is extremely informative regarding the noise in feature space present in a data set and it is independent from the method chosen for parameter selection. The log-likelihood function for bad subjects is not just much less smooth, but its range is also much smaller than for good subjects. For this reason, as described in Section 3.3, the smoothness and the variance of the log-likelihood function have been calculated as additional features indicating the noise in the data set.

No significant improvement can be seen with other preprocessing settings, even with the subject specific parameter selections, as shown in the center column of Figure 1. Applying RDE on CSP features, which consist at most on 6 channels, the feature space becomes particularly free of noise

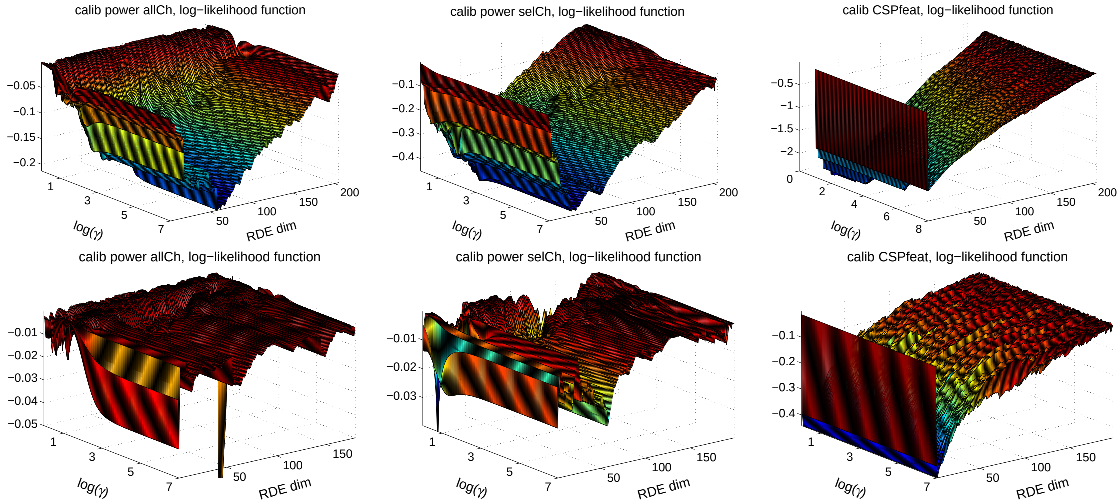


Figure 1: Negative log-likelihood function for all kernel widths and dimensions. Top: good performing BCI subject (CSP calibration error = 3.20). Bottom: bad performing BCI subject (CSP calibration error = 34.10). From left to right, three different preprocessing settings: calib-power-allCh, calib-power-selCh, calib-CSPfeat.

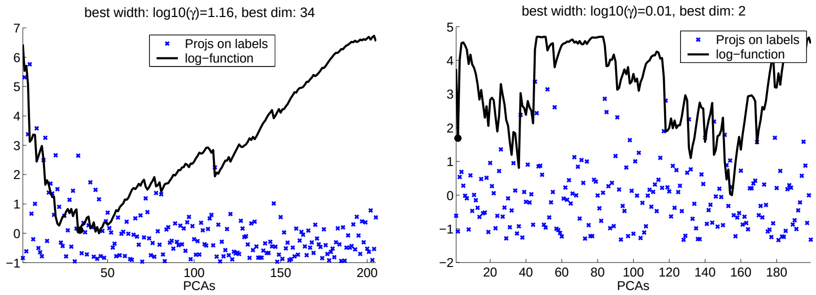


Figure 2: Negative log-likelihood function for the best kernel width. Preprocessing settings: calib-power-selCh. Left: good BCI subject. Right: bad BCI subject.

and low dimensional, so that the log-likelihood function is very smooth as shown on the right side of Figure 1. On the contrary, the surface extension is still much less for BCI subjects with poor performance, so that the variance is in fact a good feature to analyze.

In Figure 2, the negative log-likelihood function for the best kernel width is shown. The contributions of each kernel PCA component calculated as shown in Section 3.2 are visualized on the background. Also in this case, a strong difference between the two subjects can be observed. In particular, when less noise is present, the first kernel PCA components are much more informative, so that one can ideally separate the model in two components as in Equation 2, the first one containing the relevant information essential for label prediction and the second one containing mainly noise. In noisy data set as the second one, no structure can be seen in the contributions, since the noise is distributed over all components.

## 4.2 Group analysis

In order to simply confirm how much RDE features correlate with subject performance, we investigated the correlation between the features extracted by RDE with the simplest preprocessing setting calib-power-allCh and the CSP performance on the same calibration data set, i. e. the CSP

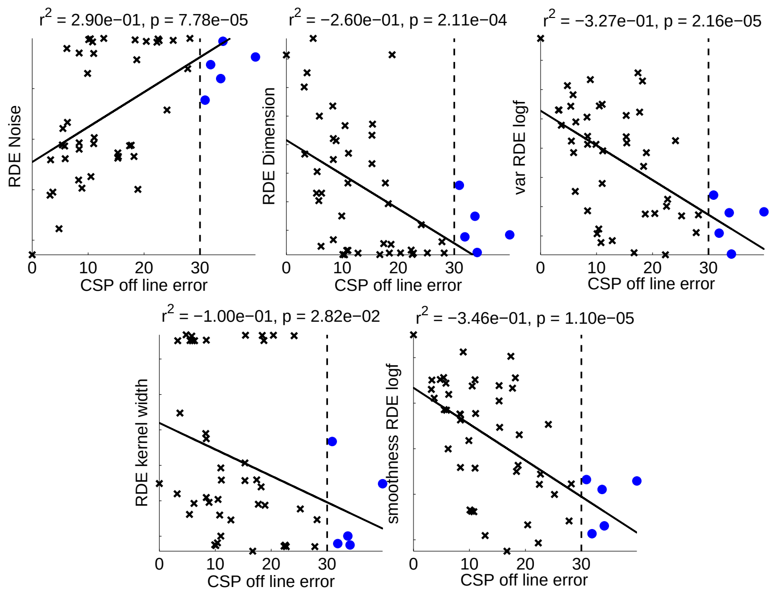


Figure 3: Correlation between RDE and CSP offline performance. Setting: calib-power-allCh.

offline error. The results are shown in Figure 3: for each subject, in each subplot, a RDE feature is plotted against the CSP offline error. Correlation and significance values are written in the titles. Already with the simplest setting, strong correlation with subject performance can be observed for all features and it becomes even stronger for the calib-power-selCh setting, not shown because of lack of space. Subjects with CSP offline classification error greater then 30 % are represented by circles, while crosses are used for the others. The two groups are divided by a vertical line. In particular, the subjects with worst performance are pretty close and can be grouped as points having the following properties: (1) high RDE noise, (2) small RDE dimensionality, (3) small kernel width, (4) small variance of the negative log-likelihood function, (5) small smoothness of the negative log-likelihood function.

A bigger challenge is to gain additional information about a subject using RDE, and try to predict from the calibration data his future online performance. For this reason, we investigated the correlation between RDE features for the calib-power-selCh setting and the CSP online error obtained from the feedback data. Results are shown in Figure 4 where the same conventions as in Figure 3 apply. Also, the correlation between CSP offline error and CSP online error is shown on the last subplot. Even if the correlation between CSP offline error and CSP online error is slightly better then for the RDE features, subjects with poor performance (CSP online error >= 30 %) can still be better characterized by (1) high RDE noise, (2) small RDE kernel width, (3) small RDE dimension, without using the CSP algorithm.

# 5 Discussion

In contrast to the hypothesis about the high dimensionality of BCI illiterate data sets, the RDE chooses very few kernel components for the feature subspace containing the label relevant information. This happens because the noise in the data set is so high that the relevant information is distributed over all components, as revealed by the structure of the projections in Figure 2. In fact, the high noise prevents RDE from choosing more components and forces RDE to choose a small kernel width. As explained in [1], particularly noisy free data set could also have very high dimensionality and very large kernel width, exactly at the opposite of BCI illiterates. This also means that illiteracy is not due to the non-stationarity present in the data, but rather due to a high intrinsic noise in the label information, meaning that the class membership cannot be

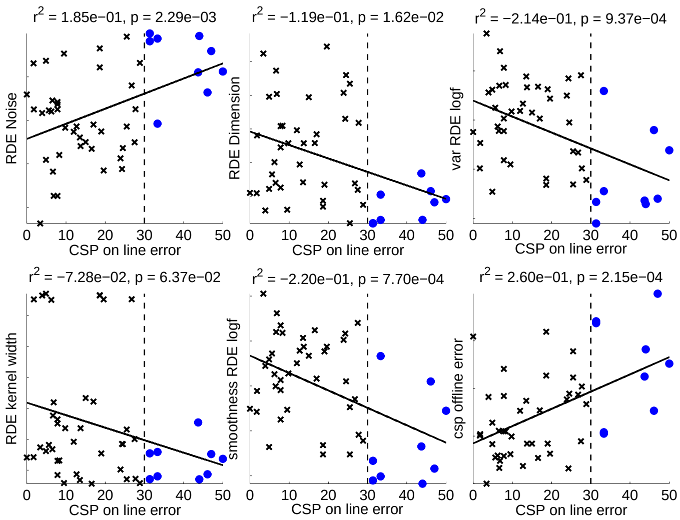


Figure 4: Correlation between RDE and CSP online performance. Setting: calib-power-selCh.

predicted well from the features over all whole range of possible scales. Finally, some subjects, not included in the illiterate group, exhibit a not so high noise, relative high dimension and kernel width would probably benefit from more training examples.

# 6 Conclusion

This study was motivated by the necessity to find new features that can predict the BCI performance of a subject with focus on an early illiteracy detection. For this reason, the RDE algorithm has applied on EEG data for the first time. The results show how RDE can be used on labeled data to understand the structure of the information contained in the data. In particular, RDE can be used to easily recognize illiterate subjects. It has been shown that the interaction among the three RDE parameters is valuable in order to understand whether a poor BCI classification performance is due to the intrinsic noise present in the data or due to a lack of training examples. Finally, the hypothesis of too high dimensionality of BCI illiterate data sets has been rejected.

**Acknowledgments:** This study was supported by the DFG (Deutsche Forschungsgemeinschaft) MU 987/3-1.

# References

[1] M. Braun, J. Buchmann, and K.-R. Müller. Denoising and dimension reduction in feature space. *Adv. Neural Inf. Process Syst. 19 (NIPS 2006)*, pages 185–192, 2007.

[2] B. Blankertz, G. Curio, and K.-R. Müller. Classifying single trial EEG: Towards brain computer interfacing. 14:157–164, 2002.

[3] B. Blankertz, G. Dornhege, M. Krauledat, K.-R. Müller, and G. Curio. The non-invasive Berlin Brain-Computer Interface: Fast acquisition of effective performance in untrained subjects. *NeuroImage*, 37:539–550, 2007.

[4] H. Ramoser, J. Müller-Gerking, and G. Pfurtsheller. Optimal spatial filtering of single trial eeg during imagined hand movement. *IEEE Trans. Rehab. Eng.*, 8(4):441–446, 2000.

[5] G. Wahba. Spline models for observational data. *Society Ind. and App. Mathematics*, 1990.

# Character identification on the P300 speller using subspace decomposition

E. Bojorges-Valdez, O. Yáñez-Suarez

Electrical Engineering Department, Universidad Autonoma Metropolitana, Mexico D.F.

bovedder@gmail.com

**Abstract**

Character identification on a P300 Speller is treated as a pattern recognition problem. SVM were used to detect ERP when character to spell were intensified. The input characteristics to SVM were the projections on an estimated signal subspace. This Subspace was estimated via eigendecomposition of correlation matrix, from a set of epochs containing ERP. ROC area for single trial ERP detection is $0.73 \pm 0.07$, and accuracy index of character identification were measure, as function of trials number.

## 1 Introduction

The P300 Speller is a BCI based on the correct identification of context update, as has been initially described by Farwell and Donchin [1] and now extended and adapted by many others [2]. This BCI presents to the user a character/symbol matrix, whose columns and rows are randomly intensified. In performing the BCI task, the subject must keep count of the number of times that a target character is intensified; this produces the context update and an event-related potential (ERP) is elicited. To identify the character, the BCI system must correctly detect the presence of the ERP, once for a column and once for a row intensification, which occur along a single trial of the task. The row and column identities give the coordinates of the target character. Several number of trials are necessary to correctly identify the character, and therefore a method that reduces required trials is desirable.

EEG recording epochs throughout the realization of a character identification task can be considered as a combination of two uncorrelated signals, an ERP, $\mathbf{s}$, and uncorrelated, zero mean additive noise $\boldsymbol{\eta}$ [3, 4], both expressed as column vectors of $M$ samples (one vector equals one epoch). Thus, the correlation matrix estimates for the intensification epochs will have the form [5]:

$$R_z = E\{\mathbf{z}\mathbf{z}'\} = E\{(\mathbf{s}+\boldsymbol{\eta})(\mathbf{s}+\boldsymbol{\eta})'\} = R_s + R_\eta \quad (1)$$

where $R_s$ is the correlation matrix estimate for the ERP, and $R_\eta$ is the noise correlation matrix estimate. Forming the *data matrix* $\mathbf{Z} = [\mathbf{z}_1 \ldots \mathbf{z}_N]$ where each column is an EEG epoch, $R_z$ can be estimated using $\hat{R}_z \approx \mathbf{Z}\mathbf{Z}'$, which is symmetric, and so the eigendecomposition

$$E\Lambda = \hat{R}_z E \quad (2)$$

can be computed. With the eigendecomposition, a set of orthogonal eigenvectors (columns of $E$) and associated eigenvalues (diagonal of $\Lambda$) are obtained. The set of eigenvectors conforms a basis that spans a space where each observation $\mathbf{z}$ resides [5].

$E$ contains the vectors that describe the ERP ($E_s$) and those that describe noise ($E_\eta$), so $E$ is a set of two subspaces, i.e. $E = [E_\eta\, E_s]$. To perform subspace decomposition of the EEG signals, it is necessary to identify which vectors correspond to each subspace. Eigenvalues are associated to the power that each eigenvector contributes to build $\mathbf{Z}$; specifically, noise eigenvalues under ideal white noise conditions have the same value ($\sigma^2$, the noise variance). If eigenvalues are sorted in ascending order, $\lambda_1 \leq \ldots \lambda_k \ldots \leq \lambda_N$ , there exists an inflection point $k$ at which both subspaces are divided. The Akaike information criterion finds this inflection point based exclusively on eigenvalues [6], by computing the minimum $k^*$ of

$$AIC(k) = -2Nk\phi(k) + 2(M+1-k)(M+1+k) \tag{3}$$

where $N$ corresponds to the number of signal vectors in $\mathbf{Z}$, $M$ is the number of samples per vector $\mathbf{z}_i$, and $\phi(k)$ is the likelihood function:

$$\phi(k) = \log\left(\frac{\prod_{i=0}^{k-1} \lambda_i^{1/k}}{\prod_{i=0}^{k-1} \frac{\lambda_i}{k}}\right) \tag{4}$$

Given $k^*$ as the minimum of equation (3), eigenvectors from 1 to $k^*$ correspond to the noise subspace, $E_\eta$, and those from $k^*+1$ to $N$ are the eigenvectors that span signal subspace $E_s$. With the identified subspaces, signal $\mathbf{z}$ can be modelled as:

$$\begin{aligned} \mathbf{z} &= \mathbf{s} + \boldsymbol{\eta} \\ &= E_s\boldsymbol{\theta} + E_{\boldsymbol{\eta}}\boldsymbol{\varphi} \end{aligned} \tag{5}$$

where $\boldsymbol{\theta}$ and $\boldsymbol{\varphi}$ are coefficients that weigh each subspace vector. Since both subspaces were obtained via eigendecomposition, the inner products with vectors in $E_s$ gives

$$\begin{aligned} E_s'\mathbf{z} &= E_s'E_s\boldsymbol{\theta} + E_s'E_\eta\boldsymbol{\varphi} \\ &= \mathbf{I}\,\boldsymbol{\theta} + 0\,\boldsymbol{\varphi} = \boldsymbol{\theta} \end{aligned} \tag{6}$$

It follows that the projections $\boldsymbol{\theta}$ are features that can be used as inputs for a pattern recognition process that identifies ERP vs. no-ERP epochs.

Some researchers have described the P300 Speller as the succession of different processes. In this perspective, five different waves are elicited by the oddball paradigm: P100, N100, P200, N200 and P300. Except for N200 and P300, the rest of the waves are related to activation of primary sensory areas [7]. Some authors have associated these waves to different sensory processes, P100 and N100 to the visual estimulation, P200 to attention, and P300 to context update [8]. These waves could serve as auxiliary information for the detection of P300, since their conjunction conforms the complete ERP, even when in some subjects elicitation of all these waves is not clearly observable. Based on these observations, three different time windows can be used to detect the presence of all these waves, one for P100 and N100, a second one for P200 and N200, and finally one more for the P300 wave. Proposed observation windows are 0–200 ms, 100–300 ms and 250–600 ms; a wider window in the P300 case is due to its more variable latency [7].

In order to achieve the detection of an ERP, and thus perform the identification of characters, a subspace estimation is carried out for each analysis window during the training phase. Then, for each epoch and window, a vector of $\boldsymbol{\phi}$ characteristics was obtained; a feature vector for each $\mathbf{z}$ is formed by concatenation of these three sets of coefficients. As described above, the number of features in each set is determined by the Akaike criterion. Finally, since more than one channel can be used to record EEG activity which might be useful for detection, feature vectors can be further expanded by gathering features from each channel for every epoch. The dimension of the complete feature vector is given by

$$D = \sum_{c=i}^{C} \sum_{w=1}^{3} N_{w,c} \tag{7}$$

where $C$ is the number of channel considered for the detection; $c$ and $w$ are the channel and window indexes respectively; and $N_{w,c}$ is the number of eigenvectors that conforms the signal subspace based on the Akaike criterion.

# 2 Methods

## 2.1 Data

Data were recorded from six healthy subjects performing the P300 speller test; for all the subjects involved this was their first contact with the BCI. Recordings were made with a g.tec USB amplifier (g.tec, Graz, Austria) using the BCI2000 platform [2], at a sampling frequency of 256 Hz, using band pass filter from 0.1 to 30 Hz, and a notch filter between 40 and 60 Hz. All subjects spell from 2 to 4 words, with a mean number of spelled characters of 12. Intensification and inter stimulus time were 125 ms and 62.5 ms, respectively. All recordings were directed, so each subject spell one word from a predefined list. Before analysis an offline processing were made, data were filtered with a low pass digital filter (FIR order 151) at 12 Hz, and normalized in amplitude between 1 and -1. Post-stimulus windows were obtained and labeled as described before.

## 2.2 Analysis

EEG channels to be included in the analysis were selected according to their SNR, and correlation index along full-word recordings; this means that those channels (up to a maximum of four) that had larger SNR and a high correlation index were selected. i. e. those channel that present the most similar behavior through different word recordings, were possible channel to be used for classification, and from that selection those with larger SNR were finally used. The classification model used was a support vector machine (SVM) with a gaussian kernel, as implemented in the LIBSVM library [9].

Three different analysis were performed: first, to determine which combination of channels gets better classification indexes; second, to optimize classifier hyper-parameters (kernel $\gamma$ and cost); and third, to evaluate accuracy on an offline P300 speller test.

Channel Combination. First analysis consisted on the utilization of 30 signals with ERP of one recording to estimate subspaces; unseen epochs from the two classes (with/without ERP) were used in an equiprobable mix to extract features. Through 10-way cross-validation, optimal classifiers were obtained for individual channels, and combinations of two to four channels, as described. The best combination, determined by ROC analysis and classification accuracy, was selected for tuning in the second analysis.

Optimization. In the second analysis, one recording was used to estimate subspaces, and the others recordings were used to map ROC area and accuracy index along various values of $\gamma$ and cost, to search for the combination with the best indexes. If more than two recordings were available, the analysis was carried out using the different combinations between registers. As result of this, cost and $\gamma$ values with best classification indexes were chosen to perform an offline P300 Speller test.

Offline P300 test. Once a channel combination and SVM hyper-parameters were determined, offline testing was performed. As for the second analysis, one recording was used to perform estimation of subspaces, and to train the SVM. The SVM training was made taking an equiprobable mix of epochs. With the trained SVM and the estimated subspaces, the remaining recordings are processed by the classifier. For each epoch that corresponds to intensification of one column or one row, class probability is calculated as function of SVM classification. A posteriori probability estimates for each column and row are computed as follows:

$$P(e) = \Phi(\mathbf{f}(\mathbf{z}_e)) \qquad P(e) \in [0, 1] \tag{8}$$

where $e$ indicates the intensification index ($[1, \ldots, 12]$ columns from 1 to 6 and rows from 7 to 12); $\Phi(\cdot)$ is a mapping function from SVM output to posterior probability [9, 10] classification function, and $\mathbf{f}(\mathbf{z}_e)$ means feature vector from post processed EEG recording at $e$-th stimulus. The posterior probability is accumulative trial by trial, so at end the correct character has a larger probability than the others. A column is selected as $\underset{e}{\operatorname{argmax}}\{P(e)\},\ e \in [1, \ldots, 6]$ and equivalently the row is selected over $e \in [7, \ldots, 12]$. ROC areas were measured as a function of trial number.

### 2.3 Results

Channels used for analysis varied depending on each subject. Except for one case, the channels that reflected best subject's activity involved at least one channel from the occipital region, together with central channels. Number of best channel combinations varied from 2 to 4. Globally, channels used were from FP1, FP2, Cz, C4, Pz, O1, Oz and O2.

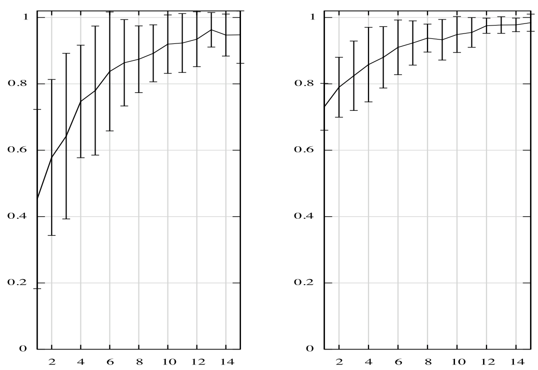

(a) accuracy (b) ROC area

Figure 1: Mean accuracy and mean ROC area for the 6 subjects.

Figure 1 shows progression of accuracy and ROC area, as function of trial number. These figures show mean value and standard deviation across the six subjects. It is noted that subjects E and F made the test twice. Detailed progression by subject could be observed in Figure 2.

## 3 Discussion

Figures 1 and 2 show that classification vary depending on subject. It is important to note that all subjects made the test for their first time ever, so they were not trained and had no previous knowledge about it. Subjects spell around 12 characters each, and since one record was taken to estimate subspaces and train the SVM, then accuracy and ROC area are estimated over the detection of eight characters on average, so a mistake in detection has a significant impact on the indexes. ROC area is an unbiased index for classification, for this the number of events has a minor impact than for accuracy. The ROC area in single trial was around 0.7, and it increased as a function of number of trials. Contrary to accuracy, ROC area had less variation between subjects.

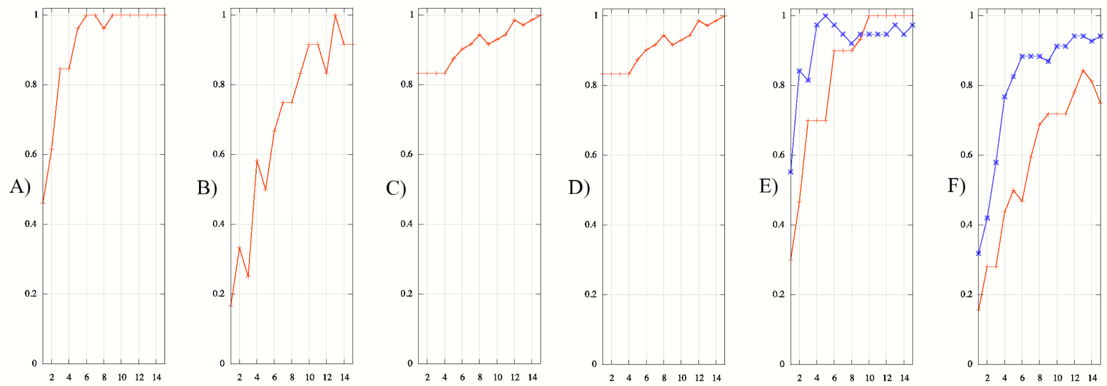

(a) accuracy

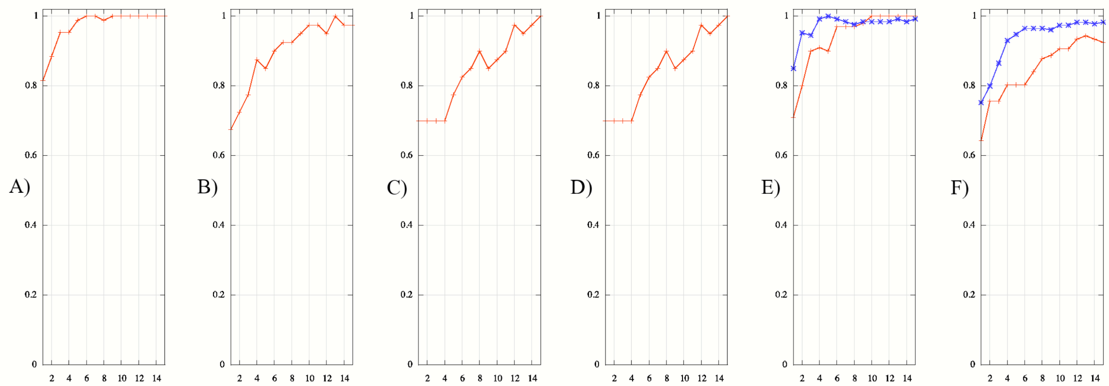

(b) ROC area

Figure 2: Accuracy and ROC area for the 6 subjects. Each subject is indicated by a capital letter. For subjects E and F, two curves are shown, each one corresponds to different session ("+" for first, and "∗" for second).

Due to the small number of characters, the SVM was trained with few patterns, while it is known that an increase in the number of training patterns would increase classification efficiency. Results show that even with this limited number of patterns, the subspace decomposition presented here has good efficiency in terms of accuracy and ROC area.

For subjects E and F, who made the test twice (in different days), an effect of increment of their respective indexes is observed, possibly due to a mild training process of these subjects. This situation hints that indexes could increase if subjects spell more characters, apart from reducing overall variance. Spelling more characters gives more epochs to improve classifier training, subjects get used to the BCI, and the impact of mistakes over accuracy index will reduce.

Results show that the proposed method is able to be included as a classification process for an online P300 Speller. Improvements from other classification methods are that few epochs (around 240) are needed to obtain good results, and the SVM could be re-trained with new patterns in a fast, efficient way. The ROC area index shows that the detection of ERP based on subspace features has good single-trial results, 0.7 on average, which naturally increases with accumulated trials. It is expected that the inclusion of language models [11] would improve the system performance.

## 4 Conclusion

The evaluation of the proposed feature extraction method has demonstrated its viability to be used in an online speller test. Around 240 epochs (half of them with ERP) were utilized for SVM training, and even with this small set, adequate results have been reached. Accuracy index in character detection is $45 \pm 27\,\%$ and ROC area of $0.73 \pm 0.07$ for ERP identification in single trial.

Subject training could increase classification indexes; if this occurs, then the number of trials for a correct identification could be reduced more. For the best subjects in this study, around 5 trials were enough to obtain 90 % of correct identification. Taking into account that all the subjects used the P300 Speller for their first time, this is a promising indicator. Training improvement could be observed in subjects E and F for whom single trial indexes increase evidently from one session to the next.

**Acknowledgments:** The authors acknowledge the support of the National Council of Science and Technology (CONACyT) through scholarship 193307 for Mr. Bojorges-Valdez, and the contribution of the Universidad Nacional de Entre Ríos (UNER, Argentina) in hosting the speller experiments.

## References

[1] L. A. Farwell and E. Donchin. Talking off the top of your head – toward a mental prosthesis utilizing event-related brain potentials. *Electroencephalogr. Clin. Neurophysiol.*, 70:510–523, 1988.

[2] G. Schalk, D. McFarlad, T. Hinterberger, N. Birbaumer, and J. R. Wolpaw. BCI2000: A general-purpose brain-computer interface. *IEEE Trans. Biomed. Eng.*, 51(6):1034–1043, 2004.

[3] P. Kisilev, Y. Y. Zeevi, and H. Pratt. Estimation of single-trial evoked signals by local transform domain filtering. *Proc. 9th Elec.tec. Conf. MELECON*, pages 658–662, 1998.

[4] P. Kisilev, Y. Y. Zeevi, and H. Pratt. Local transform processing of single-trial evoked potential. Proc. 1st BMES/EMBS Conf., 1999.

[5] C. Therrien. *Discrete Random Signal and Statistical Processing.* Prentice-Hall Signal Processing Series, 1992.

[6] M. Akay. *Detection and Estimation Methods for Biomedical Signals.* Academic Press, 1996.

[7] T. Hruby and P. Marsalek. Event-related potential – the P3 wave. *Neurobiol. Exp.*, pages 55–63, 2003.

[8] B. Kotchoubey. Event-related potentials, cognition, and behavior a biological approach. *Neurosci. Biobehav. Rev.*, pages 42–65, 2006.

[9] C.-C. Chang and C.-J. Lin. *LIBSVM: a library for support vector machines*, 2001. Software available at `http://www.csie.ntu.edu.tw/~cjlin/libsvm`.

[10] J. C. Platt. Probabilistic outputs for support vector machines and comparisson to regularized likelihood methods. *Microsoft Res., http://research.microsoft.com/~jplatt*, 1992.

[11] A. Jimenez-Ramos and O. Y. Suarez. Improving bit-rate in P300-based BCI using grammatical rules and language probability. *Proc. 3rd Int. BCI Workshop and Training Course*, pages 96–97, 2006.

# Classifying P300 paradigm data with Fisher linear discriminant and discrete wavelet transform

M. Salvaris, F. Sepulveda

BCI Group, Department of Computing and Electronic System, University of Essex, UK

mssalv@essex.ac.uk

**Abstract**

The P300 data provided by the Wardsworth centre for the BCI competition II and III have been used as a benchmark to assess the performance of many differing methods of P300 classification. In this paper the use of the discrete wavelet transform and the Fisher linear discriminant to classify data set IIb from the BCI competition II is presented. The wavelet chosen was coif3 since it closely resembles the desired wave shape and also produced good results in extracting the necessary features. The performance of the proposed method is equal to the winning one presented on the BCI competition II website, utilising the same channels but using a feature vector of almost a fifth of the size and requiring no parameter tuning. Furthermore the proposed method is considerably quicker and computationally inexpensive.

## 1 Introduction

The P3 or P300 BCI paradigm is a synchronous BCI paradigm named so due to the positive deflection of the EEG at the central electrodes around 300 ms post stimulus. The P300 or P3 is an attention based event related potential and can be caused by visual, auditory and somatosensory stimuli. The user is able to interact with the interface by paying attention to certain stimuli while ignoring others [1, 2]. The protocol used to collect the data for data set IIb is the one originally used by Farwell and Donchin [2], where the user was presented with a matrix of symbols and each row and column would flash randomly. The user would only pay attention and mentally record the row or column flashes that happened to contain the symbol they desired to select.

The Fisher Linear Discriminant (FLD), or Fisher's LDA, is a linear classifier which aims to separate the data representing two classes through hyperplanes by maximising the difference in the projected class means while reducing the variance of the projected data [3]. The linear nature of the classifier offers some advantages and disadvantages. The main advantages of the FLD are its simplicity and speed of execution. Its disadvantages are the lack of a regularisation parameter and its linearity. Despite these drawbacks, FLD and similar variants have been successfully applied to a number of BCI problems [4, 5]. The FLD function used in this work was the one provided by the statistical pattern recognition toolbox for Matlab [6].

A wavelet is a limited duration waveform with an average value of zero [7]. There are a multitude of wavelets with varying properties and suitability for certain tasks. It is very important to select the most suitable wavelet for analysing the intended signal. One way of selecting an appropriate wavelet is to observe the desired wave shape and chose one that closely matches its shape [8] (Figure 1). All the wavelet methods used to complete this work are available in the Matlab wavelet toolbox [9].

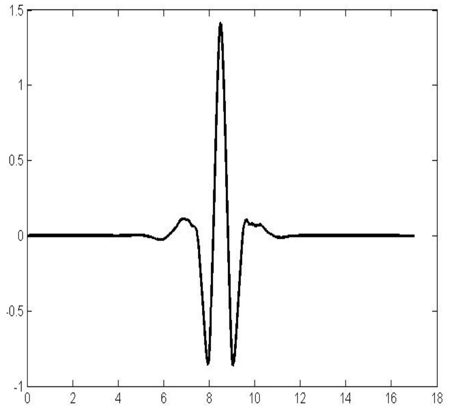


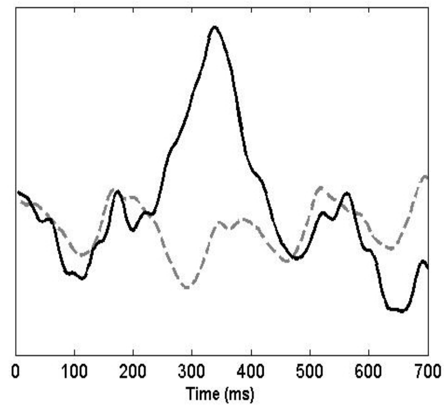


Figure 1: Left: Coif3 wavelet. Right: Grand average of the target (solid line) and non-target (dashed line) responses.

# 2 Methods

## 2.1 Signal processing

The data as provided by the BCI competition II website was sampled at 240 Hz at 64 electrode sites [10]. The data were later lowpass filtered at 30 Hz and highpass filtered at 0.1 Hz using a $8^{\text{th}}$ order Butterworth filter. The channels chosen were: Fz, Cz, Pz, Oz, C3, C4, P3, P4, PO7, PO8, due to their successful use with the BCI competition II and other P300 data sets [11, 12, 13]. The data was then downsampled to 60 Hz.

## 2.2 BCI paradigm

The subject was presented with a $6 \times 6$ matrix containing a total of 36 symbols. Each row and column of the matrix is highlighted in random order and once within a trial. For a letter to be selected the user must select one column and one row. So within a trial 2 out of the 12 row/column intensification's should contain an increased amplitude P300.

## 2.3 Data

The data provided contained 42 training symbols and 31 test symbols, each composed of 15 trials. Out of the 42 available training samples only 39 were used, since the last set of training data contained an error in the event cue information. The error was not evident in the EEG but in the matrices containing the event cue onset, offset times and type (StimulusCode, StimulusType, Flashing). It is conceivable that the erroneous cue may cause subsequent event cues to be reported at incorrect time points. Fault tolerance and prevention of such errors in an on-line system should not lie with the preprocessing and classification software, but with the software carrying out the recording from the EEG device. Therefore a solution for this type of fault is considered beyond the scope of this work.

## 2.4 DWT processing and FLD training

After the data had been preprocessed a period of 700 ms post stimulus was selected from each of the 10 chosen channels. This meant that each epoch was represented by a $10 \times 42$ sample matrix. Each 42 sample vector was then decomposed using single level wavelet decomposition, resulting in an approximation and detail vector. The approximation vector was chosen and the detail discarded. Wavelet used was coif3. This resulted in the epoch being represented by a $10 \times 21$

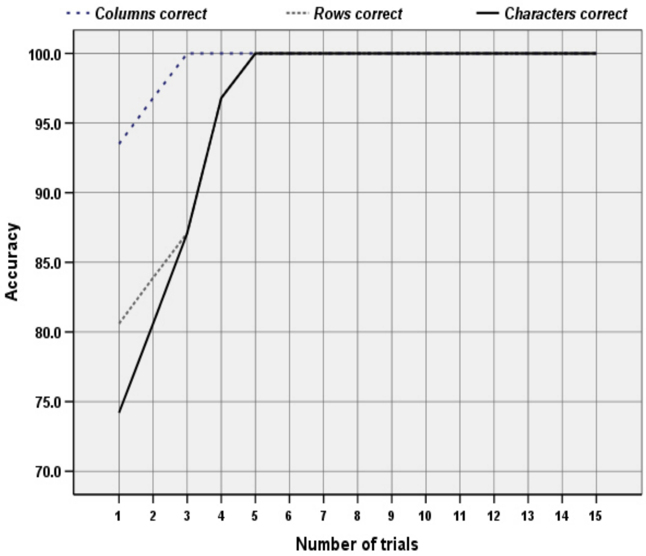


Figure 2: FLD+DWT Column/row/character accuracy across trials.

matrix. The matrix was then reshaped to make a 210 element vector. This 210 element vector would be the input to the FLD classifier. At each trial only two out of the 12 epochs should contain a target P300. Unfortunately this means that the data is unbalanced (there are more negative samples than positive). This is often solved in two ways, either by subsampling or oversampling. Although subsampling has been used successfully by a previous entrant [11] the method favoured here is oversampling due to the inclusion of all the data available. Before the data is classified it is normalised to zero mean and unit variance. The classifier is then trained to distinguish into which of the two classes the epoch belongs to. These two classes are whether a P300 exists or whether it does not.

### 2.5 Test data classification

At each epoch the 210 element feature vector is the input to the FLD and the predicted class the output (1 for P300 present 2 for P300 not present). The data is usually too noisy for the classifier to be able to correctly identify the chosen row/column from one trial alone. Multiple trials are combined by summing the discriminant function values for each row and column at each trial. The discriminant values are positive for the presence of P300 and negative for the absence. After the set number of trials the row and column with the largest values are the ones selected.

## 3 Results

This method achieved an 88.4 % correct classification rate for distinguishing between the presence or absence of the P300 in the epoch. It was also able to achieve 100 % classification of the test set after only 5 trials per symbol spelt (Figure 2). For a lower number of trials, the error increases.

## 4 Discussion

The P300 BCI paradigm provides some of the highest achievable information transfer rates using non-invasive BCI. The results achieved using the FLD and DWT combination are as good as

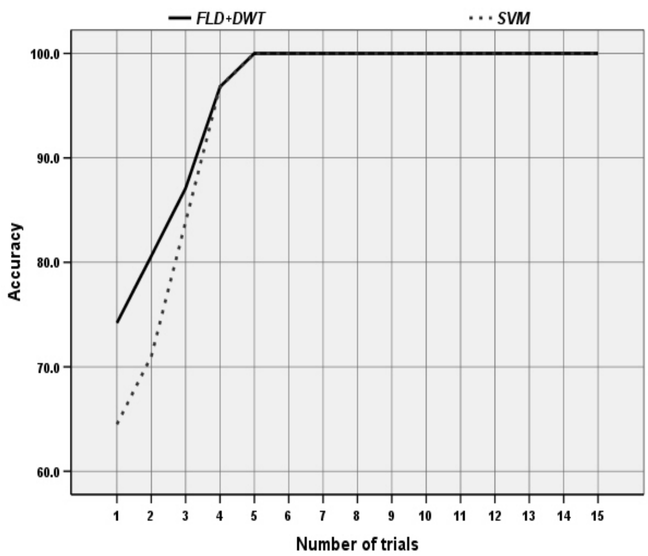


Figure 3: FLD+DWT vs. SVM character classification accuracy (SVM results taken from Kaper et. al [11]).

the results presented by the winner of the BCI competition II data set IIb, when comparing the number of trials required to achieve 100 % classification [14, 11] (Figure 3). Also Rakotomamonjy et. al [15], using the same 10 channels used in this study, achieve the same result (5 trials for 100 % accuracy), at a much greater computational cost. It is also important to emphasise the following points about the present study:

1. The feature vector was 210 samples long.
2. The same 10 channels are used as in Kaper et. al [11].
3. No channel selection method was used.
4. The classifier used was very simple and fast.
5. The classifier required no parameter tuning.
6. Only one classifier was used to classify whole test set.
7. Only 2 trials were needed to achieve 80 % character recognition (Figures 2 and 3).

Although no time estimates for the parameter tuning and training time were provided by Kaper et. al [11], using the same methods and libraries on a Q6600 at 2.4 Ghz took over 10 hours. It can be envisioned that due to the channel selection procedure and the multiple SVMs the method proposed by Rakotomamonjy et. al [15] would take even longer. In comparison the method presented here on a Q6600 at 2.4 Ghz took 6 minutes. Furthermore the time required to classify data using the FLD+DWT method is quicker than the SVM methods mentioned by Kaper et. al and Rakotomamonjy et. al [11, 15]. This makes the FLD+DWT method ideal for online BCI since it would allow the person to have a classifier ready in under 10 minutes (dependant on the amount of data provided for training and processing power of computer). Although the classification rate presented here is very high, it could possibly be further improved by replacing the FLD with an SVM or other classifiers and carrying out a channel selection method. How much improvement can be gleaned by using such computationally intensive methods would have to be seen. Also the fast execution and training of the FLD lends itself well to be used in an ensemble. The wavelet chosen has proven to be a good candidate for P300 preprocessing, but it may not be the best one. Possibly the one proposed by E. Glassman [16] or the matched Meyer ERP wavelet [8] may provide even better results.

On a final note, when observing the accuracy rates of the correct columns and rows one notices that on average the rows classification is much worse than that of the columns. In fact, if the row classification was as high as that of the columns, it is perfectly conceivable that 100 % classification could be achieved in less than 5 trials. The reason for the greater accuracy for the column classification may be due to the subject or possibly an inherent shortcoming of the Farwell and Donchin paradigm.

# 5 Conclusion

This paper has shown that the use of DWT preprocessing in EEG classification can lead to state of the art results even when combined with a simple linear classifiers such as the FLD. Furthermore the simplicity and speed of the method makes it highly suitable for online BCI applications. The use of wavelets in BCI is only beginning to be explored and although it is doubtful it will be a silver bullet for BCI it will be a very useful preprocessing tool not only for EEG data but possibly ECoG and intracortical recordings too.

**Acknowledgments:** This work was supported by the UK's EPSRC through grant number GR/T09903/01. All authors are with the BCI Group, Dept. of Computing and Electronic Systems, University of Essex, United Kingdom. Address for correspondence: F. Sepulveda, Computing and Electronic Systems, University of Essex, Wivenhoe Park, Colchester CO4 3SQ, UK (e-mail: `fsepulv@essex.ac.uk`). The authors would like to acknowledge the guidance provided by Yusuf U. Khan on the use of the Matlab wavelet toolbox.

# References

[1] J. R. Wolpaw, N. Birbaumer, D. J. McFarland, G. Pfurtscheller, and T. M. Vaughan. Brain-computer interfaces for communication and control. *Clin. Neurophysiol.*, 113:767–791, 2002.

[2] L. A. Farwell and E. Donchin. Talking off the top of your head: toward a mental prosthesis utilizing event related brain potentials. *Electroenceph. Clin. Neurophysiol.*, 70:510–523, 1988.

[3] R. O. Duda, P. E. Hart, and D. G. Stork. *Pattern Classification.* Wiley, 2001.

[4] F. Lotte, M. Congedo, A. L'ecuyer, F. Lamarche, and B. Arnaldi. A review of classification algorithms for EEG-based brain-computer interfaces. *J. Neural Eng.*, 4:R1–R13, 2007.

[5] G. Dornhege, J. del R. Millán, T. Hinterberger, D. J. McFarland, and K.-R. Müller, editors. *Toward Brain-Computer Interfacing.* MIT Press, 2007.

[6] V. Franc and V. Hlaváč. Statistical pattern recognition toolbox for Matlab. Research Report CTU–CMP–2004–08, Center for Machine Perception, K13133 FEE Czech Technical University, Prague, Czech Republic, June 2004.

[7] G. Strang and T. Nguyen. *Wavelets and Filter Banks.* Wellesley-Cambridge Press, 1997.

[8] V.J. Samar, A. Bopardikar, R. Raghuveer, and K. Swartz. Wavelet analysis of neuroelectric waveforms: A conceptual tutorial. *Brain Lang.*, 66(1):7–60, Jan 1999.

[9] Matlab wavelet toolbox. [Online]. last accesssed: 5th February 2008 http://www.mathworks.com.

[10] B. Blankertz. BCI competition 2003. [Online]. last accessed: 5th March 2008 http://ida.first.fhg.de/projects/bci/competition/.

[11] M. Kaper, P. Meinicke, U. Grossekathöfer, T. Linger, and H. Ritter. BCI competition 2003 – data set iib: support vector machines for the P300 speller paradigm. *IEEE Trans. Biomed. Eng.*, 51:1073–1076, 2004.

[12] D. J. Krusienski, E. W. Sellers, D. J. McFarland, T. M. Vaughan, and J. R. Wolpaw. Toward enhanced P300 speller performance. *J. Neurosci. Meth.*, 167:15–21, 2008.

[13] D. J. Krusienski, E. W. Sellers, F. Cabestaing, S. Bayoudh, D. J. McFarland, T. M. Vaughan, and J. R. Wolpaw. A comparison of classification techniques for the P300 speller. *J. Neural Eng.*, 3:299–305, 2006.

[14] B. Blankertz, K.-R. Müller, G. Curio, T. M. Vaughan, G. Schalk, J. R. Wolpaw, A. Schlögl, C. Neuper, G. Pfurtscheller, T. Hinterberger, M. Schröder, and N. Birbaumer. The BCI competition 2003: progress and perspectives in detection and discrimination of EEG single trials. *IEEE Trans. Biomed. Eng.*, 51:1044–1051, 2004.

[15] A. Rakotomamonjy, V. Guigue, G. Mallet, and V. Alvarado. Ensemble of SVMs for improving brain computer interface P300 speller performances. *Lect. Notes Comp. Sci.*, 3696:45–50, 2005.

[16] E. L. Glassman. A wavelet-like filter based on neuron action potentials for analysis of human scalp electroencephalographs. *IEEE Trans. Biomed. Eng.*, 52:1851–1862, 2005.

# Averaging techniques for single-trial analysis of oddball event-related potentials

N. Liang, L. Bougrain

INRIA Nancy – Grand Est, France

nanying.liang@loria.fr

**Abstract**

More and more effort is done in BCI research to improve its usability for patients, with respect to its communication speed and transmission accuracy. In this contribution, we experiment with BCI speller based on P300 evoked potential. More precisely, the typical form of event-related potential (ERP) inspires us to devise classification methods based on the similarity/dissimilarity in the time domain between single trials and one or several estimated ERP templates derived from subject recordings. The reliable estimation of template is difficult in a single trial due to the low signal-to-noise ratio (SNR) of electroencephalographic (EEG) signals. We first explicitly estimate the template using several averaging techniques: point-to-point averaging, cross-correlation alignment and dynamic time warping. Then we inexplicitly estimate several ERP templates using learning vector quantization algorithm combined with an extreme learning machine. Finally classification is realized based on the similarity/dissimilarity between the single trials and the template. Simulation is carried out using a BCI competition III data set acquired with the P300 speller paradigm. The experiments show that template-based classifiers can also obtain high accuracy.

## 1 Introduction

Brain-computer interface (BCI) system is a potentially powerful new communication and control option for those with severe motor disabilities. BCI system translates brain activity into commands for a computer or other devices. Electroencephalography (EEG) is the most studied potential non-invasive interface mainly due to its fine temporal resolution, ease of use, portability and low set-up cost. Unfortunately, non-invasive implants produce a noisy signal because the skull dampens signals. Another substantial barrier to use EEG as a brain-computer interface is the extensive training required before users can work the technology.

Oddball paradigms are used by brain-computer interfaces to generate event-related potential (ERP) on targets selected by the user. The well-known P300 speller is based on this principle [1]. The main problem is to be able to detect ERP in a noisy electroencephalographic signal recorded on human scalp. Literature proposes a set of methods to detect ERPs based on averaging. Linear or nonlinear alignment is used to deal with the variable latencies in ERPs. A good alignment allows to obtain a better averaged ERP response, named "ERP template" here, and then to be able to detect ERP faster.

Section 2 of this paper presents a set of methods of template-based classifiers. Section 3 presents the results of these techniques on a well-known third BCI2000 competition data set acquired from a P300 speller. In section 4, we conduct the conclusion and give recommendation for future works.

## 2 Methods

Methods design for ERP detection use features extracted from the responses in the time domain. To extract features from the frequency domain after any transformation is difficult in this situation because ERPs are short-time events with a local peak. Here, we discuss two types of methods using one or several templates estimated explicitly and inexplicitly in the time domain respectively.

## 2.1 Classifiers based on ERP template

In oddball paradigm, one deviant rare stimulus is presented to subjects amongst a train of standard ones. Only the deviant stimulus induces an ERP. The most common evoked potential used in BCI is the P300. Its main characteristic is a positif latency that occurs around 300 ms after the stimulus presentation. This leads us to derive a set of classifiers. All of them first explicitly estimate one ERP template by averaging the ERP responses in the time domain, and then use the distance between the response and the ERP template as the discriminant criterion.

**Point-to-point averaging (P2P) classifier:** P2P classifier discriminates the ERP responses from non-ERP responses in a straightforward way: first it estimates one ERP template by simply averaging the measurements of ERP responses point-to-point, and then calculates the Euclidean distance between responses and the ERP template. For the P300 speller, the ERP response corresponds with the one producing the minimum distance within a set of column or row responses. Then the other responses are considered as non-ERP responses.

P2P classifier is simple for implementation. However the latency of the components of ERP varies with the external factors (such as target-to-target interval). Simply averaging the measurements point-to-point could blur the component. We then seek the solution of alignment before averaging. Such alignment includes linear alignment (such as, cross-correlation alignment) and nonlinear alignment (such as, dynamic time warping).

**Cross-correlation averaging (CC) classifier:** Linear alignments can be done by shifting the measurements before the point-to-point averaging. One of the well-known linear alignments is cross-correlation. The best shift of one sequence in order to align it to the other ones is given by the one producing the highest correlation [2, 3]. CC classifier first searches the best shift for pairs of ERP responses before averaging them point-to-point to obtain one template. Then it calculates the cross-correlation between the testing response and the ERP template. The predicted ERP response corresponds with the one giving the maximum correlation value with the template. Such scheme accommodates variable linear latency. However, if one looks the ERP measurements more closely, it is found that the latency of the ERP component is nonlinear. In this case, the nonlinear alignment methods are better than the linear ones for template estimation.

**Dynamic time warping averaging (DTW) classifier:** Dynamic Time warping distance is widely used in speech domain. It is able to deal with compression/expansion by comparing the distance of each point of the first sequence to every point of the second one using the information of the amplitude and/or the first derivative of amplitude of the signals [4]. Hence, DTW classifier first finds out the best nonlinear alignment path giving the closest distance, and then averages the ERP responses according to the alignment path to obtain one ERP template [5, 6, 7]. Finally, it recognizes the ERP responses as the one producing the minimum DTW distance.

## 2.2 Methods with several templates of ERP and non-ERP

On one hand, considering the complexity of ERP responses, one template could be insufficient to capture the variability of ERP components. On the other hand, one would like to introduce non-ERP templates into decision making process done by the classifiers. Clustering methods can produce several templates. The aim of clustering methods is to split a set of patterns into clusters as homogeneous as possible, i. e., patterns are gathered by similarity. A classical rule to assign a new pattern to a cluster is based on distances between the input pattern and templates. LVQ is the most famous algorithm in this category.

**learning vector quantization (LVQ):** The first version of the learning vector quantization algorithm proposed by Kohonen [8] is a supervised clustering method designed for classification. Input weights (IW) of connections linking inputs to each neuron is a vector $m$ with the same dimension than input $x$. Each neuron is assigned to a class according to the pre-defined layer weights (LW). A classic competitive step is used to determine which neuron is the closest one to the current input with the formula: $c = arg\min_i\{||x - m_i||\}$, and only the winner neuron is updated according to the following rules:

$$m_c(t+1) = m_c(t) + \alpha(t)[x(t) - m_c(t)] \text{ if } x \text{ and } m_c \text{ belong to the same class}$$

$$m_c(t+1) = m_c(t) - \alpha(t)[x(t) - m_c(t)] \text{ if } x \text{ and } m_c \text{ belong to different classes}$$

$\alpha$ is the learning rate. To apply this algorithm, one needs to decide the value of learning rate and the number of neurons assigned to each class. Further considering the multichannel recording of EEG measurements, if one simply merges features from each channel, the dimension of IW increases with the number of channels, and it thus causes memory problem in simulation. We then consider multichannel LVQ.

**Multichannel learning vector quantization (mLVQ):** For multichannel LVQs, one LVQ model is created for each channel, and trained according to the above rules to update IWs. Thus, there are several ERP and non-ERP templates generated for each channels. In order to combine the templates in an optimal way, we further introduce an update scheme for LWs: $\mathrm{LW} = (-||X - \mathrm{IW}||)^{\dagger}T$, where $X$ is the input matrix and $T$ is the target matrix. The symbol † represents the pseudo-inverse operator. Such a solution of LW is known as minimum norm least square solution. It is originally found being used in extreme learning machine (ELM) in [9].

# 3 Results

## 3.1 Wadsworth BCI data set

The results presented here are based on the P300 speller data set from the BCI competition III [10][1]. The data set contains training and testing EEG data from two subjects. There are 85 letters for training and 100 letters for testing. For each letter, the recording consists of 15 epochs, and within each epoch, there are 12 flashings. For each epoch, a random permutation is chosen to highlight rows and columns. There is a $6 \times 6$ grid in this application containing 26 letters, 9 digits and one dash character. We are interested in the measurement window starting from the onset of the flashing and till one second, which consists of 240 samples at a sampling rate of 240 Hz. In case the row/column is highlighted exactly where the target letter is located, we got the ERP response; otherwise the non-ERP response.

## 3.2 Experimental results

### 3.2.1 ERP templates

Figure 1 shows the comparison between the ERP templates estimated by P2P averaging, CC and DTW alignment averaging, respectively. Templates are built using the first 128 trials of the training set of subject A. Indeed, the algorithms using CC and DTW prefer to pair trials in a binary tree structure. The latency of the P300 component in the estimated templates by CC and DTW alignment averaging methods is different from P2P averaging. This is the effect of aligning the component in the time domain before averaging. And we found that the template estimated by DTW was smoother than by cross-correlation.

[1]The data set is available at: `http://ida.first.fraunhofer.de/projects/bci/competition_iii/`.

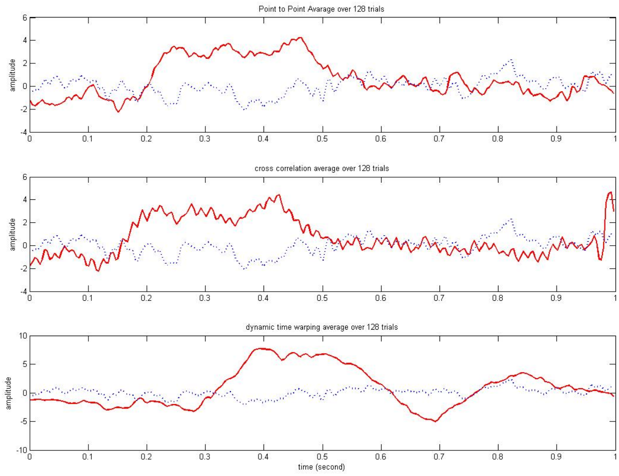


Figure 1: Comparison of ERP templates (red solid curves) and averaged background EEG activities (black dot curves) for responses recorded on channel Cz using training data from subject A. From top to bottom, templates are estimated by point-to-point averaging, cross-correlation and dynamic time warping alignment averaging, respectively.

#### 3.2.2 Classifier comparison

Simulation is carried out to compare the performance of the template-based classifiers using P2P, CC, DTW and LVQ. The result of linear discriminant analysis (LDA) is also provided for its simplicity and good performance in the application of BCIs. Table 1 shows the testing accuracy for subjects A and B. The results are based on the raw measurements from channel Cz (i. e., no pre-processing is involved). We used the full training set to estimate the ERP templates for P2P, CC and DTW; while for LVQ and LDA, they are used to estimate the parameters of the models. The full testing set is used to evaluate the performance of the classifiers. From the table, we can see that LVQ and LDA achieve similar performance and are better than the classifiers using P2P, CC, and DTW.

Table 2 shows the testing accuracy for subjects A and B based on measurements of all channels. Due to limit of memory and the large size of the input data, one needs to re-sample the signals. Thus, for Table 2, we first smooth the signal using a moving averaging filter with window size of 13, and then re-sample it with a down-sampling factor of 13. Further, multichannel version of LVQ is used here. We find that the performance of mLVQ and LDA are similar again and both increase as more channels are used for classification; while the performance of the explicit template-based classifiers using P2P, CC and DTW is bad.

From the above simulation results, we found that the performance of classifiers (such as LVQ), which take account of both ERP and non-ERP templates is better than those (such as P2P, CC, and DTW) which use only one ERP template. The optimization of the combination of the templates from different channels through assigning different weights is even more critical for improving the accuracy.

## 4 Conclusion and further work

BCI applications based on P300 ERP detection, such as the P3speller, need statistical or machine learning techniques with temporal features. ¿From a recording point of view, ERPs are graphic-elements. They have a specific waveform clearly different from EEG background activity. Thus, efficient modeling of the waveform can help to detect ERPs. Averaging techniques and clustering

| Subject | Epoch | Method | | | | |
|---|---|---|---|---|---|---|
| | | P2P | CC | DTW | LVQ | LDA |
| A | 05 | 7 % | 8 % | 15 % | 17 % | 18 % |
| | 10 | 5 % | 26 % | 28 % | 28 % | 30 % |
| | 15 | 3 % | 21 % | 39 % | 43 % | 41 % |
| B | 05 | 2 % | 6 % | 6 % | 8 % | 15 % |
| | 10 | 5 % | 9 % | 10 % | 13 % | 19 % |
| | 15 | 3 % | 16 % | 15 % | 21 % | 26 % |

Table 1: Experimental results based on channel Cz for subjects A and B. The percentage of correct classified letters contained in the testing set is shown regarding using the first 5 epochs, 10 epochs and all epochs.

| Subject | Epoch | Method | | | | |
|---|---|---|---|---|---|---|
| | | P2P | CC | DTW | mLVQ | LDA |
| A | 05 | 9 % | 7 % | 7 % | 47 % | 45 % |
| | 10 | 13 % | 6 % | 12 % | 77 % | 78 % |
| | 15 | 14 % | 7 % | 15 % | 87 % | 88 % |
| B | 05 | 3 % | 2 % | 4 % | 72 % | 76 % |
| | 10 | 3 % | 3 % | 3 % | 91 % | 92 % |
| | 15 | 4 % | 4 % | 3 % | 96 % | 96 % |

Table 2: Experimental results based on all channels for subjects A and B. The percentage of correct classified letters contained in the testing set is shown regarding using the first 5 epochs, 10 epochs and all epochs.

methods allow extracting one or several ERP templates. Averaging techniques using point-to-point averaging, cross-correlation and dynamic time warping are not efficient. They produce only one ERP template and suffer from two difficulties: first, responses are too noisy to easily distinguish ERP from non-ERP responses; second, according to the previous remark, they do not take into account the specificities of non-ERP responses to catch small differences between noisy ERP and non-ERP responses. The first difficulty exists for any classification method. But, our method mLVQ obtains similar results as LDA which is a reference technique for the P3Speller. It is because mLVQ takes into account the second remark. Thus, template-based classifiers can also obtain good results. Moreover, this approach can extract knowledge about the ERP waveform of patients.

In this article, we also evaluated the promising dynamic time warping distance. This kind of similarity measure is widely used in speech domain and align efficiently two sequences even if they differ each other from compression and/or dilatation on some segments. However, from our opinion, DTW suffers from the low SNR. The real EEG signals used in our simulation are too noisy. Many artificial peaks appear in the recording and thus it is difficult to obtain a strong alignment. In order to mitigate this difficulty, one may reduce the window of investigation to [250 ms, 650 ms] and constrain the window size of permitted distortion to short time. It should help to focus the attention on the critical zone.

In practice, it is also very interesting to reduce the number of channels in order to equip the patient with a compact system with only several necessary electrodes. Thus, channel selection will be investigated in a further work.

# References

[1] L. A. Farwell and E. Donchin. Talking off the top of your head: toward a mental prosthesis utilizing event-related brain potentials. *Electroencephalogr. Clin. Neurophysiol.*, 70(6):510–523, 1988.

[2] C. D. Woody. Characterization of an adaptive filter for the analysis of variable latency neuroelectric signals. *Med. Biol. Eng.*, 5:539–553, 1967.

[3] D. G. Wastell. Statistical detection of individual evoked responses: an evaluation of woody's adaptative filter. *Electroencephalogr. Clin. Neurophysiol.*, 42:835–839, 1977.

[4] E. Keogh and M. Pazzani. Derivative dynamic time warping, 2001.

[5] T. Picton, M. Hunt, R. Mowrey, R. Rodriguez, and J. Maru. Evaluation of brain-stem auditory evoked potentials using dynamic time warping. *Electroencephalogr. Clin. Neurophysiol.*, 71(3):212–225, 1988.

[6] K. Wang, H. Begleiter, and B. Porjesz. Warp-averaging event-related potentials. *Clin. Neurophysiol.*, 112(10):1917–1924, 2001.

[7] S. Casarotto, A. M. Bianchi, S. Cerutti, and G. A. Chiarenza. Dynamic time warping in the analysis of event-related potentials. *IEEE Eng. Med. Biol. Mag.*, 24(1):68–77, 2005.

[8] T. Kohonen. The self-organizing map. In *Proceedings of the IEEE*, volume 78, pages 1464–1480, 1990.

[9] G.-B. Huang, Q.-Y. Zhu, and C.-K. Siew. Extreme learning machine: A new learning scheme of feedforward neural networks. In *Proceedings of International Joint Conference on Neural Networks*, volume 2, pages 985–990, Budapest, Hungary, 2004.

[10] D. J. Krusienski and G. Schalk. *Wadsworth BCI Dataset (P300 Evoked Potentials).* BCI Competition III Challenge, 2004.

# Towards a noise-tagging auditory BCI-paradigm

J. Farquhar[1], J. Blankespoor[2], R. Velk[2], P. Desain[2]

[1]Biophysics Dept, Radbound University Medical School, Radbound University, Nijmegen, The Netherlands
[2]Music Mind Machine, Nijmegen Inst. for Cognition and Information, Radbound University, Nijmegen, The Netherlands

j.farquhar@nici.ru.nl

**Abstract**

Stimulus tagging is an important technique for investigating the functional operation of the brain. In this paper we propose the novel noise tagging method as an alternative to the more commonly used frequency tagging technique. Noise tagging is based on spread-spectrum signal processing techniques and has a number of theoretical advantages over frequency tagging in terms of noise robustness and temporal resolution. However, it is unclear how the brain will respond to this unpredictable aperiodic stimulus type. We present preliminary EEG experiments using auditory noise tagging which show that an attenuated version of the noise tag is detectable in EEG signals. Further, this signal is sufficient to identify; i) which noise tag was used, ii) the time lag ($\approx$ 50 ms) of the neural processing, and iii) to which tag the subject was selectively attending. The last result in particular provides encouraging evidence that noise tagging can be used as the basis for a selective attention BCI-system.

## 1 Introduction

Stimulus tagging is a commonly used technique where stimuli are modulated such that the modulation can be detected in neural activity recordings. For example, visual images can be modulated by changing their brightness. This modulation is expected to be processed alongside the stimulus in the brain. Hence, the modulation tags (or watermarks) the stimulus, allowing it to be tracked as it is processed in different brain regions at different time lags. Thus stimulus tagging is very useful for basic physiological research. It is also very useful for BCI purposes as selective attention [1] increases the neural response to the selected stimulus, and hence the strength of that tag.

There are two main types of stimulus tag, steady state [2] tags where the modulation occurs more rapidly than the subject can perceive, and transient tags which happen infrequently and evoke a transient response. Transient effects are widely used in the oddball-type BCIs, such as P300 visual spellers [3].

Steady state stimulus tags have a number of advantages from a BCI perspective. Firstly, their high speed means they can potentially give high timing accuracy. Secondly, as they are perceived by the subject as a continuous modulation they can be presented for many modulation cycles, allowing a long integration time which increases the signal-to-noise-ratio such that even very weak responses can be detected.

### 1.1 Frequency tagging

The most common form of steady state tagging [2] is the frequency tag. Here the stimulus is modulated with a simple repeating modulation, such as a sine wave. A commonly used frequency tag is the Steady State Visual Evoked Potential (SSVEP) [1] which is generated by varying the brightness of a visual stimulus in a sinusoidal fashion, a similar approach using a low frequency amplitude modulation of a higher frequency carrier is the Auditory Steady State Response (ASSR) [4, 5, 6]. Frequency tagging has the advantage that the modulator is concentrated into a very narrow frequency band which is easy to detect using a simple spectral decomposition. Further, because different frequencies are uncorrelated, multiple tags can be used simultaneously and detected with little or no interference [7].

Despite its advantages, frequency tagging has two potential disadvantages. Firstly, the narrow-band nature of the tag leaves it susceptible to interference where a noise source near the tagging frequency can mask the tag. Secondly, the short period of the stimulus may cause aliasing when time lags longer than the repetition period become indistinguishable from shorter lags[1].

### 1.2 Noise tagging

Inspired by the spread spectrum [8] techniques used extensively in wireless communication we propose to use a novel alternative steady state stimulus tagging technique, called noise tagging. The main idea is to spread the tagging signals' power over a wide range of frequencies instead of focusing it all in a narrow band. This spreading has the advantage that losing one particular part of the signal spectrum has little effect on signal detectability. In fact the reduction in signal detect-ability is roughly linear with the fraction of the signal spectrum lost. Such interference robustness is important for BCI/neuro-scientific applications where parts of the signal are likely to be lost due to either external (or neural) noise effects or simply because they are filtered out during cognitive processing. By using spread spectrum techniques we maximize the chance that some signal always remains in the recorded activity. Note, this also means the tag is robust to inter-subject variations in stimulus response.

Noise tagging has the additional advantage that the tagging signal has a much longer period, $\approx 1.5\,\mathrm{s}$ in our experiment. This is much longer than the neural processing lags that are likely to occur so temporal aliasing is no longer a problem.

The particular spread spectrum technique we use is Direct Sequence [9] spread spectrum. In this method a random "spreading code" is multiplied with the signal to spread its power over a wide band. In theory, a purely random process can be used to generate the spreading code. However, this can cause problems if the generated tag happens to repeat (i. e. be highly correlated with) itself at some point – re-introducing the temporal aliasing problem. Further, if one wishes to use more than 1 noise tag at the same time, it is hard to guarantee that they will be uncorrelated. Luckily, these problems have been solved in the telecommunications literature using specially designed Pseudo-random number generators. In our work we use a particular form of these codes, i. e. Golden codes [10], to ensure our noise tags are maximally uncorrelated in time with themselves (i. e. have low auto-correlation) and each other (i. e. have low cross-correlation). Thus we ensure the noise tags:

1. Minimize interference with other noise tags, so multiple tags can be used at the same time, e. g. in a selective parallel attention BCI.
2. Minimize temporal aliasing, so we can accurately determine neuronal processing lags.

A Golden code is produced by XOR-ing together to individual maximal pseudo-random codes. A maximal pseudo-random code can be easily made by appropriately choosing which stages of a shift-register to XOR feed-back into its input, as shown in Figure 1 lower or upper blocks, such that it shifts through all $2^n - 1$ possible states. A golden-code is produced when two appropriately chosen maximal codes are XOR-d together with an appropriate delay. A nice property of this approach is that every delay produced a different golden code.

As one cannot just look at the power in a single spectral band, detecting spread-spectrum tags is a little more complex than for frequency tagging. However, if one makes the strong assumption that the brain response is an attenuated, time-lagged version of the stimulus then the noise-tag can be detected using a simple correlation approach. That is by "sliding" the tagging signal over

[1] Using 2 tags with different can frequencies allows one to resolve this ambiguity

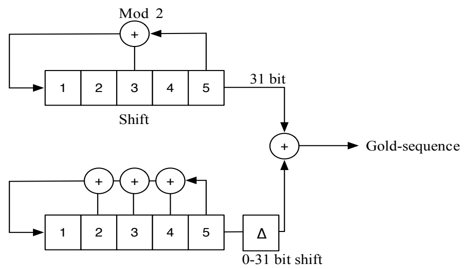


Figure 1: Block diagram of the generation of a golden common code.

the brain data to find the time lag where they are maximally correlated[2]. Note, if we believe the brain is responding to some more complex linear transformation of the tag (such as its first derivative) then more advanced techniques can be used[3]. For example in [11] Desain shows how estimating the impulse-response to the first-derivative of the tag gives impressive results.

# 2 Experiments

To test the effectiveness of the noise-tagging approach we are conducting a series of EEG based auditory selective attention experiments. The aim of these experiments is to test if the noise tag is detectable in the EEG, to compare its performance with that of a pure frequency tagging, and to see if selective attention to noise tagged stimuli can be used as the basis for a BCI. In detail the experimental design is:

- a saw-tooth tone of either 512 Hz or 768 Hz is used as a carrier[4].
- tags are applied to these carriers using binary amplitude modulation, where for the 0 bits the amplitude is reduced to 20 % of its original value
- 2 frequency tags are used for comparison with the noise tag: a) 512 Hz carrier with 42 Hz amplitude modulation and b) 768 Hz carrier with 64 Hz modulator
- 2 noise tags, called A and B, were used with a 128 bits per second modulation rate. Both were 255 bits long. The A tag used the 512 Hz carrier and the B tag 768 Hz
- each epoch was 2 seconds long, i. e. contained 1 noise tag
- two tasks are used:
  - **Serial Selective Attention** – where tags (and carriers) are presented one at a time to both ears in random order and the subject selectively attends (by counting) to one of the tags.
  - **Parallel Selective Attention** – where two tags (and carriers) are presented simultaneously, one to each ear, (512 Hz left and 768 Hz right). The subject selectively attends by counting randomly generated reduced amplitude (deviant) tags on either the left or right side.

An example of the tags used and their spectrum is shown in Figure 2.

The experiments took place in an acoustically and electrically isolated room, with EEG recorded in a 256 electrode Biosemi active electrode system sampled at 2048 Hz (though for analysis this was downsampled to 512 Hz).

[2]In fact, mathematically this is exactly what the Fourier analysis is doing behind the scenes.

[3]One advantage of the frequency tagging scheme is that a simple correlation analysis can detect any linear transformation of the signal in the output.

[4]Note, 2 carriers are necessary so the subject can perceive the difference between the different noise tags.

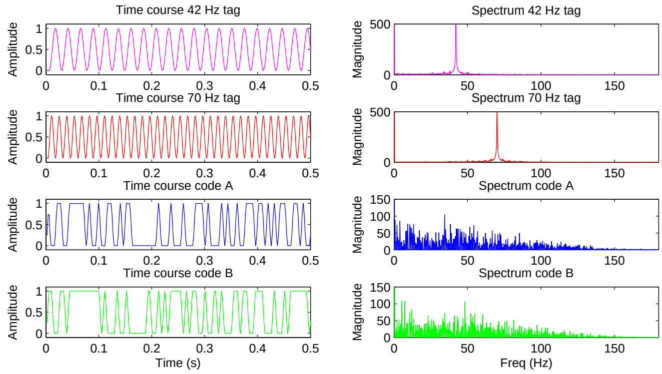


Figure 2: Example auditory tags used in the experiment. The left hand plots show the time-courses of the amplitude modulation sequences. The right hand plots show the spectral distributions of the corresponding tag, demonstrating the spread-spectrum nature of the noise tags.

We first examined the purely perceptual response to the different tags by analyzing attended and unattended tasks together for the serial selective attention task. This type of analysis gives us an indication of how strongly the tag is transmitted by the brain, and hence how useful it would be for low-level neurological investigations, but not how useful it is for a BCI. The transmission strength was estimated by simply computing the correlation between the tag and the EEG signal (band-passed between 30–80 Hz) on a channel-by-channel basis for all possible time lags. The results of this analysis are presented in Figure 3 for the frequency tags and Figure 4 for the noise tags. These results show that for both tag types which tag was used (i. e. 42 or 64 Hz, A or B code) can be easily identified from the EEG signal using this simple correlation method, though for the frequency tag is effect is about 2x stronger. The aliasing introduced by the short period of the frequency tag is also apparent. The noise tag does not suffer from this problem allowing the neural processing lag to be easily identified (50 ms in this case). Further, which of the two noise tags was used can also be seen easily. Additionally, it appears that the frontal electrodes (# 120–170) have a significantly reduced response with a different phase. The reduced amplitude is because these electrodes are furthest from the auditory cortices. The phase difference implies an additional time-lag before the signal is processed by the higher-level functions in the frontal lobes.

Next we re-analyzed the data to look for selective attentional effects, which can be used as the basis of a BCI. The approach taken was to compute the correlation between the EEG and each possible tag, and then use these correlations as inputs for a linear regularized Logistic Regression classifier. Exactly the same analysis technique was used for the pure-perceptual, serial and parallel selective attention task. The results of this analysis are presented in Table 1. These results demonstrate that there is indeed a useful attentional modulation effect for the noise-tagging which can be identified with the correlation approach. It also appears that frequency tagging, in addition to generating a larger perceptual signal than noise tagging, also generates a larger attentional modulation signal. Of course, with a more sophisticated signal analysis technique, such as the impulse response learning function of [11], we may be able to significantly improve the classification performance of the noise-tag.

# 3 Conclusion

Stimulus tagging is an important technique for investigating the operation of the brain. In this paper we proposed the novel method of noise tagging as an alternative to the more commonly used frequency tagging technique. Noise tagging is based upon spread-spectrum ideas and has a number of theoretical advantages over frequency tagging in terms of improved noise robustness

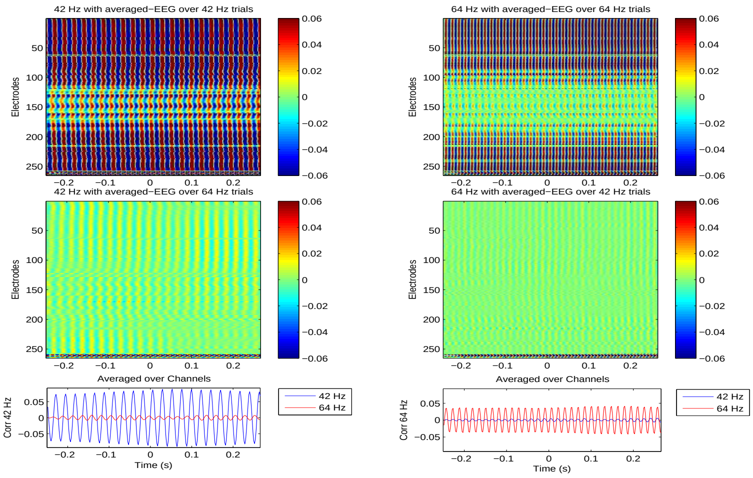


Figure 3: Correlation analysis for the frequency tagged perceptual task. For clarity only .5 s around the stimulus onset at time zero are shown. Left Plots: correlation of the 64 Hz tag with the EEG, for each channel and time averaged over 64 Hz tagged epochs (top row), resp. for over the 42 Hz tagged epochs (middle row), and for each time averaged for all channels and for the different sub-sets of epochs (bottom row). Right Plots: same as left hand plots with A and B reversed.

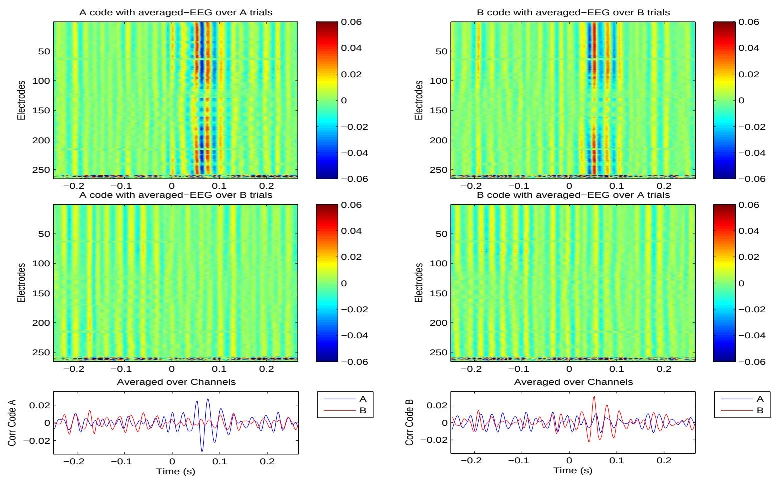


Figure 4: Correlation analysis for the noise-tagged perceptual task. Plot layout is the same as in Figure 3 but for the 2 noise tags.

| | Frequency Tagging (%) | | | Noise Tagging (%) | | |
|---|---|---|---|---|---|---|
| Subject | Perceptual | Serial | Parallel | Perceptual | Serial | Parallel |
| jf | 98 | 65 | 70 | 89 | 63 | 60 |
| mk | 85 | 48 | 64 | 58 | 52 | 54 |
| km | 98 | – | 59 | 73 | 58 | 55 |

Table 1: Selective Attention Single Trail Percentage Correct Classification Performance for the two types of stimulus tag (frequency and noise) and different types of modulation (Perceptual, Serial and Parallel) studied. Trials were 2 seconds long and performance was estimated using a 10-fold randomized cross-validation.

and temporal resolution. However, it is unclear how the brain will respond to this novel stimulus type. Our preliminary EEG experiments using auditory noise tagging show than an attenuated version of the noise tag is detectable in EEG. Further this signal is sufficient to identify the noise tag used, the time lag for the neural processing, and which noise-tag the subject was selectively attending in both parallel and serial tagging experiments. The last result in particular provides encouraging evidence that noise tagging can be used as the basis for a selective attention BCI. We are currently conducting further EEG experiments to test this possibility.

**Acknowledgments:** We gratefully acknowledge the support of the BrainGain Smart Mix Programme of the Netherlands Ministry of Economic Affairs and the Netherlands Ministry of Education, Culture and Science.

# References

[1] P. Fries, J. H. Reynolds, A. E. Rorie, and R. Desimone. Modulation of oscillatory neuronal synchronization by selective visual attention. *Science*, 291:1560–3, Feb 2001.

[2] D. Regan. Steady-state evoked potentials. *J. Opt. Soc. America*, 67:1475–89, 1977.

[3] L. A. Farwell and E. Donchin. Talking off the top of your head: Toward a mental prosthesis utilizing event-related potentials. *Electroencephalogr. Clin. Neurophysiol.*, 70:510–523, 1988.

[4] A. R. Moller. Responses of units in the cochlear nucleus to sinusoidally amplitude-modulated tones. *Exp. Neuro.*, 45:105–117, Oct 1974.

[5] B. Ross, A. T. Herdmann, and C. Pantev. The effect of attention on the auditory steady-state response. *Neuro. Clin. Neurophysiol.*, 22:1–4, 2005.

[6] T. W. Picton, M. S. John, A. Dimitrijevic, and D. Purcell. Human auditory steady-state responses. *Int. J. Audiol*, 42:177–219, 2003.

[7] O. G. Lins and T. W. Picton. Auditory steady-state responses to multiple simultaneous stimuli. *Electroencephalogr. Clin. Neurophysiol.*, 96:420–432, 1995.

[8] R. C. Dixon. *Spread Spectrum Systems.* Wiley – Interscience, 3rd edition, 1994.

[9] J. Hershey. *Direct Sequence Spread Spectrum Techniques.* Aegean Park Press, Nov 1982.

[10] R. Gold. Optimal binary sequences for spread spectrum multiplexing. *IEEE Trans. Information Theory*, 13(4):619–621, 1967.

[11] P. Desain, J. Blankespoor, J. Farquhar, and S. Gielen. Detecting spread spectrum pseudo random noise tags using a structure-based decomposition. In *Porceedings of the 4th International Brain-Computer Interface Workshop and Training Course*, 2008.

# Large scale kernel CSP algorithm for EEG feature extraction

Y. Liu, Z. Zhou, D. Hu

College of Mechatronics and Automation, National University of Defense Technology, Changsha, Hunan, P.R.China, 410073

dwhu@nudt.edu.cn

**Abstract**

Common spatial pattern (CSP) is a widely used method in movement related potentials analysis for Brain-computer interface. In this paper, a non-linear variant of CSP is introduced by kernel method, to deal with the data with complicated distributions. A large scale kernel CSP algorithm (LSKCSP) is proposed to overcome the difficulty of large memory demand in the training phase of brain-computer interface application. Experiment shows that LSKCSP algorithm is effective for large dataset training and could obtain competitive results with CSP.

## 1 Introduction

The common spatial pattern (CSP) [1] is a supervised spatial filter and is proved very useful for detecting the spatial and spectral differences between two types of electrophysiological signals [2, 3]. Nowadays CSP is successfully applied in the field of brain-computer interfaces (BCI) [4], for recognizing movement related potentials (MRP) such as ERD/ERS [5, 6, 7, 8] and slow cortical potentials (SCP) [9]. Generally speaking, like principal component analysis (PCA) and Fisher discriminant analysis (FDA), CSP is also a general purposed statistical method, which can be expected helpful to a specific kind of pattern recognition tasks. However, as we know, linear methods have their intrinsic limitation that they always make the hypothesis that the data are linear distributed. In many cases, it is the non-linear structures that exist in the data, and for which the linear methods are obvious not optimal. Kernel method [10, 11] is a sort of powerful approach that can transform the method to non-linear version, by performing the method in a usually high dimensional feature space. As one representation of kernel methods, support vector machines (SVM) have become popular in more and more applications for classification, including EEG pattern recognition [7]. At the same time, many classical linear methods are endowed with new ability to deal with non-linear problems [11]. Recently a formulation and solution of CSP in feature space are proposed and applied to ECoG/EEG classification [12]. However, the number of samples are usually very large when training kernel CSP, such that eigenvalue decomposition of the kernel matrix becomes difficult or even impossible. This paper proposes a novel kernel CSP algorithm for large scale dataset. In Section 2, CSP and kernel CSP are briefly introduced, as well as the basic algorithm. Then based on quadratic equivalent representation, the large scale kernel CSP algorithm are proposed. Experiment result of EEG classification is shown in Section 3. Section 4 provides a discussion and concludes the paper.

## 2 Methods

### 2.1 Common spatial pattern and kernel CSP

Let's consider the binary classification problem. Given two variables $x, y \in \mathcal{R}^D$ with a set of observations $\{x_i\}_{i=1}^m$ and $\{y_i\}_{i=1}^n$, the idea is to find a spatial filter $w \in \mathcal{R}^D$ such that the linear projected signals has the high variance for one class and the low variance for the other:

$$\begin{array}{ll} \max & w^T \Sigma_1 w \\ \text{s.t.} & w^T(\Sigma_1 + \Sigma_2)w = 1 \end{array} \tag{1}$$

The motivation of combining kernel method and CSP is mainly based on two facts: the success of CSP in EEG feature extraction and SVM in EEG classification. The idea is to map samples to feature space then perform CSP there.

$$\Phi : R^D \to \mathcal{H}, \quad z \to \Phi(z)$$

In $\mathcal{H}$, the covariance matrices take the form

$$\begin{array}{l} \Sigma_1 = \frac{1}{m}\sum_{i=1}^{m}[\Phi(x_i) - \bar{\Phi}_x][\Phi(x_i) - \bar{\Phi}_x]^T = \frac{1}{m}\sum_{i=1}^{m}\tilde{\Phi}(x_i)\tilde{\Phi}(x_i)^T \\ \Sigma_2 = \frac{1}{n}\sum_{i=1}^{n}[\Phi(y_i) - \bar{\Phi}_y][\Phi(y_i) - \bar{\Phi}_y]^T = \frac{1}{n}\sum_{i=1}^{n}\tilde{\Phi}(y_i)\tilde{\Phi}(y_i)^T \end{array} \tag{2}$$

and the projection vector $w$ can be expressed as a linear combination of all mapped samples:

$$w = \sum_{i=1}^{m+n}\gamma_i\tilde{\Phi}(z_i), \quad z_i = \begin{cases} x_i, \ i = 1, \ldots, m \\ y_{i-m}, \ i = m+1, \ldots, m+n \end{cases} \tag{3}$$

where $\gamma_i$ are undetermined combination coefficients. Define $(\mathbf{K})_{ij} =< \tilde{\Phi}(z_i), \tilde{\Phi}(z_j) >$ and

$$\mathbf{K} = \begin{bmatrix} \mathbf{K}_{xx} & \mathbf{K}_{xy} \\ \mathbf{K}_{yx} & \mathbf{K}_{yy} \end{bmatrix} = [\overbrace{\mathbf{K}_{zx}}^{m}\overbrace{\mathbf{K}_{zy}}^{n}] = \begin{bmatrix} \mathbf{K}_{xz} \\ \mathbf{K}_{yz} \end{bmatrix}$$

we get

$$\begin{cases} \frac{1}{m}\mathbf{K}_{zx}\mathbf{K}_{xz}\gamma = \lambda(\frac{1}{m}\mathbf{K}_{zx}\mathbf{K}_{xz} + \frac{1}{n}\mathbf{K}_{zy}\mathbf{K}_{yz})\gamma \\ \gamma^T(\frac{1}{m}\mathbf{K}_{zx}\mathbf{K}_{xz} + \frac{1}{n}\mathbf{K}_{zy}\mathbf{K}_{yz})\gamma = 1 \end{cases} \tag{4}$$

## 2.2 "Whiten and rotate" algorithm

The "whiten and rotate" algorithm is a basic algorithm for solving kernel CSP problem. We first diagonalize $\frac{1}{m}K_{zx}K_{xz} + \frac{1}{n}K_{zy}K_{yz}$, followed by a dimension reduction step, that is to say, removing the near-zero eigenvalues, which is called "whiten". Then "rotation" is performed by maximizing variance for one class. For feature extraction, similar to CSP, the filter is usually constructed by several eigenvectors $\{\gamma_i\}_{i=1}^{M}$ corresponding to the largest eigenvalues on the both ends. Finally, scale $\{\gamma_i\}_{i=1}^{M}$ by $\gamma_\mathbf{i} \leftarrow \gamma_\mathbf{i} \Big/ \sqrt{\gamma_\mathbf{i}^T(\frac{1}{m}\mathbf{K}_{zx}\mathbf{K}_{xz} + \frac{1}{n}\mathbf{K}_{zy}\mathbf{K}_{yz})\gamma_\mathbf{i}}$ for $i = 1, \ldots, M$.

For new sample $c$, the projection could be computed by

$$< \Phi(c), w^r >= \sum_{i=1}^{m+n}\gamma_i^r < \Phi(c), \tilde{\Phi}(z_i) > = \mathbf{K}_{cz}\gamma \quad \text{for } r = 1, \ldots, M. \tag{5}$$

## 2.3 Large scale kernel CSP (LSKCSP) algorithm

In applications such as brain-computer interfaces, there's usually a large number of samples, even though some techniques, e. g., downsampling, are utilized. In these cases, diagonalizing the Gram matrix $\frac{1}{m}K_{zx}K_{xz} + \frac{1}{n}K_{zy}K_{yz}$ becomes impossible on an ordinary computer.

Quadratic Equivalent Representation. Consider the data $\{x_i\}_{i=1}^{m} \subset \mathcal{R}^D$. Due to the positive definite property of the covariance matrix, it can be decomposed to product of two orthogonal matrices:

$$\sum_{i=1}^{m} x_i x_i^T = m\Sigma_x = VV^T = [v_1, v_2, ..., v_p] * [v_1, v_2, ..., v_p]^T = \sum_{i=1}^{p} v_i v_i^T \tag{6}$$

where $p = \text{rank}(\Sigma_x)$, usually $p \leq D \ll m$.

Quadratic Equivalent Representation (QER) is defined as $\{v_i\}_{i=1}^r$ plus $(m\text{-}r)$ points located in the origin. Compare it with the original set $\{x_i\}_{i=1}^m$, we have

- They have the same covariance matrix.
- The projections to any directions have the same variance.
- When some new data, centered to the same center as $\{x_i\}_{i=1}^m$, are added to the two datasets, the above two statements still hold.

Figure 1 gives a demonstration of QER in 2-D case, where large numbers of data (indicated by asterisk) are reduced to QER which contains only 2 non-zero samples (indicated by square).

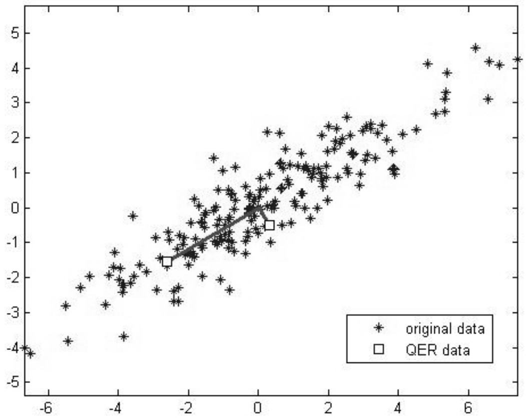


Figure 1: QER demonstration of 2-D data. The asterisk represents the original data and the square represents the QER data. The solid lines indicate the principal axes of the original data.

The LSKCSP Algorithm. The basic procedure is to compute the QER datasets of $\{\Phi(x_i)\}_{i=1}^m$ and $\{\Phi(y_i)\}_{i=1}^n$, and substitute QER for the original data to solve kernel CSP. This is achieved by the following steps.

1) Segment the whole dataset of each class into several (not too) small subsets which scale your computer could deal with.

2) Calculate the QER of each subset. Take two subsets of one class for example.

$$\begin{aligned} m_h\mathbf{\Sigma}_h &= \sum_{i=1}^{m_h} \tilde{\Phi}(x_i)\tilde{\Phi}(x_i)^T = \mathbf{U}_h\mathbf{U}_h^T = \sum_{i=1}^{s_h} \mathbf{u}_i^h(\mathbf{u}_i^h)^T \\ m_l\mathbf{\Sigma}_l &= \sum_{i=1}^{m_l} \tilde{\Phi}(x_i)\tilde{\Phi}(x_i)^T = \mathbf{U}_l\mathbf{U}_l^T = \sum_{i=1}^{s_l} \mathbf{u}_i^l(\mathbf{u}_i^l)^T \end{aligned} \tag{7}$$

where $h$ and $l$ are the indices of subsets, and $m_h$ and $m_l$ are the sizes. It shows that this procedure is essentially Kernel PCA. Note that here QER data are actually represented by the combination coefficients of the mapped original data,

$$\mathbf{u}_i^h = (\alpha_i^h)^T\Phi(\mathbf{x}_h),\ i = 1, 2, \ldots, s_h \quad \mathbf{u}_i^l = (\alpha_i^l)^T\Phi(\mathbf{x}_l),\ i = 1, 2, \ldots, s_l \tag{8}$$

3) Combine each small QERs 2 by 2 to obtain the final QER $\{u_i\}_{i=1}^r$ and $\{v_i\}_{i=1}^t$ for two classes respectively. Also take the combination of $\mathbf{U}^h$ and $\mathbf{U}^l$ for example.

$$\begin{aligned} &(s_h + s_l)\mathbf{\Sigma}_{hl} = \sum_{i=1}^{s_h} \mathbf{u}_i^h(\mathbf{u}_i^h)^T + \sum_{i=1}^{s_l} \mathbf{u}_i^l(\mathbf{u}_i^l)^T \\ &= \sum_{i=1}^{s_h} (\alpha_i^h)^T\Phi(\mathbf{x}_h)\Phi^T(\mathbf{x}_h)\alpha_i^h + \sum_{i=1}^{s_h} (\alpha_i^l)^T\Phi(\mathbf{x}_l)\Phi^T(\mathbf{x}_l)\alpha_i^l \\ &= \mathbf{U}_k\mathbf{U}_k^T = \sum_{i=1}^{s_k} u_i^k(u_i^k)^T \end{aligned} \tag{9}$$

4) In Equation 2, replace $\{\Phi(\mathbf{x}_i)\}_{i=1}^m$ and $\{\Phi(\mathbf{y}_i)\}_{i=1}^n$ by $\{u_i\}_{i=1}^s$ and $\{v_i\}_{i=1}^t$, and now the projection vector w could be expressed by

$$\mathbf{w} = \sum_{i=1}^{s+t} \eta_i r_i, \quad r_i = \begin{cases} u_i, \ i = 1, \ldots, s \\ v_{i-s} \ i = s+1, \ldots, s+t \end{cases}$$

Then Equation 4 becomes

$$\frac{1}{m}\mathbf{K}_{ru}\mathbf{K}_{ur}\eta = \lambda(\frac{1}{m}\mathbf{K}_{ru}\mathbf{K}_{ur} + \frac{1}{n}\mathbf{K}_{rv}\mathbf{K}_{vr})\eta \tag{10}$$

where the Gram matrices are all part of

$$\mathbf{K}_r = \begin{bmatrix} \mathbf{K}_{uu} & \mathbf{K}_{uv} \\ \mathbf{K}_{vu} & \mathbf{K}_{vv} \end{bmatrix} = [\overbrace{\mathbf{K}_{ru}}^{s} \overbrace{\mathbf{K}_{rv}}^{t}] = \begin{bmatrix} \mathbf{K}_{ur} \\ \mathbf{K}_{vr} \end{bmatrix}$$

# 3 Results

## 3.1 Experimental setup

In the training session or calibration measurement, each subject was asked to perform one of three motor imagery tasks: (L)eft hand, (R)ight hand and (F)oot, according to the visual indication on the screen. 4 s of 54 EEG channels of 13 subjects were recorded during the imagery. Not the following feedback phase but only the labeled data are taken into consideration in this analysis, and tasks “left hand” and “foot” are selected for we just consider binary classification here.

## 3.2 Data processing

Data are 9–14 Hz band pass filtered and downsampled to 30 Hz. Interval [0.5 s, 4 s] of each trial (i. e. data for one imagery task) is taken out. One quarter of all samples for each subject is randomly generated as the test set, the other as the training set. The size of training/test sets for each subject are: subjects 1 and 4–12: 210/70, subject 2 and 3: 202/68, subject 13: 157/53.

On the training set, all trials of the same class are concatenated according to channels, then CSP or Kernel CSP filters are computed, and applied to test set. Suppose that there are 100 trials for one class, then the scale of the Gram matrix $\frac{1}{m}K_{zx}K_{xz} + \frac{1}{n}K_{zy}K_{yz}$ in Equation 4 is $(3.5 \cdot 30 \cdot 100 \cdot 2)^2 = 21000^2$, which needs about 1.8 GB to store it if single precision is used in Matlab, and is hard to be eigenvalue decomposed, so LSKCSP algorithm is employed.

In this experiment, samples of 10 trials length are grouped when computing the QER. Gaussian kernel is chosen, for that it has a good adaptability by adjusting the variance parameter **c**. Theoretically, when $c$ becomes very large, the LSKCSP should perform like CSP.

The subset of filters are selected by median score for CSP (the number is fixed to be 6) [3]. For Kernel CSP, if the final eigenvectors are more than 6, 4 filters are selected from both ends, and if less than 6, one from each ends are selected.

Features are extracted by computing the logarithm of the variance of the projected CSP or Kernel CSP signals, and classified by LDA.

| **Method** | **CSP** | **LSKCSP** | | | | |
|---|---|---|---|---|---|---|
| | | $c = 20$ | $c = 40$ | $c = 80$ | $c = 160$ | $c = 1000$ |
| mean ± std % | $79.2 \pm 15.5$ | $67.0 \pm 12.7$ | $68.4 \pm 12.6$ | $70.2 \pm 9.6$ | $74.0 \pm 8.7$ | $73.2 \pm 8.7$ |

Table 1: Test accuracy averaged over all subjects.

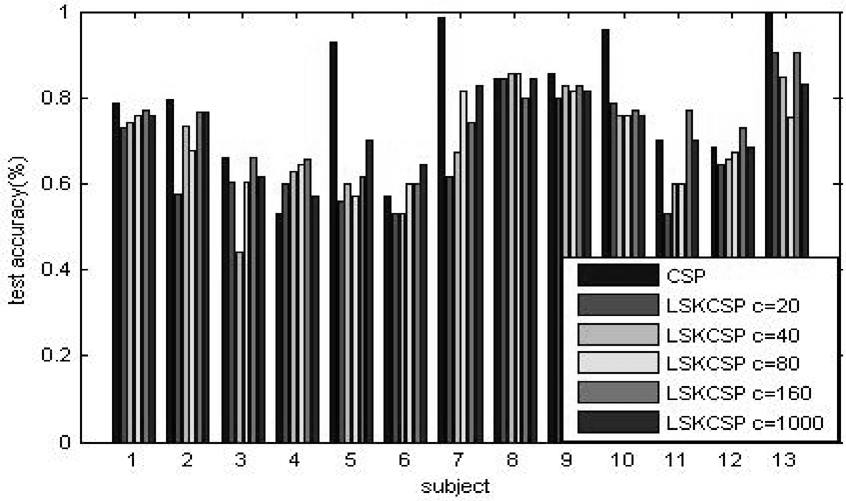


Figure 2: Test accuracy by CSP and LSKCSP algorithm with different variance parameters.

### 3.3 Results

Figure 2 shows the classification accuracy on test set for each subject. Results of LSKCSP algorithm with increasing parameter $c$ are given. For half of subjects (7/13), CSP obtains the best result, and for other subjects, LSKCSP with specific parameter performs better. Averaged results over all subjects are given in Table 1. Generally speaking, with the increase of $c$, results of LSKCSP tends to be closer to CSP, with smaller deviation.

## 4 Conclusion

This paper proposed a novel large scale algorithm to solve kernel CSP in BCI applications. Based on Quadratic equivalent representation, this method find a reduced dataset to replace the original one in the kernel CSP algorithm, which can dramatically save memory when eigenvalue decomposing. Actually, this QER method could also be applicable in kernel PCA for large dataset.

Compared with CSP, LSKCSP algorithm with Gaussian kernel get comparative results, which is not strange, for a large variance parameter makes kernel CSP approach CSP. It should be pointed out that LSKCSP so time consuming, about 20 minutes for training of one subject (processor 1.4 GHz), so it is at the limit of what is practical for online BCI training.

Another problem which should be noted is the scale of subsets in the first step of LSKCSP. Theoretically, when centering in Equation (7), the center of the whole class but not the subset should be used. Here we assume they are nearly the same. So the subset should not be too small and its samples should selected to represent the distribution of the whole class as much as possible.

As our future work, 1) a better parameter selection method should be developed for LSKCSP algorithm, 2) the influence outliers needs to be analyzed and removed, and 3) a regularization term is considered to be added to deal with the noise.

**Acknowledgments:** This work is supported by National Natural Science Foundation of China (60575044, 60771062), and National Basic Research Program of China (2003CB716104). Yang Liu would like to thank K.-R. Müller and B. Blankertz for helpful discussions as well as Berlin-BCI group for the experiment data, and also the China Scholarship Council for its financial support.

## References


[1] K. Fukunaga. *Introduction to Statistical Pattern Recognition.* Academic Press, 1990.

[2] Z. J. Koles and A. C. K. Soong. EEG source localization: implementing the spatio-temporal decomposition approach. *Electroenceph. Clin. Neurophysiol.*, 107(5):343–352, 1998.

[3] B. Blankertz, R. Tomioka, S. Lemm, M. Kawanabe, and K.-R. Müller. Optimizing spatial filters for robust EEG single-trial analysis. *IEEE Sig. Proc. Mag.*, 25(1):41–56, 2008.

[4] J. R. Wolpaw, N. Birbaumer, D. J. McFarland, G. Pfurtscheller, and T. M. Vaughan. Brain–computer interfaces for communication and control. *Clin. Neurophysiol.*, 113(6):767–791, 2002.

[5] H. Ramoser, J. Müller-Gerking, and G. Pfurtscheller. Optimal spatial filtering of single trial EEG during imagined handmovement. *IEEE Trans. Rehabil. Eng.*, 8(4):441–446, 2000.

[6] M. Cheng, W. Jia, X. Gao, S. Gao, and F. Yang. Mu rhythm-based cursor control: an offline analysis. *Clin. Neurophysiol.*, 115(4):745–751, 2004.

[7] B. Blankertz, K.-R. Müller, D. J. Krusienski, G. Schalk, J. R. Wolpaw, A. Schlögl, G. Pfurtscheller, J. del R. Millán, M. Schröder, and N. Birbaumer. The BCI competition III: validating alternative approaches to actual BCI problems. *IEEE Trans. Neural Syst. Rehabil. Eng.*, 14(2):153–159, 2006.

[8] B. Blankertz, G. Dornhege, M. Krauledat, K.-R. Müller, and G. Curio. The non-invasive Berlin Brain–Computer Interface: fast acquisition of effective performance in untrained subjects. *Neuroimage*, 37(2):539–550, 2007.

[9] G. Dornhege, B. Blankertz, and G. Curio. Speeding up classification of multi-channel brain-computer interfaces: common spatial patterns for slow cortical potentials. *First Int. IEEE EMBS Conf. Neural Eng.*, pages 595–598, 2003.

[10] B. Schölkopf and A. J. Smola. *Learning with kernels: support vector machines, regularization, optimization, and beyond.* MIT Press Cambridge, MA, USA, 2001.

[11] K.-R. Müller, S. Mika, G. Rätsch, K. Tsuda, and B. Schölkopf. An introduction to kernel-based learning algorithms. *IEEE Trans. Neural Networks*, 12(2):181–201, 2001.

[12] J. Zhang, J. Tang, and L. Yao. Optimizing spatial filters with kernel methods for BCI applications. In *MIPPR 2007: Remote Sensing and GIS Data Processing and Applications; and Innovative Multispectral Technology and Applications. Edited by Wang, Yongji; Li, Jun; Lei, Bangjun; Yang, Jingyu. Proceedings of the SPIE, Volume 6790, pp. 67903V (2007).*, volume 6790 of *Presented at the Society of Photo-Optical Instrumentation Engineers (SPIE) Conference*, November 2007.

# A method for predicting the success of a BCI training session based on the classification of the CSP filters itself

C. Grozea, S. Fazli, G. Nolte, M. Danóczy, F. Popescu

Intelligent Data Analysis, Fraunhofer FIRST, Berlin, Germany

cristian.grozea@first.fhg.at

**Abstract**

We present an offline analysis of a large set of BCI experiments, focusing on common spatial filters and patterns (CSP). First, we show that it is possible to infer from the CSP filters whether the cross-validation error of LDA-classified EEG data preprocessed by this CSP will be high or low and predict thus the future performance of the feedback sessions following the calibration. Our test is 7 to 10 times faster to compute than the cross-validation. Second, from the CSP patterns, we calculate the corresponding source localization of the activations on the cortex. We explore the possibility of applying our method towards the improvement of calibration procedure quality and thus reduce the phenomenon of BCI illiteracy.

## 1 Introduction

Common Spatial Pattern (CSP) is an established method of processing raw EEG signals in order to obtain a suitable signal projection for doing BCI in a two-class (e. g. left/right hand movement imagination) setup [1]. It has benefitted from many enhancements over the last decade, some of which are described in the context of the Berlin Brain Computer Interface (BBCI) in [2].

CSP is a supervised learning algorithm for two classes, which assumes that the signal measured by EEG sensors is a linear spatial mixture of (unknown) original sources. The rows of the unknown mixing matrix are called patterns, whereas the columns of the demixing matrix, which is the solution of the inverse problem, are called filters. The goal of CSP is to find spatial projections in sensor space that optimally demix the measured signal by maximizing the variance in one class while minimizing the variance in the other class, thereby achieving optimal discriminability for later classification. The filters are obtained by solving a generalized eigenvalue problem to simultaneously diagonalize the covariances of both classes.

A researcher experienced with CSPs is able to decide if a given CSP filter is good or not, by visual inspection – see Figure 1. By "good" we mean that the subject can perform BCI with reasonably high accuracy (80 % or higher). However, the difference is not always as clear as in this illustrative example. Moreover, it would be useful to understand, both from a machine learning perspective as well as a physiological perspective, what makes a subject – and his CSP – "bad".

In this paper we develop algorithms which can decide whether a given CSP filter is good, and predict from the first session if the subject will be able to perform BCI well in future sessions, albeit with a lower accuracy than the prediction of the quality of the CSPs.

By employing source localisation techniques we can further explain why it should be possible to detect in the CSP filters and patterns how discriminable the mental imagination of the subject was during the calibration phase.

To automatically learn the mapping between CSP filters and the cross-validation error on the training set, we used recorded data from a large corpus of BCI experiments, computed the CSP on the biggest common subset of channels and took this as the input of the mapping to be learned. As output, we took the cross-validation error, computed using information from all the channels that were recorded in the experiment.

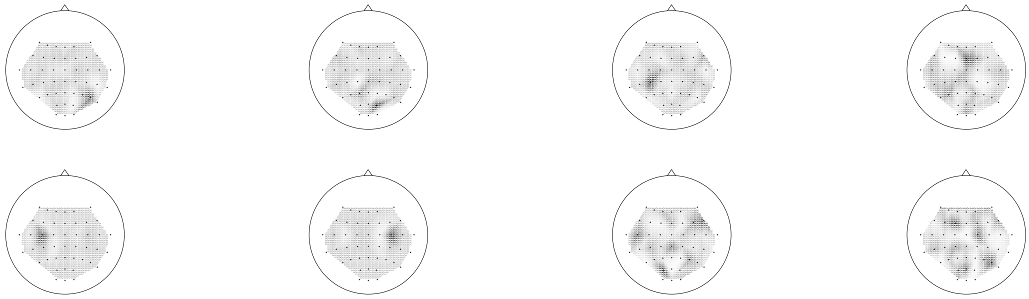

Figure 1: The 4 scalp plots on the left show a good CSP filter – cross-validation error 1 %. The 4 scalp plots on the right show a bad CSP filter – cross-validation error 50 %.

We use feature selection methods based on the Markov blanket of the target. In Bayesian networks, the Markov blanket of a node is the set of all nodes that are needed to explain that target node. It contains all parents (the direct causes) of that node, all children (direct effects) and the other parents of its children as well [3].

# 2 Methods

## 2.1 Data and preprocessing

The dataset used contains 148 experiments performed at the IDA group between 2001 and 2005 with 25 subjects. The paradigm was either LR (left/right) – 49 times, or LF (left/foot) – 53 times or RF (right/foot) – 46 times. Figure 2 shows descriptive statistics of the dataset.

The data has been filtered in the frequency domain by applying a wide-band band-pass filter from 5 to 30 Hz.

We processed these data using the Condor HTC system on a computing cluster. The processing we performed used the BBCI toolbox functions to first evaluate the cross-validation error on all channels available in the experiment. Then, only the channels common throughout the whole dataset were retained and the CSP was computed for each experiment. This was used as the initial input to the predictor. As output (binary valued), we took the membership or exclusion from the class of "good" experiments (i. e. less than 20 % cross-validation error on the trials recorded). Here are the 45 channels available in all experiments considered: F5, F3, F1, Fz, F2, F6, FC5, FC3, FC1, FCz, FC2, FC4, FC6, T7, C5, C3, C1, Cz, C2, C4, C6, T8, TP7, CP5, CP3, CP1, CPz, CP2, CP4, CP6, TP8, P5, P3, P1, Pz, P2, P4, P6, P8, PO3, POz, PO4, O1, Oz, O2.

The dataset for the learning problem we thus obtained had 148 samples each with 180 (45 channels multiplied by 4 filters) continuously valued features and a binary target.

## 2.2 Algorithms

Having more features than samples is always a problem, thus feature reduction and sparsification are to be considered. The best approach to feature reduction we found on this dataset was the "causal explorer" [4] able to provide us with Markov blanket estimations for a target feature. Out of all algorithms available in that toolkit, we used HITON, described in [5], very well suited for feature selection.

With the features thus selected, we perfomed a sparsifying linear norm-1 SVM training, by dividing the currently available training set into two equal sets, use one subset for trainig the SVM and one for testing the effect of the SVM parameters.

In order to validate the process, everything that has been described so far is wrapped into a leave-one-out cross-validation procedure, that iteratively leaves an experiment out and trains on

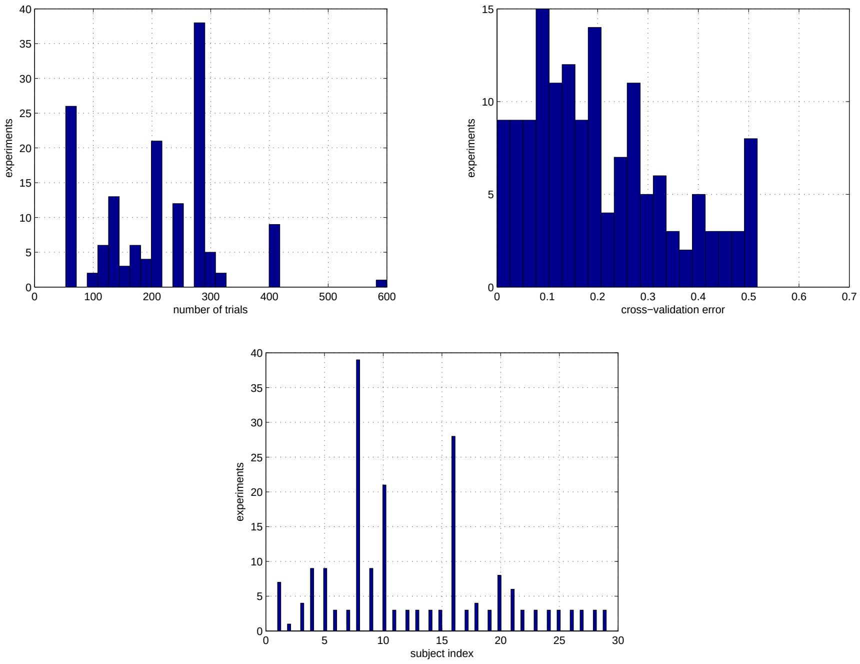


Figure 2: Left: the distribution of the number of trials. Right: The distribution of the cross-validation error. Bottom: The number of experiments per subject.

the data derived from the retained experiments, and then tests on the left out experiment (CSP), after keeping only the features inferred as important on the data used for training.

A typical such feature set contains the following channels: FC5, FC3, FC1, FC2, T7, Cz, C2, C4, CP2, CP6, P3, P1, O1. We remind the reader that we have in the dataset both experiments where the classes correspond to imaginary movements of the left and right hands and experiments where one of the classes corresponds to imaginary movements of one foot. In Figure 3(a) the approximate placement of these channels on the scalp can be seen.

**ALGORITHM 1.**
initialize the number of errors with 0
foreach experiment, $i$
    hold out the experiment $i$
    use HITON_MB to find the Markov blanket estimation of the target
    keep only the selected features, discarding all others
    split the set of remaining experiments in half
    foreach value of the SVM hyperparameter $C$ in a predefined set of 20 values,
        train a norm 1 SVM on the first half
        test it on the second half
    retain the hyperparameter value that gave the best result and the corresponding linear model
    keep only the selected features in the hold-out experiment, discarding all others
    apply the linear model on the hold-out experiment
    if classification fails to give the correct class, increase the number of errors

## 2.3 Implementation

The method has been implemented in Matlab. CVX, a package for specifying and solving convex programs [6, 7] has been used to implement and solve various flavours of norm-1 SVMs, seen as

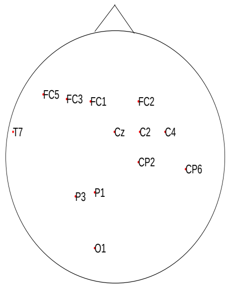


(a) Approximate placement on the scalp of the channels most relevant to predict CSP-BCI performance.

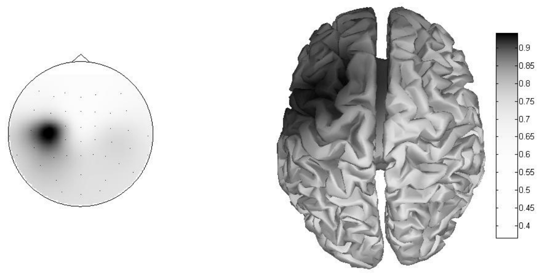


(b) Imagined movement of a limb

Figure 3: (a) The channels selected by the causal feature selection. (b) Imagined movement of a limb. On the left, CSP pattern. On the right, corresponding source localization on the cortex obtained using the MUSIC model.

convex programming instances. Causal Explorer has been used to compute the Markov blanket. Processing of the dataset (on all prefixes of each experiment) took 300 cpu-hours. The cross-validation of our method took about two hours.

### 2.4 Inverse methods

To evaluate whether the CSP-patterns correspond to focal brain sources, which we expect to be the case for useful patterns, we apply an inverse method for each pattern. We chose the well-known MUSIC approach [8] which scans a predefined grid for dipolar sources and returns for each voxel the goodness-of-fit of the best dipole placed at that voxel. The respective scan shown over the grid, which in our case was confined to be on the cortical surface, provides a qualitative picture of areas which are most likely involved in the generation of the respective CSP pattern. We emphasize that the results are too blurred to represent true brain sources and can only be understood as a rough indication of the source origin.

The calculations were done for a three-shell realistically shaped volume conductor using a semi-analytic expansion of the electric lead field [9]. The volume conductor itself was chosen to be a publically available standard head [10], and electrode locations were adjusted to this head model.

Typical appropriate locations of the sources are obtained for the good calibration sessions – Figure 3(b), and typical mistakes for the failed calibration sessions are obtained and illustrated in Figure 4. Please note that this source localisation analysis of the CSP patterns was purely qualitative, as opposed to the quantitative analysis that we did on the CSP filters.

## 3 Results

The cross-validation process produced 27 % error. Thus we expect the method to be able to identify the experiments leading to less than 20 % cross-validation error with 73 % accuracy. Note that we used only 45 channels the are common to all BCI sessions in our dataset. On the other hand, the performance to be predicted corresponds to the classifier using all electrodes for which there is recorded data.

The results are good, given the ambitious task of predicting with the less informed CSP computed on only 45 channels the performance of the (not yet computed) classifier on data processed with all electrods for which there is recorded data. As a further advantage, the classification algorithm presented here is on our data 7 to 10 times faster to compute than the 8-fold cross-validation

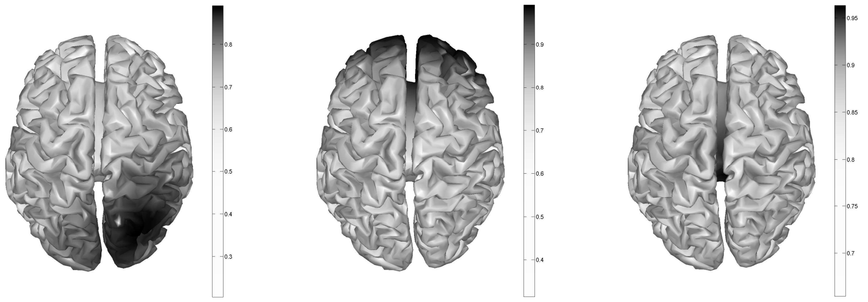

Figure 4: Source localization on the cortex obtained from the "bad" CSP patterns that are most likely related to non-movement imagination activity, using the MUSIC model. On left: seeing/eye related. On middle: abstract cognitive processing/frontal activity. On right: no (or widely distributed) cortical activity.

– in both cases the CSP calculation was included.

# 4 Discussion

About half of the experiments were under the considered threshold of 20 % used to label the subject performance as "good" or "bad". Therefore, for the learning problem, the dataset was fairly balanced, which makes the error measure used appropriate.

The use of the causal feature selection techniques to BCI sensitivity analysis is new to our knowledge and has produced set of channels that are relevant either for left hand, right hand, foot/feet movement imagination and for general alpha power level. This sensible choice of the channels further validates the use of this technique.

We have also run a different analysis where the input for the learning problem was the same set of CSP filters as explained before, but the output was 1 if the minimum cross-validation error amongst all known experiments of the same subject was below 20 %, and 0 otherwise. In other words, we tried to predict from the CSP filter of one experiment the best performance of all, future and past, experiments of the same subject. The precision we obtained in predicting whether the subject will "ever" have a good training was lower, with a cross-validation error of 35 %. What came out interesting out of this was that the set of channels usually selected was slightly different. Here is an example: F5, F3, Fz, F2, FC5, FC1, FC2, FC4, FC6, Cz, C4, T8, Pz, POz, O1. The difference seems to be the higher occurence of centro-parietal channels.

While looking at the localized sources for the CSP patterns one may easily identify the activations of cortical regions. For the low performance sessions, this enables the experimenter to pinpoint possible causes of the lack of performance in BCI for a particular subject, since he can more accurately determine the origin of activation and thus instruct the subject on how to improve his mental task performance.

# 5 Conclusion

A method to predict the success of a training session in which a subject's EEG is recorded on at least 45 channels while the subject performs imaginary limb movements in the Berlin BCI setup has been presented. By employing a causal feature selection technique, based on the Markov blanket of the target, we have been able to greatly reduce the number of features (channels) in the input CSP filters, and in this case proved critical to the success of the algorithm which mapped the CSP filters to sessions accuracy. As a result, we have been able to predict whether a BCI training was successful (low cross-validation error, i. e. below 20 %), with 73 % accuracy.

Furthermore, source localization has been employed to qualitatively inspect the CSP patterns and explain individual performances of subjects. Whereas good CSPs correspond to expected cortical sources, “bad” ones may be due to a variety of mental task performance “errors” which are explainable.

This justifies the claim of the experienced BCI lab researchers of being able to see the success of a training session from the initial CSP filters. Also, this opens the perspective – to be confirmed with further online studies – of being able to reduce the BCI illiteracy by instructing properly (e. g. “try to imagine a concrete movement.” or “are you vizualizing the scene?”) the subjects who, initially, do not have a very good performance.

**Acknowledgments:** This work was supported by the European Commission’s Marie Curie Excellence Team grant MEXT-CT-2004-014194 “Brain2Robot”.

## References

[1] J. Müller-Gerking, G. Pfurtscheller, and H. Flyvbjerg. Designing optimal spatial filters for single-trial EEG classification in a movement task. *Clin. Neurophysiol.*, 110(5):787–798, 1999.

[2] B. Blankertz, R. Tomioka, S. Lemm, M. Kawanabe, and K.-R. Müller. Optimizing spatial filters for robust eeg single-trial analysis. *IEEE Sig. Process. Mag.*, 25:41–56, 2008.

[3] J. Pearl. *Probabilistic Reasoning in Intelligent Systems: Networks of Plausible Inference.* Morgan Kaufmann Publishers, 1988.

[4] C. F. Aliferis, I. Tsamardinos, A. Statnikov, and L. E. Brown. Causal Explorer: A Causal Probabilistic Network Learning Toolkit for Biomedical Discovery. *Int. Conf. Math. Eng. Tech. Med. Biol. Sci. (METMBS’03)*, pages 371–376, 2003.

[5] C. F. Aliferis, I. Tsamardinos, and A. Statnikov. HITON: A Novel Markov Blanket Algorithm for Optimal Variable Selection. *AMIA. Annu. Symp. Proc.*, 2003:21, 2003.

[6] M. Grant and S. Boyd. CVX: Matlab software for disciplined convex programming (web page and software), 2008.

[7] M. C. Grant and S. P. Boyd. Graph implementations for nonsmooth convex programs. *Rec. Adv. Learn. Control*, 2008.

[8] J. C. Mosher, P. S. Lewis, R. M. Leahy, and R. B. TRW. Multiple dipole modeling and localization from spatio-temporal MEGdata. *IEEE Trans. Biomed. Eng.*, 39(6):541–557, 1992.

[9] G. Nolte and G. Dassios. Analytic expansion of the EEG lead field for realistic volume conductors. *Phys. Med. Biol.*, 50(16):3807–3823, 2005.

[10] A. C. Evans, M. Kamber, D. L. Collins, and D. MacDonald. An MRI-based probabilistic atlas of neuroanatomy. *Magn. Reson. Scanning and Epilepsy*, 264:263–274, 1994.

# Optimizing common spatial pattern for a motor imagery-based BCI by eigenvector filteration

A. Satti, D. Coyle, G. Prasad

Intelligent Systems Research Centre, University of Ulster

satti-ar@ulster.ac.uk

**Abstract**

One of the fundamental criterion for the successful application of a brain-computer interface (BCI) system is to extract significant features that confine invariant characteristics specific to each brain state. Distinct features play an important role in enabling a computer to associate different electroencephalogram (EEG) signals to different brain states. To ease the workload on the feature extractor and enhance separability between different brain states, the data is often transformed or filtered to maximize separability before feature extraction. The common spatial patterns (CSP) approach can achieve this by linearly projecting the multi-channel EEG data into a surrogate data space by the weighted summation of the appropriate channels. However, choosing the optimal spatial filters is very significant in the projection of the data and this has a direct impact on classification. This paper presents an optimized pattern selection method from the CSP filter for improved classification accuracy. Based on the hypothesis that values closer to zero in the CSP filter introduce noise rather than useful information, the CSP filter is modified by analyzing the CSP filter and removing/filtering the degradative or insignificant values from the filter. This hypothesis is tested by comparing the BCI results of eight subjects using the conventional CSP filters and the optimized CSP filter. In majority of the cases the latter produces better performance in terms of the overall classification accuracy.

## 1 Introduction

Brain-computer interface (BCI) involves transforming signals from the brain into control signals for transmission of messages or commands, thus offering a new communication pathway between human brain and the computer system [1]. Patients suffering from motor impairments, severe cerebral palsy and spinal chord injuries (SCI) may use a BCI system as a substitute communication pathway which relies only on the mental imagination and not on neuromuscular control. The main difference between BCI techniques and human-computer interface (HCI) tasks lies in not relying on muscular response, but only on detectable signals representing responsive or intentional brain activity. Recently there has been a significant growth in BCI technology but there are a significant number of issues and areas that need to be improved [2] – reasons being the complexity and ambiguity of the EEG signals recorded from the brain [3].

Many BCIs are based on EEG signals which are modified by motor related brain activity, as these signals exhibit significant and lateralized event related activity. Event related desynchronization (ERD) is the phenomenon which results in amplitude attenuation of certain EEG rhythms when an event is initiated or is taking place in the brain [4, 5]. On the other hand, event-related synchronization (ERS) is an amplitude enhancement of a certain EEG rhythm when cortical areas are not specifically engaged in a given mode of activity at a certain instant of time [4].To capture only these rhythms, a band pass filter between 8–26 Hz can be applied to filter out the non-event related data. Even though hand movement (motor) imagery-related ERD/ERS forms a centre close to the hand representation area in close proximity to the electrodes C3 and C4, one or two

EEG signals recorded from both hemispheres are insufficient to completely describe the state of brain activation during motor imagery [6]. Thus when using only 2 or 3 electrodes, it is difficult to obtain the same accuracy as compared to multichannel EEG which captures most of the event related information [6]. On the contrary, using a large number of electrodes adds more irrelevant data but choosing good spatial patterns helps to reinforce the event related information. Common Spatial Pattern (CSP) filtering provides an efficient solution for a larger number of channels. The goal of CSP is to devise spatial filters that lead to new time series whose variances are optimal for the discrimination of different brainstates or EEG classes. The CSP method is used to estimate spatial filters that reflect the specific activation of cortical areas during movement imagination (cf. Section III for more details on CSP).

In this work, the CSP method is used to find the appropriate CSP filter for a 60 channel EEG recorded during motor imagery-based BCI experiments. The most significant CSP filters are then statistically analyzed and each filter is optimized by removing the values from the filter which are assumed to introduce noise rather than enhancing separability between different classes of EEG. The technique developed for doing this is based on the hypothesis that values closer to zero in the common spatial pattern are not significant and introduce noise. This hypothesis is then tested by comparing results for the conventional CSP filters and the optimized one.
The remainder of the paper is organized into four sections. Section II contains details on the BCI Competition III multichannel/multiclass datasets and acquisition procedure. Section III discusses the CSP method and a novel CSP optimization technique. Results are plotted in section IV for the comparison of CSP and its variant. Section V provides the conclusion.

## 2 Data acquisition and configuration

The datasets used in this analysis are datasets IIIa and IVa provided for the third International BCI Competition [7]. A berief description of these datasets is as under:
The dataset IIIa was recorded from three subjects using a 64 channel amplifier from Neuroscan, and was filtered between 1 and 30 Hz. The subject sat on a comfortable chair and had to perform left, right hand, tongue and foot movement imagination according to the cue on the screen.

Each trial begins with a black screen and a beep sounds at $t = 2\,\mathrm{s}$, at which time a fixation cross appears on the screen which is indication for the subject to get ready. At $t = 3\,\mathrm{s}$ an arrow appears on the fixation cross indicating the imagined movement to be executed, pointing left, right, up or down for left/right hand, foot and tongue imagery, respectively. The subject performs the imagery task until $t = 7\,\mathrm{s}$. Each of these four tasks was performed 10 times in a random order in each run.
Dataset IVa was recorded with slight variation from dataset IIIa. 118 EEG channels were used for data acquisition and arrows were displayed for 3.5 s indicating the corresponding task to be performed. The presentation of target arrows were intermitted by periods of random length, 1.75 to 2.25 s, in which the subject could relax [7].
In this work, which is only a 2 class analysis, the data was filtered between 8–26 Hz to remove the components which are generally not event-related.

## 3 Methodology

The purpose of CSP is to filter the original data using the optimally designed CSP filter into new time series i. e., to produce the surrogate data space for the discrimination of two populations. The patterns designed in this way help to maximize the variance for the ‘left motor imagery’ trials and minimize the variance for the ‘right motor imagery’ in the surrogate data space [6, 8, 9, 10, 11, 12].

### 3.1 Common spatial patterns

CSP filtering involves linearly projecting the multichannel EEG data into a surrogate data space by a weighted summation of the appropriate channels. This projection is based on the simultaneous

diagonalisation of the covariance matrices from both classes [6, 8, 9, 10, 11]. This diagonalisation is achieved by the following three steps.
Let $X$ be a single trial EEG matrix for N-channel EEG of size $N \times T$ where $T$ is the number of samples in a trial. A single trial is one specific imagined movement in a cue based paradigm depending on the direction of the arrow. The normalized covariance for the two classes $\sum_L$ and $\sum_R$ can be represented as:

$$\sum_k = \frac{1}{n} \sum_{i=1}^{n} X_i X_i^t \ (k \in \{L, R\}) \tag{1}$$

where $n$ is the total number of trials for the class $k$, respectively. For the simultaneous diagonalisation of these two covariance matrices, the first step is to perform the whitening transformation i. e., finding a matrix $P$ such that:

$$P \left( \sum_L + \sum_R \right) P^T = I \tag{2}$$

where $P^T$ represents the transpose of $P$.
According to spectral theory, using $P$ the matrices $Q$ and $D$ can be calculated using (4) below. The columns of the matrix $Q$ are the eigenvectors and the diagonal matrix $D$ contains the eigenvalues.

$$P \sum_R Q \cdot P^T = Q \cdot D \cdot Q^T \tag{3}$$

From Equation 1 and 2

$$P \sum_L Q \cdot P^T = Q(1 - D)Q^T \tag{4}$$

The mixing matrix $W$ can be calculated as :

$$W = Q^T \times P \tag{5}$$

With the mapping matrix $W$, the trial $X$ is projected as

$$Z = W \times X \tag{6}$$

From Equation 4 and 5 it is clear that the eigenvalues of the transformed covariance matrices sum to one. By construction, the variance for a left movement imagination is largest in the first row of Z and decreases for the subsequent rows [6]. The opposite is the case for a trial with right motor imagery. Thus those eigenvectors whose corresponding eigenvalues are close to 1 or 0 are chosen as spatial filters [6]. This can be achieved by arranging the eigenvalues in ascending or descending order and matching corresponding columns of the W matrix. The appropriate number of eigenvectors from both sides is chosen as filters; generally between 2 to 6 from either side of the eigenvector matrice is optimal.

### 3.2 Optimizing the CSP filter

The chosen eigenvectors represent the filters whose values symbolize the weights to be applied to corresponding channel for mapping the data to the surrogate data space. It is important that the spatial pattern be used efficiently for optimal mapping. For this reason, in this work the CSP filter has been analyzed and filtered to improve the performance. Table 1 portrays the range of values in the CSP filter (4 eigenvectors – 2 from either end of the eigenvector matrix). It is important to note that the greater the weight of the eigenvector value, the greater the impact the corresponding channel would have on the surrogate data space. The values in the eigenvector which are closer to zero have a very small impact in the surrogate data space and can often introduce noise and

| Statistics | Eigenvector 1 | Eigenvector 2 | Eigenvector 3 | Eigenvector 4 |
|---|---|---|---|---|
| Range | $-3.808 \rightarrow 1.873$ | $-3.579 \rightarrow 4.112$ | $-2.971 \rightarrow 6.367$ | $-4.485 \rightarrow 4.288$ |
| Threshold | 0.5241 | 0.7697 | 0.9348 | 0.8703 |

Table 1: Statistics for CSP filter of Subject 1.

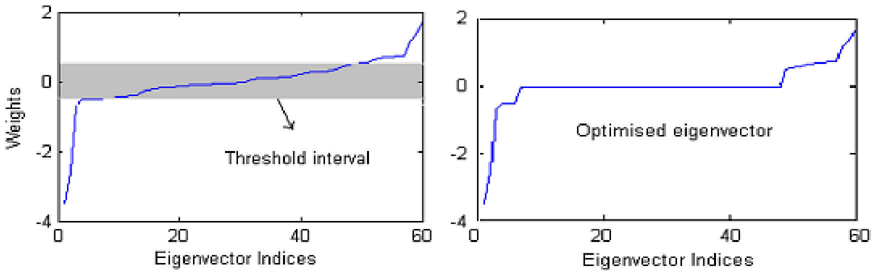


Figure 1: Eigenvector optimization of CSP vector 1 for Subject 1.

degrade the effectiveness of CSP filter. Based on this observation, the modified CSP matrix, $\Psi$, can be extracted from the CSP filter W based on the significance of the weights in the filter.

The threshold value for removing superfluous weights is chosen based on the hypothesis that the values closer to zero in the eigenvector curve (cf. Figure 1 for example) are non significant and add noise rather than useful information and thus should be discarded. To illustrate this, Figure 1 shows plotted values for first eigenvector from the CSP filter W for subject 1 and the modified eigenvector with values close to zero set to zero. To achieve this, the values of the eigenvector are first arranged in ascending order.

Let $w = w_1, \ldots, w_n$ be the values of the eigenvector population. To obtain the values closer to zero in the eigenvector curve the range $\gamma$ of the eigenvector w, is given as:

$$\gamma = \max(w_j) - \min(w_i) \tag{7}$$

If $\lambda$ is the percentile of the range $\gamma$ close to zero to be discarded, then the interval used for thresholding the eigenvectors is calculated as

$$\text{Threshold interval} = \left[0 - \frac{\lambda \cdot \gamma}{2}, 0 + \frac{\lambda \cdot \gamma}{2}\right] \tag{8}$$

Thus the optimized matrix $\Psi$ is extracted from $W$ as;

$$\Psi_{i,j} = W_{i,j} \quad \text{for } |W_{i,j}| > \text{Threshold} \tag{9}$$

$$\Psi_{i,j} = 0 \quad \text{for } |W_{i,j}| < \text{Threshold} \tag{10}$$

where,

$$\text{Threshold} = \frac{\lambda \cdot \gamma}{2} \tag{11}$$

All the values lying in this interval are truncated to zero. The resulting CSP pattern will then contain only the significant values which lie outside the threshold obtained via the above analysis. Note that the columns of $\Psi$ (the mixing matrix) are the modified common spatial patterns which are time-invariant EEG source distribution vectors.

To apply the filters, $X$, the input trial, which is spectrally pre-filtered between 8–26 Hz is fed to the modified CSP filter $\Psi$ which maps the original EEG data into new surrogate space $Z$

$$Z = \Psi \times X \tag{12}$$

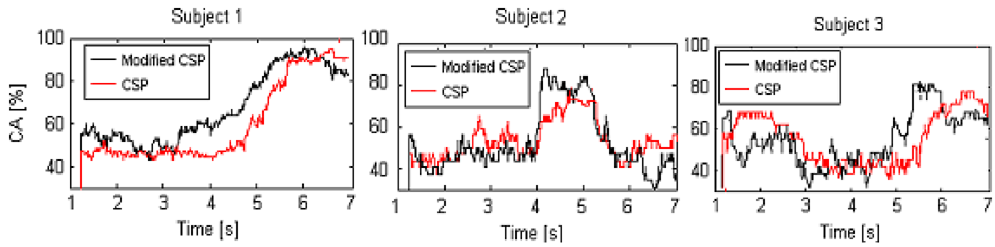


Figure 2: Classification accuracies for 3 subjects (IIIa) across sessions.

| | | Cross-validation | | Test data (unseen) | |
|---|---|---|---|---|---|
| | | CSP | Modified CSP | CSP | Modified CSP |
| Dataset IIIa | Sub1 | 92.4 | 95.2 | 93.3 | 96.1 |
| | Sub2 | 82.3 | 90.1 | 78.9 | 87.3 |
| | Sub3 | 78.8 | 83.2 | 70.0 | 74.1 |
| Dataset IVa | Sub4 | 81.4 | 83.2 | 62.1 | 69.7 |
| | Sub5 | 97.8 | 93.8 | 88.5 | 82.4 |
| | Sub6 | 67.1 | 74.8 | 68.0 | 78.5 |
| | Sub7 | 75.0 | 78.5 | 79.1 | 76.1 |
| | Sub8 | 90.7 | 88.5 | 80.1 | 82.0 |
| | Mean | 83.2 | 86.4 | 77.5 | 80.8 |

Table 2: Classification accuracies.

For feature extraction, the log-variance of the surrogate data is used as the feature vector for classification. The CSP filters and feature extraction are continually calculated from a 1s wide window slid across the trials.

$$V = \log\{(\mathrm{var}(Z)\} \tag{13}$$

## 4 Results and discussion

To assess the modified method, data from the right and left hand imagination trials from the BCI competition are utilized. 5-fold cross-validation was carried out for each subject, where the data was partitioned into a training set (80 %) and a validation set (20 %). Tests were performed five times using a different validation partition each time. Information obtained using the maximum mean-CA (mCA) rates on the 5-folds of validation data was used to setup the CSP filter and classifier for a final single trial test on unseen test data (as per the BCI competition splits ). The modified CSP was setup by varying $\lambda$ between 10–40 % of the range of the vector during cross-validation and it was observed that generally $\lambda \approx 10\,\%$ provides the optimal performance.
Table 2 lists the classification accuracy rates for the comparison between the traditionally used CSP method and the modified CSP for the eight subjects. These results indicate that for six subjects out of eight, the classification accuracy is improved by applying eigenvector filtration indicating that elimination of non- event related information from the surrogate dataspace using modified CSP is beneficial for a BCI. Figure 2 also shows that the response latency is reduced by the modified CSP (only subjects 1–3 are shown). It is notable that the modified CSP pattern helps improve the classification accuracy on average by $\sim 4\,\%$. These results indicate that the hypothesis that weights closer to zero in the CSP eigenvector are non-significant and can be degradative to performance although statistical significance cannot be shown due to the small subject samples and the large variation in results across subjects. Further fine tuning of $\lambda$ could improve the performance but it has been observed that, in general, removing ~5–20 % of the values closer to zero yields an acceptably optimized CSP filter.

## 5 Conclusion

The results presented in this work indicate that appropriately modifying the eigenvectors of the most significant CSPs can have a significant influence on the CSP filter. Eigenvectors values around zero should be removed as they can be a noise source and degrade the separability of motor imagery in the surrogate data space. To the best of the author's knowledge this aspect of CSP filtering is not accentuated in the literature. The results could be enhanced through a more detail investigation into the optimal number of CSPs or subject-specific frequency filter selection [8, 9]. Further statistical analysis on the CSP pattern could enhance the BCI accuracy by introducing adaptive thresholds, which could help suppressing insignificant information for online systems.

## References

[1] J. R. Wolpaw, N. Birbaumer, D. J. McFarland, G. Pfurtscheller, and T. M. Vaughan. Brain-computer interfaces for communication and control. *Clin. Neurophysiol.*, 113:767–791, 2002.

[2] S. G. Mason, A. Bashashati, M. Fatourechi, K. F. Navarro, and G. E. Birch. A comprehensive survey of brain interface technology designs. *Ann. Biomed. Eng.*, 35:137–169, 2007.

[3] D. Coyle, T. M. McGinnity, and G. Prasad. A multi-class brain-computer interface with SOFNN-based prediction preprocessin. *IEEE World Congress Comput. Intell.*, 2008.

[4] G. Pfurtscheller and F. H. Lopes da Silva. Event-related EEG/MEG synchronization and desynchronization: basic principles. *Clin. Neurophysiol.*, 110:1842–1857, 1999.

[5] D. Coyle. Intelligent preprocessing and feature extraction techniques for a brain computer interface. PhD Thesis, University of Ulster, N. Ireland, 2006.

[6] C. Guger, H. Ramoser, and G. Pfurtscheller. Real-time EEG analysis with subject-specific spatial patterns for a brain-computer interface (BCI). *IEEE Trans. Neural Syst. Rehabil. Eng.*, 8:447–450, 2000.

[7] A. Schlögl, F. Lee, H. Bischof, and G. Pfurtscheller. Characterization of four-class motor imagery EEG data for the BCI-competition 2005. *J. Neural Eng.*, 2:L1–L9, 2005.

[8] B. Blankertz, F. Losch, M. Krauledat, G. Dornhege, G. Curio, and K.-R. Müller. The Berlin Brain-Computer Interface: accurate performance from first-session in BCI-naive subjects. *IEEE Trans. Biomed. Eng.*, in press, 2008.

[9] B. Blankertz, R. Tomioka, S. Lemm, M. Kawanabe, and K.-R. Müller. Optimizing spatial filters for robust EEG single-trial analysis. *IEEE Sig. Process. Mag.*, 25:41–56, 2008.

[10] J. Müller-Gerking, G. Pfurtscheller, and H. Flyvbjerg. Designing optimal spatial filters for single-trial EEG classification in a movement task. *Clin. Neurophysiol.*, 110:787–798, 1999.

[11] H. Ramoser, J. Müller-Gerking, and G. Pfurtscheller. Optimal spatial filtering of single trial EEG during imagined hand movement. *IEEE Trans. Rehabil. Eng.*, 8:441–446, 2000.

[12] Y. Wang, Z. Zhang, Y. Li, X. Gao, S. Gao, and F. Yang. BCI competition 2003 – data set IV: An algorithm based on CSSD and FDA for classifying single-trial EEG. *IEEE Trans. Biomed. Eng.*, 51, 2004.

# Mathematical morphological multi-resolution analysis of EEG signals during misoperation of BCI system

K. Inoue[1], M. Fujio[1], T. Yamaguchi[1] and G. Pfurtscheller[2]

[1]Department of Systems Design and Informatics,
Kyushu Institute of Technology, Iizuka, Fukuoka, Japan
[2]Institute for Knowledge Discovery, BCI Lab, Graz University of Technology, Graz, Austria

inoue@ces.kyutech.ac.jp

**Abstract**

Recently, there are a lot of researches on Brain Computer Interface (BCI) system, and some systems have already been put to practical use. However, the development of the fail safe function is indispensable to be able to use the BCI system more safely. In this paper, we try to detect misoperation of BCI system by analyzing electroencephalogram (EEG) signals recorded during misoperation. Mathematical morphological multi- resolution analysis is adopted as a tool of EEG analysis. This method is a kind of wavelet analysis with non-linear characteristics. In this study, it is investigated about optimal data length, electrode position and feature extraction method. Effectiveness of a proposed method is confirmed through experimental studies. As the results, we found out that construction of BCI system with fail safe function is possible.

## 1 Introduction

Electroencephalogram (EEG) signals can be used to move a cursor to a target on a computer screen. Such an EEG-based brain computer interface (BCI) can provide a new communication channel to replace an impaired motor function [1]. It can be used by e. g., handicapped users with amyotrophic lateral sclerosis (ALS). In such a BCI system, information (e. g. ERD/ERS, P300 etc.) which is included in EEG signals related to a cognitive task or motor imagery is used in order to estimate the will of humans. For the EEG signals recognition method, there are many methods have been proposed. For example, Pfurtscheller et al. extracted ERD/ERS from EEG during right and left hand motor imagery and made it use for the pattern recognition for single-trial wave form by a neural network [2]. We also have studied pattern recognition method based on autoregressive (AR) model about right and left hand motor imagery [3, 4]. However, it seems to be impossible to construct a complete BCI system, since it depends on human state. Therefore, some compensation function is needed in BCI system. The research about error potential by Schalk et al. [5] is useful to construct such function. However, the estimation of will of human and the detection of misoperation must be done simultaneously in the BCI system in order to enable a continuous operation with the fail safe function. In other words, the operation of the machine based on the estimation of the will must be always executed, and the detection result of machine misoperation must be used to stop machine as a fail safe function. From the viewpoint of such BCI system, the error potential seems to be insufficient, because the detection period of error is different from the estimation period of human's will. Such different information seems to be able to be extracted at a time, by using either multi channel EEG signals or different frequency band signals.

Therefore, in this paper, we try to detect misoperation of BCI system by applying mathematical morphological multi-resolution analysis [6, 7] to EEG signal as a basic research. And it is

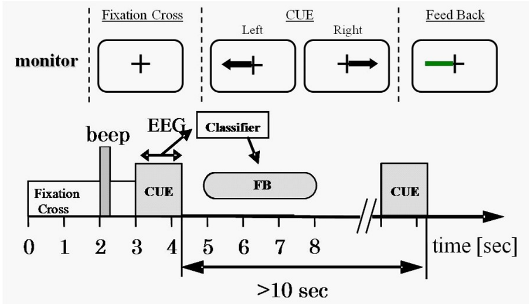


Figure 1: Timing chart.

investigated about optimal data length, electrode position, feature extraction method. Effectiveness of a proposed method is confirmed through experimental studies. As the results, we found out that construction of BCI system with fail safe function is possible.

## 2 Experimental paradigm

During the experiment, subject fixated a computer monitor 100 cm in front of him. Each trial was 10 s long and started with the presentation of a fixation cross at the center of the monitor, followed by a short warning tone ('beep') at 2000 ms (see Figure 1). At 3000 ms, the fixation cross was overlaid with an arrow at the center of the monitor for 1250 ms, pointing to the left or to the right. Depending on the direction of the arrow, subject was instructed to imagine a movement of the left or the right hand. At 5000 ms, the monitor displays the feedback as result of discrimination of BCI system for 3000 ms.

In this study, two kinds of experiments are executed. One is "Motor Imagery Discrimination Experiment (Exp. I)" and this purpose is to train subject. The other is "Pseudo Feedback Experiment (Exp. II)" and this is executed to obtain EEG data during misoperation of BCI system. Exp. I has been executed in the past for other purpose (EEG-based control of robot [4]). Therefore, the specifications of Exp. II are different from the specifications of Exp. I, although they should be set to be same. Three subjects (N, U, Y) participated in these experiments. They are 20–23 years old and free of medication and central nervous system abnormality.

### 2.1 Experiment I (motor imagery discriminate experiment)

Two subjects (N, U) participated in this experiment. Each of the subjects participated in 10 sessions, all on different days. Each session consisted of 3 experimental of 60 trials (30 'left' and 30 'right') and lasted for about 1.5 hours. The sequence of 'left' and 'right' trials, as well as the duration of the breaks between consecutive trials (ranging between 500 and 2500 ms.), were randomized throughout each experimental run. In 2–10 sessions, the feedbacks are executed based on the parameter estimated from the previous experimental data. Feedback is refreshed every 250 ms on the monitor. Sampling frequency of EEG signals acquisition is 500 Hz. EEG recording electrode positions are shown in Figure 2(a).

Right hand movement or left hand movement were able to be discriminated about 90 % on both of these subjects at tenth experimental day. These two subjects participated in the following Exp. II. The method of this experiment is the same as in [3]. Therefore, the detailed explanation of this experiment is omitted in this paper.

### 2.2 Experiment II (pseudo feedback experiment)

Three subjects (N, U, Y) participated in this experiment. Subject Y did not have the experience of Exp. I, but he was well informed of the experimental situation and system. In this experiment,

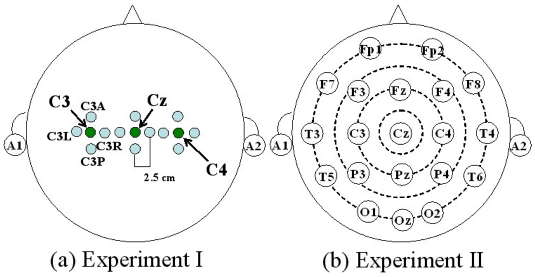


Figure 2: Electrode positions.

the feedback has displayed only one direction for 3000 ms. All subjects are told that feedback has to do with motor imagery before the experiment (as Exp. I). However, feedback was generated artificially at random regardless of subject's motor imagery.

"Correct-Class" data is defined as EEG signals obtained when the direction of feedback arrow on monitor is same as the direction of instruction arrow. "Error-Class" data is defined as EEG data obtained when the direction of feedback arrow on monitor is different from the direction of instruction arrow. The presentation ratio of "Correct-Class" to "Error-Class" is 8:2. The sampling frequency is 512 Hz. EEG recording electrode positions are shown in Figure 2(b).

# 3 Signal analysis and pattern recognition method

## 3.1 Mathematical morphological multi-resolution analysis

In this study, we use the mathematical morphological multi-resolution analysis. These are captured as a unified manner [7]. In this section, mathematical morphological multi-resolution analysis is described. As basic operations, we employ Minkowski addition $\oplus$ and Minkowski subtraction $\ominus$, those are respectively defined as follows.

$$[f \oplus g](t) = \max_{t-u \in F} f(t-u) + g(u) \tag{1}$$

$$[f \ominus g](t) = \min_{u \in G} f(t-u) - g(u) \tag{2}$$

Here, $f(t)$ is the input signal and $g(t)$ is the structural function which characterizes the filters which will be constructed below. The sets $F$ and $G$ denote the domains of $f(t)$ and $g(t)$, respectively. Conventionally, it is assumed that every signal takes the value $-\infty$ out of its domain. By combining these operations, we define two morphological filters:

$$\text{Opening}: f_g(t) = [(f \ominus g^s) \oplus g](t), \tag{3}$$

$$\text{Closing}: f^g(t) = [(f \oplus g^s) \ominus g](t), \tag{4}$$

where $g^s(t) := g(-t)$ . The opening process for $f(t)$ by $g(t)$ removes the parts in the positive direction of the wave form of $f(t)$ those are too narrow to fit for the wave form of $g(t)$ attached below. In contrast, the closing filter removes the narrow negatively directed parts. In other words, opening (resp. closing) smooth $f(t)$ from the positive (resp. negative) direction by $g(t)$. Furthermore, the open-closing filter consisting of successive applications of the opening followed by the closing provides an effect of low pass filter. Thus, we can also construct a high pass filter by taking the difference between the input signal and its open-closed result.

$$\text{Low pass}: \Psi^{\uparrow}(t) = (f_g)^g(t) \tag{5}$$

$$\text{High pass}: \omega^{\uparrow}(t) = f(t) - \psi(t) \tag{6}$$

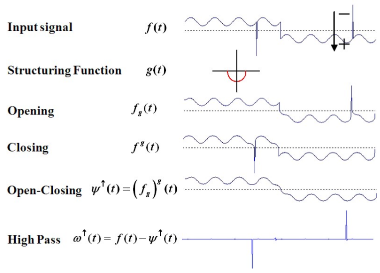


Figure 3: Properties of morphological filter.

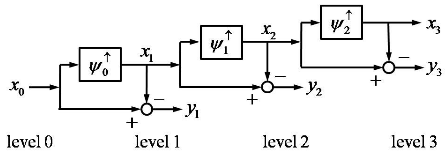


Figure 4: Schematic diagram of three-level signal analysis.

Notations are borrowed from [6]. The up arrow indicates increasing of the level in multi-resolution. The schematic figures of morphological operations are shown in Figure 3.

It is necessary to set out the structural function to use morphological filters. By the convention, the structural function has finite values only in the processing window and takes $-\infty$ on the outside. In this paper, we use the Haar type structural functions. The Haar type structural function is defined with a constant parameter $c$ and the width of window $2n+1$ as follows.

$$g(t) = \begin{cases} c & -n \leq t \leq n \\ -\infty & \text{otherwise} \end{cases} \tag{7}$$

A sequence of successive processes with varying structural functions constitutes a multi-resolution signal analysis. To describe this more precisely, let us assume that there exist sets $V_j$ and $W_j$ for each level $j$ ($j = 0, 1, \ldots, L$). We refer to $V_j$ (resp. $W_j$) as the signal space (resp. detail space) at the level $j$. Then, for a given input signal $x_0 \in V_0$ , we obtain the following recursive analysis scheme.

$$x_0 \rightarrow \{x_1, y_1\} \rightarrow \{x_2, y_2, y_1\} \rightarrow \cdots \rightarrow \{x_k, y_k, y_{k-1}, \ldots, y_1\} \rightarrow \cdots \tag{8}$$

where $x_{j+1} = \psi_j^{\uparrow}(x_j) \in V_{j+1}$, $y_j = x_j - x_{j+1} \in W_{j+1}$, for $x_j \in V_j$, $x_{j+1} \in V_{j+1}$.

Conversely, the input signal $x_0$ can be reconstructed by summing up the detail signals at every level. A three-level signal analysis scheme is depicted in Figure 4. In this study, we increase the width of windows by 2 to the power of levels. And two types of multi-resolution analysis are adopted. One is a method which uses the closing morphological filter (CMF) $f^g(t)$ as a low-pass filter. The other is a method which uses the closing-opening morphological filter (COMF) $(f^g)_g(t)$ as a low-pass filter. The former method and the later method will be called MRA-CMF, MRA-COMF respectively as an abbreviation.

## 3.2 Pattern recognition method

### 3.2.1 Notations

We summarize the notations used in this section. $M$ is the number of trials. $x_0(t), x_j(t), y_j(t), \tilde{y}(t)$ are EEG signals, low frequency component signals of level $j$, high frequency component signals of level $j$ and reconstructed signals from $\{y_\alpha(t), y_\beta(t), y_\gamma(t), \ldots\}$ , respectively. The discrete time parameter $t$ runs from 1 through $N$.

### 3.2.2 Feature extraction

At first, EEG signals are reconstructed by using $y_j(t)$. In this study, 11 kind of reconstructed signals are used for feature extraction (see Table 1). In the table, 'Lu', 'Lv', and 'Lw' are the definitions of sets of signals. For example, level 'Lu' means sets of signals $\{y_4, y_5, y_6\}$.

| Reconstructed signal | 0 | 1 | 2 | 3 | 4 | 5 | 6 | 7 | Lu | Lv | Lw |
|---|---|---|---|---|---|---|---|---|---|---|---|
| Signals used | $x_0$ | $y_1$ | $y_2$ | $y_3$ | $y_4$ | $y_5$ | $y_6$ | $y_7$ | $y_4, y_5, y_6$ | $y_5, y_6, y_7$ | $y_4, y_5, y_6, y_7$ |

Table 1: List of reconstructed signals used in experiments.

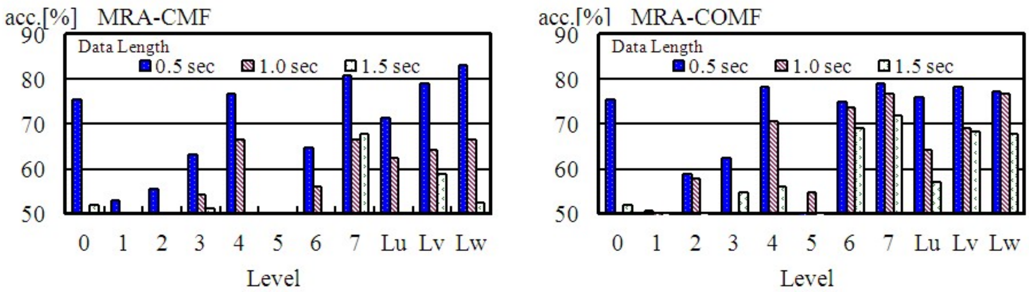


Figure 5: Pattern recognition results based on each reconstructed signal (subject Y).

Next, the following value is estimated from the reconstructed signals as a feature parameter related to event related potential (where $H(\cdot)$ is Heaviside function).

$$s = \sum_{t=1}^{N} \{H(\tilde{y}(t)) \cdot \tilde{y}(t)\} \tag{9}$$

### 3.3 Decision rule

Bayes classifier is adopted as the pattern recognition method with the assumption that the feature value $s$ is a random variable with normal distribution. The discrimination function is as follows:

$$k^* = \arg\max_k \Pr(C_k|s) = \arg\min_k \left\{ \ln(\sigma_k) + \frac{1}{2\sigma_k^2}(s - m_k)^2 - \Pr(C_k) \right\} \tag{10}$$

# 4 Results

The period of processing data is set to be the period from 5000 ms to 5500, 6000 and 6500 ms (processing data length is 0.5, 1.0 and 1.5 seconds), since feedback arrow is shown at 5000 ms. Pattern recognition result based on each reconstructed signals are shown in Figure 5. Figure 5(a) and 5(b) show the result based on MRA-CMF and MRA-COMF respectively. The pattern recognition results in each subject are shown in Figure 6.

Figure 5 shows that optimal data length is 0.5 seconds for recognition. High accuracies are obtained by signals reconstructed from Level $4^{\text{th}}$, Level $7^{\text{th}}$ or Level Lw (4, 5, 6, 7) signals.

This fact suggests that Level $4^{\text{th}}$ signal and Level $7^{\text{th}}$ signal has an essential information about the reaction of subject related to misoperation of BCI system. Figure 6 shows that optimal filter (closing filter or close-opening filter) is depend on each subject. The optimal electrode position seems to be Cz, C3 or C4. These electrodes are used to determine right-hand movement or left-hand movement. This fact suggests that detection of subject's motion imaging and detection of subject's reaction of misoperation of BCI system are possible by using the signals obtained from the same electrode.

# 5 Conclusion

In this paper, we tried to detect misoperation of BCI system by applying mathematical morphological multi-resolution analysis to EEG signal. Although more precise investigation about optimal method (e. g. tuning method, optimal filter etc.) is needed yet, it was confirmed that detection of

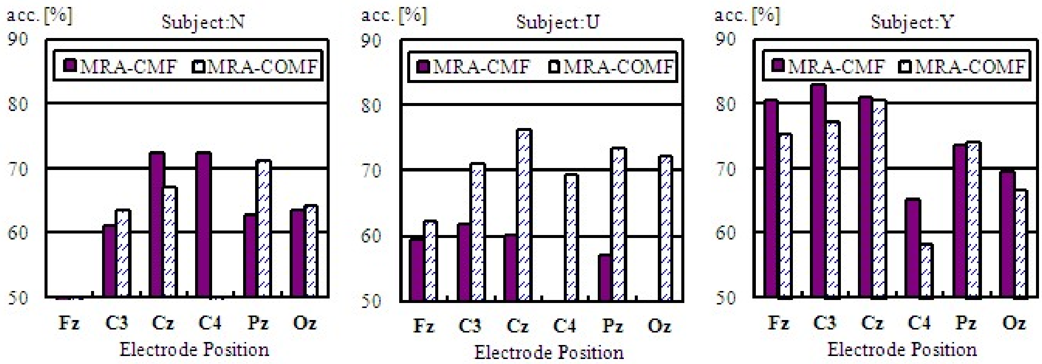


Figure 6: Pattern recognition result in each subject (target signal is reconstructed by using level Lw signals, data length: 0.5 s.)

subject's reaction related to misoperation of BCI system was possible. Our results suggest that the will of human may be able to be estimated by using the reconstructed signals (level 2 and/or 3) and the misoperation may be able to be detected by using the reconstructed signals (level 4 or Lw). A BCI system with the fail-safe function will be able to be achieved by advancing this research further.

## References


[1] J. J. Vidal. Toward direct brain-computer communication. *Ann. Rev. Biophys. Bioeng.*, 2:157–180, 1973.

[2] G. Pfurtscheller, C. Neuper, D. Flotzinger, and M. Pregenzer. EEG-based discrimination between imagination of right and left hand movement. *Electroencephalogr. Clin. Neurophysiol.*, 103:642–651, 1997.

[3] K. Inoue, D. Mori, G. Pfurtscheller, and K. Kumamaru. Pattern recognition of EEG signals during right and left motor imagery learning effects of the subjects. In *Proc. First Int. Conf. Complex Med. Eng.*, pages 665–670, 2005.

[4] K. Inoue, K. Kumamaru, and G. Pfurtscheller. Robot operation based on pattern recognition of EEG signals. In *3rd Int. BCI Workshop and Training Course*, pages 116–117, 2006.

[5] G. Schalk, J. R. Wolpaw, D. J. McFarland, and G. Pfurtscheller. EEG-based communication: presence of an error potential. *Clin. Neurophysiol.*, 111:2138–2144, 2000.

[6] J. Serra. Image analysis and mathematical morphology. London, U.K. Academic, 1994.

[7] H. J. A. M. Heijmans. Nonlinear multiresolution signal decomposition schemes-part II: Morphological wavelets. *IEEE Trans. Image Process.*, 9, 2000.

# Detecting spread spectrum pseudo random noise tags in EEG/MEG using a structure-based decomposition

P. Desain[1], J. Farquhar[1,2], J. Blankespoor[1], S. Gielen[2]

[1]Music Mind Machine, Nijmegen Institute for Cognition and Information, Radbound University, Nijmegen, The Netherlands
[2]Biophysics Department, Radbound University Medical School, Radbound University, Nijmegen, The Netherlands

desain@nici.ru.nl

**Abstract**

A method is presented to tag (watermark) stimuli with carefully chosen binary pseudo random noise codes, and to decompose the EEG response into short waveforms for each rising or falling transition in the stimulus. This decomposition can be used for EEG classification by computing the class which has maximum correlation between the measured and predicted EEG response. Classification performance when a single class is present is excellent (85 %), and very robust when a small pass band or short time interval is used. A unique feature of this method is that, while it is easy to generate tags for any number of classes, training the classifier is needed only for responses to one stimulus class, and few trials (up to about a minute of data) suffice for training.

## 1 Introduction

The neural responses of stimuli with a repetitive character have been well studied in EEG and MEG. These "Steady State Evoked Potentials" (SSEP) are thought to reflect the frequency- and phase-locked responses of neural circuits to periodic stimulation [1]. This has been shown in the tactile, visual, and auditory domains [2, 3, 4]. As certain features of these stimuli, such as power and phase at the stimulation frequency, are modulated by (selective) attention, SSEPs have been used as the basis of BCIs [5]. Furthermore, the phase difference between stimulus and response can be used as a probe for cognitive processing time and order (modulo the stimulation period).

However, interesting frequencies in the various domains ($\tilde{1}0$–140 Hz) are in the same range as spontaneous oscillations that occur in the brain (alpha, theta, gamma) which may complicate analysis. One approach to attenuating the relatively narrow band noise from other cognitive process would be to use a spectrally spread stimulus. One could think of chirps, frequency hopping, pseudo random noise and other signals that have a broadband spectral character. This will only work if the underlying hypothesis of an attuning process claimed to explain SSEP does not hold: oscillators cannot attune to non-periodic or fast changing signals. Thus a test with this signal is valuable both for scientific reasons to explore the dynamics of interacting neuronal populations and for the pragmatic aim to increase the robustness of BCI systems.

Broadband signals have already been used for single cell behavior [6]. In [7] this approach is elaborated for amplitude modulated auditory stimuli and EEG responses. In this paper we focus on the classification process and a way to structurally decompose the noise codes and demonstrate how they form a powerful new method for probing cognitive processing.

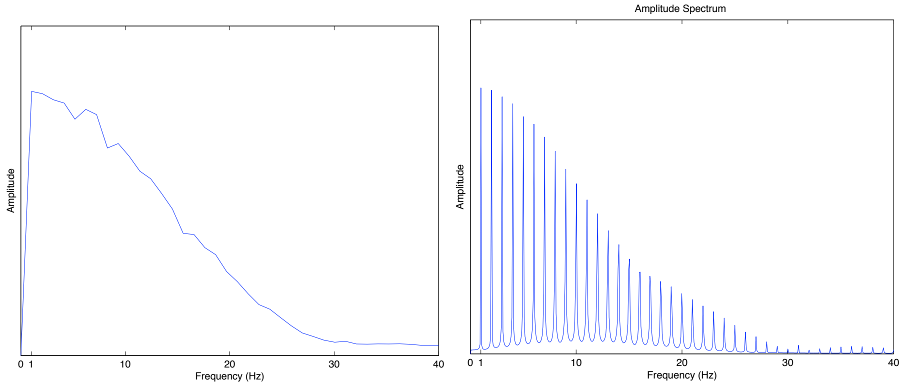


Figure 1: a) Average spectrum of a set of 31 golden codes of 31 bits long, presented at a bit rate of 31 Hz. b) Average spectrum of long sequence of a repeating golden code.

## 2 Pseudo random codes

Pseudo random noise is an optimal deterministic periodic signal with statistical properties close to that of Gaussian White Noise. For applications in signal detection the random bit codes need certain properties. To be able to detect the time-lag of a code in a response, the auto-correlation of a code should be close to zero for all time lags different from zero. To distinguish different codes easily, the cross-correlation between codes should be minimal at all time lags. There is a family of codes, golden common codes [8], which have this property and is used heavily in broadband communication systems (WIFI, cell phones). The spectrum of these codes is shown in Figure 1.

## 3 Decomposition of the signal

One nice property of purely periodic stimuli, such as the more commonly used frequency tags, is that they can be detected by simply looking for an increase in signal power at the stimulation frequency in the neural response. This is possible because the total response after the current stimulus is simply the sum of the appropriately delayed responses to all previous stimuli. As the delays between stimuli are set the terms in this sum are constant hence giving a fixed total response. Thus purely periodic stimuli generate a periodic response with the same frequency. This is true even if the responses to individual stimuli have a much longer duration than the inter-stimulus interval, i. e. the stimulus responses overlap.

Unfortunately for non-period stimuli, such as Pseudo-Random noise tags, this is no-longer true because the delays between stimuli are no-longer fixed. When inter-stimulus interval is much longer than the stimulus response, then this is not a problem as one can directly learn an estimate of individual stimulus responses. This is the approach taken in Event Related Potential BCI systems such as visual P300 spellers. However, as stimulus response durations can be quite long, e. g. in P300 systems significant response lasts up to 700 ms after stimulation [9], this non-overlapping requirement places quite a strong limit on the stimulation rates and hence system bit-rates.

What we would like is to estimate a single isolated stimulus's individual impulse-response from an over-lapping set of training responses. We can the used the impulse-response to re-construct the estimated total response to a known overlapping stimulus sequence, and use the correlation between the recorded and estimated responses as the basis of a classification system. This paper presents such an approach where we decompose the response to a stimulus sequence as a sum of overlapping impulse-responses to the stimulus events contained in the sequence. We learn the individual impulse responses using a least-squares technique. The effectiveness of the technique is demonstrated with classification results on EEG data derived from pseudo-random-noise tagging experiments.

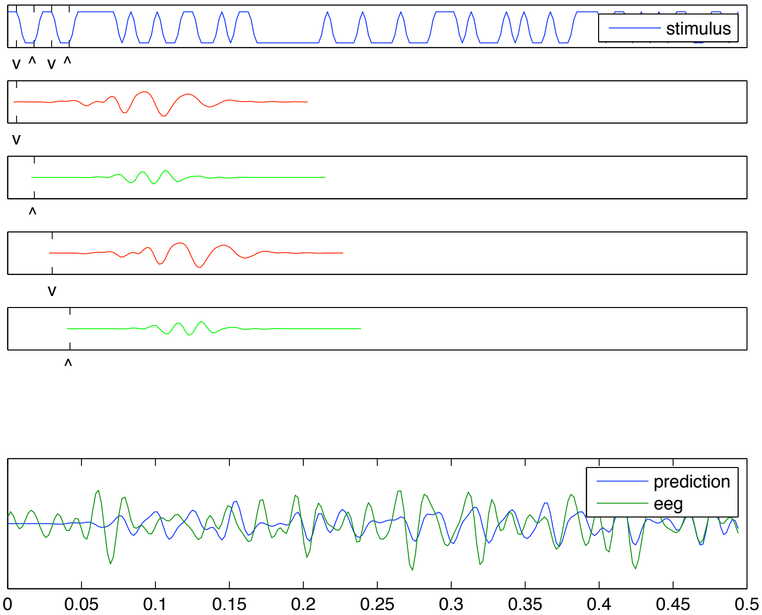


Figure 2: The decomposition of a mean EEG into its structural components and fit to the data.

The input stimulus is a binary modulation sequence. As we believe the brain responses mainly to changes in input, we treat the transitions in this bit sequence as the stimulus events. Further, we postulate that the brain responds differently to rising (0–1) and falling (1–0) transitions. Finally, assume that each transition contributes a time-limited impulse-response waveform which combine linearly to give the total stimulus response. Figure 2 illustrates this model. The same decomposition model was used for timing signals in [10]. In algebraic terms this model can be written as:

$$x(t) = \sum_{\tau=1}^{L} \mathrm{I}_r(t) r(t-\tau) + \mathrm{I}_f(t) f(t-\tau) \tag{1}$$

where, $x(t)$ is the total response at time $t$, $L$ is the duration of the response, $r(.)$,$f(.)$ are the temporal responses of the brain to a rising (resp. falling) edge in the stimulus, and $\mathrm{I}_r(t)$, $\mathrm{I}_f(t)$ are indicator functions which have the value 1 if there is a rising/falling edge at time, $t$, and 0 otherwise. This model can more compactly be expressed in matrix notation using a structure matrix $M$ to encode the indicator functions $\mathrm{I}_r, \mathrm{I}_f$, as,

$$x = \left[ \begin{array}{c|c} \vdots & \vdots \\ \mathrm{I}_r(i:i+L) & \mathrm{I}_f(i:i+L) \\ \vdots & \vdots \end{array} \right] \left[ \frac{r}{f} \right] = Mp \tag{2}$$

where, $x$ is the column vector of modeled response for each time, the rows of $M$ signify sample times with each row being the previous row shifted 1 element to the right, and $p$ is the concatenation of the two types of response function. Equation 2 is linear in the temporal responses, $r$ and $p$, so these parameters can be found using a least-squares regression with the average measured response.

## 4 Experiments

We collected the 128 channel EEG responses for 140 trials of listening to a saw-tooth carrier wave of 420 Hz, AM modulated by one of two cosine filtered pseudo random noise modulators presented

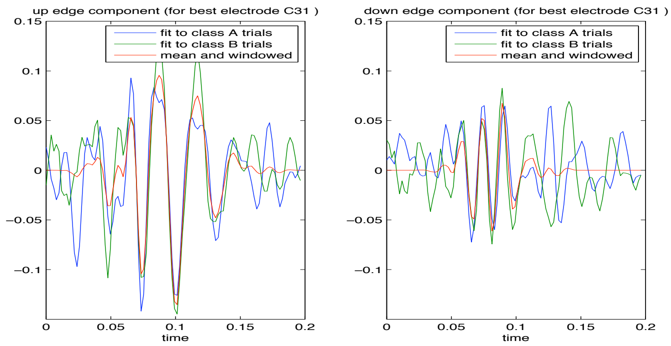


Figure 3: Edge components derived from the regression fit, for two classes and the averaged and windowed waveform used for classification.

at 168 bits/second. For details of the experimental procedure see [7]. Two noise-tags were used, called code A and B, in a sequential purely perceptual mode. The classification problem was to identify which stimulus the subject was exposed to at each point in time. All classification results are estimated using 3 seconds of EEG data with 10-fold cross validation, with 20 testing trials, from a dataset containing 280 trials (140 per class).

To classify EEG signals we use a simple correlation approach, where the predicted class is that which has maximal correlation with its class prototype. We present results for 2 types of class-dependent prototypes. The first is simply the mean EEG response for this class. This is used as a base-line for comparison. The second is the decomposition approach presented above, where the decomposition was conducted independently for each channel[1] This yielded very good fits: predictions explained up to 33 % of the variance for the best electrode. In Figure 3 the impulse-response functions are shown for the two classes. It can be seen how the responses are similar in the central region but differ towards the edges. We believe these differences are due to overfitting, and use a simple cosine window (parameters) and the mean of the two waveforms to suppress these differences. Note, using an appropriately regularized parameter estimate may be a better approach to deal with this overfitting issue. We intend to pursue this approach in future work.

## 4.1 Results

To estimate classification performances a subset of the channels were used, where the subset was found using two different strategies. The first used a stepwise forward selection procedure to incrementally add the single best electrode until training set performance was maximized. The second approach used first used Independent components analysis to determine create a set of "virtual electrodes" from which the forward selection procedure was again used.

In terms of classification performance using the mean EEG response obtained 79 % correct, using all 128 channels. Using the decomposition with electrode selection on the raw EEG channels gave a significantly better 85 % correct, whereas using ICA derived virtual channels gave 94% (using on average 9 ICA components). In Figure 4(a) it is shown which channels were used in the decomposition classification. The topology of the most often selected ICA component is shown in Figure 4(b). This shows a clear dipole nature over the auditory cortex, as would be expected for an auditory stimulus.

To demonstrate the robustness of the decomposition approach (and the pseudo-random noise tags) Figure 5 shows the classification performance as a function of the pass-band of a spectral

[1]Note these different approaches have different advantages and disadvantages. The decomposition approach treats all rising and falling edges as the same and so cannot represent any non-linearity or history dependence of the response. However, because it uses an order of magnitude fewer parameters, the decomposition may extract underlying regularities better and be less prone to over-fitting.

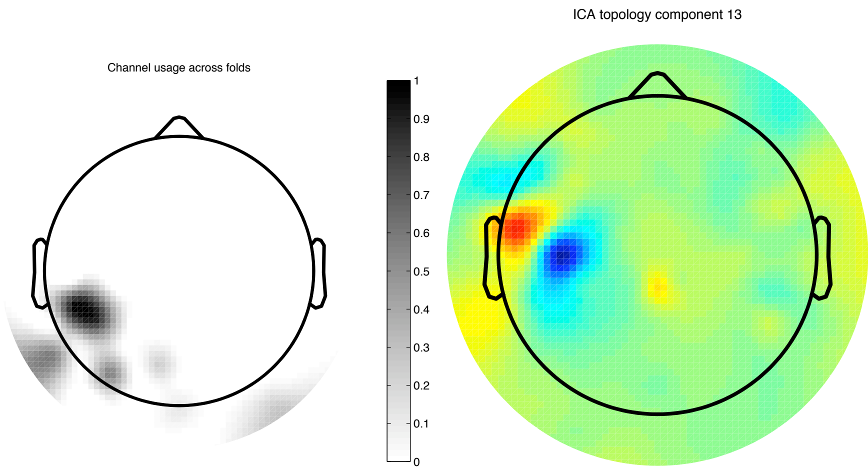


Figure 4: a) Channels used in the various folds of the cross-validation, b) Topology of the most often selected ICA component.

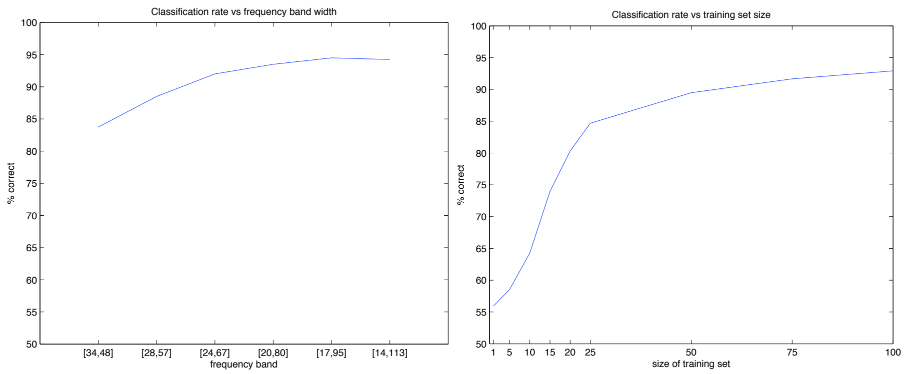


Figure 5: a) Classification rate for octave-wide pass-band signals. b) classification rate vs. training set size.

filter and as a function of the training set size. This clearly shows that classification performance gracefully degrades as more of the signal it attenuated away (i. e. the pass band narrows). Further, only a very small amount of training data, 25 trials which is 75 s of data, are required to obtain 75 % of the full-training set performance.

Finally, to demonstrate that impulse-responses learned on one stimulus sequence can be used with another, we trained the decomposition using only data from one code and tested it on the other. Classification rates only dropped by only a few percent (from 94 to 91 %). This proved the validity of the approach and limits the amount of time needed for collecting training data in multi-class setups considerably. This is not possible in the mean EEG method which uses complete induced or evoked responses directly.

## 5 Conclusion

We have demonstrated how pseudo random noise sequences with certain characteristics can be exploited as a stimulus tagging method. Furthermore, the EEG response can be predicted from a decomposition based on the structure of rising and falling edges in the tag. For auditory amplitude modulation this decomposition technique proved very successful: classification rates are high and can be reached with very little data, and even from data obtained from a different tagging sequence. Furthermore, the detection is robust with shorter durations or small pass bands causing a slow and graceful degradation of the classification rate. These properties show that noise tagging represents a very promising approach for the development of a BCI. It is usable in the tactile and visual domain as well. For P300 spellers the possibility to handle overlapping responses at fast flashing rates seems promising to optimize these types of BCIs [9]. One possible improvement that we are investigating is the construction of bit codes which preserve their low auto and cross correlation properties when short sub-sequences are used.

Noise tagging is also potentially very useful for tracing and decomposing cognitive processing through a set of sequential modules, each with their own location and time delay. Further the systematic comparison of this new method to the use fixed frequency tags, would allow us to gain insight in how far and where in the brain oscillatory attunement present, if at all. We intend to investigate this issue further in future work. This investigation could further be enhanced by decomposing the individual electrode responses as weighted and time delayed versions of an individual edge response.

**Acknowledgments:** We gratefully acknowledge the support of the BrainGain Smart Mix Programme of the Netherlands Ministry of Economic Affairs and the Netherlands Ministry of Education, Culture and Science.

## References

[1] D. Regan. Steady-state evoked potentials. *J. Opt. Soc. America*, 67:1475–89, 1977.

[2] T. W. Picton, M. S. John, A. Dimitrijevic, and D. Purcell. Human auditory steady-state responses. *Int. J. Audiol*, 42:177–219, 2003.

[3] P. Fries, J. H. Reynolds, A. E. Rorie, and R. Desimone. Modulation of oscillatory neuronal synchronization by selective visual attention. *Science*, 291:1560–3, Feb 2001.

[4] M. Bauer, R. Oostenveld, M. Peeters, and P. Fries. Tactile spatial attention enhances gamma-band activity in somatosensory cortex and reduces low-frequency activity in parieto-occipital areas. *J. Neurosci.*, 26(2):490–501, 2006.

[5] P. Desain, A. M. G. Hupse, M. G. J. Kallenberg, B. J. de Kruif, and R. S. Schaefer. Brain-computer interfacing using frequency tagged stimuli. In *Proc. 3rd Int. Brain-Computer Interface Workshop and Training Course*, 2006.

[6] A. R. Möller. Use of pseudorandom noise in studies of frequency selectivity: The periphery of the auditory system. *Biol. Cybernet.*, 47:95–102, 1983.

[7] J. Farquhar, J. Blankespoor J. and R. Vechk, and P. Desain. Towards a noise-tagging auditory BCI-paradigm. In *Proc. 4th Int. Brain-Computer Interface Workshop and Training Course*, 2008.

[8] R. Gold. Optimal binary sequences for spread spectrum multiplexing. *IEEE Trans. Information Theory*, 13(4):619–621, 1967.

[9] J. Hill, J. Farquhar, S. Martens, F. Bießmann, and B. Schölkopf. Balancing psychophysiological and information-theoretic effects in the design of a visual brain-computer interface speller. Technical report, Max Planck Institute for Biological Cybernetics, 2008.

[10] W. L. Windsor, P. Desain, A. Penel, and M. Borkent. A structurally guided method for the decomposition of expresssion in music performance. *J. Acoust. Soc. Am.*, 119(2):1182–1193, 2006.

# Online comparison of wavelet transforms and band power features for brain-computer communication

R. Leeb, G. Pfurtscheller

Institute for Knowledge Discovery, BCI Lab, Graz University of Technology, Graz, Austria

robert.leeb@tugraz.at

**Abstract**

In this paper, the application of online wavelet transform for the detection of motor imagery tasks in real-time brain-computer interface (BCI) experiments is described for the first time. Wavelet packet (WP) features were compared with band power (BP) features, both selected with Distinction Sensitive Learning Vector Quantization (DSLVQ). Unlike other studies, online performances are compared in this work. Thereby the WP/BP features were used to detect oscillatory patterns in ongoing EEG during different motor imagery tasks and to generate real-time-feedback in the BCI experiments. The WP method performed slightly better than the standard BP method in the online experiments and in the subsequent offline cross-validation analysis, but no statistically significant difference could be found in the performance increase.

## 1 Introduction

An electroencephalogram (EEG) based brain-computer interface (BCI) is a communication system that provides a direct connection between the human brain and a computer [1]. Thereby the bioelectrical activity of the human brain is modified by mental activity (thoughts) without requiring any physical movement. Different EEG signals can be used as input to a BCI, either event-related potentials (ERPs) or transient oscillatory changes in the ongoing EEG. Motor imagery (MI) can induce event-related desynchronization (ERD, amplitude suppression) and/or event-related synchronization (ERS, amplitude enhancement) in alpha and beta frequency bands and has been shown to represent an efficient mental strategy for operating a BCI [1, 2].

Feature extraction is one of the key issues in BCI research and its goal is to find a suitable representation (signal features) of the EEG data that simplifies the subsequent detection of MI patterns. Ideally, the signal features should encode the brain patterns just associated with the MI performed by the user. Traditionally, signals are analyzed in either the time domain or in the frequency domain. Wavelet transforms overcome these problems by providing a multi-level time-frequency decomposition of signals, which allows the simultaneous use of longer duration intervals for low-frequency information and shorter duration intervals for high-frequency information. Wavelet transform has already been used for the detection and de-noising of ERPs [3, 4, 5] and recently also for offline analysis of oscillatory EEG [6, 7]. The outcome of these studies was that wavelet transforms improve the detection performance compared to other existing feature extraction methods. Up until only Hsu [5] reported results of an online BCI for the detection of ERPs during real finger movements, but no one has reported on the online analysis of oscillatory EEG components during MI.

The goals of this paper are (i) to demonstrate that wavelet transforms using wavelet packet analysis (WP) can be used for online BCI experiments, and (ii) to conduct an online comparison study to explore whether wavelet transform features perform better than standard band power (BP) features. Therefore all subjects performed BCI feedback experiments with BP features as well as with WP features.

# 2 Methods

## 2.1 Subjects, data recording and experimental paradigm

Five subjects (2 males and 3 females, age 26.0 ± 3.7 years) participated in this study. Three bipolar EEG derivations (C3, Cz and C4; 2.5 cm anterior and posterior to the position of the 10/20 system; ground electrode at Fpz) were recorded with a sensitivity of 50 µV, band pass filtered between 0.5 and 100 Hz (activated power line notch) and sampled at 250 Hz. The BCI system consisted of an EEG amplifier (g.tec, Guger Technologies, Graz, Austria) and one data acquisition card (E-Series, National Instruments Corporation, Austin, USA). The BCI algorithms were implemented in MATLAB 6.5 and Simulink 5.0 (The MathWorks, Inc., Natick, USA) using the open source package BIOSIG (`http://biosig.sourceforge.net/`).

The participants were instructed to imagine either a kinesthetic left or right hand movement, depending on a visual cue stimulus (arrow pointing to the left or right between seconds 3 and 4.25). Visual feedback between seconds 4 and 7 was presented continuously (sample-by-sample) by using a horizontal bar graph, in which the length of the bar was proportional to the classification output. The exact timing scheme is illustrated in Figure 1.A. Each run consisted of 40 trials (20 left and 20 right cues), whereby the sequence of right and left cues was randomized within each run. The subjects participated on five different days (called sessions) and in each session, four experimental runs were performed. The data of the first training session (tr) was recorded without feedback and used for the offline analysis. In all other sessions (fb1-fb4) online feedback was provided. The task of the subject was to keep the MI task over the entire feedback period. In each session, two runs with feedback based on BP features and two runs with feedback based on WP features were performed. The order of feature extraction type has been permuted for each subject and session.

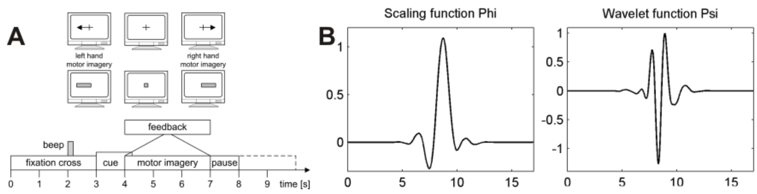


Figure 1: (A) Timing of the paradigm. (B) Symlet "sym9" mother wavelet.

## 2.2 Feature extraction: band power (BP)

For each of the three bipolar channels 16 non-overlapping frequency components between 6–38 Hz were calculated with a bandwidth of 2 Hz. The frequency components were computed by digitally band pass filtering the EEG signal (Butterworth IIR filter of order 5), squaring and averaging the samples over the past second. Finally, the logarithm was computed from this time series.

## 2.3 Feature extraction: wavelet packet analysis (WP)

For each of the three bipolar EEG channels the wavelet coefficients obtained by a wavelet packet analysis were calculated as features. A symlet (sym9) mother wavelet was used (see Figure 1.B), which has already been used for the detection of oscillatory changes in the electrocorticogram [8]. One level of wavelet decomposition separated the original signal into two complementary halves, i. e. approximation and detail. In each half, the number of samples was reduced by half because of dyadic down-sampling. Thereby the frequency range was also reduced by half. Due to the sampling frequency of 250 Hz, the theoretical frequency content was 0–125 Hz. After the first level of decomposition the resulting approximation component contained signals from 0–62.5 Hz and the detail component contained signals from 62.5–125 Hz (so the bandwidth was reduced to 62.5 Hz). After the second step the bandwidth was reduced to 31.3 Hz, after the third step to 15.6 Hz and so on. Decomposition up to level 4 was performed to have on the one hand a reasonable frequency resolution (e. g. beta band 15.6–23.4 Hz) and on the other hand to keep the number of features and therefore the computational effort small. Not only the 16 wavelet packet features from the fourth decomposition level were used, but also the components from higher levels, resulting in a total number of 31 features for each EEG channel. It was only necessary to consider the half of the components (fifteen), because of the interest in the alpha and beta band components (same frequency range of interest as used by BP features). The WP signals were reconstructed, squared and logarithm transformed to achieve power values [8]. For the last online-session a decomposition up to level 5, with a reduced subset of 15 components in the interesting frequency range (similar to [4]), has been used.

### 2.4 Feature selection with DSLVQ and classifier setup

The feature extraction procedure used yielded up to 16 BP features and 15 WP features for each EEG channel. For selection of the most informative features the 'Distinction Sensitive Learning Vector Quantization' (DSLVQ) was used (for details see [9]). The major advantage of DSLVQ is that it neither requires expertise, nor any a priori knowledge nor assumption about the distribution of the data. Furthermore, not only relevant features, but also feature combinations are identified. Features were selected according to following criteria (with the precondition of a symmetrical arrangement [2]): (i) large mean feature relevance and small variance, (ii) only important during MI, (iii) two features per channel, (iv) same features for all channels, (v) adjacent BP features were combined to one feature (e. g. 20–22 Hz and 22–24 Hz were combined to 20–24 Hz). In case of WP features condition (v) is changed to: use features of lower decomposition level if both lower and higher level features are equally important. The selected features were used to set up a Fisher's linear discriminant analysis (LDA) classifier to discriminate between the two different mental states; for each feature extraction method one classifier was setup. The accuracy rates were estimated by a 10 times 10-fold cross-validation LDA-training.

After each feedback session, a classifier update (DSLVQ selected feature set and LDA weights) was performed for both feature extraction methods (BP and WP) based on all data recorded in the previous session. The updated classifier with the modified feature set was only used in the next session if the classification accuracy could have been increased (see last column in Table 1).

## 3 Results

In Figure 2 the feature relevance of the extracted wavelet packets up to decomposition level 4 is given over the trial time for one channel. Each row corresponds to a feature and the value in each cell is the feature relevance. The cells are plotted in dark if the feature is important during this 0.5 seconds time period. In this dataset the important features are the wavelet packets with the number 26 (∼16–31 Hz), 27 (∼16–23 Hz), 28 (∼23–31 Hz) and 30 (∼8–15 Hz), whereby feature 26 is a feature after decomposition level 3 and decomposed into feature 27 and 28 by the next wavelet decomposition step. Therefore only feature 26 and 30 have been selected. The features selected and used for BP and WP for all sessions and subjects are given in Table 1.

After each experimental session the online performance of each run was estimated by plotting the classification accuracy over the trial time. The highest classification accuracy during the feedback time of this accuracy was extracted and used as a performance measure. In Figure 3.A the classification accuracy is displayed; beginning with second 4.5 it climbs above 95 %, but single class accuracy goes up to 100 %. The point with the largest accuracy during the feedback time is marked. The accuracy for all runs and subjects is given in Table 1 together with the cross-validated classification accuracies. Either band power (BP) or wavelet packet (WP) features were used in each run, and the order of feature type was alternated (the used method for each run is indicated in Table 1). The box plots of all online accuracies in Figure 3.B shows that WP slightly performed better than BP.

Paired sample $t$-tests showed no significant differences between the conditions (BP and WP) for the online classification accuracy ($t_{(4)} = 1.776$, n. s.). The grand average of the classification

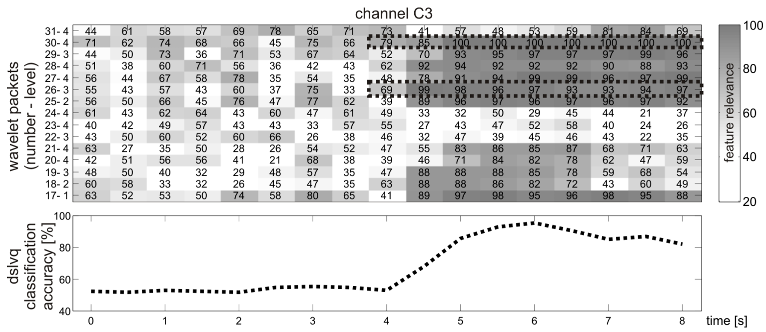


Figure 2: DSLVQ feature relevance map over the trial time for channels C3 using wavelet features (decomposition level 4) extracted from data of subject s1 (session fb1). The maps of channel Cz and C4 are not displayed because of lack of space. The number in each cell is the feature relevance and important features are highlighted with a darker background. The classification performance over the trial time is given in the last row. The selected features are marked with dotted rectangles (feature 26 and 30).

accuracy of wavelet features (mean $\pm$ SD = 91.15 % $\pm$ 8.37 %) is slightly larger than for band power features (90.08 % $\pm$ 8.84 %). One phenomenon that was also reported by the subjects was that the wavelet features needed slightly more time to move the feedback bar to the correct side, but were more accurate compared to the band power features. A more detailed analysis showed that in session fb2 wavelet was significant better than band power ($t_{(4)} = 2.450$; $p = 0.07$; with BP mean = 87.63 % and WP mean = 90.63 %) and as well in session fb3 ($t_{(4)} = 2.449$; $p = 0.07$; with BP mean = 90.27 % and WP mean = 93.75 %). The paired sample $t$-tests of the offline cross-validation accuracy showed again no significant differences ($t_{(4)} = 0.376$, n. s.) between the two conditions.

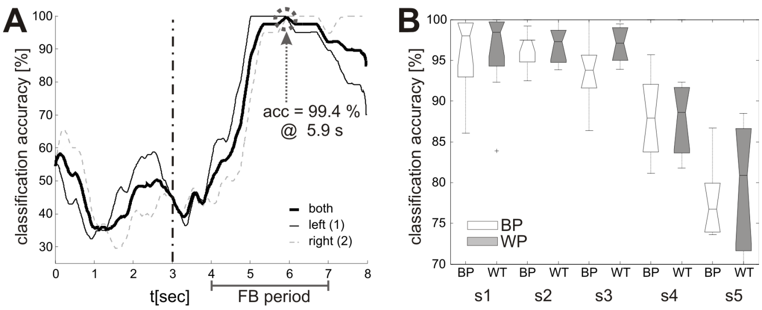


Figure 3: (A) Online Performance (classification accuracy) of run 2 in session fb3 of subject s1 using wavelet features (20 trials per condition). The cue onset is indicated at second 3 with a dot dashed line. The feedback (FB) was given from second 4 to 7. The indicated highest classification accuracy during the feedback time is marked (99.4 % at second 5.9) and used in Table 1. (B) Box-plots of the classification accuracy for both conditions (band power [BP] or wavelet packet [WP]) of each subject.

# 4 Discussion and conclusion

The goals of this study were (i) to investigate whether wavelet transform can be used for online BCI feedback experiments and (ii) to compare the online BCI performance between wavelet features and standard band power features. The results presented show that the proposed method based on wavelet-packet decomposition in combination with a DSLVQ feature selection process can be used

Table 1: Online classification accuracy in percent of each run and session. In brackets the used feature extraction method either band power (B) or wavelet packet decomposition (W) is indicated. The BP frequency bands and the WP feature numbers are specified. Cross validation accuracy in percent of each session for BP and WP features WP is given in the right part of the Table. In the last session (fb4) a wavelet decomposition till level 5 was used. The last column (update) indicates if a new classifier (C) with a different feature set (F) based on the current data was used for the following online session.

| | | online results | | | | | | cross validation results | | |
|---|---|---|---|---|---|---|---|---|---|---|
| | | run 1 [%] | run 2 [%] | run 3 [%] | run 4 [%] | BP band [Hz] | WP nr. | BP [%] | WP [%] | update BP / WP |
| s1 | tr | | | | | | | 87.0 | 88.0 | CF / CF |
| | fb1 | 97.5 (W) | 86.0 (B) | 89.4 (B) | 92.3 (W) | 10–14 20–28 | 28 30 | 96.9 | 97.5 | CF / CF |
| | fb2 | 98.5 (B) | 96.3 (W) | 99.3 (W) | 99.1 (B) | 10–14 22–26 | 26 30 | 98.8 | 100.0 | – / – |
| | fb3 | 100.0 (B) | 99.4 (W) | 97.5 (B) | 100.0 (W) | 10–14 22–26 | 26 30 | 99.4 | 100.0 | – / CF |
| | fb4 | 100.0 (W) | 100.0 (B) | 83.9 (W) | 96.5 (B) | 10–14 22–26 | 54 60 | 97.5 | 96.9 | |
| s2 | tr | | | | | | | 90.0 | 88.1 | CF / CF |
| | fb1 | 97.5 (B) | 95.0 (W) | 97.1 (W) | 92.5 (B) | 10–16 19–27 | 27 30 | 94.4 | 93.8 | CF / CF |
| | fb2 | 92.5 (B) | 93.8 (W) | 97.5 (B) | 99.1 (W) | 10–12 16–24 | 20 26 | 95.6 | 95.0 | – / CF |
| | fb3 | 100.0 (W) | 99.2 (B) | 97.5 (B) | 97.4 (W) | 10–12 16–24 | 20 28 | 97.5 | 96.3 | CF / CF |
| | fb4 | 94.5 (W) | 97.1 (B) | 98.3 (W) | 97.5 (B) | 10–12 20–24 | 52 54 | 97.5 | 96.9 | |
| s3 | tr | | | | | | | 96.3 | 94.4 | CF / CF |
| | fb1 | 92.2 (B) | 97.5 (W) | 98.7 (W) | 100.0 (B) | 11–14 17–23 | 26 30 | 94.4 | 95.0 | – / – |
| | fb2 | 86.4 (B) | 96.3 (B) | 95.0 (W) | 99.4 (W) | 11–14 17–23 | 26 30 | 95.0 | 96.3 | – / – |
| | fb3 | 95.0 (B) | 95.0 (W) | 91.0 (B) | 96.8 (W) | 11–14 17–23 | 26 30 | 93.1 | 93.8 | CF / CF |
| | fb4 | 93.9 (W) | 92.5 (B) | 95.0 (B) | 99.4 (W) | 10–14 22–28 | 50 60 | 95.6 | 96.9 | |
| s4 | tr | | | | | | | 83.5 | 84.0 | CF / CF |
| | fb1 | 88.9 (B) | 89.3 (B) | 81.8 (W) | 81.9 (W) | 10–14 22–26 | 27 30 | 81.9 | 81.3 | C / C |
| | fb2 | 86.1 (W) | 81.4 (B) | 81.1 (B) | 85.3 (W) | 10–14 22–26 | 27 30 | 82.5 | 82.5 | CF / CF |
| | fb3 | 92.3 (W) | 87.0 (B) | 91.2 (W) | 86.1 (B) | 10–14 20–26 | 28 30 | 86.3 | 86.3 | C / CF |
| | fb4 | 94.9 (B) | 91.1 (W) | 92.2 (W) | 95.7 (B) | 10–14 20–26 | 52 59 | 88.8 | 84.4 | |
| s5 | tr | | | | | | | 78.5 | 79.6 | CF / CF |
| | fb1 | 77.8 (B) | 74.3 (B) | 72.7 (W) | 70.5 (W) | 10–14 22–30 | 26 28 | 73.1 | 76.9 | – / – |
| | fb2 | 82.6 (W) | 79.5 (B) | 69.9 (W) | 64.1 (B) | 10–14 22–30 | 26 28 | 68.8 | 70.0 | CF / C |
| | fb3 | 73.6 (B) | 79.1 (W) | 75.8 (B) | 86.4 (W) | 10–14 24–32 | 26 28 | 77.5 | 80.6 | CF / CF |
| | fb4 | 88.5 (W) | 86.9 (W) | 80.4 (B) | 86.7 (B) | 10–14 22–30 | 55 60 | 80.6 | 83.1 | |

to detect oscillatory patterns in the ongoing EEG. Single trial classification of different MI tasks is possible and accurate online feedback based on these wavelet features can be given. Online classification accuracies between 70 % and 100 % were achievable. Therefore the statement of Hinterberger et al. [10] that "wavelet transformed data cannot be fed back on-line before the end of a trial. . . " and "wavelet transformed data should serve for BCIs without immediate feedback. . . " is not longer valid.

In the online experiments, the wavelet features performed slightly better than band power features (in two subjects better and in three subjects equal), but because of the performance variations of the subjects over the runs, no statistically significant difference could be found in the performance increase. In the offline evaluation only for one subject WP features were not superior to BP ones. These findings are consistent with the results of existing offline studies, in which wavelet analysis outperformed other methods [4, 5, 7, 8].

When comparing the online classification results and the accuracy rate obtained by the offline analysis, several differences need to be considered. The main difference between both is that online results are given for each run and the cross validated offline results only for each session. Although in single online runs performances with 100 % accuracy could be achieved in subject s1, s2 and s3, only the data of s1 could be separated offline with 100 % accuracy. The reason for this result are, that the time course of the classification accuracy varies in each run, so the time point of the best classification is slightly different for each run. If the data of all four runs per session are analyzed together, an averaged time course exists. Subjects s4 and s5 improved with both methods over the sessions, in contrast to subjects s1 and s2 which retained their high classification accuracy over the sessions but could not improve further. In the case of the offline performances, a general improvement for all subjects and methods could be achieved, except for session fb4 in subject s1 and fb3 in subject s3. In case of subject s1 it was nearly impossible to exceed the result of fb3 with 100 % accuracy, but fb4 was very good with 97 % classification accuracy.

In general, the difference between published offline studies and this online study is that in the offline studies only the best possible separability of the data rather than the performance achieved is given (see also difference in this work between online and cross-validated offline results). Clearly a large number of methods and parameters can be compared in an offline study and various optimization procedures can be applied to find the best separation between the different MI tasks. Nevertheless it is not guaranteed that the subject would perform better with the optimized method. In contrast to that, in this work both feature extraction methods have been used in online experiments and it could be demonstrated, that the wavelet packet features selected in the offline analysis can be applied and successfully in online sessions. The prediction out of the first training session that wavelet and band power features should work and perform similarly has been proved. In summary, it could be demonstrated for the first time that a wavelet transform can be used for an online EEG-based brain-computer interface to detect oscillatory patterns in ongoing EEG during MI.

**Acknowledgments:** This work was carried out as part of the PRESENCCIA project, an EU funded Integrated Project under the IST programme (Number 27731) and the EU COST Action BM0601: Neuromath.

## References

[1] J. R. Wolpaw, N. Birbaumer, D. J. McFarland, G. Pfurtscheller, and T. M. Vaughan. Brain-computer interfaces for communication and control. *Clin. Neurophysiol.*, 113(6):767–791, 2002.

[2] G. Pfurtscheller, C. Neuper, G. R. Müller, B. Obermaier, G. Krausz, A. Schlögl, R. Scherer, B. Graimann, C. Keinrath, D. Skliris, M. Wörtz, G. Supp, and C. Schrank. Graz-BCI: state of the art and clinical applications. *IEEE Trans. Neural. Syst. Rehabil. Eng.*, 11(2):177–180, 2003.

[3] V. Bostanov and B. Kotchoubey. The t-CWT: a new ERP detection and quantification method based on the continuous wavelet transform and student's t-statistics. *Clin. Neurophysiol.*, 117(12):2627–2644, 2006.

[4] M. Fatourechi, G. E. Birch, and R. K. Ward. Application of a hybrid wavelet feature selection method in the design of a self-paced brain interface system. *J. Neuroeng. Rehabil.*, 4:11, 2007.

[5] W. Y. Hsu, C. C. Lin, M. S. Ju, and Y. N. Sun. Wavelet-based fractal features with active segment selection: application to single-trial EEG data. *J. Neurosci. Methods*, 163(1):145–160, 2007.

[6] S. Lemm, C. Schafer, and G. Curio. BCI competition 2003 – data set III: probabilistic modeling of sensorimotor mu rhythms for classification of imaginary hand movements. *IEEE Trans. Biomed. Eng.*, 51(6):1077–1080, 2004.

[7] L. Qin and B. He. A wavelet-based time-frequency analysis approach for classification of motor imagery for brain-computer interface applications. *J. Neural Eng.*, 2(4):65–72, 2005.

[8] B. Graimann, J. E. Huggins, S. P. Levine, and G. Pfurtscheller. Toward a direct brain interface based on human subdural recordings and wavelet-packet analysis. *IEEE Trans. Biomed. Eng.*, 51(6):954–962, 2004.

[9] M. Pregenzer and G. Pfurtscheller. Frequency component selection for an EEG-based brain to computer interface. *IEEE Trans. Rehabil. Eng.*, 7(4):413–419, 1999.

[10] T. Hinterberger, A. Kübler, J. Kaiser, N. Neumann, and N. Birbaumer. A brain-computer interface (BCI) for the locked-in: comparison of different EEG classifications for the thought translation device. *Clin. Neurophysiol.*, 114(3):416–425, 2003.

# BCI preprocessing of EEG signals based on time-frequency ratio of mixtures

M. Naeem[1], C. Brunner[1], B. Graimann[1,2], R. Leeb[1], G. Pfurtscheller[1]

[1]Institute for Knowledge Discovery, BCI Lab, Graz University of Technology, Graz, Austria
[2]Institute for Automation, University of Bremen, Bremen, Germany

naeem6500@yahoo.com

**Abstract**

A recently introduced blind source separation concept called time-frequency ratio of mixtures (TIFROM) is employed to build spatial filters for brain-computer interfaces (BCI) preprocessing. TIFROM works on the concept of sparsity, that is, it seeks to locate single source zones by finding few adjacent low variance areas in the time-frequency decomposed mixtures. The method presented in this paper is under-determined and is adapted with some modifications to the need of BCI preprocessing for two class motor imagery tasks. Two distinct groups of electrodes (5 each) around and including $C_3$ and $C_4$ (from the international 10-20 system) were chosen a priori for estimating corresponding filters.

The mean accuracy values of 8 subjects in 2 sessions are compared with CSP and Infomax. The pairwise *t*-test concluded that CSP performed significantly better than Infomax in both sessions. However, with respect to TIFROM, CSP was found to be significantly better in only one of the session. Moreover, no significant difference was found between the results of TIFROM and Infomax.

## 1 Introduction

A new blind source separation (BSS) concept called time-frequency ratio of mixtures (TIFROM) [1] is introduced in this paper. It was already shown [2] that TIFROM can separate dependent, Gaussian or non-stationary signals and there exist some areas in the time-frequency plane where single sources occur, that is, the signals are sparse in the time-frequency domain. Moreover, the method is reported to be particularly successful in separating linear instantaneous under-determined mixtures [2]. It is this under-determined approach of TIFROM that will be employed to build spatial filters for BCI preprocessing in this study. More specifically, TIFROM seeks to build two spatial filters for the two class motor imagery data representing discriminative task-related activity in regions contra-lateral to the movement side. In this regard, two distinct groups of electrodes (5 each) around and including $C_3$ and $C_4$ (from the international 10-20 system) were utilized to estimate corresponding filters. The results of the TIFROM are compared with Infomax [3] and common spatial patterns (CSP) [4, 5]. The reason for choosing Infomax as BSS method was its better performance in comparison with other ICA-based algorithms in recent years [6, 7]. On the other hand CSP, which is a supervised method, is considered as the best performing algorithm in BCI preprocessing.

## 2 Methods

### 2.1 Experiment

The electrode montage, illustrated in Figure 1 (right), consists of electrodes for recording the EEG signals. The 22 signals were sampled with 250 Hz and filtered between 0.5 and 100 Hz. Moreover,

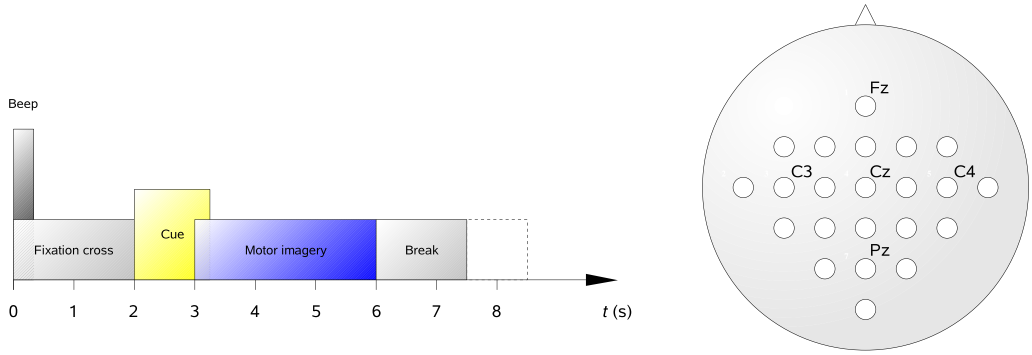


Figure 1: Left: Timing of a trial of the training paradigm. Right: EEG electrode setup, some labels corresponding to positions in the international 10–20 system are indicated.

line noise was suppressed by enabling a 50 Hz notch filter. This study was conducted on datasets recorded from eight healthy subjects, not experienced with BCI training. They were seated in a comfortable armchair in front of a computer screen.

The experimental paradigm consisted of two different tasks, that is, right and left hand movement imagination. The beginning of each trial (at $t = 0$ s) was indicated by an acoustic tone along with the display of a fixation cross on the screen. After two seconds (at $t = 2$ s), a visual cue (an arrow pointing either left or right) appeared for 1.25 s on the screen. Each position of the arrow required the subject to perform the corresponding imaginary movement. Specifically, they were asked to keep up the imagination of the movement between seconds 3 and 6. After six seconds (at $t = 6$ s), the fixation cross disappeared indicating the subject to relax. The next trial started after a short break of 1.5–2.5 seconds. The experimental paradigm is illustrated in Figure 1 (left). Two sessions of each subject were recorded on different days, each session comprising 6 runs. Each of the two types of cues was displayed 12 times within each run (which yields a total of 72 trials per session for each class) in a random order. All the runs of each session were concatenated. Overall, there were 144 trials in each session for every subject.

## 2.2 Time-frequency ratio of mixtures

For the sake of simplicity, a model of linear instantaneous mixtures of two sources is considered first. Signal mixtures are denoted by $x_1(t)$ and $x_2(t)$. Each is a linear combination of the source signals denoted by $s_1(t)$ and $s_2(t)$:

$$x_1(t) = a_{11}s_1(t) + a_{12}s_2(t) \tag{1}$$

$$x_2(t) = a_{21}s_1(t) + a_{22}s_2(t) \tag{2}$$

In matrix notation these equations can be written as $\mathbf{x} = \mathbf{A}\mathbf{s}$, where $\mathbf{A}$ is a mixing matrix whose inverse is directly estimated, up to a scaling and permutation factor, by using the time-frequency information contained in the observations. More specifically, TIFROM seeks to estimate the inverse of the mixing matrix [2]:

$$\tilde{\mathbf{A}}^{-1} = \begin{pmatrix} 1 & 1 \\ 1/c_1 & 1/c_2 \end{pmatrix}^{-1} \tag{3}$$

Here, $c_1 = a_{11}/a_{21}$ and $c_2 = a_{12}/a_{22}$, which give estimated separated sources $\mathbf{y}$ as follows:

$$\mathbf{y}(t) = \tilde{\mathbf{A}}^{-1}\mathbf{x}(t) = [a_{11}s_1(t), a_{12}s_2(t)]^T \tag{4}$$

The coefficients $c_i$ in the estimated inverse of the mixing matrix are automatically determined by using time-frequency information in the observations. To this end, the short-time Fourier transform (STFT) of the observations $x_i$, denoted by $X_i(t_j, \omega_k)$, is computed:

$$X_i(t, \omega) = \frac{1}{\sqrt{2\pi}} \sum_{-\infty}^{+\infty} x_i(\tau) h(\tau - t) e^{-j\omega\tau} \tag{5}$$

$X_i(t, \omega)$ is the contribution of the signal $x_i$ in the short time and frequency windows respectively centered at time $t$ and frequency $\omega$. The STFT decomposition only requires a single source to occur alone in a few adjacent time-frequency windows for its resolution [2]. This leads to the fundamental assumption of the TIFROM approach:

For each source $s_i$, there exist some adjacent time-frequency windows $(t_j, \omega_k)$ where only $S_i$ occurs:

$$S_l(t_j, \omega_k) \ll S_i(t_j, \omega_k), \forall l \neq i$$

TIFROM then seeks to make those single source areas obvious by calculating the complex ratio:

$$\alpha(t_j, \omega_k) = \frac{X_1(t_j, \omega_k)}{X_2(t_j, \omega_k)} \tag{6}$$

The linearity of the STFT operator allows to write the complex ratio $\alpha$ as follows:

$$\alpha(t_j, \omega_k) = \frac{a_{11} S_1(t_j, \omega_k) + a_{12} S_2(t_j, \omega_k)}{a_{21} S_1(t_j, \omega_k) + a_{22} S_2(t_j, \omega_k)} \tag{7}$$

The coefficients are computed in the following way: For each frequency $\omega_k$ (or time $t_j$), the sample variance of the complex ratio $\alpha(t_j, \omega_k)$ is calculated on the series $\Gamma_q$ of $M$ short overlapping time windows (or frequency windows):

$$\mathrm{Var}[\alpha](\Gamma_q, \omega_k) = \frac{1}{M} \sum_{j=1}^{M} \| \alpha(t_j, \omega_k) - \overline{\alpha}(\Gamma_q, \omega_k) \|^2 \tag{8}$$

The sample mean $\overline{\alpha}$ of the complex ratio $\alpha$ is defined as:

$$\overline{\alpha}(\Gamma_q, \omega_k) = \frac{1}{M} \sum_{j=1}^{M} \alpha(t_j, \omega_k) \tag{9}$$

What remains to be done is to sort the values of $\mathrm{Var}[\alpha](\Gamma_q, \omega_k)$ in ascending order. The lowest value directly gives a time-frequency domain $(\Gamma_q, \omega_k)$ with only one source. The corresponding coefficient $c_i$ is then given by $\overline{\alpha}(\Gamma_q, \omega_k)$. The second coefficient can be found by searching the next lowest value of $\mathrm{Var}[\alpha](\Gamma_q, \omega_k)$ associated with a significantly different value of $\overline{\alpha}(\Gamma_q, \omega_k)$ by using a threshold of minimum difference between the two values. The separated signals thus can be obtained by applying the inverted mixing matrix.

The extension of the basic model ($2 \times 2$ case) to the $N \times N$ case can be done elegantly by considering the coherence property of time-frequency maps [2]. More specifically, the areas $(\Gamma_q, \omega_k)$ where a single source appears alone in one observation are the same for all observations. That is, a single source manifesting itself in some adjacent time-frequency windows of one channel, will be present in all the channels in the same areas. As a consequence of this coherence, single source areas can be detected by analyzing the variance of the ratio $\alpha(t, \omega) = X_i(t, \omega)/X_j(t, \omega)$ associated to only one pair of observation. The inverse of the mixing matrix for the $N \times N$ case is depicted below:

$$\tilde{\mathbf{A}}^{-1} = \begin{pmatrix} 1 & \dots & 1 \\ 1/c_{12} & \dots & 1/c_{N2} \\ \vdots & \ddots & \vdots \\ 1/c_{1N-1} & \dots & 1/c_{NN-1} \\ 1/c_{1N} & \dots & 1/c_{NN} \end{pmatrix}^{-1} \tag{10}$$

## 2.3 TIFROM for BCI preprocessing

Ideally speaking, for a single source to occur alone in a time-frequency domain $(\Gamma_q, \omega_k)$ the corresponding variance $\mathrm{Var}[\alpha](\Gamma_q, \omega_k)$ should be zero in that region. However, there is always a small interference from other sources and the variance values will be different from exactly zero. This suggests that the method needs a variance threshold in addition to the threshold value required for the separability between the sources. In the case of EEG-related brain patterns, both of these thresholding criteria are subject-specific. Therefore, in order to circumvent this problem, the TIFROM method was adopted for BCI preprocessing with some modifications. The modified method is described in the following paragraphs.

First of all, STFT decomposition was performed on each single trial. The STFT of the signals was computed with the full sampling frequency of 250 Hz using 250 points. These parameters ensured a maximum frequency resolution of 1 Hz. In the next step, only time-frequency bins that fell in the range of 7–30 Hz and 3–6 s (motor imagery period) were chosen for further analysis. Next, the ratio of these STFT-transformed signals were computed according to (6). To this end, we computed the ratios with respect to the two contra-lateral channels $C_3$ and $C_4$ corresponding to positions in the international 10–20 system. Due to their importance in the method, channels $C_3$ and $C_4$ were termed as pivot channels. To be more specific, $X_1$ in (6) means pivot channel ($C_3$ or $C_4$) whereas $X_2$ is a symbol for the remaining channels. Each of these time-frequency ratios of decomposed signals with respect to $C_3$ or $C_4$ will be processed separately with the aim of building spatial filters, one for each of them. For further processing, one group will be considered and the same procedure will be true for the other one.

For one pair of observation, i. e. one pair among $C_3$–c1, $C_3$–c2, ... (where c1, c2, ... represent 5 channels, including and surrounding $C_3$ – see Figure 1), the sample variance of the complex ratio $\alpha$ was calculated on $M$ short adjacent frequency bins for each time $t_j$. The parameter $M$ in this study was chosen to be 4, with the aim of estimating 11 overlapping 4 Hz frequency bands in one pair of observation. Specifically, the adjacent frequency bands thus obtained were different from each other by 2 Hz (e. g. 7–10 Hz, 9–12 Hz, ... ). The process described in the lines above was repeated for all pairs of observations in a group. Thereafter, the algorithm seeks to find for each frequency band the averaged time-frequency bin where the variance is smallest. The corresponding coefficient was then determined by the sample mean of the complex ratio $\alpha$ according to (9) (here the summation is performed over $k$). The procedure was repeated for each frequency band and all the respective coefficients $c_i$ were estimated along with the corresponding observation pairs. The next step consisted of filling the coefficients in the mixing matrix as represented in (10). In this context, it should be mentioned that due to the coherence property, the averaged time-frequency area where a source appears alone in one observation is the same for all observations. Therefore, the mixing matrix is obtained with columns corresponding to distinct frequency bands and rows to observations (5 channels), according to (10). Each column represents a unique averaged time-frequency bin where the variance is smallest at one of the pair of observations. It can readily be seen that the method is under-determined as one pair of observations can correspond to two or more columns. The same procedure as described in the preceding paragraphs is applicable to the other group ($C_4$–c1, $C_4$–c2, ... ), thereby obtaining a second mixing matrix.

## 2.4 Feature extraction and classification

For the computation of spatial filters with Infomax preprocessing, the entire data (i. e. a whole session) for each subject was used. The unmixing matrix (i. e. spatial filter) thus obtained was then multiplied to the entire (raw) data. As a next step, for each of these twenty-two components, logarithmic band-power features were calculated. The frequency band selected was 7–30 Hz for all subjects. Overall, there were 22 band-power features corresponding to 22 ICA components. In contrast to the Infomax, TIFROM utilized only the motor imagery period (3–6 s) and a frequency band of 7–30 Hz to calculate unmixing matrices. It has already been mentioned that TIFROM calculates two unmixing matrices based on two distinct group of channels including and surrounding the two contra-lateral pivot channels. Therefore each of these unmixing matrices were then

| | Session 1 | | | Session 2 | | |
|---|---|---|---|---|---|---|
| Subject | TIFROM | Info | CSP | TIFROM | Info | CSP |
| s1 | 80.4 | 76.8 | 79.5 | 87.0 | 84.4 | 91.0 |
| s2 | 59.6 | 58.7 | 58.9 | 59.0 | 60.4 | 64.4 |
| s3 | 92.4 | 93.2 | 98.0 | 94.6 | 92.8 | 96.1 |
| s4 | 92.7 | 93.3 | 95.9 | 95.9 | 97.5 | 98.9 |
| s5 | 96.5 | 93.0 | 93.4 | 93.7 | 92.2 | 94.0 |
| s6 | 74.3 | 72.8 | 73.1 | 66.7 | 74.0 | 74.6 |
| s7 | 63.5 | 55.8 | 59.0 | 59.2 | 59.8 | 56.4 |
| s8 | 66.2 | 70.9 | 75.2 | 75.9 | 79.6 | 91.4 |
| Mean | 78.2 | 76.8 | 79.1 | 79.0 | 80.0 | 83.4 |

Table 1: Overall accuracies (in %) of TIFROM, Infomax and CSP.

multiplied to EEG data of corresponding channels. The number of components so obtained in each case was 11 – a total of 22 components. Finally, for each of these 22 components one band-power feature was calculated by utilizing a frequency band of 7–30 Hz.

After feature extraction, the next step is the same for both preprocessing methods. For this purpose, 90 % of the data was used to train a linear statistical classifier (Fisher's linear discriminant analysis, LDA) [8]. Within each trial, samples between seconds 4.5 and 5.5 were used to train the classifier. This classifier was then applied to the remaining 10 % of the data and the classification accuracy was calculated. The whole procedure was repeated 10 times, i. e. a $10\times10$ cross-validation procedure [8] was performed.

In the case of CSP, signals were first band-pass filtered in the range of 7–30 Hz, then the samples were partitioned into 10 parts before building two CSP spatial filters. Each part was used as test set only once in the following way. The (two) spatial filters were calculated on the basis of the 90 % portion (nine parts) and were then applied to this data. In the next step, 6 components (the first and last three) were chosen and log-transformed normalized variances were calculated for each of the components. Next, these features were forwarded to a linear statistical classifiers (Fisher's linear discriminant analysis, LDA). The classifier weights were calculated and along with two spatial filters was then applied to the remaining 10 % of the data. The whole procedure was repeated 10 times, i. e. a $10 \times 10$-fold cross-validation procedure was performed and classification accuracies were determined. The same time slice (between second 4.5 and 5.5) was used to train the classifier like in the case of Infomax and TIFROM. It should be mentioned that in the case of CSP like TIFROM the time slice of (3–6 s) was used to calculate the spatial filters.

## 3 Results

The accuracy values for TIFROM, Infomax and CSP for all the subjects and two sessions are shown in Table 1.

In this comparison the pairwise $t$-test was applied to the data (Table 1) for each session separately at a 5 % significance level. The results revealed that CSP performed significantly better than TIFROM in the second session. On the other hand, CSP performed significantly better than Infomax in both sessions. Similarly, pairwise $t$-tests did not find significant differences between TIFROM and Infomax in either of the session.

## 4 Discussion and conclusion

It has been shown that TIFROM performed comparably with Infomax in both session and with CSP in session 1. However, as expected CSP remained the best performing algorithm. The method can be easily extended to 3 class problems by preselecting an additional group of electrodes including and around $C_z$. This pre-selection of reduced number of electrodes can come very handy in practical applications of BCI systems. Therefore, as a direction of further research it can be worthwhile investigating how other algorithms such as CSP performs in comparison with TIFROM for reduced number of electrodes.

Apart from TIFROM, hardly any method in BCI preprocessing is available that utilizes time-frequency decomposed information for building spatial filters. Sparsity is only one concept that proved to be useful in extracting relevant information from time-frequency decomposed signals. Its relative success at least in comparison with Infomax, can be seen as an encouragement for exploring other hitherto unexploited concepts that can be utilized for extracting useful information from time-frequency decomposed signals.

**Acknowledgments:** This work was funded by the Higher Education Commission (HEC), Pakistan, the European projects Presenccia (IST-2006-27731) and Eye-To-IT (IST-2006-517590), and the Styrian government project GZ A3-16 B 74-05/1.

## References

[1] F. Abrard and Y. Deville. Blind separation of dependent sources using the TIme-frequency ratio of mixtures approach. In *Proceedings of the 7th International Symposium on Signal Processing and its Applications (ISSPA 2003)*, 2003.

[2] F. Abrard and Y. Deville. A time-frequency blind signal separation method applicable to underdetermined mixtures of dependent sources. *Signal Process.*, 85:1389 –1403, 2005.

[3] A. J. Bell and T. J. Sejnowski. An information-maximization approach to blind separation and blind deconvolution. *Neural Comput.*, 7:1129–1159, 1995.

[4] Z. J. Koles, J. C. Lind, and A. C. Soong. Spatio-temporal decomposition of the EEG: a general approach to the isolation and localization of sources. *Electroencephalogr. Clin. Neurophysiol.*, 95:219–230, 1995.

[5] J. Müller-Gerking, G. Pfurtscheller, and H. Flyvbjerg. Classification of movement-related EEG in a memorized delay task experiment. *Clin. Neurophysiol*, 111:1353–1365, 2000.

[6] M. Naeem, C. Brunner, R. Leeb, B. Graimann, and G. Pfurtscheller. Seperability of four-class motor imagery data using independent components analysis. *J. Neural Eng.*, 3:208–216, 2006.

[7] C. Brunner, M. Naeem, R. Leeb, B. Graimann, and G. Pfurtscheller. Spatial filtering and selection of optimized components in four class motor imagery EEG data using independent components analysis. *Pattern Recogn. Lett.*, 28:957–964, 2007.

[8] R. O. Duda, P. E. Hart, and D. G. Stork. *Pattern classification.* Wiley, 2001.

# A new general weighted least-squares algorithm for approximate joint diagonalization

M. Congedo, C. Jutten, R. Sameni, C. Gouy-Pailler

GIPSA-lab, UMR5216-CNRS, Université Joseph Fourier, Université Pierre Mendès-France, Université Stendhal, INPG, Grenoble, France

marco.congedo@gmail.com

**Abstract**

Independent component analysis (ICA) and other blind source separation (BSS) methods are important processing tools for multi-channel processing of electroencephalographic data and have found numerous applications for brain-computer interfaces. A number of solutions to the BSS problem are achieved by approximate joint diagonalization (AJD) algorithms, thus the goodness of the solution depends on them. We present a new least-squares AJD algorithm with adaptive weighting on the separating vectors. We show that it has good properties while keeping the greatest generality among AJD algorithms; no constraint is imposed either on the input matrices or on the joint diagonalizer to be estimated. The new cost function allows interesting extensions that are now under consideration.

## 1 Introduction

Given a set of matrices $C\colon \mathbf{C}_k, k = 1 \ldots K$, $K > 2$, the approximate joint diagonalization (AJD) constis in finding a matrix $\mathbf{B}$ such that all $K$ products $\mathbf{B}\mathbf{C}_k\mathbf{B}^T$ result in matrices as close as possible to diagonal form. The AJD is an important algebraic tool extending the generalized eigenvalue problem (two-matrix diagonalization). As such, it is enjoying considerable interest and several efficient algorithms have been proposed [1, 2, 3, 4, 5, 6, 7, 8, 9]. In the context of brain-computer interface (BCI) the AJD provides a natural extension of the common spatial pattern to multi-class feature extraction [8]. Furthermore, since many matrices can be jointly diagonalized, one may optimize the spatial filter not only with respect to the signal diversity across classes [8], but also with respect to other kinds of signal diversity such as coloration and non-stationarity [9].

Recently a least-squares (LS) AJD algorithm has been proposed almost simultaneously in [6] and [8]. This algorithm does not impose restrictions either on the input matrices $\mathbf{C}_k$ (e. g., real, positive-definite, symmetric, etc.) or on the joint diagonalizer $\mathbf{B}$ (e. g., orthogonality), thus it is the most flexible among existing AJD algorithms. In [7] a similar LS idea has been used to perform simultaneous joint diagonalization and zero-diagonalization on two matrix sets, an approach that suits time-frequency data expansions. More generally, AJD algorithms are well adapted to expansion of the signal in several dimensions, enhancing the ability of capturing the source of diversity in a given data-set, hence offering a powerful approach for feature extraction. We anticipate that AJD algorithms will acquire a prominent role in feature extraction methods for BCI and we feel that a general approach may prove advantageous, which motivated us pursue further LS algorithms. The criterion used in [6] and [8] is

$$\Im^{\mathrm{Off}}(\mathbf{B}) = \sum_k \left\|\mathrm{Off}\left(\mathbf{B}\mathbf{C}_k\mathbf{B}^T\right)\right\|^2 \tag{1}$$

where $\|\cdot\|$ indicates the Frobenius norm and the Off operator zeros the diagonal entries of the matrix argument. The minimization of this criterion with respect to $\mathbf{B}$ evidently yields an AJD solution in the LS sense.

## 2 Method

For simplicity of exposition in the following we assume that the $N$-dimensional input matrices $\mathbf{C}_k$ are real and square, but not necessarily symmetric. The non-square/complex case is easily derived thereupon. We propose a weighted and normalized version of (1) given by the minimization of

$$\wp^{\mathrm{Off}}(\mathbf{B}) = \frac{\sum_k \|\mathrm{Off}\,(\mathbf{W}\mathbf{B}\mathbf{C}_k\mathbf{B}^T\mathbf{W})\|^2}{\sum_k \|(\mathbf{W}\mathbf{B}\mathbf{C}_k\mathbf{B}^T\mathbf{W})\|^2} \tag{2}$$

where $\mathbf{W}$ is and $N$-dimensional diagonal matrix holding the weights for each row vector of $\mathbf{B}$. Since $\sum_k \|(\mathbf{W}\mathbf{B}\mathbf{C}_k\mathbf{B}^T\mathbf{W})\|^2 = \sum_k \|\mathrm{Off}\,(\mathbf{W}\mathbf{B}\mathbf{C}_k\mathbf{B}^T\mathbf{W})\|^2 + \sum_k \|\mathrm{Diag}(\mathbf{W}\mathbf{B}\mathbf{C}_k\mathbf{B}^T\mathbf{W})\|^2$, where the Diag operator zeros the off-diagonal entries of the matrix argument, the minimization of (2) is equivalent to the maximization of

$$\wp_{\mathrm{Diag}}(\mathbf{B}) = \frac{\sum_k \|\mathrm{Diag}(\mathbf{W}\mathbf{B}\mathbf{C}_k\mathbf{B}^T\mathbf{W})\|^2}{\sum_k (\mathbf{W}\mathbf{B}\mathbf{C}_k\mathbf{B}^T\mathbf{W})\|^2} \tag{3}$$

Denoting by $\mathbf{b}_i^T$ the $i$-th row vector of $\mathbf{B}$ and by $\mathbf{b}_i$ its transpose (stil the row vector but in column representation) and following [7] we expand (3) such as

$$\sum_k \|\mathrm{Diag}(\mathbf{W}\mathbf{B}\mathbf{C}_k\mathbf{B}^T\mathbf{W})\|^2 = \sum_{k=1}^{K}\sum_{i=1}^{N}(w_i\mathbf{b}_i^T\mathbf{C}_k\mathbf{b}_i w_i)^2 = \sum_{i=1}^{N} w_i\mathbf{b}_i^T\left[\sum_{k=1}^{K}(\mathbf{C}_k\mathbf{b}_i w_i^2\mathbf{b}_i^T\mathbf{C}_k)\right]\mathbf{b}_i w_i \tag{4}$$

and

$$\sum_k \|(\mathbf{W}\mathbf{B}\mathbf{C}_k\mathbf{B}^T\mathbf{W})\|^2 = \sum_{k=1}^{K}\sum_{i=1}^{N}\sum_{j=1}^{N}(w_i\mathbf{b}_i^T\mathbf{C}_k\mathbf{b}_j w_j)^2 = \sum_{i=1}^{N} w_i\mathbf{b}_i^T\left[\sum_{k=1}^{K}(\mathbf{C}_k\mathbf{B}^T\mathbf{W}^2\mathbf{B}\mathbf{C}_k^T)\right]\mathbf{b}_i w_i \tag{5}$$

Now by defining

$$\mathbf{M}_i = \sum_{k=1}^{K}(\mathbf{C}_k\mathbf{b}_i w_i^2\mathbf{b}_i^T\mathbf{C}_k) \tag{6}$$

and

$$\mathbf{M} = \sum_{k=1}^{K}(\mathbf{C}_k\mathbf{B}^T\mathbf{W}^2\mathbf{B}\mathbf{C}_k^T) \tag{7}$$

and substituting (4) and (5) in (3), we can write

$$\wp^{\mathrm{Diag}}(\mathbf{B}) = \sum_i \frac{w_i\mathbf{b}_i^T\mathbf{M}_i\mathbf{b}_i w_i}{\mathrm{tr}(\mathbf{W}\mathbf{B}\mathbf{M}\mathbf{B}^T\mathbf{W})} \tag{8}$$

Similarly as in [6, 7, 8] the optimization of $\mathbf{B}$ according to 8 may proceed iteratively row-by-row. For each vector of $\mathbf{B}$ a step consists in sphering $\mathbf{M}$ (fixing the denominator) and finding the optimal direction $\mathbf{b}_i$ maximizing $\mathbf{b}_i^T\mathbf{M}_i\mathbf{b}_i$. Updating $\mathbf{b}_i$ will results in different $\mathbf{M}$ and $\mathbf{M}_i$, to which a new $\mathbf{b}_i$ will correspond and so on iteratively. The process sequentially applies to all $N$ vectors of $\mathbf{B}$ within each iteration, resulting in mutual restrictions. The following sphered weighted diagonalization (SWDiag) algorithm makes use of adaptive weighting:

Initialize **B** by a clever guess or by **I** (the identity matrix) if no guess is available. Initialize **W** by **I**.

**While not** Converge **do**

**For** $i = 1$ to $N$ **do twice**

(A: Sphering): Find **H** such that $\mathbf{HMH}^T = \mathbf{I}$

(B: Optimal Direction): Find the principal eigenvector $\mathbf{u}_i$ and associated eigenvalue $\lambda_i$ of $\mathbf{HMH}^T$

Update the $i$-th row of **B** as $\mathbf{b}_i^T \leftarrow \mathbf{u}_i^T \mathbf{H}$

**End For**

Update all diagonal elements of **W** as $w_i \leftarrow \lambda_i^{-\frac{1}{2}}$ and normalize them so as $\sum_i w_i^2 = N$, $i = 1 \ldots N$

**End While**

This family of algorithms has good convergence properties (see [6, 7, 8]). Note that $\mathbf{M}$ in (7) and $\mathbf{M}_i$ in (6) are updated at each pass of the for loop. If each pass of the for loop is not repeated twice, as suggested, the algorithm still converges, but the stopping criterion (see below) displays a "saw" (non-monotonically decreasing) behavior. The eigenvalues associated with the principal eigenvectors of Step B are by definition comprised between 0 and 1.0 and equals 1.0 if the off criterion is zero, which happens if the input matrices can be diagonalized exactly, that is, if they have exactly the same eigenstructure. If not, or more in general due to sampling error, which will always happen in practice, the eigenvalues will converge to a value smaller than 1.0. This ensures numerical stability of the algorithm and provides the rationale for the weighting scheme: at each iteration the diagonalization achieved by each row vector of $\mathbf{B}$ is proportional to the magnitude of the associated eigenvalue. In (7) $\mathbf{C}_k\mathbf{B}^T\mathbf{W}^2\mathbf{B}\mathbf{C}_k^T$ can be written as $\mathbf{C}_k \sum_i w_i^2 \mathbf{b}_i \mathbf{b}_i^T \mathbf{C}_k^T$, thus we see that the adaptive weighting emphasizes the search of vectors attaining a lower eigenvalue at the expense of those attaining an higher eigenvalue, which steers the algorithm toward a more balanced solution. See also the discussion on balanced solutions in [6]. As for the stopping criterion of the algorithm, we stop as soon as the change of the $N$ eigenvalues $\lambda_i$ is negligible.

Each eigenvector (optimal direction) in step B can be successfully updated toward convergence if matrix $\mathbf{M}_i$ does not have multiple maximum eigenvalues. In this case the optimal direction eigenvector cannot be found uniquely. This is also the case of the LS algorithm of [6] and [8], which minimizes

$$\Im^{\mathrm{Off}}(\mathbf{B}) = \sum_k \|\mathrm{Off}(\mathbf{B}\mathbf{C}_k\mathbf{B}^T)\|^2 \text{ with constraint } \mathrm{Diag}(\mathbf{BEB}^T) = \mathbf{I} \tag{9}$$

where $\mathbf{E}$ is any positive definite matrix. Since the matrix $\mathbf{E}$ is disjoint to matrix $\mathbf{B}$, their algorithm consists in performing the sphering once at the beginning and then iteratively finding the optimal directions by minor component analysis and scaling to match the constraint. However, if after sphering there are multiple minor eigenvalues this algorithm is more likely trapped. On the other hand in our optimization scheme the matrices $\mathbf{HM}_i\mathbf{H}^T$ change at each pass due to the fact that the sphering step (step A) depends on the previous estimation of $\mathbf{B}$ in (7), thus our algorithm may be trapped only if the multiplicity of maximum eigenvalues happens close to convergence, whence the changes caused by the sphering update are small and cannot correct the multiplicity issue anymore.

# 3 Results

We compared our SWDiag algorithm and its unweighted version SDiag (obtained setting all weights to 1.0 and not updating them at each iteration) to the well-established FDiag algorithm of [5] and QDiag of [6]. We performed simulations using synthetic input matrices and a real-data example.

For the synthetic matrices simulation we generated 12 6-dimensional square diagonal matrices with each diagonal entry distributed as a chi-squares random variable with one degree of freedom. Each of these matrices, named $\mathbf{D}_k$, may represent the error-free covariance matrix of six inde-

| Perturbation | **FDiag** | **QDiag** | **Sdiag** | **WSDiag** |
|---|---|---|---|---|
| **None** | 0.9999 | 0.9999 | 1.0 | 1.0 |
| | (0.0000) | (0.0011) | (0.0) | (0.0) |
| **Mixing** | 0.9926 | 0.9927 | 0.9915 | 0.9928 |
| | (0.0107) | (0.0104) | (0.0119) | (0.0102) |
| **Independence** | 0.8057 | * | 0.7961 | 0.8002 |
| | (0.0676) | | (0.0698) | (0.0683) |

Table 1: Mean and standard deviation (within parentheses) of the performance index (11) across 500 repetitions of the synthetic input matrices simulation with and without perturbation. The higher the index the better. *: QDiag resulted in a false solution 87 out of 500 repetitions in this case.

pendent standard Gaussian processes (zero mean and unit variance). The 12 input matrices were obtained as

$$\mathbf{C}_k = \mathbf{A}\mathbf{D}_k\mathbf{A}^T \tag{10}$$

$k = 1\ldots12$, where each entry of the 6-dimensional square mixing matrix $\mathbf{A}$ is randomly distributed as a standard Gaussian.

We considered three cases:

**No perturbation:** the exact AJD problem as described by (10)

**Perturbation of the mixing matrix:** input matrices were generated as $\mathbf{C}_k = \mathbf{A}_k\mathbf{D}_k\mathbf{A}_k^T$, where each entry of the mixing matrix $\mathbf{A}$ in (10) is perturbated as $\mathbf{A}_{kij} \leftarrow \mathbf{A}_{ij} + \phi\zeta\mathbf{A}_{ij}$, where $\phi$ is $+1$ or $-1$ with equal probability and $\zeta$ is uniformly distributed in $[0.001\ldots0.1]$, for all $k = 1\ldots K$ and for all $i$, $j = 1\ldots N$.

**Perturbation of independence:** with probability 0.2 each off-diagonal symmetric pair of the input matrices $\mathbf{D}_k$ is perturbated as $\mathbf{D}_{kij} = \mathbf{D}_{kji} \leftarrow \phi(\sqrt{\mathbf{D}_{kii}}\sqrt{\mathbf{D}_{kjj}})/\delta$, where $\phi$ is $+1$ or $-1$ with equal probability and $\delta$ uniformly distributed in $1\ldots8$, for all $k$ and $i > j$.

Given true mixing $\mathbf{A}$, each AJD algorithm estimates demixing $\mathbf{B}$, which should approximate the inverse of $\mathbf{A}$ out of row scaling (including sign) and permutation. Then, matrix $\mathbf{G} = \mathbf{B}\mathbf{A}$ should equal a scaled permutation matrix. At each repetition we computed the performance index such as

$$\text{Performance Index} = \frac{2(N-1)\sum_i\sum_j \mathbf{G}_{ij}^2}{\sum_i \max_j(\mathbf{G}_{ij}^2) + \sum_j \max_i(\mathbf{G}_{ij}^2)} \tag{11}$$

which is positive and reaches its maximum 1.0 if $\mathbf{G}$ has only one non-null elements in each row and column. For QDiag as per (9), we used $\mathbf{E} = \mathbf{I}$ for this simulation. The mean and standard deviation across 500 repetitions are reported in Table 1.

The real data example concerns an eyes open EEG recording of a 12 year-old boy comprising 19 electrodes and 11 seconds sampled at 128 samples per second. The recording (Figure 1, top) displays a rapid sequence of eye blinks and bilateral jaw muscle contamination visible at temporal leads T3 and T4. We performed AJD of 44 Fourier co-spectral matrices corresponding to frequencies 1 Hz to 44 Hz in 1 Hz steps. For QDiag we used the sum of the cospectra in this range as $\mathbf{E}$ in (9). EEG data was previously whitened and the 16 most energetic components were retained. Such an AJD procedure corresponds to exploiting the different coloration of EEG source components. In fact, the AJD of cospectral matrices successfully estimates the inverse of the mixing matrix if the source components have non-proportional power spectra (characteristic coloration). Out of random permutations, FDiag, QDiag and WSDiag gave very similar results (Figure 1).

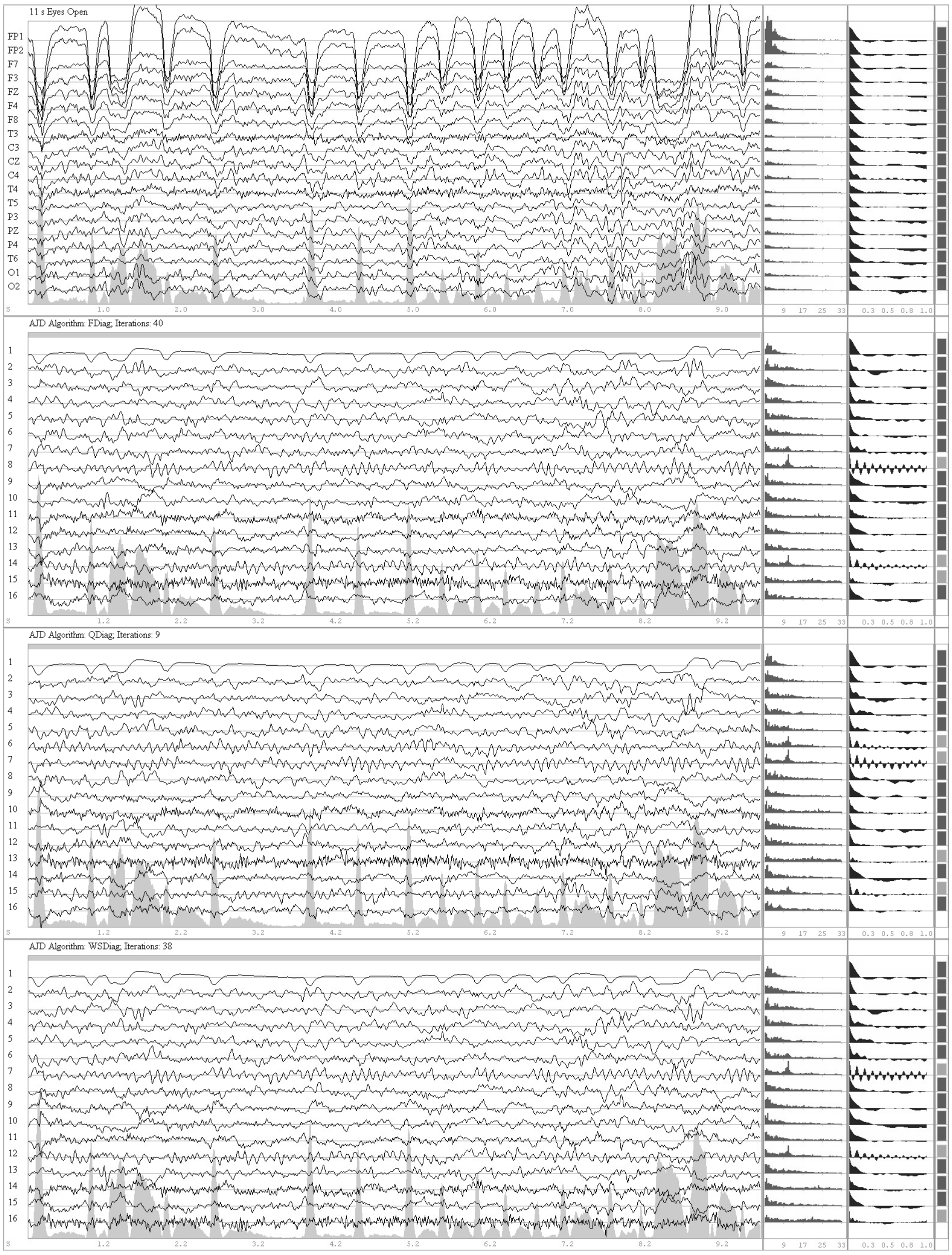

Figure 1: Top: about 9 s of a 11 s epoch extracted from the raw EEG recording of a 12 year-old male. From left to right, electrode labels according to the 10–20 international system, raw EEG tracing (upward deflection is negative potential; the space between two horizontal centering lines is 70 µV), average power spectrum (from zero to 32 Hz; arbitrary units) and autocorrelation function (the space between two horizontal centering lines is autocorrelation = 1 in the upward direction and −1 in the downward direction). The gray shaded area in the background of EEG tracings is the global field power, the sum of the square of potentials across electrodes for each sample (arbitrary units). The next three plots are the sources estimated using FDiag, QDiag and WSDiag on the same set of Fourier cospectral matrices. For all methods sources were standardized (unit variance) and plotted on the same scale.

# 4 Discussion

We have presented a new least-squares approximate joint diagonalization algorithm with adaptive weighting for the row vectors of the matrix to be estimated. Simulations on synthetic input matrices and a real-data example indicate the good performance of WSDiag when compared to FDiag and QDiag. Our new LS optimization scheme allows interesting manipulations, besides the adaptive weighting here proposed, which are now under investigation. We are currently considering weighting also the input matrices and solving block diagonalization problems. We are also working on the convergence properties of the algorithms and on its link to cost function (3).

# 5 Conclusion

The proposed AJD algorithm may prove useful for the extraction of electroencephalographic features. Application of source separation methods making use of AJD algorithms has been recently introduced in the brain-computer interface field [10, 11] and appears a promising approach.

# References

[1] J. F. Cardoso and A. Souloumiac. Jacobi angels for simultaneous diagonalization. *SIAM J. Matrix Anal. Appl.*, 17(1):161–164, 1996.

[2] D. T. Pham. Joint approximate diagonalization of positive definitive matrices. *SIAM J. Matrix Anal. Appl.*, 22(4):1136–1152, 2001.

[3] E. Moreau. A generalization of joint-diagonalization criteria for source separation. *IEEE Trans. Signal Proc.*, 49(3):530–541, 2001.

[4] A. Yeredor. Non-orthogonal joint diagonalization in the least-squares sense with application in blind source separation signal processing. *IEEE Trans. Signal Proc.*, 50(7):1545–1553, 2002.

[5] A. Ziehe, P. Laskov, G. Nolte, and K.-R. Müller. A fast algorithm for joint diagonalization with non-orthogonal trnasformations and its application to blind source separation. *J. Mach. Learn. Res.*, 5:801–818, 2004.

[6] R. Vollgraf and K. Obermayer. Quadratic optimization for simultaneous matrix diagonalization. *IEEE Trans. Signal Process.*, 54(9):3270–3278, 2006.

[7] E. M. Fadaili, N. T. Moreau, and E. Moreau. Nonorthogonal joint diagonalization/zero diagonalization for source separation based on time-frequency distributions. *IEEE Trans. Signal Process.*, 55(5):1673–1687, 2007.

[8] S. Degerine and E. Kane. A comparative study of approximate joint diagonalization algorithms for blind source separation in presence of additive noise. *IEEE Trans. Signal Process.*, 55(6):3022–3031, 2007.

[9] X.-L. Li and X. D. Zhang. Nonorthogonal joint diagonalization free of degenerate solution. *IEEE Trans. Signal Process.*, 55(5):1803–1814, 2007.

[10] M. Grosse-Wentrup and M. Buss. Multi-class common spatial pattern and information theoretic feature extraction. *IEEE Trans. Biomed. Eng.*, In Press.

[11] C. Gouy-Pailler abd M. Congedo, C. Brunner, C. Jutten, and G. Pfurtscheller. Multi-class independent common spatial patterns: exploiting energy variacions of brain sources. *Proc. 4th Int. BCI Workshop*, In Press.

# Single-trial P300 detection in healthy and ALS subjects by means of a genetic algorithm

B. Dal Seno[1], M. Matteucci[1], L. Mainardi[2], F. Piccione[3], S. Silvoni[3]

[1]Department of Electronics and Information, IIT-Unit, Politecnico di Milano, Italy
[2]Department of Bioengineering, IIT-Unit, Politecnico di Milano, Italy
[3]IRCSS San Camillo, Venezia, Italy

bernardo.dalseno@polimi.it

**Abstract**

P300 is a potential widely used in brain-computer interfaces (BCI), as P300 is an innate response that does not require training on the part of the user. In the literature several classification algorithms have been used (e. g., Linear Discriminant Analysis, Stepwise Discriminant Analysis, Support Vector Machines), and, typically, first the P300 relevant features are extracted from the EEG signal, then they are fed into the classifier. From this, it becomes clear that feature extraction is the key point, and doing it by hand can be at the same time cumbersome and suboptimal. In this paper, we face the issue of automatic feature extraction by using a genetic algorithm (GA) able to retrieve the relevant aspects of the signal to be classified in an automatic fashion. We do not use GA for feature selection or classifier optimization; instead, we learn directly from the signal which are the features we should use in our classifier. The approach has been used for single-sweep classification with a logistic classifier on a group of 10 subjects affected by ALS (amyotrophic lateral sclerosis), hospitalized in the S. Camillo structure, and a group of 4 healthy subjects, voluntarily participating to the study. Results are promising, reaching up to 95 % accuracy for some subjects; moreover, the features extracted by the GA turn out to be related to the P300 activity and can provide insights about the most interesting regions and time to classify P300s.

## 1 Introduction

A brain-computer interface (BCI) [1] is an interface that does not entail muscle movements, but it bypasses any muscle or nerve mediation and connects a computer directly with the brain by picking up signals generated by the brain activity.

In this study, we focus on the P300 [2], an event-related potential (ERP) that can be recorded through an electroencephalogram (EEG). This potential is a late positive wave that occurs between 250 and 800 ms after the onset of a meaningful stimulus; the wave elicitation occurs in response to task-relevant events, and its latency depends on the stimulation paradigm.

The P300 has been widely used for BCIs, with many variations, but in all cases the paradigm is the same: the BCI system presents the user with some choices, one at a time; when it detects a P300 potential, the associated choice is selected. The user is normally asked to count the number of times the choice of interest is presented, so as to remain concentrated on the task. As the P300 is an innate response, it does not require training on part of the user.

In [3], Donchin and colleagues presented the first P300-based BCI, called also P300 speller, which permits to spell words. A grid of letters and symbols is presented to the user, and entire columns or rows are flashed one after the other in random order. Classification is made through stepwise discriminant analysis (SWDA) applied to averages of samples from epochs relative to the same stimulation (same row or same column).

In [4], a virtual-reality system is presented where users operates objects selected through the P300. Classification is made by comparing the correlation of single responses with the averages of all target and nontarget responses.

In [5], tests have been made both with healthy and impaired subjects. The subjects control a cursor by choosing among four commands (up, down, left, right) via the P300. Single-sweep detection is performed; independent component analysis (ICA) is used to decompose the EEG signal, a fuzzy classifier identifies a candidate P300 component among the ones extracted by ICA, and a neural network classifies it as target or non-target. The system is more effective with healthy subjects, though no exact reason could be pinpointed.

In [6], an initial attempt at using a BCI in a home environment is reported: a person with ALS uses a P300 speller on a daily basis. The system is very similar to the original Donchin's speller, with a few differences in the detection algorithm.

Many techniques for detecting the P300 extract relevant features from the EEG signal and feed those features into a classifier. In these approaches, feature extraction becomes the key point, and doing it by hand can be at the same time cumbersome and suboptimal. In this paper we face the issue of feature extraction by using a genetic algorithm (GA) able to retrieve the relevant aspects of the signal to be classified in an automatic fashion.

GAs have been used already in the BCI field, although differently from the present work: in [7], the best combination between different features and different classifiers is sought for a motor-imagery task, while in [8], a classifier operating on P300 features is selected by a GA.

In the following section, we present the paradigm used to collect the EEG data for the present study, while Section 3 gives a brief overview of the GA. Section 4 presents the performance achieved by the GA and a graphical interpretation of evolved classifiers.

# 2 Experimental setup

## 2.1 Subjects

A group of 10 subjects affected by ALS, hospitalized in the S. Camillo structure, and a group of 4 healthy subjects voluntarily participated to the study (ALS group: 3 females and 7 males, mean age of 55 years, range 31–73 years; control group: 2 females and 2 males, mean age of 36 years, range 27–41 years). The research was approved by the ethical committee of the S. Camillo Hospital; informed consent was obtained according to the Declaration of Helsinki. All participants underwent neuropsychological evaluation and auditory odd-ball P300 testing, in order to exclude cognitive deficits. We assessed that all participants had preserved auditory, visual, and cognitive functions, including adequate language comprehension.

## 2.2 BCI paradigm

An experiment was carried on to test the ability of the subjects to use a BCI based on P300 elicitation with an on-line single-sweep classifier. The paradigm consisted of a presentation of finite sequences of visual stimuli on a computer screen to the subjects. They were asked to control the movement of a virtual object (a blue ball) from the center of the monitor to one out of four peripheral target images representing generic needs. The initial distance between the virtual object and the target image encompassed four discrete steps. Upward, rightward, downward and leftward arrows in peripheral positions of the monitor (see Figure 1 a) were flashed in random order. Each arrow indicated one out of four possible directions for the movement of the ball. Participants had to pay attention to the arrow indicating the target image direction (target arrow; probability of occurrence: 25 %), but to ignore the arrows indicating wrong directions (distracting arrows; probability of occurrence: 75 %). The subjects had to move the blue ball along only one direction, according to the target image specified by the examiner.

Each trial comprised the flashing of one arrow for 150 ms (see Figure 1 b), followed by the data processing necessary for P300 recognition, and finally the generation of the feedback consisting in

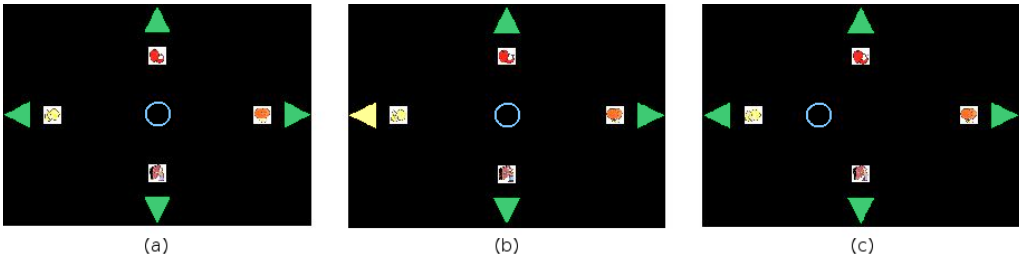


Figure 1: Representation of a trial. (a) The blue ball, the target images and the four directions arrows; (b) the flashed arrow; (c) the movement of the ball after a P300 recognition.

the movement of the ball (see Figure 1 c). The interval between the presentation of two arrows (inter-trial interval – ITI) was 2.5 s, in order to achieve optimal on-line data processing. A session was defined as the complete sequence of trials sufficient to reach the target image (range: 13–92 trials). We hypothesized that every target arrow should elicit a P300 wave. Every time a P300 was detected during the trial, the ball moved on the graphical interface in the direction of the flashed arrow. Each participant performed eight learning sessions (LS) in the first day, and sixteen testing sessions (TS) spread over the following 11 days (more precisely, first day: 8 LS → second day: 4 TS → two days interval → fifth day: 4 TS → two days interval → eighth day: 4 TS → two days interval → eleventh day 4 TS). Learning sessions were characterized by an ideal feedback (after each target stimulus the ball moved), while all testing sessions were characterized by a real feedback (the movement of the ball depended on the classification algorithm).

### 2.3 Data acquisition

EEG electrodes were placed according to the international 10–20 system at Fz, Cz, Pz and Oz; the EOG was placed at SO2; all electrodes were referenced to the left earlobe. The five channels were amplified, band-pass filtered between 0.15 Hz and 30 Hz, sampled at 200 Hz, and digitized (with a 16 bit resolution). Every ERP epoch, synchronized with the stimulus, began 500 ms before the stimulus onset, and ended 1000 ms after the stimulus onset (1500 ms total). Thus, after each stimulus (trial) the system recorded 300 samples per each of the 5 channels, available for on-line and off-line processing.

## 3 Genetic algorithm

We applied the genetic algorithm described in [9] to the data described in the previous section in an offline fashion. In this section, only a very brief description of the algorithm is given; details are given for the fitness function, as it differs from the one used in the cited work.

Genetic algorithms are a class of optimization algorithms that mimic the way natural evolution works. In a genetic algorithm, a set of possible solutions to an optimization problem are coded in strings called chromosomes solutions are evaluated, and the best ones (those with highest fitness) are selected and combined together to form new possible solutions, in a process that mimics evolution among living beings. After some repetitions of the procedure, good solutions emerge.

In the genetic algorithm used in this work, each individual (chromosome) represents a set of possible features for discriminating the presence of a P300 in EEG recordings. Each gene encodes a feature and an EEG channel from which to extract it; a feature is obtained by multiplying the EEG channel by a weight function, whose exact shape is encoded by parameters in genes (see Figure 2 for examples of weight functions). Genetic operators are a variant of 1-point crossover and uniform mutation, and tournament selection with elitism is used.

The fitness of a chromosome is computed by evaluating the performance of a logistic classifier on the features it encodes. To have a fair estimate of the performance, a 4-fold cross-validation

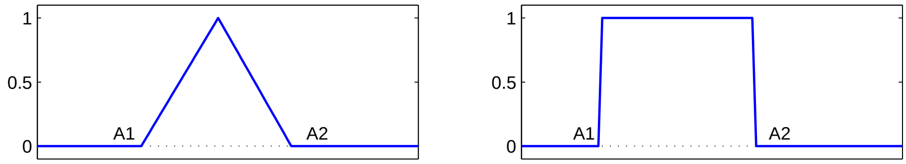


Figure 2: Weight functions used for feature extraction

| Subject | Training | | Test | | Recall | | Exp. | Perf. |
|---|---|---|---|---|---|---|---|---|
| | **Targ.** | **Non-T.** | **Targ.** | **Non-T.** | **Targ.** | **Non-T.** | **Targ.** | **Len.** |
| S1 | 204 | 703 | 99 | 284 | 61 %±3 % | 66 %±2 % | 57 % | 22.9 |
| S2 | 121 | 354 | 58 | 166 | 96 %±1 % | 95 %±1 % | 100 % | 13.1 |
| S3 | 98 | 277 | 57 | 206 | 63 %±5 % | 77 %±3 % | 77 % | 23.3 |
| S4 | 175 | 492 | 61 | 178 | 86 %±4 % | 83 %±3 % | 93 % | 16.4 |
| S5 | 114 | 325 | 32 | 94 | 75 %±7 % | 78 %±3 % | 85 % | 19.5 |
| S6 | 124 | 356 | 52 | 148 | 87 %±3 % | 85 %±5 % | 95 % | 16.0 |
| S7 | 144 | 433 | 50 | 138 | 82 %±4 % | 76 %±3 % | 85 % | 17.8 |
| S8 | 112 | 340 | 39 | 112 | 82 %±7 % | 72 %±5 % | 80 % | 17.9 |
| S9 | 185 | 529 | 50 | 154 | 94 %±2 % | 86 %±2 % | 96 % | 14.6 |
| S10 | 219 | 690 | 47 | 142 | 97 %±2 % | 82 %±2 % | 94 % | 14.5 |
| S11 | 86 | 228 | 30 | 84 | 75 %±4 % | 81 %±2 % | 88 % | 19.3 |
| S12 | 116 | 327 | 34 | 95 | 85 %±5 % | 90 %±3 % | 98 % | 15.8 |
| S13 | 218 | 617 | 84 | 240 | 77 %±3 % | 77 %±2 % | 84 % | 19.0 |
| S14 | 165 | 489 | 61 | 170 | 55 %±7 % | 73 %±4 % | 63 % | 26.0 |

Table 1: Means and standard deviations of recall for targets and non-targets obtained in 14 runs of the GA.

scheme on the training set is used, and the mean performance on the 4 folds is used as the fitness. The "performance" $f$ of a classifier is obtained by combining precision $p_{\mathrm{T}}$ and recall $r_{\mathrm{T}}$ for targets according to this formula:

$$f = \frac{2}{3}\,p_{\mathrm{T}} + \frac{1}{3}\,r_{\mathrm{T}} \tag{1}$$

The definitions of precision and recall in terms of *true positives* ($TP$), *false positives* ($FP$), and *false negatives* ($FN$) are:

$$p_{\mathrm{T}} = \frac{TP}{TP+FP} \qquad\qquad r_{\mathrm{T}} = \frac{TP}{TP+FN} \tag{2}$$

An analysis of the combination of the features extracted by the genetic algorithm and the classifier trained on the training set allows to compute weights assigned to individual EEG samples.

# 4 Results and conclusions

The GA was applied in an offline fashion to the data recorded as described in Section 2. EEG data were decimated to half of the original frequency; epochs were trimmed to the interval from $-0.2$ s to $+0.8$ s (i. e., half a second was thrown away), and the linear trend was removed. No normalization of data was performed; we tried to normalize EEG data before running the GA, but it did not change the test performance significantly, so we chose the way that required less computation.

The GA was trained on the first three quarters of the available data for each subject, and the features encoded by the best chromosome and the corresponding classifier trained on the training set were applied to the remaining quarter of the data. This procedure was repeated with 14 independent runs of the GA on each subjects.

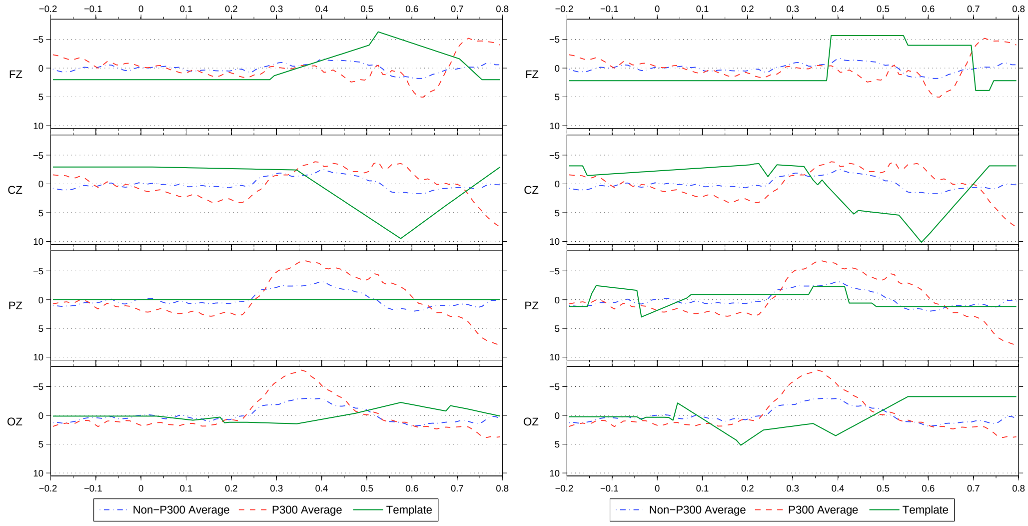


Figure 3: Examples of templates obtained in two different GA run for Subject S2

The results are shown in Table 1: the mean values and the standard deviation of the recall of targets and non-targets over all the 14 runs are presented. Subjects S11, S12, S13, S14 are healthy, while all the others are affected by ALS. For most subjects, the performance of the GA is good, achieving consistently more than 70 % of recall in 8 subjects (i. e., the mean is at least two standard deviations over 70 %). In 6 subjects, the classifiers achieved often more than 80 % of correct answers.

The last two columns of Table 1 show how effective this BCI can be for the various subjects; the first of the two is the expected fraction of times a user reached the desired target, and the second is the expected number of trials needed to reach a target. These numbers have been obtained with a Montecarlo simulation of the BCI done with the mean recall values obtained by the GA. Only 3 subjects reach an accuracy in the task performance lower than 80 %, so we can consider the classifier performance satisfactory in at least 11 cases. For a comparison, a perfect classifier (with 100 % recall) reaches the target always, in 12 trials on average; a random classifier (50 % recall) reaches the target in 25 % of the cases, and each selection takes almost 21 trials on average.

Figure 3 shows what the GA has found: the continuous green lines represent the weight assigned to individual EEG samples in the final logistic classifier, while the averages of targets and non-targets epochs are given as references. Units are µV and s; the templates have been scaled to fit in the graphs. The plots regard two classifiers that reached over 90 % of correct epochs for Subject S2; although the averages are not very different, the algorithm found good classifiers concentrating more on the Fz and Cz channels. By comparing the averages of targets and non-targets in the plots, it is possible to see that they have important differences in the Fz and Cz channels between 400 and 800 ms after the stimulus. The P300 complex includes other subcomponents besides P3b, which has its maximal amplitude in parietal regions, as P3a and the slow wave post P3b, which have their maximal amplitude over fronto-central regions. P3a occurs when the changes in physical properties of the novel stimulus are task relevant and attention is switched to the stimulus source. The slow wave post P3b occurs in the latency range from 500 to 1400 ms, and its amplitude increases as the task becomes more demanding and difficult [10, 11]. This suggests that the characteristics of the task and the attention requirement determine strong response in the front-central region, which is exploited by the classifiers found by the GA.

We think that the results obtained offline are very promising and could be confirmed in future online tests. The GA is very suitable for an online application; for the data set used in the present work and on a low-end PC, a single run of the GA takes between 5 and 15 minutes, depending on the subject, and the classification of an epoch less than 1 ms.

**Acknowledgments:** This work has been partially supported by the Italian Institute of Technology (IIT), and by the grant "Brain-Computer Interfaces in Everyday Applications" from Politecnico di Milano and Regione Lombardia. We are thankful to all the participants in our study.

## References

[1] J. R. Wolpaw, N. Birbaumer, D. J. McFarland, G. Pfurtscheller, and T. M. Vaughan. Brain-computer interfaces for communication and control. *Clin. Neurophysiol.*, 113:767–791, 2002.

[2] S. Sutton, M. Braren, J. Zubin, and E. R. John. Evoked-potential correlates of stimulus uncertainty. *Science*, 150(3700):1187–1188, 1965.

[3] E. Donchin, K. M. Spencer, and R. Wijesinghe. The mental prosthesis: Assessing the speed of a P300-based brain-computer interface. *IEEE Trans. Rehabil. Eng.*, 8(2):174–179, June 2000.

[4] J. D. Bayliss, S. A. Inverso, and A. Tentler. Changing the P300 brain computer interface. *Cyberpsychol. Behav.*, 7(6):694–704, 2004.

[5] F. Piccione, F. Giorgi, P. Tonin, K. Priftis, S. Giove, S. Silvoni, G. Palmas, and F. Beverina. P300-based brain computer interface: reliability and performance in healthy and paralysed participants. *Clin. Neurophysiol.*, 117(3):531–537, March 2006.

[6] T. M. Vaughan, D. J. McFarland, G. Schalk, W. A. Sarnacki, D. J. Krusienski, E. W. Sellers, and J. R. Wolpaw. The Wadsworth BCI research and development program: At home with BCI. *IEEE Trans. Neural Syst. Rehabil. Eng.*, 14(2):229–233, 2006.

[7] R. Boostani, B. Graimann, M. H. Moradi, and G. Pfurtscheller. A comparison approach toward finding the best feature and classifier in cue-based BCI. *Med. Biol. Eng. Comput.*, 45(4):403–412, April 2007.

[8] L. Citi, R. Poli, C. Cinel, and F. Sepulveda. Feature selection and classification in brain computer interfaces by a genetic algorithm. In *Late-breaking papers of the Genetic and Evolutionary Computation Conference (GECCO-2004)*, volume CD-ROM, 2004.

[9] B. Dal Seno, M. Matteucci, and L. Mainardi. A genetic algorithm for automatic feature extraction in P300 detection. In *2008 Int. Joint Conf. Neural Networks (IJCNN)*, pages 3144–3151, 2008.

[10] J. Polich. Updating P300: an integrative theory of P3a and P3b. *Clin. Neurophysiol.*, 118:2128–2148, 2007.

[11] E. Altenmüller. Psychophysiology and EEG. In E.t Niedermeyer and F. H. Lopes Da Silva, editors, *Electroencephalography*. Williams & Wilkins, Baltimore, USA, 3rd edition, 1993.

# Approximate entropy for EEG-based movement detection

M. Dyson, T. Balli, J. Q. Gan, F. Sepulveda, R. Palaniappan

BCI Group, Department of Computing and Electronic System, University of Essex, UK

{mdyson,tballi}@essex.ac.uk

**Abstract**

An approximate entropy feature is tested with parameters appropriate for online BCI – a short calculation window and use of the running standard deviation of the EEG signal. Features are extracted from self-paced real movement data, with various values of the embedding dimension and tolerance of comparison. Two alternative features, band power and reflection coefficients, are extracted for comparative purposes. Class separability is measured using classification results from $k$-means clustering for individual features and linear discriminant analysis for multiple features, as selected by sequential forward floating search. Results show this method of calculating approximate entropy to be a candidate for online movement detection in self-paced BCI systems.

## 1 Introduction

In many traditional feature extraction methods it is assumed that the fundamental signal characteristics are contained in the amplitude and the frequency spectrum. However for some signals these features are insufficient as signals belonging to different classes have different bandwidths. Such signals can be best distinguished using complexity measures which are independent of the precise frequency content of the signal [1].

In recent years, there have been many research studies on nonlinear complexity measures for analysis of EEG signals [1, 2, 3]. These methods are used for analysis of the electrophysiological condition of subjects, discrimination of mental tasks, and diagnosis of different pathological conditions such as epilepsy, memory impairments and sleep disorders. It is reported that signal complexity is correlated with the mental and physiological condition of subjects.

In this paper the detection of index finger movement using a nonlinear complexity measure, approximate entropy, is investigated. Detection rates using two linear features, band power and reflection coefficients, are included for comparison.

## 2 Methods

### 2.1 Approximate entropy

Approximate entropy (ApEn) is a recently developed method that measures the irregularity of time series data [4]. This measure of irregularity is obtained by comparing the original time series with time shifted versions of itself. For this purpose the original signal is reconstructed in phase space using time delay embedding. The number of previous data points used for making the prediction of the next data point is termed the embedding dimension, m.

Assuming we have EEG data from a single channel;

$$x = [x(1), x(2), \ldots, x(N)] \tag{1}$$

with $N$ data points, a sequence of vectors are constructed with time delay embedding as follows;

$$y = [y_1, y_2, y_3, \ldots, y_M] \tag{2}$$

where

$$y_i = [x(i), x(i+\tau), x(i+2\tau), \ldots, x(i+(m-1)\tau)]^T \tag{3}$$

for $i = 1, 2, \ldots, N-(m-1)\tau$. The next step is the calculation of the correlation integral using the reconstructed vectors, which is defined by

$$C_i^m(r) = \sum_{j=1}^{N-(m-1)} \frac{\Theta(r - \|y_i - y_j\|)}{N-(m-1)} \tag{4}$$

where $N$ is the length of time series, $r$ is the tolerance of comparison, $y_i$ and $y_j$ are vectors constructed in phase space, $\|\cdot\|$ represents the Euclidean distance between vectors and $\Theta(x)$ is the heaviside function such that $\Theta(x) = 1$ if $x > 0$ and $\Theta(x) = 0$ if $x \leq 0$. The approximate entropy $\mathrm{ApEn}(m, r)$ is obtained by;

$$\mathrm{ApEn}(m, r) = \Phi^m(r) - \Phi^{m+1}(r), \tag{5}$$

where

$$\Phi^m(r) = \frac{1}{N-(m-1)} \sum_{i=1}^{N-(m-1)} \ln[C_i^m(r)]. \tag{6}$$

## 2.2 Recording

Signals were acquired at 256 Hz. Five bipolar EEG channels were recorded over the motor cortex at locations C3, C1, Cz, C2 and C4 as shown in Figure 1. EMG was recorded from the flexors of the left forearm. A right mastoid reference channel was used. Signals were acquired using a Guger Technologies g.BSamp. Data was recorded from eleven right handed subjects, three subjects were female, ages ranged from 23 to 46. Subject 1 was experienced using a BCI system based on self-paced movement, Subjects 7 to 11 had experience in offline BCI experiments, the remaining subjects were naive to BCI use.

As data was un-cued the number of trials performed within each run was variable. Each subject performed three runs in a single session. A run lasted 610 seconds. After a five second pre waiting period a fixation cross appeared on the screen. The fixation cross remained on the screen for 10 minutes during which time data was acquired. A five second post waiting period was used.

Within each run subjects were instructed to perform self paced flexion/extension of the left index finger whilst the fixation cross was visible. Subjects were requested to perform each movement for between 5 and 10 seconds and to rest for at minimum 10 seconds between movements. Instructions were given to concentrate on the fixation cross as much as possible during each run. After each run EMG recordings were assessed to ensure subjects understood requirements and could moderate actions accordingly.

## 2.3 Feature extraction and parameter initialisation

ApEn was calculated using a window of 32 samples with an overlap of 31 samples; a 1 second averaging window was applied. Prior testing had determined that this window size demonstrated promising results whilst retaining a calculation time appropriate for online use.

The calculation of ApEn involves selection of three parameters namely the embedding dimension $m$, time delay $\tau$, and the distance within which the neighboring trajectory points must lie (tolerance of comparison) $r$. There is no fixed manner of determining $m$ and $\tau$ values used in the phase space reconstruction of the time series. In this study ApEn values were calculated for $m$ values ranging from 1 to 10, with $\tau$ fixed at 1, as suggested in [5].

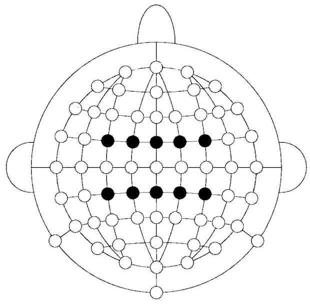

Figure 1: Electrode layout.

In previous studies it has been suggested that $r$ should be calculated via the product of the standard deviation of the original signal [4] with a coefficient value. In order to estimate an appropriate range of coefficient values for $r$ a prior investigation was performed using data recorded from three subjects (2 channel: C3, C4) during use of an online BCI system utilising self paced movement. ApEn values were derived for 10 embedding dimensions over a set of coefficient values, ranging from 1 to 4 incremented by 0.1. Class separation was determined by calculating Bhattacharyya distances [6]. Based on class separation results the maximum coefficient value for testing was increased to 5 and the increment step to 0.2.

As the standard deviation of the entire signal is not an appropriate parameter for use in an online BCI system we substitute the use of the running standard deviation of the relevant EEG channel. The running standard deviation is calculated and updated sequentially based on prior data up to and including the sample point for which features are extracted. As subjects perform three runs the standard deviation value of each channel is recalculated for each run. As the standard deviation of a signal takes time to converge we tested $k$-means classification accuracy over time during the prior investigation to ensure results would not be detrimentally affected.

## 2.4 Classification

Class labels were derived through manual markup of the EMG channel. At the point of each class transition 32 samples prior and post were dropped. To ensure equal sample sizes for each class we obtain the number of samples for each class within a run, take the minimum $N$, and use $n = 1 \ldots N$ from each class. As we are interested in comparative class separability cross-validation was not applied. Classification results are representative of training classifiers using the entire dataset.

To examine the relationship between class separation, embedding dimension and $r$ values classification results for single electrode-feature pairs were obtained by use of $k$-means clustering (Mathworks Matlab, default settings). To compare feature separability using multiple electrode-features a sequential forward floating search (SFFS) algorithm [7] was applied using a linear discriminant analysis (LDA) classifier. A maximum of six features were selected, corresponding to lightweight online use.

Classification results were also calculated for ten band power features (BP) corresponding to the delta (0.1–0.5 Hz), theta (5–8 Hz), alpha (8–12 Hz), sigma (12–15 Hz), beta (15–25 Hz) bands along with five gamma bands (25–35, 35–45, 45–55, 55–65, 65–75 Hz) and autoregressive reflection coefficients ($K$), orders 1 to 10. To determine if ApEn complexity information could be complementary to these features a SFFS was run using all three features.

# 3 Results

Maximum $k$-means classification results for each subject are presented in Table 3 along with associated electrode site and related parameter values. Optimal $r$ values all fall within the range 1.2 to 3.8 whilst $m$ values cover all possible embedding dimensions. No significant differences were found between classification accuracies obtained for approximate entropy when compared to band power and reflection coefficient features ($p > 0.05$, paired $t$-test, $df = 10$). From $k$-means classification results we obtained optimal $r$ coefficients for each embedding dimension, Figure 2 shows the relationship between these values for subjects demonstrating classification dominance in channel C4.

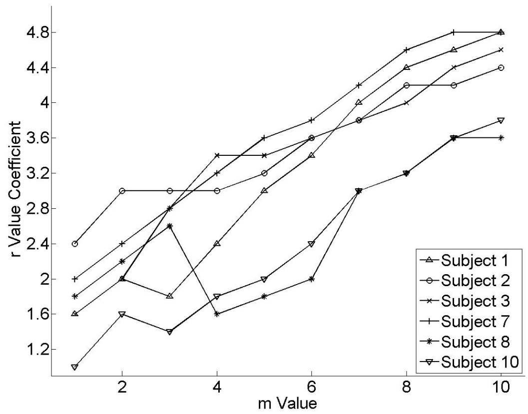


Figure 2: Optimal $r$ coefficients for $m$ values, C4 dominant subjects.

Class separation as measured by multiple feature LDA classification is shown in Table 2. Classification accuracy is shown for BP, $K$, ApEn, the maximum classification result using a single feature (Max) and classification accuracy achieved when all three features are made available to SFFS (Comb). The column 'Comb Used' outlines the combination of features used for each subject.

When comparing use of multiple features within feature groups we find significant differences in class separation across subjects for AE and BP ($p < 0.05$, paired $t$-test, $df = 10$), AE and $K$ ($p < 0.05$, paired $t$-test, $df = 10$), no significant differences were found between BP and $K$ features.

| | Band Power | | | Reflection Coefficients | | | Approximate Entropy | | | |
|---|---|---|---|---|---|---|---|---|---|---|
| Subject | Acc % | Site | Band | Acc % | Site | Order | Acc % | Site | $r$ Coeff | $m$ Value |
| 1 | 81.42 | C4 | 5 | 80.40 | C4 | 3 | 82.56 | C4 | 1.8 | 3 |
| 2 | 66.79 | C4 | 4 | 61.18 | C4 | 1 | 62.37 | C4 | 2.4 | 1 |
| 3 | 58.60 | Cz | 10 | 60.72 | C2 | 2 | 64.37 | C4 | 2.8 | 3 |
| 4 | 63.61 | C4 | 7 | 71.99 | C1 | 5 | 72.25 | C2 | 2.2 | 7 |
| 5 | 65.94 | C3 | 10 | 70.67 | C3 | 5 | 66.11 | C3 | 1.2 | 9 |
| 6 | 56.58 | C2 | 1 | 64.30 | C3 | 5 | 62.18 | Cz | 3.8 | 9 |
| 7 | 61.21 | C4 | 5 | 60.41 | C1 | 3 | 62.02 | C4 | 2.8 | 3 |
| 8 | 65.55 | Cz | 10 | 71.01 | Cz | 6 | 66.76 | C4 | 3.6 | 10 |
| 9 | 58.54 | C1 | 9 | 63.83 | C4 | 6 | 59.55 | Cz | 1.6 | 3 |
| 10 | 57.08 | C4 | 3 | 61.08 | C4 | 3 | 63.03 | C4 | 2.0 | 5 |
| 11 | 59.14 | C4 | 5 | 60.49 | C2 | 4 | 57.33 | C1 | 1.2 | 8 |
| $\bar{x}$ ($\sigma$) | 63.13 (7.09) | | | 66.01 (6.59) | | | 65.32 (6.93) | | | |

Table 1: $k$-means classification: maximum for each subject.

| | Classification Accuracy % | | | | | Comb Used | | |
|---|---|---|---|---|---|---|---|---|
| Subject | BP | $K$ | ApEn | Max | Comb | BP | $K$ | ApEn |
| 1 | 83.47 | 86.56 | 87.06 | 87.06 | 87.97 | 2 | 0 | 4 |
| 2 | 75.44 | 64.92 | 73.87 | 75.44 | 77.25 | 3 | 0 | 3 |
| 3 | 61.27 | 62.51 | 69.90 | 69.90 | 70.18 | 1 | 0 | 5 |
| 4 | 76.78 | 79.85 | 81.11 | 81.11 | 83.07 | 1 | 1 | 4 |
| 5 | 75.40 | 75.67 | 79.71 | 79.71 | 80.95 | 1 | 1 | 4 |
| 6 | 63.19 | 67.65 | 66.45 | 67.65 | 69.17 | 0 | 3 | 3 |
| 7 | 65.79 | 62.46 | 68.62 | 68.62 | 67.52 | 4 | 1 | 1 |
| 8 | 70.31 | 72.15 | 74.50 | 74.50 | 76.01 | 0 | 1 | 5 |
| 9 | 61.74 | 62.52 | 61.70 | 62.52 | 63.65 | 0 | 2 | 4 |
| 10 | 66.07 | 64.22 | 63.17 | 66.07 | 66.79 | 4 | 0 | 2 |
| 11 | 66.97 | 65.53 | 66.65 | 66.97 | 68.02 | 3 | 0 | 3 |
| $\bar{x}$ | 69.68 | 69.46 | 72.07 | 72.69 | 73.69 | 1.73 | 0.82 | 3.45 |
| $\sigma$ | 7.20 | 8.11 | 7.99 | 7.53 | 7.84 | | | |

Table 2: LDA classification accuracy using six features selected by SFFS.

Significant differences were found between accuracy rates obtained using combined features against BP ($p < 0.01$, paired $t$-test, $df = 10$), $K$ ($p < 0.01$, paired $t$-test, $df = 10$) and AE ($p < 0.01$, paired $t$-test, $df = 10$).

# 4 Discussion

Maximum $k$-means classification results for each subject, obtained for a single feature, show no significant difference in class separability when using approximate entropy as compared to the more traditional features, band power and autoregressive reflection coefficients. Demonstrating that, given optimal parameters, signal complexity may be comparable to these linear features.

We use the classification rates from $k$-means to investigate the relationship between parameters varied in the approximate entropy calculation and class separability. As the selection of these parameters is a non-trivial problem, we calculated approximate entropy with a range of $m$ and $r$ coefficients in an exhaustive manner. The results of $k$-means classification, as shown in Figure 2 show parameters $m$ and $r$ are proportionally related to one another; as the distance between embedding vectors increases with $m$ it is necessary to increase $r$ for optimal performance.

Significant differences were found between the degree of class separability, as measured by LDA classification accuracy, when comparing the use of multiple features of a single type. The difference in classification accuracy found between approximate entropy and the linear features are likely to be attributable to the difference in granularity in the search spaces. Parallel work using an increased feature space for band power has failed to find a significant difference in class separability between the features.

When comparing classification accuracy obtained for approximate entropy with the use of all available features, in our case augmenting the approximate entropy feature space with information from band power and reflection coefficients, we find significant differences in classification accuracy with relatively comparative feature spaces. This suggests that the linear features used provide further characterization of EEG time series which is complementary to approximate entropy. Across subjects the use of combined features demonstrates a bias towards the approximate entropy feature, followed by band power which is represented around twice as often as reflection coefficients. The bias towards approximate entropy is again, likely to be influenced by the increased search space for the feature. We did not utilize cross-validation in this study as we are interested in separability of features rather than the generalisation ability of a particular BCI system. An attempt to counter the overfitting problem, to some extent, was made through the use of linear

LDA classifiers. We plan on using cross-validation in future tests and during online BCI system design.

The classification results achieved using approximate entropy demonstrate that, although computationally expensive, promising results may be obtained using parameters appropriate for online use. A short window was used to investigate the applicability of approximate entropy for online BCI use where the detection latency and the number of channels to be processed are important factors. Increasing the window size should lead to a greater accuracy at the cost of latency of onset detection and the feasible number of channels used.

The main constraint to the use of approximate entropy for BCI use is in the estimation of the correct range of parameters. Based on the subjects tested it appears that optimal $r$ coefficient and $m$ values are subject dependant. In this study we used a fixed $\tau$ value of 1, this was employed to restrict the search space of the feature. Using methods such as the first local minimum of mutual information and first zero crossing of the autocorrelation function it may be possible to obtain an optimal $\tau$ value [8, 9]; we expect this to increase the characterization ability of the approximate entropy method.

# 5 Conclusion

Based on a limited number of subjects approximate entropy features using a short calculation window appear appropriate for detection of real finger movement. Classification results suggest that the complexity information derived may be complementary to the linear features tested. Further research is necessary to determine if methods used are applicable to imaginary movements.

# References

[1] S. J. Roberts, W. Penny, and I. Rezek. Temporal and spatial complexity measures for EEG-based brain-computer interfacing. *Med. Biol. Eng. Comput.*, 31(1):93–99, 1998.

[2] I. A. Rezek and S. J. Roberts. Stochastic complexity measures for physiological signal analysis. *IEEE Trans. Biomed. Eng.*, 45:1186–1191, 1998.

[3] V. Srinivasan, C. Eswaran, and N. Sriraam. Approximate entropy-based epileptic EEG detection using artificial neural networks. *IEEE Trans. Inf. Technol. Biomed.*, 11:288–295, 2007.

[4] S. M. Pincus. Approximate entropy as a measure of system complexity. *Prc. Natl. Acad. Sci.*, 88:2297–2307, 1991.

[5] J. Bhattacharyya. Complexity analysis of spontaneus EEG. *Acta Neurobiol. Exp.*, 60:495–501, 2001.

[6] A. Bhattacharyya. On a measure of divergence between two statistical populations defined by probability distributions. *Bull. Calcutta Math. Soc.*, 35:99–109, 1943.

[7] P. Pudil, J. Novovicova, and J. Kittler. Floating search methods in feature selection. *Pattern Recognition Lett.*, 15:1119–1125, 1994.

[8] J. C. Sprott. *Chaos and Time-Series Analysis.* Oxford University Press, 2003.

[9] H. Kantz and T. Schreiber. *Nonlinear Time Series Analysis.* Cambridge University Press, 1997.

# Comparison of three methods for adapting LDA classifiers with BCI applications

C. S. L. Tsui and J. Q. Gan

BCI Group, Department of Computing and Electronic System, University of Essex, UK

csltsu@essex.ac.uk

**Abstract**

Due to the non-stationarity of electroencephalogram (EEG) signals, online training and adaptation is essential to EEG based brain-computer interface (BCI) systems. Three methods were used to adapt linear discriminant analysis (LDA) classifiers during simulated online training for a comparative study. One method generates a new classifier based on updated means and variances of the BCI data of different classes, and the other two are Kalman filter and extended Kalman filter based methods that adapt LDA's parameters directly. Cue-based motor imagery BCI experiments were carried out with 9 naive subjects. Results show that all methods returned comparable improvement during online training, but the mean-variance updating based method is much simpler than the other two methods.

## 1 Introduction

A brain-computer interface (BCI) is a communication system in which an individual sends commands to the external world by generating specific patterns in brain signals and a computer detects and translates the brain signal patterns into commands that accomplish the individual's intention.

It is well-known that electroencephalogram (EEG) signals, particularly in EEG-based BCI systems, are non-stationary. The non-stationarities may be caused by the subject's brain conditions or dynamically changing environments. To some extent, a realistic BCI system has to be trained online and adaptive even in application phases where the true labels of ongoing EEG trials are unknown. Therefore, adaptation of feature extraction [1, 2, 3, 4] or classification is very important for BCI. Classifiers were manually updated or re-trained with new recorded data in between runs [5], or automatically updated online [6, 7, 8, 9].

This paper compares three online training methods for adapting parameter values of the linear discriminant analysis (LDA) classifiers of the BCI systems to deal with non-stationary EEG signals. Cue-based motor imagery BCI data were used to simulate online training for the purpose of comparison, so that true labels are available for supervised adaptation. The first adaptation method regenerates a new LDA classifier based on the newly updated means and variances of the BCI features of different classes. The second and third methods are Kalman filter and extended Kalman filter based adaptation methods. Experimental results shown that all methods returned comparable improvement on performance, but the first method is much simpler than the other two methods. We also investigated the issue of 'when' to adapt, by repeating the experiments with systems updated only when the prediction mismatches the true label at each trial.

## 2 Methods

### 2.1 Synchronous data acquisition and offline training

The experiments were carried out with able-bodied subjects who sat on an armchair at 1m distance in front of a computer screen. The EEG recording was made with a g.tec amplifier (Guger

Technologies OEG Austria). Five bipolar EEG channels using 10 electrodes were measured over C3 (FC3 vs. CP3), C1 (FC1 vs. CP1), Cz (FCz vs. CPz), C2 (FC2 vs. CP2), and C4 (FC4 vs. CP4). The EEG was sampled at 250 Hz.

A simple synchronous BCI paradigm, proposed by the Graz BCI Lab [10], was used to record data for training classifiers offline. The subjects were asked to imagine left versus right hand movements. The experiment consisted of 6 runs with 40 trials each. In each trial the subjects relaxed until a green cross appeared on screen at $t = 2$ s (s for second). At $t = 3$ s, a red arrow (cue) pointing either left or right direction appeared on screen for 2 seconds. The subject's task was to respond to the arrow by imagining left or right hand movements until the green cross disappeared at $t = 8$ s. The order of left and right cues was random, and there was a random interval of 2–3 seconds between trials.

Logarithmic band power features were extracted from EEG signals and used to classify the imagery movements into left or right class. Frequency bands that give good separation were manually or automatically selected for each subject. Using the selected frequency bands, EEG signals were digitally bandpass filtered, squared, averaged over a 1 second sliding window, and a natural logarithm was then applied to obtain the features. Using the extracted features and their corresponding class labels (from the cue signals), two LDA classifiers were trained, with one to distinguish left imagery movement from others (right imagery movement or no imagery movement) and the other to separate right imagery movement from others.

It was shown in the BCI competitions 2003 and 2005 that LDA performs as well as (sometimes even outperforms) non-linear classifier, and almost all the winning classifiers are linear [11]. Therefore, we chose to use and adapt LDA in this study.

## 2.2 Adaptation methods

The advantage of using LDA is that it is completely determined by means and variances of the BCI data from individual classes and the number of samples from each class. Therefore, it can be updated incrementally and robustly with new input data without explicit history of previous training data. We employ the following method [12, 13], called MCLDA, for updating means and variances that define a LDA classifier, with an additional learning parameter $C$.

$$\mu_{k|k} = \mu_{k|k-1} + C \cdot \frac{x - \mu_{k|k-1}}{N + C} \tag{1}$$

$$\Sigma_{k|k} = \frac{(N-1)\Sigma_{k|k-1} + C(x - \mu_{k|k})(x - \mu_{k|k})^T}{N + C - 1} \tag{2}$$

where $\mu_{k|k-1}$ and $\Sigma_{k|k-1}$ are the mean and variance before updating at time step $k$, and $k|k$ denotes after adaptation at time step $k$. $N$ is the number of samples, which will be increased by $C$ after the above updating. It can be seen from the above equations that the learning parameter $C$ multiplies the involvement of new data $x$ for the newly generated classifier.

On the other hand, Kalman filter based adaptation method, KALDA [7], adjusts adaptation speed dynamically in respect to the linear response from the current model, $w_{k|k-1}$ and $A_{k|k-1}$. The update equations are briefly shown below, where $p$ is the number of elements of $w_{k|k-1}$, $z$ is the current class label. As can be seen from ( 6), when a true positive trial is predicted, the algorithm enhances the classifier, otherwise, the system makes correction if the prediction is incorrect.

$$K = \frac{A_{k|k-1}x}{x^T A_{k|k-1}x + (1 - C)} \tag{3}$$

$$\widetilde{A} = A_{k|k-1} - Kx^T A_{k|k-1} \tag{4}$$

$$A_{k|k} = \mathrm{trace}(\widetilde{A}) \cdot C/p + \widetilde{A} \tag{5}$$

$$w_{k|k} = w_{k|k-1} + K(z - xw_{k|k-1}) \tag{6}$$

In extended Kalman filter (EKF) the state transition and observation models need not be linear functions but may instead be differentiable functions. Lowne et al. [14] used a logistic regression function in the observation model. The update equations for EKF are shown below:

$$P_{k|k-1} = P_{k-1|k-1} + \max\left\{u_{k-1|k} - u_{k-1|k-1}\ ,\ 0\right\} \cdot I \tag{7}$$

$$K = \frac{P_{k|k-1}x}{ux^T P_{k|k-1}x + C} \tag{8}$$

$$P_{k|k} = P_{k|k-1} - Ku(P_{k|k-1}x)^T \tag{9}$$

$$w_{k|k} = w_{k|k-1} + K(z - y) \tag{10}$$

where $u = y(1-y)$ is the uncertainty of the moderated logistic regression output $y$, $I$ is an identity matrix, and $u_{k-1|k} - u_{k-1|k-1}$ is information gain from the last update step.

# 3 Simulated online synchronous BCI experiments

We tested 3 adaptation algorithms with offline cue-based BCI data recorded using the methods described in Section 2.1. The experiments were carried out with 9 able-bodied subjects without previous BCI experience. A total of 6 runs of data, with 40 trials each, were recorded for each subject. The first 4 runs were recorded within one day, and the last 2 runs were recorded later on another day.

For each subject, a classifier was trained based on the data from the first 4 runs. Adaptation algorithms were tested on the fifth and sixth runs, with 80 testing trials in total. The benefit of the adaptation can be demonstrated because the training and testing data were recorded on different days.

Both manual and automatic feature selection methods have been tried. The same frequency bands, 7–15 Hz, 15–25 Hz and 25–45 Hz, were manually chosen for band power feature extraction for subjects S1, S2, S3, S7 and S8; Different frequency bands were chosen by automatic feature selection method for other subjects in order to achieve better classification results. Band power in 10 frequency bands was initially extracted from raw EEG signals, where 7–25 Hz was separated every 3 Hz, and 25–45 Hz was separated every 5 Hz, resulting in a vector of 10 features from each channel. For 5 channels, there are 50 features in total. The Sequential Floating Forward Selection (SFFS) method [15] was used to select up to 10 features that return the best 4 fold cross-validation performance.

In synchronous BCI the user's intention is triggered by a cue. At each trial, instead of sample-by-sample update, the data within the 2 seconds after the cue is averaged for prediction and adaptation; thus the classifier is updated once at each trial. For simplicity, we choose the start of the 2 seconds period at 1, 2, or 3 seconds after the cue, respectively for different subjects. It was selected manually based on the single trial analysis of the training data such that the chosen period gives maximum accuracy across all training trials.

The testing was performed offline in order to compare the performance of different adaptation methods, but in a way that online testing is simulated. At each trial, the prediction was made and recorded for evaluation before supervised learning adapts the classifiers for the next trial.

Two different adaptation schemes were tested. In one scheme, the adaptation can take place at every trial, so that the adaptation performs both enhancement and correction depending on whether the prediction at each trial matches the true label or not. In the other scheme, the adaptation is restricted to when the classification mismatches the true label only. By doing this, the system adjusts with correction only (without enhancement).

The experiment is evaluated by comparing the performance between with and without adaptation. Two performance indexes are provided. The first is based on event-by-event analysis, which shows the performance as if the system was running for real online application where a decision has to be made based on the predefined decision time instant or interval. The second performance index is max-accuracy, which shows the maximum accuracy that can be achieved at a proper decision time point.

| Subject | No Adapt | Always Adapt MCLDA | Always Adapt KALDA | Always Adapt EKF | Adapt when False MCLDA | Adapt when False KALDA | Adapt when False EKF |
|---|---|---|---|---|---|---|---|
| S1 | 73.75 | 76.25 | 73.75 | 73.75 | 73.75 | 76.25 | 76.25 |
| S2 | 70.00 | 70.00 | 70.00 | 75.00 | 71.25 | 70.00 | 71.25 |
| S3 | 70.00 | 72.50 | 72.50 | 75.00 | 75.00 | 70.00 | 72.50 |
| S4 | 70.00 | 72.50 | 77.50 | 72.50 | 71.25 | 77.50 | 73.75 |
| S5 | 70.00 | 70.00 | 71.25 | 70.00 | 70.00 | 71.25 | 75.00 |
| S6 | 67.50 | 67.50 | 75.00 | 68.75 | 70.00 | 67.50 | 71.25 |
| S7 | 60.00 | 63.75 | 68.75 | 63.75 | 62.50 | 62.50 | 62.50 |
| S8 | 58.75 | 63.75 | 62.50 | 65.00 | 63.75 | 63.75 | 65.00 |
| S9 | 56.25 | 61.25 | 65.00 | 63.75 | 66.25 | 65.00 | 65.00 |
| mean | 66.25 | 68.61 | 70.69 | 69.72 | 69.31 | 69.31 | 70.28 |
| variance | | 4.08 | 13.72 | 7.34 | 10.20 | 10.98 | 5.38 |
| $p$ value | | 0.003999 | 0.003490 | 0.002452 | 0.010411 | 0.012219 | 0.000407 |

Table 1: Event-by-event analysis (%).

| Subject | No Adapt | Always Adapt MCLDA | Always Adapt KALDA | Always Adapt EKF | Adapt when False MCLDA | Adapt when False KALDA | Adapt when False EKF |
|---|---|---|---|---|---|---|---|
| S1 | 76.25 | 78.75 | 76.25 | 76.25 | 77.50 | 77.50 | 78.75 |
| S2 | 73.75 | 75.00 | 78.75 | 75.00 | 76.25 | 77.50 | 77.50 |
| S3 | 73.75 | 78.75 | 75.00 | 75.00 | 76.25 | 75.00 | 77.50 |
| S4 | 72.50 | 78.75 | 75.00 | 76.25 | 73.75 | 77.50 | 77.50 |
| S5 | 72.50 | 75.00 | 72.75 | 72.50 | 72.50 | 75.00 | 75.00 |
| S6 | 70.00 | 72.50 | 71.25 | 72.50 | 71.25 | 72.50 | 72.50 |
| S7 | 67.50 | 72.50 | 71.25 | 68.75 | 70.00 | 71.25 | 72.50 |
| S8 | 65.00 | 67.50 | 68.75 | 68.75 | 66.25 | 68.75 | 66.25 |
| S9 | 63.75 | 70.00 | 67.50 | 68.75 | 70.00 | 66.25 | 68.75 |
| mean | 70.56 | 74.31 | 72.94 | 72.64 | 72.64 | 73.47 | 74.03 |
| variance | | 3.52 | 3.16 | 3.13 | 3.13 | 1.56 | 1.87 |
| $p$ value | | 0.000162 | 0.001887 | 0.003835 | 0.003835 | 0.000056 | 0.000031 |

Table 2: Maximum accuracy analysis (%).

# 4 Results

The results of the simulated synchronous online training under event-by-event analysis are given in Table 1, and under max-accuracy analysis are given in Table 2. Mean and variance of improvement and $t$-test (paired and tailed) were used to compare the effect of adaptation. In the case of event-by-event analysis, the performance was improved from 66.25 % to 68.61 % (MCLDA), 70.69 % (KALDA), and 69.72 % (EKF) when adaptation was performed at every trial (Always Adapt). EKF achieved the best $p$-value 0.00245, but MCLDA returned lowest variance on improvement at 4.08 %. A 70.28 % accuracy was achieved by EKF when the system adapted only when the prediction was incorrect at each trial (Adapt when False), and the lowest variance on improvement and $p$-value were also achieved by EKF at 5.38 % and 0.00041 respectively.

The improvement under the maximum accuracy analysis is similar. The system was improved from 70.56 % to 74.31 % (MCLDA), 72.94 % (KALDA), and 72.64 % (EKF) when adaptation was performed at every trial. MCLDA returned the best averaged accuracy and lowest p-value at 0.00016, and KALDA and EKF acheived marginally lower variance of improvement. When the system was adapted only when the prediction was incorrect at each trial, EKF achieved the highest overall improvement with 74.03 % accuracy and lowest $p$-value at 0.000031.

Good improvements are achieved by subjects whose performance were low when there were no adaptation. Subject 8 produced 58.75 % without adaptation, and the improvement by adaptation

| | Event-by-Event | | Maximum Accuracy | |
|---|---|---|---|---|
| | Always | False | Always | False |
| MCLDA vs KALDA | 0.0502(KALDA) | 0.5000(same) | 0.0666(MCLDA) | 0.1497(KALDA) |
| MCLDA vs EKF | 0.0768(EKF) | 0.1140(EKF) | 0.0111(MCLDA) | 0.0106(EKF) |
| KALDA vs EKF | 0.2375(KALDA) | 0.1221(EKF) | 0.3063(KALDA) | 0.1561(EKF) |

Table 3: $t$-test on methods against each other. At each entry, the method with higher mean value is shown in a basket. Always: always adapt adaptation scheme. False: adapt when false only adaptation scheme.

was 6.25 % by EKF under event-by-event analysis for both adaptation schemes. Similarly for Subject 9, the improvements for different adaptation schemes were up to 8.75 % and 10 % respectively under event-by-event analysis by different adaptation methods.

On the other hand, adaptation offers less improvement for subjects who have already achieved good accuracy without adaptation. For instance, the result for Subject 1 was improved by 2.5 % by KALDA and EKF with correction only adaptation scheme. Performance improvements for other subjects vary from 1.25 % to 5 %.

Overall, both performance indexes have demonstrated that better results have been achieved with correction only adaptation.

We preformed $t$-test to show the improvement from each adaptation method against no-adaption. It was also used to compare the three adaptation methods, each against another (see Table 3). Since the $t$-test is non-directional, the method achieved higher mean value is shown at each comparison. It can be seen that EKF beats KALDA and MCLDA on performance indexes under "Adapt when False" adaptation scheme, with 0.0106 being the lowest $p$-value against MCLDA. KALDA beats EKF when the system always adapt, but only marginally in terms of mean and $p$-values. MCLDA performs better than KALDA and EKF under Maximum Accuracy analysis when the system always adapt, with relatively low $p$-value at 0.0666 and 0.0111. Roughly speaking, these three methods achieve comparable performance.

# 5 Conclusion

We tested 3 adaptation methods to update LDA's parameters online at each trial. It is clear that all adaptation methods are able to return good increases in performance, even with short online training period. While no method performs significantly better than others, EKF seems to perform better with lowest $p$-value from 3 out of 4 tests, and highest accuracy improvement from 2 out of 4 tests. This is also confirmed when T-test was carried out to compare the methods with one against another. KALDA returned highest improvement for some subjects (S4, S7 and S9). The performance of MCLDA is similar to that of KALDA or EKF, while its implementation is simpler.

In this paper, a cue-based BCI system was used for our experiments. Our ongoing work is to implement adaptive classifier for self-paced BCI. It is a great challenge to train and adapt a self-paced BCI online because the user's control intention and timing are usually unknown to the self-paced BCI system. Furthermore, the system should be switched to unsupervised learning once the online training reaches a satisfactory level, or true labels are unavailable.

**Acknowledgments:** The authors would like to thank Matthew Dyson, Tao Geng, and Steve Roberts for constructive discussions and comments.

# References

[1] R. Tomioka, G. Dornhege, K. Aihara, and K.-R. Müller. An iterative algorithm for spatio-temporal filter optimization. In *Proc. 3rd Int. Brain-Computer Interface Workshop*, pages

22–23, Graz, Austria, September 2006.

[2] S. Sun and C. Zhang. Adaptive feature extraction for EEG signal classification. *Med. Biol. Eng. Comp.*, 44(10):931–935, 2006.

[3] M. Grosse-Wentrup, K. Gramann, and M. Buss. Adaptive spatial filters with predefined region of interest for EEG based brain-computer interfaces. In B. Schoelkopf and J. C. Platt, editors, *19th Advances in Neural Information Processing Systems (NIPS)*, pages 537–544, Cambridge, 2007. MIT Press.

[4] J. Farquhar. Learning optimal EEG features across time, frequency and space. In B. Schoelkopf and J. C. Platt, editors, *19th Advances in Neural Information Processing Systems (NIPS)*, Cambridge, 2007. MIT Press.

[5] G. Pfurtscheller, C. Neuper, C. Guger, W. Harkam, H. Rampser, A. Schlögl, B. Obermaier, and M. Pregenzer. Current trends in graz brain-computer interface (BCI) research. *IEEE Trans. Rehabil. Eng.*, 8(2):216–219, 2000.

[6] A. Buttfield, P. W. Ferrez, and J. del R. Millán. Towards a robust BCI: Error potentials and online learning. *IEEE Trans. Neural Syst. Rehabil. Eng.*, 14(2):164–168, 2006.

[7] C. Vidaurre, A. Schlögl, R. Cabeza, R. Scherer, and G. Pfurtscheller. Study of on-line adaptive discriminant analysis for EEG-based brain computer interfaces. *IEEE Trans. Biomed. Eng.*, 54(3):550–556, 2007.

[8] J. del R. Millán. On the need for on-line learning in brain-computer interfaces. In *Int. Joint Conf. Neural Networks (IJCNN)*, pages 2877–2882, Budapest, 2004.

[9] P. Sykacek, S. Roberts, and M. Stokes. Adaptive BCI based on variational Bayesian Kalman filtering: An empirical evaluation. *IEEE Trans. Biomed. Eng.*, 51(5):719–729, 2004.

[10] G. Pfurtscheller and C. Neuper. Motor imagery and direct brain-computer communication. *Proc. IEEE*, pages 1123–1134, 2001.

[11] B. Blankertz, K.-R. Müller, D.J. Krusienski, G. Schalk, J.R. Wolpaw, A. Schlögl, G. Pfurtscheller, J. del R. Millán, M. Schröder, and N. Birbaumer. The BCI competition III: Validating alternative apporaches to actual BCI problems. *IEEE Trans. Neural Syst. Rehabil. Eng.*, 14(2):153–159, 2006.

[12] J. Q. Gan. Self-adapting BCI based on unsupervised learning. In *Proc. 3rd Int. Brain-Computer Interface Workshop*, pages 50–51, Graz, Austria, September 2006.

[13] D. H. D. West. Updating mean and variance estimates: An improved method. *Communications of the ACM*, 22(9):532–535, 1979.

[14] D. R. Lowne, C. J. Haw, and S. J. Roberts. An adaptive, sparse-feedback EEG classifier for self-paced BCI. In *Proc. 3rd Int. Brain-Computer Interface Workshop*, pages 58–59, Graz, Austria, September 2006.

[15] P. Pudil, J. Novovicova, and J. Kittler. Floating search methods in feature-selection. *Patt. Recogn. Lett.*, 15:1119–1125, 1994.

# Unsupervised adaptation of the LDA classifier for brain-computer interfaces

C. Vidaurre[1], A. Schlögl[2], B. Blankertz[3,1], M. Kawanabe[1], K.-R. Müller[3,1]

[1]Intelligent Data Analysis, Fraunhofer FIRST, Berlin, Germany
[2]Institute for Human Computer Interfaces, Graz University of Technology, Graz, Austria
[3]Department of Machine Learning, Berlin Institute of Technology, Berlin, Germany

carmen.vidaurre@first.fraunhofer.de

**Abstract**

This paper discusses simulated on-line unsupervised adaptation of the LDA classifier in order to counteract the harmful effect of non-class related non-stationarities in EEG during BCI sessions. Three types of adaptation procedures were applied to the two large BCI data sets from TU Graz and Berlin BCI project. Our results demonstrate that the unsupervised adaptive classifiers can improve performance substantially under different BCI settings. More importantly, since label information is not necessary, they are applicable to wide ranges of practical BCI tasks.

## 1 Introduction

A Brain Computer Interface (BCI) has to be robust against non-stationary changes [1] or adapted to these [2, 3, 4]. Some BCI users, especially at early training stages, might not generate stable EEG patterns. The system requires then supervised classifiers that can "follow" unexpected class-related changes of EEG and successfully help in the learning process [2]; however, class information is usually not available in practical BCI tasks. On the other hand, when subjects can generate stable patterns, task related EEG information might not change so drastically, but different electrode montages or task unrelated factors affect the signals. In this case, class information might not be required for the adaptation of the system. This motivated us to study whether unsupervised adaptation based on extra assumptions works in practical BCI scenarios. In BCI experiments one of the main problems from session to session or from calibration to feedback within the same session, is the bias adaptation. Typically the features move in the feature space and the classifier should be re-adjusted [2, 4, 5]. Even during a feedback session the bias must be recalculated after some time. When a subject generates almost stable patterns, one could expect the change between the vectors connecting the two class means to be small. This difference can be measured by the angle formed between the vectors connecting the mean values of each class (see Figure 1(b)).

All data processing methods used in this paper are causal and suitable for on-line and real-time realization. We describe adaptive unsupervised classifiers based on the simple and robust linear discriminant analysis (LDA). For this we exploit the fact that adapting parameters of LDA without label information is possible. The improvement in performance on two large data sets using these classifiers indicates that there exist underlying background activity that negatively affects the system performance, but that can be counteracted with the proposed methods.

# 2 Material and methods

## 2.1 The datasets

### 2.1.1 Graz data

Experiments were carried out with 21 subjects without previous BCI experience. They performed motor imagery of the left and right hand to control a “basket feedback”, [6]. Each subject conducted three sessions of 9 runs and 40 trials per run (we used second and third sessions). Two bipolar channels, C3 and C4 were recorded.

### 2.1.2 BBCI data

We took 19 datasets recorded from 10 subjects who performed motor imagery (left-right hand, right foot) according to visual cues without feedback. The pair of tasks with best discrimination was chosen. These datasets were used because they revealed non-stationarities in a previous study [7]. Brain activity was recorded with multi-channel EEG using 55 Ag/AgCl electrodes.

## 2.2 Feature extraction techniques

We selected a standard choice in each laboratory: Adaptive autoregressive parameters (AAR) for the Graz data and Common spatial patterns (CSP) for the BBCI data.

### 2.2.1 Adaptive autoregressive parameters

To extract AAR parameters from the EEG [8], an adaptive filter based on a stable version of Recursive Least Squares (RLS) was used. AAR parameters of model order 5 were computed from two bipolar channels over C3 and C4. The logarithmic variance of the innovation process (which resulted from the adaptive filtering used) was also concatenated because it provides further information, see formula of the auto-regressive spectrum.

### 2.2.2 Common spatial patterns (CSP)

CSP is a technique to analyze multichannel data based on recordings from two classes (tasks). It yields a data-driven supervised decomposition of the signal $\boldsymbol{x}(t)$ parameterized by a matrix $\boldsymbol{W}$ that projects the signal in the original sensor space to a surrogate sensor space $\boldsymbol{x}_{\mathrm{CSP}}(t)$, [9]: $\boldsymbol{x}_{\mathrm{CSP}}(t) = \boldsymbol{x}(t) \cdot \boldsymbol{W}$. Each column vector of a $\boldsymbol{W}$ is a spatial filter. CSP filters maximize the variance of the spatially filtered signal under one task while minimizing it for the other task. Since the variance of a band-pass filtered signal is equal to band-power, CSP analysis is applied to band-pass filtered signals to obtain an effective discrimination of mental states that are characterized by ERD/ERS effects. Detailed information about this technique can be found in [9].

## 2.3 Classifiers

We concentrate on a binary classification problem with linear classifiers which are specified by discriminant functions. LDA assumes the covariance matrices of both classes to be equal, $\boldsymbol{\Sigma}$. We denote the means by $\boldsymbol{\mu}_1$ and $\boldsymbol{\mu}_2$, and arbitrary feature vector by $\boldsymbol{x}$ and define:

$$
\begin{aligned}
D(\boldsymbol{x}) &= [b; \boldsymbol{w}]^T \cdot [1; \boldsymbol{x}] && (1)\\
\boldsymbol{w} &= \boldsymbol{\Sigma}^{-1} \cdot (\boldsymbol{\mu}_2 - \boldsymbol{\mu}_1) && (2)\\
\boldsymbol{b} &= -\boldsymbol{w}^T \cdot \boldsymbol{\mu} && (3)\\
\boldsymbol{\mu} &= \frac{1}{2} \cdot (\boldsymbol{\mu}_1 + \boldsymbol{\mu}_2) && (4)
\end{aligned}
$$

Then $D(\boldsymbol{x})$ is the difference in the distance of the feature vector $\boldsymbol{x}$ to the separating hyperplane described by its normal vector $\boldsymbol{w}$ and the bias $b$. If $D(\boldsymbol{x})$ is greater than 0, the observation $\boldsymbol{x}$ is classified as class 2 and otherwise as class 1. Note that using a "pooled covariance matrix" instead of an averaged one does not affect the classification result. We consider five on-line aptation schemes: two of them require label information (supervised) and the other three can update the classifier without knowing performed tasks.

#### 2.3.1 Supervised adaptive LDA

In the supervised scenario, we can update the class means $\boldsymbol{\mu}_1$, $\boldsymbol{\mu}_2$ and the common covariance matrix $\boldsymbol{\Sigma}$ in on-line manner. LDA relies on the inverse $\boldsymbol{\Sigma}^{-1}$ of the covariance matrix $\boldsymbol{\Sigma}$ (see (2) and (3)), which can be recursively estimated applying the matrix inversion lemma, where UC is the update coefficient and $\boldsymbol{x}(t)$ is the current sample vector without the mean.

$$\boldsymbol{\Sigma}(t)^{-1} = \frac{1}{(1-\mathrm{UC})} \cdot \left( \boldsymbol{\Sigma}(t-1)^{-1} - \frac{1}{\frac{1-\mathrm{UC}}{\mathrm{UC}} + \boldsymbol{x}(t)^T \cdot \boldsymbol{v}(t)} \cdot \boldsymbol{v}(t) \cdot \boldsymbol{v}(t)^T \right) \tag{5}$$

with $\boldsymbol{v}(t) = \boldsymbol{\Sigma}(t-1)^{-1} \cdot \boldsymbol{x}(t)$. Note, the term $\boldsymbol{x}(t)^T \cdot \boldsymbol{v}(t)$ is a scalar, and no costly matrix inversion is needed. To estimate the class-specific adaptive mean $\boldsymbol{\mu}_1(t)$ and $\boldsymbol{\mu}_2(t)$ one can use:

$$\boldsymbol{\mu}_i(t) = (1-\mathrm{UC}) \cdot \boldsymbol{\mu}_i(t-1) + \mathrm{UC} \cdot \boldsymbol{x}(t) \quad \text{with } i := \text{class of } \boldsymbol{x}(t) \tag{6}$$

We also consider a simpler adaptive classifier (Mean classifier) which only updates the class means $\boldsymbol{\mu}_1$ and $\boldsymbol{\mu}_2$ by (6), while the covariance matrix $\boldsymbol{\Sigma}$ is kept constant.

#### 2.3.2 Unsupervised adaptive LDA I: common mean changes

As shown in [10], there are changes which affect the mean of the features. One can modify part of the bias given in (3) by adapting the common mean $\boldsymbol{\mu}(t)$ (the average of the two class means). We update the global mean $\boldsymbol{\mu}(t)$ by the same rule as (6) except that all trials from both tasks are used. This classifier is called CMean in this paper.

$$b(t) = -\boldsymbol{w}^T \cdot \boldsymbol{\mu}(t) \tag{7}$$

#### 2.3.3 Unsupervised adaptive LDA II: common mean and covariance changes

We update the global mean and covariance matrix (CMean-CCov classifier), and keep the difference between the two class means constant. We estimate the inverse of the "pooled covariance matrix" for which no class information is needed, as in (5). We only need to substract the common mean estimator to the current feature vector $\boldsymbol{x}(t)$. The LDA bias and weights are modified:

$$\boldsymbol{w}(t) = \boldsymbol{\Sigma}(t)^{-1} \cdot (\boldsymbol{\mu}_2 - \boldsymbol{\mu}_1) \quad b(t) = -\boldsymbol{w}(t)^T \cdot \boldsymbol{\mu}(t) \tag{8}$$

#### 2.3.4 Unsupervised adaptive LDA III

A scaling happening in the feature space can be accounted for by using a parallel formula to that explained in [11] for the case of adaptive CSP filters:

$$\boldsymbol{w}(t) = \boldsymbol{\Sigma}(t)^{-1/2} \cdot \boldsymbol{\Sigma}^{-1/2} \cdot (\boldsymbol{\mu}_2 - \boldsymbol{\mu}_1) \quad b(t) = -\boldsymbol{w}^T \cdot \boldsymbol{\mu}(t) \tag{9}$$

In which one should use the "normalization assumption" of [11].

$$\boldsymbol{\Sigma}(t)^{-1/2} \cdot (\boldsymbol{\mu}_2 - \boldsymbol{\mu}_1) \quad = \quad \boldsymbol{\Sigma}^{-1/2} \cdot (\boldsymbol{\mu}_2 - \boldsymbol{\mu}_1) \tag{10}$$

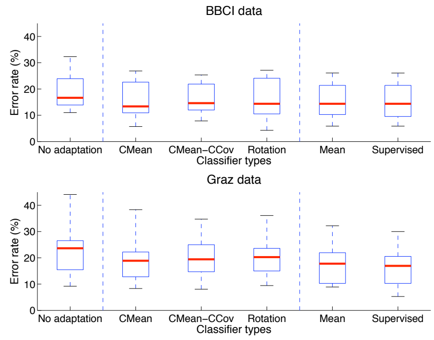


(a) Percentiles 5, 25, 50, 75 and 95 of error rates for the two data sets. No adaptation is separated from unsupervised versions and these from the two supervised classifiers.

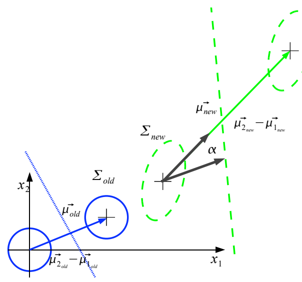

(b) Angle $\alpha$ between vectors connecting the two means, features were recorded at two different moments.

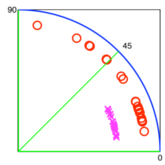


(c) Angles between training and testing data.

Figure 1: Left plot: percentiles of classification error rates. Middle plot: angle formed between the vectors connecting the mean values of the two classes at two different time points. Right plot: computed angles for the two datasets.

#### 2.3.5 Parameter selection

For each method, the update coefficient UC, the number of samples used to adapt the classifiers and the initial time for adaptation had to be selected (see [2]). All tuning parameters of "Graz data" were optimized based on the runs in session 2 for each subject and applied to session 3. The initial classifiers were calculated using the data from the previous session. For "BBCI data", the sessions were divided into two halves. The parameters were optimized in the first half and applied to the second one.

### 2.4 Investigating the nonstationarities

The proposed unsupervised adaptive LDAs (Section 2.3.2–2.3.4) are based on the assumption that the means of the two feature distributions drift in a similar way, i. e. the difference between the two means is nearly constant. In order to quantify the validity of this assumption, the angle formed between the vectors connecting the mean values of each class of the first half and the corresponding vector of the second half is determined for each dataset.

## 3 Results

Figure 1(c) summarizes the results of the angles computed for every dataset. With "Graz data" the mean values were calculated using the data of session 2 for the first vector and session 3 for the second. With the "BBCI data" we used the first half against the second.

Figure 1(a) shows the percentiles 5, 25, 50, 75 and 95 of the classifiers. A significance test with a Sidak corrected $p$-value for multi-comparison of 1.74 % revealed that no adaptation is significantly worse than all the other options. The supervised classifier was found significantly better than the rest of classifiers. Adapting the mean with and without class information did not show significant differences, although using class-labels for adapting the mean was better than CMean-CCov and Rotation classifiers. However, no differences were found between CMean and CMean-CCov, although Rotation was worse than the first one. Finally, no significant differences showed between CMean-CCov and Rotation.

Figure 2 depicts error rates of each of the classifiers versus no adaptation except in the bottom-right corner, where the mean and common mean classifiers are compared. The time in which the

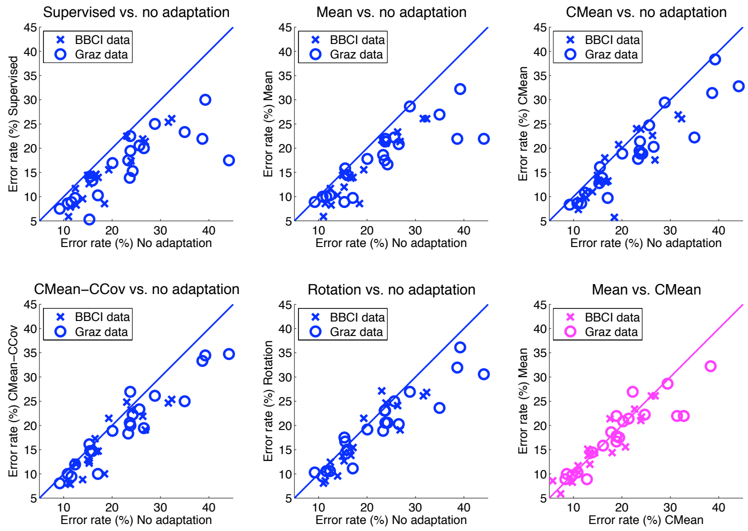


Figure 2: Comparison of classifiers based in error rates. All of them are compared to no adaptation except the bottom-right corner, in which adaptation with and without class labels are compared.

performance was calculated was fixed beforehand to assure causality of the results. The values below the diagonal mean that the classifier of the y-axis performs better than the one of the x-axis.

# 4 Discussion

Results presented in Figure 1(c) show that angles for BBCI subjects vary from 8 to 25 degrees. The features used were not adaptive and were computed with a fixed spatial filter after which band power estimates in a narrow band were calculated. Some of the subjects were naive, but did not present bigger angle-differences than experienced ones. Also, the two datasets used to estimate this difference come from the same session which would be an explanation for the small change. However, this is a realistic setting because many BCI systems record calibration and feedback runs in the same session. In contrast, all Graz subjects were inexperienced, besides the features were adaptive. These subjects show angles varying from 9 to 81 degrees.

Figures 1(a) and 2 suggest that supervised adaption is the best option, followed by the supervised adaptation of the means. All unsupervised classifiers seem to perform very similarly, with a slight advantage of the CMean classifier, which might be due to a lower number of parameters to be adapted. It is interesting to note that adapting means with and without class-labels was not found significantly different, which is explained by the small difference between the vectors connecting the two means (small angles) found in most of the subjects. Looking at the comparison between the Mean and CMean classifiers in Figure 2 one can see that especially for 4 subjects (all of them from the Graz dataset) Mean was better than CMean. Finally, the Rotation classifier exhibits the worst average error rate of the unsupervised classifiers, and was found to be significantly worse than CMean. This might be caused because the assumptions to define problem are too strong.

# 5 Conclusion

When operating a BCI there is considerable fluctuation in the underlying statistics. This observation is subject- and even task-dependent. Compensating such non-stationary effects and investigating their underlying cause is an important mile-stone on the way to more robust BCI systems. Our focus in this paper is to study non-task related fluctuations, for which unsupervised data analysis methods can contribute to compensating such non-stationarity. We consider three unsupervised classifiers that are shown to successfully counteract the effect of non-class related EEG changes. These unsupervised classifiers can perform well under very different settings using CSP or AAR features for preprocessing and training and test sets from within the same session and from different ones. This is in line with the small fluctuations that can be found when analysing the change in the vectors that connect the class means at different time points. In other words, for the majority of subjects considerable signal variation is task unrelated and can thus be tackled in an unsupervised manner.

**Acknowledgments:** Work supported by the EU Marie Curie grant 040666 FP6, the BMBF, FKZ 01IBE01A/B, and by the IST Programme of the European Community, under the PASCAL2 Network of Excellence, ICT-216886. This publication only reflects the authors' views.

## References

[1] B. Blankertz, M. Kawanabe, R. Tomioka, F. Hohlefeld, V. Nikulin, and K.-R. Müller. Invariant common spatial patterns: Alleviating nonstationarities in brain-computer interfacing. In *Ad. in NIPS 20*. MIT Press, Cambridge, MA, 2008. in press.

[2] C. Vidaurre, A. Schlögl, R. Scherer, R. Cabeza, and G. Pfurtscheller. Study of on-line adaptive discriminant analysis for EEG-based brain computer interfaces. *IEEE Trans. Biomed. Eng.*, 54:550–556, 2007.

[3] M. Sugiyama, M. Krauledat, and K.-R. Müller. Covariate shift adaptation by importance weighted cross validation. *JMLR*, 8:1027–1061, 2007. accepted.

[4] J. del R. Millán, A. Buttfield, C. Vidaurre, R. Cabeza, A. Schlögl, G Pfurtscheller, P. Shenoy, P. N. Rao, and B. Blankertz. Adaptation in brain-computer interfaces. In *Toward Brain-Computer Interfacing*, pages 303–326. MIT Press, Cambridge, MA, 2007.

[5] J. Blumberg, J. Rickert, S. Waldert, A. Schulze-Bonhage, A. Aersten, and C. Mehring. Adaptive classification for brain computer interfaces. In *Proc 29th Ann Int Conf of the IEEE EMBS*, pages 2536–2539, 2007.

[6] G. Krausz, R. Scherer, G. Korisek, and G. Pfurtscheller. Critical decision-speed and information transfer in the Graz brain-computer-interface. *Appl. Psychophysiol. Biofeedback*, 28:233–240, 2003.

[7] M. Krauledat. *Analysis of Nonstationarities in EEG signals for improving BCI performance*. PhD thesis, TU-Berlin, Fakult. IV – Elektrotech. und Inf., 2008.

[8] A. Schlögl. *The electroencephalogram and the adaptive autoregressive model: theory and applications*. Shaker Verlag, Aachen, Germany, 2000.

[9] B. Blankertz, R. Tomioka, S. Lemm, M. Kawanabe, and K.-R. Müller. Optimizing spatial filters for robust EEG single-trial analysis. *IEEE Sign. Process Mag.*, 25:41–56, 2008.

[10] M. Kawanabe, M. Krauledat, and B. Blankertz. A bayesian approach for adaptive BCI classification. In *Proc. 3rd Int. BCI Workshop and Training Course*, pages 54–55, 2006.

[11] R. Tomioka, J. Hill, B. Blankertz, and K. Aihara. Adapting spatial filtering methods for nonstationary BCIs. In *Proc. of IBIS2006)*, pages 65–70, 2006.

# Recognition of anticipatory behavior from human EEG

G. Gangadhar[1,2], R. Chavarriaga[1], J. del R. Millán[1,2]

[1]IDIAP Research Institute, Rue Marconi 19, C.P. 592, CH-1920 Martigny, Switzerland
[2]Ecole Polytechnique Fédérale de Lausanne, Lausanne, Switzerland

gangadhar.garipelli@idiap.ch

**Abstract**

Anticipation increases the efficiency of a daily task by partial advance activation of neural substrates involved in it. Single trial recognition of this activation can be exploited for a novel anticipation based Brain Computer Interface (BCI). In the current work we compare different methods for the recognition of Electroencephalogram (EEG) correlates of this activation on single trials as a first step towards building such a BCI. To do so, we recorded EEG from 9 subjects performing a classical Contingent Negative Variation (CNV) paradigm (usually reported for studying anticipatory behavior in neurophysiological experiments) with GO and NOGO conditions. We first compare classification accuracies with features such as Least Square fitting Line (LSFL) parameters and Least Square Fitting Polynomial (LSFP) coefficients using a Quadratic Discriminant Analysis (QDA) classifier. We then test the best features with complex classifiers such as Gaussian Mixture Models (GMMs) and Support Vector Machines (SVMs).

## 1 Introduction

Anticipation is a process that not only depends on past and current states but also on future expectations. Without anticipation everyday cognitive tasks would become exclusively reactive. Conversely, this process increases the efficiency of daily tasks by partial advance activation of the neural substrates involved [1]. We hypothesize that the recognition of this activation can be exploited for Brain Computer Interaction (BCI). For example, consider a scenario of a brain-actuated wheelchair [2] driving towards a table with breakfast lying among several other tables. Using the onboard sensors the intelligent controller in the wheelchair can detect the presence of a table in front but it cannot decide by itself whether to dock or avoid. If the controller is integrated with anticipation recognition algorithms, the user can issue the docking command just by anticipating the docking event to happen. Otherwise, the controller triggers the obstacle avoidance behavior.

To the best of our knowledge, anticipation related potentials in human EEG are well studied in the context of clinical science and functional neurophysiological studies [3] but not well explored in the context of BCI, excepting one early attempt based on neurofeedback [4]. In the current work we compare different methods for the recognition of these potentials on single trials as a first step towards the design of an anticipation-based BCI.

To record these potentials we have considered a classical Contingent Negative Variation (CNV) paradigm [3] as an experimental procedure. A vast amount of literature describes the CNV potentials (the potentials recorded using CNV paradigm) as related to anticipation [3, 5, 6]. In this paradigm a warning stimulus (S1) predicts the appearance of an imperative stimulus (S2) in a predictable inter-stimulus-interval (ISI). A negative shift in the cortical activity with a centro-medial distribution (under the vertex electrode, Cz) usually develops between S1 and S2 depending on contingency of stimuli and task parameter relevance [5, 6]. This signal has been shown to be stable over several days and in different conditions (e. g., amount of sleep time) [5]. In addition, one neurofeedback experiment suggests that humans are able to modulate its amplitude [4]. The stability of this potential, and the human's ability to modulate its amplitude, support the possibility of using this phenomenon for the design of anticipation-based BCI. To this end, it is first necessary to ascertain the feasibility of achieving reliable recognition of CNV potentials on single trials; this is the goal of the present study. In the following sections we describe the experimental setup, along with classification techniques used in recognizing these potentials.

# 2 Methods

## 2.1 Experimental setup

We used the CNV paradigm with relevant (GO) and irrelevant (NOGO) conditions for simulating anticipatory and non-anticipatory behaviors (e. g., the table with food corresponds to a relevant condition). Figure 1(a) and Figure 1(b) describe the CNV paradigm used in the current study. The EEG signals of nine male subjects (22–27 years) were recorded in four consecutive sessions with 50 trials each (equiprobable GO and NOGO trials in random order separated by an inter-trial interval of $4 \pm 4\,\mathrm{s}$).

## 2.2 Data acquisition and preprocessing

The EEG signals were acquired for 9 subjects using 32 (subjects 4, 5 and 9) or 64 (remaining 6 subjects) electrodes according to the 10/20 international system with a sampling rate of 512 Hz. Raw EEG signals were first spatially filtered by using common average reference (CAR). The signals were then filtered using a low pass filter with cut off frequency of 15 Hz and then the trials were extracted and separated into GO and NOGO trials using S1 as the reference (i. e., onset of S1 considered as at 0.0 s) with $[-1.0, 5.0]\,\mathrm{s}$ as total trial interval. Average voltage of the time window from $-1000\,\mathrm{ms}$ to $0\,\mathrm{ms}$ was used as a baseline.

## 2.3 EEG grand averages

The EEG grand averages at Cz electrode computed over subjects for GO and NOGO conditions show clear differences (see Figure 1(c) for grand averages using 64 electrode set-up). Similar differences are observed in the case of 32 electrode set-up. From the topographic plots of average scalp distribution we observed an increasing negativity under this electrode in GO condition and a smaller negativity in NOGO condition. An evoked response due to S1 is observed at this electrode around 0.3 s to 0.4 s in both conditions. The potential at Cz during GO condition is composed of an early peak around 1s and a late peak between 3.5 s and 4.0 s which is consistent with previous studies [6]. Although clear differences are observed in grand averages, the use of these potentials for BCI imposes the challenge of recognizing them on single trial. The methods developed for addressing these challenges are described in the next section.

# 3 Classification

As the subjects were instructed to press a button on the arrival of S2 (at 4 s) the recognition methods evaluated here are based on the EEG potentials up to 3.5 s after the onset of S1 (0.0 s) in order to avoid any movement preparation potential that could contaminate the recognition of anticipation processes. In the scope of the current work we restrict to features computed from the potential at Cz electrode alone ($v_{\mathrm{Cz}}(t)$, where $t$ is time, $t \in [0\ \ T_{\max}]$ and $T_{\max} = 3.5\,\mathrm{s}$).

## 3.1 Feature selection

Since slope and peak negativity are usually reported as features of CNV potentials [1], we first test Least Square Fitting Line (LSFL) parameters with the help of a Quadratic Discriminant

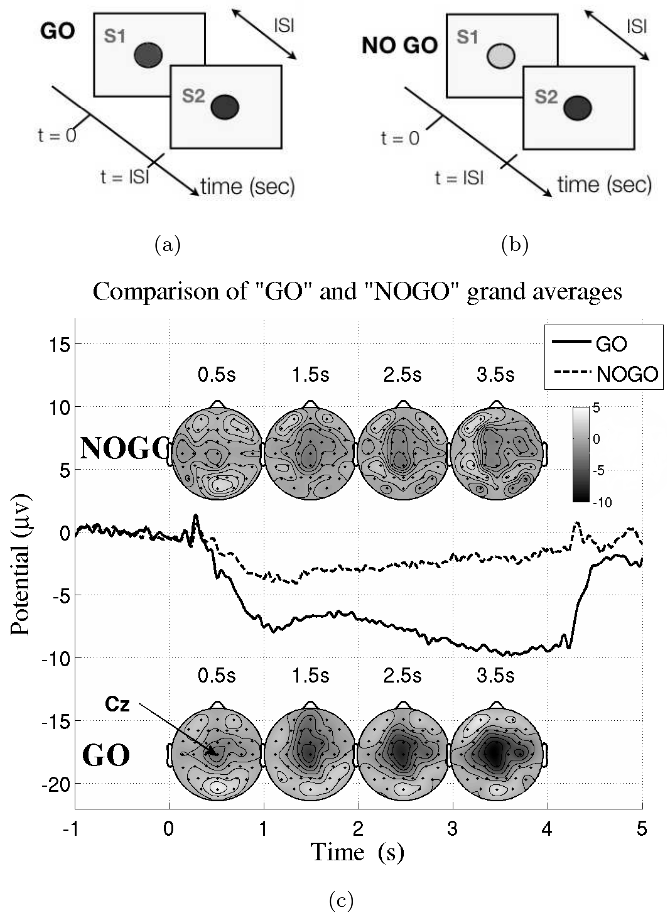


(a) (b)

(c)

Figure 1: CNV experimental setup and ERP grand averages. (a) In the GO condition a warning stimulus (S1) with a green dot at time $t = 0\,\mathrm{s}$ is displayed and then an imperative stimulus (S2) with a red dot on the screen is presented with ISI of 4 s. Subjects are instructed to anticipate and press a button as soon as S2 is presented. (b) To differentiate the NOGO condition from the GO condition S1 is replaced with a yellow dot. The subjects are instructed to do nothing for this condition. (c) The grand averages of GO and NOGO trials for six subjects recorded with 64 electrode configuration at Cz electrode. The circular figures are the topographic representation of average scalp distribution at different time scales for GO (bottom) and NOGO (top) conditions.

Analysis (QDA) classifier. We then compare higher order features such as Least Square Fitting Polynomial (LSFP) features computed as the coefficients of $n^{\text{th}}$ order LSFP ($\alpha_i$, where $i = 1 \ldots n$ of $\tilde{v}_{\text{Cz}} = \alpha_0 + \alpha_1 t^1 + \alpha_2 t^2 + \ldots + \alpha_n t^n$). Each trial is then described by feature vector, $\mathbf{x} = [\alpha_0 \;\; \alpha_1 \;\; \alpha_2 \;\; \ldots \;\; \alpha_n]^T$, where $\mathbf{x} \in \mathbb{R}^{n+1}$. The best polynomial order for each subject is chosen by comparing training accuracies of classifiers calculated for $n \in \{2, 3, \ldots, 6\}$ (the maximal order for search is 6 due to the limited amount of training samples). The LSFL features are equivalent to the LSFP features with order one.

## 3.2 Classifiers

We compare classification of anticipation related potentials using the features described above with the help of different classifiers described in the following paragraphs. Due to space limitations we give only a very brief introduction of these classifiers.

**Quadratic Discriminant Analysis (QDA).** Similar to Linear Discriminant Analysis (LDA) classifier, the QDA classifiers assumes that the features are normally distributed and relaxes the assumption that the covariance of each class is identical. For the current problem, we first project the features onto a canonical space with the help of a projection matrix, that maximizes between-class variance and minimizes within-class variance, which can be obtained by maximizing Fisher's criterion [7]. We then calculate QDA classifiers on the projected features.

**Gaussian Mixture Model (GMM).** The GMM is a generative model widely used for clustering and classification applications. In the current study we first model each class distribution with a separate GMM and using these models we build a classifier. The initial estimates of means are obtained using a $k$-means algorithm and we then use the Expectation Maximization (EM) algorithm [7] for estimating the mean ($\boldsymbol{\mu_k}$), covariance ($\boldsymbol{\Sigma_k}$) and mixing coefficients ($\pi_k$) of each Gaussian component of the GMM. Due to limited number of training samples we reduce the number of free parameters to estimate by constraining the covariance matrix to be diagonal and sharing it among all the components. The best number of Gaussian components for each subject is obtained by exhaustive search in the range $\{1, 2, \ldots, 4\}$ based on training accuracies. Since this classifier suffers from the problem of local minima for complex data that are not well clustered, we built 100 different models with random initial Gaussian centers. The best model from all the 100 models was then chosen using the training accuracy and considered for testing with test data.

**Support Vector Machine (SVM).** SVMs are supervised learning methods that simultaneously minimize empirical classification error and maximize the geometrical margin between two classes [8]. In the present study we report classification results based on linear kernel (SVM-linear) and Radial Basis Function kernel (SVM-RBF). The free parameters of the classifier are estimated by 10-fold cross validation on training trials.

# 4 Results

To assess the classification performance across sessions we did a 4-fold cross-validation study where each fold corresponds to a separate session. The results of this study are summarized in Table 1. We first did feature comparison with the help of QDA classifiers trained separately for each subject. We observed that the LSFP features outperform the LSFL features (Wilcoxon test $p = 0.01$, over all the subjects and sessions), suggesting that these features describe the anticipation related potential better than the LSFL features that are usually computed for the characterization of the CNV potential in neurophysiological studies [1, 4]. It is worth noting that no specific differences are observed for EEG setup with 32 or 64 electrodes.

Since LSFP features performed better, we tested them on the other complex classifiers such as GMM and SVM-linear and SVM-RBF classifiers to compare with the performance of the QDA classifier (see Table 1). The classification accuracies of the QDA classifier are significantly better than the other three classifiers (Wilcoxon test, $p = 0.01$ among all the subjects and sessions). Coming to individual subjects, the accuracies for subjects 6, 8 and 9 are close to random for all the methods. For subjects 1, 2, 3 and 5 the QDA classifier with LSFP features performed significantly better than the other classifiers (the best being subject 5, $75.86 \pm 6.45\,\%$). On average the SVM classifier with linear kernel is the next best classifier. However, this classifier gives accuracies above $65\,\%$ only for one subject whereas the QDA classifier does so for 3 subjects. The SVM classifier with RBF kernel and GMM classifier perform worse compared to the QDA classifier.

Although the QDA classifier with LSFP features performs best compared to all the other methods, the results of cross-validation show that the recognition method is not reliable enough for a BCI. Nevertheless, most subjects exhibit an increasing performance over sessions (we excluded the subjects 6, 8 and 9 from this study due to the classification accuracies are close to random in all sessions with all the classifiers). Figure 2 illustrates this trend with the help of accuracies averaged over all the 6 subjects separately for each session. The accuracies in the 3$^{\text{rd}}$ and 4$^{\text{th}}$ session are significantly higher ($67.06 \pm 12.30\,\%$ and $66.77 \pm 7.77$) as compared to the first two

| | LSFL | LSFP | | | |
|---|---|---|---|---|---|
| **Subject** | **QDA** | **QDA** | **GMM** | **SVM-linear** | **SVM-RBF** |
| **1** | $62.15 \pm 8.62$ | $66.14 \pm 6.78$ | $58.02 \pm 9.44$ | $58.02 \pm 5.69$ | $58.52 \pm 7.92$ |
| **2** | $64.61 \pm 13.17$ | $66.04 \pm 6.90$ | $64.55 \pm 5.68$ | $64.55 \pm 6.31$ | $54.37 \pm 5.44$ |
| **3** | $47.57 \pm 5.56$ | $59.91 \pm 10.97$ | $46.87 \pm 1.82$ | $46.87 \pm 7.37$ | $45.93 \pm 7.68$ |
| **4** | $50.50 \pm 5.74$ | $58.00 \pm 7.48$ | $61.00 \pm 5.29$ | $61.00 \pm 12.48$ | $51.00 \pm 3.83$ |
| **5** | $68.83 \pm 8.95$ | $75.86 \pm 6.45$ | $66.31 \pm 7.36$ | $66.31 \pm 6.60$ | $46.73 \pm 4.11$ |
| **6** | $53.64 \pm 8.40$ | $53.09 \pm 9.55$ | $43.54 \pm 4.00$ | $43.54 \pm 6.43$ | $52.44 \pm 3.03$ |
| **7** | $44.64 \pm 3.01$ | $54.77 \pm 11.93$ | $57.04 \pm 7.20$ | $57.04 \pm 10.03$ | $53.75 \pm 4.44$ |
| **8** | $53.82 \pm 9.39$ | $51.28 \pm 4.25$ | $44.01 \pm 9.09$ | $44.01 \pm 9.36$ | $47.11 \pm 6.40$ |
| **9** | $51.00 \pm 8.08$ | $51.00 \pm 5.29$ | $51.00 \pm 9.59$ | $51.00 \pm 12.70$ | $53.00 \pm 8.25$ |

Table 1: Comparison of cross-validation accuracies with different features and classifiers.

sessions ($58.60 \pm 13.96$ and $61.37 \pm 5.61$). Observing this trend, we argue that the features of this potential are becoming stable and well separable over time due to subjects adaptation to the experimental paradigm. This suggests that, similar to BCI systems, a good training method is a key component for subjects to learn to provide stable EEG patterns. Proper training of the subjects is likely to enhance the classification accuracies with the methods studied in the current work.

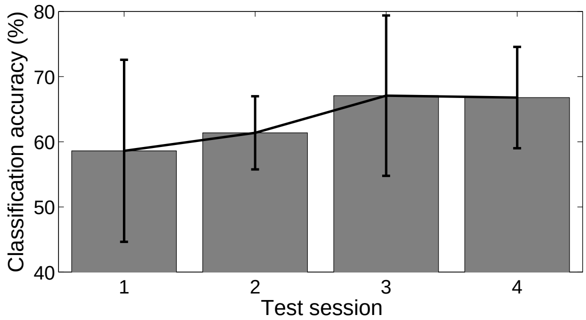


Figure 2: Average classification accuracies in different sessions using QDA classifier with LSFP features for subjects 1–5 and 7.

# 5 Conclusions

We compared different classification techniques for the recognition of anticipation related potentials from human EEG as a first step towards the design of a novel BCI. From the off-line studies on these potentials using the QDA classifier we observed that the LSFP features perform better than the LSFL features. This result suggests that LSFP features describe the anticipation related potential better than the LSFL features, the latter being those usually computed in neurofeedback and neurophysiological studies for the characterization of CNV potentials [4, 1]. We also compared the classification accuracies of LSFP features with QDA, GMM, SVM-linear and SVM-RBF classifiers. The 4-fold cross validation, with each fold corresponding to a separate session, showed that the QDA classifiers perform significantly better than the other classifiers

It is worth noting that none of the subjects considered in the current study had previous experience with the CNV protocol. The systematic observation of the performance in each session showed an increasing trend in classification accuracy for most (6 out of 9) subjects. We argue that this trend is due to subjects' adaptation to the experimental paradigm. However, for the remaining subjects the classification accuracy is at chance level which is most likely due to lack of practice (note that the CNV paradigm is a learned task and subjects need to practice for a few sessions). As some subjects learn faster than others the classification accuracies also differ in the same way. Moreover, as there is a learning component, the classifier calculated using the later sessions does not perform well for the early session, whereas the classifier calculated using early sessions performs better for the later session (see Figure 2).

Proper training of the subjects is likely to enhance the performance of the recognition methods compared in the current study. Moreover, an early study based on neurofeedback showing that the subjects were able modulate these potentials [4]. Based on this knowledge we hypothesize that the closed loop implementation of the current recognition methods can improve the subject's training yielding to more stable and well separable features. We consider this implementation as next immediate step for further research. In addition, we will extend these methods to multi-electrode features in order to improve the classification accuracies. Also, fast recognition of these potentials is another crucial factor for building a reliable BCI application. We plan to achieve this by extending the current methods to multi-classifier based recognition techniques in which each classifier looks at different temporal blocks of EEG and makes a decision as quickly as possible.

**Acknowledgments:** This work is supported by the EC-contract number BACS FP6-IST-027140 and the Swiss National Science Foundation NCCR "IM2".

# References

[1] G. J. M. Van Boxtel and K. B. E. Böcker. Cortical measures of anticipation. *J. Psychophysiol.*, 18:61–76, 2004.

[2] G. Vanacker, J. del R. Millán, E. Lew, P. Ferrez, F. Galán, J. Philips, H. V. Brussel, and M. Nuttin. Context-based filtering for assisted brain-actuated wheelchair driving. *Comput. Intel. Neurosci.*, 2007:Article ID 25130, 2007.

[3] W. G. Walter, R. Cooper, V. J. Aldridge, W. C. McCallum, and A. L. Winter. Contingent negative variation: an electric sign of sensorimotor association and expectancy in the human brain. *Nature*, 203:380–4, 1964.

[4] L. Bozinovska, S. Bozinovski, and G. Stojanov. Electroexpectogram: Experimental design and algorithms. In *Proceedings IEEE Biomedical Engineering Days, 1992*, pages 58–60, 1992.

[5] P. Kropp, A. Kiewitt, H. Göbel, P. Vetter, and W. D. Gerber. Reliability and stability of contingent negative variation. *Appl. Psychophysiol. Biofeedback*, 25:33–41, 2000.

[6] B. Rockstroh, T. Elbert, A. Canavan, W. Lutzenberger, and N. Birbaumer. *Slow Cortical Potentials and Behaviour.* Urban and Schwarzenberg, 2nd edition, 1989.

[7] C. M. Bishop. *Pattern Recognition and Machine Learning.* Springer, 2006.

[8] C. J. C. Burges. A tutorial on support vector machines for pattern recognition. *Data Mining Knowledge Discov.*, 2:121–167, 1998.

# Theoretical and ethical issues on brain-computer interfaces

E. Hildt

Chair for Ethics in the Life Sciences, University of Tübingen, 72074 Tübingen, Germany

elisabeth.hildt@uni-tuebingen.de

**Abstract**

In approaches in which there is direct interaction and mutual interdependence between human brain and technical devices manifold anthropological, philosophical and ethical issues arise, some of which will be discussed in the following. These relate to human self-perception, to the enormous dependence of the individual person from the computer system and to problems that may arise in case of technological disturbances and dysfunction. For as opposed to the traditional use of tools and technical instruments, brain-computer interfaces (BCIs) and other neurotechnological devices are technical tools which are in direct contact with the human brain and body or which even enter the human brain and body.

## 1 Introduction

During the past decades, our knowledge of the structure and function of the human brain has increased considerably. This has prompted the development and use of various pharmacological and technological procedures to be used in medical contexts, among them neurotechnological approaches. These include direct brain-computer interfaces (BCIs) which allow brain signals to be used for communication and control of movement [1, 2, 3]. Apart from non-invasive approaches such as the so-called thought translation device, which is a biofeedback communication system used by locked-in patients [4], invasive brain-computer interfaces are currently being developed which aim at enabling the brain to exert direct motor control. In animal experiments using microelectrode arrays implanted in the motor cortex, it has been possible to control movements merely by "thinking them through" [5]. There are also some reports of successful clinical studies with prosthetic limbs [6].

## 2 Discussion

In the following, medical, anthropological and ethical issues of BCIs will be discussed. In this, after a short paragraph on risks and benefits, the focus will be on implications which the direct interplay between man, brain and technical devices might have for our conceptions of human identity and authenticity.

### 2.1 Risks and benefits

The BCI approach is a very promising technology that raises enormous hopes for patients suffering from severe diseases such as amyotrophic lateral sclerosis (ALS), stroke, spinal cord injury or cerebral palsy. The clinical applications of this technology have been facilitated by the availability of small high-performance computers and other small, biocompatible devices. In the use of BCIs the risk-benefit-ratio is essential.

Possible benefits include positive effects on autonomy, communication and mobility, which are all aspects of central relevance for persons. Of particular importance is the influence of the devices on the quality of life of the individuals involved, on their independence and on their possibility to participate in family and social life.

Compared to non-invasive procedures, the invasive methods involve considerable risks. These include the risk for brain lesions going along with the implantation or removal of electrodes and other technical devices, and the risk for infections or immunological reactions. Also long-term functionality is a crucial issue. There may be situations, however, in which non-invasive BCIs cannot be used for practical reasons or in which invasive BCIs go along with greater benefits.

It should not be forgotten that in invasive BCIs, there is an implantation of technical material into the human brain, this being the organ which determines, like no other, an individual's overall existence. Only those uses in which considerable benefit can reasonably be expected and in which the expected benefits clearly outweigh the risks can be considered acceptable. This requires an adequate amount of basic research and animal experiments carried out before beginning to do clinical trials. Before invasive procedures are chosen for an individual patient, all other less invasive options should have been taken into consideration.

## 2.2 Brain-computer interfaces and human self-perception

As opposed to the customary, traditional use of tools and technical instruments, BCIs are technical tools which are in direct contact with the human brain. By way of this intensive interaction between technical devices and the human brain, the distinction normally drawn between tools and the subject who uses them is blurred. This holds in particular in invasive BCIs in which a "tool" is integrated directly into the human brain. BCIs may be characterized to be hybrids of man and machine: The BCI results from intensive interdependence between a person and a computer system. Most often, it involves complex mutual learning and adaptation processes.

In view of this intensive interaction between person and technical devices the question arises: In how far can the technical system be integrated into the self-conception of the person involved? In how far may a person consider the artificial actuator, for example a prosthetic limb, to be part of herself? Is this bodily extension an aim worth pursuing?

These are complicated issues, for from an external perspective there is no answer to the question: What is it like to live with a BCI? In order to find an answer to that question, the internal perspective of the person involved is necessary. The philosopher Thomas Nagel has explicated this in his famous article: "What is it like to be a bat?" in which he argues that it is impossible for human beings to know what it is like to be a bat because human beings will never be able to have a bat's internal perspective and a bat's consciousness [7]. In spite of these difficulties, self-perception and identity are very fundamental issues for persons which need detailed reflection in the context of BCIs.

The idea of bodily extension is most obvious in the use of prosthetic limbs, but it plays a central role in all forms of BCIs: The neuromotor prosthesis may be considered to be an additional limb over which – by way of the BCI – the person gains control. At least in the beginning of an individual's BCI use, however, there is an obvious difference between a prosthesis and a person's body: The prosthesis clearly is not part of the person's body, which is not just any body, but the body experienced by the person to be her own body. In this, self-experience plays a central role, a person's experience that this body is her own body.

Maurice Merleau-Ponty [8] has used the term "Leib" for this particular perception of one's own body from the internal perspective. For bodily self-perception, physiological as well as mental aspects are important. For Helmuth Plessner's position [9], the internal perspective, the external perspective and border-drawing, achieved by oscillations between internal and external perspective, are central for an individual's self-conception. In how far can a person's bodily perception be extended to a tool that the person uses regularly? In the 1940s, Maurice Merleau-Ponty had such an extension of a person's bodily experience in mind when he discussed the integration of a blind person's cane into that person's bodily perception ("Erweiterung der Leibessynthese", [8], p. 182).

This idea of integration is supported by recent studies such as the one carried out by Iriki et al., [10]. In this study, in macaque monkeys there has been an extension of the visual receptive fields of bimodal cortical neurons along the length of a rake used by the monkeys as a tool to retrieve distant objects. This supports the idea that tools can become incorporated into the body schema, i.e., the internal representation of one's body, constructed by proprioceptive, somatosensory and visual signals.

Also other experiments carried out in animals and humans encourage this idea [11, 12]. In view of these results it seems possible that prosthetic devices can be incorporated into the body representation [3]. Probably, an assimilation of the prosthetic device as if it were part of the person's own body will be facilitated by providing the brain with multiple sensory feedback from the artificial actuator.

As Lebedev and Nicolelis ([3], p. 542) put it:

"Altogether, these results suggest that long-term usage of an artificial actuator directly controlled by brain activity might lead to substantial cortical and subcortical remapping. As such, this process might elicit the vivid perceptual experience that the artificial actuator becomes an extension of the subject's body rather than a mere tool."

So, in the long-term usage of a BCI, the person involved may no longer consider the artificial actuator to be a mere tool, but to be an extension of her body, to be part of her own body. It seems that incorporation of the prosthetic device into the body representation is even necessary for adequate BCI functioning.

## 2.3 Hybrids of man and machine: ethical aspects

What are the ethical implications of such a direct interdependence between man and computer in a brain-computer interface?

Apart from medical aspects relating to the risks of the procedure: Is a person harmed by the intensive interrelation with a computer or by the incorporation of technical devices into the brain? Manifold concerns, fears and fantasies stem from the option to integrate computers and other technical instruments into the brain and other parts of the human body. These involve aspects such as the technicalization of the human body, the encouragement of a reductionist, technological view on human beings, the fear of losing human identity, and speculations relating to *cyb*ernetic *org*anisms, *cyborgs* [13].

Undoubtedly, these concerns relating to a technicalization of the human body reveal that there are ethical limits to the amount and range of human body parts to be substituted by technical devices. These issues clearly need broad and intensive interdisciplinary discussion. This holds in particular since in BCI use an incorporation of the artificial actuator into the person's body representation and a modification of the person's self-conception are to be expected.

In my opinion, however, it is not adequate to reject neurotechnological approaches such as BCIs merely because of the technical nature of these devices. Instead, the functions achieved by the technological system are crucial. In clinical contexts, BCIs aim at substituting basic human functions that have been lost due to disease or accident. For the persons involved, the ability for communication or for motor control conferred by the BCI are of central relevance for their independence and overall room for manoeuvre in everyday life. In this, the decisive criterion is not whether biological or technical material is used, but whether the system is able to substitute for the lost function at an acceptable risk-benefit-ratio.

In BCI use, a patient's quality of life, ability to communicate, motor performance or room for manoeuvre strongly depend on the correct functioning of the BCI. In order to allow the patient to control his overall situation as far as possible, it is necessary to secure continuous functioning of the system without any disruptions or technical problems. For dysfunctions and failures have direct negative impact on the person involved. Consider for example the sudden disruption of a person's sole possibility to communicate with her surroundings. An impression of this enormous dependence and of the central relevance of communication for persons is given by Jean-Dominique Bauby's captivating book "The Diving Bell and the Butterfly" [14].

## 3 Conclusion

BCIs are a very fascinating technological approach which raises enormous hopes for patients suffering from severe diseases. The intensive interdependence between man and computer system in these hybrid devices implicates manifold theoretical and ethical issues relating to human self-perception, identity, and technicalization that need further discussion.

## References

[1] J. R. Wolpaw, N. Birbaumer, D. J. McFarland, G. Pfurtscheller, and T. M. Vaughan. Brain-computer interfaces for communication and control. *Clin. Neurophysiol.*, 113:767–791, 2002.

[2] M. A. L. Nicolelis. Brain-machine interfaces to restore motor function and probe neural circuits. *Nat. Rev. Neurosci.*, 4:417–422, 2003.

[3] M. A. Lebedev and M. A. L. Nicolelis. Brain-machine interfaces: past, present and future. *Trends Neurosci.*, 29:535–546, 2006.

[4] N. Birbaumer, N. Ghanayim, T. Hinterberger, I. Iversen, B. Kotchoubey, A. Kübler, J. Perelmouter, E. Taub, and H. Flor. A spelling device for the paralysed. *Nature*, 398:297–298, 1999.

[5] M. A. L. Nicolelis. Actios from thoughts. *Nature*, 409:403–407, 2001.

[6] L. R. Hochberg, M. D. Serruya, G. M. Friehs, J. A. Mukand, M. Saleh, A. H. Caplan, A. Branner, D. Chen, R. D. Penn, and J. P. Donoghue. Neuronal ensemble control of prosthetic devices by a human with tetraplegia. *Nature*, 442:164–171, 2006.

[7] T. Nagel. What is it like to be a bat? *Philos. Rev.*, 83:435–450, 1974.

[8] M. Merleau-Ponty. De Gruyter:Berlin, 1st. edition 1945 edition, 1974.

[9] M. Plessner. De Gruyter:Berlin, 1st. edition 1928 edition, 1975.

[10] A. Iriki, M. Tanaka, and Y. Iwamura. Coding of modified body schema during tool use by macaque postcentral neurones. *Neuroreport*, pages 2325–2330, 1996.

[11] A. Maravita and A. Iriaki. Tools for the body (schema). *Trends Cogn. Sci.*, 8:79–86, 2004.

[12] M. Maruishi, Y. Tanaka, H. Muranaka, T. Tsuji, Y. Ozawa, S. Imaizumi, M. Miyatani, and J. Kawahara. Brain activation during manipulation of the myoelectric prosthetic hand: a functional magnetic resonance imaging study. *Neuroimage*, 21:1604–16011, 2004.

[13] E. Hildt. Computer, Körper und Gehirn: Etische Aspekte eines Wechselspiels. In E. M. Engels und E. Hildt, editor, *Neurowissenschaften und Menschenbild*, pages 121–137. mentis:Paderborn, 2005.

[14] J. D. Bauby. *The diving bell and the butterfly. A memoir of life in death.* B&T, 1998.

# Examining causes for nonstationarities: the loss of controllability is a factor which induces nonstationarities

S. Jatzev[1], T. O. Zander[1], M. De Filippis[2], C. Kothe[1], S. Welke[1], M. Roetting[1]

[1]Department of Psychology and Ergonomics, Chair of Human-Machine Systems, Team PhyPA, Berlin Institute of Technology, Berlin, Germany
[2]Department of Psychology and Ergonomics, Chair Cognitive Psychology, Berlin Institute of Technology, Berlin, Germany

sja@mms.tu-berlin.de

**Abstract**

While allowing for a control of a feedback device via brain activity, Brain-Computer Interfaces (BCI) still suffer from performance decrements during an online session. As a possible cause for this problem, nonstationarities in the statistical properties of the EEG data have been identified. There are numerous studies claiming that new methods of adaptation have to be found [1, 2, 3, 4, 5], in order to confine the influence of statistical nonstationarities on the classification accuracy, but so far no heuristic-based approaches have been developed. With this study we were able to isolate one cognitive factor responsible for statistical nonstationarities in EEG data: the Loss of Controllablity (LoC). LoC refers to the perceived control the user has over a feedback device. We induced this factor artificially in a highly controlled experimental setup. Phases with reduced controllability induced a highly significant deviance of Event Related Desynchronisation BCI features but had no significant effects on features from Slow Cortical Potentials. Data based adaptation approaches are lacking an explanation for the causes of statistical nonstationarities. Hence these approaches run the risk of overfitting the adaptation to factors not relevant for the features. By identifying possible causes, like the factor LoC, we follow a new theoretical perspective on a heuristic based approach, applicable to a broader context of settings. Our results also show that statistical nonstationarities in EEG signals can be traced back to a functional background, and are not random noise. The identified cause for nonstationarities, LoC, could help to develop new methods of adaption by serving as an indicator for a change in the statistical properties of the EEG data. With this heuristic-based approach other factors could also be identified, in order to improve BCI online adaptation.

## 1 Introduction

Subject of investigation – Nonstationarities: In recent years nonstationarities in statistical properties of Electroencephalogram (EEG) data (in the following referred to as nonstationarities) became an increasingly relevant issue in BCI (Brain-Computer Interface) research. These nonstationarities are likely to occur in the course of time of an experimental session, causing drastic changes in BCI relevant features, hence leading to a serious decline in the classification accuracy. There are several studies claiming that they have to be further investigated to find new solutions of online adaption e. g. [1, 2, 3, 4, 5]. A first systematic quantitative study was given by Shenoy et al. [3]. They found evidence for nonstationarities in the statistical properties of the relevant extracted features. Shenoy et al. [3] point out the need of an investigation of neurophysiological and psychological causes. Various adaptation methods have been developed, following a data based approach. Here some of the parameters of the translation algorithm are updated during an online session [4, 5, 2, 6]. Nevertheless, apart from [3], none of these investigated possible causes for nonstationarities and are therefore vulnerable to an overfitting to factors irrelevant for classification. Likewise, in this study we want to investigate nonstationarities on a new theoretical basis, proposing a heuristic approach. Causes for these effects have to be identified at first, in order to find relevant indicators. As a result, a new adaptation scheme could be followed by changing parameters of the translation algorithm, whenever the crucial factor is denoting the need for adaptation.

Factor of interest – Loss of Controllability: This study investigated the factor of perceived Loss of Controllability (LoC). By controllability we refer to the perceived control the user has over a feedback device. Noticing classification errors, the user is trying to regain control over the machine. Perceived LoC could cause a change in the mental state of the subject, and therefore have an impact on the feature distributions. The idea of perceived controllability has been stated before, for it refers directly to the classification accuracy of a BCI system [7, 3]. Data based methods face the problem of complexity in online BCI systems. These consist of two strongly interacting components, namely the user and the machine, which creates a closed feedback loop. Each of the interacting systems has to optimize for the same goal – hence ideally adaptations of both systems should converge. But in the other case, it can happen that both systems diverge from one another, as demonstrated here. LoC is a result of the static translation algorithms confronted with the variable brain trying to optimize during phases of classifier errors. LoC can be defined as the classifier output being inconsistent with expected feedback. Hence, in a new experimental setup, the RLR (Rotation-Left-Right) paradigm, we manipulated the rate by which the user was able to predict the feedback under controlled conditions, by artificially inserting machine errors. The study was held in offline mode, to ensure the control of possible intervening factors and to avoid phases of loss of control over the feedback device, as they occur in online sessions (for details see methods section). This study has found evidence for a crucial factor causing nonstationarities.

# 2 Methods

An offline analysis approach [8] was utilized, replacing the usual online session which follows the initial calibration measurement. Thereby subjects performed a series of clearly defined control actions, while the EEG was only recorded and not fed back to the user. Therefore, the subject is not influenced by the performance of a particular algorithm and multiple algorithms can later on be compared on exactly the same data.

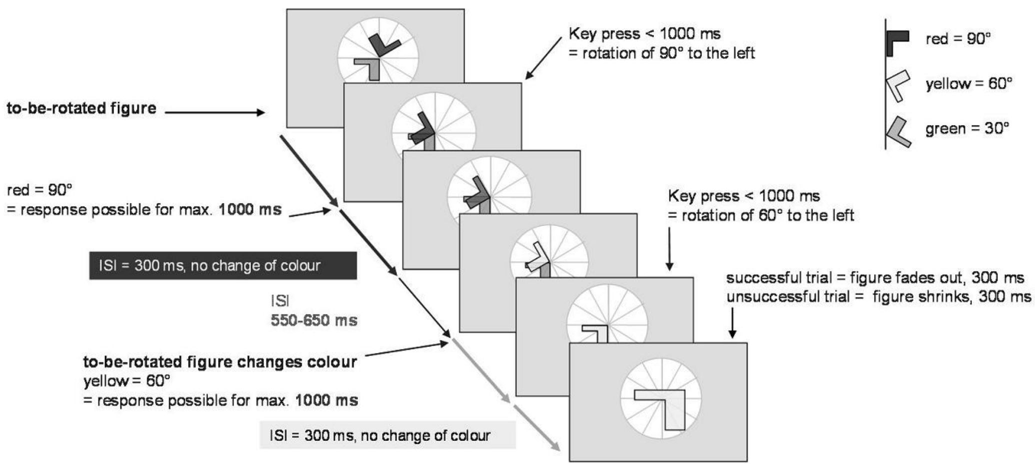


Figure 1: Experimental task of the RLR paradigm, section of one sample trial.

## 2.1 Experimental task and setup

The experimental task was to rotate a letter with left or right key press until it corresponded to a target figure. This was either the letter L or R, indicating both left or right key press (Ctrl keys, standard keyboard) and direction of rotation (left- or right wise) (Figure 1). Change of stimulus colour was an indicator for different angles of rotations: red indicating 90 degrees, yellow 60 degrees and green 30 degrees. Every 1000 ms the letter changed colour indicating the possibility of rotation. The stimulus would not rotate automatically, but only if a key was pressed. Therefore, participants were able to build up a strategy, in order to achieve the goal: to rotate the starting stimulus as fast as possible to the target stimulus. After rotation, the letter remained in its colour for 300 ms, changed into grey for a variable inter-stimulus interval (ISI) of 550 to 650 ms, while no key press was possible. The inter-trial interval (ITI) was 1000 ms. Faulty trials were defined rotating the stimulus too far or pressing the non appropriate key. Mapping rules of colours and size of rotations were kept constant until loss of controllability via a wrong mapping of colours and angles was introduced, leading to machine errors and thus faulty trials.

Experimental setup: The first block (LR, 5 minutes) was a typical BCI calibration measurement, for left/right keypresses prompted by letters L/R, which was not used for online control, but served as a baseline for subsequent comparisons [7]. Afterwards, a short practice block (P) of two minutes duration was introduced (RLR paradigm). The following sessions were divided in three blocks (A1,A2,B). For each block, the RLR paradigm had to be performed. A pause of 5 minutes each was inserted. The first two blocks (A1,A2, 12 minutes duration each) were identical. During the third block (B, 29 minutes duration) LoC was introduced. After 7 minutes, LoC was gradually raised from 0–30 percent (transition of four minutes). This probability of error was held constant for another 7 minutes (Buc) and recovered in a second transition phase. Another final phase of 7 minutes of correct feedback followed (Ba2).

Experimental Paradigm: The new RLR paradigm parallels features of typical online feedback scenarios in BCIs (e. g. Basket Feedback [7]), as it mimics an asynchronous BCI (internally paced, user-initiated) [9], there is an iterative decision process within each trial, and it has a defined goal and therefore provides motivation for participation in the game.

Recording: In this study 22 healthy subjects (age range 19–40) took part. EEG was recorded from scalp with multi channel EEG amplifiers (BrainAmp DC by Brain Products), using Ag/AgCl electrodes (reference at nasion), sampled at 1000 Hz, with a band pass filter from 0.05 to 200 Hz. The electrodes were distributed on standard 10/20 based caps with 32 positions. Electromyogram (EMG) and electrooculogram (EOG) data, as well as ambient temperature and noise level have been recorded, controlling for external effects such as measurement artifacts and for class correlated eye movements.

## 2.2 Analysis of EEG data

As formerly stated, we follow an approach which is widely known as offline analysis. This is realized by crossvalidation (CV) [10]. The continuous EEG data for a session is segmented into a set of blocks, one for each trial. The recorded trials are repeatedly partitioned into disjoint training and corresponding testing sets, used to train an instance of a classifier and then estimate its performance on the unknown data of the test set. We used a $10\times(10,5)$-fold nested CV.

Features and Feature Extractors: The EEG features that allow left and right hand movements to be discriminated fall into two categories: Slow Cortical Potentials (SCPs) and Event-Related Desynchronization (ERD) features.

SCP feature extraction: SCPs are low-frequency changes (1–5 Hz) [11], in this case localized over motor cortex. A slow negativity can be observed prior to a movement, and the relative strength of this negativity in the channels over the left versus right cortical hemisphere can be used to infer the laterality of the upcoming movement [12].

The CSP Algorithm: As ERD feature extractor the Common Spatial Patterns (CSP) algorithm was utilized. A variant of this algorithm, CSP for SCP (CSPfSCP), was used for the SCPs [8]. CSP aims to find linear combinations (patterns) of EEG channels such that the variance (deflection in the SCP case) of each trial projected according to these patterns is most discriminative (i. e., differs maximally between the two classes).

The SpecCSP algorithm: For the extraction of ERD features we used Spectrally Weighted CSP (SpecCSP) [13]. SpecCSP iteratively alternates between optimizing spatial and spectral criteria.

This way, the algorithm calculates a set of subject-specific spatial projections together with a set of frequency filters.

LDA was used as a classifier for all of the above feature extractors, as it was shown to be well suited for them [13, 8].

### 2.3 Dependent measures of nonstationarities

To assess the impact of LoC on the classifier's performance, we calculated pseudo online classification rates (POC) over time. POC rates were calculated by offline analysis serving as estimation for online classification results. POC was determined as following: The appropriate CSP derivate was used, with a time window of 300 ms, six patterns and a band-pass filter of [7–30] Hz. A classifier was trained on the initial calibration block (LR). Then, this classifier was applied to every key press, which happened over the course of the main experiment (i. e. blocks A1,A2 and B). An average of approx. 100 gradual classifier outputs in a one-second window before each key press was averaged and taken as the classifier's decision for this key press. The sign of this decision value (by default, left keys were assigned − 1, right keys +1) was remapped according to the key actually pressed, such that correct decisions were assigned positive values and wrong decisions were assigned negative values. By this, we got a real number for each key that was pressed by the subject. The plot in Figure 3 shows the aggregation of all values over all 22 subjects. The classifier outputs were forward/backward – filtered with a moving average window of 25 seconds, to obtain smooth plots. Therefore, positive values in the plot indicate overall correct classifier decisions, while values close to zero or negative indicate overall wrong decisions. We also calculated the Kullback- Leibler divergence (KLD) (for details see [3]) of the classifier's feature distributions. All measures were calculated relative to the training data's distribution of the initial calibration measurement, the LR-block. We used the KLD to measure the divergence of the CSP feature distributions as they build up over the course of the main experiment. Note that these KLD results have been determined in a classical offline fashion, i. e. one for each key press.

## 3 Results

Class correlation of the eye movements during the RLR sessions were all below $r = 0.012$, showing no significant difference to the class correlation of the LR design. This ensures that the result of the classifier output is not contaminated by class correlated eye movements. In RLR-designed sessions the well known $\alpha$ -rhythm is less pronounced than in the standard LR-Training. It slightly increases through the course of time Figure 2. $T$-tests were calculated for the CSPfSCP and for the SpecCSP features for the blocks A1, A2 and B (including LoC). For the SpecCSP features based on the Event Related Desynchronization, phases including the LoC (Buc, Block uncontrollable) showed a significant ($p = 0.0083$) increase in KLD of the SpecCSP features. Also the pseudo-online classification rate shows a decrease over time and it correlates significantly ($p = 0.0092$) to that of the KLD in block B (Figure 3). For the CSPfSCP there was no significant change for the phases with Loss of Controllability (Figure 3).

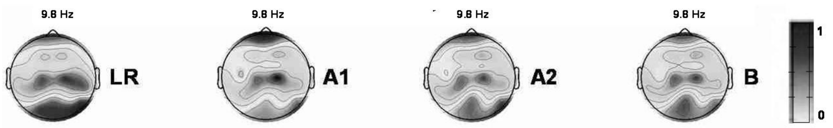


Figure 2: Topographical plots: spatial distribution of 10 Hz activity (one subject) over all blocks.

# 4 Discussion

Due to the new experimental design of the RLR paradigm, we were able to isolate one factor responsible for BCI relevant nonstationarities. With increasing LoC the KLD increases, disclosing nonstationarities in the EEG signal. But LoC has only a significant impact on features extracted with SpecCSP. This effect could not be found in features based on CSPfSCP. Hence, the choice of feature extraction methods is crucial for controlling the impact that nonstationarities have on the classification results. We are able to replicate the change in background activity of the brain, typically occurring in the transition from offline to online session. This change manifests itself in a less pronounced $\alpha$ -rhythm during the online session than in the calibration measurement (e. g. LR-Training). Shenoy et al. [3] identified this shift of data in feature space as a main cause for statistical nonstationarities and traces this change back to the fact that the calibration measurement is more monotonous than the online session. Our results ensure that our RLR-design mimics typical online sessions, also showing a less pronounced $\alpha$ -rhythm. Hence we were able to discriminate this effect from our new factor of investigation – LoC – which had an additional influence, giving rise to statistical nonstationarities.

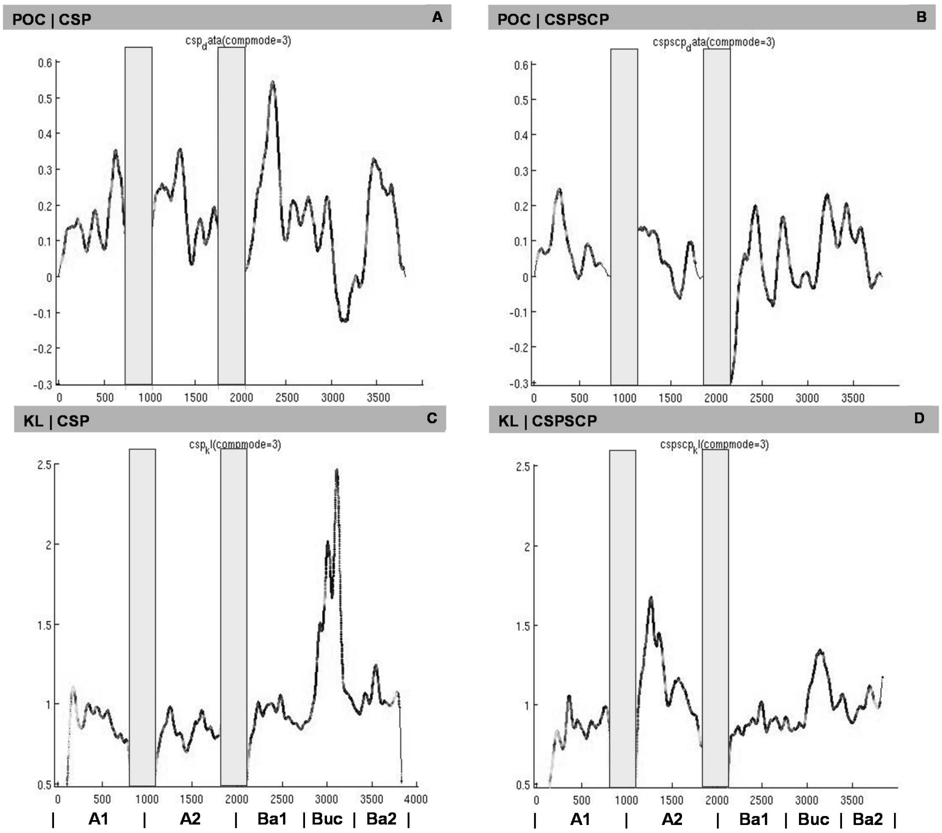


Figure 3: (A,B,C,D): Smoothed versions of the grand average. Figures A and B show POC accuracy, figures C and D show KLD. Left hand is ERD based, right hand is SCP based.

# 5 Conclusion

The LoC study reveals that the two systems taking part in BCI sessions – the translation algorithm and the brain – can diverge while trying to optimize for better results. Here, simulated errors of the computer lead to an attempt by the subject to adapt, causing a change in brain patterns. As an unavoidable consequence, with proceeding interaction, classification is getting more and more problematic, leading to even more errors by the computer. Hence, this loop contains a significant portion of positive feedback, which leads to steadily increasing classification errors once a certain threshold is passed. By identifying starting points for this viscious cycle, there will be new possible solutions of online adaptation. LoC could serve as an indicator for statistical nonstationarities and thereby overfitting would be avoided, while providing an additional theoretical basis for adaptation. This adaptation is characterized by a passive approach, with no need for an active action of the subject directed towards the BCI. Anyhow, it provides relevant informations about the current mental state of the user, making an improved interaction possible. The RLR paradigm can be utilized for recording signals from executed movements without generating a parietal $\alpha$ -rhythm. It gives the opportunity to manipulate BCI relevant factors in a controlled way, EEG allowing for the investigation of yet unknown other influences.

## References


[1] B. Blankertz, R. Tomioka, S. Lemm, M. Kawanabe, and K.-R. Müller. Optimizing spatial filters for robust EEG single-trial analysis. *IEEE Sig. Process. Mag.*, 25:41–56, 2008.

[2] C. Vidaurre, A. Schlögl, R. Cabeza, R. Scherer, and G. Pfurtscheller. Study of on-line adaptive discriminant analysis for EEG based brain computer interfaces. *IEEE Trans. Biomed. Eng.*, 54:550–556, 2007.

[3] P. Shenoy, M. Krauledat, B. Blankertz, Rajesh, P. N. Rao, and K.-R. Müller. Towards adaptive classification for BCI. *J. Neural Eng.*, 3:R13–R23, 2006.

[4] J. R. Wolpaw and D. J. McFarland. Control of a two-dimensional movement signal by a noninvasive brain-computer interface in humans. *PNAS*, 101:17849–17854, 2004.

[5] J. del R. Millán, F. Renkens, J. Mourino, and W. Gerstner. Noninvasive brain-actuated control of a mobile robot by human EEG. *IEEE Trans. Biomed. Eng.*, 51:1026–1033, 2004.

[6] G. Dornhege, J. del R. Millán, T. Hinterberger, D. J. McFarland, and K.-R. Müller. *Toward Brain-Computer Interfacing*, pages 305–309. MIT Press, Cambridge, MA, 2007.

[7] G. Dornhege. *Increasing Information Transfer Rates for Brain-Computer Interfacing, PhD thesis.* University of Potsdam, 2006.

[8] G. Dornhege, B. Blankertz, and G. Curio. Speeding up classification of multi-channel brain-computer interfaces: Common spatial patterns for slow cortical potentials. *Proc. 1st Int. IEEE EMBS Conf. Neural Eng.*, pages 591–594, 2003.

[9] G. Pfurtscheller, C. Neuper, and N. Birbaumer. *Human Brain-Computer Interface*, pages 367–401. CRC Press, New York, 2005.

[10] R. O. Duda amd P. E. Hart and D. G. Stork. *Pattern classification.* J. Wiley and Sons, 2001.

[11] R. Q. Cui, D. Huter, W. Lang, and L. Deecke. Neuroimage of voluntary movement: topography of the bereitschaftspotential,a 64-channel dc current source density study. *Neuroimage*, 9:124–134, 1999.

[12] B. Blankertz, G. Curio, and K.-R. Müller. Classifying single trial EEG: Towards brain computer interfacing. *Adv. Neural. Inf. Process. Syst.*, 14:157–164, 2002.

[13] R. Tomioka, Dornhege, G. Aihara, K. K. Aihara, and K.-R. Müller. An iterative algorithm for spatio-temporal filter optimization. *Proc. 3rd. Int. BCI Workshop and Training Course*, pages 22–23, 2006.

# Enhancing human-machine systems with secondary input from passive brain-computer interfaces

T. O. Zander[1,2], C. Kothe[1], S. Welke[1,2] and M. Roetting[1,2]

[1]Department of Psychology and Ergonomics, Chair for Human-Machine Systems, Team PhyPA, Berlin Institute of Technology, Berlin, Germany
[2]Center of Human-Machine Systems, GRK prometei, Berlin Institute of Technology, Berlin, Germany

thorsten.zander@mms.tu-berlin.de

**Abstract**

The introduction of methods from statistical machine learning [1] to the field of brain-computer interfacing (BCI) had a deep impact on classification accuracy. It also minimized the effort needed to build up the skill of controlling a BCI system [2]. This enabled other fields of research to adapt methods from BCI research for their own purposes [3, 4]. Team PhyPA, the research group for physiological parameters of the chair for Human-Machine Systems (HMS) of the Technical University of Berlin, focuses on enabling new communication channels for HMS. Especially the use of passive BCIs (pBCI) [3, 4], not dependent on any intended action of the user, showed a high potential for enhancing the interaction in HMS [5]. Additionally, as actual classification rates are still below the threshold for efficient primary control [6, 7] in HMS, we focus on establishing a secondary, BCI based communication channel. This kind of interaction does not necessarily disturb the primary mode of interaction, providing a low usage cost and hence a efficient way of enhancement. We have designed several applications following this approach. Here we are going to present briefly the results from two studies, which show the capabilities arising from the use of passive and secondary BCI interaction. First, we show that a pBCI can be utilized to gain valuable information about HMSs, which are hard to detect by exogenic factors. By mimicing a typical BCI interaction, we have been able to identify and isolate a factor inducing non-stationarities with a deep impact on the feature dynamics. The retained information can be utilized for automatically triggered classifier adaptation. And second, we show that pBCIs are indeed capable to enhance common HMS interaction outside the laboratory. With this, we would like to feed back our experiences made with passive interaction to the BCI community. We hope to povide new and useful information about brain dynamics which might be helpful for ongoing BCI research.

## 1 Introduction

Team PhyPA aims at the combining the technologies from Brain-Computer Interfacing (BCI) [8, 9, 1] and those from the context of Human-Machine Systems (HMS). HMS is the science of interaction between humans and technical systems. Therefore, an interdisciplinary team of mathematicians, psychologists and engineers works on currently seven projects investigating non-stationarities, efficiency and general applicability of feature extraction methods, single trial detection of motor and non-motor patterns e. g. error-responses and defining support systems enhancing HMS. As we focus on the applicability of BCI while interacting in typical HMS environments we augment the field of Brain-computer Interfaces to the field of Brain-Computer Interaction. Therefore, we have developed several tools allowing us to detect intended and non-intended user states and integrate them into existing and new HMS. We categorize the methods derived from BCI research into active and reactive. By the term active BCI (aBCI) we denote BCIs which utilize brain activity of direct correlates of intended actions as input. This includes the detection of motor imagery or execution as well as the control over slow cortical potentials. A reactive BCI (rBCI) is still controlled via intended actions. In contrast to the aBCI features are not derived from direct correlates to these actions, but from cognitive reactions on exogenic stimuli, as e. g. in

| Type of BCI | Based on features from | Used for |
|---|---|---|
| Active | intended generated cognition | direct control |
| Reactive | unintended changes in cognition by voluntary focussing on exogenic stimuli | direct control, brain switch |
| Passive | unintended changes in cognition induced by common interaction | supporting systems, user-state detection |

Table 1: Categorization of BCI Systems and their fields of of application.

the P300 speller. The rBCI features seem to be more robust in general. This might be due to the fact, that they usually depend on automatic processes of cognition which are not as easily modulated by conscious processes. According to this line of thought [3, 4], we now define passive BCI (pBCI). pBCIs are based not on intended actions of the user, but instead on reactive states of the user's cognition automatically induced while interacting in the surrounding system. Hence, the underlying features used by pBCIs are mostly independent of the primary mode of interaction within an HMS, be it BCI based or not.

# 2 Methods

## 2.1 Specifications of our BCI system and experimental design

### 2.1.1 Recording

The EEG system has 32 channels of Ag/AgCl conventional (EasyCap) or impedance optimized (ActiCap) electrodes. Signals are amplified by a BrainAmp DC system and recorded by the BrainVision Recorder (BrainProducts). The electrodes are distributed on standard 10/20 based caps with 128 positions. Depending on the type of experiment they are placed over according parts of the cortex. Additionally, we record electrooculogram (EOG) for controlling feedback-induced correlated eye movements, and electromyogram (EMG) on the relevant limbs, for protocolling correlated movements. Both are bipolarly multiplexed by a BrainAmp (ExG) system and derived with Ag/AgCl electrodes. In order to retain information on exogenic factors, we also record ambient temperature and noise level within the laboratory.

### 2.1.2 Analyses

For offline analyses, all feature extraction methods, especially methods for filtering and resampling, are applied in a strictly causal way. Classifiers are chosen from several linear (LDA, RDA, SVM) and non-linear (kernel SVM, rQDA, GMM) methods. In all analyses presented subsequently, (regularized) LDA was the best performing classifier and was therefore selected. Classification accuracy was estimated by $10\times(10[\times5])$ [nested] crossvalidation if not otherwise stated. Results from offline analysis are derived from strictly separated training and test blocks. Significance statements are substantiated by standard $T$-Tests and $F$-Tests without assumptions on the type of underlying distributions.

### 2.1.3 Experimental design

The stimulus presentation in calibration phases before online feedback is designed for providing high control over exogenic and correlating factors besides the one of interest. This control is relaxed in certain online feedback sessions to allow for a more realistic mode of interaction. Notice, that this decrement of control might allow for a higher number of artifacts but does decrease the signal to noise ratio. Subjects have been introduced to the main factor of investigation by an instructor. Experimental tasks have been presented in a standardized way on the screen of the Feedback Unit. The course of the experiments contained several breaks for relaxation and recovering of the subjects. Subjects gave information on their overall state and their impressions on different blocks of the experiment by answering questionnaires. All subjects are from age 18 to 45 with german as primary language. All groups of subjects are of balanced or selected sex. After all sessions the subject has been paid (20 Euro).

### 2.2 The RLR paradigm and its directed restriction, the RLR-Game

In the Rotation-Left-Right (RLR) paradigm [10] a stimulus on a starting position has to be rotated left- or rightwise (by a left or right key press) until it corresponds to a given target figure. The stimulus is either the letter "L" or "R", indicating the direction of rotation. While the colour of the stimulus is grey, it can not be rotated. However, every 1000 ms it changes into one of three colours, indicating A) the possibility to be rotated by a keypress and B) the degree of rotation. If the stimulus lights up in red, the stimulus will rotate 90 degree, if it is yellow 60 degree and if it is green 30 degree. Please notice, that each rotation has to be triggered, which only can be done once per colour change. The subject has to build up an efficient strategy for reaching the target: to rotate the starting stimulus as fast as possible on the target stimulus without rotating too far. A derivate of the RLR paradigm is the RLR-Game, defined in two modes: The first was restricted to standard states and the second with additional error states. The standard states are restricted to the colours green and red. The mapping of angles in the error states is directed downwards, hence an error induces a smaller angle of rotation than indicated by the colour. Goal of the game is to reach the target stimuli as fast as possible. Two players can play against each other. Their performance is measured and fed back in points. A player get a point when hitting the target earlier than his opponent.

## 3 Experimentel setups

### 3.1 A pBCI for retaining interaction relevant endogenic information

#### 3.1.1 Motivation

Shifting BCI applications from laboratory environment to interactive scenarios enforces losing the control over most of the interfering factors. Hence, one faces problems connected to the interaction between man and machine. The use of pBCI might give insights into the correlation between mental states and system states which are hard to infer from exogenic factors.

#### 3.1.2 Factor of investigation

One class of problems is that of non-stationarities resulting from shifts in cognitive states, which have not been represented in the data of the calibration phase. These might be induced by changes in the mode of interaction or mental processing of exogenic factors. As stated by Dornhege, Shenoy and Krauledat (see `www.bbci.de`) the loss of controllability (LoC) might be one of these factors.

#### 3.1.3 Experimental design

By utilizing the RLR paradigm we have been able to artificially induce phases of reduced controlability (BUc, see Figure 1) in experiments with 24 subjects by permuting the mapping between colours and angles of rotation. We tracked features representing the primary mode of interaction, pressing a key, in the EEG data. One representing the event-related desynchronization (ERD) and one representing a slow cortical potential (SCP) prior to the movement. Details on this study can be found in [10].

#### 3.1.4 Features

Features have been extracted by Common Spatial Patterns for SCP (CSPfSCP) [11] and Spectrally Weighted CSP (SpecCSP) [12] for ERD from 200 ms of data prior to the button press.

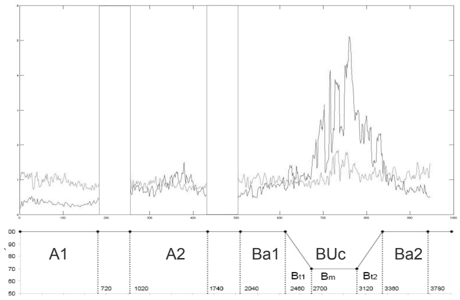


Figure 1: Grand average of the KL divergence using features for ERD (dark) and SCP (light).

## 3.2 Applicability of a pBCI for enhancement of efficiency in HMS

### 3.2.1 Motivation

Errors in communication are highly relevant factors regarding the efficiency of HMS. Especially in automated adaptation of the machine to the interaction mode of the user [13]. A wrong decision induces effects of surprise and frustration and in this respect, adaptation reduces the performance and the safety in HMS [14]. Additionally it triggers a correction action which enforces a shift in the intention focus of the user. According to this it reduces the overall acceptance of the adaptation and of the whole system.

### 3.2.2 Factor of investigation

In this study we have shown that pBCIs are capable of enhancing such an adaptation. For this we have designed the RLR-Game which mimics the interaction in an HMS and allows for modelling an unexpected and negative effect, the error states. While this game is based on common interaction channels we have added a secondary and passive BCI channel capable of correcting the effect of error states. This correction was triggered by an event related potential reflecting the mental processing of an error trial. If it is correctly detected by the pBCI during an error trial, the rotation angle was set to the correct mapping. In case of a false positive the angle was reduced to that of an error state. Hence, each correct detection of an error speeds the player up and a false positive slows him down. Therefore, if the classifier works properly, it will enhance the performance of the player and it will reduce it otherwise.

### 3.2.3 Experimental design

For keeping the environment as realistic as possible, we have chosen the Open House of the TU Berlin (LNdW 2007) as the setting. Four times two different players from the audience played the game against each other. Each pair played three sessions of 50 trials. One for user training, without error states. In the second session we introduced the error trials. The automatic adaptation has been applied in the last session, only for one player.

### 3.2.4 Features

Features have been extracted by a derivate of the pattern matching algorithm ([15]) extended for detection of several extrema of SCPs. 600 ms of data after the rotation have been selected.

# 4 Results

The results of the LoC study (Figure 1) show that in phases with full control (A1, A2, Ba1, Ba2) the variance of the averaged Kullback-Leibler divergence (KLD) of both features is bounded. In

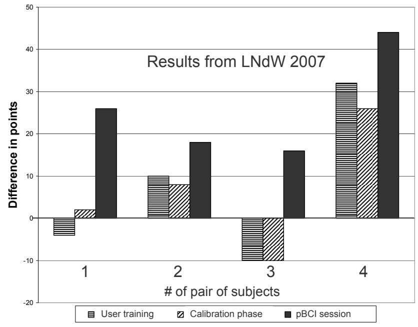


Figure 2: Differences of points from two opponents playing the RLR-Game at the Open House 2007.

contrast, the phases of reduced controlability (BUc) shows an significant increase of the KLD for ERD based features. Hence, the KLD of these features is a measure representing the perception of controlability. Figure 2 shows the results from the sessions from the open house of the TU Berlin 2007. In the third session one player has been supported by the pBCI. While the points have been equally distributed between session 1 and 2, the performance of all pBCI supported players has been increased significantly.

# 5 Discussion

Here we gave examples of two types of pBCIs. One establishing an information flow from the human brain to the HMS reflecting user states correlated to current modes of interaction. The other one extracting the actual interpretation of dedicated system states from the users cognition. Both can be applied in the context of BCI for enhancing classification accuracy. First, for an automated adaptation of the classifier and second, for correcting machine errors as proposed in [15, 16]. Also, for application in the field of HMS, it provides information about the user, which can only hardly be inferred by typical information channels in HMS. Especially the idea of utilizing the human brain as sensory for the subjective interpretation of current states within the HMS seems to be very promising. These studies are hopefuly a starting point for a whole series of new approaches. Currently we are investigating pBCIs for detection of mental workload, cognitive interpretation of the perception of human movements [17] and information on driver intentions. Please, see `www.phypa.org` for details.

# 6 Conclusion

Our experiences with pBCIs show, that these enable new channels of information within the interaction between man and machine. These can be utilized for both BCI and HMS research. Additionaly it seems to be very fruitful to exchange experiences between these two fields of research, which will hopefully will be done extensively in the near future.

# References

[1] B. Blankertz, G. Curio, and K.-R. Müller. Classifying single trial EEG: towards brain computer interfacing. In *Advances in Neural Inf. Proc. Systems (NIPS 01)*, volume 14, pages 157–164, 2002.

[2] B. Blankertz, G. Dornhege, M. Krauledat, K.-R. Müller, and G. Curio. The non-invasive Berlin brain-computer interface: fast acquisition of effective performance in untrained subjects. *Neuroimage*, 37:539–550, 2007.

[3] T. O. Zander, C. Kothe, S. Jatzev, R. Dashuber, S. Welke, M. de Fillippis, and M. Roetting. Team phypa: Developing applications for brain-computer interaction. In *Proc. CHI-Conference*, 2008.

[4] E. Cutrell and D. Tan. BCI for passive input in HCI. In *Proc. CHI-Conf.*, 2008.

[5] T. O. Zander, C. Kothe, S. Jatzev, M. Luz, and A. Mann. Das PhyPA-BCI: ein Brain-Computer-Interface als kognitive Schnittstelle in der Mensch-Maschine-Interaktion. *Prosp. Gestaltung Mensch-Tech.-Interaktion*, 13:183–185, 2007.

[6] C. Guger, G. Edlinger, W. Harkam, I. Niedermayer, and G. Pfurtscheller. How many people are able to operate an EEG-based brain-computer interface (BCI)? *IEEE Trans. Neural Syst. Rehabil. Eng.*, 11:145–147, 2003.

[7] B. Blankertz, G. Dornhege, M. Krauledat, K.-R. Müller, and G. Curio. The berlin brain-computer interface: Report from the feedback sessions. Technical report, Technical Report 1, Fraunhofer FIRST, 2005.

[8] J. J. Vidal. Toward direct brain-computer communication. *Annu. Rev. Biophys. Bioeng.*, 2:157–180, 1973.

[9] J. R. Wolpaw, N. Birbaumer, D. J. McFarland, G. Pfurtscheller, and T. M. Vaughan. Brain-computer interfaces for communication and control. *Clin. Neurophysiol.*, 113:767–791, 2002.

[10] S. Jatzev, T. O. Zander, M. DeFlilippis, C. Kothe, S. Welke, and M. Roetting. Examining causes for non-stationarities: The loss of controllability is a factor which induces non-stationarities. *Proc. 4th Int. BCI Workshop and Training Course*, 4, 2008.

[11] G. Dornhege, B. Blankertz, and G. Curio. Speeding up classification of multi-channel brain-computer interfaces: common spatial patterns for slow cortical potentials. In *Proc. 1st Int. IEEE EMBS Conf. Neural Eng.*, pages 591–594, 2003.

[12] R. Tomioka, G. Dornhege, G. Nolte, B. Blankertz, K. Aihara, and K.-R. Müller. Spectrally weighted common spatial pattern algorithm for single trial EEG classification. *Math. Eng. Tech. Reports*, METR 2006-40:1–6, 2006.

[13] R. Parasuraman, T. B. Sheridan, and C. D. Wickens. A model for types and levels of human interaction with automation. *IEEE Trans. Syst. Man Cybern. Part A*, 30:286–297, 2000.

[14] N. B. Sarter, D. D. Woods, and C. E. Billings. Automation surprises. *Handbook of Human Factors and Ergonomics*, 2:1926–1943, 1997.

[15] B. Blankertz, G. Dornhege, C. Schafer, R. Krepki, J. Kohlmorgen, K.-R. Müller, V. Kunzmann, F. Losch, and G. Curio. Boosting bit rates and error detection for the classification of fast-paced motor commands based on single-trial EEG analysis. *IEEE Trans. Neural Syst. Rehabil. Eng.*, 11:127–131, 2003.

[16] P. W. Ferrez and J. del R. Millán. Error-related EEG potentials in brain-computer interfaces. In *Towards Brain-Computer Interfacing*, pages 291–301. The MIT Press, 2007.

[17] M. Gärtner, T. Klister, and T. O. Zander. Classifying the observation of feasible and unfeasible human motion. *Proc. 4th Int. BCI Workshop and Training Course*, 4, 2008.

# Effects of long-term feedback training on oscillatory EEG components modulated by motor imagery

S. Kanoh[1], R. Scherer[2,3], T. Yoshinobu[1], N. Hoshimiya[4], G. Pfurtscheller[2]

[1]Graduate School of Engineering, Tohoku University, Sendai, Japan
[2]Institute for Knowledge Discovery, Graz University of Technology, Graz, Austria
[3]Computer Science & Engineering, University of Washington, Seattle, WA, USA
[4]Tohoku Gakuin University, Sendai, Japan

kanoh@ecei.tohoku.ac.jp

**Abstract**

An EEG-based BCI (brain-computer interface) system named "Brain Switch" was developed which detects motor imagery of subjects' own limbs by the increase of beta band power from one-channel EEG data. In this paper, the effect of long-term on-line feedback training on two healthy subjects using the Brain Switch is reported. Two subjects with normal motor ability took part in the experiments which consisted of screening sessions without feedback and training sessions with feedback. In the screening sessions, 32 channel EEG, 3 channel EOG and 4 channel EMG were measured simultaneously to review the EEG activation due to motor imagery and to choose one EEG channel related to limb motor imagery and one proper frequency band as a source of feedback training. In the feedback training session, EEG was measured from the selected channel. The length of a bar graph, presented on-line on an LCD as a feedback, was proportional to the EEG band power in the pre-defined frequency band. Training were executed for 50 or 40 sessions within 6 or 7 months, and a screening session was executed every 10 training sessions for checking and changing conditions for feedback. The EEG band power and the results of threshold-based command detection are investigated and discussed.

## 1 Introduction

A brain-computer interface (BCI) is a non-muscular communication channel which allows physically disabled people to re-establish interaction with their surrounding environment. One way to realize such a BCI is to detect motor imagery of users' limbs from the electroencephalogram (EEG) [1].

The BCI presented in this work is based on the detection of changes in oscillatory EEG components (event-related synchronization/desynchronization, ERS/ERD) induced by motor imagery [2]. From an engineering point of view, the simplest way to transfer information is to use binary control signals. For the realization of this binary signal, the authors have developed the system named "Brain Switch", which detects the presence of a user-specific motor imagery. This system detects the enhancement of EEG activities in a user-specific frequency component (ERS) in a user-specific bipolar EEG channel on a threshold basis [3, 4]. The Brain Switch has already successfully been employed to restore the grasp function of a spinal cord injury patient [3].

However, one crucial issue to gain control of a BCI is the training protocol. It is known that the feedback training, in which information on target brain activation is presented to the subjects during the task, is effective to modulate neuronal activities on motor imagery [3]. Due to the non-stationarity and inherent variability of brain signals, the user has to learn to reliably generate the requested patterns by feedback training. For the best feedback effects, the three above mentioned parameters (frequency range, EEG channel, threshold) need to be specifically selected for each user.

In this paper, the process and effect of long-term on-line feedback training on two healthy subjects using the Brain Switch is reported. The EEG band power during experiments and the results of threshold-based command detection were investigated by off-line analyses.

# 2 Methods

## 2.1 Subjects

Two able-bodied subjects (male, 23 and 24 years old) took part in the experiments, which consisted of EEG screening and BCI feedback training sessions (experiments with additional subjects are in progress). The study was reviewed and approved by the Ethics Committee on Clinical Investigation, Graduate School of Engineering, Tohoku University.

## 2.2 Screening sessions

Screening sessions were used to collect EEG activity from subjects during cue-guided motor imagery and to set up the parameters for the feedback training. Thirty-two EEG channels were recorded from Ag/AgCl electrodes placed over positions AFZ, FZ, F1, F2, F3, F4, FCZ, FC1, FC2, FC3, FC4, FC5, FC6, CZ, C1, C2, C3, C4, C5, C6, CPZ, CP1, CP2, CP3, CP4, CP5, CP6, PZ, P1, P2, P3, and P4 (reference and ground were left and right earlobe, respectively). Additionally, 3 EOG channels and 4 bipolar EMG channels (left forearm, right forearm, left leg, right leg) were recorded. The measured signals were bandpass-filtered between 0.5 and 100 Hz and sampled at 250 Hz.

The subjects were sitting in a comfortable armchair in an electromagnetically shielded room watching a computer screen from a distance of about 2 m. In each trial, a fixation cross was displayed at time 0 s until the end of the trial at time 8 s. A short warning tone occurred at 2 s, and one second later (3 s), an arrow pointing either to the left, right or down representing one of three different motor imagery tasks (left hand, right hand, both feet, respectively) was displayed for 1.25 s. The period between trials varied randomly between 5 and 6 s. The subjects were instructed to perform the indicated motor imagery task up to time 8 s, while remaining relaxed and avoiding any motion during performance. The number of trials in one run was 10 for each limb (totally 30 trials per run), and three runs were conducted in one session. Within each run, the order of the tasks was randomized.

Time-frequency ERS/ERD maps [5] of monopolar recordings and bipolar re-referenced channels (pairs of nearest neighboring electrodes) were computed and visually inspected. The following three conditions were selected for feedback experiments: motor imagery task (left hand, right hand or both feet), single bipolar EEG channel (one pair of electrodes) and frequency band with major ERS activity during motor imagery as a source of feedback information. These conditions were chosen manually by experimenters, and if the target activity was weak and not significant, a default frequency band (25–30 Hz) was adopted.

Screening sessions were recorded on the first and after every tenth feedback training session. The identified conditions were fixed and the same conditions were used during the following 10 training sessions.

## 2.3 Training sessions

In feedback training sessions, the length of a bar graph, continuously presented on a computer screen, was proportional to the power in the chosen frequency band. The subjects were requested to extend the length of the bar graph by performing the selected motor imagery task. The band power was estimated by bandpass filtering (Butterworth order 5) of the found EEG channel, squaring the samples and averaging over the past 1 s period.

In each trial, a scale consisting of two lines appeared at time 0 s until 6 s. During the presence of the scale, the subjects were instructed to perform the pre-defined motor imagery. The number of trials in one run was 20, and three runs were conducted in one session. In addition, two asynchronous (self-paced) runs in which subjects were allowed to imagine at free will, were executed at the beginning of each session (5 minutes per run).

After each session, time-frequency ERS/ERD maps were computed and an off-line Brain Switch simulation was calculated to evaluate the effect of feedback training. A Brain Switch accepts a command each time the power in the pre-defined band exceeds a threshold for a certain period of time (dwell time [6]). After a detection, a refractory period follows with the aim to reduce the same command a second time.

These parameters for command detection (threshold, dwell time, and refractory period) were optimized by ROC analysis [6], and the command detection was simulated. If the band power exceeded the threshold in the motor imagery period (time 0 s until 6 s) and it resulted the detection of the first command in each trial, it was counted as a desired command detection (true positive), otherwise detected command were treated as an unexpected one (false positive). The number of true and false positives (NTP and NFP, respectively) were calculated and evaluated by the simulation.

# 3 Results and discussion

Subject 1 and 2 participated in 50 and 40 training sessions within 6 and 7 months, respectively. All the raw data to be analyzed and its power spectrum were carefully reviewed to avoid contamination by EMG or other artifacts. The epoch data with excess artifacts or noise was excluded from further analysis and simulation.

## 3.1 Initial conditions for feedback training

Data taken from the first screening session (day 1) was analyzed to determine the initial conditions for feedback training. ERS with large magnitude was not observed at the beginning from both subjects. In Subject 1, a weak ERS component was observed at 18–23 Hz on bipolar montage CZ–C3 by motor imagery of right hand, and they were set as initial conditions for feedback. In Subject 2, the initial conditions were set to: motor imagery of feet, CZ–FCZ and 25–30 Hz.

## 3.2 ERS changes during training sessions

The results of time-frequency analysis on training sessions in both subjects are shown in Figure 1.

In Subject 1, no significant ERS response was observed by motor imagery of right hand during the first 10 training sessions. In the second screening session (day 12), ERS was induced by motor imagery of feet at 25–35 Hz on bipolar montage CZ–FCZ. Then the condition for feedback training was changed to feet, CZ–FCZ and 25–35 Hz from 11$^{th}$ training session (day 13).

It was observed that the frequency band of such narrow-band ERS during motor imagery increased as training went on. The ERS elicited by motor imagery initially appeared at around 28–30 Hz in about 15$^{th}$ to 17$^{th}$ training session (Figure 1(b)). The frequency band gradually increased to around 30 Hz and finally went up to about 35 Hz (Figure 1(h)). Due to such increase of frequency band of target ERS, the frequency band for feedback was changed to 30–35 Hz, 32–37 Hz from 21$^{th}$, 49$^{th}$ session, respectively (limb for imagery and EEG channel location were fixed from 11$^{th}$ session). It seemed that the change at 21$^{th}$ training session was quite effective for feedback training.

In Subject 2, ERS on vertex at 30–35 Hz was observed during feet motor imagery on the first few training sessions (Figure 1(i)). The observed ERS frequency band was 5 Hz higher than that for feedback (25–30 Hz) which was initially set by the results on first screening session (day 1). This ERS was gradually reduced during the first 10 training sessions, and such decrease of ERS was supposed to occur because the frequency band used for feedback training was different from that of the target ERS activation.

Based on the results of the second screening session (day 12), the frequency band for feedback was changed to 25–35 Hz from 11$^{th}$ training session. From 11$^{th}$ training session, stronger ERS on

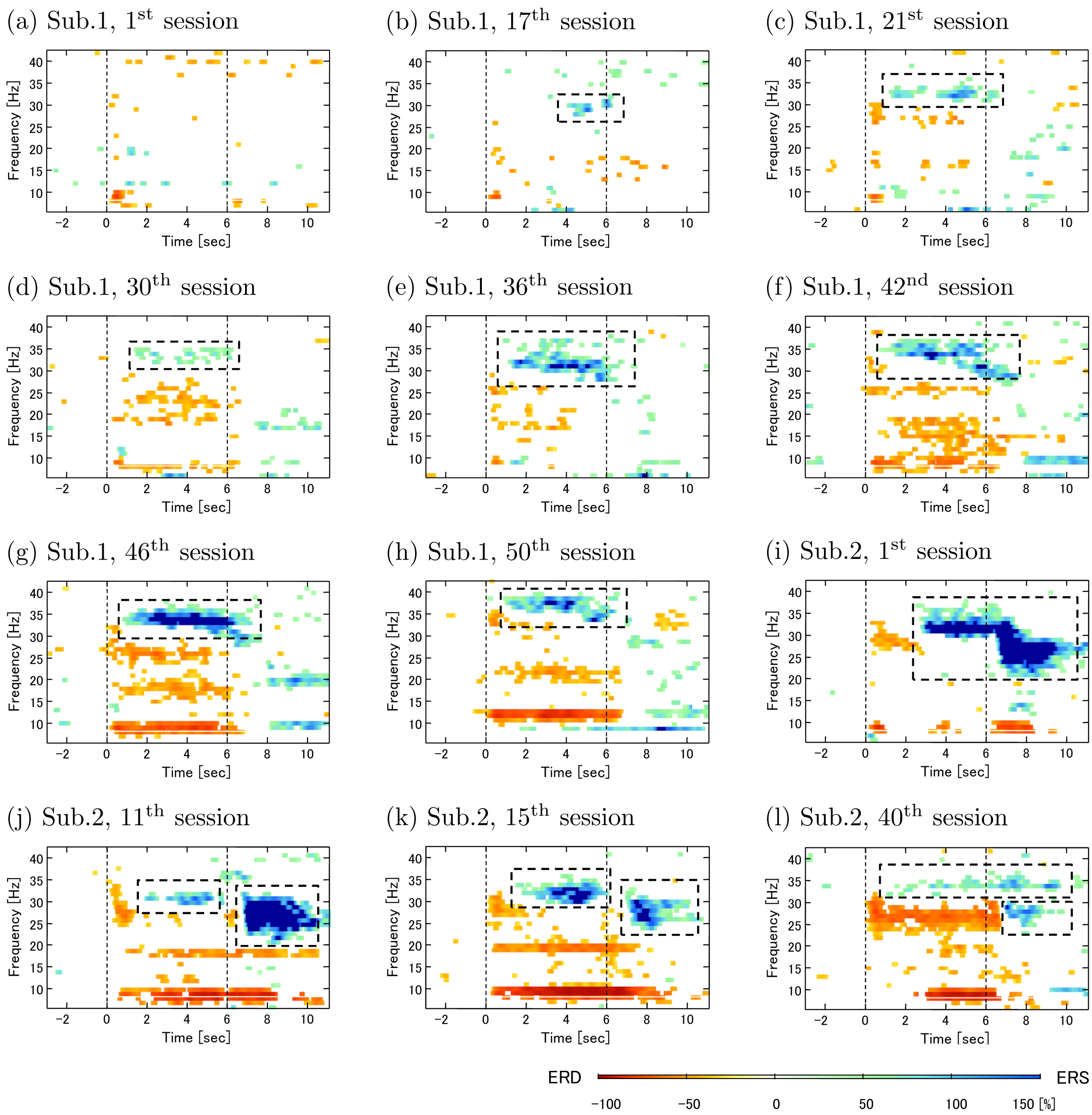


Figure 1: Result of time-frequency analysis of the data on training sessions on Subject 1 (a)–(h) and Subject 2 (i)–(l). Only significant ERS and ERD responses from reference period ($-1.5 \ldots -0.5$ s) are shown. Source of analysis and object of motor imagery were: CZ–C3, right hand (a, b), and CZ–FCZ, feet (c)–(l). Open dashed boxes denote ERS activities during motor imagery (time 0–6 s).

30–35 Hz appeared and the frequency band for feedback was finally changed and fixed to 30–35 Hz from 15$^{\text{th}}$ training session.

## 3.3 Performance of command detection

The number of true positives and false positives on each training session are shown in Figure 2. The three parameters for command detection were set by ROC analysis. As the total duration of the resting state was much longer than that for the imagery state (6 s per trial), NFP was corrected to that in the same duration of imagery state.

(a) Subject 1

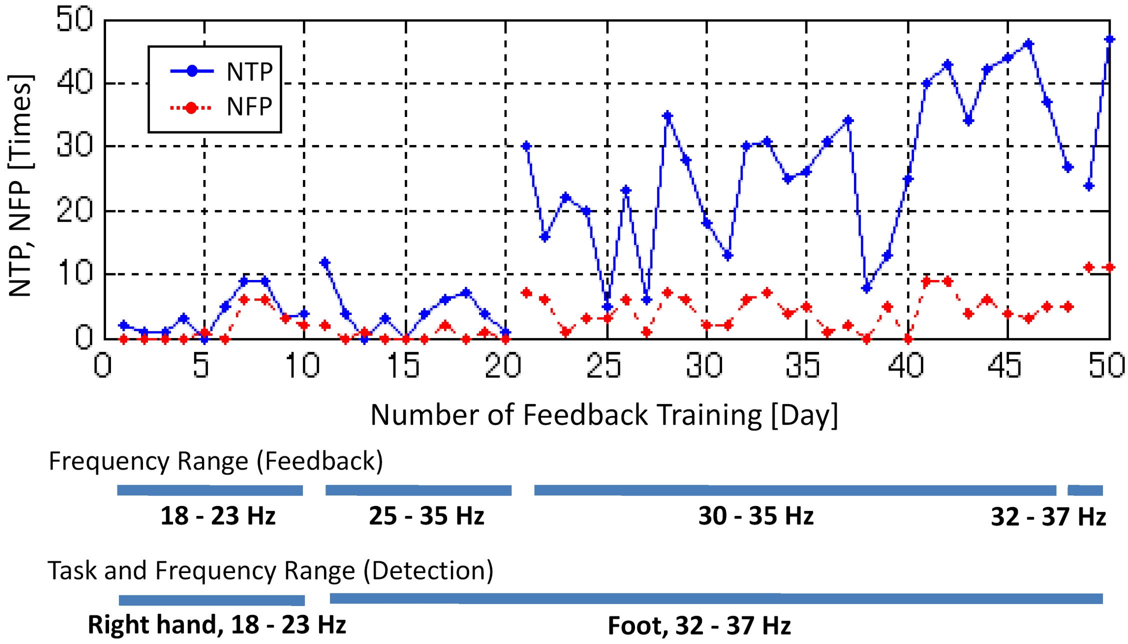


(b) Subject 2

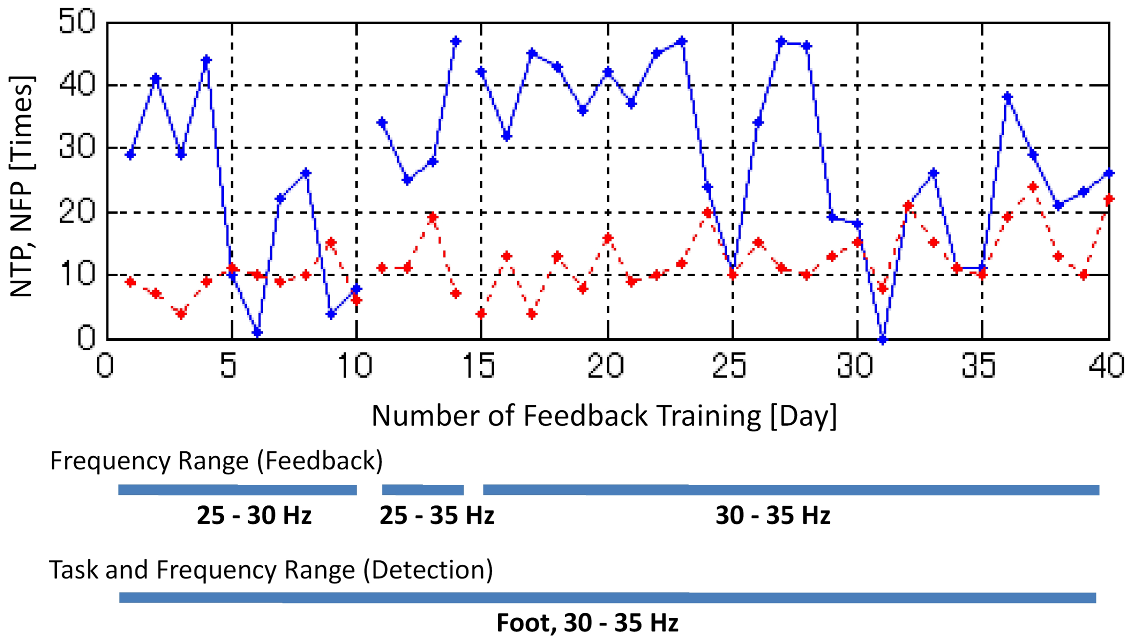


Figure 2: Result of command detection on training sessions. Number of true and false positives (top), frequency band for feedback training, task of motor imagery and frequency band for command detection used (bottom) are shown. The number of trials in each training session (i. e. possible maximum NTP) was 60.

In Subject 1, NTP increased from the 21$^{\text{th}}$ training session, nevertheless the NFP did not change. It was found from interviews after each training session that the subject sometimes had a feeling that he could control the length of the bar graph displayed on a computer screen during experiments. As there were no significant ERS responses for this subject before taking part in this experiment, it was found that this subject gained the ability to generate ERS on motor area voluntarily by motor imagery of feet.

In Subject 2, NTP decreased until the 10$^{\text{th}}$ training session. By the result of the second screening session (day 12) which was executed between 10$^{\text{th}}$ and 11$^{\text{th}}$ training sessions, the condition on the frequency band was changed to 30–35 Hz from the 11$^{\text{th}}$ training session. From the 11$^{\text{th}}$ training session, more NTP was obtained and was kept during the training session.

For this subject, the feedback training was executed regularly until 24$^{\text{th}}$ training session. But due to his schedule, there were two long distances between 23$^{\text{rd}}$ and 24$^{\text{th}}$, and 30$^{\text{th}}$ and 31$^{\text{st}}$ training sessions (about 4 and 3 weeks, respectively). The performance of command detection deteriorated by such a distance during training sessions for this subject.

## 4 Conclusion

In this study, the process and effect of long-term feedback training for BCI based on motor imagery were investigated in two subjects. The information on band power in specific frequency bands was presented to the subjects during training sessions as a feedback. From the result of one of the subjects, such a feedback could enhance the band power in the same frequency band. It was found that subjects where no EEG response related to motor imagery was observed initially could acquire the ability to produce enhancement of EEG band power during motor imagery.

In this study, the conditions for feedback training (especially the target frequency band) were chosen empirically by experimenters by taking the results of previous sessions into account. Moreover, the present training paradigm was rather boring for the subjects. The proposal of efficient training strategies and protocols to boost the effects of feedback training is left for further studies.

## References

[1] G. Pfurtscheller, C. Neuper, and N. Birbaumer. Human brain-computer interface. *In: A. Riehle and E. Vaadia (Eds.), Motor cortex in voluntary movements: a distributed system for distributed functions*, pages 367–401, 2005.

[2] G. Pfurtscheller and F. H. Lopes da Silva. Event-related EEG/MEG synchronization and desynchronization: basic principles. *Clin. Neurophysiol.*, 110:1842–1857, 1999.

[3] G. Pfurtscheller, G. R. Müller-Putz, J. Pfurtscheller, and R. Rupp. EEG-based asynchronous BCI controls functional electrical stimulation in a tetraplegic patient. *EURASIP J Appl. Sig. Proc.*, 19:3152–3155, 2005.

[4] S. Kanoh, R. Scherer, T. Yoshinobu, N. Hoshimiya, and G. Pfurtscheller. "Brain switch" BCI system based on EEG during foot movement imagery. *Proc. 3rd Int. BCI Workshop and Training Course 2006*, pages 64–65, 2006.

[5] B. Graimann, J. E. Huggins, S. P. Levine, and G. Pfurtscheller. Visualization of significant ERD/ERS patterns in multichannel EEG and ECoG data. *Clin. Neurophysiol.*, 133:43–47, 2002.

[6] G. Townsend, B. Graimann, and G. Pfurtscheller. Continuous EEG classification during motor imagery – simulation of an asynchronous BCI. *IEEE Trans. Rehabil. Eng.*, 12:258–265, 2004.

# Sequential selection in a sensorimotor rhythm-based brain-computer interface

E. V. C. Friedrich[1,2], D. J. McFarland[1], C. Neuper[2,3], T. M. Vaughan[1], P. Brunner[1,3], J. R. Wolpaw[1]

[1]Laboratory of Nervous Systems Disorders, The Wadsworth Center, New York State Department of Health, Albany, NY 12201-0509, USA
[2]Institute of Psychology, University of Graz, Graz, Austria
[3]Institute for Computer Graphics and Vision, Graz University of Technology, Graz, Austria

elisabeth.friedrich@uni-graz.at

**Abstract**

In a novel protocol of a sensorimotor rhythm (SMR)-based brain-computer interface (BCI), the so-called "scanning protocol", the participant views a screen that shows four choices in a linear array with one marked as the target. The four choices are highlighted in succession for 2.5 s each. When a target is highlighted, the user could select it by modulating the SMR. Participants trained for ten 30 min sessions over five weeks. The results demonstrated that the frequency of correct selections was inversely related to the target position. The reanalysis of the data of three participants showed that this effect can be led back to the sequential selection of the target positions which results in a dependence of correct selections of the target positions from each other. If the correct selections are calculated relatively to how often the scan actually highlights the target, there is no difference in correct selections between the first and the fourth target position anymore. The detailed analyses of the false alarms showed that for each position the non-target box just before the target box was selected most often. This result indicates that the reason for the false alarms is very likely a problem of anticipation that causes the users to desynchronize the brain rhythms slightly too early no matter which position is marked as target.

## 1 Introduction

A brain-computer interface (BCI) provides people with severe motor disabilities, such as amyotrophic lateral sclerosis (ALS), spinal cord injury or brainstem stroke, with a new non-muscular channel for communication and control [1]. In this study, the brain's electrophysiological signals were recorded from the scalp with electroencephalography (EEG) and the users were asked to control the task by modulation of mu (8–12 Hz) or beta (18–25 Hz) rhythms over sensorimotor cortex (i. e. sensorimotor rhythms (SMR)) [2, 3]. Previous studies showed that participants were able to do so and to achieve control of a computer cursor in order to select targets at the edge of the screen [4, 5, 6]. Recently, a novel protocol of a SMR-based selection task was implemented that allowed users to select multiple alternatives by modulating a single EEG feature [7]. The work showed that the so-called "scanning protocol" could be useful and effective but still faces some problems. The main issue was the impact of the target positions. So the aim of this study was to analyze the problem of sequential selection and the resulting dependence of the target positions more detailed. For these analyses the data of the $8^{th}$, $9^{th}$ and $10^{th}$ session of three participants who achieved significant control of the scanning protocol was taken.

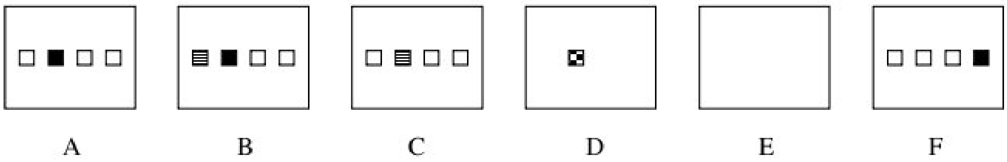


Figure 1: Scanning protocol.

# 2 Methods

## 2.1 Scanning protocol

The used four-choice one-dimensional scanning protocol is illustrated in Figure 1. At 0 s, four square-box choices were presented on the screen. The target appeared in red (black in Figure 1A) and the non-targets appeared in blue (white in Figure 1A). At 1 s, the scan started at the left edge of the screen and successively highlighted each choice in yellow (striped in Figure 1B) for 2.5 s. The scanning sequence was repeated without pause until a selection was made or until the time-out occurred after 30 s (i. e. after a total of three full scans). The participants were instructed to relax while the scan advanced automatically and to make their selection by motor imagery when the target choice was highlighted (Figure 1C). If the selection was correct, the target turned green (checkerboard pattern in Figure 1D) for 1 s while the other choices disappeared and a "hit" was registered. If a choice other than the target was selected, the screen immediately turned blank for 1 s and a "false alarm" was registered. The 1 s disappearance of the other choices after a "hit" or the blanking of the screen after a "false alarm" provided post-trial feedback to the user. One time passing a target without its being selected was counted as a "miss" and three full scans of the four choices without a selection being made (30 s total time) was called "time out". The screen remained blank for 1.5 s (Figure 1E) before the start of the next trial (Figure 1F). Each session contained eight three-minute runs (containing 7–29 trials) with one-minute breaks in between.

## 2.2 Participants

For this study, the data of three naïve users (ages 39–61, 2 women and 1 man), who achieved control within ten sessions, was taken from the original sample of 10 naïve participants. Each user participated in one screening and ten 30 minutes sessions of the scanning protocol. The participants performed the task on average twice a week over a period of 4–6 weeks. All gave informed consent for the study, which had been reviewed and approved by the New York State Department of Health Institutional Review Board.

## 2.3 Procedure and EEG recordings

First, each of the participants performed the standard BCI screening [2]. The users sat back in a reclining chair facing a $38 \times 28$ cm monitor at a distance of 2 m, and wore an elastic electrode cap seeded with tin scalp electrodes in the 64 positions standard for EEG recording according to the modified 10–20 system [8]. The data was referred to the right earlobe, grounded at the right mastoid, filtered (0.1–50 Hz), amplified (20.000 times) and digitized (160 Hz). While EEG was recorded, the users were asked to perform several motor actions or to imagine performing them. Based on the analysis of this screening, the centrally located electrode position over sensorimotor cortex and the frequency band between 8 and 28 Hz with the highest $r^2$ (Pearson's correlation between the amplitude of the EEG signal at the feature and the class information whether the stimuli was or was not the target choice) was determined as the feature for the online control of the following ten sessions of the scanning protocol.

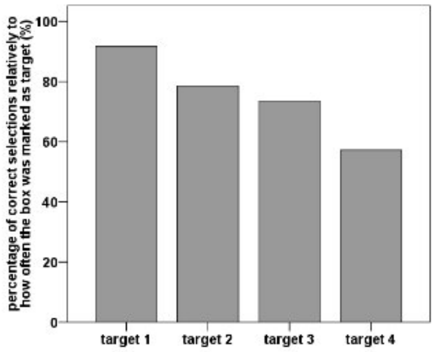


Figure 2: Percentage of correct selections relatively to how often the box was marked as target.

### 2.4 Signal processing and data analyses

The task was implemented in the BCI2000 software platform [9], and all recorded data were stored for offline analysis. Online, one selected channel over sensorimotor cortex was filtered with a large Laplacian spatial filter [10]. Every 50 ms, the most recent 400 ms segment from each channel was analyzed by a $16^{th}$-order autoregressive model (MEM) to determine the amplitude in a 3 Hz-wide mu or beta frequency band. The used feature locations and center frequencies of the features of these three users in their last three sessions were CP3 and 16 Hz, CP4 and 15 Hz and C1 and 25 Hz.

The selection was based on one feature varying among users and across sessions. The selection was made by reduction in feature amplitude. A selection was determined by whether feature amplitude was under a proportion of the threshold. This threshold was defined as the average of the feature amplitudes for the last three 2.5 s periods of each target position in which a choice was highlighted. In this study, the proportion was 0.9 in the first and 0.8 in the subsequent sessions for all participants regardless of their performance.

## 3 Results

These results were based on the data of the last three sessions ($8^{th}$ to $10^{th}$ session) of three participants (A, C and D) who achieved control in the scanning protocol. First, the percentage of correct selections (%) for each target position was calculated as the ratio between the number of correct selections of a target position achieved by the users and the total number of how often this position was marked as target. In general, the frequency of correct selection was inversely related to the target position. This means that the first target position (farthest to the left of the screen) was selected most often, whereas the last target position (farthest to the right of the screen) was selected least often (see [7]). Individual analyses of the data showed that there were some exceptions: User A selected the fourth target position in three out of the ten sessions approximately as often as the first one correctly (within a range of 5 percentage points) and user C selected the fourth target position even slightly more often (1 percentage point difference) than the first one in one session. Figure 2 shows that the three participants selected on average the first target position with an accuracy of 92 %, the second with an accuracy of 79 %, the third with an accuracy of 74 % and the fourth with an accuracy of 57 % in their last three sessions.

However, these results do not take the unequal a priori probabilities of the different target positions into account. To select the first target position correctly, just one correct selection is required, whereas for the fourth target position, four correct selections are required, because the scan has to pass the first three non-target boxes correctly before a selection of the fourth target position

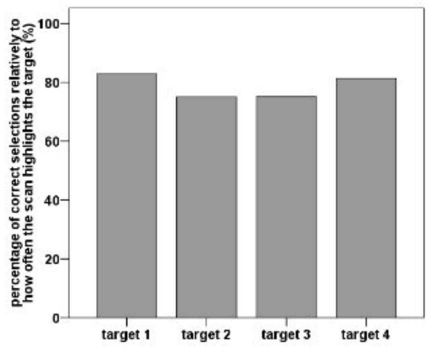


Figure 3: Percentage of correct selections relatively to how often the scan highlights the target position.

gets possible. So the correct selection of one target position can not be seen independent from the others. Therefore, the correct selections were additionally calculated as the ratio between the number of correct selections (%) of a target position achieved by the users and the total number of how often the scan actually highlighted this target position. Relatively to how often the scan actually highlighted the target, the participants selected the first target with an accuracy of 83 %, the second and third with an accuracy of 75 % and the fourth with an accuracy of 81 % (Figure 3).

Each position was marked as target on average 32–34 times per session. Of these about 132 possible correct selections per session, the participants made on average about 31 false alarms and 27 misses. Generally, the further the target position was to the right, the less often the target position was actually highlighted and the more false alarms were made. However, the scan passed all three non-target positions and highlighted the fourth target position about 23 times on average in one session and got selected correctly then about 19 times. Furthermore, the fourth target position was missed least often in comparison with the other target positions. That shows that performance was clearly above chance level for all target positions [11].
The detailed analyses of the false alarms showed that for each target position the non-target box just before the target box was selected most often (Figure 4). The number of false alarms was not distributed randomly upon the first, the second and the third position when the fourth box was marked as the target, for example, but more false alarms were made on the third position than on the other two non-target positions. Even if the first box was the target, slightly more false alarms were made on the fourth position. Thus the first target was missed at the beginning and after the fourth position the scan would have highlighted the first position again and a selection of the target would have been possible again.

# 4 Discussion

The target position had a considerable influence on performance. Although the individual analyses showed that in some few cases the target positions were selected correctly equally often (which can be seen as proof that it is practically possible for the users to select the fourth target position as often as the first one), generally the first target position was selected most often, whereas the last target position was selected least often (see [7]). This effect can be led back to the sequential selection of the target position which results in a dependence of correct selections between the target positions. If the correct selections are calculated relatively to how often the scan actually

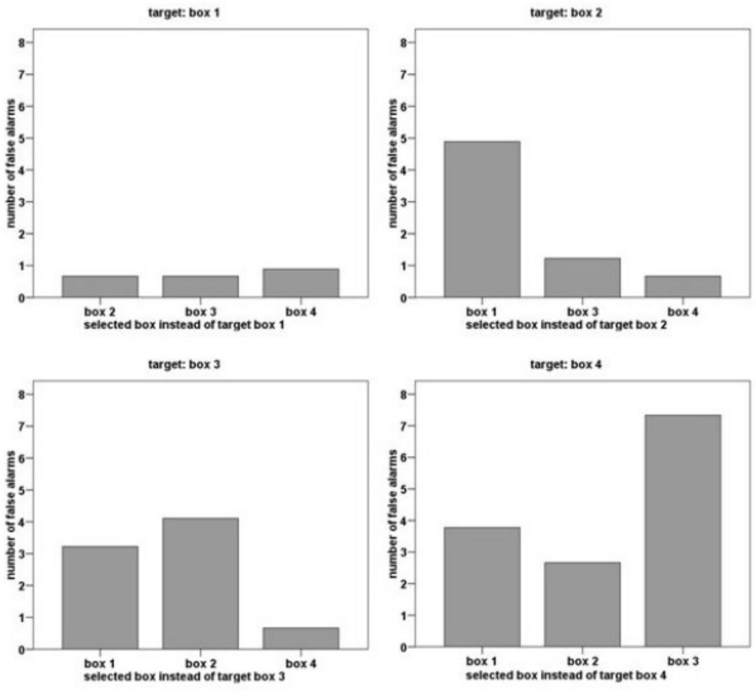


Figure 4: Mean number per user and session of false alarms per each position

highlighted the target, there is no difference between the first and the fourth target position anymore. The problem is that the scan did not always reach the last position due to early false alarms, whereas the first was always highlighted.
The performance of these three users in their $8^{th}$ to $10^{th}$ session was clearly above chance level for all target positions [11]. They achieved very good control, made about as many false alarms as misses and the scan came in 71 % to the last box position if it was marked as target.
The non-target box just before the target was selected erroneously more often than the other non-target boxes. This result suggests that the false alarms were not the result of random selections but demonstrate a certain level of control. Even if the first box was the target, slightly more false alarms were made on the fourth position. This indicates that the reason for the false alarms might not be that users found it hard to relax long enough and wait for the scan to pass the non-target boxes, but a problem of anticipation that causes the users to desynchronize slightly too early [12]. Of course, these results have to be interpreted carefully due to a small number of cases and this effect might not be seen in the first sessions of participants or in users who did not achieve sufficient control, because they were mainly selecting only the first position. However, one solution could be to take only the first second of the 2.5 s selection window into account for the decision if a selection is made or not for online control instead of the mean value of the whole 2.5 s. This suggestion is based on the analyses of the 2.5 s selection window that showed that the amplitudes at the feature of a user during a target box were most distinguishable from these during a non-target box (e. g. the highest $r^2$ was displayed) in the period between 0.4 to 0.8 s after stimuli onset (see [7]); replicated on these three sessions of these three participants as well). Further studies could implement this suggestion and try to decrease the number of false alarms due to the too early start of desynchronization of brain rhythms for the next position. Another very important aspect concerns the training of the participants. A pre-training to prepare the users with the ability to make a difference between relaxation and selection before they are confronted with a complex task might be useful.

## 5 Conclusion

The sensorimotor rhythm-based scanning protocol might become a promising option for a BCI communication for people with severe motor disabilities. Therefore further studies should address to the problem of sequential selection and the resulting dependence of the target positions.

**Acknowledgments:** This work was supported by the National Center for Medical Rehabilitation Research, NICHD, NIH (Grant HD30146), the NIBIB/NINDS, National Institutes of Health (Grant EB00856), the James S. McDonnell Foundation, the ALS Hope Foundation, the NEC Foundation, the Altran Foundation, the Helen Hayes Hospital and the University of Graz.

## References

[1] J. R. Wolpaw, N. Birbaumer, D. J. McFarland, G. Pfurtscheller, and T. M. Vaughan. Brain-computer interfaces for communication and control. *Clin. Neurophysiol.*, 113:767–791, 2002.

[2] D. J. McFarland, L. A. Miner, T. M. Vaughan, and J. R. Wolpaw. Mu and beta topographies during motor imagery and actual movements. *Brain Topogr.*, 12:177–186, 2000.

[3] C. Neuper, A. Schlögl, and G. Pfurtscheller. Enhancement of left-right sensorimotor EEG differences during feedback-regulated motor imagery. *J. Clin. Neurophysiol.*, 16:373–382, 1999.

[4] D. J. McFarland, W. A. Sarnacki, and J. R. Wolpaw. Brain-computer interface (BCI) operation: optimizing information transfer rates. *Biol. Psychol.*, 63:237–251, 2003.

[5] C. Neuper, G. R. Müller, A. Kübler, N. Birbaumer, and G. Pfurtscheller. Clinical application of an EEG-based brain-computer interface: a case study in a patient with severe motor impairment. *Clin. Neurophysiol.*, 114:399–409, 2003.

[6] J. R. Wolpaw, D. J. McFarland, G. W. Neat, and C. A. Forneris. An EEG-based brain-computer interface for cursor control. *Electroencephalogr. Clin. Neurophysiol.*, 78:252–259, 1991.

[7] E. V. C. Friedrich, D. J. McFarland, C. Neuper, T. M. Vaughan, P. Brunner, and J. R. Wolpaw. A scanning protocol for a sensorimotor rhythm-based brain-computer interface. *Biol. Psychol.*, in press, 2008.

[8] F. Sharbrough, C. E. Chatrian, R. P. Lesser, H. Luders, M. Nuwer, and T. W. Picton. American electroencephalographic society guidelines for standard electrode position nomenclature. *J. Clin. Neurophysiol.*, 8:200–202, 1991.

[9] G. Schalk, D. J. McFarland, T. Hinterberger, N. Birbaumer, and J. R. Wolpaw. BCI2000: a general-purpose brain-computer interface (BCI) system. *IEEE Trans. Biomed. Eng.*, 51:1034–1043, 2004.

[10] D. J. McFarland, L. M. McCane, S. V. David, and J. R. Wolpaw. Spatial filter selection for EEG-based communication. *Electroencephalogr. Clin. Neurophysiol.*, 103:386–394, 1997.

[11] G. R. Müller-Putz, R. Scherer, C. Brunner, R. Leeb, and G Pfurtscheller. Better than random? a closer look on BCI results. *Int. J. Bioelectromagn.*, 10:52–55, 2008.

[12] M. C. M. Bastiaansen, C. H. M. Brunia, and K. B. E. Böcker. ERD as an index of anticipatory behaviour. *Electroencephalogr. Clin. Neurophysiol.*, 6:203–217, 1999.

# Temporal localization of stimulated cognitive processes in BCIs

S. Welke[1,2], T. O. Zander[2], C. Kothe[2], and M. Roetting[2]

[1]Center of Human-Machine Systems, GRK prometei, Berlin Institute of Technology, Berlin, Germany
[2]Department of Psychology and Ergonomics, Chair of Human-Machine Systems, Team PhyPA, Berlin Institute of Technology, Berlin, Germany

swe@zmms.tu-berlin.de

**Abstract**

A necessary step in the data processing of a BCI is to extract temporal segments of the EEG data which contain the desired information, and preferably only that information. In most BCIs, the time boundaries of these segments are determined by some form of data-driven optimization, e. g. via automated parameter search, or ad hoc by experience. Though, it is known that data-driven parameter optimization suffers from a heightened risk of overfitting on the training data, e. g. coincidential noise patterns or training conditions. The worst case in this respect, and also the most commonly used, is when the optimization criterion is the actual discrimination performance of the classifier being trained. Therefore, our goal was to find a different subject-specific criterion for the determination of EEG time boundaries, orthogonal to classifier performance. We have identified aspects of the mental information processing of presented stimuli, particularly the timing of the event-related N400 component, as a possible source for such a heuristic. This potential, known to indicate the processing of linguistic stimuli, allows for the temporal delimitation of the preparation and execution of the class-specific task against the stimulus processing. This makes the approach immediately applicable in the stimulus-driven BCI calibration phase, but potentially for online phases in synchronous BCIs, too. Another benefit of this method is that it is unlikely to waste valuable information directly following the stimulus processing, by the choice of the time boundary. A preliminary offline study with 9 subjects, instructed to perform imagined movements, was carried out. In this, we could show that the presented method leads to classification error rates which are well contained in the expected range of error rates of that paradigm. This suggest that our method does not obviously affect the BCI performance in a negative way and is in fact practically applicable.

## 1 Introduction

A major goal of Brain-Computer Interface (BCI) research is the robust discrimination of electroencephalogram (EEG) patterns correlated to different mental states. The application of ideas from statistical machine learning to this problem has proven to be very practical for efficient online control via EEG signals, especially for naive subjects [1]. Nevertheless, the machine learning approach suffers from the problem of overfitting on the training data, typically coincidential noise patterns or conditions. This behaviour effectively degrades the possible online BCI performance. Based on experience, several common techniques do increase the danger of overfitting, most of them involving the data-driven optimization of one or more meta-parameters, subject to classification performance. According to machine learning theory [2], this effect can be mitigated by optimizing parameters based on different criteria instead, which are less directly related to discriminability, a popular application being crossvalidation (CV) guided parameter search. Still, the scope of that method is limited since its goal remains to be the classification performance, just in a different part of the training data. For example, learning on experimental conditions which just coincidentially but consistently improve the classification performance in the training set cannot be avoided by CV.

One such classification parameter which must be determined in almost every BCI application is the temporal location of the EEG segments which contain the desired information. The classical approach of determining this parameter is to either optimize it in a data-driven way, or to specify it ad hoc based on experience. In the latter case, in stimulus-driven BCIs, it is typically set to be several hundred miliseconds past the stimulus presentation.

The focus of this paper is therefore to find a different criterion based on which this parameter – the beginning of the discriminative EEG segment – can be determined. We found the human information processing of presented stimuli to be applicable for this challenge. The N400 component, which is correlated to the processing of linguistic stimuli, can be used to infer the time at which the stimulus processing is finished (see Section 1.1 for more details). Consequently, this time is also the best conservative estimate for the beginning of the subsequent task execution, and thus of the EEG segment of interest.

As an example application for our method, we considered the BCI calibration phase, which usually relies on stimulus-based instructions. Two different experimental sessions have been carried out. The first to find out whether typical BCI training stimuli are in fact able to induce stimulus processing ERPs, and to identify ERP components which best represent the completion of stimulus processing. In the second experiment, the new method was applied to the classical paradigm of training on imagined movements. Here we used SpecCSP/LDA [3] as a representative feature extractor/classifier in order to assess the quality of the windows which are estimated by our heuristic. See Section 2.1 for details.

## 1.1 Neurophysiological background

It is well known that aspects of the human information processing can be examined by means of event-related potentials (ERPs). These potentials not only reflect direct brain activity with a latency and precision in the range of milliseconds, but also allow for a qualitative discrimination of various stimulus-related cognitive processes. Consequently, a suitable choice of stimuli may induce ERPs indicative of information processing. In particular, the ERP N400 is assumed to be correlated to the processing of linguistic stimuli. This ERP is a negative polarity component whose maximum amplitude is found over the centro-parietal cortex. It usually begins at around 250 ms after the presentation of the stimulus and reaches its maximum amplitude at around 400 ms.

Further studies in this field revealed that the processing of any type of semantic information is accompanied by an N400 [4, 5, 6]. In the context of language comprehension, another hot topic of ERP components is the P600. Following the N400, this positive polarity ERP component with maximum amplitude at around 600 ms relative to the stimulus can be observed in linguistic ERP experiments. Such waveforms were reported in association with syntactic anomalies and ambiguities [7, 8]. It can be assumed that the brain distinguishes between semantic and syntactic representation and processes.

The literature also suggests that the process of normal language comprehension may rely on at least two complementary neural processing streams: a semantic memory-based mechanism, and a combinatorial mechanism that identifies the structure of a sentence [9]. Consequently, both components might be useful to some degree for temporally separating the instruction comprehension from the task performance, and it has to be determined which of them is best suited for our approach.

Although both amplitude and latency of the P600 component depend on the processing of linguistic stimuli, other studies have shown that the basal ganglia – intricately involved in the task execution – seem to play a crucial role in the modulation of the P600 [10], an indication that its interpretation with respect to the stimulus processing and task execution is not yet sufficiently understood.

# 2 Methods

Current BCIs allow for control over devices by discriminating, or classifying, different mental states. These states could be intentional thoughts like e. g. movement imagination, mathematical calculations or mental rotations, as in active BCIs (see [11] for a definition). Both of our experiments were cases of typical BCI calibration phases for active BCIs, in which a series of stimuli is presented to the subject in randomized order. In these, the subject is instructed to immediately carry out the task indicated by the type of the stimulus. This phase is crucial for machine learning based BCIs, since in it, the training data for building the classification model is collected.

## 2.1 Experimental designs

### 2.1.1 Preliminary ERP experiment – executed movements

In a preliminary ERP experiment with one subject, a suitable kind of stimulus presentation was identified. The brain activity was recorded with 32 Ag/AgCl impedance-optimized electrodes (ActiCap, Brain Products), referenced to the nasion, sampled at 1000 Hz and wide-band filtered. Electromyogram (EMG) was recorded from both forearms. No data was rejected due to artifacts. The task was to move upper limbs according to a preceding instruction, which was drawn from one of the investigated stimulus sets {'Left', 'Right'} and {'L', 'R'}. In both cases the instruction was to close the appropriate fist. At this stage we analyzed the EEG data of subject A for the selection of a set of linguistic stimuli suitable for ERP induction. Also, the temporal relation of the P600 component to the movement execution was to be explored based on this data. Another focus of this experiment was to infer the duration of the movement executions according to the EMG channels, as a preparation to the subsequent imagined movement experiments.

### 2.1.2 ERD experiments – imagined movements

In the following experiments we collected EEG data from "classical" BCI calibration phases – the instructed imagination of left and right upper limb movements [12]. These were used to apply our parameter estimation method in a subsequent offline analysis. Nine healthy subjects took part in the EEG measurement, which consisted of three blocks, separated by a d2 test and a pause of several minutes each. In each block, a different kind of movement imaginations was to be performed to capture much of the spectrum of possible imaginations. The chosen types of imaginations were closing the left/right fist, moving the left/right thumb and bending the left/right arm. A block was structured as a randomized sequence of trials, each lasting for 4 seconds, with stimuli chosen from the set {'L', 'R', 'X'}. 'L' and 'R' prompted for the appropriate movement imagination, while 'X' allowed for relaxation. In each block there were 45 trials per class (i. e. $45 \times 3$). Furthermore, subjects performed 15 trials of physically executed movements in the beginning of each block, in order to facilitate the subsequent imaginations.
The brain activity was recorded using 59 Ag/AgCl electrodes (reference to the nasion) in an extended 10–20 system sampled at 1000 Hz with a band-pass filter going from 0.05 to 200 Hz. Additionally, EMG was recorded from both forearms and thumbs as well as the horizontal and vertical electrooculogram (EOG). The EMG channels were used to monitor for physical limb movements that could correlate with the mental task, and thus influence the EEG signals in this part. Though, again, no trials had to be rejected due to artifacts.
Based on this data we applied the well-known SpecCSP classifier [3], in order to assess the quality of our window estimation. SpecCSP is a recent variant of the known Common Spatial Patterns (CSP) feature extractor [13]. It pinpoints relevant oscillatory features in time, space and frequency and has only two free scalar parameters: the beginning of the class-specific time window and the window length.
The beginning of the time window was estimated according to the proposed method, specifically by averaging the subject's ERP over Cz relative to the stimulus presentation, applying a [0.1–15] Hz band-pass filter, and taking the time of the minimum amplitude in the interval of [250–450] ms as the value of interest.

The duration of the movement was set to be 1.75 times the duration of an executed movement, as measured in the first experiment. LDA was chosen as the classifier for SpecCSP, as this was shown to be effective on this type of features [3]. Also, the data that was fed into SpecCSP was subsampled to 200 Hz for efficiency reasons.

# 3 Results

## 3.1 Preliminary ERP experiment - execution of movements

Figure 1 shows the averaged EEG signal over 270 trials of the preliminary experiment (subject A) at the electrode Cz, superimposed with the left EMG channel. Note that negative voltages are plotted above the zero line. Stimuli were presented as words, though a very similar figure can be derived from the other condition (single-letter stimuli). Clearly pronounced and detectable N400 and P600 peaks are visible in the ERP. It is interesting to note that the EMG onset (dashed line) begins at the same time as the P600 component peak. Also, it has to be noted that the N400 appears relatively early, at 340 ms after the stimulus presentation.

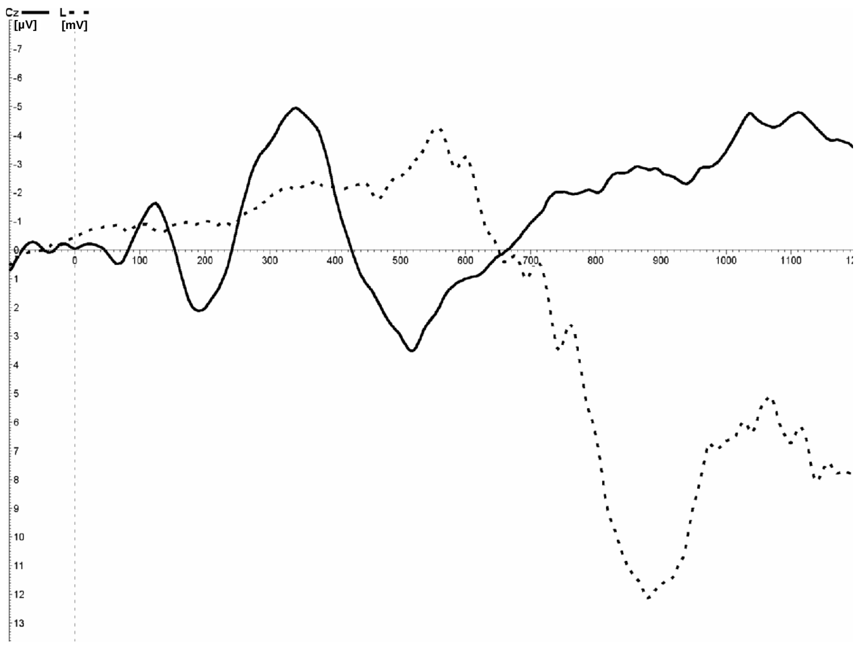


Figure 1: Subject $A$: Average (270 trials) of the N400 effect elicited by target words, followed by the execution of upper limb movements at electrode Cz and the corresponding EMG signal [L] (preliminary ERP experiment).

## 3.2 ERD experiments - imagination of movements

To define the time point where the subjects began to perform the imagination of movements, the ERP peak locations were determined from each subject's averaged EEG data. For seven out of nine subjects, a negative and positive component around 320 ms and 470 ms, respectively, were found. A standard deviation of 97 ms in the latency of the N400 components across subjects was measured. For two subjects, no clear peaks could be found by averaging. Table 1 shows the leave-one-out cross-validation test error rate for all remaining seven subjects. The mean error rate is 22.49 %.

| Subject | loo-cross-validation test error | Imagined movement |
|---|---|---|
| **1** | 33.00 % | thumb |
| **2** | 24.44 % | arm |
| **3** | 20 % | arm |
| **4** | 16.67 % | arm |
| **5** | 28.89 % | thumb |
| **6** | 24.44 % | fist |
| **7** | 10 % | fist |
| **Average** | **22.49 %** | |

Table 1: Leave-one-out cross-validation test error for SpecCSP and estimated epochs by N400 (peak) and a duration of less than the double of a corresponding executed movement.

# 4 Discussion

The early appearance of the observed N400 peak (Figure 1) can in part be explained by over-learning the given semantic stimuli. The EMG onset shows that the movement execution starts after the N400 and directly after the P600 component peak. Consequently, the movement preparation phase must be overlapped with the P600 component, as we anticipated. This underpins the decision to estimate the ending of the stimulus processing phase directly at the N400 peak. Since the ERP is also clearly pronounced, this component is a viable basis for the separation of stimulus processing from movement preparation and execution or imagination.
The fact that the classification results are very well contained in the expected range for SpecCSP on imagined movemements backs up the theoretical claim that the method should be sane and shows that it is also practically applicable. From a machine learning standpoint, this method has the inherent benefit that it only takes information into account which is in some way orthogonal to that embedded in the discriminative features, and is therefore thought to be less prone to classifier overfitting. A practical example for the possible benefits of this method in e. g. the calibration phase of an asynchronous BCI is that it can help to train only on the relevant features – in particular, it can help to prevent feeding uncorrelated or even falsely correlated information from the stimulus processing, such as stimulus-evoked visual potentials, into the training function. And on the other hand, valuable information following the stimulus processing is retained, a guarantee that cannot be provided by the ad-hoc approach. In fact, the high variance of stimulus processing duration across subjects shows that no a priori window can be optimally suited for all subjects. Another, totally unrelated benefit compared to the CV-guided optimization method is its relative computational simplicitly, which can save costly time in the critical machine training phase.

# 5 Conclusion

The presented idea allows for estimating the beginning of movement imagination within a standard BCI calibration session using a heuristic model. We believe that this approach provides a substantial improvement with respect to overfitting. Furthermore, this heuristic has a lot of potential for an automated estimation of designated time windows in the context of BCIs.
The next step will be an extensive comparison to the most prevalent contemporary window estimation procedures, potentially in an online setting, in order to ultimately measure the effectiveness of our method compared to established practices. The results from the calibration example can then in principle be carried over to synchronous BCI applications, except that in these cases the stimuli do not encode the actual type of the following task, but instead just mark its beginning. Another interesting future direction is to use the results the other way round, and instead identify the time window of the stimulus processing, in order to supplement BCIs based on such features, e. g. passive BCIs [11].

## References


[1] B. Blankertz, F. Losch, M. Krauledat, G. Dornhege, G. Curio, and K.-R. Müller. The Berlin brain-computer interface: Accurate performance from first-session in BCI-naive subjects. *IEEE Trans. Biomed. Eng.*, 2007.

[2] R. O. Duda, P. E. Hart, and D. G. Stork. *Pattern Classification (2nd Edition)*. Wiley-Interscience, 2000.

[3] R. Tomioka, G. Dornhege, G. Nolte, B. Blankertz, K. Aihara, and K.-R. Müller. Spectrally weighted common spatial pattern algorithm for single trial EEG classification. *Math. Eng. Tech. Reports*, (METR 2006–40), 2006.

[4] T. Curran, D. M. Tucker, M. Kutas, and M. I. Posner. Topography of the N400: brain electrical activity reflecting semantic expectancy. *Electroencephalogr. Clin. Neurophysiol./Evoked Potentials Sec.*, 88:188–209, 1993.

[5] M. Kutas and V. Iragui. The N400 in a semantic categorization task across 6 decades. *Electroencephalogr. Clin. Neurophysiol./Evoked Potentials Sec.*, 108:456–471, 1998.

[6] M. Kutas and K. D. Federmeier. Electrophysiology reveals semantic memory use in language comprehension. *Trends Cogn. Sci.*, 4:463–470, 2000.

[7] L. Osterhout and P. J. Holcomb. Event-related brain potentials elicited by syntactic anomaly. *J. Mem. Lang.*, 31:785–806, 1992.

[8] L. Osterhout. On the brain response to syntactic anomalies: Manipulations of word position and word class reveal individual differences. *Brain Lang.*, 59:494–522, 1997.

[9] G. R. Kuperberg. Neural mechanisms of language comprehension: Challenges to syntax. *Brain Res.*, 1146:23–49, 2007.

[10] S. Frisch, S. A. Kotz, D. Yves von Cramon, and A. D. Friederici. Why the p600 is not just a P300: the role of the basal ganglia. *Clin. Neurophysiol.*, 114:336–340, 2003.

[11] T. O. Zander, C. Kothe, S. Welke, and M. Roetting. Enhancing human-machine systems with secondary input from passive brain-computer interfaces. In *4th Int. BCI Workshop and Training Course*, 2008.

[12] G. Dornhege, B. Blankertz, G. Curio, and K.-R. Müller. Combining features for BCI. *Adv. Neural. Inf Process Syst. (NIPS 02)*, 15:1115–1122, 2003.

[13] J. Müller-Gerking, G. Pfurtscheller, and H. Flyvbjerg. Designing optimal spatial filters for single-trial EEG classification in a movement task. *Clin. Neurophysiol.*, 110(5):787–798, 1998.

# Classifying the observation of feasible and unfeasible human motion

M. Gärtner, T. Klister, T. O. Zander

Department of Psychology and Ergonomics, Chair of Human-Machine Systems, Team PhyPA, Berlin Institute of Technology, Berlin, Germany

mga@mms.tu-berlin.de

**Abstract**

The present study has been carried out by graduate students of the Berlin Institute of Technology. After attending an introductory lecture about Brain-Computer Interfaces (BCI) in the department of Human-Machine Systems the task was to develop a BCI experiment to gain hands-on experience. It has been decided to develop an experimental design concerning the observation of human motion. It is a well-known phenomenon that motor imagery causes desynchronization of the $\mu$-rhythm. This phenomenon has been used in the BCI context to develop a new communication and control modality for individuals with severe motor deficits. According to Neuper et al. and Hammon et al. desynchronization of the $\mu$-rhythm can be enhanced when motor imagery and movement observation are combined. In the experiment presented here it was tested, if movement observation alone leads to $\mu$-rhythm desynchronization that is detectable on a single trial basis. For averaged trials this has been shown by Ulloa and Pineda. They showed that desynchronization of the $\mu$-rhythm is stronger during the observation of feasible and meaningful human motion than during the observation of unfeasible and useless human motion. In the presented study this difference has been classified using point-light human animations versus scrambled versions of these animations as stimuli. Although this is work in progress, preliminary results for three subjects indicate that it is possible to detect the observation of point-light human motion on a single trial basis.

## 1 Introduction

It has been shown that the $\mu$-rhythm in the alpha-band (7–13 Hz) over the sensorimotor cortex is modulated by execution, imagination and observation of movements [1]. In the BCI context motor imagery is commonly used to discriminate different imagined movements that lead to lateralized modulations of the $\mu$-rhythm [2]. Neuper et al. [3] as well as Hammon et al. [4] have shown that motor imagery combined with the observation of movement leads to better classification rates in BCI experiments than solely motor imagery. Furthermore there is evidence that the observation of movement leads to modulations of the $\mu$-rhythm [5]. The idea of the experiment that is presented here was to combine the above mentioned findings and to test if $\mu$-rhythm modulations that are based on the observation of movements are detectable on a single trial basis.

To realize this idea point-light videos were used. A couple of studies deal with the question up to what degree human motion can be defamiliarized so that it is still recognized as a feasible human motion. A detailed review of these studies can be found in Blake and Shiffrar [6].

It has been discovered that point-light videos showing human motion can be identified correctly even under hard conditions [6]. Section 2.4 provides further information about point-light videos. The common assumption is that due to the lack of additional information about the shape of the moving persons, the bare movement has a huge effect in the perception of these videos.

Studies involving point-light animations usually use scrambled defamiliarized versions of those animations that provide the same amount and the same kind of information, but are not recognized as feasible human motions.

Grossman et al. [7] investigated that disturbance of the spatio-temporal coherences of dots makes it most difficult to identify human motion. According to Pavlova [8] rotations between 180 and ±90 degrees makes it even harder. These empiric findings were used as a base for the creation of the point-light animations in the presented experiment.
In an fMRI study Saygin et al. [9] discovered that activity in sensorimotor areas of the prefrontal cortex can be found during the observation of normal human motion and during the observations of point-light human motion as well. They also compared point-light videos showing natural movements to scrambled versions of the same movements (cp. 2.4). They discovered lateral and inferio-temoral areas that are more responsive to point-light videos showing natural movements than to scrambled versions of those.
Ulloa et al. [5] presented five point-light videos based on those of Saygin et al. to subjects of an EEG study. Two of them showed normal human motion, while two showed scrambled versions of these movements and one showed white noise as the baseline (cp. 2.4). They examined modulations of the $\mu$-rhythm while subjects were observing these videos. Their results revealed a strong desynchronization of the $\mu$-rhythm during the observation of the point-light videos that showed normal human motion and a much lower desynchronization for scrambled versions of these videos.
In the present experiment it was tested if the findings of Ulloa et al. [5] could be transferred to a BCI experiment, meaning that the observation of human motion can be discriminated from a scrambled version of this human motion on a single trial basis.

# 2 Methods

## 2.1 Subjects

The experiment was carried out with three subjects (two female and one male). The age of the subjects was between 29 and 38 years. Two of the subjects were students of the Berlin Institute of Technology and knew about the hypothesis. All subjects were paid 20 euros for their participation in the experiment.

## 2.2 Experimental setup

The experiment took place in the EEG laboratory of the Berlin Institute of Technology. Subjects were placed in a sound insulating cabinet to avoid background noise. They viewed the point-light animations on a projection screen that was placed approximately 80 cm in front of their main field of view. The animations consisted of three different conditions that appeared in random order. Detailed information about the stimuli can be found in Section 2.4. The animations were shown for three seconds and the inter-stimulus interval lasted five seconds. In total, subjects viewed 80 animations for each condition in blocks of 5 minutes. The three different conditions appeared in randomized order. In between these blocks there were short breaks that could be aborted any time the subject was feeling ready to continue. In order to keep the subjects motivated, target stimuli have been introduced. While the dots of the point-light animations usually were yellow, their color was changed to green for 10 % of all stimuli after 0.0, 0.5, 1.0, 1.5, 2.0 and 2.5 seconds after stimulus onset respectively. The target stimulus appeared for half a second. The subjects had been instructed to press a button (SPACE of a standard keyboard) as quickly as possible after the target had been discovered. Since this target stimulus was only for motivational purposes all trials containing the target were removed before classification.

## 2.3 Materials

EEG data was recorded from 32 scalp electrodes, which have been placed on a standard 10/20 cap with 128 positions focusing the motor cortex. The Acticap system of the company Brainproducts was used. Additionally horizontal and vertical eye movements were recorded with two bipolar electrodes. Furthermore arm movements were recorded from both arms with two additional bipolar electrodes (EMG). All EEG data was recorded with the Brain Vision Recorder.

## 2.4 Stimuli

Videos showing point-light animated figures have been used as visual stimuli. Point-light figures are common visual stimuli showing distinct positions of joints of the human skeleton that have been used for several experiments concerning the presentation of movements (cp. Saygin et al. (2004) [9], Blake and Shiffrar (2007) [6] and Ulloa and Pineda (2007) [5]).
The motion capturing data used for the presented study was taken from the CMU Graphics Lab Motion Capturing Database of the Carnegie Mellon University that can be found on the internet.[1]
Three conditions can be differentiated ('Running Condition', 'Scrambled Condition' and 'Noise Condition'). The first condition, which stood for the feasible human motion showed an animated point-light figure running.

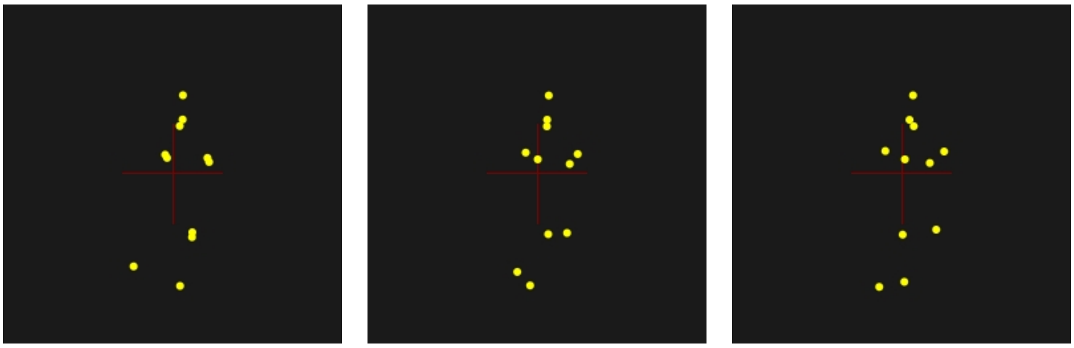

Figure 1: Example of three frames of the point-light animations for the 'Running Condition'.

The second condition was based on the same movement data as the first condition. However the initial positions of the dots were randomized as well as their direction of movement was changed, i. e. the x- and y-components of the positions of randomly selected positions were swapped.

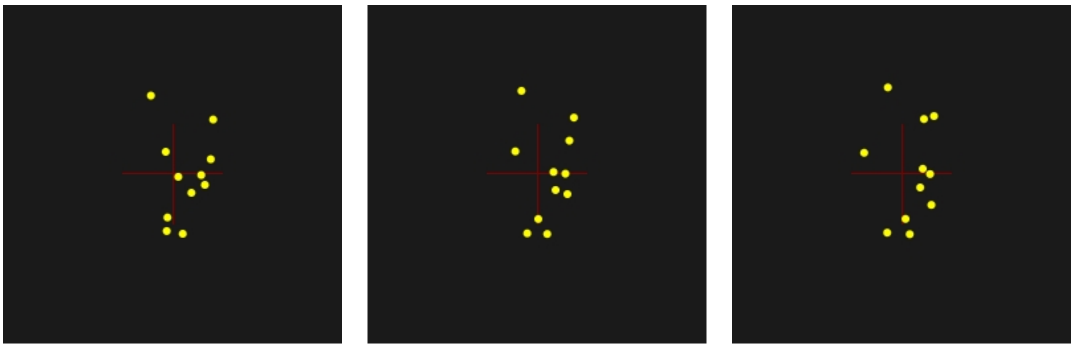

Figure 2: Example of three frames of the point-light animations for the 'Scrambled Condition'.

The third condition, which was used as a control condition showed Gaussian noise. Since every two frames of this animated Gaussian noise were pairwise independent, a discontinuous animation arose, which led to a 'flickering' subjective visual impression, that was completely different from the other two conditions. In order to compensate this 'flickering', the number of dots was dynamically

[1] http://mocap.cs.cmu.edu/

altered from at least one up to a maximum of eleven dots per figure. Furthermore the number of frames per second for these animations was 15, i. e. half of the number of frames per second for the other two conditions. Thus, the general subjective visual impression has been brought much more in line with the other conditions. Examples of pictures of the point-light animations used are shown in Figure 1, 2 and 3.

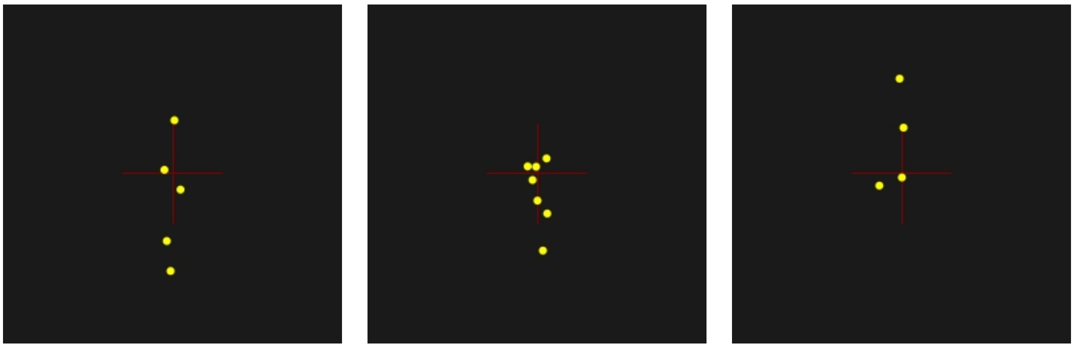

Figure 3: Example of three frames of the point-light animations for the 'Noise Condition'.

### 2.5 Data analysis

Analysis of the data was carried out with the PhyPA Toolbox[2] in MATLAB. In a preprocessing step the data was reduced to epochs of 3 seconds. Starting point of each epoch was the marker position that was set when a point-light sequence appeared on the screen. Furthermore the data was filtered to a frequency spectrum of 7–30 Hz using an FFT-bandpass filter. Epochs were weighted with a Gaussian window function so that the data in the center of each epoch became most relevant for classification.
After preprocessing of the data the 'Running Condition' was tested against the 'Scrambled Condition' and against the 'White Noise Condition' for separability. To maximize the discriminable information between conditions the Spec-CSP algorithm by Tomioka et al. [10] was used. The algorithm is an extension of the CSP algorithm by Ramoser et al. [11]. Spec-CSP is a spatio-temporal filter that maximizes the difference of the variance between classes. Until now it has mainly been used to discriminate lateralized ERD/ERS. Nevertheless the algorithm can be applied to other phenomena as well. In the next step we defined a linear classifier based on linear discriminant analysis (LDA) that was validated on the data. The method of validation that was used was a leave-one-out crossvalidation. A search for optimal parameters was included in the procedure. The parameters included in this search were the time frame and the number of pattern pairs generated by the Spec-CSP algorithm[3]. Examples for the spatio-temporal filtering of the Spec-CSP algorithm are shown in Figure 4. Three different time frames were tested and three different combinations of pattern pairs.

## 3 Results

The 'Running Condition' was tested against the 'Scrambled Condition'. The mean classification error was 29.63 (standard deviation 1.45). The classification error for subject 1 was 31.25 %. The optimal parameters for subject 1 were a timeframe of 0.5–2.5 seconds and two pairs of Spec-CSP patterns. The classification error for subject 2 was 29.17 %. Optimal parameters for this subject were a timeframe of 0.5–2.5 seconds and two pairs of Spec-CSP patterns. For subject 3 the classification error was 28.47 %. Optimal parameters were a timeframe of 0.8–2.2 seconds and

[2]The PhyPA Toolbox was developed by Christian Kothe and Thorsten Zander at the Berlin Institute of Technology. It consists of various functions that support data analysis in the BCI context.
[3]Detailed information about how the patterns were generated can be found in Tomioka et al. [10]

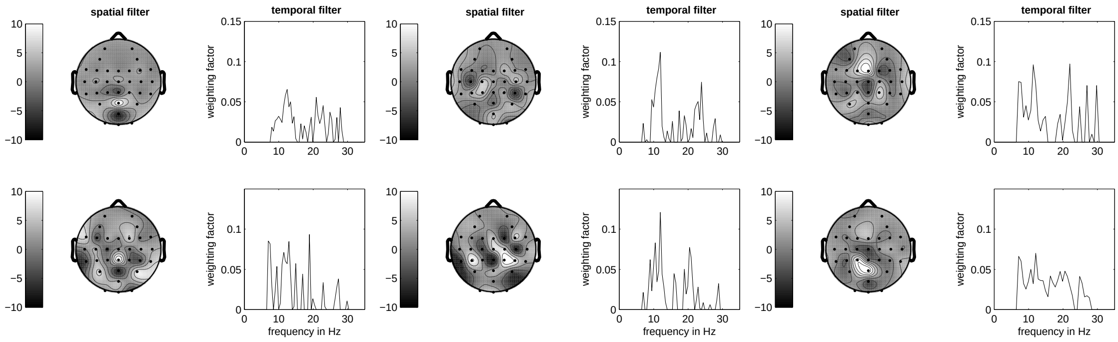


Figure 4: Spatial and temporal filters for subject 1 (left), subject 2 (middle) and subject 3 (right) computed by Spec-CSP. Both, the spatial and the temporal filters are weighting factors and therefore unit-less. Upper row: 'Running Condition'. Lower row: 'Scrambled Condition'.

three pairs of Spec-CSP patterns. The patterns of subject 2 are shown in Figure 4.
The 'Running Condition' was also tested against the 'White Noise Condition'. For these two classes the results are not clear-cut. The classification errors were 38.62 % for subject 1, 35.41 % for subject 2 and 47.22 % for subject 3.

# 4 Discussion

First results indicate that the 'Running Condition' and the 'Scrambled Condition' are separable by our BCI system. Clearly a larger number of subjects is needed to further validate these findings. In most of the patterns electrodes over sensorimotor areas are highly weighted. Especially the results of subject 2 are clear-cut. This indicates that a desynchronisation of the $\mu$-rhythm might be involved in the classification process. Furthermore frequencies in the alpha- and in the beta-band are highly weighted. Since the $\mu$-rhythm consists of these two frequency-bands, this weighting further enhances the assumption that a modulation of the $\mu$-rhythm is involved in classification.
The 'Running Condition' and the 'White Noise Condition' were separable for two of the three subjects, but the Spec-CSP patterns for this classification were less clearly distributed than those of the first classification.

# 5 Conclusion

The results of the presented experiment are in line with other findings which have shown that the observation of human motion evokes a desynchronisation of the $\mu$-rhythm [5]. Furthermore it has been shown that the observation of feasible human motion causes different modulations over sensorimotor areas than the observation of motion that is not feasible [5]. In the presented experiment these findings were advanced by showing that it is possible to detect this difference on a single trial basis. An experiment with a suitable number of subjects is going to be carried out during the next two months.
The subjects in this experiment were not instructed to imagine the human motion they were observing. This indicates that the observation of human motion per se is dectectable on a single-trial basis. Whether the classification is based on modulations of the $\mu$-rhythm has to be verified with a band power analysis that has not been carried out yet. Nevertheless the highly weighted electrodes over sensorimotor areas, as well as the highly weighted alpha and beta frequency-bands strongly indicate that the classification is based on modulations of the $\mu$-rhythm.
In contrast to the study of Hammon et al. [4] the observation of human motion is not used to further enhance classification rates of a BCI system that is based on motor imagery. The single

trial detection of an observed human motion could be used in a so called passive BCI system. Such a system is designed to extract information of the subject's brain activity, without the need of any intended action by the subject. Possible applications for passive BCI systems are currently being researched in Team PhyPA at the Berlin Institute of Technology.
Although this study is work in progress and our results are preliminary, we can conclude that it seems to be possible to distinguish between feasible and non-feasible movements. We can not assume to have based our classification on the $\mu$-rhythm only. There are wide inter individual differences in classifiability as well as in the patterns of the topo plots.

## References

[1] J. A. Pineda. The functional significance of mu rhythms: Translating "seeing" and "hearing" into "doing". *Brain Res. Rev.*, 50:57–68, 2005.

[2] J. R. Wolpaw, D. J. McFarland, G. W. Neat, and C. A. Forneris. An EEG-based brain-computer interface for cursor control. *Electroencephalogr. Clin. Neurophysiol.*, 78:252–9, 1991.

[3] C. Neuper, R. Scherer, M. Reiner, and G. Pfurtscheller. Imagery of motor actions: differential effects of kinesthetic and visual-motor mode of imagery in single-trial EEG. *Brain Res. Cogn. Brain Res.*, 25:668–77, 2005.

[4] P. S. Hammon, J. A. Pineda, and V. R. de Sa. Viewing motion animations during motor imagery: effects on motor imagery. In G. R. Mueller-Putz, C. Brunner, R. Leeb, R. Scherer, A. Schloegl, S. Wriessneggger, and G. Pfurtscheller, editors, *Proc. 3rd Int. BCI Workshop and Training Course 2006*, pages 62–63, 2006.

[5] E. R. Ulloa and J. A. Pineda. Recognition of point-light biological motion: Mu rhythms and mirror neuron activity. *Behav. Brain Res.*, 183:188–194, 2007.

[6] R. Blake and M. Shiffrar. Perception of human motion. *Annu. Rev. Psychol.*, 58:47–73, 2007.

[7] E. D. Grossman and R. Blake. Perception of coherent motion, biological motion and form-from-motion under dim-light conditions. *Vision Res.*, 39:3721–3727, 1999.

[8] M. Pavlova and A. Sokolov. Orientation specificity in biological motion perception. *Percept. Psychophys.*, 62(5):889–899, 2000.

[9] A. P. Saygin, S. M. Wilson, D. J. Hagler Jr, E. Bates, and M. I. Sereno. Point-light biological motion perception activates human promotor cortex. *J. Neurosci.*, 24(27):6181–6188, 2004.

[10] R. Tomioka, G. Dornhege, G. Nolte, B. Blankertz, K. Aihara, and K.-R. Müller. Spectrally weighted common spatial pattern algorithm for single trial EEG classification. Technical Report 40, Dept. of Mathematical Engineering, The University of Tokyo, 2006.

[11] H. Ramoser, J. Müller-Gerking, and G. Pfurtscheller. Optimal spatial filtering of single trial EEG during imagined hand movement. *IEEE Trans. Rehabil. Eng.*, 8:441–446, 2000.

# The importance of individual features for motor-imagery based BCI

V. Attina[1,2,3], E. Maby[1,2,3], R. Bouet[1,2,3], G. Gibert[1,2,3], J. Mattout[1,2,3], O. Bertrand[1,2,3]

[1]INSERM, U821, Lyon, F-69500, France
[2]Institut Fédératif des Neurosciences, Lyon, F-69000, France
[3]Université Lyon 1, Lyon, F-69000, France

virginie.attina@inserm.fr

**Abstract**

The aim of the present study is to investigate the influence of various experimental parameters and features for future use in motor-imagery based BCI. Three types of movement are investigated: index tapping, sustained clenching and repetitive clenching. Real and imaginary movement executions are also compared. Finally, interindividual variability is addressed by comparing features common to all subjects with individually optimized ones. Results show that individual features, namely in the spatial and frequency domain, yield on average significantly enhanced differences between experimental conditions that could be exploited to optimize a future motor-imagery based BCI.

## 1 Introduction

Motor imagery is one of the most investigated process to implement an efficient and direct brain-computer interface (BCI) (see [1, 2] for a review). These BCI are generally based on mu rythm (8–12 Hz) desynchronization as observable with EEG over motor areas during motor imagery, in a similar way as in movement preparation or execution. Although a lot of studies have focused on signal processing techniques to reduce classification error in motor-based BCI, very few studies have provided insights on the role of movement types.

In the present study, we compare mu power desynchronization during the realization or imagination of three different movements: index tapping (IT), sustained clenching (SC) and repetitive clenching (RC). Movements are performed either with the right or the left hand. Our main goal is to identify crucial guidelines for optimizing a future motor-imagery based BCI. Therefore and since BCIs are meant to be optimized for individual usage, we investigate signal feature space, namely in the spatial and frequency domain. Hence we focus on subject differences in terms of scalp region of interest (ROI) for data acquisition and mu frequency range. In a multi-subject statistical analysis, we compare those individual features with some literature-based definitions of classical motor related ROIs and mu rhythms.

In this paper, we focus on the quantitative comparison between different possible features to discriminate between movement types. It tackles the preliminary question: do the considered movements exhibit significant differences at the single trial level, on average? We address this question with a classical factorial design and analysis of variance. We hoped the answer would be positive so that we can contemplate building a BCI paradigm based on the identified features. Evaluation of such a BCI will be the focus of future work that will then tackle the following question: how well can we classify single trial responses based on those features? This is typically addressed using cross validation.

# 2 Methods

## 2.1 Subjects

Six healthy right-handed female subjects (range age: 21–29 years, mean age: 22.7) participated in the experiment. They were all free of neurological diseases and had no previous experience with motor-imagery paradigms. All subjects signed an informed consent approved by the local Ethical Committee and received monetary compensation for their participation. Because she failed in performing the imaginary movement task, one subject was excluded from the analysis.

## 2.2 Experimental paradigm

During the recording, subjects were sitting in a comfortable armchair in an electrically shielded room. Task execution was monitored with the PsyScope software [3], using an Apple Macintosh G4 computer for visual display of instructions and cues within the acquisition room. Each subject started the experiment with a short training session to ensure they correctly understood the task. Then, the actual experiment was divided into 12 blocks whose order was randomized. Each block was made of 16 trials of 20 seconds each and was dedicated to one of the three movement types only. Each trial consisted in 2 seconds of rest (R), followed by 5 seconds of actual movement (M), 5 seconds of rest (R), 5 seconds of motor imagery (I) and 3 seconds of rest (R) (Figure 1). Within trial, imagery was always performed after the exact same real movement in order to ease the imaginary task. The hand to be used was randomly chosen and equally balanced within block. It remained the same within trial and was indicated by a right or left arrow during the whole task periods (M and I). The subject was also asked to fixate a cross at the middle of the screen to minimize eye movements. In total each participant underwent 192 trials, hence about one hour of experiment.

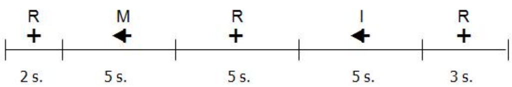


Figure 1: Timing of a trial.

## 2.3 Data acquisition and preprocessing

EEG activity was recorded from 32 scalp active electrodes (actiCAP, BrainProduct GmBH, Munich, Germany) placed at standard locations of an extended 10–10 international system (Figure 2). All electrodes were referenced to the nose and grounded to the forehead. Horizontal and vertical electrooculograms (EOG) were recorded from the right eye. Ag/AgCl bipolar electrodes were used on both arms and located in order to get EMG signals for each movement type. Electrode impedances were kept below 10 kΩ. EEG was amplified (BrainProduct GmBH, Munich), filtered (0.1–150 Hz), and digitized online with a sampling frequency of 1000 Hz.

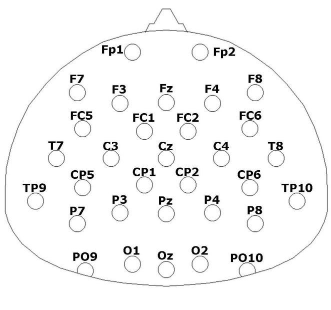


Figure 2: Electrode montage.

| Subject | Mu band (Hz) | Left ROI | Right ROI |
|---|---|---|---|
| 1 | 9–12 | CP1, P3 | C4, CP2, P4, CP6 |
| 2 | 8–10 | CP1, P3, CP5 | C4, CP2, P4 |
| 3 | 9–13 | C3, CP1, CP5 | C4, CP2, CP6 |
| 4 | 7–9 | C3, CP1 | C4, CP2 |
| 5 | 12–14 | C3, CP5 | C4 |

Table 1: Individual features.

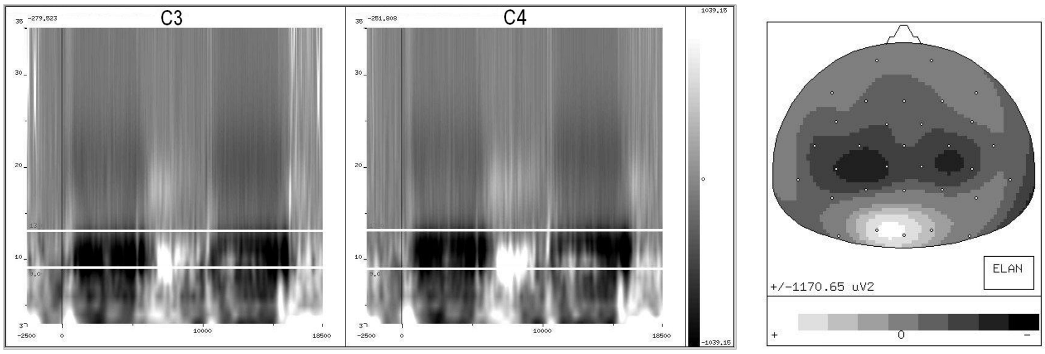


(a) (b)

Figure 3: (a) Grand mean time-frequency plots over C3 and C4 for subject 3. The most important mu desynchronization can be observed between 9 Hz and 13 Hz. (b) Topographical distributions of the averaged mu power during actual movement. Mu desynchronization can be observed over the C3, CP1 and CP5 electrodes (left ROI) and over the C4, CP2, CP6 electrodes (right ROI).

After epoching, all trial data with large muscular activity were rejected from further analyses. The eye blink component was automatically removed using ICA [4]. This preprocessing step left at least 26 clean trials for each participant, each hand and each movement type.

## 2.4 Data analysis

Data analysis focused on mu power during movement (desynchronization) relatively to mu power during rest. For each condition, the averaged time-frequency transform across single trials [5] was computed for both real and imaginary movements, using a three-second-length time window (from 1 to 4 seconds after movement cue onset). Data from the same trial were baseline corrected using the same initial resting period (from 1500 to 500 ms before the real movement cue onset). Two different spectral analysis were performed from the time-frequency representations: a common-feature based analysis and an individual-feature based one. In the first one, mu power was computed in the 8–12 Hz frequency band from electrodes C3 and C4 [6]. In the subject specific procedure, individual features (specific mu range and ROIs) were identified from the averaged time-frequency plots over all conditions (see Table 1). Individual mu range was first determined from individual time-frequency plots over centro-parietal electrodes (Figure 3(a)) and then individual ROIs were selected from the ensuing mu power topographies (Figure 3(b)).

Using R software [7], linear mixed effect modeling [8, 9] was applied to both data sets, with Movement Type (real vs. imaginary movement), Movement (IT, RC and SC), Hand (left vs. right) and ROI (left vs. right) as fixed effects and Subject as random effect to account for between subject variability. An analysis of variance was then computed separately on both estimated fixed effects.

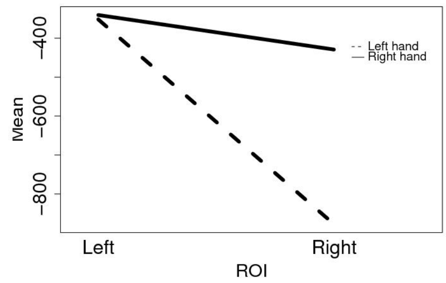


Figure 4: Two-way interaction (Hand × ROI) when considering the common mu-range definition.

# 3 Results

## 3.1 Towards a routine-based BCI

From spatial and frequency features common to all subjects, results showed a main effect of Hand ($p < 0.001$), with lower mu power during left hand compared to right hand movement. The interaction between Hand and ROI factors proved also significant ($p < 0.05$; Figure 4), showing a larger decrease in mu power on C4 than on C3 for left hand movements. Surprisingly, a similar pattern was observed for right hand. No other significant main effects or interactions were found, suggesting no significant differences in mu power due to movement type or between real and imaginary movements.

## 3.2 Towards a subject-specific BCI

Here considering individual features in terms of both mu frequency range and ROIs, a significant mu desynchonization was again observed for left hand movements ($p < 0.0001$). Furthermore, significant interactions were observed: Hand × ROI ($p < 0.01$) and ROI × Movement ($p < 0.05$). Contrary to what was evidenced from the use of common features, a clear controlateralization for each hand is revealed (see Figure 5(a)). This suggests that common features may fail to extract informative signals that can be revealed by subject specific features.

Moreover and contrary to the previous analysis, the ROI × Movement interaction proved significant here (see Figure 5(b)). Indeed, while RC and SC movements reveal a similar pattern of relative mu power from left to right ROI, this pattern is inverted for IT movements. This may be due to the difference in either the movement effectors (index vs. full hand movement) or the kind of movement (tapping vs. clenching).

On the other hand and as revealed by a significant main effect of Movement ($p < 0.01$), a global mu power was found greater for SC compare to both IT and RC, and for IT compare to RC. This may be explained by the difference in performing a sustained versus repeated movement.

Finally, a significant main effect of Movement Type was found with individual features ($p < 0.01$), due to lower mu power values for real compare to imaginary movements. Note however that mu power values are all negative (compare to resting periods), suggesting that the motor-imagery task was well performed.

# 4 Discussion and conclusion

Although more subjects would need to be tested in order to confirm our findings, the present study provides clear evidence in favor of the use of individual features to optimize a motor-imagery based BCI.

Indeed, our comparison of common and individual features in the spatial and frequency domains revealed the following statistical differences. The difference between controlateral and ipsilateral mu desynchronization was only significant when considering individual features, as observed with

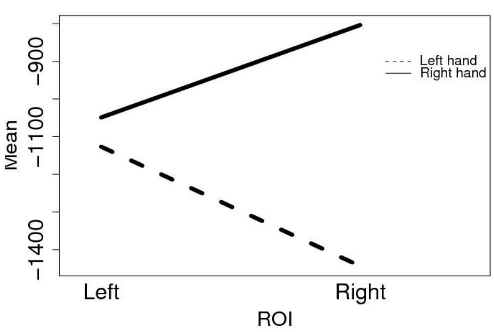


(a)

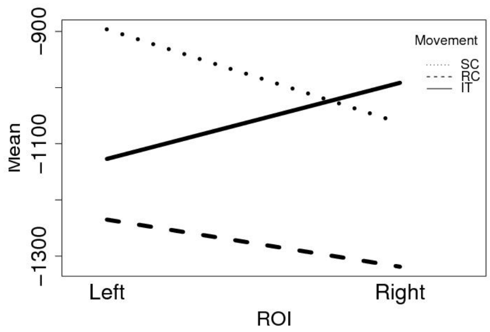


(b)

Figure 5: Plot of the two-way interactions (a) Hand × ROI and (b) ROI × Movement in the mu band for individual features.

both the left and right hand movements. This is probably due to the optimization of the ROI since C3 did not appear to be informative for both subjects 1 and 2 (see Table 1). This finding holds true for either real or imaginary movements. Note also, that in all cases, left movements induced a larger mu desynchronization than right movement, maybe reflecting the right-handedness of the subjects.

This study suggests, whatever the strategy (see e. g. [10] for a binary-command BCI based on the contrast between bilateral imagery and rest) that subtle and carefully indentified individual features or preferences (e. g. in the type of movements) could optimize motor-imagery based BCI in a significant way [6, 11]. According to our results, lateralization of imaginary movements as well as movement type (e. g. clenching vs. tapping) are relevant parameters to be looked at individually.

To further assess the differences between conditions, we contemplate to analyze the dynamics of mu desynchronization during movements. It might be that the full period between 1 and 4 seconds after movement cue onset is not specific enough or subject dependent and could be also individually optimized. Indeed, the visual comparison of time-frequency plots during real and imaginary movements indicate a less stable mu desynchronization during motor imagery. This may be due to the fact that all the subjects were untrained and naïve regarding motor imagery.

Although it was designed in the perspective of optimizing a BCI application, the current experiment was performed offline and involved a classical factorial design with several-second-long trials. In BCI practice, decision would need to be taken more rapidly, on a few hundred of milliseconds basis. Therefore, studying and exploiting the temporal structure of the identified features will be crucial. One possible direction we are currently investigating is temporal integration in probabilistic decisions using dynamical classification models (see [12]).

Finally, we focussed the current analysis on mu rythm and motor related electrode sites. Further improvement could be obtained from including other locations and frequencies, such as beta (around 16–24 Hz) desynchronization, or faster rythms as proposed in [13].

**Acknowledgments:** The authors are grateful to Amélie Da Costa for her valuable contribution in collecting the data. This work was supported by the French National Research Agency and the National Network for Software Technologies within the Open-ViBE project and grant ANR05RNTL01601.

# References

[1] G. Pfurtscheller and C. Neuper. Motor imagery and direct brain-computer communication. *IEEE J. Proc.*, 89:1123–1134, 2001.

[2] J. R. Wolpaw, N. Birbaumer, D. J. McFarland, G. Pfurtscheller, and T. M. Vaughan. Brain-computer interfaces for communication and control. *Clin. Neurophysiol.*, 113:767–791, 2002.

[3] J. D. Cohen, B. MacWhinney, M. Flatt, and J. Provost. Psyscope: A new graphic interactive environment for designing psychology experiments. *Behav. Res. Methods, Instruments and Computers*, 25:257–271, 1993.

[4] A. Delorme and S. Makeig. Eeglab: an open source toolbox for analysis of single-trial eeg dynamics including independent component analysis. *J. Neurosci. Methods*, 134:9–21, 2004.

[5] C. Tallon-Baudry and O. Bertrand. Oscillatory gamma activity in humans and its role in object representation. *Trends Cogn. Sci.*, 3:151–162, 1999.

[6] G. Pfurtscheller, C. Neuper, D. Flotzinger, and M. Pregenzer. Eeg-based discrimination between imagination of right and left hand movement. *Electroencephalogr. Clin. Neurophysiol.*, 103:642–651, 1997.

[7] R Development Core Team. *R: A language and environment for statistical computing.* R Foundation for Statistical Computing, Vienna, Austria, 2005. ISBN 3-900051-07-0.

[8] J. C. Pinheiro and D. M. Bates. *Mixed-Effects Models in S and S-Plus.* Springer, 2000. ISBN 0-387-98957-0.

[9] J. Pinheiro, D. Bates, S. DebRoy, and D. Sarkar. *nlme: Linear and nonlinear mixed effects models*, 2006. R package version 3.1-78.

[10] J. Mellinger, G. Schalk, C. Braun, H. Preissl, W. Rosenstiel, N. Birbaumer, and A. Kübler. An meg-based brain-computer interface (bci). *Neuroimage*, 36:581–593, 2007.

[11] C. Neuper, R. Scherer, M. Reiner, and G. Pfurtscheller. Imagery of motor actions: differential effects of kinesthetic and visual-motor mode of imagery in single-trial EEG. *Brain Res. Cogn. Brain Res.*, 25:668–677, 2005.

[12] J. Mattout, G. Gibert, V. Attina, E. Maby, and O. Bertrand. Probabilistic classification models for brain computer interfaces. In *14th Annual Meeting of the Organization for Human Brain Mapping*, 2008.

[13] R. Grave de Peralta Menendez, Q. Noirhomme, F. Cincotti, D. Mattia, F. Aloise, and S. Gonzalez Andino. Modern electrophysiological methods for brain-computer interfaces. *Comput. Intell. Neurosci.*, 2007:56986, 2007.

# Repeated BCI sessions without new training

M. Tangermann[1], M. Krauledat[1], B. Blankertz[1], K.-R. Müller[1,2]

[1]Machine Learning Laboratory, Berlin Institute of Technology, Germany
[2]Intelligent Data Analysis Group, Fraunhofer FIRST, Berlin, Germany

schroedm@cs.tu-berlin.de

**Abstract**

In this paper we suggest a new method that overcomes the requirement of time-consuming calibration recordings at the start of every new Brain-Computer Interface (BCI) session for long-term users. The method takes advantage of knowledge collected in previous sessions about spatial filters and classifiers: By a novel technique, prototypical spatial filters are determined which have better generalization properties compared to single-session filters. In particular, they can be used in follow-up sessions without the need to recalibrate the system. This way the calibration periods can be dramatically shortened or even completely omitted for these "experienced" BCI users. The feasibility of our novel approach is demonstrated with a series of online BCI experiments. Although performed without any calibration measurement at all, no loss of classification performance was observed.

## 1 Introduction

In the machine learning approach to BCI ([1]) a statistical analysis of a calibration measurement is used to adapt the system to the specificities of the user's current brain signals at the beginning of each session. This approach allows for an effective performance from the first session on without user training ([2]). As the signals vary between sessions even for the same user, BCI systems rely on the calibration procedure for an optimal performance (machine training).

Besides the montage of the EEG cap, the recording of calibration data is the most time-consuming preparational step at the beginning of every new session. It will be addressed by the so-called the Zero-Training method in the present online study.

The basic idea of the method is as follows: In the case of long-term BCI users, who repeatedly perform BCI sessions with the same mental tasks, one can exploit data from previous sessions in order to learn most of the calibration parameters. In more detail, we show how to learn good spatial filters and classifiers from data of previous sessions which eliminates the necessity of going through a new calibration phase during each new session (see Figure 1).

In the current work, we expand the work of Krauledat et al. [3] to the online scenario. The Zero-Training method is tested against the standard approach where spatial filters and classifiers are trained anew on the calibration data of a new session.

## 2 Methods

The exact location, the exact frequency band of the sensorimotor rhythm and the way it can be influenced by motor imagery (resulting e. g. in event-related desynchronization (ERD) or synchronization (ERS) [4]), is subject-specific. Hence individually optimized filters can increase the signal-to-noise ratio dramatically [5]. To this end, the Common Spatial Patterns (CSP) technique has proven to be a useful tool for BCI.

**Common Spatial Pattern** and its extensions (e. g. [6, 5]) is a technique to analyze multi-channel data based on recordings from two classes (conditions). It is, e. g. used in BCI systems based on the modulation of brain rhythms. CSP filters maximize the EEG signal's variance under one condition while simultaneously minimizing it for the other condition. In the example of left vs. right hand motor imagery, the CSP algorithm will find two groups of spatial filters. The first

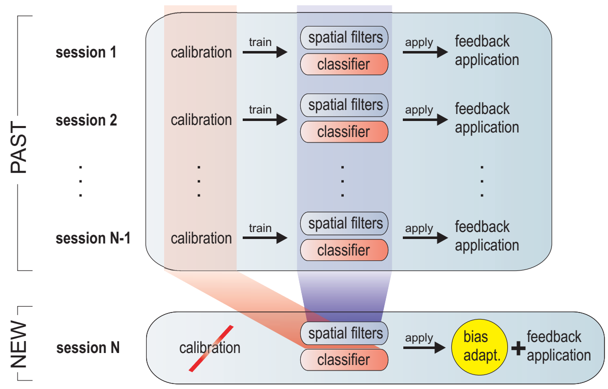


Figure 1: Sessions 1 to N-1 follow a standard BCI procedure: spatial filter and classifiers are learned each session anew from a calibration recording before they are applied during a feedback application. The new Zero-Training method eliminates the calibration recording: spatial filters and a classifier are predetermined before session $N$ starts. The spatial filters for session $N$ are extracted from old filters (blue), the classifier for session $N$ is calculated from old calibration recordings (red). The feedback application of session $N$ is preceded by a quick bias adaptation.

will show high band power during left hand motor imagery and low band power during right hand motor imagery, and the second vice versa.

Let $\mathbf{\Sigma}_i$ be the covariance matrix of the trial-concatenated matrix of dimension $[C \times T]$ (where $C$ is the number of electrodes and $T$ is the number of concatenated samples) belonging to the respective class $i \in \{1, 2\}$. The CSP analysis consists of calculating a matrix $\mathbf{W} \in I\!R^{C \times C}$ and a diagonal matrix $\mathbf{D}$ with elements in $[0, 1]$ such that

$$\mathbf{W}^\top \mathbf{\Sigma}_1 \mathbf{W} = \mathbf{D} \quad \text{and} \quad \mathbf{W}^\top \mathbf{\Sigma}_2 \mathbf{W} = \mathbf{I} - \mathbf{D} \tag{1}$$

where $\mathbf{I} \in I\!R^{C \times C}$ is the identity matrix. This can be solved as a generalized eigenvalue problem. The projection that is given by the $i$-th column of matrix $\mathbf{W}$ has a relative variance of $d_i$ ($i$-th element of $\mathbf{D}$) for trials of class 1 and relative variance $1 - d_i$ for trials of class 2. If $d_i$ is near 1, the filter given by the $i$-th column of $W$ (i. e., the $i$th spatial filter) maximizes the variance for class 1, and since $1 - d_i$ is near 0, it also minimizes the variance for class 2. Typically one would retain projections corresponding to two or three of the highest eigenvalues $d_i$, i. e., CSP filters for class 1, and projections corresponding to the two or three lowest eigenvalues, i. e., CSP filters for class 2. For a detailed review of the CSP technique with respect to the application in BCI see [5].

Krauledat et al. [3] showed in an offline analysis on data from repeated sessions for a number of subjects, that spatial filters computed via CSP can be clustered into physiologically relevant groups using a specialized metric [7] in the CSP filter space.

Extracting prototypical CSP filters from regions with a high density of CSP filters and applying them to data of an unseen new session of the same user, those prototypical filters result in very good offline classification performance. For the present online study, we used the same methods for creating the CSP filter space and for determining cluster prototypes.

## 3 Experimental setup

To demonstrate the feasibility of the Zero-Training approach, a BCI feedback study was designed to compare the proposed approach with the classical CSP approach in terms of feedback performance. The specific construction of the two classification setups is described in Section 3.1.

The BCI experiments were performed with 6 healthy subjects, aged 26–41 who previously had performed at least 5 motor imagery BCI sessions with the Berlin Brain-Computer Interface

| Subject | #chan-nels | #past sessions | #train trials | Classes | FQ band (CSP) | ($ZT$) | Interval (CSP) | ($ZT$) |
|---|---|---|---|---|---|---|---|---|
| *zq* | 46 | 7 | 845 | LR | [9 14] | [9 25] | [810 4460] | [500 3000] |
| *ay* | 46 | 4 | 324 | LR | [8 22] | [9 25] | [710 2650] | [500 3000] |
| *zp* | 46 | 5 | 704 | LR | [10 25] | [9 25] | [2750 5000] | [500 3000] |
| *al* | 44 | 9 | 684 | FR | [11 25] | [9 25] | [1600 4690] | [500 3000] |
| *aw* | 44 | 13 | 1075 | LF | [11 17] | [10 25] | [1500 4500] | [500 3000] |
| *zk* | 46 | 7 | 240 | LR | [8 31] | [9 25] | [920 4390] | [500 3000] |

Table 1: Subject-specific parameters for CSP and Zero-Training (ZT)

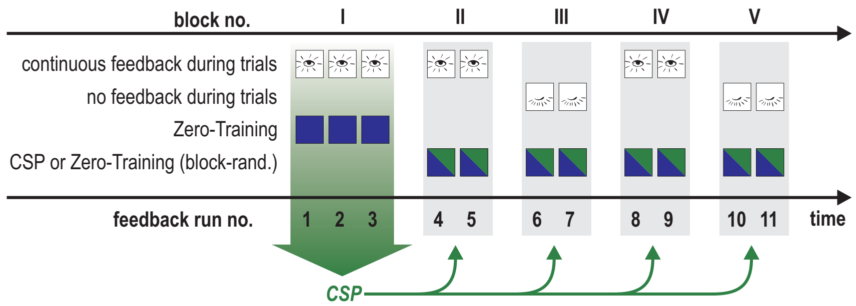


Figure 2: Sequence of the 11 runs and the two methods used for calculating feedback.

(BBCI). The availability of a large amount of experimental data is a prerequisite for the extraction of prototypical CSP filters, since the cluster density in the CSP filter space can only be estimated reliably with a sufficient number of sample points.

The visual feedback of horizontal cursor control was given in 11 runs of 100 trials each (50 per class). The runs were grouped in five experimental blocks (see Figure 2). In three runs of block I, continuous feedback was given by a classifier that had been pre-computed with the Zero-Training method, see Section 3.1. Data collected in these runs were used to determine spatial filters and a classifier using the ordinary CSP method as described in Section 3.1 for use in some runs of the following blocks. Blocks II to V each contained one run with Zero-Training feedback and one run with CSP feedback. Within a block, the order of the two feedback methods was chosen randomly and remained unknown to the subject. To represent two different widespread approaches, the use of continuous visual feedback and no continuous visual feedback alternated regularly between blocks II to V, as indicated in Figure 2.

During the experiment the subjects were sitting in a comfortable chair in front of a computer screen. EEG was recorded with 64 Ag/AgCl electrodes, downsampled to 100 Hz, bandpass-filtered at a subject-specific frequency band (see Table 1) and spatial CSP filters, as described in Section 2, were applied. Finally, the logarithmic band power of the spatially and temporally filtered signals was estimated by calculating the logarithm of the squared sum of the filter outputs. These features were fed into a linear classifier. We used least squares regression (LSR). At a rate of 25 Hz, graded LSR outputs were calculated for the last 1000 ms, and averaged over 8 samples. A scalar factor was multiplied to the result, and finally a real-valued bias term was added.

CSP filters are not adapted during the online operation. The system allows for a stable performance even for several hours ( [8]), but the bias of the classifier might need to be adjusted. Guided by our experience with non-stationary bias, a bias adaptation was performed at the beginning of every run. Therefore, the subject controlled the cursor for 20 trials (10 per class), and the bias was adapted at the end of this period. The procedure corresponds to the initial calibration of the bias as presented in [9]. A thorough investigation of this topic can be found in [10].

### 3.1 Construction of classifiers

Both approaches, the proposed new Zero-Training approach and the classical CSP use only a small number of spatial filters (two or three per class) from the total set of filters provided by CSP, as the restriction to a small number of filters per class is known to be helpful [5].

#### The Zero-Training filters and classifier

For every subject, we performed the following: for each class and for each historic session of the subject, we calculate the three filters with the largest Eigenvalues using the CSP algorithm in Section 2. Depending on the number of past sessions, this procedure creates a larger set of filters. Then 6 so-called prototype filters are chosen from the set by applying the clustering method described in [3]. Those filters constitute the first 6 dimensions of the final feature space for the Zero-Training method. In addition we pool all data from past experiments of the subject and calculate the ordinary CSP filters on this collection. The resulting CSP filters (3 per class) are concatenated to the 6 prototype filters gained from the clustering approach.

With this approach, filtering the EEG data of the pooled data set (all past sessions of the subject) results in a 12-dimensional feature space. Finally, a linear LSR classifier is calculated on the features. If necessary we could also use nonlinear classification here (cf. [11]).

#### The ordinary CSP filters and classifier

For each subject, we also build a set of ordinary CSP filters and a corresponding classifier. In contrast to the Zero-Training solution, they can not be prepared beforehand. Their construction is done on the fly during a new experimental session and does not involve data from past sessions.

For the training of a regular CSP classifier, we first record three runs of feedback data (with feedback provided by the output of the Zero-Training classifier), totalling to more than 150 trials per class. According to the cross-validation error on this data, the optimal frequency band is selected, as well as some additional parameters like length and starting point of the training time interval for estimating the band power. The Common Spatial Patterns are computed on this data and the two spatial filters representing the most extreme eigenvalues are chosen for each class. Finally a LSR classifier was trained using the preprocessed data from the first three runs.

## 4 Results

The first three runs of feedback showed that all subjects under study were able to operate the BCI with the pre-computed classifier at a high accuracy (only 10 trials per class from the current day were required to update the bias for the classification scenario). For every subject Fig. 3 shows the percentage of successful ("hit") trials from each run. After the third run, the subjects could not know in advance, which one of the two classifiers (Zero-Training or ordinary CSP) was used for the generation of the feedback.

For subjects *zq*, *al* and *zk*, the CSP feedback performed better than the Zero-Training feedback. In *ay* and *aw*, the feedback performance on the four blocks is very similar with both classifiers, whereas in subject *zp*, the Zero-Training feedback even outperformed the CSP feedback.

The performance over all subjects is shown in Fig. 4, where the feedback performance in each run of the four blocks is collected in a single boxplot for each classifier. The CSP performance is slightly higher on average, although this difference is not very significant: a Wilcoxon ranking test yields a significance level of $p = 0.05$.

Extensive offline tests, that simulated different levels of bias adaptation between runs, showed that the bias adaptation was indispensable for two of the six subjects and did not degrade the performance for the other subjects. This result matches with results of previous studies [9, 10].

No systematic difference in performance could be observed between the continuous visual feedback in blocks II and IV compared to no continuous visual feedback in blocks III and V.

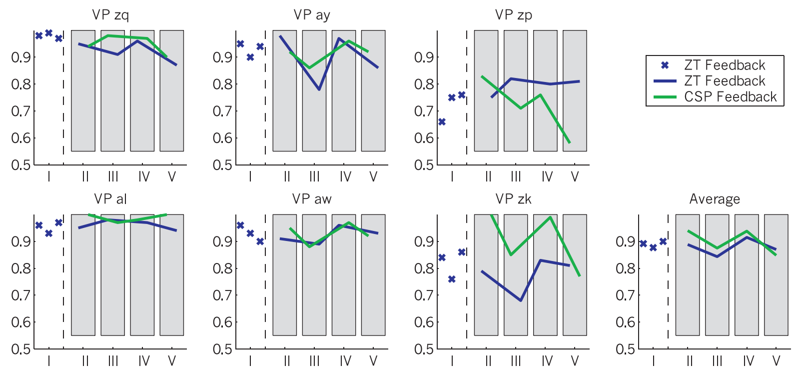


Figure 3: Feedback results for the six subjects and 100 trials per run. Three initial runs (block I), were done with the Zero-Training classifier. In following blocks II–V the order of the classifiers was randomly permuted. The shift of the blue curve relative to the green curve within the shaded areas indicates the order of the classifiers within each block.

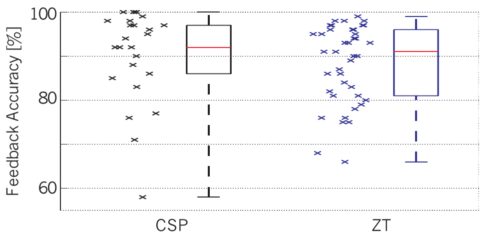


Figure 4: Feedback performance of CSP and *Zero-Training* over all subjects and runs.

# 5 Discussion

The final validation of BCI algorithms can only be provided in online experiments. However, in contrast to offline evaluation, only one classifier can be applied to the same data set. This makes a comparison especially hard, since the differences between data sets (high inter-subject and inter-session variability) add to the variability of the performance. Therefore it is required to record all data sets under similar conditions. All presented online experiments for one subject were therefore carried out on the same day. We evaluated the performance of our new classifier by comparing it to the standard CSP method that is typically used for the classification of band power features in motor imagery paradigms (see e. g. [2]).

The aim of this study was to construct and evaluate a classification method that can be applied without a lengthy calibration measurement. We could show, that the features chosen via Zero-Training are discriminative for the classification task at hand, but also that the bias adaptation was indispensable for two of the six subjects.

It has been shown in recent publications [5], that the optimization of spatial and temporal parameters can result in a significantly increased classification accuracy. For the training of the Zero-Training classifier however, some of the parameters were not specifically optimized, such as the frequency band, the training window for parameter estimation on the previous sessions, and the movement type combination used for the feedback. These parameters were fixed beforehand. In contrary to this, the subject-dependent parameters of the standard CSP method were selected individually based on the same day's training data. We are fully aware, that this comparison strategy may have resulted in a slight advantage in favor of the standard CSP method, but we accepted this advantage in order to have a maximally strong adversary method available for the comparison with our new Zero-Training method.

## 6 Conclusion

In this contribution we went one step further towards the goal of avoiding subject training altogether and proposed novel algorithms to transfer knowledge between BCI sessions. Our study shows that the results from prior off-line analysis, successfully carry over to the present set of online experiments, where subjects use decoders that were constructed from past data instead of calibrating anew. Our findings thus show that information from prior session can indeed be used profitably for constructing better individual mental state decoders. Note that the loss in performance (bitrate) is negligible when contrasted to employing a fully calibrated decoder (after 30 minutes of training) in a blind protocol.

Our work opens therefore a highly promising path for the ultimate goal of Zero-Training. While the proposed methods work well for session to session transfer for an individual subject, it remains still open, whether inter-subject information could also be successfully transferred. Ideally a data base consisting of individualized decoders could be appropriately combined as an ensemble decoder and thus help to avoid training completely. In combination with dry electrodes, Zero-Training would again provide a large step forward when striving towards more general applicability of BCI technology for daily use in man machine interaction.

## References


[1] B. Blankertz, G. Dornhege, M. Krauledat, K.-R. Müller, and G. Curio. The non-invasive Berlin Brain-Computer Interface: Fast acquisition of effective performance in untrained subjects. *Neuroimage*, 37(2):539–550, 2007.

[2] B. Blankertz, F. Losch, M. Krauledat, G. Dornhege, G. Curio, and K.-R. Müller. The Berlin Brain-Computer Interface: accurate performance from first-session in BCI-naive subjects. *IEEE Trans Biomed Eng*, 2008. in press.

[3] M. Krauledat, M. Schröder, B. Blankertz, and K.-R. Müller. Reducing calibration time for brain-computer interfaces: A clustering approach. In B. Schölkopf, J. Platt, and T. Hoffman, editors, *Advances in Neural Information Processing Systems 19*, pages 753–760, Cambridge, MA, 2007. MIT Press.

[4] G. Pfurtscheller, C. Brunner, A. Schlögl, and F. H. Lopes da Silva. Mu rhythm (de)synchronization and EEG single-trial classification of different motor imagery tasks. *Neuroimage*, 31(1):153–159, 2006.

[5] B. Blankertz, R. Tomioka, S. Lemm, M. Kawanabe, and K.-R. Müller. Optimizing spatial filters for robust EEG single-trial analysis. *IEEE Signal Proc. Mag.*, 25(1):41–56, January 2008.

[6] Z. J. Koles. The quantitative extraction and topographic mapping of the abnormal components in the clinical EEG. *Electroencephalogr. Clin. Neurophysiol.*, 79(6):440–447, 1991.

[7] S. Harmeling, G. Dornhege, D. Tax, F. C. Meinecke, and K.-R. Müller. From outliers to prototypes: ordering data. *Neurocomp.*, 69(13–15):1608–1618, 2006.

[8] K.-R. Müller and B. Blankertz. Toward noninvasive brain-computer interfaces. *IEEE Signal Proc. Mag.*, 23(5):125–128, September 2006.

[9] P. Shenoy, M. Krauledat, B. Blankertz, R. P. N. Rao, and K.-R. Müller. Towards adaptive classification for BCI. *J. Neural Eng.*, 3(1):R13–R23, 2006.

[10] M. Sugiyama, M. Krauledat, and K.-R. Müller. Covariate shift adaptation by importance weighted cross validation. *J. Mach. Learn. Res.*, 8:1027–1061, 2007.

[11] K.-R. Müller, C. W. Anderson, and G. E. Birch. Linear and non-linear methods for brain-computer interfaces. *IEEE Trans. Neural Syst. Rehabil. Eng.*, 11(2):165–169, 2003.

# Motor imagery induced changes in oscillatory EEG components: speed vs. accuracy

R. Scherer[1,2,3], G. Pfurtscheller[1], C. Neuper[1,2]

[1]Institute for Knowledge Discovery, BCI Lab, Graz University of Technology, Graz, Austria
[2]Institute of Psychology, University of Graz, Graz, Austria
[3]Computer Science and Engineering, University of Washington, Seattle, WA, USA

reinhold.scherer@tugraz.at

**Abstract**

Two important issues for Brain-Computer Interface-based (BCI) communication are the information transfer rate and user training. While the former needs to be maximized, a minimization of the latter is mandatory to enhance usability and practicality. In this paper we analyze the relationship between communication speed and classification accuracy of electroencephalographic (EEG) signals recorded during cue-guided left hand and right hand motor imagery. The methods of common spatial patterns (CSP) and Fisher's linear discriminant analysis classifier (LDA) were applied off-line to EEG recordings of sixty-nine ($N = 69$) naive subjects. The results suggest that 2000 ms of EEG data is required to get the best possible discrimination (average accuracy of about 80 %) for the majority of user (61 %).

## 1 Introduction

A Brain-Computer Interface (BCI) allows users to interact with the surrounding environment without the need of any peripheral nerve or muscle activity. Compared to communication aids operated by muscular activity, the information transfer rate (ITR) of a BCI is low. Furthermore, to gain direct brain-computer control, both the human brain and the machine need training. The former to reliably generate distinctive brain patterns and the later to detect them. Depending on the experimental strategy, such a training may require hours or, when working with patients, even days or months. To increase the user acceptance it is therefore crucial to increase the ITR and at the same time to reduce the training period.

The Graz-BCI is based on the single-trial classification and detection of transient oscillatory changes, modulated by motor imagery (MI), in the ongoing electroencephalogram (EEG) [1]. For such a MI-based system one obvious question related to the above mentioned issues is "How much time is required to induce MI modulated brain patterns?" or in other words "How much time is required to reliably discriminate between different mental MI tasks?" The aim of this paper is to research the relationship between classification speed and classification accuracy of MI induced brain patterns in EEG signals. Results of an extensive off-line analysis based on cue-guided trials recorded from sixty-nine ($N = 69$) naive subjects during left hand and right hand MI are presented.

## 2 Methods

### 2.1 Subjects and signal recording

Sixty-nine naive volunteers between 19 and 51 years old ($26 \pm 5$ years, 32 female and 37 male) participated in this study. The volunteers were right handed, had normal or corrected to normal vision and and gave informed consent after the experimental procedure had been explained to them.

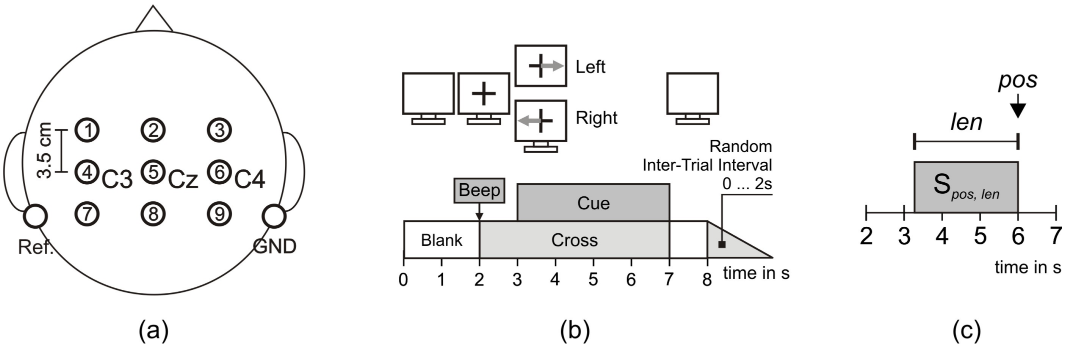


Figure 1: (a) EEG electrode placement. Reference was placed on the left and ground on the right mastoid. (b) Timing of the experimental paradigm used to collect motor imagery related EEG signals. (c) Definition of examined segments.

Each volunteer was seated in an armchair placed about 0.80 m in front of a computer monitor. Nine sintered Ag/AgCl electrodes were placed over sensorimotor areas. The electrode locations included the position C3, Cz and C4, as well as positions 3.5 cm anterior and posterior to these (Figure 1(a)). The EEG was analog band pass filtered between 0.5 and 100 Hz (60 dB/decade, dynamic range ±100 µV, notch at 50 Hz) and sampled at a rate of 250 Hz.

## 2.2 Experimental paradigm

Following a fixed repetitive time scheme, subjects had to imagine left hand and right hand movements. Each trial started with the presentation of a blank screen. After two seconds a fixation cross was displayed in the middle of the screen and an acoustical warning tone was presented. Subjects were told to fixate the cross, avoiding eyes and body movements. One second later, an arrow (cue) pointing to the left (left hand) or to the right (right hand) specified the motor imagery task to perform. Volunteers had to perform motor imagery repetitively for 4 s, until the screen content was erased. After a random inter-trial interval (0–2 s) introduced after second 8 the the next trial started (Figure 1(b)). Each training run consisted of 40 trials with 20 trials per class (left/right) presented in randomized order. Five training runs were recorded for each subject.

## 2.3 Data analysis

All trials were visually inspected for EEG artifacts and trials containing (task-related) EMG or EOG activity were omitted from further analysis. The mean (median) ± SD (standard deviation) number of trials left for analysis were 81.0(85.0) ± 11.6 and 80.8 (83.0) ±12.3 for left hand and right hand motor imagery, respectively.

In order to identify the optimal time interval needed to induce MI-related EEG rhythms and thus achieving best possible discrimination between left hand and right hand MI, the method of Common Spatial Patterns (CSP) was applied. CSP designs spatial filters in such a way that the variances of the filtered time series are optimal (in the least squares sense) for discrimination. For more details refer to [2, 3, 4]. The recorded EEG signal was band pass filtered between 8 and 30 Hz ($5^{\text{th}}$ order Butterworth) and segments $S_{\text{pos}}^{\text{len}}$ of the length len were extracted with the same time lag pos to the begin of a trial (Figure 1(c)). For the analysis the time lag pos was varied from $\text{pos} = 2.0\,\text{s}$ to $\text{pos} = 9.0\,\text{s}$ in steps of $\Delta\text{pos} = 0.125\,\text{s}$. For each pos the segment length len was changed from $\text{len} = 250\,\text{ms}$ to $\text{len} = 4000\,\text{ms}$ in steps of $\Delta\text{len} = 250\,\text{ms}$. Independent CSP analyses were performed for each combination $(\text{pos}, \text{len})$ by using a $10 \times 10$-fold cross validation statistic. This means that 90 % of the segements were used to compute the CSP projection matrix $W$. The $m = 2$ projections resulting form the $m$ largest and $m$ smallest eigenvalues were retained ($W_{2m}$), the logarithm of the normalized variance ($\log \text{NV}^{\text{len}}$) over the segment length len was computed and a Fisher's linear discriminant analysis (LDA) [5] classifier was trained. The computed projection

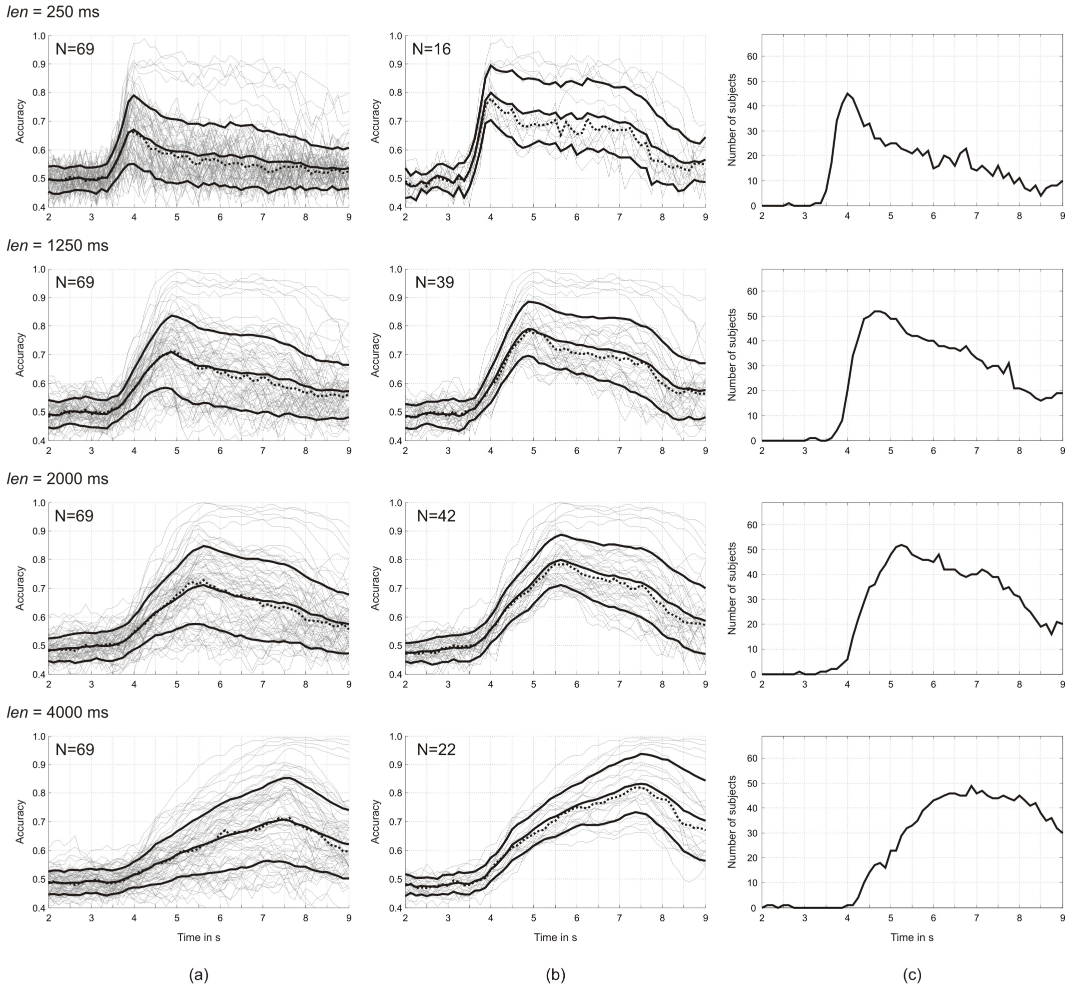


Figure 2: (a) Individual (gray), mean ± SD (bold) and median (dotted) curves of the classification accuracy for different segment window lengths. (b) Accuracies of subjects which performed better than random for at least 2 s out of the 4 s of motor imagery (3.0, . . . , 7.0 s). (c) Number of subjects over time which were better than the individual random level.

matrix $W_{2m}$ was applied to the remaining 10 % of the segments, $\log \mathrm{NV}^{\mathrm{len}}$ was computed and classified. The performance for each $S_{\mathrm{pos,len}}$ was computed by averaging the individual accuracies.

# 3 Results

Exemplarily the discriminative power between left hand and right hand MI as function of time for four different window lengths len are plotted in Figure 2(a). Individual results, as well as the mean ± SD (standard deviation) and median curves are shown. Independently of the segment length len, the maximum average classification accuracy over time is about 70 %. Furthermore, one can see that for five subects the performance was higher than average independently of len. Table 1 summarizes results for subjects (column 2) which maximum accuracy within the MI-period was higher than the chance classification level (computed according [6] and a significance level $\alpha = 0.01$). Most subjects, i. e., 59 out of 69 achieved accuracies better than random when using a segment length of 1250 ms. Highest accuracies were computed by using a 2500 ms window. The average level of chance classification for all subjects was approximately 61 %.

Figure 2(b) shows only the curves of subjects which performance was better than random for

| | | Accuracy | | pos |
|---|---|---|---|---|
| len | $N$ (%) | Mean (Median) ± SD | StdError | Mean (Median) ± SD |
| 250 | 55 (80) | 74.81 (73.60) ± 8.39 | 1.13 | 4.323 (4.000) ± 0.791 |
| 500 | 58 (84) | 76.09 (75.53) ± 9.34 | 1.23 | 4.373 (4.125) ± 0.609 |
| 750 | 58 (84) | 76.78 (75.93) ± 9.45 | 1.24 | 4.666 (4.375) ± 0.718 |
| 1000 | 58 (84) | 77.08 (76.77) ± 9.62 | 1.26 | 4.957 (4.688) ± 0.727 |
| 1250 | **59 (86)** | 77.04 (76.61) ± 9.84 | 1.28 | 5.121 (4.875) ± 0.702 |
| 1500 | 57 (83) | 77.88 (77.06) ± 9.62 | 1.27 | 5.338 (5.125) ± 0.686 |
| 1750 | 57 (83) | 77.88 (75.84) ± 9.64 | 1.28 | 5.540 (5.375) ± 0.610 |
| 2000 | 55 (80) | 78.47 (75.76) ± 9.58 | 1.29 | 5.743 (5.625) ± 0.623 |
| 2250 | 55 (80) | 77.64 (76.20) ±10.00 | 1.35 | 5.828 (5.875) ± 0.677 |
| 2500 | 53 (77) | **79.05 (78.47)** ± 9.25 | 1.27 | 6.061 (6.125) ± 0.466 |
| 2750 | 54 (78) | 78.67 (78.02) ± 9.47 | 1.29 | 6.229 (6.375) ± 0.658 |
| 3000 | 53 (77) | 78.54 (78.52) ± 9.77 | 1.34 | 6.377 (6.500) ± 0.560 |
| 3250 | 55 (80) | 77.89 (78.29) ±10.17 | 1.37 | 6.464 (6.750) ± 0.803 |
| 3500 | 54 (78) | 77.49 (77.07) ±10.27 | 1.40 | 6.600 (6.875) ± 0.810 |
| 3750 | 51 (74) | 76.96 (77.23) ± 9.73 | 1.36 | 6.792 (7.000) ± 0.463 |
| 4000 | 51 (74) | 75.40 (75.78) ± 9.48 | 1.33 | 6.664 (6.875) ± 0.497 |

Table 1: Mean (median) ± SD of the maximum accuracies (in %) which are better than the subject-specific chance classification level. Additionally the standard error (StdError) and mean (median) ± SD time (in s) are presented.

at least 2 s out of the 4-s MI period. Since subjects were told to perform continuous MI for 4 s this criteria reflects the task to perform better than single peak values. Table 2 summarizes the mean peak accuracies of the curves and corresponding time for all segment lengths. Most subjects, i. e. 42 out of 69 (61 %), achieved best results by using a 2000/2250 ms time window. The last column represents the percentage of time during MI (from 3.0 s to 7.0 s) in which subjects were better than random. Figure 2(c) illustrates the underlying distribution. The highest value was achieved by using a 1250 ms time window.

# 4 Discussion

The aim of the study was to research the relationship between speed and accuracy of MI-based BCIs. The method of CSP was selected because default parameters achieve satisfying results over subjects [3] without the need of computational demanding optimization. Additional channels or user-specific optimization, however, potentially increase the classification accuracy [4].

Interesting and already demonstrated is the early classification peak about one second after cue-onset. This peak, clearly visible in Figure 2(a) for segment length len = 250 ms, results very likely from an early contralateral dominant event-related desynchronization (ERD) at electrode positions overlaying the hand representation area. Müller-Gerking et al. [2] reported such an early ERD in a delayed movement task and Pfurtscheller and Neuper [7] during right vs. left hand motor imagery.

Average classification accuracies of approximately 70 % (Figure 2(a)) give evidence that basically each of the analyzed segment lengths can be used to operate a BCI. Longer segments obviously delay the time of highest classification which is varying from about 1 s to approx. 4.5 s after cue-onset. The individual curves show that only a minority of subjects ($< 10$ %) are able to achieve very good control (about 90 %) from the very beginning and during the whole MI-period.

From Table 2 and the mean curves in Figure 2(b) it is visible that the time window needed to obtain a good discrimination, i. e., about 80 %, is best for most subjects by analyzing EEG segments of 1250 ms to 2500 ms length. Table 2 suggests that the best choice in terms of speed, accuracy and number of subjects is a window length of 2000 ms: Forty-two subjects (61 %) achieved

| | | Accuracy | | | |
|---|---|---|---|---|---|
| len | $N$ (%) | Mean (Median) ± SD | StdError | pos | > RND |
| 250 | 16 (23) | 79.90 (77.86) ± 9.46 | 2.37 | 4.000 | 32.11 |
| 500 | 28 (41) | 77.69 (76.78) ± 9.71 | 1.84 | 4.125 | 39.90 |
| 750 | 35 (51) | 78.36 (78.46) ± 9.35 | 1.58 | 4.375 | 43.89 |
| 1000 | 36 (52) | 79.15 (78.76) ± 9.13 | 1.52 | 4.625 | 45.97 |
| 1250 | 39 (57) | 79.05 (78.65) ± 9.42 | 1.51 | 4.875 | 47.46 |
| 1500 | 40 (58) | 79.87 (79.46) ± 9.17 | 1.45 | 5.125 | 47.01 |
| 1750 | 40 (58) | 80.24 (78.83) ± 9.01 | 1.42 | 5.375 | 46.06 |
| 2000 | 42 (61) | 79.92 (78.23) ± 8.80 | 1.36 | 5.625 | 45.52 |
| 2250 | 42 (61) | 80.01 (79.32) ± 9.34 | 1.44 | 5.875 | 44.75 |
| 2500 | 40 (58) | 80.84 (81.51) ± 9.15 | 1.45 | 6.125 | 43.93 |
| 2750 | 34 (49) | 80.80 (80.91) ± 9.45 | 1.62 | 6.375 | 42.39 |
| 3000 | 32 (46) | 81.65 (82.22) ± 9.18 | 1.62 | 6.500 | 41.03 |
| 3250 | 30 (43) | 81.35 (83.32) ± 10.55 | 1.93 | 6.875 | 40.04 |
| 3500 | 28 (41) | 82.00 (82.12) ± 10.01 | 1.89 | 7.000 | 37.77 |
| 3750 | 24 (35) | 82.22 (81.69) ± 9.78 | 2.00 | 7.000 | 35.82 |
| 4000 | 22 (32) | 80.95 (78.91) ± 9.96 | 2.12 | 7.000 | 33.74 |

Table 2: Mean (median) ± SD classification accuracy (in %), standard error (StdError in %) and time (in s) are reported. Only subject which performed better than random in $\leq 2$ s out of the 4-s motor imagery period were considered ($N$). Column RND shows the percentage (over all subjects) within the 4-s MI period in which the performance was higher than random.

an average classification accuracy of about 80 % approximately 2.6 s after cue-onset.

# References


[1] G. Pfurtscheller, G. R. Müller-Putz, A. Schlögl, B. Graimann, R. Scherer, R. Leeb, C. Brunner, C. Keinrath, F. Lee, G. Townsend, C. Vidaurre, and C. Neuper. 15 years of BCI research at Graz University of Technology: current projects. *IEEE Trans. Neural Syst. Rehabil. Eng.*, 14(2):205–210, Jun 2006.

[2] J. Müller-Gerking, G. Pfurtscheller, and H. Flyvbjerg. Designing optimal spatial filters for single-trial EEG classification in a movement task. *Clin. Neurophysiol.*, 110(5):787–798, May 1999.

[3] H. Ramoser, J. Müller-Gerking, and G. Pfurtscheller. Optimal spatial filtering of single trial EEG during imagined hand movement. *IEEE Trans. Rehabil. Eng.*, 8(4):441–446, Dec 2000.

[4] B. Blankertz, R. Tomioka, S. Lemm, M. Kawanabe, and K.-R. Müller. Optimizing spatial filters for robust EEG single-trial analysis. *IEEE Signal Process. Mag.*, 25(1):41–56, 2008.

[5] R. Duda, P. Hart, and D. Stork. *Pattern Classification (2nd ed.).* Wiley Interscience, 2000.

[6] G. R. Müller-Putz, R. Scherer, C. Brunner, R. Leeb, and G. Pfurtscheller. Better than random? a closer look on bci results. *Int. J. Bioelectromagnetism*, 10 (1):52–55, 2008.

[7] G. Pfurtscheller and C. Neuper. Motor imagery activates primary sensorimotor area in humans. *Neurosci. Lett.*, 239(2-3):65–68, Dec 1997.

# A multiclass BCI using MEG

M. Bensch[1], J. Mellinger[2], M. Bogdan[3], W. Rosenstiel[1]

[1]Wilhelm-Schickard Institute, Department of Computer Engineering, Eberhard-Karls-Universität, Tübingen, Germany
[2]Institute of Medical Psychology and Behavioral Neurobiology, MEG Center, Eberhard-Karls-Universität, Tübingen, Germany
[3]Department of Computer Engineering, Universität Leipzig, Leipzig, Germany

bensch@informatik.uni-tuebingen.de

**Abstract**

Classification of MEG brain signals has been used in the past to drive brain-computer interfaces with healthy subjects. We present a multi-class study with offline results. We investigate which combinations of classes are suitable for classification and show that this result is subject-specific, although a general trend to particular combinations of patterns exists. For the current set of offline results, information transfer rate increases in eight of ten subjects going from 2-class to 3-class communication.

## 1 Introduction

Brain-Computer Interface (BCI) research is largely concerned with increasing the communication speed, or bit rate. Attempts to increase the bit rate of BCIs based on spontaneous brain activity by increasing the number of classification tasks naturally suffer from a higher misclassification rate. In an experiment with 10 subjects and 7 classification tasks, we find the best trade-off concerning the number of tasks for each subject.

High signal quality and sensor resolution inspired us to use MEG. Other BCIs based on MEG using binary classification have already been presented [1, 2]. The work presented here is a multi-class approach.

An extensive multi-class investigation is performed in [3]. A 3-class asynchronous BCI using three motor tasks for spelling was shown to produce an average of 1.99 letters/minute [4], but is difficult to compare with synchronous BCIs. A study using two motor and two non-motor imagery tasks concludes that non-motor task pairs can be discriminated easier than others [5].

The following sections explain our experimental setup and artifact analysis. Thereafter, a summary of the results obtained so far is given. The aim of this work is to find combinations of imagination tasks particularly well-suited to multi-class BCIs.

## 2 Methods

### 2.1 Experimental paradigm and data acquisition

Data was recorded with the BCI2000 software [6] at a sampling rate of 586 Hz from 10 subjects aged between 24 and 34 on two different days for each subject. Each of the two sessions included 3 runs of data acquisition, with 7 imagination tasks being presented in a block-randomised order. Cues were given in textual form on a screen positioned in front of the seated subject. Subjects were instructed to focus on a cross in the centre of the screen during the imagination phase to prevent movement artifacts. The trial structure is as follows: display of a fixation cross ("get ready", 0.7 s)

| Category | Class | Task | Description |
|---|---|---|---|
| Motor | 1 | Foot | Rotate both feet |
| Motor | 2 | Left hand | Open and close hand in repetitive motions |
| Motor | 3 | Right hand | Open and close hand in repetitive motions |
| Motor | 4 | Tongue | Lick ice-cream with tongue in repetitive motions |
| Non-motor | 5 | Subtraction | Start at 99 and repeatedly subtract 7 from answer. Do not visualise numbers, do the calculation each time. Start at a new number once the sequence has been memorised too well. |
| Non-motor | 6 | Navigation | Walk around a well-known location (e. g. the house you grew up in). Recognise objects in the rooms. |
| Non-motor | 7 | Visual scene | Imagine a green scene, e. g. a lawn or green landscape. |

Table 1: Categorisation of the imagination tasks.

| Subject | BCI experience | EMG measured | Handedness | Hardest task |
|---|---|---|---|---|
| A | 0 | Session 1 | RH | 5 |
| B | 0 | Session 2 | RH | – |
| C | 0 | – | RH | – |
| D | 4 | Session 1 | RH | 7 |
| E | 0 | Session 2 | RH | 6 |
| F | 0 | Session 1 | RH | 7 |
| G | 0 | Session 2 | RH | 7 |
| H | 0 | – | RH | – |
| I | $> 5$ | Session 1 | RH | – |
| J | 0 | Session 2 | LH | 5,6 |

Table 2: Subject details. The second column indicates the number of times the subject had participated in previous BCI experiments. The "Hardest task" column lists the task that the subject reported as the most difficult to perform.

– text cue overlayed on fixation cross ("prepare for task", 2 s) – fixation cross ("mental imagery", 4 s) – blank screen ("inter-trial interval", 2 s). Due to the exploratory nature of this study, no feedback was given. A 275-channel whole-head MEG-system (VSM MedTech Ltd.) was used.

We chose 7 imagination tasks as a trade-off between high number of classes (to test which tasks work best for the participants) and being able to collect enough data for each task to train a classifier. With 7 tasks we were able to collect 102 trials per class and keep each recording session around two hours. Each of the three runs per session lasted 17 minutes, enough to make most subjects feel tired after every run. A description of the imagination tasks is given in Table 1. As suggested in [5], functional motor tasks (some related to a subject's specific skills) were endorsed to make the task more interesting.

Some subject-specific details are given in Table 2. The only female subject was F. Note the high number of first-time BCI users. EMG was measured for 8 subjects in only one of the two recording sessions due to the increased preparation time. Head position was measured before each run. To recreate the previous session's or run's head position, the subject was given the opportunity to reposition his/her head according to an online head position display (CTF Systems).

## 2.2 Artifact rejection

Artifacts could be a major contributor to the fact that healthy subjects mostly achieve higher bit rates than patients when using BCIs. We precluded the outer MEG channels close to eyes and neck muscles and focussed on the inner 168 channels. Additionally, we investigated the effect that trials containing electromyographic (EMG) hand movement artifacts had on classification

| Subject | Total per run | | | 1 | 2 | 3 | 4 | 5 | 6 | 7 | Total |
|---|---|---|---|---|---|---|---|---|---|---|---|
| A | 20 | 11 | 21 | 8 | 4 | 8 | 7 | 8 | 8 | 9 | 52 |
| B | 7 | 14 | 3 | 3 | 4 | 2 | 4 | 2 | 4 | 5 | 24 |
| D | 7 | 9 | 5 | 0 | 16 | 2 | 0 | 2 | 1 | 0 | 21 |
| E | 1 | 6 | 8 | 0 | 2 | 2 | 3 | 3 | 3 | 2 | 15 |
| F | 1 | 1 | 6 | 1 | 0 | 0 | 1 | 0 | 3 | 3 | 8 |
| G | 4 | 7 | 5 | 1 | 0 | 1 | 3 | 5 | 6 | 0 | 16 |
| I | 7 | 16 | 9 | 7 | 4 | 5 | 2 | 7 | 2 | 5 | 32 |
| J | 13 | 12 | 7 | 7 | 2 | 4 | 1 | 5 | 5 | 8 | 32 |
| Mean | 60 | 76 | 64 | 27 | 32 | 24 | 21 | 32 | 32 | 32 | 200 |

Table 3: Number of artifacts, listed separately for runs 1–3 of the EMG session (columns 2–4) and for each task. Note the tasks 2 and 3 are the hand motor imagery tasks.

performance.

In the sessions shown in Table 2, one pair of EMG electrodes was placed on each forearm on either the lateral or medial antibrachial muscle. The EMG time series was high-pass filtered at 0.5 Hz.

To find trials containing EMG artifacts, we used a threshold-based algorithm on the EMG time series. Because the noise level of the EMG signal varied with time (due to stress on electrode cables and other effects), we used a sliding window to determine the noise level for each trial separately and standardised it accordingly. The window size was 250 samples (0.43 s) and the step size was 50 samples. Each window's score was computed as the average of the 10 highest peaks. The window with the lowest value was assumed to be free of artifacts and therefore used as noise level for the scaling. If the maximum peak in the standardised signal of a particular trial was further than $n$ standard deviations from the mean, the trial was labelled as an artifact. After a visual inspection of some artifacts, $n$ was set to 3 for most subjects.

The contaminated trials found by this method are listed in Table 3. Refer to Table 2 to see in which sessions the EMG was measured.

### 2.3 Feature extraction and classification

Multiple cross-validation runs were done with the following features extracted from the data: Autoregressive (AR) coefficients (model order 2) exclusively, spectral bandpower features exclusively, phase locking features exclusively, AR coefficients combined with bandpower features, AR coefficients combined with phase locking features, bandpower features combined with phase locking features.

The feature selection algorithm worked independently of the type of feature in those validations where multiple feature types were used. Using all the 168 inner channels, there were 336 AR coefficients in total. The mean number of features selected was 7.7 ($\pm$5.4) in the 2-class case and 44 ($\pm$27) in the 3-class case.

The best results were obtained by using solely the AR features and will be presented in the next section.

We performed a nested cross-validation (CV) with a feature selection in the inner loop (recursive feature elimination, 10-fold CV) and 5 outer folds, similar to the method described in [1]. The outer fold consisted of a random split of the data into 80 % train and 20 % test set. To obtain 3-class results, we used the MATLAB spider toolbox [7] implementation of the one-vs-all SVM with ridge regularisation.

## 3 Results

The information transfer rate (ITR) measured in bits/minute (we use the Wolpaw bit rate [8]) for all the binary combinations of the 7 classification tasks are shown in Figure 1. It is interesting that the ITR is three times higher after feature selection.

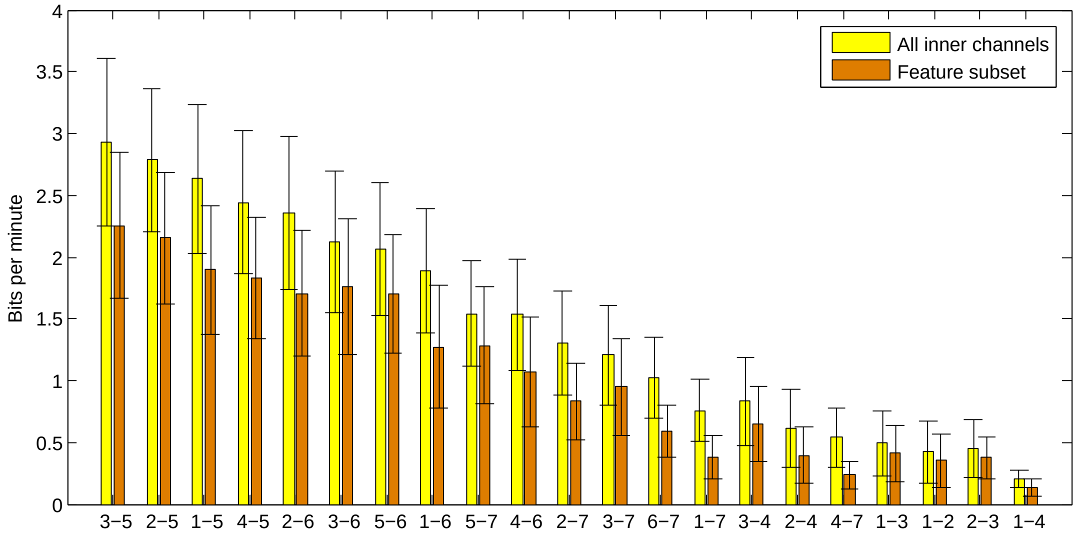


Figure 1: ITR in bits/minute (mean over 10 subjects) for each 2-class combination shown for all features and a feature subset. The error bars depict standard error. Bars are labelled with the class combination.

Subject-specific results for the 3-class and 2-class error estimates can be seen in Table 4. The column description "Inner channels" refers to the fact that we did not include the outermost MEG sensors. We do not expect the outer MEG sensors to contribute class-discriminative information, except possibly for artifacts, which we wanted to preclude anyway. The feature selection is needed for the online case, where processing speed is important.

| | 3-class Inner channels | | 3-class Subset of features | | | 2-class Inner channels | | 2-class Subset of features | | |
|---|---|---|---|---|---|---|---|---|---|---|
| Subject | Error | Comb. | Error | Comb. | ITR | Error | Comb. | Error | Comb. | ITR |
| A | 0.34 | 1–5–6 | 0.40 | 3–5–6 | 1.50 | 0.19 | 3–6 | 0.23 | 3–6 | 1.53 |
| B | 0.16 | 2–5–6 | 0.23 | 1–2–6 | 4.00 | 0.08 | 2–6 | 0.11 | 3–5 | 3.37 |
| C | 0.29 | 1–5–7 | 0.29 | 1–5–7 | 2.98 | 0.15 | 2–5 | 0.21 | 2–5 | 1.77 |
| D | 0.32 | 2–3–6 | 0.39 | 3–5–6 | 1.61 | 0.22 | 3–5 | 0.24 | 3–5 | 1.41 |
| E | 0.25 | 2–5–7 | 0.23 | 2–5–6 | 3.94 | 0.10 | 1–5 | 0.14 | 2–5 | 2.90 |
| F | 0.23 | 4–5–6 | 0.23 | 1–5–6 | 3.94 | 0.10 | 3–5 | 0.15 | 3–5 | 2.65 |
| G | 0.16 | 1–5–6 | 0.21 | 4–5–6 | 4.39 | 0.06 | 2–5 | 0.10 | 2–5 | 3.68 |
| H | 0.16 | 1–5–6 | 0.20 | 2–5–6 | 4.70 | 0.05 | 3–5 | 0.09 | 5–7 | 3.90 |
| I | 0.48 | 2–3–5 | 0.50 | 3–5–6 | 0.59 | 0.26 | 3–5 | 0.31 | 2–5 | 0.75 |
| J | 0.09 | 3–5–6 | 0.12 | 3–5–6 | 6.47 | 0.03 | 3–5 | 0.06 | 3–6 | 4.64 |
| Mean | 0.25 | | 0.28 | | 3.41 | 0.12 | | 0.16 | | 2.66 |

Table 4: Results for the best combination of three classes per subject, in terms of classification error (and ITR when applying feature selection). The error estimate is by 5-fold cross-validation. The 2-class results are given as a comparison.

Removal of artifact-trials increased the offline classification error to 0.11 (subject J) and 0.35 (subject D) using all inner channels, and to 0.125 (subject J) and 0.41 (subject D) with feature selection.

A comparison with other multi-class BCI results is shown in Table 5. The results shown for our study are after feature selection (which we require for online operation of the BCI). The error using all inner channels is slighty lower.

| | | ITR: bits per trial | | | ITR: bits per min | | | |
|---|---|---|---|---|---|---|---|---|
| Study | Classes | worst | best | mean | worst | best | mean | N |
| Dornhege et al. [3] | 3 | 0.5 | 1.15 | 0.78 | 6.7 | 15.3 | 10.32 | 5 |
| Dornhege et al., feature comb. | 3 | 0.6 | 1.19 | 0.92 | 8.0 | 15.9 | 12.2 | 5 |
| This study | 3 | 0.09 | 0.95 | 0.5 | 0.59 | 6.47 | 3.41 | 10 |

Table 5: Comparison of 3-class results. The three columns for the bit rates are worst/best/mean result of the subject population, whose size is given in the final column. Each subject's best combination is regarded.

# 4 Discussion

The analysis of artifacts showed that, with the exception of subject D, the EMG hand movement artifacts were evenly distributed across all tasks. This implies that hand movements did not unfairly bias the classifier during the offline analysis. However, we cannot rule out the possiblity that eye or head movement artifacts could have influenced the result. Furthermore, there is no guarantee that the subject did not move his/her tongue or feet during the recording.

The error estimates using feature selection are higher than without feature selection in the 2-class as well as the 3-class setting (Table 4). Feature selection is needed for the online BCI to reduce the computational load, especially if combinations of various feature types are to be used. The ITR estimates with feature selection are higher in the 3-class setting for all except the worst two subjects. An online spelling session was performed with one subject up to now.

The task combinations shown in Table 4 are the best on a per-subject basis. It is interesting to see that for most subjects, a motor task combined with the two non-motor tasks "subtraction" and "navigation" was the best combination (even though subjects reported difficulties with the non-motor mental tasks, see Table 2). This might have to do with the fact that cortical activation for these tasks is spatially far apart - we plan to investigate this in more detail. The best 2-class pairs were "subtraction" together with a motor task in eight of ten cases. This is in contrast to [5], where the most discriminable pair consisted of two non-motor tasks. The difference could be explained by the fact that (1) we did not include the "auditory" task, or (2) we allowed functional motor tasks (subjects A, B, F, H, J used functional motor tasks for the hand imagery). Our results suggest that some patterns of class combinations exist that generally lead to a higher discriminability (motor/non-motor task combination).

We acknowledge the fact that measuring MEG in people from the current target group for BCIs, namely paralyzed patients, is expensive and time-consuming. However, the focus of this study was to explore the multi-class paradigm. Furthermore, future BCIs may be based on a contactless measuring technique similar to MEG.

# 5 Conclusion

The bit rates found for the 3-class setting presented in this study are an improvement over the 2-class results, yet must still be compared with other studies. Additionally, a comparison with existing 3-class BCIs based on motor imagery alone has to be undertaken. This could show whether there is an advantage to using non-motor tasks combined with motor tasks, as suggested by the results presented here.

We found that it is possible to select a subset from a larger group of mental tasks individually to obtain a higher bit rate for each BCI user. In the offline analysis, eight subjects benefit by using a 3-task combination instead of binary decision tasks. The mean improvement in the ITR for these eight subjects is 32 % when using 3 classes instead of 2. This motivates us to continue measurements where the subjects spell a word by selecting letters from a ternary decision tree.

**Acknowledgments:** The authors thank J. Hill for providing analysis software and M. Spüler for his assistance in preparing the results and programming the online interface.

## References


[1] T. N. Lal, M. Schröder, N. J. Hill, H. Preissl, T. Hinterberger, J. Mellinger, M. Bogdan, W. Rosenstiel, T. Hofmann, N. Birbaumer, and B. Schölkopf. A brain computer interface with online feedback based on magnetoencephalography. In *ICML*, pages 465–472, 2005.

[2] J. Mellinger, G. Schalk, C. Braun, H. Preissl, W. Rosenstiel, N. Birbaumer, and A. Kübler. An MEG-based Brain-Computer Interface (BCI). *Neuroimage*, 36:581–593, 2007.

[3] G. Dornhege, B. Blankertz, G. Curio, and K.-R. Müller. Boosting bit rates in non-invasive EEG single-trial classifications by feature combination and multi-class paradigms. *IEEE Trans. Biomed. Eng.*, 51(6):993–1002, 2004.

[4] R. Scherer, G. R. Müller, C. Neuper, B. Graimann, and G. Pfurtscheller. An asynchronously controlled EEG-based virtual keyboard: Improvement of the spelling rate. *IEEE Trans. Biomed. Eng.*, 51(6), 2004.

[5] E. Curran, P. Sykacek, M. Stokes, S. Roberts, W. Penny, I. Johnsrude, and A. Owen. Cognitive tasks for driving a brain computer interfacing system: a pilot study. *IEEE Trans. Rehabil. Eng.*, 12(1), 2003.

[6] G. Schalk, D. McFarland, T. Hinterberger, N. Birbaumer, and J. Wolpaw. BCI2000: a general-purpose brain-computer interface (BCI) system. *IEEE Trans. Biomed. Eng.*, 51:1034–1043, 2004.

[7] J. Weston, A. Elisseeff, G. Bakir, and F. Sinz. The spider machine learning toolbox. http://www.kyb.mpg.de/bs/people/spider/, 2005.

[8] J. R. Wolpaw, N. Birbaumer, W. J. Heetderks, D. J. McFarland, P. H. Peckham, G. Schalk, E. Donchin, L. A. Quatrano, C. J. Robinson, and T. M. Vaughan. Brain-computer interface technology: A review of the first international meeting. *IEEE Trans. Rehabil. Eng.*, 8:164–173, 2000.

# Simultaneous real-time detection of motor imagery and error-related potentials for improved BCI accuracy

P. W. Ferrez[1,2] and J. del R. Millán[1,2]

[1]IDIAP Research Institute, Martigny, Switzerland
[2]Ecole Polytechnique Fédérale de Lausanne, Lausanne, Switzerland

{pierre.ferrez,jose.millan}@idiap.ch

**Abstract**

Brain-computer interfaces (BCIs), as any other interaction modality based on physiological signals and body channels (e. g., muscular activity, speech and gestures), are prone to errors in the recognition of subject's intent. An elegant approach to improve the accuracy of BCIs consists of a verification procedure directly based on the presence of error-related potentials (ErrP) in the EEG recorded right after the occurrence of an error. Two healthy volunteer subjects with little prior BCI experience participated in a real-time human-robot interaction experiment where they were asked to mentally move a cursor towards a target that can be reached within a few steps using motor imagery. These experiments confirm the previously reported presence of a new kind of ErrP. These "Interaction ErrP" exhibit a first sharp negative peak followed by a positive peak and a second broader negative peak ($\sim$270, $\sim$330 and $\sim$430 ms after the feedback, respectively). The objective of the present study was to simultaneously detect erroneous responses of the interface and classifying motor imagery at the level of single trials in a real-time system. We have achieved online an average recognition rate of correct and erroneous single trials of 84.7 % and 78.8 %, respectively. The off-line post-analysis showed that the BCI error rate without the integration of ErrP detection is around 30 % for both subjects. However, when integrating ErrP detection, the average online error rate drops to 7 %, multiplying the bit rate by more than 3. These results show that it's possible to simultaneously extract in real-time useful information for mental control to operate a brain-actuated device as well as correlates of cognitive states such as error-related potentials to improve the quality of the brain-computer interaction.

## 1 Introduction

People with severe motor disabilities (spinal cord injury (SCI), amyotrophic lateral sclerosis (ALS), etc.) need alternative ways of communication and control for their everyday life. Over the past two decades, numerous studies proposed electroencephalogram (EEG) activity for direct brain-computer interaction [1, 2]. EEG-based brain-computer interfaces (BCIs) provide disabled people with new tools for control and communication and are promising alternatives to invasive methods. However, as any other interaction modality based on physiological signals and body channels (e. g., muscular activity, speech and gestures), BCIs are prone to errors in the recognition of subject's intent, and those errors can be frequent. Indeed, even well-trained subjects rarely reach 100 % of success. In contrast to other interaction modalities, a unique feature of the "brain channel" is that it conveys both information from which we can derive mental control commands to operate a brain-actuated device as well as information about cognitive states that are crucial for a purposeful interaction, all this on the millisecond range. One of these states is the awareness of erroneous responses, which a number of groups have recently started to explore as a way to improve the performance of BCIs [3, 4, 5, 6, 7].
In particular, [6] recently reported the presence of error-related potentials (ErrP) elicited by erroneous feedback provided by a BCI during the recognition of the subject's intent. In this off-line

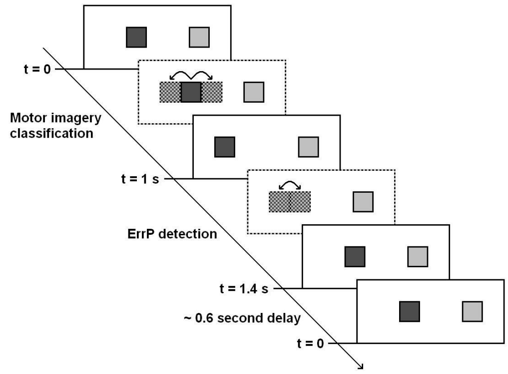


Figure 1: Timing of the protocol.

study, six subjects were asked to mentally drive a cursor towards targets that can be reached within a few steps using motor imagery. However, since the subjects had no prior BCI experience, the system was not moving the cursor following the mental commands of the subject, but with a 20 % error rate, to avoid random or totally biased behavior of the cursor. The main components of these "Interaction ErrP" are a negative peak 290 ms after the feedback, a positive peak 350 ms after the feedback and a second broader negative peak 470 ms after the feedback. This study shows the feasibility of simultaneously and satisfactorily detecting erroneous responses of the interface and classifying motor imagery for device control at the level of single trials. Indeed, the recognition rate of correct and erroneous single trials are 81.8 % and 76.2 %, respectively while the average recognition rate of the subject's intent is 73.1 %. Finally, the average theoretical increase of the BCI performance (in terms of bit rate) when integrating ErrP detection is over 100 %.
The objective of the present study is to simultaneously detect erroneous responses of the interface and classifying motor imagery at the level of single trials in a real-time BCI system. In this paper we report new experimental results recorded with two healthy volunteer subjects with little prior BCI experience during a simple real-time human-robot interaction that confirm similar results obtained off-line [6], as explained above. We have achieved online an average recognition rate of correct and erroneous single trials of 84.7 % and 78.8 %, respectively. The off-line post-analysis showed that the BCI error rate without the integration of ErrP detection is around 30 % for both subjects. However, when integrating ErrP detection, the average online error rate drops to 7 %, multiplying the bit rate by more than 3. These results confirm that it's possible to simultaneously extract in real-time useful information for mental control to operate a brain-actuated device as well as correlates of cognitive states such as error-related potentials to improve the quality of the brain-computer interaction.

# 2 Materials and methods

To test the ability of BCI users to concentrate simultaneously on a mental task and to be aware of the BCI feedback at each single trial, we have simulated a human-robot interaction task where the subject has to bring the robot to targets located 3 steps away, either to the left or to the right. This virtual interaction is implemented by means of a green square cursor that can appear on any of 20 positions along a horizontal line. The goal with this protocol is to bring the cursor to a target that randomly appears either on the left (blue square) or on the right (red square) of the cursor. The target is no further away than 3 positions from the cursor (symbolizing the current position of the robot). This prevents the subject from habituation to one of the stimuli since the cursor reaches the target within a small number of steps. Each target corresponds to a specific mental task. Subjects were asked to imagine a movement of their left hand for the left target and to imagine a movement of their right foot for the right target.

**Subject 1** (Cz, C2, C4 and 12 Hz, 14 Hz)

| | | I | II | III | IV | Average | SD |
|---|---|---|---|---|---|---|---|
| **ErrP detection** | **Error trials [%]** | 74.8 | 83.7 | 76.1 | 67.5 | **75.5** | **6.6** |
| | **Correct trials [%]** | 88.3 | 82.1 | 91.1 | 81.6 | **85.8** | **4.7** |
| **BCI without ErrP** | **Error rate [%]** | 33.0 | 27.5 | 34.3 | 39.0 | **33.5** | **4.7** |
| | **Rejection rate [%]** | 0.0 | 0.0 | 0.0 | 0.0 | **0.0** | **0.0** |
| **BCI with ErrP** | **Error rate [%]** | 8.3 | 4.5 | 8.2 | 12.7 | **8.4** | **3.4** |
| | **Rejection rate [%]** | 32.5 | 36.0 | 32.0 | 37.6 | **34.5** | **2.7** |
| **Performance** | **BpT initial** | 0.09 | 0.15 | 0.07 | 0.04 | **0.09** | **0.05** |
| | **BpT final** | 0.31 | 0.41 | 0.32 | 0.17 | **0.30** | **0.10** |
| | **Increase [%]** | 244 | 173 | 357 | 325 | **275** | **83** |

**Subject 2** (Cz, C4, CP4 and 12 Hz, 24 Hz, 26 Hz)

| | | I | II | III | IV | Average | SD |
|---|---|---|---|---|---|---|---|
| **ErrP detection** | **Error trials [%]** | 94.8 | 76.6 | 76.5 | 80.2 | **82.0** | **8.7** |
| | **Correct trials [%]** | 68.0 | 88.5 | 86.1 | 91.4 | **83.5** | **10.6** |
| **BCI without ErrP** | **Error rate [%]** | 31.3 | 30.2 | 31.1 | 29.2 | **30.5** | **1.0** |
| | **Rejection rate [%]** | 0.0 | 0.0 | 0.0 | 0.0 | **0.0** | **0.0** |
| **BCI with ErrP** | **Error rate [%]** | 1.6 | 7.6 | 7.6 | 5.8 | **5.7** | **2.8** |
| | **Rejection rate [%]** | 51.6 | 32.5 | 33.1 | 29.5 | **36.7** | **10.1** |
| **Performance** | **BpT initial** | 0.10 | 0.12 | 0.11 | 0.13 | **0.12** | **0.01** |
| | **BpT final** | 0.38 | 0.36 | 0.33 | 0.42 | **0.37** | **0.04** |
| | **Increase [%]** | 280 | 200 | 200 | 223 | **226** | **38** |

Table 1: Classification rates and performance increase. For both subjects, this table presents the classification rates for ErrP detection (error and correct single trials) for the four groups of recordings and for the average of them. It also shows the error rates and the rejection rates for motor imagery, with and without ErrP detection. Finally the increase in performance is also shown. The ErrP detection rate is around 80 % and the error rate of the standard BCI is around 30 %. When integrating ErrP detection, this error rate is below 10 % with an acceptable rejection rate of 30–35 %. Finally, for both subjects the bit rate is multiplied by more than 3 when using ErrP detection.

After the presentation of the target, the subject focuses on the corresponding mental task until the cursor moves. The system uses a 1 second window to determine the subject's intent. Then the system uses a 400 ms window to detect the presence of ErrP just after the presentation of the feedback (movement of the cursor). If no ErrP are detected, nothing happens and about 600 ms later, the system starts to accumulate data for the next classification of motor imagery. If ErrP are detected, the movement is canceled, and again after about 600 ms the system starts accumulating data for the next step. Figure 1 illustrates this timing. At $t = 0$, the target is 3 steps on the right of the cursor. The subject is therefore imagining a movement of his right foot. At $t = 1$ second, the system makes a mistake and moves the cursor to the left while the subject was imagining a movement of his right foot. At $t = 1.4$ second, the system detects ErrP and cancels the wrong movement. It is to note that the system is only canceling the movement, not replacing the wrong command (left) by the opposite one (right). After a delay of about 600 ms, the system starts accumulating data for the next motor imagery classification, i. e. for the next single trial.

In any case, the cursor is moving on average every 2 seconds, and some movements are canceled if ErrP are detected. When the cursor reached a target, it briefly turned from green to light green and then a new target is randomly selected by the system. If the cursor didn't reach the target after 10 steps, a new target is selected. Two healthy volunteer subjects performed 10 sessions of 15 targets ($\sim$ 90 single trials per session) on 2 different days, the delay between the two days of measurements was about 2 weeks. The 20 sessions were split into 4 groups of 5. For the first day (Groups I & II) we used classifiers built with data recorded during a previous off-line study described above [6], and for the second day (Groups III & IV) we used the data of the first day to build classifiers. This rule applies for both motor imagery classification and for ErrP detection. The data acquisition and processing as well as the classification procedures can be found in [6]. For both subjects we used a 150 ms window starting 250 ms after the feedback for channels FCz and Cz for ErrP detection. For motor imagery classification, we used EEG channels Cz, C2, C4 and frequencies 12 Hz, 14 Hz for Subject I and EEG channels Cz, C4, CP4 and frequencies 12 Hz, 24 Hz, 26 Hz for Subject II.

# 3 Results

## 3.1 Performances

For both subjects, Table 2 shows the classification rates for ErrP detection (error and correct single trials) for the four groups of recordings and for the average of them. It also shows the error rates and the rejection rates for motor imagery, with and without ErrP detection. Finally the increase in performance expressed in bits per trials (BpT) is also shown. For both subjects, ErrP detection rate is around 80 % and pretty stable over the different groups. Without the use of ErrP detection, Subject I shows a stable error rate of 34 % for motor imagery, whereas for Subject II this rate is just above 30 %. These rates are relatively high for a two tasks BCI, but keeping in mind that the subjects had very little BCI experience and that these are real-time experiments performed using classifiers built with data from previous sessions recorded several weeks before, they are satisfactory. When integrating ErrP detection, the error rates drop below 10 % for both subjects with acceptable rejection rates around 35 %. This clearly shows the benefit of using ErrP detection to filter out wrong decisions. This benefit is clear in term of performance, the bit rate is multiplied by more than 3 for both subjects.

## 3.2 Motor imagery

Subjects were asked to imagine a movement of their left hand when the left target was proposed and to imagine a movement of their right foot when the right target was proposed. The most relevant EEG channels and frequencies were selected by a simple feature selection algorithm based on the overlap of the distributions of the different classes. The data recorded during the off-line study [6] mentioned in Section 1 and 2 was used to select the relevant features (EEG electrodes and frequencies) for motor imagery classification as well as to build the initial statistical classifier used for these real-time experiments. For Subject I the relevant features are EEG channels Cz, C2, C4 and frequencies 12 Hz, 14 Hz whereas for Subject II we used EEG channels Cz, C4, CP4 and frequencies 12 Hz, 24 Hz, 26 Hz. Previous studies confirm these results. Indeed, alpha and beta rhythm over left and/or right sensorimotor cortex have been successfully used for BCI control [8]. Event-related de-synchronization (ERD) and synchronization (ERS) refer to large-scale changes in neural processing. During periods of inactivity, brain areas are in a kind of idling state with large populations of neurons firing in synchrony resulting in an increase of amplitude of specific alpha (8–12 Hz) and beta (12–26 Hz) bands. During activity, populations of neurons work at their own pace and the power of this idling state is reduced, the cortex has become de-synchronized [9, 10]. In our case, the most relevant electrodes for both subjects are in the C4 and Cz area. These locations confirm previous studies since C3 and C4 areas usually show ERD/ERS during hands movement or imagination whereas foot movement or imagination are focused in the Cz area [9, 10].

Figure 2 shows the discriminant power (DP) of frequencies (top) and electrodes (bottom) for both subject. The DP was calculated off-line after the real-time recordings to check the stability of the selected features. For Subject I, the best frequencies are 12 Hz and 14 Hz, whereas for Subject II the best ones are 12 Hz, 24 Hz and 26 Hz. This matches exactly the selected frequencies. For both subjects, the best EEG electrodes are located around C4, matching relatively well the selected ones. These results indicates that the relevant features are stable over time.

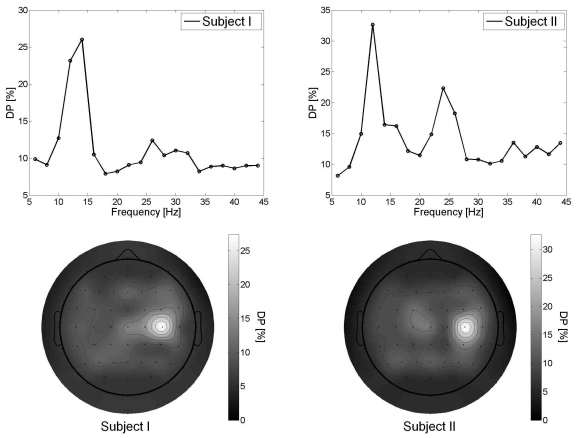


Figure 2: Top: Discriminant power (DP) of frequencies. Sensory motor rhythm (12–16 Hz) and some beta components are discriminant. Bottom: Discriminant power (DP) of electrodes. The most relevant electrodes are in the central area (C4 and Cz) according to the ERD/ERD location for hand and foot movement or imagination.

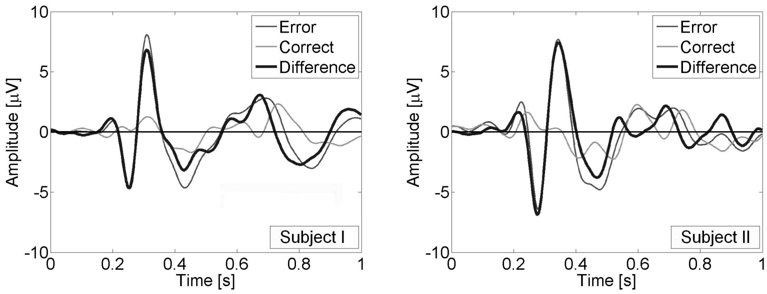


Figure 3: Grand averages of error trials, of correct trials and the difference error-minus-correct for channel FCz for both subjects. Both subjects show similar ErrP time courses whose amplitudes slightly differ from one subject to the other.

### 3.3 Error-related potentials

Figure 3 shows the grand averages of error trials, of correct trials and the difference error-minus-correct for channel FCz for both subjects). A first small positive peak shows up about $\sim 200$ ms after the feedback ($t = 0$). A negative peak clearly appears $\sim 270$ ms after the feedback. This negative peak is followed by a positive peak $\sim 330$ ms after the feedback. Finally, a second negative peak appears $\sim 430$ ms after the feedback. Both subjects show very similar ErrP time courses whose amplitudes slightly differ from one subject to the other. These experiments seem to confirm the existence of a new kind of error-related potentials [7].

# 4 Discussion

In this study we have closed the loop using a previously described protocol [6] for real-time experimentations, i. e. with statistical classifiers for motor imagery and ErrP detection running in real-time and simultaneously. Two subjects were able to control the cursor using motor imagery with an average accuracy just below 70 %. In parallel, the system was able to detect the presence of ErrP with an accuracy above 80 % to improve the quality of the brain-computer interaction.

Indeed, in terms of bit rate, the integration of ErrP detection multiplies the performance by a factor 3. The features used for classification were those selected in [6]. They show a relatively good stability, in particular the potentials used for ErrP detection.
More generally, the ErrP potentials described in this study are relatively similar for all subjects. We could therefore maybe build a general ErrP classifier that we would use for all subjects. This would simplify the training sessions, since no preliminary ErrP recordings to build classifiers would be needed anymore. The duration of the window used for motor imagery classification was 1 second. This could probably be shortened to 0.5 second or maybe even less without decreasing performances, so that if we reduce the delay after ErrP detection, we could be able to deliver a feedback almost every second. In this study, ErrP detection was used to filter out erroneous responses of the system. ErrP could also be used as learning signals for an unsupervised online adaptation of the BCI classifier. Finally, the work described in this paper suggests that it could be possible to recognize in real-time high-level cognitive and emotional states from EEG (as opposed, and in addition, to motor commands) such as alarm, fatigue, frustration, confusion, or attention that are crucial for an effective and purposeful interaction. Indeed, the rapid recognition of these states will lead to truly adaptive interfaces that customize dynamically in response to changes of the cognitive and emotional/affective states of the user.

# References


[1] J. R. Wolpaw, N. Birbaumer, D. J. McFarland, G. Pfurtscheller, and T. M. Vaughan. Brain-computer interfaces for communication and control. *Clin. Neurophysiol.*, 113:767–791, 2002.

[2] J. del R. Millán, F. Renkens, J. Mouriño, and W. Gerstner. Non-invasive brain-actuated control of a mobile robot by human EEG. *IEEE Trans. Biomed. Eng.*, 51:1026–1033, 2004.

[3] G. Schalk, J. R. Wolpaw, D. J. McFarland, and G. Pfurtscheller. EEG-based communication: Presence of and error potential. *Clin. Neurophysiol.*, 111:2138–2144, 2000.

[4] B. Blankertz, G. Dornhege, C. Schäfer, R. Krepki, J. Kohlmorgen, K.-R. Müller, V. Kunzmann, F. Losch, and G. Curio. Boosting bit rates and error detection for the classification of fast-paced motor commands based on single-trial EEG analysis. *IEEE Trans. Neural Syst. Rehabil. Eng.*, 11:127–131, 2003.

[5] L. C. Parra, C. D. Spence, A. D. Gerson, and P. Sajda. Response error correction – a demonstration of improved human-machine performance using real-time EEG monitoring. *IEEE Trans. Neural Syst. Rehabil. Eng.*, 11:173–177, 2003.

[6] P. W. Ferrez and J. del R. Millán. EEG-based brain-computer interaction: Improved accuracy by automatic single-trial error detection. *21st Ann. Conf. Neural Information Process. Syst. (NIPS)*, 2007.

[7] P. W. Ferrez and J. del R. Millán. Error-related EEG potentials generated during simulated brain-computer interaction. *IEEE Trans. Biomed. Eng.*, 55:923–929, 2008.

[8] D. J. McFarland and J. R. Wolpaw. Sensorimotor rhythm-based brain-computer interface (BCI): feature selection by regression improves performance. *IEEE Trans. Neural Syst. Rehabil. Eng.*, 13(3):372–379, 2005.

[9] G. Pfurtscheller and F. H. Lopes da Silva. Event-related EEG/MEG synchronization and desynchronization: basic principles. *Clin. Neurophysiol.*, 110:1842–1857, 1999.

[10] G. Pfurtscheller and C. Neuper. Motor imagery and direct brain-computer communication. *Proc. IEEE*, 89:1123–1134, 2001.

# Towards a virtual 4-class synchronous BCI using motor prediction and one motor imagery

T. Geng and J. Q. Gan

BCI Group, Department of Computing and Electronic Systems, University of Essex, UK

tgeng@essex.ac.uk

**Abstract**

Multi-class EEG-based BCIs (brain-computer interfaces) usually use a set of different mental tasks to generate different commands. This study shows that, after training with a specially designed BCI paradigm using one motor imagery, humans can learn to predict the time course of band power features of the EEG signals. With this newly-obtained prediction skill, subjects can use only one motor imagery to select one of the four targets on screen in each trial that lasts 3.4 seconds on average, which is functionally analogous to a 4-class synchronous BCI.

## 1 Introduction

Most of the current EEG (electroencephalogram)-based BCI systems use various mental tasks, which are classified and translated into different computer commands using various pattern classification algorithms. An increased number of mental tasks or brain patterns, if classified reliably, can potentially boost the communication speed of the BCI systems. This is because as the number of classes grows, the potential number of class combinations grows exponentially. Unfortunately, with the number of classes increased, the accuracy of the BCI decreases evidently because every additional EEG pattern to be classified brings up more difficulty to the classifier. Most BCIs use synchronous paradigms, where the control is externally paced. In each trial, there is a cue telling the user to start the desired mental state/task and keep it for some predefined length of time. The EEG phenomena and the system are time-locked to the cue. A trial lasts a relatively long period, from 4 to 10 or more seconds, because the EEG phenomena need time to develop and recover. In this study, we have designed a new synchronous BCI paradigm that can realize the function of a 4-class BCI but use only one motor imagery. The study presented in this paper shows that, after training with a specially designed BCI paradigm, humans can learn to predict the time course of band power feature of the EEG signals. It is also shown that, with this newly-obtained prediction skill, subjects can use one motor imagery only to choose one of the four targets on screen in each trial that lasts 3.4 seconds on average. The BCI paradigm in this study is different from other synchronous BCIs in that it explicitly depends on subjects' prediction skill in the control of the EEG pattern.

## 2 Synchronous experiments

There are two BCI paradigms used in this study. One is a conventional synchronous paradigm which is used to collect offline data for each subject. The other is our specially designed prediction paradigm which will be described later in the next section. Before taking part in the motor prediction experiment, three healthy subjects (one is female) participated in two-day synchronous experiments.

## 2.1 The first day synchronous experiments

In each experiment, the subject sat in a comfortable arm chair, one meter away from a 19 inch screen. EEG signals were recorded from 5 channels of bipolar electrode positions with respect to the international 10–20 systems: FC3–PC3, FC1–PC1, Cz–Pz, FC2–PC2, FC4–PC4. The recording was made with a 16-channel EEG amplifier from g.tec. The EEG was sampled at 250 Hz. The first-day synchronous experiment consisted of 8 runs with 20 trials each. In each trial, from $t = 3\,\mathrm{s}$ an arrow pointing to down or a circle was displayed on the screen. The subject was instructed to imagine feet movement or relax until $t = 8\,\mathrm{s}$. This paradigm is similar to that reported in [1]. The band power of each channel is calculated using the same method of [2].
The time-frequency maps of the band power were calculated using the data collected from the first-day synchronous experiment for each subject. By visually checking these maps, we chose the band power of one or two frequency bands for each subject as the features. These band power features of the recorded EEG data were used to train an LDA (Linear Discriminant Analysis) classifier for each subject, which can be described as

$$F = \sum W_i B_i + C \tag{1}$$

where $F$ is the LDA score, $W_i$ is the weight for the $i^{\text{th}}$ band power feature, $B_i$ is the band power of the selected band of a channel, and $C$ is a constant. The value of $F$ calculated online will be used as the online feedback in the second day experiments and the motor prediction experiments later on. For each subject, after trained with the data of the first-day synchronous experiments, the values of $W_i$ and $C$ were fixed in all subsequent experiments of this subject.

## 2.2 The second day synchronous experiments

On the second day, the subjects continued to take part in synchronous BCI experiments. The paradigm was similar to that of the first day and each trial still lasted 8 seconds. But, this time, a feedback bar was displayed on the screen from $t = 3\,\mathrm{s}$ to $t = 8\,\mathrm{s}$. Its length was proportional to the band power calculated online from the single frequency band of the single channel chosen for the subject. In each trial, at second 3, a cue appeared on the screen. The cue was randomly chosen by the system to be an arrow or a circle. If the cue is an arrow, the subject should start a motor imagery of feet immediately and try to make the feedback bar over the threshold as soon as possible. If the cue is a circle, the subject should relax and perform no motor imagery.
The threshold for the feedback of each subject is calibrated daily in all experiments. Before experiments on a day, the subject was instructed to keep relaxing without performing any motor imagery for 3 minutes. The band power of the selected single band from the single channel was calculated sample by sample using the data recorded from this 3-minutes idling period. Then the mean, m, and standard deviation, S, of the band power were calculated. The threshold for that day's experiments, T, was set to:

$$T = m + \alpha \cdot S \tag{2}$$

where $\alpha$ is a constant and is manually set by trial and error in experiments, which were chosen to be 3.5 in the second-day experiments and all later experiments using the motor prediction paradigm.
The aim of the synchronous experiments is to make the subject familiar with how fast the feedback bar responds to his motor imagery of feet. The time course of the LDA score averaged from 80 or 60 trials of motor imagery of feet of each subject in the second-day experiments is shown in Figure 1. It can be seen that the averaged LDA score (feedback) needs about 1.5–2.1 seconds after the cue to reach the threshold. This time- length for the development of band power features is in agreement with experimental results of other BCI studies involving motor imagery of feet in healthy subjects [3, 4] and a tetraplegic patient [5].

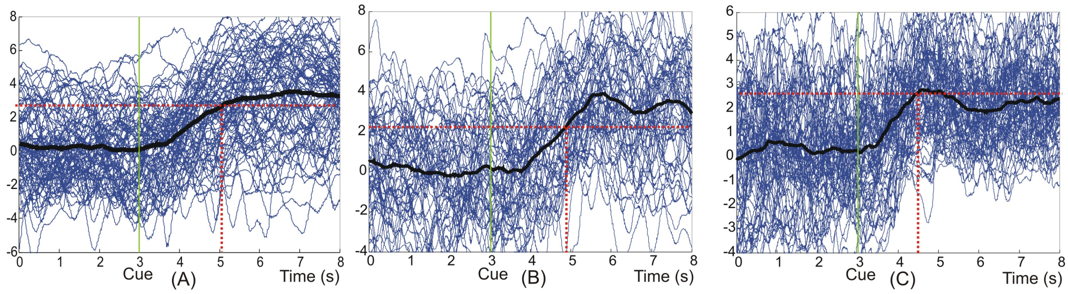


Figure 1: The time course of the LDA score of the second-day experiments (averaged over 80 trials for subjects 1 and 3, and 60 trials for subject 3) : (A) Subject 1, (B) Subject 2, (C) Subject 3. The red line is the threshold.

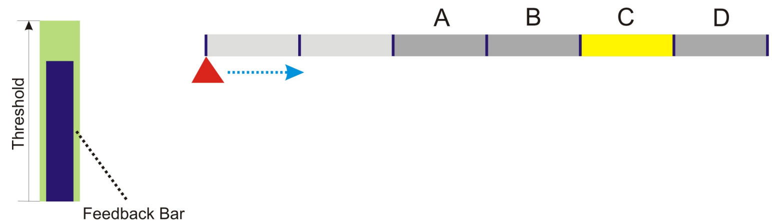


Figure 2: The feedback bar, the cursor, and the target areas (A, B, C, D) shown on the screen. The target selected by the system in a trial (here, it's the "C" area) was highlighted.

## 3 Prediction experiments

On the third day, the subjects participated in online motor prediction experiments. In this paradigm, a straight horizontal line with a triangle cursor on it was displayed on the screen (see Figure 2). The straight line was equally divided to 6 areas. The 3$^{rd}$, 4$^{th}$, 5$^{th}$, and 6$^{th}$ areas were labeled with A, B, C, D, respectively, and used as the four target areas. Beside the straight line there is a feedback bar whose height is proportional to a weighted combination of the band power of the 5-channel EEG signals (see Equation 1), which is the same as the feedback bar in the second day experiments.

In this online prediction training experiments, each trial lasts no more than 4.8 seconds, and there is a break of 5–6 seconds between trials. At the beginning of each trial, there is a sound alert, and a target area randomly chosen by the system was highlighted. At the same time, the cursor appeared at the left end of the straight line and started moving along the line at a fixed speed of 0.8 seconds per area (4.8 seconds for all 6 areas). Whenever the feedback bar was over a threshold for 0.1 seconds, the cursor stopped moving and the trial was finished. If the feedback bar was not over the threshold in a trial, the trial would end when the cursor reached the right end of the straight line (which was 4.8 seconds). A trial was regarded as a successful one only if the cursor was stopped in the highlighted target area during that trial. All the following occasions were regarded as a failed trial: (1) the cursor was stopped before entering the target area (see Figure 2); (2) the cursor stopped in a wrong target area (not the highlighted one); (3) the cursor was not stopped during the trial.
The task of the subject is to make the cursor stop in the highlighted target area by controlling the feedback bar using motor imagery of feet. Because the moving cursor only stays in the target area for 0.8 seconds during each trial and the combined band power feature of motor imagery (the feedback bar) needs about 1.5–2.1 seconds to develop to reach the threshold (see Figure 1), the subject has to start motor imagery well before the cursor enters the target area. But exactly how much in advance the subject should start the motor imagery is a prediction skill, which the subject must learn in the training using this paradigm.

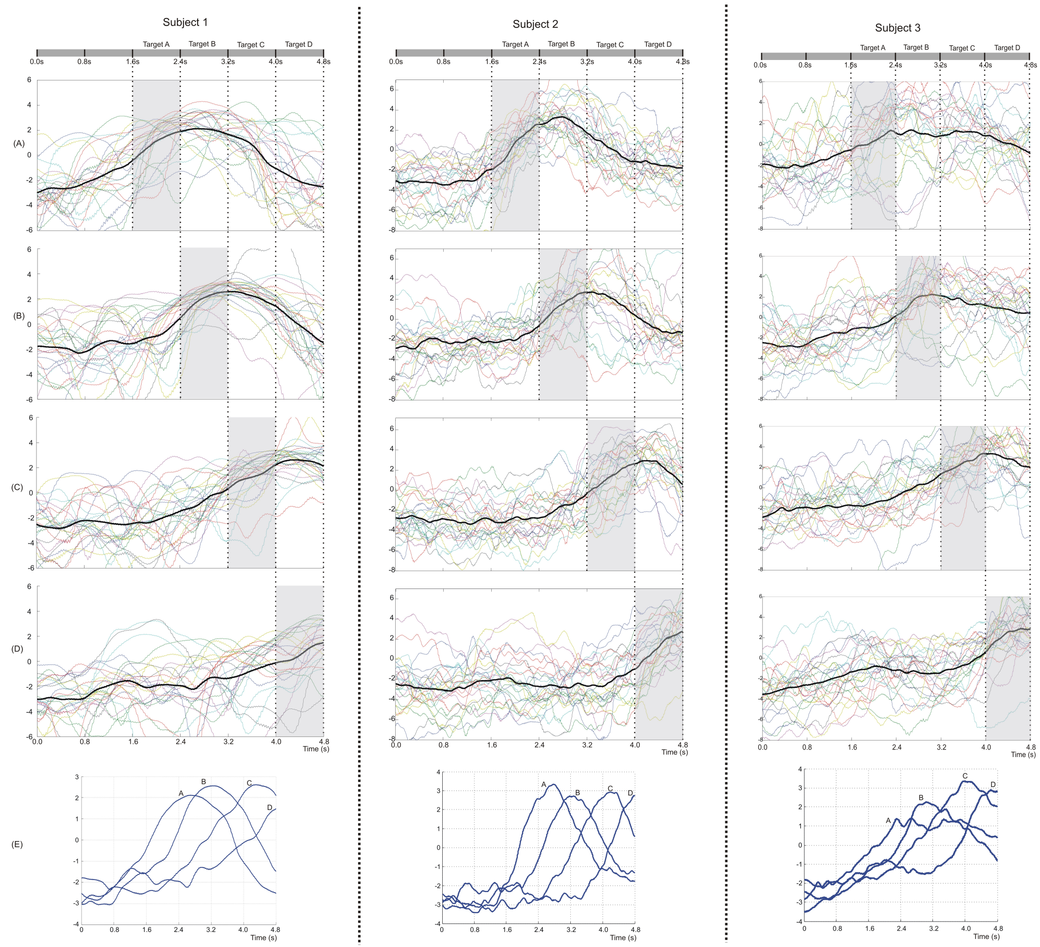


Figure 3: The LDA score (feedback) recorded form the 100 trials of each subject.

After one hour of free training with this prediction paradigm, each subject took part in five sessions of online experiments for evaluating how accurate the subjects can choose targets by the newly obtained prediction skill. Each session had 20 trials. Although the target was chosen randomly in each trial, the number of trials in each session for each target area is 5. The LDA scores of the five sessions (100 trials) from each subject are shown in Figure 3. For each subject, the LDA score (feedback) recorded from 0 s to 4.8 s in each trial were grouped to be shown in Figure 3 A, B, C and D, respectively, according to the highlighted target of that trial (A, B, C, or D). For example, the left figure in Figure 3 A shows all the 25 trials of subject 1 in which the target chosen by the system was target A. The thick black lines in Figure 3 A–D were the averaged LDA scores of each target group. They are also redrawn in Figure 3 3E and labeled with their corresponding targets, A, B, C, and D, in order to show more clearly the timing differences between the four target groups of trials. The accuracy of each subject over the five sessions (100 trials) were 72 %, 59 %, 67 % for subjects 1, 2, and 3, respectively, which are much higher than the chance rate (25 % for a four-class problem, or 16.7 % for each of the 6 areas in Figure 2). The averaged time-length of all 300 trials for the three subjects is 3.4 seconds.

## 4 Conclusion

This study has revealed that the prediction capability can be trained for subjects to predict the time course of the band power feature in the EEG signals. It has also been shown that subjects can employ this newly obtained prediction skill to realize the function of a 4-class synchronous BCI while using one motor imagery.

## References

[1] G. Townsend, B. Graimann, and G. Pfurtscheller. A comparison of common spatial patterns with complex band power features in a four-class BCI experiment. *IEEE Trans. Biomed. Eng.*, 53:642–651, 2006.

[2] G. Pfurtscheller, C. Neuper, C. Guger, W. Harkam, H. Ramoser, A. Schlögl, B. Obermaier, and M. Pregenzer. Current trends in Graz brain-computer interface (BCI) research. *IEEE Trans. Rehabil. Eng.*, 8:216–219, 2000.

[3] G. Pfurtscheller and F. H. Lopes da Silva. Event-related EEG/MEG synchronization and desynchronization: basic principles. *Clin. Neurophysiol.*, 110:1842–1857, 1999.

[4] G. Pfurtscheller. Induced oscillations in the alpha band: Functional meaning. *Epilepsia*, 44:2–8, 2003.

[5] G. Pfurtscheller, C. Guger, G. Müller, G. Krausz, and C. Neuper. Brain oscillations control hand orthosis in a tetraplegic. *Neurosci. Lett.*, 292:211–214, 2000.

# Motor imagery training system for BCI using real – time cortical rhythmic activity monitoring system

H.-J. Hwang, G. H. Seo, K. J. Choi, E. B. Kim, K. Kwon, C.-H. Im

Department of Biomedical Engineering, Yonsei University, Wonju, Korea

han-jeong@yonsei.ac.kr

**Abstract**

In the present study, we propose a novel approach to training motor imagery tasks in EEG-based brain computer interface (BCI), based on a recent technique named a real-time cortical rhythmic activity monitoring system. In this preliminary experimental study, four healthy participants, who had difficulty in performing the motor imagery tasks, could successfully perform the motor imagery tasks after only a few training sessions. We recorded continuous EEG signals while the subjects were imagining left or right hand movements, before and after the training session. The subjects' intentions were then detected using a conventional time-frequency analysis technique. The analysis results showed significant differences at mu rhythm between signals obtained before and after the training session. These preliminary results demonstrated that our proposed system is effective in training motor imagery tasks for BCI applications.

## 1 Introduction

There are many people with disabilities who cannot freely move or control their specific parts of the body. Brain-computer interface (BCI) can help them to drive external devices using their brain activities without any actual movements of the body [1]. Diverse kinds of brain activities have been used to realize BCI such as slow cortical potential [2], P300 [3], steady-state visual evoked potential (SSVEP) [4, 5, 6], and so on. Among them, one of the most widely used brain activities in BCI applications has been the mu rhythm related with motor actions or motor imagery (MI) [7, 8], which has peaks around 10 Hz (alpha) and 20 Hz (beta) and is generated around motor cortex [7, 8, 9]. The mu rhythm can be voluntarily generated by subjects with quicker response time than the other brain activities.

However, it is still very difficult to make a subject get the feel of MI which can generate a mu-rhythm activity on motor cortex without any actual movements of the body. When subjects are asked to perform MI, most of them do not recognize how to have a concrete feeling of MI and tend to imagine the image of moving their hands or legs [7]. Therefore, one of the challenging issues in EEG-based BCI is how well we can train subjects to perform the MI task.

Over the last decade, various feedback systems for the MI training have been proposed, most of which were based on visual [8, 10, 11, 12] or auditory feedbacks [12, 13]. Suppose that subjects are instructed to perform MI of left or right hand. In the conventional feedback system, reference features for each left and right hand MI are extracted and the subjects' intentions are classified by comparing the reference features with the current features. The subjects then get visual or auditory feedback according to the classification results. Although in this example it may be sometimes possible to categorize the subjects' intentions, it is difficult to conclude that the subjects actually performed MI tasks without an off-line analysis of the stored EEG data. According to Pfurscheller and Neuper [14], some subjects cannot generate a typical activity patterns on motor cortex, even after extensive MI training processes. One typical reason of the wrong MI is that subjects imagine visual image of the movement itself (visual motor imagery: VMI), which generates completely

different brain activity patterns from MI [7]. Therefore, even when each subject attempts a same MI task, individual differences are observed because the results depend on their feeling and perception about MI (i. e., large inter-subject variability), as described by Annett [15].
In the present study, we propose a kind of neurofeedback system to train MI using the real-time cortical rhythmic activity monitoring system recently introduced by the authors [16]. The real-time monitoring system can visualize spatiotemporal changes of cortical rhythmic activity of a specific frequency band on a subject's cortical surface, not on the subject's scalp surface, with a high resolution. In our experiment, able-bodied four volunteers, who had no experience of BCI experiments before, were asked to imagine either left or right hand movement while they were watching their cortical activation maps through the real-time monitoring system. During the experiment, they tried to increase mu-rhythm (8–12 Hz) activation around the motor cortex. We investigated the changes of mu-rhythm activities in the time-frequency domain before and after the MI training to demonstrate the effect of our MI training system.

# 2 Materials and methods

## 2.1 Experimental environments

Four healthy participants (all male, 26 years old and right handed) took part in this experiment. None of them had a previous history of neurological, psychiatric or other severe diseases and they had signed a written consent. All subjects had not known the preliminary background knowledge about BCI and they had never participated in any experiments related to EEG or neurofeedback system. The experiments were conducted in the Bioelectromagnitcs and Neuroimaging Laboratory of Yonsei University. EEG was recorded at 15 electrode locations (Cz, C1, C2, C3, C4, CPz, CP1, CP2, CP3, CP4, FCz, FC1, FC2, FC3, FC4) using 32-channel EEG acquisition system (WEEG-32, Laxtha Inc., Daejeon, Korea) with a sampling rate of 256 Hz. We also recorded EMG at both forearms in order to observe the subjects' movements during MI.
The experiment consisted of two parts: training session and data acquisition session. One subject (EB) participated in five 0.5 h training sessions on separate days. The others had only one 30 minute training session. In the training session, all subjects sat on an armchair facing 17 inch monitor and watched time-varying maps of their cortical rhythmic activity updated every 350 ms, while they were attempting either left or right hand MI. In the data acquisition session, continuous EEG data were recorded before and after the training session with our experimental paradigm to examine the MI training effect.

## 2.2 EEG-based real-time cortical rhythmic activity monitoring system

An EEG-based real time cortical rhythmic activity monitoring system which was used in the training session consists of three parts: data acquisition, pre-processing, and real-time processing including visualization. In the data acquisition part, a subject's structural magnetic resonance imaging (sMRI) data are acquired prior to the EEG data recording and then the relative locations of the electrodes and important anatomical landmarks are measured using a 3D digitizer system after multi-channel EEG electrodes are attached on the subject's scalp. The sMRI data and electrode configurations are then transferred to the pre-processing part. If the individual subject's sMRI data were not available, MNI standard brain was utilized. The pre-processing part plays a role in constructing an inverse operator in which the subject's anatomical information is reflected. Once the linear inverse operator is constructed and saved to a data-storage unit, spatiotemporal changes of cortical rhythmic activities can be monitored in real time by means of a unified processing and visualization part. The processing and visualization part is composed of three independent programs: the FFT program, the frequency domain minimum norm estimation (FD-MNE) solver and the visualization program – which are executed one after the other at each time slice [13].

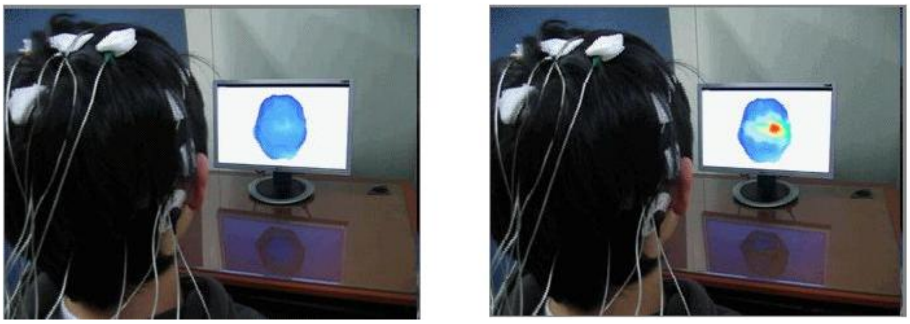

Figure 1: Screenshots of real-time cortical mu-rhythm activation monitoring: (left) normal cortical activation map, (right) cortical activation map during motor imagery.

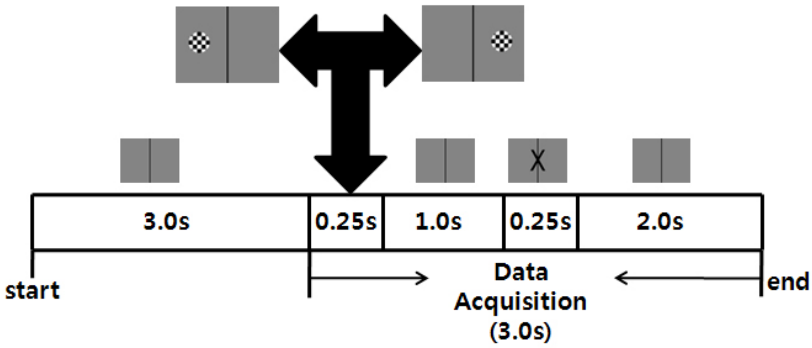


Figure 2: Experimental paradigm.

## 2.3 Training session

All participants first observed their brain activity maps on the sensorimotor cortex when they actually raise their left or right hand. We then instructed them to remember the feeling of their motor movement and perform left or right hand MI. In the beginning of the training session, all of them failed to generate the brain activity maps around the sensorimotor cortex. Through the repetitive trials, however, all subjects succeeded in generating brain activity on their sensorimotor cortex without any actual movement. Figure 1 shows the screenshots of the experiment, where a subject, EB, activated his motor cortex without actual movements.

## 2.4 Data acquisition

EEG was recorded before and after the training session to confirm the effect of our MI training. Figure 2 shows the experimental paradigm used in the present study. During the first 3 s, a gray blank appeared. A circle with a checkerboard pattern then appeared randomly on either left or right side of the screen for next 0.25 s, indicating which hand movement a subject has to imagine. After 1 s preparation time, a letter 'X' appeared and lasted for 0.25 s. At that time, the subject was asked to perform either left or right hand MI. This paradigm was repeated 180 times, when 90 trials were for the right hand MI and the other 90 trials were for the left hand MI.

## 2.5 Data analysis

We have used a 3 s segment depicted in Figure 2 for the data analysis because a subject might start the imagination right after a circle with a checkerboard pattern appeared [17]. The raw EEG signals were converted to common average reference (CAR) to compensate common noise components. The CAR method has shown good performance for the noise reduction purpose along

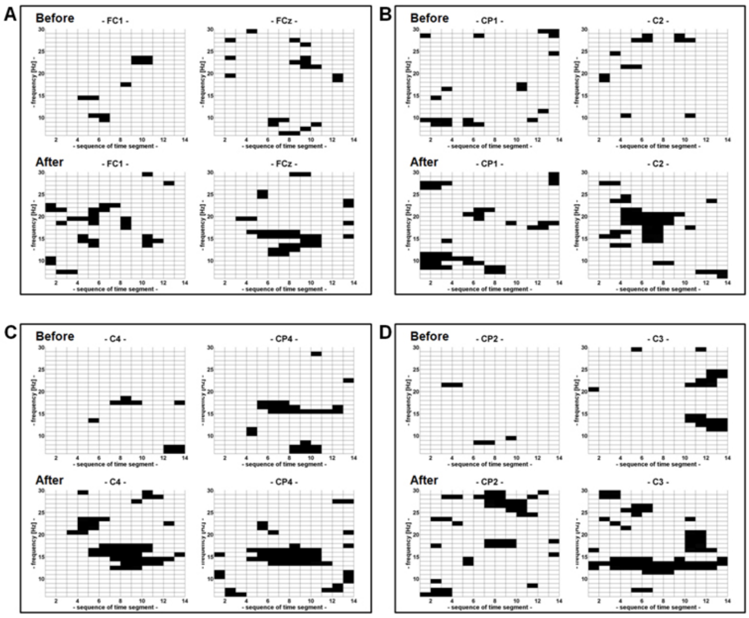


Figure 3: Distribution of time-frequency patterns showing significant difference ($p < 0.05$, black rectangles) between right and left hand motor imagery. 'A', 'B', 'C' and 'D' show the time-frequency patterns of each subject before and after the training session.

with surface Laplacian filtering [18, 19].

For the time-frequency analysis, we used fourth order Butterworth band-pass filters, in which the span of a frequency band was 2 Hz with 50 % overlapping. The selected frequency bands were 6–30 Hz, including mu and beta bands. In order to reduce the sampling rate containing original information of EEG signals, envelopes of the signals were calculated at each bin. Moving average filter was then applied to the time domain signals with 400 ms intervals to smooth the envelopes. Finally, we obtained a new time-frequency pattern map by integrating the enveloped signals at each time segment and bin. Two-tailed $t$-test was then applied to every possible combination of frequency bins, time segments, and electrodes in order to find the combinations showing significant differences ($p < 0.05$) between left and right hand MI. EMG power recorded during MI was compared with that recorded before MI, to check if the subjects actually moved their hands during the experiment.

# 3 Results

Figure 3 shows all subjects' time-frequency maps, where black colors represent time-frequency blocks which showed significant difference ($p < 0.05$) between left and right MI. After the training session, the number of black blocks was increased in most electrode positions of all four subjects. As seen in the figure, the time-frequency map did not show any distinguished feature before the training session. On the contrary, we can observe that the number of the black blocks was increased and the blocks were clustered around the mu rhythm (10 and 20 Hz) after the training session, which indirectly demonstrates that the subject succeeded in performing MI. Figure 4 shows the change of EMG power (integration of 3 s EMG segments) recorded before and during MI. The results verify that the all subjects did not move their hands during the MI experiments.

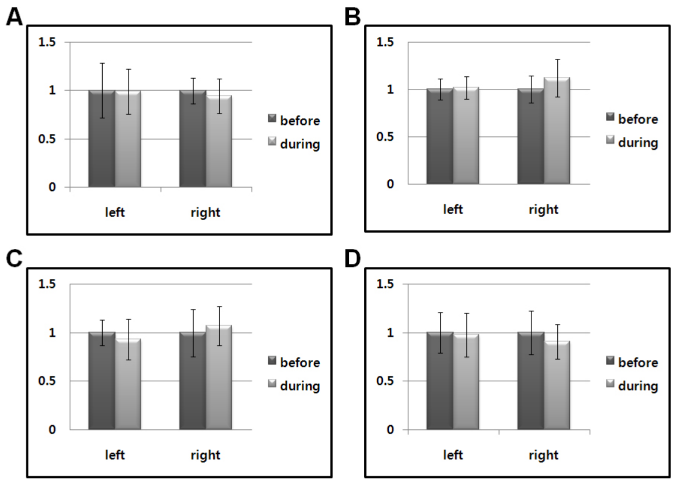


Figure 4: Relative EMG power of each subject recorded before and during the motor imagery task.

# 4 Conclusion

In the present study, we proposed a novel motor imagery training system for EEG-based BCI on the basis of a real-time cortical rhythmic activity monitoring system. A subject could get the feel of motor imagery while he was trying to activate his motor cortex presented in the computer screen. From the preliminary experimental results obtained from four subjects, we could confirm that our training system is effective in training MI to subjects who have not experienced BCI.

# References

[1] J. R. Wolpaw, N. Birbaumer, D. J. McFarland, G. Pfurscheller, and T. M. Vaughan. Brain-computer interfaces for communication and control. *Clin. Neurophysiol.*, 113:767–791, 2002.

[2] T. Hinterberger, J. M. Houtkooper, and B. Kotchoubey. Effects of feedback control on slow cortical potentials and random events. In *Parapsych. Assoc. Convention Proc.*, 2004.

[3] U. Hoffmann, J. M. Vesin, T. Ebrahimi, and K. Diserens. An efficient P300-based brain-computer interface for disabled subjects. *J. Neurosci. Methods*, 167:115–125, 2008.

[4] J. D. Bayliss. Use of the evoked potential P3 component for control in a virtual apartment. *IEEE Trans. Rehabil. Eng.*, 11:113–116, 2003.

[5] E. Lalor, S. Kelly, C. Finucane, R. Burke, R. Smith, and R. B. Reilly. Steady-state vep-based brain-computer interface control in an immersive 3D gaming environment. *EURASIP J. Appl. Sig. Process.*, 19:3156–3164, 2005.

[6] M. Middendorf, G. McMillan, G. Calhoun, and K. S. Jones. Brain-computer interfaces based on the steady-0state visual-evoked response. *IEEE Trans. Rehabil. Eng.*, 8:211–214, 2000.

[7] C. Neuper, R. Scherer, M. Reiner, and G. Pfurtscheller. Imagery of motor actions : Differential effects of kinesthetic and visual-motor mode of imagery in single-trial EEG. *Cogn. Brain Res.*, 25:668–667, 2005.

[8] J. A. Pineda, D. S. Silverman, A. Vankov, and J. Hestenes. Learning to control brain rhythms: Making a brain-computer interface possible. *IEEE Trans. Neural Syst. Rehabil. Eng.*, 11:181–184, 2003.

[9] C. Neuper and G. Pfurtscheller. Event-related desynchronization (ERD) and event-related synchronization (ERS). In *Electroencephalography: basic principles, clinical applications and related fields*. Williams & Wilkins, 2005.

[10] R. Leeb, C. Keinrath, D. Friedman, C. Guger, R. Scherer, C. Neuper, M. Garau, A. Antley, A. Steed, M. Slater, and G. Pfurtscheller. Walking by thinking: The brainwaves are crucial, not the muscles. *Presence*, 15:500–514, 2006.

[11] B. Blankertz, G. Dornhege, M. Krauledat, K.-R. Müller, and G. Curio. The non-invasive Berlin brain-computer interface: Fast acquisition of effective performance in untrained subjects. *Neuroimage*, 37:539–550, 2007.

[12] F. Nijboer, I. Gunst, S. von Hartlieb, D. McFarland, N. Birbaumer, and A. Kübler. A comparison between auditory and visual feedback of sensorimotor rhythms (SMR) for a brain-computer interface (BCI) in healthy participants. *Psychophysiol.*, 43:S71–S71, 2006.

[13] F. Nijboer, A. Furdea, I. Gunst, J. Mellinger, D. J. McFarland, N. Birbaumer, and A. Kübler. An auditory brain-computer interface (BCI). *J. Neurosci. Methods*, 167:43–50, 2008.

[14] G. Pfurtscheller and C. Neuper. Motor imagery activates primary sensorimotor area in humans. *Neurosci. Lett.*, 239:1123–1134, 2001.

[15] J. Annett. Motor imagery: Perception or action? *Neuropsychologia*, 33:1395–1417, 1995.

[16] C. H. Im, H. J. Hwang, H. J. Che, and S. H. Lee. An EEG-based real-time cortical rhythmic activity monitoring system. *Physiol. Meas.*, 28:1101–1113, 2007.

[17] B. Kamousi, A. N. Amini, and B. He. Classification of motor imagery by means of cortical current density estimation and von neumann entropy. *J. Neural Eng.*, 4:17–25, 2007.

[18] B. Hjorth. An on-line transformation of EEG scalp potentials into orthogonal source derivations. *Clin. EEG Neurosci.*, 39:526–530, 1975.

[19] D. J. McFarland, L. M. McCane, S. V. David, and J. R. Wolpaw. Spatial filter selection for EEG-based communication. *Electroencephalogr. Clin. Neurophysiol.*, 103:386–394, 1997.

# Ensembles of temporal filters enhance classification performance for ERD-based BCI systems

S. Fazli[1], C. Grozea[1], M. Danóczy[1], B. Blankertz[2], K.-R. Müller[2], F. Popescu[1]

[1]Fraunhofer First, Kekuléstr. 7, 12489 Berlin, Germany
[2]Technical University, Franklinstr. 28/29, 10587 Berlin, Germany

fazli@first.fhg.de

**Abstract**

Finding suitable subject-dependent temporal and spatial filters is of paramount importance for achieving high information transfer rates in BCI systems, depending on event-related (de-)synchronization (ERD/ERS). The temporal filter can be chosen manually, or automatically by use of a heuristic. We employ a multi-classifier system (MCS), based on a predefined filter-bank of temporal filters and apply it to 91 datasets, comprising 2-class experiments from 45 subjects. Our results indicate that this approach is a viable alternative to existing methods and can completely automate the temporal filter choice while promising higher performance than either a broad, subject-independent frequency band choice or the current heuristic.

## 1 Introduction

Classical BCI systems relied on subject-training, i. e. the subject was equipped with a BCI system and had to adapt to the system in order to learn how to use it, a method termed operant conditioning [1, 2]. Reducing the subject-training time has been and is still one of the goals of the BCI community, for the achievement of which Machine learning has proved to be a suitable method [3, 4]. Very recently, a technique emerged, where reusage of subject-specific training data of previous sessions is utilized, not only enabling expert BCI subjects to engage in feedback sessions without the need of a calibration session, but also yielding highly competitive accuracies [5]. However, for naïve users, ERD-based BCI systems such as the Berlin Brain Computer Interface (BBCI) require a calibration phase, where the subject is instructed to imagine movements of their respective limbs a number of times. The types of imaginations, called classes, are chosen with respect to their topography on the motor-cortex. This calibration data is then examined and machine learning methods are employed to build subject-dependent spatial and temporal filters as well as a classifier, in order to be able to discriminate the classes as accurately as possible in a real-time feedback paradigm.

Instead of using a single temporal filter that can be identified heuristically or adjusted manually via an expert user from the calibration data, we identified multiple temporal filters which have proven to be effective over a large set of subjects. As can be seen in Figure 1, the calibration data are filtered by one of the predefined temporal filters. Subsequently, corresponding spatial filters and classifiers are calculated for each of the given temporal filters. The individual outputs thus obtained are then combined by a final gating function to yield the resulting output. The final gating function may be a simple voting scheme, but can also be designed in a more complex fashion.

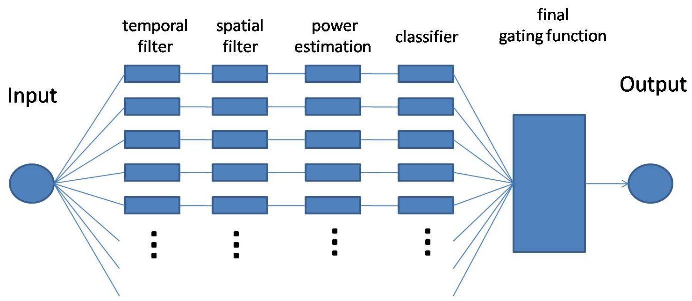


Figure 1: The flowchart shows the general setup of the method. Data is run through predefined temporal filters, and subsequently filtered by a spatial filter, which was obtained by the training set and classified, once the spectral power has been estimated. A gating function combines the outputs from the individual classifiers to a single output.

| number of datasets/subject | 1 | 2 | 3 | 5 | 8 | 9 | 13 |
|---|---|---|---|---|---|---|---|
| occurance | 32 | 5 | 3 | 2 | 1 | 1 | 1 |
| percentage [%] | 39.0 | 11.0 | 11.6 | 12.5 | 6.8 | 8.0 | 11.1 |

Table 1: The first row gives the numbers of experiments that exist for a single subject, while the second row shows how often this occurs, i. e. 32 times a particular subject carried out only a single experiment, 5 subjects carried out 2 experiments, and so on. The third row show the percentage of all trials that fall into each category (not every experiment contains the same number of trials).

# 2 Methods

## 2.1 Datasets used

We used 91 experiments of 45 individual subjects, all of which have been recorded at the IDA group. For each dataset the number of trials ranged from 70 to 600 trials and in total $\approx$ 22000 trials were examined. Each trial was referenced by 500–3500 ms, relative to stimulus onset. We considered only datasets with 2 classes of movement imaginations: left hand versus right hand. 45 channels were identified to be present in all datasets and only these were used for reasons of consistency. The channels we used are: 'F5', 'F3', 'F1', 'Fz', 'F2', 'F6', 'FC5', 'FC3', 'FC1', 'FCz', 'FC2', 'FC4', 'FC6', 'T7', 'C5', 'C3', 'C1', 'Cz', 'C2', 'C4', 'C6', 'T8', 'TP7', 'CP5', 'CP3', 'CP1', 'CPz', 'CP2', 'CP4', 'CP6', 'TP8', 'P5', 'P3', 'P1', 'Pz', 'P2', 'P4', 'P6', 'P8', 'PO3', 'POz', 'PO4', 'O1', 'Oz' and 'O2'. Individual experiments consisted of different training paradigms. While there were minor differences for the various paradigms, generally speaking visual cues were presented to the subject, and she was intructed to perform the cued imagination upon appearance. For further details we refer the reader to [6].

We would like to draw the readers attention to the fact that the dataset, considered here is biased towards subjects, for which BCI generally works, since the subjects who were chosen to take part in more than one of experiment were generally not BCI-illiterates. Please refer to Table 1 to see how many experiments per subject are present in the data we used.

## 2.2 Selection of a frequency band

### 2.2.1 Heuristic

As has been shown in [7] a heuristic can be very useful in detecting the most discriminant frequency range for a given subject. In short the method's steps are the following:

1. Use Laplacian or bipolar channels, from motor cortex related electrodes

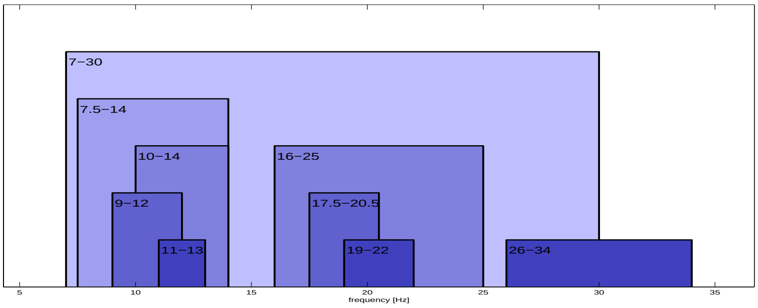


Figure 2: The Figure shows all temporal filters, used in the ensemble. Note that the heights of the patches are not related to the orders or the magnitude responses of the filters. All filters are order 5 butterworth filters.

| Frequency (Hz) | Loss (%) | Best performance (%) |
|---|---|---|
| 7.5–14 | **12.4** | 16.5 |
| 11–13 | 19.6 | 9.9 |
| 10–14 | 12.8 | **30.8** |
| 9–12 | 18.6 | 11.0 |
| 19–22 | 42.9 | 1.1 |
| 16–25 | 31.8 | 6.6 |
| 26–34 | 46.4 | 2.2 |
| 17.5–20.5 | 41.4 | 2.2 |
| 7–30 | 14.8 | 19.8 |

Table 2: The Table summarizes the median loss of each temporal filter, we chose to include for the ensemble over all subjects. The first column gives the actual frequency band, the second column represents the median, x-validated loss over all datasets and the third column shows for how many datasets the given filter performed best. Note that for seemingly unsuitable filters, some datasets score their best validation loss.

2. For each trial, channel and frequency in the range from 7 to 35 Hz, calculate the log-bandpower
3. Calculate the correlation coefficient between the log-bandpowers and their true labels
4. Find the frequency with the highest correlation coefficient and broaden the band step-wise in both diretions, until the next frequency bin is smaller than 5 % of the peak

### 2.2.2 Filter bank

From neurophysiology we know, that the $\mu$-rhythm (9–14 Hz) and synchronized components in the beta band (16–22 Hz) are macroscopic idle-rhythms, that occur when a subject is at rest and are located over the postcentral somatosensory cortex and precentral motor cortex, respectively. Imaginations of movements as well as actual movements are known to suppress this idle rhythm contralaterally. However the motoric $\mu$-rhythm as well as the beta-rhythm can have a slightly different frequency ranges for individual subjects. From empirical considerations we identified 9 different band-pass filters that have proven to discriminate best over a large range of subjects. Figure 2 shows the filters we used to generate the ensemble, Table 2 summarizes how well each of the chosen filters performs on average. Also in the same table it can be seen how often each one of the proposed filters acts best on all experiments, percentagewise.

| | CSP | | Ensemble | | | |
|---|---|---|---|---|---|---|
| | broad | auto | mean | max | maj | med |
| 25 %-tile | 7.2 | 4.1 | **3.6** | 6.8 | 24.1 | 5.1 |
| median | 14.8 | 15.5 | **11.2** | 17.3 | 43.8 | 11.3 |
| 75 %-tile | 31.7 | 36.7 | **30.7** | 32.7 | 64.9 | 31.4 |

Table 3: The results given above were calculated for each subject individually and then averaged. The left part of the table shows the loss of the baseline, using CSP and a broad band-pass filter (7–30 Hz) and the automatic heuristic. On the right hand side of the table the results of the ensemble are presented. "mean" uses the mean of all classifiers, "max" uses only the classifier output with the highest absolute value, "maj" stands for majority voting and "med" for median voting

### 2.3 Validation

Every dataset was split into two chronological halves, i. e. each method was trained on the first half and then validated on the second half.

### 2.4 Final gating function

The final gating function can be realized in different ways, for a intuitive review of the most common methods, we would like to refer the reader to [8]. Given the classifier outputs for a single trial $X \in R^{d \times t}$, one approach is to average out the resulting outputs of the individual classifiers $\hat{y}_m = \sum_{j=1}^{d} X$. However, we may also choose to let only the classifier with highest absolute value take the decision or let the majority decide or the median of the individual outputs. Table 3 shows the validation results of these combination rules.

## 3 Results

Each LDA output for a given trial indicates how far the feature is from the hyperplane. This can be interpreted as how confident a classifier is. In this sense the weighting of the individual classifiers is already optimal. It is therefore not surprising that the ensemble mean yields the best results, as can be seen from Table 3. For good subjects the heuristic performs very well, while for subjects, where the discriminativities are not so well detectable, a broadband CSP perfoms favourably.

## 4 Discussion

The principal aim of this work is to make classifier tuning as automatic and fast as possible. Certainly, the mean ensemble method obviates the need to find any extra parameter estimation for the weighting of the individual classifier outputs.
The motivation of the ensemble of temporal filters was, that for small numbers of training trials, or for subjects, where the detection of the correct frequency band is difficult, it is certainly possible that the heuristic fails. By using the ensemble we introduce prior information from neurophysiology and BCI classifier calibration experience and let the ensemble of classifiers decide which band scores the highest confidence at minimal computational cost.
It would be unrealistic to claim that the data presented here can be seen as an unbiased sample of society, as only successful BCI subjects are likely to participate in more than one experiment. However, since most of the BCI community is interested in well performing subjects, the results presented here should be of interest. Furthermore, when possible we look at individual subject performance as well as experiment performance, as to reduce this bias as much as possible.
While this study is solely based on offline results, it can be of significant value only if designed in a

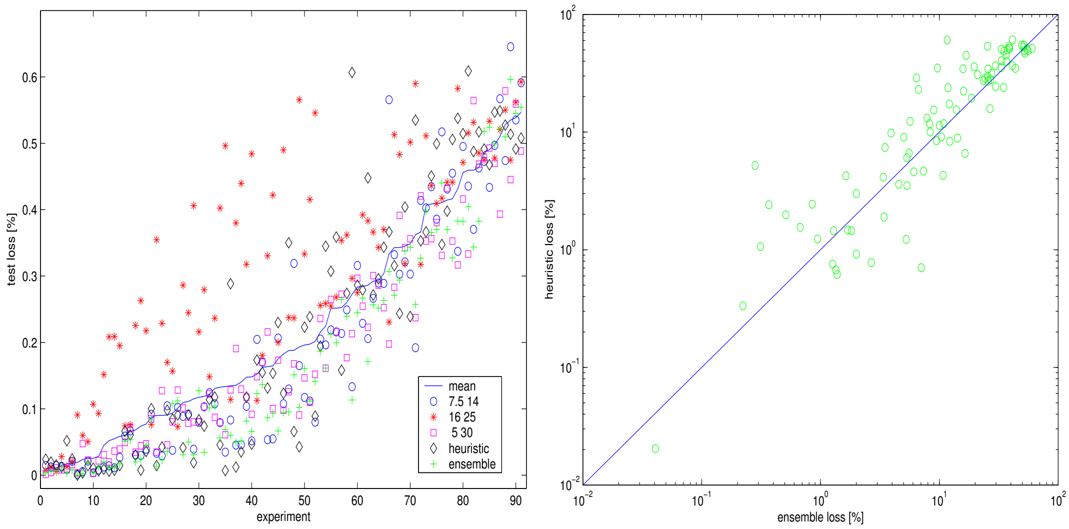


Figure 3: The Figure on the left shows the resulting loss of 4 different frequency bands, data is sorted by the mean performance of all bands. The Figure on the right shows the test loss for each individual experiment for the best ensemble method, versus the classical procedure, with the automatic heuristic

meaningful manner. The implementation of the presented method is computationally manageable and in fact we plan to validate the presented results by online experiments in novel subjects.

## 5 Conclusion

Ensemble methods have only recently been applied to BCI related data [9, 10] with promising results, but to our knowledge not using the filter-bank approach presented here. We show that our approach of parallelizing the decoding of ERD-based EEG signals has a beneficiary effect on the classification performance. Furthermore, we see that the combination of the individual classifier outputs can be realized in a very simple and effective manner. Using ensemble methods has an increased but manageable computational cost, while it has the inherent advantage over optimization of the correct band pass filter that it is less prone to overfitting.
It remains to be seen, if by this method, the resulting architecture is more robust to non-stationarities, which may occur over long feedback sessions. Whatever the nonstationarities, it is less likely that a particular subject changes his frequency band corresponding to motor imagination over time. Furthermore, this could be easily tested by applying the presented method to datasets where non-stationarities are known to exist or by putting the method into practice in a feedback environment.
In the more likely case that slightly different cortical regions are active and encode information with different frequencies, the approach we present here ensures that these type of effects are taken into account and can be tracked in the nonstationary case.

## References

[1] N. Birbaumer, N. Ghanayim, T. Hinterberger, I. Iversen, B. Kotchoubey, A. Kübler, J. Perelmouter, E. Taub, and H. Flor. A spelling device for the paralysed. *Nat.*, 398:297–298, 1999.

[2] T. Elbert, B. Rockstroh, W. Lutzenberger, and N. Birbaumer. Biofeedback of slow cortial potentials. i. *Electroencephalogr. Clin. Neurophysiol.*, 48:293–301, 1980.

[3] B. Blankertz, G. Curio, and K.-R. Müller. Classifying single trial EEG: Towards brain computer interfacing. In T. G. Diettrich, S. Becker, and Z. Ghahramani, editors, *Advances in Neural Inf. Proc. Systems (NIPS 01)*, volume 14, pages 157–164, 2002.

[4] K.-R. Müller, M. Krauledat, G. Dornhege, G. Curio, and B. Blankertz. Machine learning techiques for brain-computer interfaces. *Biomed. Tech.*, 49(1):11–22, 2004.

[5] M. Krauledat, M. Schröder, B. Blankertz, and K.-R. Müller. Reducing calibration time for brain-computer interfaces: A clustering approach. In B. Schölkopf, J. Platt, and T. Hoffman, editors, *Advances in Neural Inf. Proc. Systems (NIPS 07)*, volume 19, pages 753–760, 2007.

[6] B. Blankertz, M. Kawanabe, R. Tomioka, F. Hohlefeld, V. Nikulin, and K.-R. Müller. Invariant common spatial patterns: Alleviating nonstationarities in brain-computer interfacing. In *Advances in Neural Inf. Proc. Systems (NIPS 08)*, volume 20, 2008.

[7] B. Blankertz, R. Tomioka, S. Lemm, M. Kawanabe, and K.-R. Müller. Optimizing spatial filters for robust eeg single-trial analysis. *IEEE Sig. Process. Mag.*, 25(1):41–56, January 2008.

[8] R. Polikar. Ensemble based systems in decision making. *IEEE Circuits and Syst. Mag.*, 6(3):21–45, 2006.

[9] M. Fatourechi, R. K. Ward, and G. E. Birch. A self-paced brain-computer interface system with a low false positive rate. *J. Neural Eng.*, 5:9–23, 2008.

[10] A. Rakotomamonjy and V. Guigue. Bci competition iii: dataset ii- ensemble of svms for bci p300 speller. *IEEE Trans. Biomed. Eng.*, 55(3):1147–1154, March 2008.

# Steady-state movement related potentials for BCI – an exploratory approach in the STF domain

K. Nazarpour[1], P. Praamstra[1], R. C. Miall[1], S. Sanei[2]

[1] Behavioural Brain Sciences Centre, School of Psychology, University of Birmingham, Birmingham, UK
[2] Centre of Digital Signal Processing, School of Engineering, Cardiff University, Cardiff, UK

k.nazarpour@bham.ac.uk

**Abstract**

Classification of the steady-state movement related potentials (ssMRP) is proposed here as a potential approach to real-time brain computer interfacing (BCI). We briefly review the neurological background of ssMRPs which are typically studied by means of averaged electroencephalogram (EEG) signals. A simple feature extraction method is then suggested for single trial ssMRP processing. The Fisher's linear discriminant (FLD) classifier is utilized here in order to test the proposed BCI. The novelty and promise of this approach is mainly in the application of rhythmic cues for BCI, the simple recording setup, and straightforward computations which make the real-time implementations plausible.

## 1 Introduction

Potentially effective hybrid space-time-frequency (STF) approaches to EEG analysis have attracted an increasing interest within BCI community recently [1, 2, 3, 4, 5]. The main rationale behind those is that by combining the information from the three domains – space, time, and frequency – the finger movement related changes in EEGs can be robustly extracted. Fundamentally, there are two approaches for extracting the EEG features in the STF domain. Supervised optimization methods, as in [5, 6, 7, 8], spectrally regularize the conventional spatio-temporal common filters for EEG classification. The unsupervised methods [3, 9] mainly utilize parallel factor analysis [10] to identify the movement related factor in the EEG measurements. However, they either suffer from the implied computational complexity as in [2, 4] or sophisticated optimization schemes should be followed [5]. On the other hand, noticing exceptional performances of STF tensor decomposition methods in sensor array processing and wireless communications [11], the prime question is: "Do (un)supervised STF-based approaches consistently outperform the conventional time-space or time-frequency methods for BCI applications?" In reply, the implementation of STF methods provides promising results if the signal of interest occurs sparsely in the STF domain or at least in a sub-domain. This does not seem to be very likely in the uncertain and highly nonstationary nature of real-time BCI.

Temporal and spatial characteristics of spectrally band limited readiness potentials (RP) during the execution of self-paced voluntary movement have been well investigated [12, 13]. Blankertz et al. [14] introduced a sparse feature extraction method by mining a set of heuristically selected data points from multichannel EEGs in the frequency band of RP [12]. The selected feature points in the STF domain were then introduced to a classifier. The results [5] are promising, however, the approach suffers from high inter- and intra-subjects variability. On the other hand, since RPs are generally low frequency signals, their recording is not easy. For instance, DC drifts (due to sweating or electrode displacement) are not easily distinguished from slow 1 or 2 Hz RP signals in short windows of 0.5 second length before the movement onset [5].

The second problem arises from the nature of the RP. In order to allow the RP build up over time, the inter-movement interval should be several seconds. Aiming at increasing the information transfer rate (ITR), measured in bits per minute (bpm), recently, it was attempted to modify the conventional RP-based BCI paradigms by asking the subjects to respond at faster rates; the movement intervals were reduced to 0.5 second. However, that inevitably has led to a decrement in the correct classification rates. For instance, as reported in [14], in classification of RP features, mis-classification will be $5\,\%$ (ITR $\approx 18.6$ bpm) and $19\,\%$ (ITR $\approx 52.9$ bpm) when the respective inter-tap intervals (ITI) are 2 and 0.5 seconds.

An alternative approach based on the steady-state movement related potentials recorded during real finger movements is proposed here. The main idea is to modify the EEG recording protocol in order to produce continuous spatio-spectrally localized motor related potentials. It overcomes the above mentioned limitations and provides desirable classification rates in a high ITR framework. This approach does not imply greater computational load and therefore its real-time implementation is possible.

In the following paragraphs, the main motivation and the neurological background of using ssMRPs for BCI applications are presented. In Section 2, the data recording and processing procedures are fully described. We subsequently report the results in Section 3 followed by the concluding remarks in Section 4.

Behavioral neuroimaging studies on rhythmic movements have led to the hypothesis that there are distinct brain structures which perform automatic vs. cognitively controlled timing for repetitive movements [15, 16]. The automatic control system is primarily involved in continuous movements with frequencies greater than 1 Hz, i. e. sub-second intervals. It is highly likely to recruit neural circuits within the primary motor system that measure the time without attentional modulation. On the other hand, the cognitively controlled timing system is more exploited in controlling the movements with frequencies much smaller than 1 Hz, i. e. supra-seconds intervals. Cognitively controlled timing structure requires the activation of additional prefrontal and parietal lobes. In [15, 16], we have concluded that once a fast rhythmic task is selected and initiated, it may be executed without direct attention. The timing control of a continuous series of fast and predictable movements should therefore require attention merely during the selection and initiation phases.

In an fMRI study, Schaal et al. [17] have verified that even in slow single-joint rhythmic movements higher brain levels such as working memory (the dorsolateral prefrontal cortex), recall (the ventrolateral prefrontal cortex), and attention (the intraparietal sulcus and inferior parietal lobe) may be recruited. In contrast, high frequency ($> 1$ Hz) rhythmic movements show much less cerebral activity; the only significantly active region is the contralateral motor cortex. On the other hand, it has been documented [18] that execution of simple unimanual repetitive finger movements is associated with activity within the Rolandic fissure of the contralateral hemisphere corresponding to the primary sensorimotor cortex, termed ssMRPs.

For BCI purposes, it is hypothesized that during fast repetitive finger tapping, ssMRPs are highly confined to the contralateral motor areas. This, in turn, implies that non-motor related activities will be attenuated. Therefore, if the subjects carry out (or just imagine) the motor task in synchrony with a flashing stimulus, movement related EEG signals are modulated with the frequency of the flashing cue over the motor cortex. This synchronization is stronger on the hemisphere contralateral to the moving finger. In this paper, we only analyze ssMRPs recorded during real finger movements.

## 2 Methods

Four right-handed healthy individuals (one female) participated in the experiment; all gave informed consent. No one had any previous BCI experience. Each subject first underwent a practice block of 20 trials. The main recording session was comprised of eight blocks, each contained 40 trials, resulting in 320 trials for further analysis. Each trial lasted 7 seconds which includes one second for initial fixation and another 6 seconds for EEG recording during the motor task. In the first second of each trial a fixation cross was shown in the center of the screen. Afterward, while

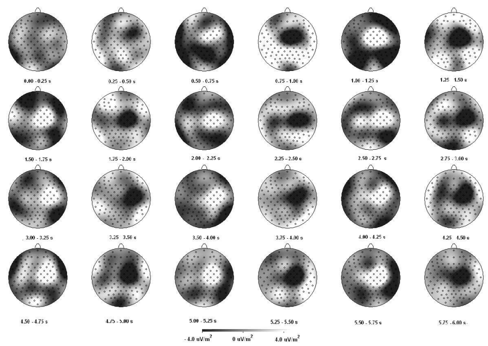

Figure 1: Averaged pre-processed EEGs during repetitive left finger movement for a single representative participant. Topographical maps have been depicted in consecutive 0.25 s time windows. The top-left map illustrates the averaged EEGs over 0 and 0.25 seconds time window and the bottom right ones present those of the last 0.25 seconds window, i. e. 5.75 to 6 seconds. Notice the rapid development of a lateralized signal over the right hemisphere whose polarity alternates every 250 ms.

the cross was kept constant in the center, two flashing cues (as "X") appeared at left and right sides of the cross for 6 seconds; each was 10 cm apart from the center. Flashing frequency was set to 2 Hz. The participants were instructed to tap (real movement) on two force transducers under left or right index fingers at a constant rate of 2 Hz synchronous to the flashing cues. The rest interval between trials was approximately one and half seconds, randomly changing so that the subjects would not guess the start of next trial. Choice between right or left finger tapping was made freely by the participants in each trial. However, they were asked to be fair between right and left responses.

The main reason for showing the flashing cues was to give the subjects a 2 Hz pace. Bilaterally equidistant cues on either side from the center should not cause development of asymmetric potentials over the motor cortex. Moreover, in order that the subjects did not concentrate on these cues, the subjects were asked to maintain fixation on the central cross during the course of tapping. This approach was adopted in order to attenuate any undesired steady-state visual evoked potential (ssVEP). Force transducers were utilized instead of conventional response switches in order to provide a setup in which the subjects did not actually press any switch, just performed repetitive tapping, which maintained the continuity of the repetitive finger movement.

EEG potentials were recorded continuously using 128 Ag/AgCl scalp electrodes with respect to an (off-line) averaged left and right mastoids reference. The electrodes were placed according to the $10-5$ system [19], using a carefully positioned nylon cap. Eye movement and eye-blink artifacts were monitored by bipolar horizontal and vertical electro-oculogram (EOG) derivations. EEG and EOG signals were amplified with a bandpass of 0–128 Hz using BioSemi Active-Two amplifier, and sampled at 512 Hz. Continuous EEG recordings were off-line segmented in epochs from 0–6 s after trial onset.

Of primary interest were the steady-state movement-related potentials developing by rhythmic tapping. Therefore, the averaged bandpass filtered (1.5–2.5 Hz) EEGs recorded during repetitive left and right finger movement trials were used to visualize ssMRPs in the time domain. The topographic maps (Figure 1) show rapid development of a lateralized signal over contralateral sensorimotor cortex whose polarity alternates every 250 ms, i. e. at 2 Hz, during left index rhythmic movements. Similarly, in the case of right finger movement, the 2 Hz signal is detectable from the left contralateral hemisphere, see Figure 2.

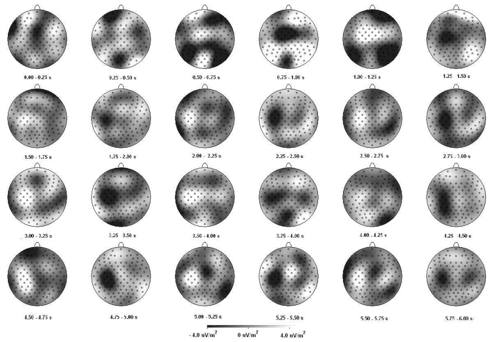

Figure 2: Averaged pre-processed EEGs during repetitive right finger movement for a single representative participant. Topographical maps have been depicted in consecutive 0.25 s time windows. The top-left map illustrates the averaged EEGs over 0 and 0.25 seconds time window and the bottom right ones present those of the last 0.25 seconds window, i. e. 5.75 to 6 seconds. Notice the rapid development of a lateralized signal over the left hemisphere whose polarity alternates every 250 ms.

## 2.1 Feature extraction and classification

Each trial was temporally segmented into ten overlapping windows comprising of three short early windows, i. e. 0–0.5 s, 0–1.5 s, and 0–2.5 s and seven overlapping windows of 3 seconds length. The latter seven windows have 83 % temporal overlap, i. e. 0–3 s, 0.5–2.5 s, 1–4 s, 1.5–4.5 s, 2–5 s, 2.5–5.5 s, and finally 3–6 s. Finally, the energy features were computed from multi-channel EEGs. First three windows, namely 0–0.5 s, 0–1.5 s, and 0–2.5 s, were considered to investigate the approximate time needed for the subjects to select and initiate tapping synchronous to the 2 Hz flashing cues. We would expect that a relatively poor classification performance would be achieved during the selection and initiation phases in each trial. The performance would eventually increase after first few seconds. Note that first two time windows, 0–0.5 s and 0–1.5 s, are too short to provide a reliable estimate of the spatially distributed 2 Hz rhythm. However, they can provide an indication of ITR lower bound of the proposed scheme.

The conventional Fisher linear discriminant (FLD) [20] classifier was utilized for classification of the extracted features. In FLD the main motive is to maximize the between-class distance while minimizing the within-class distance of the samples.

# 3 Results

Individual trials containing eye-blink and eye-movement artifacts were discarded (on average 15 % from each subject) and the remaining trials were considered for feature extraction and classification stages. EEG measurements from 45 scalp electrodes over the sensorimotor cortex were bandpass filtered between 1.5–2.5 Hz and the energies (variance) calculated. In order to reduce the feature space dimensionality, we have experimentally found that using the first three principal components of the feature space lead to acceptable classifications results. For each temporal segment, we randomly selected 60 % of computed feature vectors as training samples and the classifiers were tested with the remaining 40 %. The percentage of correct classified feature vectors over all test segments was considered to be the ratio of correct decisions over total number of decisions. This procedure was repeated 400 times. Average rates of correct classification are illustrated in Figure 3.

In all four subjects, the steady incremental trends of classification rates in early segments, 0–0.5 s, 0–1.5 s, and 0–2.5 s, are evident. In the very first seconds of each trial the subjects attempt to adopt the correct 2 Hz pace which causes activities from areas of the brain other than the contralateral motor cortex resulting in slight degradation in BCI classification performance. Although the subjects had a short 5 minutes training block before the actual recording, they

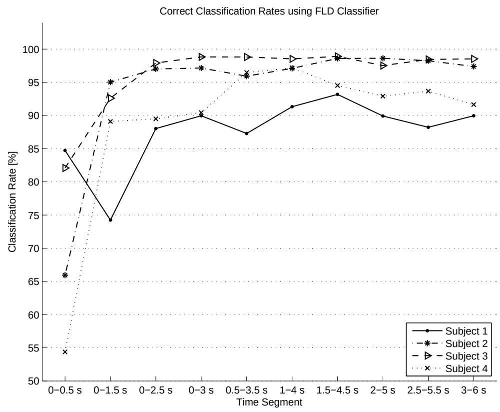


Figure 3: The correct classification rates of the temporally segmented EEGs recorded from four subjects using FLD classifier.

still reported afterwards they had to attend to the pace or the onset of each trial. When they acquire the correct pace, taps are carried out at almost the correct frequency which lead to high classification results.

# 4 Conclusions

This work shows that ssMRPs can be utilized as a suitable approach for a real-time high accuracy BCI. Here, ssMRP-based BCI has been tested for four subjects. The subjects were asked to cyclically move one of their fingers at a pre-determined frequency. Therefore, the continuous and spectrally band limited signal of interest can be extracted from the motor cortex. In the point of view of STF tensor processing, fast detection and localization of such movement related potentials is a technical challenge.

Considering the aforementioned results, the main advantages of the ssMRP-based BCI over other approaches are its simple recording setup and straightforward computations. In addition, ssMRP recording is not difficult for the subjects since in each trial they are actively involved in the experiment rather than waiting for several seconds before the exertion of a single discrete movement. Moreover, very limited training would be required.

The large number of electrodes utilized in this research should not be regarded as a hindrance towards end-product BCI. We would like here to stress that although conventional data driven common spatial patterns (CSP) [20] and their variations [6] which inherently would increase the performance may be used, they have not been considered.

In this papers, ssMRPs recorded during real finger movement were exploited for BCI. The physiologic background and simplicity of the recording setup support the repeatability of the experiments during imagery movements.

**Acknowledgments:** This work is supported by The Wellcome Trust, UK. The work of S. Sanei is supported by The Leverhulme Trust, UK.

# References

[1] S. Sanei and J. A. Chambers. *EEG signal processing.* Wiley, 2007.

[2] K. Nazarpour, L. Shoker, and S. Sanei. Brain computer interfacing in space-time-frequency domain. In *3rd International BCI Workshop and Training Course*, 2006.

[3] K. Nazarpour, S. Sanei, L. Shoker, and J. A. Chambers. Parallel space-time-frequency decomposition of EEG signals for brain computer interfacing. In *Proceedings EUSIPCO 06*, 2006.

[4] T. Ebrahimi, J.-M. Vesin, and G. Garcia. Brain-computer interface in multimedia communication. *IEEE Sig. Process. Mag.*, 20:14–24, 2003.

[5] B. Blankertz, G. Dornhege, M. Krauledat, K.-R. Müller, V. Kunzmann, F. Losch, and G. Curio. The Berlin Brain-Computer Interface: EEG-based communication without subject training. *IEEE Trans. Neural Syst. Rehabil. Eng.*, 14:147–152, 2006.

[6] S. Lemm, B. Blankertz, G. Curio, and K.-R. Müller. Spatio-spectral filters for improving the classification of single trial EEG. *IEEE Trans. Biomed. Eng.*, 52:1541–1548, 2005.

[7] R. Tomioka, G. Dornhege, K. Aihara, and K. R. Müller. An iterative algorithm for spatio-temporal filter optimization. In *3rd International BCI Workshop and Training Course*, 2006.

[8] R. Tomioka, G. Dornhege, K. Aihara, and K. R. Müller. Classifying matrices with a spectral regularization. In *Proc. ICML07*, pages 895–902, 2007.

[9] M. Mørup, L. K. Hansen, C. S. Herrmann, J. Parnas, and S. M. Arnfred. Parallel factor analysis as an exploratory tool for wavelet transformed event-related EEG. *Neuroimage*, 29(3):938–947, 2006.

[10] R. Bro. *Multi-way analysis in the food industry: models, algorithms and applications.* PhD thesis, University of Amsterdam, Royal Veterinary and Agricultural University, 2001. Toolbox available at `http://www.models.kvl.dk/users/rasmus/`.

[11] N. D. Sidiropoulos, R. Bro, and G. B. Giannakis. Parallel factor analysis in sensor array processing. *IEEE Trans. Sig. Process.*, 48(8):2377–2388, 2000.

[12] M. Jahanshahi and M. Hallet, editors. *The Bereitschaftspotential movement-related cortical potentials.* Kluwer Academic, 2003.

[13] P. Praamstra, D. F. Stegeman, A. R. Cools, and M. W. I. M. Horstink. Reliance on external cues for movement initiation in Parkinson's disease. Evidence from movement-related potentials. *Brain*, 121:167–177, 1998.

[14] B. Blankertz, G. Dornhege, S. Lemm, M. Krauledat, G. Curio, and K.-R. Müller. The Berlin Brain-Computer Interface: machine learning based detection of user specific brain states. *J. Univ. Comp. Sci.*, 12:581–607, 2006.

[15] P. A. Lewis and R. C. Miall. Distinct systems for automatic and cognitively controlled time measurement: evidence from neuroimaging. *Curr. Opin. Neurobiol.*, 13:250–255, 2003.

[16] R. C. Miall and R. Ivry. Moving to a different beat. *Nat. Neurosci.*, 7:7–8, 2004.

[17] S. Schaal, D. Sternad, R. Osu, and M. Kawato. Rhythmic arm movement is not discrete. *Nat. Neurosci.*, 7(10):1137–1144, 2004.

[18] C. Gerloff, C. Toro, N. Uenishi, L. G. Cohen, L. Leocani, and M. Hallett. Steady-state movement-related cortical potentials: a new approach to assessing cortical activity associated with fast repetitive finger movements. *Electroencephalogr. Clin. Neurophysiol.*, 102:106–113, 1997.

[19] R. Oostenveld and P. Praamstra. The five percent electrode system for highresolution EEG and ERP measurements. *Clin. Neurophysiol.*, 112:713–719, 2001.

[20] K. Fukanaga. *Introduction to statistical pattern recognition.* Academic Press, 2nd edition, 1990.

# Robotic simulation platform for BCI application: a wheelchair driving example using P300 paradigm

G. G. Gentiletti-Faenze[1,2], J. G. Gebhart[1], M. Richard[1], E. García-Cossio[3]
R. C. Acevedo[1] V. Medina-Bañuelos[2]

[1]Universidad Nacional de Entre Ríos, Argentina
[2]Universidad Autónoma Metropolitana – Iztapalapa, México
[3]Escuela de Ingeniería de Antioquia, Colombia

ggentiletti@bioingenieria.edu.ar

**Abstract**

Recently, some researches in BCI are using robotic technologies with the aim of providing a physical interaction of the individual with his environment. This paper presents a platform that will allow the development of BCI applications in this field, particulary at their early stage, using a realistic simulation of robotic devices and their environment. As a first example of its potential, a control of a simulated electrical powered wheelchair through the visual P300 paradigm using the BCI2000 software is presented. The matrix of Donchin speller was modified using icons suitable for commanding the wheelchair movements. Our preliminary result suggest that the use of this platform is a powerful tool for design, performance test and feasibility evaluations of BCI robotic applications.

## 1 Introduction

In recent years several investigations on BCI have been directed towards applications that go beyond the interface with the computer [1]. Within these applications, some of them are making use of robotic technologies [2] trying to provide the user not only with possibilities for communication but also a direct physical interaction with their environment [2, 3].

However, these new BCI applications mean new challenges and problems. Among them two relevant items can be cited as important factors in order to reach some success to address basic research in this new area of application:

- Errors in driving online robotic applications may lead to situations of risk in the security of users and others.
- Increased costs in conducting tests on real applications, requiring elements more expensive than ubiquitous personal computer, including the use of sophisticated robotic systems [4].

In this realm, a platform derived from combining the well-known BCI2000 software [5], along with sophisticated simulation systems of robotics modules able to reproduce an extremely high level of reality, the behavior of sensors and actuators with respect to real properties in a physical environment [6], seems to be an optimal starting point.

The objective of this work is the set up of a platform able to support research in the exploration of possible online robotics BCI applications, based on sufficient and flexible simulation of robotics devices and their environment. As a pilot example we present a wheelchair driving based on the P300 visual paradigm, using a presentation matrix obtained by modifications of the classical Donchin Speller [7].

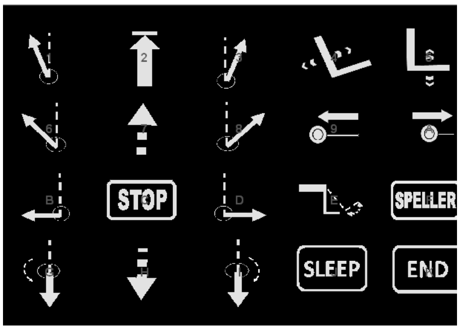


Figure 1: Modified stimulus matrix.

# 2 Methods

## 2.1 EEG recording and experimental paradigm

The EEG recording set up was based on a GRASS (model 8–18–36) module of electroencephalogram amplifiers, connected to a 6 channel analog to digital converter (DataTranslation, USB DT9816 model). Eight gold plated type reusable single disc electrodes have been used.

The software BCI2000 v2.0 has been used [5]. Changes have been made in the DTADC source module code in order to create a new DT9816 acquisition module compatible with the new board.

As the robotic simulation module we have chosen the Marilou Robotics Studio System (RSS) [6] (see 2.3), and the communications between both software (see 2.4) were established using the AppConnector functionality of BCI2000 and special functions developed on the robotic module side.

The six EEG channels (Fz, Cz, Pz, Oz, C3 and C4) were derived from electrodes located at the standard 10–20 positions, with the ground and reference electrodes located on the left and right mastoids (M1, M2) respectively. The amplifier band pass filters were set at 0.1 Hz (Low-pass) and 15 Hz (Hi-pass). The sampling frequency was 1024 Hz in order to reach a good compromise between block size (set to 32) and timing resolution for data processing in the BCI2000.

## 2.2 Stimulus matrix for a wheelchair driving interface

The classical stimulus matrix of Donchin Speller was modified, replacing character by icons in order to get a graphic user interface according to the need of establishing a set of commands to drive a simulation of the Smart Electrical Powered Wheelchair (SEPW). In Figure 1 the proposed stimulus matrix can be seen.

The duration of the stimulus used was 93.75 ms and the inter-stimulus interval (ISI) was randomly variable between 187.5 and 281.2 ms.

## 2.3 Robotics simulation module

The Robotics Simulation Module (RSM) is composed bysimulation software and control software. The simulation software used was Marilou Robotic Studio (MRS) developed by Anykode company, a modeling and simulation environment for robots operating in real-world and real-time conditions that respect the laws of physics. MRS has totally graphical handling of robots and environment models (physics parts and 3D models) and provides simulated embedded robotic components like motors, odometers, distance sensors (US, IR, Laser), bumpers, actuating cylinders, air pressure forces, cameras, GPS and accelerometers. MRS uses the Open Dynamics Engine as physical simulator to manage dynamic of physical geometries and contacts and forces among them. The control software allows robot models to be controlled using the open source MODA library provided by Anykode which can be programmed in various languages (C/C++, VB#, J#, C#, C++ CLI and URBI).

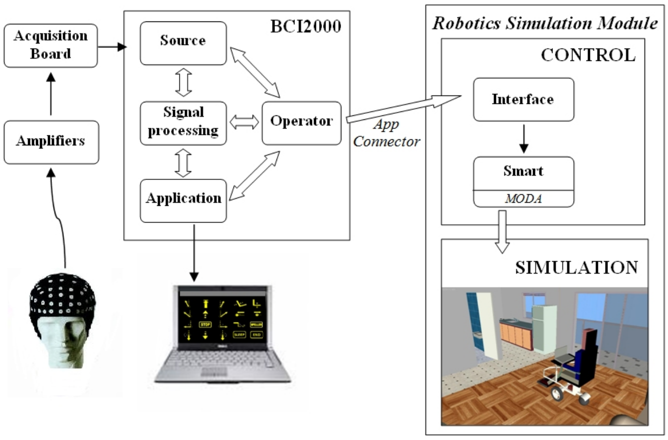


Figure 2: Components modules of proposed platform.

The control software has been developed in C++ language and is composed of two others different units, the Interface unit and the Smart unit.

The interface unit manages the communication with BCI2000 using its external application interface (App Connector). The App Connector provides a bi-directional link via an UDP based transmission protocol to exchange information with external processes running on the same machine, or on a different machine over a local network. This unit receives BCI2000 states and picks up the user's selected targets from the arrived information.

The Smart unit manages the robot control algorithms and communicates with the simulation software using MODA library to receive sensor information and send commands to actuators. This unit uses the selected targets to control the simulated wheelchair when it navigates in a simulated world. Each of the selected targets are interpreted as a control command. The wheelchair behavior not only depends on the command, but also on the ambient conditions.

Obstacles are recognized by the Smart unit using eighteen infrared sensors situated around the wheelchair in different directions. In Figure 2 a full diagram of components involved in the proposed platform in this work is shown.

## 2.4 Simulation of a smart electrical powered wheelchair

As a first example of application of the RSM, a SEPW model was created. It included structure (motors, chassis, wheels and its kinematics), dynamics (real chairs plus average human mass distributions) and sensory (18 IR sensors) elements as well as a basic obstacle avoidance control. The sensors and control give some basic capability of semiautonomous behaviors in order to prevent the user from harmful collision situations and facilitate its control with a minimum of commands.

Figure 3 shows a table with the relationship between icons in the stimulation matrix and the designed commands.

This approach allows a very basic behavior for the wheelchair, which reacts to the commands and the IR sensors states. For example, when moving forward, if the IR sensors indicate that there is something in front of the wheelchair at a distance less than half a meter, the wheelchair will stop moving. The steps forward and backward commands make the wheelchair go forward or backward respectively a distance of one meter. However, if the IR sensors detect an obstacle far less than one meter, the wheelchair will move just ten centimeters from its position in the command direction.

| Selected Target code | Icons | Commands description | IR Sensors States |
|---|---|---|---|
| 1/6/11/16 |  | turn left 15°, 45°, 90°,180° | |
| 2 |  | forward | * |
| 3/8/13/18 |  | turn right 15°, 45°, 90°, 180° | |
| 4 |  | seat rotation 0°-15° | |
| 5 |  | seat up/down | |
| 7 |  | step forward | ** |
| 9/10 |  | pull out/in back wheel | |
| 12 |   | stop | |
| 14 |  | leg rest rotation 45°-85° | |
| 15 |   | go to speller matrix | |
| 17 |  | step backward | ** |
| 19/20 |   | Sleep / End | |

Figure 3: Table of command function and Icons relationship. (∗) Move forward until IR sensors detect obstacles at distance less than half a meter from the wheelchair. (∗ ∗) If IR sensors detect distances of less than one meter in the front/back of the wheelchair, it only moves ten centimeters.

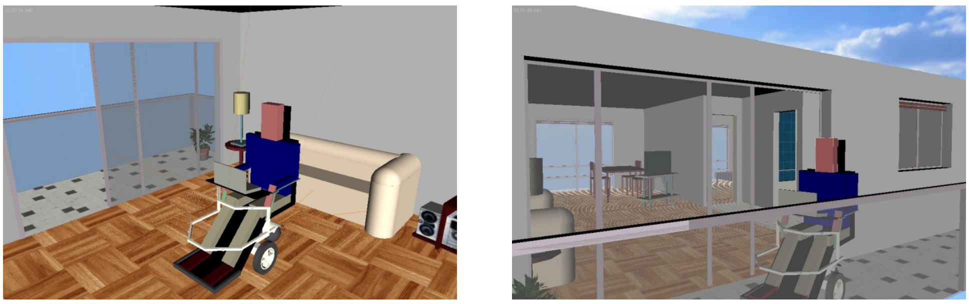

(a) View inside the simulated world. (b) View from outside of the simulated world.

Figure 4: Views of the simulated SEPW inside and outside of the simulated world.

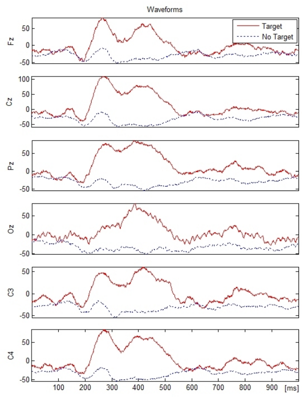


(a) Waveforms of Target vs. No-target.

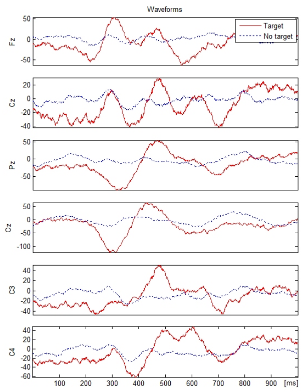


(b) Waveforms of Target vs. No-target.

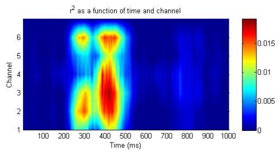


(c) Maps of $r^2$ for six channels.

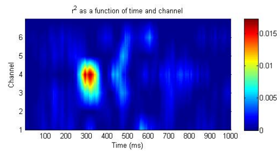


(d) Maps of $r^2$ for six channels.

Figure 5: Analysis of data in the training sets for Subject S1 (left) and S2 (right).

| Subject | Classifier | Time window | Spatial filter | Resampling freq. Hz | Channel set |
|---|---|---|---|---|---|
| S1 | SWLDA | 102–717 ms | row | 128 | 1 2 3 4 6 |
| S2 | SWLDA | 102–717 ms | row | 128 | 1 2 3 4 5 6 |

Table 1: Classifier parameters for each subject.

### 2.5 Training and online tests

Once the full platform was configured, two healthy volunteer subjects (S1 and S2) were proposed to drive the SEPW. Each subject, after being instructed, did a set of six sessions, registering four preselected icon targets (copy mode) in each session. The numbers of sequences stimulus repetition was set to 10. With this slight database, and using the BCI2000's own tool P300GUI, one classifier for each subject was trained. Both subjects remain with the same electrodes, including the time of online free mode testing (about 2hs in total). Subjects were sited in front of a two monitors arrangement, one presenting the stimulus matrix, and one showing the SEPW simulation views.

## 3 Results

The grand average waveform plots and $r^2$ maps for the six recorded channels obtained from the training database on both subjects are shown in Figure 5. Using the P300GUI provided by BCI2000 over this data base, a relatively brief search for a good set of classifiers models parameters was conducted. The set of selected parameters for each subject are detailed in Table 1

Finally, with the trained classifier and the SEPW simulation with the BCI2000 running online together, one session test was conducted on each subject. Each session consisted in trying a sequence of consecutive commands that was used by the subjects when asked to freely drive the SEPW from one place to another. Both subjects were interrupted when they reach the number of eighteen commands selected. The accuracy in the online classification task was 69.44 and 100.00 percent for S1 and S2 respectively.

## 4 Discussion

The wheelchair system has been designed to test the initial platform start up and its performance, but it will be improved in further researches. In the future, an intelligent wheelchair control system will be developed in order to improve user safety and decrease delays and user efforts. S1's performance was affected by the enthusiasm caused when he sent successful commands to the SEPW. Subject S2 was able to address the SEPW in an impressive way. The result are quite preliminary but very encouraging at this stage.

## 5 Conclusion

This first experience at our lab suggests that the use of this platform becomes a powerful tool for the design, performance test and feasibility evaluations of BCI robotics applications. This platform can be used prior to any physical construction and real assessment without compromising the safety of users, saving cost and time during the research stage.

**Acknowledgments:** The authors are grateful to the Wadsworth Center for Materials Use Agreement of BCI2000 and to Laurent Ricatti for the support with Marilou Robotic Studio. We would also like to mention the professor Erika Weiss, who has contributed improving the English writing of this article.

## References

[1] S. Mason, A. Bashashati, M. Fatourechi, K. Navarro, and G. Birch. A comprehensive survey of brain interface technology designs. *Ann. Biomed. Eng.*, 35:137–169, 2007.

[2] J. del R. Millán, F. Renkens, J. Mourino, and W. Gerstner. Noninvasive brain-actuated control of a mobile robot by human EEG. *IEEE Trans. Biomed. Eng.*, 51(6):1026–1033, 2004.

[3] J. Philips, J. del R. Millán, G. Vanacker, E. Lew, F. Galan, P. W. Ferrez, H. Van Brussel, and M. Nuttin. Adaptive shared control of a brain-actuated simulated wheelchair. In *Proc. Rehab. Robotics, 2007. ICORR 2007. IEEE 10th Int. Conf.*, number 104, pages 408–414, 2007.

[4] K. Inoue, K. Kumamaru, and G. Pfurtscheller. Robot operation based on pattern recognition on EEG signals. In *Proc. 3rd Int. BCI Worshop and Training Course 2006, Graz University of Technology, Austria*, pages 116–117, 2006.

[5] G. Schalk, D. J. McFarland, T. Hinterberger, N. Birbaumer, and J. R. Wolpaw. BCI2000: A general purpose brain-computer interface (BCI) system. *IEEE Trans. Biomed. Eng.*, 51:1034–1043, 2004.

[6] L. Ricatti. Marilou robotics studio, http://www.anykode.com.

[7] E. Donchin, K. M. Spencer, and R. Wijesinghe. The mental prosthesis: Assessing the speed of a P300-based BCI. *IEEE Trans. Rehabil. Eng.*, 8:174–179, 2000.

# Combined classification and channel/basis selection with L1-L2 regularization with application to P300 speller system

R. Tomioka[1,3] and S. Haufe[2,3]

[1]Computer Science, Tokyo Institute of Technology, Tokyo, Japan
[2]Computer Science, Technische Universität Berlin, Berlin, Germany
[3]Fraunhofer FIRST.IDA, Berlin, Germany

tomioka@sg.cs.titech.ac.jp; haufe@cs.tu-berlin.de

**Abstract**

We propose a method that combines single-trial classification and channel/basis selection in a single regularized empirical risk minimization problem. We use the linear sum of the Euclidian norms of the columns of the coefficient matrix as the regularizer. This penalty enables us to select rows and columns of the coefficient matrix, which correspond to a subset of the channels or a subset of basis functions, in a systematic manner. Moreover, the parameter learning can be performed in a convex optimization problem with second order cone constraints. The method is demonstrated on P300 speller dataset (dataset II) from the BCI competition III. The method performs reasonably well with small number of electrodes/basis functions.

## 1 Introduction

Interpretability is one of the key issues in brain-computer interfacing (BCI). A machine learning technique for BCI, though how powerful it might be, can be unacceptable unless it provides insight into the way it functions. Therefore, dimensionality reduction or feature selection techniques, such as independent component analysis or common spatial pattern have become important tools for BCI research (see e. g., [1]). However, these techniques are often developed based on criteria that have little direct connection to the task that we actually need to solve, such as classification or prediction of brain signals. In this paper, we propose a combined approach that enables us to reduce the number of channels or basis functions through regularization of the classifier. We use the linear sum of the Euclidian norms of the rows or columns of the coefficient matrix as the regularizer. This regularization enforces the weight matrix to have small number of non-zero rows or columns. Selecting rows and columns correspond to selecting channels or temporal basis functions. The same idea has also been used in other contexts to achieve joint sparsity of groups of variables (not necessarily rows or columns of a matrix) [2, 3]. The proposed method is applied to P300 speller dataset from the BCI competition III [4] and shows a reasonable performance at small number of channels. Moreover, the inference can be done in a convex optimization problem which can be solved with CVX [5], which is a freely available toolbox for MATLAB.

### 1.1 P300 speller system

Here we briefly describe the P300 speller system designed by Farwell and Donchin [6]. The subjects are presented a $6 \times 6$ table of 36 characters on the screen (see Figure 1); they are instructed to focus on the characters they wish to spell for some specified period for each character; during that period the rows and columns of the table are intensified in a random order. It is known that the subject's brain shows a characteristic reaction called P300 when the row or column that includes the character that the subject is focusing is intensified. Thus we can predict the character that the subject is trying to spell by detecting the P300 response. Each intensification lasts 100 ms with an interval of 75 ms afterwards; the intensifications of all 6 rows and 6 columns (in a random order) are repeated 15 times; hence one character takes 175 ms $\times$ 12 $\times$ 15 = 31.5 sec. Note that the period of intensification (175 ms) is shorter than the expected reaction of the brain (300 ms). Thus the intervals we analyze are usually overlapped to the next intensification and to each other.

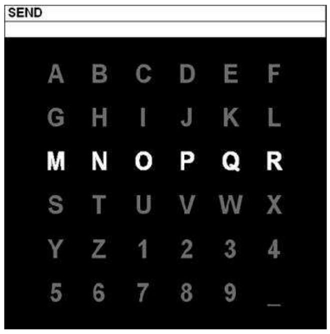


Figure 1: Table of characters shown on the display in the P300 speller system [6]. The third row is intensified.

# 2 Method

## 2.1 Detection model

Let $\tilde{\boldsymbol{X}} \in \mathbb{R}^{C \times T}$ be a short segment of EEG with $C$ channels and $T$ time-points and let $\boldsymbol{X} = \boldsymbol{P}_S \tilde{\boldsymbol{X}} \boldsymbol{P}_T$ be the input matrix preprocessed with a fixed spatial and temporal filters, which are defined with regular matrices $\boldsymbol{P}_S \in \mathbb{C}^{C \times C}$ and $\boldsymbol{P}_T \in \mathbb{C}^{T \times T}$. Basic goal in many BCI problems is to detect a characteristic spatio-temporal pattern of some activity in $\boldsymbol{X}$. Let us write a model for this detection as follows:

$$f_\theta(\boldsymbol{X}) = \Re(\langle \boldsymbol{W}, \boldsymbol{X} \rangle) + b, \tag{1}$$

where $\theta = (\boldsymbol{W}, b) \in \Theta$ and we call $\boldsymbol{W} \in \mathbb{C}^{C \times T}$ the coefficient matrix and $b \in \mathbb{R}$ the bias term; $\langle \boldsymbol{W}, \boldsymbol{X} \rangle = \sum_{ij} (\boldsymbol{W})_{ij} (\boldsymbol{X})_{ij}$ is the inner product between two matrices $\boldsymbol{W}$ and $\boldsymbol{X}$; $\Re(\cdot)$ denotes the real part of the argument. Note that we use complex coefficients only for the spatio-spectral component selection regularizer (see next section).

## 2.2 Learning with the L1-L2 regularization

Given $n$ training examples $\{\boldsymbol{X}_i, y_i\}_{i=1}^n$, where $\boldsymbol{X}_i$ can be the input matrix or a collection of matrices and $y_i \in \mathcal{Y}$ are the target values we would like to predict, let us introduce the following regularized empirical risk minimization [7] problem,

$$\underset{\theta \in \Theta}{\text{minimize}} \quad \sum_{i=1}^{n} \ell(z_i, \theta) + \lambda \Omega(\theta), \tag{2}$$

where $z_i = (\boldsymbol{X}_i, y_i) \in \mathcal{Z}$ $(i = 1, \ldots, n)$. The function $\ell : \mathcal{Z} \times \Theta \to \mathbb{R}$ is called the loss function and it measures how good a parameter configuration $\theta$ explains a training example $z$. The function $\Omega : \Theta \to \mathbb{R}$ is called the regularizer and it measures the complexity of the parameter configuration $\theta$. Our goal here is to minimize the sum of losses that we incur on the whole training examples and the complexity measured by the regularizer $\Omega(\theta)$. The trade-off between the two terms is controlled by the regularization constant $\lambda\,(\geq 0) \in \mathbb{R}$.

In this paper we discuss the following three regularizers:

$$\Omega_C(\theta) = \sum_{c=1}^{C} \|\boldsymbol{W}(c,:)\|_2, \tag{3}$$

$$\Omega_T(\theta) = \sum_{t=1}^{T} \|\boldsymbol{W}(:,t)\|_2. \tag{4}$$

$$\Omega_{CT}(\theta) = \sum_{c=1}^{C}\sum_{t=1}^{T} |\boldsymbol{W}(c,t)|. \tag{5}$$

The first regularizer is called channel selection regularizer and it is a linear sum of the Euclidian norms of the row vectors (which correspond to electrodes) of the coefficient matrix $\boldsymbol{W}$. The second regularizer is called basis selection regularizer and it is a linear sum of the norms of the column vectors (which correspond to time-points) of the coefficient matrix $\boldsymbol{W}$. The third regularizer is the sum of absolute values $|\boldsymbol{W}(c,t)| = \sqrt{\Re(\boldsymbol{W}(c,t))^2 + \Im(\boldsymbol{W}(c,t))^2}$ and selects single complex entries of $\boldsymbol{W}$ and is equivalent to conventional $\ell_1$-norm regularization of the vectorized coefficients (see e.g., [8]) if the coefficient matrix $\boldsymbol{W}$ is real. It is here called spatio-spectral component (SSC) selection regularizer, as we will use it to select pairs of informative electrodes and temporal frequencies.

### 2.3 P300 decoding model

Let us denote by $\mathcal{A}$ the set of all characters on the screen (see Figure 1); thus $|\mathcal{A}| = 36$. We denote by $\boldsymbol{X} = (\boldsymbol{X}^{(1)}, \ldots, \boldsymbol{X}^{(12)})$, where $\boldsymbol{X}^{(l)} \in \mathbb{C}^{C\times T}$, a collection of short segments of EEG recorded after each intensification (1-6 corresponds to columns and 7–12 corresponds to rows). Note that we sort the responses $\boldsymbol{X}^{(l)}$ ($l = 1, \ldots, 12$) according to the indices of rows and columns, which were recorded in the randomized order that the intensifications took place. Additionally let $a \in \mathcal{A}$ be the true character that the subject intend to spell during the intensifications. We formulate the problem of decoding the character $a \in \mathcal{A}$ out of 36 candidates as a direct product of two six-class classification problem as follows:

$$p_\theta(a|\boldsymbol{X}) = \frac{e^{f_\theta(\boldsymbol{X}^{(\mathrm{col}(a))})}}{\sum_{l=1}^{6} e^{f_\theta(\boldsymbol{X}^{(l)})}} \cdot \frac{e^{f_\theta(\boldsymbol{X}^{(\mathrm{row}(a)+6)})}}{\sum_{l=7}^{12} e^{f_\theta(\boldsymbol{X}^{(l)})}} \tag{6}$$

where $\mathrm{col}(a) \in \{1, \ldots, 6\}$ and $\mathrm{row}(a) \in \{1, \ldots, 6\}$ are the indices of the column and the row of the character $a$ on the display (see Figure 1). Here $f_\theta(\boldsymbol{X})$ is the linear model in Eq. (1) and outputs a scalar value for each intensification; note that the parameter $\theta = (\boldsymbol{W}, b)$ is *shared* among all inputs $\boldsymbol{X}^{(l)}$ ($l = 1, \ldots, 12$). In other words, the above model is a direct product of a column classifier and a row classifier in which the scalar value of the model Equation (1) is interpreted as the degree of P300 response after each intensification. In order to predict a character assuming that we have a detection model $f_\theta(\boldsymbol{X})$, we maximize the posterior probability $p(a|\boldsymbol{X})$ given $\boldsymbol{X}$ with respect to $a$ as follows:

$$\begin{aligned}\hat{a} &= \underset{a\in\mathcal{A}}{\mathrm{argmax}} \log p_\theta(a|\boldsymbol{X}) \\ &= \underset{a\in\mathcal{A}}{\mathrm{argmax}} \left(f_\theta(\boldsymbol{X}^{(\mathrm{col}(a))}) + f_\theta(\boldsymbol{X}^{(\mathrm{row}(a)+6)})\right),\end{aligned}$$

which is simply to choose the column and row with maximum response.

### 2.4 Learning the decoding model

Our training data consists of controlled trials where the subjects are instructed to spell some predefined sequences of characters. Given training examples $\{\boldsymbol{X}_i, a_i\}_{i=1}^{n}$, where $\boldsymbol{X}_i = (\boldsymbol{X}_i^{(1)}, \ldots, \boldsymbol{X}_i^{(12)})$, and $a_i \in \mathcal{A}$, our task is to learn the coefficients $\boldsymbol{W}$ and $b$. To this end, the most straightforward approach is to use the above decoding model as the conditional likelihood of the training examples. We take the negative logarithm of the likelihood and define the following loss function $\ell(z, \theta)$ as $\ell(z, \theta) := -\log p_\theta(a|\boldsymbol{X})$, where $z = (\boldsymbol{X}, a)$. Plugging this loss function into Eq. (2) we obtain the following optimization problem:

$$\begin{aligned}
\text{minimize} \quad & \sum_{i=1}^{n} \left\{ -f_{i,\mathrm{col}(a_i)} + \log\left(\sum_{l=1}^{6} e^{f_{i,l}}\right) - f_{i,(\mathrm{row}(a_i)+6)} + \log\left(\sum_{l=7}^{12} e^{f_{i,l}}\right) \right\} + \lambda \sum_{c=1}^{C} u_c, \\
\text{subject to} \quad & f_{i,l} = \left\langle \boldsymbol{W}, \boldsymbol{X}_i^{(l)} \right\rangle + b \quad (i = 1, \ldots, n, \quad l = 1, \ldots, 12), \\
& u_c \geq \sqrt{\sum_{t=1}^{T} w_{ct}^2} \quad (c = 1, \ldots, C),
\end{aligned}$$

where $w_{ct}$ is the $(c, t)$ element of $\boldsymbol{W}$, in the case of channel selection regularizer (Eq. (3)); the optimization problem for the basis selection regularizer (Eq. (4)) can be obtained similarly. The above optimization problem is a convex problem with second order cone constraints (see e. g., [9]) and can be solved using CVX toolbox [5] for MATLAB. The above approach that uses the decoding model as the likelihood function for training contrasts sharply with conventional approach that firsts train a binary classifier that detects P300 response and then combines them to predict a character.

## 2.5 Data acquisition and preprocessing

We use the P300 datasets (dataset II) provided by Jonathan R. Wolpaw, Gerwin Schalk, and Dean Krusienski in the BCI competition III [4]. The dataset includes two subjects namely A and B. The signal is recorded with a multi-channel EEG amplifier with 64 channels. We low-pass filter the signal at 20 Hz, down sample the signal to 60 Hz, and cut out an interval of 600 ms from the onset of each intensification as an epoch $\tilde{\boldsymbol{X}}^{(l)} \in \mathbb{R}^{C \times T}$ where $C = 64$ and $T = 37$ $(l = 1, \ldots, 12)$. A trial $\boldsymbol{X} \in (\mathbb{C}^{C \times T})^{12}$ consists of 12 preprocessed epoches $\boldsymbol{X}^{(l)} = \boldsymbol{P}_S \tilde{\boldsymbol{X}}^{(l)} \boldsymbol{P}_T$ $(l = 1, \ldots, 12)$ and is assigned a single character $a \in \mathcal{A}$. For each character, trials (each consisting of 12 epochs) are repeated 15 times. We average out these repetitions and get 85 training examples $(12 \cdot 85 = 1020$ epochs); although we can also consider each repetition as an individual example in the learning framework (Equation (2)) as in [10], at the moment we are not able to handle a large training set due to the computational burden. In order to further reduce the training set size we partition 85 trials into 8 sets of 40 trials (480 epochs) regularly overlapped and randomly sampled. We learn $\boldsymbol{W}$ and $b$ in our discriminative framework with the loss function derived from the decoding model; the outputs of 8 classifiers are simply averaged. Although in [10] it was reported that making an ensemble of SVMs improves performance, such comparison was not possible in our case.

The test data consists of 100 characters; also 12 different intensifications are repeated 15 times (in a random order) in the test set. We report the results of (a) averaging all the 15 repetitions and (b) averaging only the first 5 repetitions in the prediction of each character.

For the channel selection regularizer, we use identity matrices for $\boldsymbol{P}_S$ and $\boldsymbol{P}_T$. For the basis selection regularizer, we use the whitening matrices for $\boldsymbol{P}_S$ and $\boldsymbol{P}_T$ as $\boldsymbol{P}_S = \boldsymbol{\Sigma}_S^{-1/2}$ and $\boldsymbol{P}_T = \boldsymbol{\Sigma}_T^{-1/2}$, respectively. Here $\boldsymbol{\Sigma}_S$ and $\boldsymbol{\Sigma}_T$ are the pooled covariance matrices between channels and time-points, respectively, and are defined as $\boldsymbol{\Sigma}_S = \frac{1}{12n}\sum_{i=1}^{n}\sum_{l=1}^{12} \mathrm{cov}((\tilde{\boldsymbol{X}}_i^{(l)})^\top)$, $\boldsymbol{\Sigma}_T = \frac{1}{12n}\sum_{i=1}^{n}\sum_{l=1}^{12} \mathrm{cov}(\tilde{\boldsymbol{X}}_i^{(l)})$, where cov denotes the covariance along the rows (MATLAB cov function). Finally, for the SSC selection regularizer, we use the identity matrix for $\boldsymbol{P}_S$ and for $\boldsymbol{P}_T$ we use the unitary matrix given by the complex Fourier transform, i.e. $\boldsymbol{P}_T(t_1, t_2) = \exp(-\imath 2\pi \frac{(t_1-1)(t_2-1)}{T})$ $t_1, t_2 = 1, \ldots, T$. As $\boldsymbol{P}_T$ is complex, we also allow complex coefficients $\boldsymbol{W}$, although only real parts enter the loss function. Note that minimization of Eq. (5) is still convex for complex $\boldsymbol{W}$ and can again be accomplished using second order cone constraints.

# 3 Results

Figure 2 shows the classification accuracy and the number of active components for channel, basis and SSC selection regularizer from left to right, respectively. Subjects A and B are shown in the left and the right part of each figure, respectively. The top part shows the classification accuracy. Note that a random guess would give $100/36 = 2.8\,\%$ accuracy. We can see that the number of non-zero channels, basis, or SSC decreases as the regularization constant $\lambda$ increase; however the accuracy is almost constant until the regularization shuts off all the coefficients. Figure 3 shows the coefficient matrix topographically mapped on the scalp (nose pointing upwards) for the different regularizers considered. We can see that the coefficients are tightly concentrated around Cz and CPz for the channels selection regularizer (Eq. (3)). On the other hand, since the basis defined by the whitening transformation is fairly localized, the coefficients for the basis selection regularizer (Eq. (4)) are very much concentrated around the time interval from 200 to 300 ms. The frequencies selected by the SSC regularizer are mainly below 5 Hz. The time-courses of the coefficients are therefore very smooth, reflecting the shape of the P300 component. We note that the best accuracy obtained by Rakotomamonjy et al. at the competition was 72 % and 97 % for subject A and 75 % and 96 % for subject B for 5 repetitions and 15 repetitions, respectively [10].

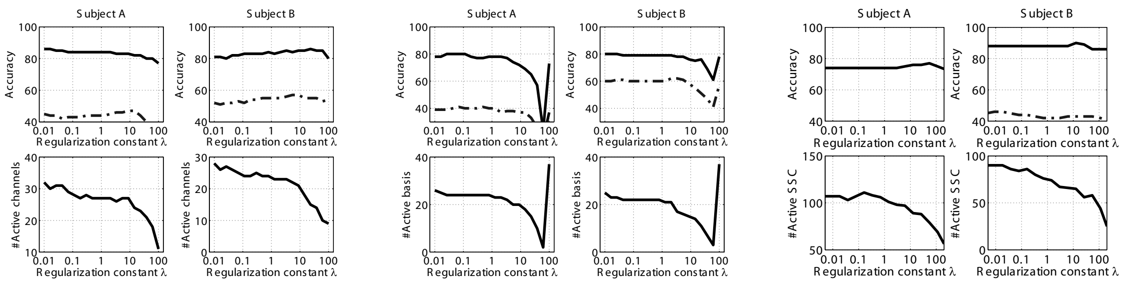


Figure 2: Performance and the number of active channels (left), active basis (center) and active spatio-spectral components (right) with the respective regularizers. In the top part, solid and dash-dotted curves show results of averaging 15 and 5 repetitions, respectively.

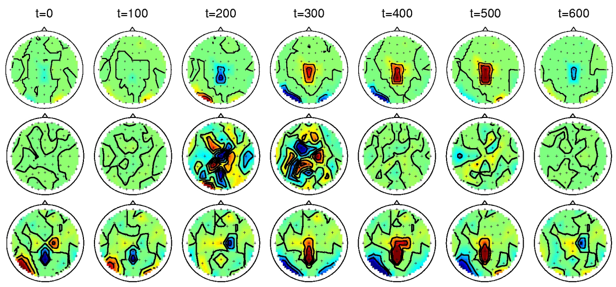


Figure 3: Scalp plots of the coefficients obtained with the along time. Top Row: channel selection regularizer (Subject A; $\lambda = 61.6$). Center Row: basis selection regularizer (Subject B; $\lambda = 8.86$). Bottom row: SSC selection regularizer (Subject B; $\lambda = 12.74$).

# 4 Conclusion

In this paper, we have proposed a method that performs channel or basis selection jointly with the training of a brain-signal decoding model. We use the linear sum of the Euclidian norms of the rows or columns of the coefficient matrix as the regularizer and perform learning in an empirical risk minimization problem. The regularizer enforces many rows or columns of the coefficient matrix to be simultaneously zero. This row- or column-wise selection contrasts sharply with the element-wise selection that can be obtained with the lasso-regularization [8]. Moreover the training can be done in a convex optimization problem. The proposed method is applied to P300 speller dataset and has shown reasonable performance at small number of electrodes/basis functions. However compared to the best results from the competition the performance was not satisfactory especially when the number of repetition is small. One reason for this might be the fact that we averaged all the repetitions in the training examples and trained the classifier on the averaged data. Thus the classifier underestimates the variability within repetitions. In the future we plan to make the optimization more efficient so that we can handle the original set of training examples without averaging.

**Acknowledgments:** Ryota Tomioka is supported by Microsoft CORE3 Project. This work was supported in part by grants of the Bundesministerium für Bildung und Forschung (BMBF), FKZ 01IBE01A (BCI III) and 01GQ0415 (BCCNB-A4), and by the IST Programme of the European Community, under the PASCAL Network of Excellence, IST-2002-506778. This publication only reflects the authors' views.

# References

[1] G. Dornhege, J. del R. Millán, T. Hinterberger, D. McFarland, and K.-R. Müller, editors. *Toward Brain-Computer Interfacing.* MIT Press, 2007.

[2] M. Yuan and Y. Lin. Model selection and estimation in regression with grouped variables. *J. R. Stat. Soc. Ser. B*, 68(1):49–67, 2006.

[3] S. Haufe, V. V. Nikulin, A. Ziehe, K.-R. Müller, and G. Nolte. Combining sparsity and rotational invariance in EEG/MEG source reconstruction. *Neuroimage*, 2008. In press.

[4] B. Blankertz, K.-R. Müller, D. Krusienski, G. Schalk, J. R. Wolpaw, A. Schlögl, G. Pfurtscheller, J. del R. Millán, M. Schröder, and N. Birbaumer. The BCI competition III: validating alternative approaches to actual BCI problems. *IEEE Trans. Neural Sys. Rehab. Eng.*, 14(2):153–159, 2006. See also the webpage: `http://ida.first.fhg.de/projects/bci/competition_iii/`.

[5] M. Grant, S. Boyd, and Y. Ye. CVX: Matlab software for disciplined convex programming, 2007. `http://www.stanford.edu/~boyd/cvx/`, Version 1.1 build 520.

[6] L. A. Farwell and E. Donchin. Talking off the top of your head: toward a mental prosthesis utilizing event-related brain potentials. *Electroencephalogr. Clin. Neurophysiol.*, 70(6):510–523, 1988.

[7] V. N. Vapnik. *Stat. Learn. Theory.* Wiley-Interscience, 1998.

[8] R. Tibshirani. Regression shrinkage and selection via the lasso. *J. R. Stat. Soc. Ser. B*, 58(1):267–288, 1996.

[9] S. Boyd and L. Vandenberghe. *Convex Optimization.* Cambridge Univ. Press, 2004.

[10] A. Rakotomamonjy and V. Guigue. BCI competition III : dataset II – ensemble of SVMs for BCI P300 speller. *IEEE Trans. Biomed. Eng.*, 55(3):1147–1154, 2008.

# Automatic recognition of error potentials in a P300-based brain-computer interface

G. Visconti[1], B. Dal Seno[1], M. Matteucci[1], L. Mainardi[2]

[1]Department of Electronics and Information, IIT-Unit, Politecnico di Milano, Italy
[2]Department of Bioengineering, IIT-Unit, Politecnico di Milano, Italy

bernardo.dalseno@polimi.it

**Abstract**

An error potential (ErrP) is an innate event-related potential generated when a subject makes a mistake, and, more relevant to brain-computer interface (BCI) applications, when the BCI itself behaves differently from the user intent. For this reason, error potentials are nowadays attracting attention in the BCI field and the presence of ErrPs has been studied already in a few BCI paradigms. In this paper we investigate the presence and the detection of error potentials in a P300-based BCI speller similar to the one described in [1], where 36 symbols are disposed on a $6 \times 6$ grid, and entire rows and columns of symbols are flashed one after the other in random order. The aim of our research is twofold; first of all, we are interested in developing a method for the automatic detection of ErrPs in a P300 speller, and, secondly, we want to evaluate the real improvement of the performance obtained when ErrP detection is used. Experiments are conducted on five subjects in a controlled scenario, where the outcome of the BCI is actually programmed to generate errors with a 20 % probability; users are unaware of this, and they believe to be interacting with a real BCI. Results show that it is indeed possible to recognize an ErrP in an automated fashion when a user interacts with a P300-based BCI, and we also provide a measure of how an automatic error correction based on ErrPs impacts on the overall BCI performance.

## 1 Introduction

An error potential (ErrP) is an event-related potential generated when a subject makes a mistake, and, more relevant to BCI applications, when the machine behaves differently from the user intent. They are known since the late 80s [2, 3] when they were described as a negative shift in the electric potential over the fronto-central region (from Fz to Cz of the 10–20 system) occurring 50–100 ms after an erroneous response (error negativity Ne or error-related negativity ERN) and a subsequent positive shift in the parietal region [2], whose maximum occurs between 200 and 500 ms after the error (error positivity Pe). Many experiments have been done, and a high variability in shape, size, and delay of the Ne and Pe components has been observed. The two components are thought to be the effect of different underlying mechanism, whose nature is not yet certain [4].

Error potentials are obviously attracting attention for BCI applications. In [5] the presence of ErrPs in a BCI paradigm (cursor movement by mu and beta rhythms) was revealed, as a positive peak at Cz 40 ms after the end of erroneous trials. Although the features of this potential are rather different from the ErrP mentioned above, this finding suggests an interesting application: the automatic detection of the errors a BCI makes in recognizing the user's intent. Millán and colleagues worked on this possibility to improve a BCI performance [6]: they made experiments with a simulated BCI, which made an incorrect choice 20 % of the times, independently of the user's EEG. They trained a Gaussian classifier to automatically recognize ErrPs reaching an accuracy of about 80 %.

In this paper we investigate the presence of error potentials in a P300-based BCI speller with two aims: first, the development of a method for the automatic detection of ErrPs in a real BCI,

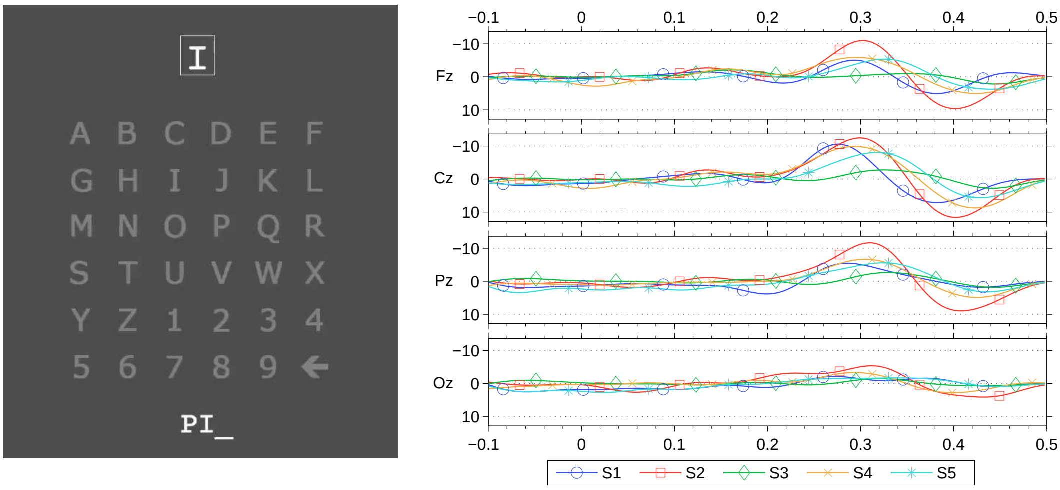


(a) (b)

Figure 1: (a) Graphical interface of our P300 speller. (b) Error-minus-correct means for the five subjects; units are seconds and microvolts; time 0 is feedback time.

i. e., a P300 speller, and, second, evaluating the possible increase of the real performance obtained when such an ErrP automatic detection is included in the speller. Section 2 of this paper describes our experimental setup, the P300 speller used, and the designed interactions between user and machine; Section 3 describes the methodologies used to identify ErrPs in the experimental data, while the obtained results are shown in Section 4.

## 2 Experimental setup

In this study, we used an experimental paradigm similar to the one described by Donchin [1]: 36 symbols are disposed on a $6 \times 6$ grid, and entire rows and columns of symbols are flashed one after the other in random order. The grid of symbols (see Figure 1.a) includes letters from the alphabet, digits, and the backspace symbol, represented by the small arrow in the right bottom corner.

The spelling of a single letter is divided in repetitions, with each repetition being composed of 12 stimulations. A single stimulation is obtained by flashing a row or a column (the intensification lasts 100 ms and the inter-stimulus interval is 100 ms). Each row/column is flashed only once during a repetition, and a series of 5 repetitions is performed. There is no pause between repetitions. At the end of the fifth repetition, the P300 system detects the (hopefully) desired row and column, and selects the letter at the intersection. After a pause of 1 s, the letter is displayed in the rectangular frame visible in the top part of Figure 1.a, and added to the word at the bottom of the screen. The presentation of the letter should elicit an ErrP whenever the letter is different from the user intention. If the error-detection system recognizes an ErrP, it overrides the P300 speller and cancels the last spelled letter. After a 2 s pause, the speller starts a new series of stimulations for the next letter. A single trial is therefore composed of 60 P300 stimulations and 1 ErrP stimulation.

In our study, the interaction between user and BCI was conducted in a controlled scenario in order to reach a desired number of errors and easily acquire the experimental ground truth without the user knowing it. Subjects were told to pay attention to a given letter at the beginning of each trial, and they were informed that the system would recognize their intention. However, the BCI system was programmed to select the right letter with a probability of 80 % and a wrong one with 20 % probability, without considering the EEG recordings at all. When a wrong letter was spelled, subjects had to choose the backspace symbol in the next trial. An accuracy of 80 %

was selected because it was considered reasonable for this BCI protocol: this accuracy value is low enough to have a sufficient number of error epochs without frustrating the users or inducing them to think that the BCI was not working.

Five subjects took part in this experiment. EEG data were recorded with an EBNeuro BE Light system at Fz, Cz, Pz, Oz referenced to right mastoid, and EOG with two bipolar electrodes near the right eye, sampled at 512 Hz, in the band 0.1–230 Hz. Each subject participated to three separate recording sessions, separated by a few days or also some weeks. Figure 1.b shows the error-minus-correct means (i. e., the differences between the averages of ErrP epochs and the averages of non-ErrP epochs), filtered in the 1–10 Hz band. Four out of five subjects have a strong Ne with a peak at about 300 ms, followed by a proportionate Pe some 100 ms after. The response of Subject 3 is rather weak, with peaks of less than 3 μV in absolute value.

# 3 Signal analysis and classification

Recorded data are segmented in epochs ranging from 100 ms before the stimulation instant (feedback onset) to 500 ms after it. Epochs containing strong EOG activity (> 100 μV at any point) are automatically discarded before further analysis. The implication of discarding epochs in a BCI is that in those cases there is no way to correct possibly wrong responses. Obviously, robustness with respect to EOG contamination is a desirable property for a detection algorithm, but we preferred to concentrate first on producing something working, and leave the improving of its robustness for the future. Data are then filtered in the band 1–10 Hz to improve the signal-to-noise ratio by eliminating frequency components extraneous to ErrPs.

On average, a difference between ErrP and non-ErrP epochs is observable only in some intervals of the segmented epoch, and these intervals depend on the subject. For these reasons we developed a way to automatically determine significant intervals in the ErrP for classification. For each channel $c$ and time point $t$, the signals $s_{c,1}(t)$ from ErrP epochs and $s_{c,0}(t)$ from non-ErrP epochs can be viewed as two sets of random variables. A $t$-test is used to check if, for any given $t$ and $c$, the mean of $s_{c,1}(t)$ differs significantly from the mean of $s_{c,0}(t)$; the significance level has been chosen to be 0.01, but much smaller $p$-values have been often found in analyzing data.

The $t$-test requires the distributions of the samples under test to be normal with equal variance. The significance of the $t$-test is not used to classify epochs, but only to find promising time intervals. For this reason, only a preliminary analysis has been done to verify that the $t$-test preconditions, so as to be sure that the $t$-test results would be meaningful. Normal probability plots drawn for a subset of time instants have been used to verify normality; although in some cases the tails of the observed distributions are longer than the Gaussian ones, the departure from normality is never dramatic. Equality of variance has been tested by applying the $F$-test to data from some subjects, and it is verified at a significance level around 0.01.

The points detected by the $t$-test tend to lie in groups, because the filtered signals have a strong autocorrelation for short lags. However, many intervals of different sizes, with "holes" in between (see the top part of Figure 2 for an example) are usually detected, while we are interested only in finding one contiguous time interval containing all the interesting features of signals. For this reason, a clustering algorithm is run on the time points found by the $t$-test to fill holes and discard isolated points or small intervals. For this purpose, we used DBSCAN [7], a clustering algorithm based on density, because it clusters together nearby points and ignores outliers, which is exactly what we need.

For our application, a cluster is transformed in an interval by taking the smallest interval containing the cluster; in other words, any gap is filled (see Figure 2). For the DBSCAN parameters, we have chosen $k = 10$ and $\varepsilon = 60$ ms; $k$ defines the minimum number of points in a cluster, so the smallest interval found was $10/512$ Hz $\approx 20$ ms. $\varepsilon$ defines the minimum distance between two points in different clusters, hence sequences of contiguous points from the $t$-test less than 60 ms apart are fused together; when Ne and Pe components are present, they generate (more or less) contiguous sequences of points passing the $t$-test, and these sequences are fused by clustering, as they are closer than 60 ms.

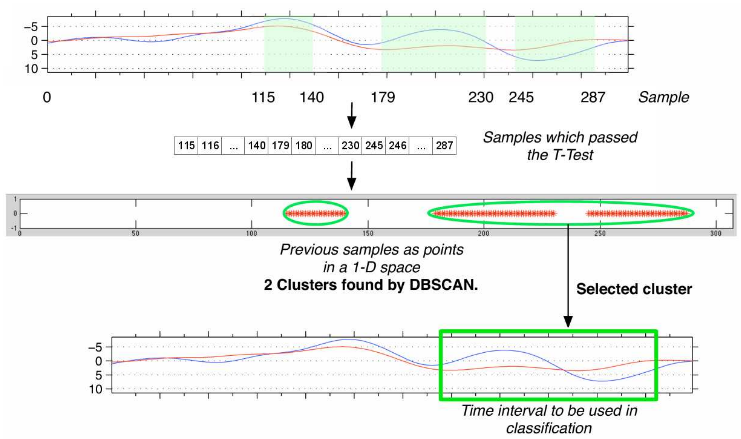


Figure 2: Procedure for the identification of significant intervals. Top: shadowed areas contain the samples that passed the $t$-test with a $p$-value of 0.01 or less. Middle: clustering of samples. Bottom: the interval used for classification.

The channels with the most significant interval found by the $t$-test have been Cz and Fz, in accord with the literature. For this reason, we use only these two channels for automatic epoch classification. As a further simplification, the intervals found by DBSCAN for the two channels are fused together (the minimum interval encompassing both is taken), and used for both channels.

The significant intervals are then used to extract two different kinds of features: raw sample values and coefficients of polynomial approximation. Features of the first kind are just all the samples of the EEG signals falling within the time interval found as previously explained. The second kind of features is computed by fitting (in the least square sum sense) two third-grade polynomials to the EEG signals from the Fz and Cz channels of each epoch; the 8 (4+4) coefficients of both polynomials represent the extracted features. Features are then fed into classifiers.

We used two standard classifiers, linear discriminant analysis (LDA), and $k$ nearest neighbor ($k$-NN), and two methods from the literature, which were already been applied to detect other event-related potentials: the Bayesian method described in [8], and the SVM-based approach [9]. LDA was applied to both kind of features, while $k$-NN only to raw samples. The SVM-based method was applied to all the four channels of whole epochs, as a sort of a check that the selection of channels and time interval would not lower the classification performance.

# 4 Results and conclusions

Table 1 shows the classification results, as the mean values of recall (fraction correctly classified) for ErrP and non-ErrP epochs obtained with a 3-fold cross-validation scheme applied to the three sessions of each subject. The column labeled size shows the number of epochs, either ErrP or non-ErrP, that remained after discarding the most noisy ones followed by their original number (please recall that we discared epochs affected by relevant EOG artifacts). The column labeled LDA is for LDA applied to raw samples, while P. LDA stands for LDA applied to polynomial coefficients. Except for Subject 3, the best classifiers (SVM and LDA with polynomial coefficients) reach about 80 % of recall, which is quite good. The performance for Subject 3, whose responses in Figure 1.b are the weakest, is just slightly better than random.

It should be evident that a BCI elicits ErrPs and it is possible to automatically detect them. The question is, can ErrP detection improve the overall performance of a BCI? We estimated the impact of ErrP detection by modeling how this affects the performance of the BCI used in this study.

We considered the case where the user selects the backspace command in the letter grid to correct all the errors made by the P300 speller, and we computed the expected number of trials

| Subject | | Size | LDA | Bayes | $k$-NN | P. LDA | SVM |
|---|---|---|---|---|---|---|---|
| S1 | ErrP | 90 / 92 | 72 % | 74 % | 63 % | 77 % | 84 % |
| | N-ErrP | 440/450 | 86 % | 75 % | 88 % | 87 % | 82 % |
| S2 | ErrP | 83 / 90 | 64 % | 72 % | 60 % | 72 % | 70 % |
| | N-ErrP | 384/426 | 83 % | 81 % | 85 % | 84 % | 84 % |
| S3 | ErrP | 56 / 97 | 50 % | 46 % | 50 % | 54 % | 52 % |
| | N-ErrP | 284/477 | 68 % | 55 % | 64 % | 67 % | 56 % |
| S4 | ErrP | 89 / 92 | 69 % | 65 % | 71 % | 69 % | 79 % |
| | N-ErrP | 352/450 | 86 % | 75 % | 87 % | 83 % | 84 % |
| S5 | ErrP | 41 / 88 | 61 % | 73 % | 63 % | 80 % | 71 % |
| | N-ErrP | 245/443 | 85 % | 76 % | 86 % | 91 % | 80 % |

Table 1: 3-fold cross-validated results of ErrP detection in P300-speller tasks

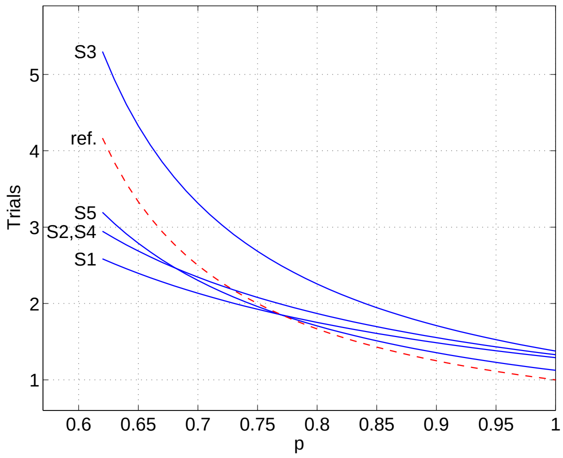


Figure 3: Trials per letter in a P300 speller with error correction vs. accuracy of the base speller classifier. The lines for Subjects 2 and 4 almost coincide and have been collapsed.

needed to correctly spell a letter. We derived a formula for this (the derivation is based on the modeling of the BCI as a simple stochastic process that is beyond the scope of this paper):

$$t_{\mathrm{L}} = \frac{1}{p \cdot r_{\mathrm{C}} + (1-p) \cdot r_{\mathrm{E}} + p - 1}\,, \tag{1}$$

where $p$ is the accuracy of the selection of the letter, i. e., the BCI accuracy, $r_{\mathrm{E}}$ is the recall of ErrP epochs, and $r_{\mathrm{C}}$ the recall for non-ErrP epochs (i. e., correct letters). To be fair, the recall values in Table 1 cannot be used directly, as they are calculated after throwing away some epochs. If we treat discarded epochs as if they were classified as non-ErrP, then we have

$$r_{\mathrm{E}} = f_{\mathrm{E}}\, r'_{\mathrm{E}} \qquad\qquad r_{\mathrm{C}} = 1 - f_{\mathrm{C}}\,(1 - r'_{\mathrm{C}})\,, \tag{2}$$

where $f_{\mathrm{E}}$ and $f_{\mathrm{C}}$ are the fraction of epochs kept, and $r'_{\mathrm{E}}$ and $r'_{\mathrm{C}}$ are the recall values computed on the epochs kept.

The improvement in BCI given by ErrP detection can be measured as the reduction in the number of trials needed to properly spell a letter; Figure 3 shows the expected number of trials needed to spell a letter correctly, as a function of the precision $p$, for the five subjects of the study. We used Equations (1) and (2) applied to the results obtained with the LDA classifier applied to polynomial coefficients, which is a reasonably simple system with good performance. The dashed red line is a reference that represents the expected outcome with no automatic error correction ($r_{\mathrm{E}} = 0$, $r_{\mathrm{C}} = 1$). While Subject 3 seems not to get any benefit from automatic error detection, the other subjects can benefit from it when the accuracy of the P300 speller is no more than 75 %.

We have described a procedure to recognize ErrPs in an automated fashion when a user interacts with a P300-based BCI. Our results are encouraging, but further work is needed to improve the performance. First of all, epochs containing EOG activity were excluded from the analysis, and robustness and validity of our method against EOG contamination should be tested. In addition, we limited the search of ErrPs in a 0.5 s window after the stimulus, but longer windows could be explored as done in previous research [10]. Nevertheless, the obtained results show the feasibility of detecting ErrPs, and we quantitatively show how the automatic error correction based on ErrPs may impact the overall BCI performance.

**Acknowledgments:** This work has been partially supported by the Italian Institute of Technology (IIT), and by the grant "Brain-Computer Interfaces in Everyday Applications" from Politecnico di Milano and Regione Lombardia. We are thankful to EBNeuro S.p.A. for the use of their BE Light EEG system and their support. We are also thankful to all the participants in our study.

## References

[1] E. Donchin, K. M. Spencer, and R. Wijesinghe. The mental prosthesis: assessing the speed of a P300-based brain-computer interface. *IEEE Trans. Rehab. Eng.*, 8(2):174–179, June 2000.

[2] M. Falkenstein, J. Hohnsbein, J. Hoormann, and L. Blanke. Effects of crossmodal divided attention on late ERP components. II. Error processing in choice reaction tasks. *Electroenceph. Clin. Neurophysiol.*, 78(6):447–455, June 1991.

[3] W. J. Gehring, B. Goss, M. G. H. Coles, D. E. Meyer, and E. Donchin. A neural system for error detection and compensation. *Psych. Sci.*, 4(6):385–390, 1993.

[4] M. Falkenstein. ERP correlates of erroneous performance. In Markus Ullsperger and Michael Falkenstein, editors, *Errors, Conflicts, and the Brain. Current Opinions on Performance Monitoring*, pages 5–14, 2004.

[5] G. Schalk, J. R. Wolpaw, D. J. McFarland, and G. Pfurtscheller. EEG-based communication: presence of an error potential. *Clin. Neurophysiol.*, 111(12):2138–2144, 2000.

[6] P. W. Ferrez and J. del R. Millán. EEG-based brain-computer interaction: Improved accuracy by automatic single-trial error detection. In *Advances in Neural Information Processing Systems 20*, pages 441–448, 2007.

[7] M. Ester, H.-P. Kriegel, J. Sander, and X. Xu. A density-based algorithm for discovering clusters in large spatial databases with noise. In *Proc. 2nd Int. Conf. Knowledge Discovery and Data Mining*, pages 226–231, Portland, Oregon, USA, August 1996. AAAI Press.

[8] J. Kohlmorgen and B. Blankertz. Bayesian classification of single-trial event-related potentials in EEG. *Int. J. Bifur. Chaos*, 14(2):719–726, 2004.

[9] M. Kaper, P. Meinicke, U. Grossekathoefer, T. Lingner, and H. Ritter. BCI competition 2003 – data set IIb: support vector machines for the P300 speller paradigm. *IEEE Trans. Biomed. Eng.*, 51(6):1073–1076, June 2004.

[10] P. W. Ferrez and J. del R. Millán. Error-related EEG potentials generated during simulated brain-computer interaction. *IEEE Trans. Biomed. Eng.*, 55(3):923–929, March 2008.

# Are eye movements mandatory to elicit a P300 event-related brain potential in a visual search?

V. Braunstein, S. C. Wriessnegger, C. Neuper

Institute of Psychology, University of Graz, Graz, Austria

verena.braunstein@uni-graz.at

**Abstract**

This study examined the P300 event-related brain potential elicited during a visual search. The aim of the study was to determine whether the P300 component and eye movements are related and how eye movements influence the P300. The results are of importance for the Brain Computer Interface device called P300-Speller. Only by concentrating on selected letters in a matrix a P300 event-related brain potential is elicited. If there is no dependency on eye movements and the P300 component, the P300-Speller could be used by ALS patients in their late stage of disease, where eye movement control is limited. 17 subjects executed a visual search paradigm on a $6 \times 6$ letter matrix. The set size of the matrix was varied between 8, 16 and 36 letters. The subjects searched for letters in a parallel and serial search under the condition "free search", where eye movements were allowed and the condition "fixation", where subjects had to focus their gaze on the fixation cross in the middle of the screen. While performing the visual search, the EEG and eye movements of the subjects were recorded. Though the "free search"-condition produced a larger P300 amplitude, a distinct P300 could also be seen in the "fixation"-condition. The latency was nearly the same in both conditions. This work shows that there are differences in the P300 amplitude between the conditions "free search" and "fixation", but eye movements are not a prerequisite to elicit a P300.

## 1 Introduction

The aim of this study was to determine whether event-related brain potentials (ERPs) – especially the P300 component – are dependent on eye movements in a visual search paradigm and to what extent eye movements modulate ERPs. Practical implications of this study concern the application of a Brain Computer Interface device called P300-Speller for Amyotrophic Lateral Sclerosis (ALS) patients in their late stage of this neurodegenerative disease. In this stage, patients have lost control of all voluntary muscle movements except for reduced eye movements. The P300-Speller can help them to communicate with their environment only by their brain activity. The concentration on randomly flashing target letters in a letter matrix, produces an ERP component named P300, which is related to attention processes [1].

This study provides basic information of whether a flashing target letter, only recognized in the peripheral vision without fixating the letter itself elicits a P300. It is well known that people are able to shift attention between visual stimuli without shifting gaze (i. e. covert attention). An early ERP study, however, showed that visual evoked potentials were larger for stimuli at the attended location [2]. Additionally, a recent study [3] can confirm these results: for steady-state visual evoked potentials (SSVEP) subjects produced a much stronger response to stimuli they could shift their gaze to than to overlapping stimuli. Kaper et al. [4] assume that not only cognitive processes play a role for eliciting a P300 component in the P300-Speller but also sensory information from different highlightings of focused and unfocused symbols are likely to result in different stimulations in the visual cortex.

The P300 component is the third positive deflection in voltage at a latency roughly between 350 and 500 ms after stimulus-onset. In general, a distinction can be made between a novelty

P300 (P3a) and a target P300 (P3b, or "classical" P300). The focus of this study is on the P3b – henceforth called P300: With a maximum peak at the centroparietal site the P300 amplitude is smaller for difficult tasks where low stimulus discriminability is given. Under condition of attention a P300 is elicited after randomly presented rare target stimuli which appear less frequently than the non-target stimuli. This scheme is called oddball-paradigm [5]. As studies showed, a larger P300 amplitude is seen in target trials than in non-target trials [6, 7]. The oddball-paradigm is used with the P300-Speller.

Visual search is the act of searching for a target among non-targets on a screen. In general, one distinguishes between a parallel pop-out search and a serial search [8]. The parallel search is an easy task where the target is detected in a short time independent of the set size in contrast to the serial search. Although there are no differences in reaction times, Luck and Hillyard [6] showed in their EEG-studies on visual search that the set size had an effect on the P300 amplitude in both search tasks. The P300 amplitude was larger for small set sizes in parallel search and for larger set sizes in serial search.

The main research question of this study is focused on the P300 component characteristics between the conditions "fixation" and "free search". Results of EEG-studies with a visual search paradigm derive all from a fixation condition due to the artefacts that eye movements cause in the EEG. It is the goal of this study to see how the P300 component varies between a free search vs. a fixation condition and, further, if there are differences depending on set size and search task.

# 2 Methods

## 2.1 Subjects

Twenty volunteers (2 male) took part in this study. They were between 20 and 34 years old ($M = 25.15$, SD = 3.95), right-handed and had normal or corrected-to-normal vision. Fifteen of them were undergraduate students of Psychology at Graz University. To eliminate those subjects with colour deficiency, participants completed the Tests for Colour Blindness by Ishihara (1962) beforehand. Three subjects had to be excluded due to technical problems.

## 2.2 Stimuli

Similar to the P300-Speller [1] a $6 \times 6$ letter matrix filled with white capital and lower case letters of the Latin alphabet from A to Z was used. There were two types of targets: Green or red letters used in the parallel search and the capital letters 'E' or 'B' used in the serial search. Non-targets were randomly picked white letters on a black background. Eight, sixteen or thirty-six letters were placed in every matrix; the targets had a fixed position in the matrix although not in the near vicinity of the fixation cross, whereas the non-targets were randomly put in. On positive trials ($p = 0.33$) one of the letters described above was the target and the others were distractors; on the negative trials ($p = 0.66$) all letters were distractors.

The matrices had a resolution of $960 \times 720$ pixels and were positioned in the centre of the screen which had a resolution of $1280 \times 1024$ pixels. The distance between subject and screen was 60 cm and the letters were located within an imaginary matrix 10.2° wide and 9.7° high. An example of one matrix can be seen in Figure 1.

## 2.3 Procedure

The serial and parallel search tasks were run in separate blocks of trials, each consisting of 144 matrices presented in random order. All in all 8 blocks were performed, 4 blocks of each condition (fixation vs. free search) which were divided into 2 blocks for each search task (parallel vs. serial). Half of the subjects started with 4 blocks of free search, the other half with the fixation condition. Within the condition, the search task blocks were randomized.

Subjects were instructed to respond to each matrix by pressing two different buttons indicating either a non-target or a target trial. Furthermore the participants were instructed separately for the free search and the fixation condition: They should focus their gaze on the fixation cross in the middle of the screen in the fixation condition whereas in the free search they had no limitation.

### 2.4 Data acquisition and analysis

34 Ag/AgCl electrodes were mounted in an elastic cap according to the international 10-20 system. For ocular artefact correction the vertical and horizontal EOG was recorded. The electrodes were referenced to the left mastoid. All channels were band-pass filtered between 0.5 and 70 Hz, and digitized at a sampling rate of 500 Hz.

Off-line preprocessing was performed with the Brain Vision Analyzer (version 1.02.0002) using an automatic artefact detection system after the ocular correction; bad intervals were rejected. Epochs from 100 ms prestimulus to 600 ms poststimulus were used for analyses separately for all conditions. Peak detection for a positive deflection between 300 and 500 ms was carried out through all target segments for all subjects. These peak values were taken for the statistical analyses of differences in the P300 amplitude.

All electrophysiological measures were analysed with repeated measures analyses of variance (ANOVAs). For the initial data analyses the P300 component was analysed with three factors: SEARCH TASK (parallel vs. serial), CONDITION (fixation vs. free search) and SET SIZE (8, 16, 36 letters).

The participant's eye gaze was recorded with the Tobii 1750 eye tracker to provide information about whether subjects actually fixated the fixation cross during the fixation condition. The percentage of fixations landing on or next to the fixation cross for the two conditions "fixation" vs. "free search" was analysed with paired sample $t$-test.

## 3 Results

### 3.1 Eye gaze data

Significantly higher numbers of fixations were found on or next to the fixation cross in the fixation condition than in the free search ($t(16) = 13.62$, $p < 0.001$). The percentage of eye fixations for each subject including mean value and standard deviation over all subjects is shown in Table 1. Furthermore an example of a target trial is given in Figure 1 where one can see the difference in the fixation pattern.

| Subject | Fixation | Free Search | Subject | Fixation | Free Search |
|---|---|---|---|---|---|
| B01 | 42.2 | 12.9 | B11 | 64.0 | 30.9 |
| B02 | 38.8 | 22.5 | B12 | 60.2 | 27.3 |
| B03 | 27.6 | 11.1 | B16 | 70.3 | 20.7 |
| B04 | 44.2 | 4.1 | B17 | 55.5 | 20.3 |
| B05 | 58.6 | 12.8 | B18 | 60.2 | 23.5 |
| B06 | 47.7 | 21.0 | B19 | 61.8 | 9.6 |
| B07 | 78.2 | 33.7 | B20 | 59.8 | 20.3 |
| B08 | 64.5 | 19.8 | | | |
| B09 | 60.8 | 26.8 | MEAN | 56.04 | 20.2 |
| B10 | 44.5 | 18.8 | SD | 12.61 | 7.83 |

Table 1: Percentage of fixations for each subject on or next to the fixation cross for the free search and the fixation condition.

Figure 1: Examples of one target trial with eye fixations indicated by white rings for the free search (left) and the fixation condition (right).

## 3.2 EEG data

Statistical analyses of the P300 peak amplitude for both conditions, separately for the search tasks, showed a highly significant main effect CONDITION ($F(1, 16) = 16.02$, $p = 0.001$) with a larger P300 amplitude in the free search ($M = 11.81\,\mu\text{V}$, SD = 3.37) than in the fixation condition ($M = 9.36\,\mu\text{V}$, SD = 3.28). The parallel search ($M = 15.61\,\mu\text{V}$, SD = 4.62) elicited a larger P300 than the serial search ($M = 5.59\,\mu\text{V}$, SD = 3.06) as revealed by a significant main effect SEARCH TASK ($F(1, 16) = 184.83$, $p < 0.001$). No significant main effect or interaction involving SET SIZE was obtained ($p > 0.6$). Stimulus-locked ERP averages for the fixation condition and free search are shown in Figure 2.

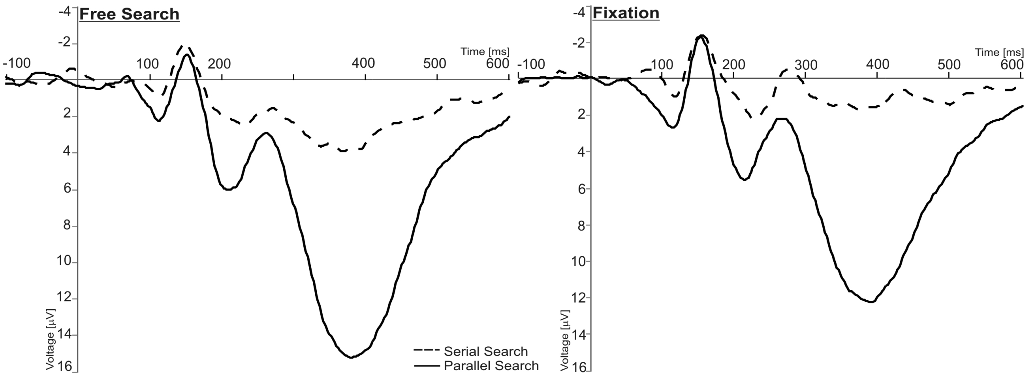


Figure 2: Grand-average ERP amplitudes at electrode site Pz for the parallel (complete line) and serial search task (dashed line) in the free search (left) and the fixation condition (right).

Separate statistical analyses were performed only for the fixation condition. The main effect SEARCH TASK ($F(1, 16) = 126.79$, $p < 0.001$) revealed a larger P300 amplitude for the parallel search ($M = 14.09\,\mu\text{V}$, SD = 4.63) than for the serial search ($M = 4.63\,\mu\text{V}$, SD = 3.26) as seen for both conditions combined. A significant SET SIZE×SEARCH TASK ($F(2, 32) = 3.77$, $p < 0.05$) interaction was observed displaying a larger P300 amplitude for 16 letter matrices ($M = 15.11\,\mu\text{V}$, SD = 4.92) than for 36 letter matrices ($M = 13.22\,\mu\text{V}$, SD = 4.86) in parallel search. The average ERP waveforms are displayed in Figure 3. Additionally, no significant main effect of interactions involving the P300 latency were found (p>0.9).

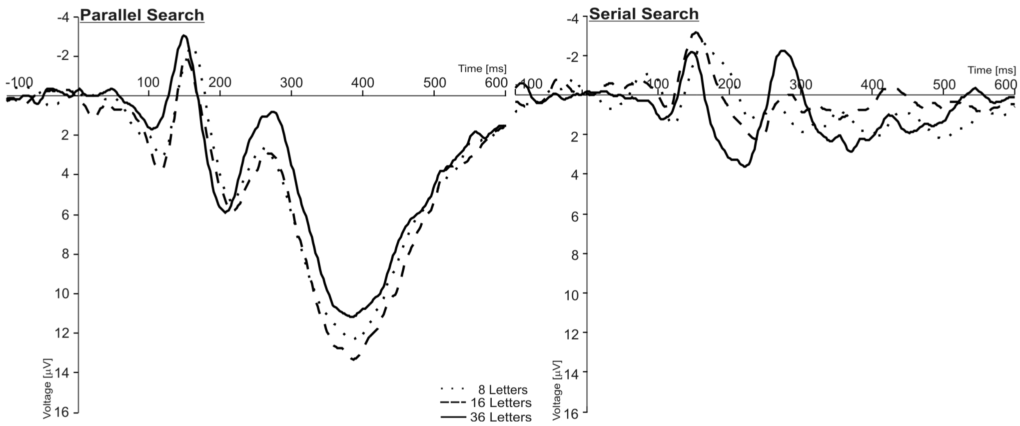


Figure 3: Grand-average ERP amplitudes for the fixation condition elicited by parallel search tasks (left) and serial search tasks (right) at set sizes of 8 (dotted line), 16 (dashed line) and 36 letters (complete line).

# 4 Discussion

The P300 component varies within both the search task and the condition. The free search condition with no limitations in eye movements elicited a larger P300 amplitude than the fixation condition. It can be said that the task was easier in the free search as seen in much faster reaction times. Therefore, the target could be recognized much more easily and the decision on the presence of a target was made with more confidence.

As seen in Figure 3 the P300 amplitude is much larger in the parallel search than in the serial search. This could result from a difference in complexity of the two tasks. Figure 3 displays differences of the P300 amplitude concerning the set size as according to the significant set size×search task interaction: A smaller set size elicited a larger P300 amplitude for parallel search trials. Additionally, the opposite can be seen, albeit not as distinct, for the serial search task. A study done by Allison and Pineda [9] confirms this result with an increase in P300 amplitude as the size of the matrix increased.

Table 1 shows that all participants focused the fixation cross in the fixation condition as instructed by the operator. It is also seen that in the free search condition where eye movements were allowed the fixation cross is often focused as well. One explanation can be that it was not necessary to shift one's gaze away from the cross to find the coloured letter especially when the subjects started with the fixation condition and were used to find letters while fixating the cross.

Concerning the latency of the P300 no significant differences were found. Although the P300 latency is thought to index classification speed, which is proportional to the time required to detect and evaluate a target stimulus [5], no correlation between the latency and reaction times could be discovered.

# 5 Conclusion

This work shows that there are differences in the P300 amplitude between fixation (i. e. detection of target letter in peripheral vision) and free search (i. e. target letter in gaze focus) though eye movements are not mandatory to elicit a P300. According to the results of this study it can be said that ALS patients with limited control of their eye movements may still be able to use the P300-Speller. However, it must be considered that there may be abnormal evoked potentials in ALS patients besides individual differences in P300 amplitude and latency [10]. Only further experiments will show whether the P300 component can be classified in single EEG trials despite limited eye movements on letter matrices.

## References


[1] E. Donchin, K. M. Spencer, and R. Wijesinghe. The mental prosthesis: Assessing the speed of a P300-based brain-computer interface. *IEEE Trans. Rehabil. Eng.*, 8:174–179, 2000.

[2] S. Van Voorhis and S. A. Hillyard. Visual evoked potentials and selective attention to points in space. *Percept. Psychophys.*, 22:54–62, 1977.

[3] B. Z. Allison, D. J. McFarland, G. Schalk, S. D. Zheng, M. M. Jackson, and J. R. Wolpaw. Towards an independent brain-computer interface using steady state visual evoked potentials. *Clin. Neurophysiol.*, 119:399–408, 2008.

[4] M. Kaper, P. Meinicke, U. Grossekathoefer, T. Lingner, and H. Ritter. BCI competition 2003 – data set IIb: Support vector machines for the P300 speller paradigm. *IEEE Trans. Biomed. Eng.*, 51:1073–1076, 2004.

[5] J. Polich. Updating P300: An integrative theory of P3a and P3b. *Clin. Neurophysiol.*, 118:2128–2148, 2007.

[6] S. J. Luck and S. A. Hillyard. Electrophysiological evidence for parallel and serial processing during visual search. *Percept. Psychophys.*, 48:603–617, 1990.

[7] S. J. Luck and S. A. Hillyard. Electrophysiological correlates of feature analysis during visual search. *Psychophysiol.*, 31:291–308, 1994.

[8] A. M. Treisman and G. Gelade. A feature-integration theory of attention. *Cogn. Psych.*, 12:97–136, 1980.

[9] B. Z. Allison and J. A. Pineda. ERPs evoked by different matrix sizes: Implications for a brain computer interface (BCI) system. *IEEE Trans. Neural Syst. Rehabil. Eng.*, 11:110–113, 2003.

[10] H. A. Hanagasi, I. H. Gurvit, N. Ermutlu, G. Kaptanoglu, S. Karamurseld, H. A. Idrisoglua, M. Emrea, and T. Demiralp. Cognitive impairment in amyotrophic lateral sclerosis: evidence from neuropsychological investigation and event-related potentials. *Cogn. Brain Res.*, 14:234–244, 2002.

# Size enhancement coupled with intensification of symbols improves P300 speller accuracy

G. Gibert[1,2,3], V. Attina[1,2,3], J. Mattout[1,2,3], E. Maby[1,2,3], O. Bertrand[1,2,3]

[1]INSERM, U821, Lyon, F-69500, France
[2]Institut Fédératif des Neurosciences, Lyon, F-69000, France
[3]Université Lyon 1, Lyon, F-69000, France

guillaume.gibert@inserm.fr

**Abstract**

The P300 Speller was proposed in 1988 by Farwell and Donchin [1]. In this Brain Computer Interface (BCI), a matrix of symbols is presented whose rows and columns are sequentially intensified. In this study, we investigated the influence of three stimulation parameters: the enhancement of the symbols while intensified, the inter-stimulus interval (ISI) and the reduction of flash duration. Results indicate that symbol enhancement increase P300 amplitude and the ensuing classification accuracy by a Fisher LDA. P300 amplitude and classification accuracy decrease with faster ISI. Finally, reduction of flash duration do not increase the P300 amplitude but yielded a better classification accuracy.

## 1 Introduction

Farwell and Donchin presented in 1988 [1] a BCI based on the P300 EEG evoked response. This BCI is used for communication by spelling words. The subject looks at a $6 \times 6$ matrix of grey symbols (letters, numbers, ...) on a black background. The subject's task is to focus attention to one of the symbols in the matrix (the target). Each row and column is flashed sequentially in a random manner and the subject has to count the number of intensifications of the same target. Each flash of the row or the column containing the target symbol produces a P300 response while non-target flashes do not. Averaging over responses to each row and each column and feeding a classifier with these average responses enables to detect the target symbol.

A large amount of work has been devoted to feature extraction [2] and classification [3] but only few studies have provided insights on the influence of stimulation parameters. Allison and Pineda [4] studied the effect of matrix size on the amplitude of the P300 response. Larger matrices evoked larger P300 amplitude but did not improve classification accuracy [5]. It was also shown that the P300 amplitude increases with slower ISI [6]. But again, it didn't improve the classification accuracy [5]. Finally, the symbol size was manipulated with no effect on classification accuracy [7].

The purpose of this study is to examine the impact of two new stimulus properties: the enhancement of the symbols coupled with intensification and the flash duration. We also manipulated the ISI. In this paper, we focus on the quantitative evaluation of experimental parameters on the ensuing features to detect the P300 response in single trial responses. Features are first compared on average. Then, an online analysis is mimicked and a linear classifier is applied to estimate the relative performance of the experimental manipulations as a function of the number of accounted observations.

## 2 Methods

### 2.1 Subjects

Four healthy volunteers (four women 21, 22, 20 and 22 years old) were paid to participate. All subjects reported normal vision. They had no previous experience with the P300 speller paradigm, nor with any other BCI paradigm. The protocol of this experiment was approved by the regional Ethical Committee and each subject signed an informed consent, prior to the experiment.

## 2.2 Stimulation device

Stimulation was handled by a C++/SDL software on a dedicated computer. While visual stimulation was sent to a CRT screen (vertical screen refresh equal to 60 Hz, resolution $1024 \times 768$), a trigger (for the flashed row or column, from 1 to 12) was sent to the EEG amplifier via parallel port. Since the trigger clock was based on the refresh screen VGA signal, the jitter between visual stimulations and triggers was less than 0.1 ms (as measured by an optoelectronic sensor).

## 2.3 Data acquisition and preprocessing

EEG activity was recorded continuously from 32 active electrodes (actiCap, Brain Products GmbH, Munich) at standard locations following the extended 10/10 international system, referenced to the nose and grounded to the forehead. Horizontal and vertical electro-oculograms (EOG) were recorded from the right eye. All impedances were kept below 10 kΩ throughout the experiments. EEG signals were bandpass filtered between 0.1–150 Hz (EOG signals were bandpass filtered between 0.01–150 Hz), amplified and digitized at a rate of 1 kHz using a BrainAmp amplifier (Brain Products GmbH, Munich). The EEG was collected and stored using BrainVision Recorder software from Brain Products.

## 2.4 Experimental setup and design

The subjects were seated in a comfortable chair at 1.2 m from the CRT screen. They were watching a $6 \times 6$ matrix of letters (a–z), numbers (1–9) and symbol (_) (see Figure 1 (a)). The experiment was divided into runs. Each run corresponded to one word (or non-word). Before each run, the entire word to be spelt was displayed at the top of the screen. The subject was instructed to focus his attention on the current target symbol (which was displayed in between brackets next to the target word) and to count the number of times this symbol was intensified. After each symbol, there was a 3 s delay. During this period, the subject indicated the outcome of his counting and then focused his attention on the next symbol. The subject could make a short break after each run. Before and after the experiment, a resting period of 3 minutes was recorded, during which the subject was instructed to remain still and to watch a black screen.


(a) Stimulation matrix. (b) Enhancement of a row while intensified.

Figure 1: On the left, stimulation matrix for the word SIX with current target S. On the right, an example of the *enhanced* condition, symbols on the second row are larger while intensified.

Five conditions were tested in blocks, randomly presented across subjects. Conditions are detailled in Table 1. In each condition, the user had to spell 5 words (or non-words) made of 2 to 4 letters (or numbers) such that each condition involved the same following 15 symbols [A E I L M O P R S T U V X 9 5] to be spelt in. These 15 selected symbols were evenly distributed all over the screen matrix. There was at least 3 symbols in each quarter of the screen. For each symbol, each row and each column was flashed 15 times in a random sequence. The angular

| Condition | Flash duration | ISI | Font size | Accuracy (%) | Bitrate (bits/min) |
|---|---|---|---|---|---|
| enhanced slow | 100 ms | 500 ms | +5 | 91.25 | 2.86 |
| enhanced medium | 100 ms | 350 ms | +5 | 91.11 | 4.08 |
| enhanced fast | 100 ms | 200 ms | +5 | 85.83 | 6.42 |
| classic | 100 ms | 200 ms | +0 | 81.66 | 5.90 |
| short flash | 50 ms | 200 ms | +0 | 85.13 | 6.34 |

Table 1: Description and mean results (accuracy and bitrate for 15 repetitions using a LDA classifier and the entire ERP from 0 to 500 ms) of the different conditions of stimulation.

dimension of the matrix was 8.67°H × 11.33°W. Each symbol subtended 0.48°H × 0.48°W of visual angle and the distance between each character was 1.24°H × 1.62°W. In the enhanced conditions, symbols were larger (font size +5) while intensified (see Figure 1 (b)). In that case, they subtended 0.62°H × 0.62°W of visual angle. Three inter-stimulus intervals (ISI) and 2 flash durations were tested in different blocks (see Table 1).

### 2.5 Evoked potential analysis

Averaging was done separately for each of the 12 rows and columns in a time window ranging from 300 ms before to 1000 ms after stimulus onset. A baseline correction was applied to each event-related potential (ERP) using random epochs of 300 ms from the resting period recorded at the beginning of the experiment. Then, another average was performed across the 15 symbols in each condition, leading to one ERP by condition and subject computed over 15symbols × 15flashs × 2 (1 target row + 1 target column), i. e., 450 trials. Finally, these evoked potentials were digitally filtered with a band-pass filter (butterworth filter, 0.2–30 Hz, slope 24 dB/octave).

### 2.6 Fisher linear discriminant analysis

Single trials were epoched between 0 and 500 ms after stimulus onset. For each condition, averaging within symbol and row/column was performed using 1 up to all 15 trials When averaging less than all 15 trials, the trials were randomly selected. Evoked potentials were digitally band-pass filtered (butterworth filter, 0.2–30 Hz, slope 24 dB/octave) and downsampled at 120 Hz. Two kinds of features were used: the vector of 60 samples (corresponding to the whole ERP) and the maximum amplitude of the ERP between 300 ms and 500 ms. This yielded 15 symbols ×2 (1 target row and 1 target column) = 30 target samples and 15 × 10 = 150 non-target samples for each subject and condition. A leave-one-out strategy for cross-validation was adopted. This means that the data were split into a training set of size $N - 1$ (where $N$ is the total number of samples) and a test set of size 1. Then the average of the squared error on the left-out pattern over the $N$ possible ways of obtaining such a partition was used as test and the rest as training of a Fisher LDA classifier.

## 3 Results

### 3.1 Behavioral measure

The subjects were asked to report the number of flashes they counted for each target. Of course, no information about the actual number of flashes per symbol was delivered to the subject prior the experiment. Even though there were always 30 flashes per target, subjects made errors. The accuracy of this counting was used as a behavioral measure of task difficulty as well as a measure of attention. The performance rate were: enhanced slow (98.2 %±0.7) > enhanced medium (98.1 %± 1.0) > enhanced fast (97.8 % ± 1.2) > classic (96.9 % ± 1.7) > short flash (96.3 % ± 1.9). Note that, as expected, the worst result was obtained in the most difficult task: short flash (short ISI and short flash duration) whereas the best result was obtained in the easiest condition: enhanced slow (longer ISI).

### 3.2 Evoked potential comparison

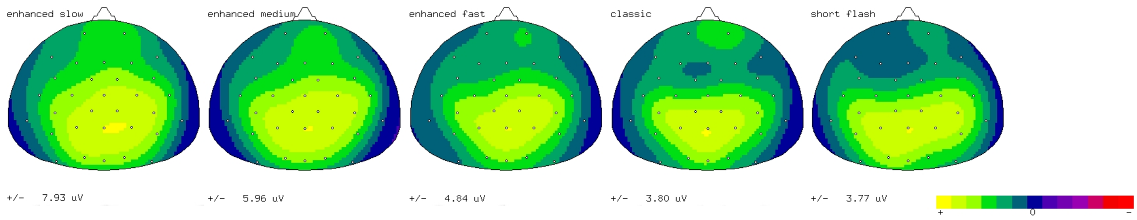


(a) P300 topographies for all conditions.

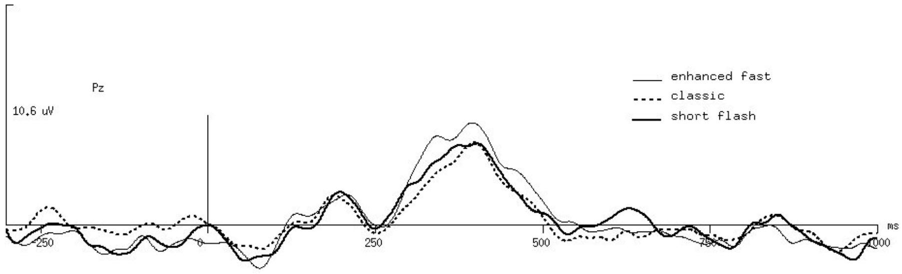


(b) ERPs for enhanced fast, classic and short flash conditions.

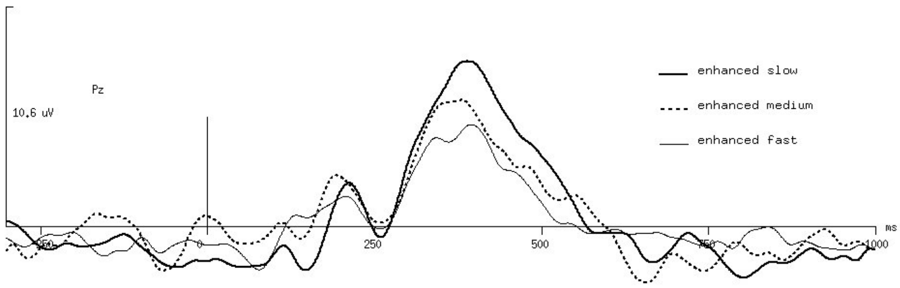


(c) ERP for each enhanced conditions.

Figure 2: Grand-average ERP (over subjects) for target stimulus recorded at Pz electrode and global topographies in the different conditions.

ERP scalp topographies at the maximum of the P300 (389 ms) were computed using spherical spline interpolation [8] for each condition (see Figure 2 (a)). The maximum of the P300 response is located on the Pz electrode for all the conditions. Therefore, the study focuses on this particular electrode.

The averaged waveforms over subjects for the classic, the enhanced fast and the short flash conditions are shown in Figure 2 (b). We observe that the enhanced fast condition elicits larger positivity than the classic condition. Across the 4 subjects, the mean rank of condition enhanced fast and classic are significantly different for the maximum amplitude (Kruskall-Wallis test, $p = 0.0264$) and the mean amplitude (Kruskall-Wallis test, $p = 0.0264$) between 300 ms and 500 ms.

The averaged waveforms over subjects are shown in Figure 2 (c) for the three enhanced conditions. We observe that the longer the ISI, the larger the positivity between 300 and 500 ms. The maximum amplitude of the P300 response is also a function of the ISI. However, across the 4 subjects, the difference between the three enhanced conditions appeared not to be significant, neither in terms of maximum amplitude (Kruskall-Wallis test, $p = 0.1462$), nor in terms of mean amplitude between 300 and 500 ms (Kruskall-Wallis test, $p = 0.2106$).

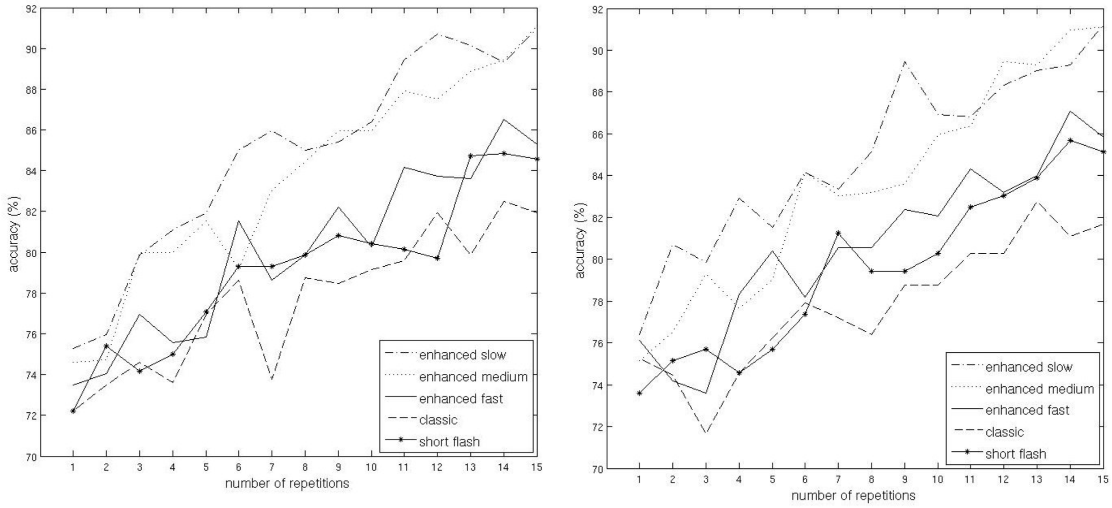


(a) Maximum of Amplitude. (b) Window 0–500 ms.

Figure 3: Mean accuracy over the four subjects of the Fisher LDA classifier for each condition and for two kinds of feature (on the left, the maximum of amplitude between 300 and 500 ms and on the right, the entire ERP from 0 to 500 ms).

### 3.3 Classification performance

The averaged accuracy over subjects of the Fisher LDA output is represented in Figure 3 for both the maximum amplitude and the entire ERP features. Consistent with [9], the accuracy grows with the number of flashing repetitions (i. e. with the quantity of information) used for averaging whatever the condition or feature type. Furthermore, whatever the type of feature and the number of accounted repetitions, the best results were obtained with the enhanced slow condition closely followed by the enhanced medium condition. Finally, the enhanced fast condition elicited better accuracies than the classic and the short flash conditions for most of the number of accounted repetitions. These results are consistent with our observations derived from the averaged waveforms, either based on amplitudes or areas under the curves.

## 4 Discussion

This study demonstrates several points. First, the size enhancement of the symbol during intensification both affects the amplitude of the P300 response and increases the accuracy of a LDA classifier. As the symbols increase in size when intensified, the stimulus intensity is higher. One possible explanation would be that the amplitude of the P300 response increases with stimulus intensity [10]. A way to confirm this hypothesis would be to vary the intensity difference between target and non target symbols by manipulating the color or the contrast. Second, short flash stimulation (50 ms) renders task more difficult than the classical paradigm. Incorrect number of counts is higher than for the classical paradigm but there is no statistical difference in terms of P300 amplitude. LDA accuracy is higher maybe because this stimulation yields shorter peak latency. To confirm this hypothesis, different time windows of analysis should be compared. Third, increasing ISI leads to increased amplitude of the P300 response as well as increased accuracy. However, increasing the ISI yields a slower BCI. The optimal compromise in terms of bitrate [11] is the enhanced fast condition (see Table 1). We are currently acquiring more subjects in order to confirm and generalize these findings. Finally, applying other classifiers should enable us to assess which are the most relevant parameters and to ensure that the results do not depend on the type of classifier.

## 5 Conclusion

This study has proposed three modifications of the classical P300 paradigm: the size enhancement of the symbols during intensification, the use of longer ISI and the reduction of the flash duration. Results have shown that variations of the flash duration has no effect on the amplitude of P300 response but that the accuracy of a Fisher LDA is higher than in the classical condition. Moreover, the symbol size enhancement during intensification yields bigger amplitude of the P300 and very high classification rates.

**Acknowledgments:** We would like to thank Gaëlle Charles for her help during the experiments. This work was supported by grant ANR05RNTL01601 of the French National Research Agency and the National Network for Software Technologies within the Open-ViBE project.

## References

[1] L. A. Farwell and E. Donchin. Talking off the top of your head: toward a mental prosthesis utilizing event-related brain potentials. *Electroencephalogr. Clin. Neurophysiol.*, 70(6):510–523, Dec 1988.

[2] B. Rivet and A. Souloumiac. Subspace estimation approach to P300 detection and application to brain-computer interface. *Conf. Proc. IEEE Eng. Med. Biol. Soc.*, 2007:5071–5074, 2007.

[3] D. J. Krusienski, E. W. Sellers, F. Cabestaing, S. Bayoudh, D. J. McFarland, T. M. Vaughan, and J. R. Wolpaw. A comparison of classification techniques for the P300 speller. *J. Neural. Eng.*, 3(4):299–305, Dec 2006.

[4] B. Z. Allison and J. A. Pineda. ERPs evoked by different matrix sizes: implications for a brain computer interface (BCI) system. *IEEE Trans. Neural Syst. Rehabil. Eng.*, 11(2):110–113, Jun 2003.

[5] E. W. Sellers, D. J. Krusienski, D. J. McFarland, T. M. Vaughan, and J. R. Wolpaw. A P300 event-related potential brain-computer interface (BCI): the effects of matrix size and inter stimulus interval on performance. *Biol. Psychol.*, 73(3):242–252, Oct 2006.

[6] B. Z. Allison and J. A.Pineda. Effects of SOA and flash pattern manipulations on ERPs, performance, and preference: implications for a BCI system. *Int. J. Psychophysiol.*, 59(2):127–140, Feb 2006.

[7] M. S. Salvaris and F. Sepulveda. Robustness of the Farwell & Donchin bci protocol to visual stimulus parameter changes. *Conf. Proc. IEEE Eng. Med. Biol. Soc.*, 2007:2528–2531, 2007.

[8] F. Perrin, J. Pernier, O. Bertrand, M.-H. Giard, and J.-F. Echallier. Mapping of scalp potentials by surface spline interpolation. *Electroencephalogr. Clin. Neurophysiol.*, 66(1):75–81, Jan 1987.

[9] J. Cohen and J. Polich. On the number of trials needed for P300. *Int. J. Psychophysiol.*, 25(3):249–255, Apr 1997.

[10] J. W. Covington and J. Polich. P300, stimulus intensity, and modality. *Electroencephalogr. Clin. Neurophysiol.*, 100(6):579–584, Nov 1996.

[11] J. R. Wolpaw, N. Birbaumer, D. J. McFarland, G. Pfurtscheller, and T. M. Vaughan. Brain-computer interfaces for communication and control. *Clin. Neurophysiol.*, 113(6):767–791, Jun 2002.

# Single-trial movement-related cortical potentials are modulated by rate of torque development in lower extremity amputees

O. F. do Nascimento[1], C. R. Andersen[2], D. Farina[1]

[1]Center for Sensory-Motor Interaction, Department of Health Science and Technology, Aalborg University, Aalborg, Denmark
[2]Department of Occupational Therapy and Physiotherapy, Aalborg Hospital, Aalborg, Denmark

omar@hst.aau.dk

**Abstract**

This article describes the first step in the development of a brain-computer interface that discriminates variations of speed for movements of phantom limbs in amputees. This approach is intended for controlling prosthesis and/or for treating phantom limb pain by preventing the cortical reorganization that follows amputation. EEG activity was recorded from six patients with unilateral lower limb amputation, while they plantar-flexed their ankle (of the phantom limb) at two rates of torque development. Movement-related cortical potentials (MRCPs) were classified using a novel pattern recognition approach that uses adaptive wavelet decomposition for feature extraction and support vector machine (SVM) for classification. Misclassification rates of less than 5 % could be obtained from single channels overlying sensorimotor cortical regions in the two subjects with most recent amputations whereas the misclassification rate was substantially higher for the other subjects. The results suggest that cortical reorganization occurring after the amputation prevents the ability of cortically expressing movements of phantom limbs.

## 1 Introduction

Amputated patients could benefit from the use of Brain-Computer Interfaces (BCI) either for controlling prosthetic devices or for therapeutic purposes. For example, the use of a BCI may prevent or reduce cortical reorganization following the amputation, which has been shown to be associated to phantom limb pain [1, 2, 3]. Cortical reorganization could be attenuated by training with a BCI system that uses cortical potentials related to movement of the phantom limb. For this purpose, the steady-state movement-related cortical potentials (MRCPs) seem to be a reasonable type of cortical expression. These cortical potentials reflect preparation, execution and control of performance of a movement and are modulated by movement variables, such as perceived effort, movement speed and intensity [4, 5].

This article presents the preliminary attempts for developing a BCI system dedicated to the rehabilitation of lower extremity amputees. The MRCPs associated to the performance of movements with the amputated limb at different speeds are investigated and classified on a single-trial basis with a recently proposed pattern recognition approach [6].

## 2 Methods

### 2.1 Experimental procedure

Electroencephalographic (EEG) recordings were performed in six patients on discharge from treatment after amputation of one of their lower limbs (details in Table 1). All experimental procedures

| Subject # | Age (years) | Amputation | Time after amputation | Phantom sensation | Phantom limb pain | Cause of amputation |
|---|---|---|---|---|---|---|
| 1 | 21 | left transtibial | 1.5 years | intense | mild | Infection |
| 2 | 56 | left transfemoral | 8 years | weak* | absent | Infection |
| 3 | 58 | left transtibial | 3 years | n/a | n/a | Diabetes |
| 4 | 59 | right transfemoral | 9 months | intense | intense | Infection |
| 5 | 26 | left transtibial | 3 years | n/a | absent** | Accident |
| 6 | 66 | left transtibial | 5 months | n/a | n/a | Diabetes |

Table 1: Clinical patient data. Phantom limb sensation and pain scores have been subjectively reported by the patients; *This patient describes the phantom limb permanently locked at a certain position; **Chronic pain patient because of a spinal injury from the accident; n/a = not available.

were approved by the local ethical committee and all patients gave their written informed consent before participation.

Subjects were initially asked to execute isometric plantar-flexions with their able leg on a pedal instrumented with strain gauges for torque measurement. These trials comprised two rates of torque development (RTD) at a constant target torque (TT). Submaximal torques were defined as percentages of the average torque expressed in 5 maximum voluntary contractions (MVC), performed with 3-min rest intervals. The two RTDs were defined as ballistic (as fast as possible) and moderate (15 % MVC / s) with TT equal to 60 % MVC. These contractions – 25 for each RTD, performed in random order – were used for priming the subjects on the tasks to perform with their phantom limb.

Subjects were then released from the pedal and asked to perform the same tasks using their phantom limb. They performed 75 randomized trials of the "kinesthetic imagery" for each of the two RTDs (ballistic and moderate), with short resting intervals every 25 trials. Feedback on torque (for the real tasks), instruction on which task to perform at each trial, randomization of trials and timing guidance were controlled by a custom-made software developed in Labview (National Instruments). In this application, a text instruction indicated to the subject which task should be performed at the coming trial. Then, following a random period from 1 to 5 s, a progression bar crossing fixed markers indicated when the subjects should initiate and terminate the task. After every run of the progression bar, subjects should confirm if the current trial was valid, by pressing a button. When trials were not valid (by no button press or time out), they were re-included in the randomization procedure, so that they were accomplished at a later stage. The experimental session ended when all trials were executed and reported by the patient as valid.

The EEG activity was recorded using a 40-channel digital amplifier (Nuamps, Neuro Scan Labs) and a 32-channel tin electrode cap (Electro-Cap International), with electrodes arranged according to the international 10–20 system [7]. Vertical and horizontal electrooculographic (EOG) activity was also recorded. All electrodes were referenced to linked tin electrodes at the earlobes and grounded at AFz. Signals were digitized at 500 Hz, notch filtered at 50 Hz, and band-pass filtered between 0.01 and 30 Hz. The recordings were segmented in epochs from 1 s before to 3 s after the task onset. Epochs with EOG activity exceeding 125 µV were discarded. Only trials related to the imagined movement of the phantom limb were further analyzed.

## 2.2 Signal processing

The pattern recognition method was based on wavelet transformation (feature extraction) and support vector machine (SVM) (classification) and is described in detail elsewhere [6, 8]. Briefly, a discrete wavelet transform (DWT) over 9 scales (512 signal samples) was applied to the EEG signals. The mother wavelet was parameterized from the scaling filter [8] and optimized in order to minimize the estimated (from the training set) probability of error. The features were the marginal distribution over time of the DWT. Supervised classification was performed using SVM with Gaussian kernel, optimized on the basis of the probability of error estimated on the training

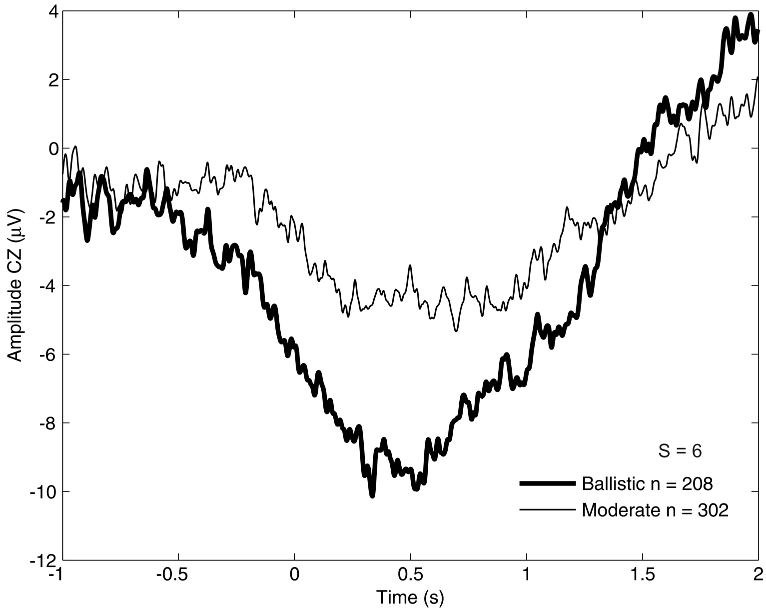


Figure 1: Grand average of MRCPs at location Cz.

set [6, 9]. Thus, the pattern recognition system was based on two optimization processes performed on the training set of signals: for each selection of the mother wavelet the parameters of the classifier were optimized (internal optimization) and the optimal mother wavelet was chosen as that leading to minimum estimated probability of error (external optimization).

Performance was evaluated with cross-validation by dividing the entire set of available signals in three subsets, two used for training and one for testing. The sets were permuted and the average error rate from the 3 test set classifications was used as a measure of performance.

# 3 Results

The grand average of MRCPs at location Cz over all subjects is presented in Figure 1. The average potentials show a clear difference between MRCPs generate under the two different RTDs.

The topographical distributions of misclassification rates are presented in Figure 2, where arrow markers indicate focal regions corresponding to the lowest misclassification rates. The lowest error rates were obtained in subjects 4 and 6 and corresponded to 3.3 % (at P4) and 0 % (at CPP2, between CP2 and P2), respectively. The location CPP2 presented also the lowest averaged misclassification rate (25.6 %±13.3) over all subjects, followed by the location P4 (28.6 %±14.9).

The lowest misclassification rates were obtained from subjects who were recently amputated (subjects 4 and 6, see Table 1). Figure 3 presents the misclassification rates at locations CPP2 and P4 as a function of time after the amputation.

# 4 Discussion

This article shows the preliminary results of a comprehensive study for recording and classifying MRCPs associated to movement of phantom limbs in lower extremity amputees, which is a preceding step for the development of a BCI system for therapeutic and functional purposes.

The MRCPs associated to movement of phantom limbs are very similar (in shape and amplitude, Figure 1) to those associated to imaginary and real movements of intact limbs in able-bodied subjects [5, 10]. Our results also confirm previous functional imaging studies which found that movement of amputated and intact limbs generated similar levels of cortical activity [11, 12].

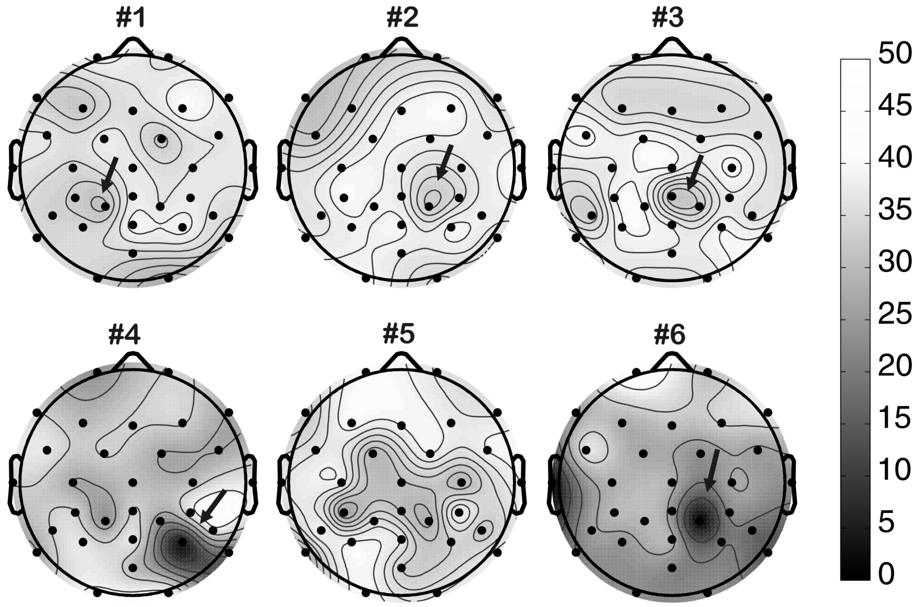


Figure 2: Topographical distributions of misclassification rates for each of the participants (#1 to #6). Grey scale expressed in percentage (%). Arrow markers indicate focal regions where the lowest misclassification rates were obtained.

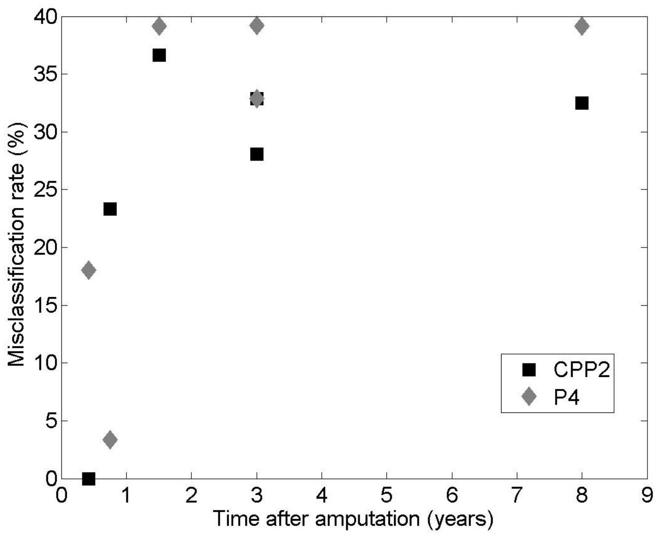


Figure 3: Misclassification rates as a function of time after amputation.

The classification approach adopted has proven to efficiently separate single-trial MRCPs related to different RTDs in all subjects (33.2 %±7; average missclassification rate over all subjects and channels), with exceptionally low misclassification rates in two of the participants (as low as 0 %). The lowest misclassification rates were predominantly localized in centro-parietal electrodes (mainly CPP and P lines) in all subjects, indicating that the discriminations are related to sensorimotor processes. Except for subject 4, all subjects had the left leg amputated, but there is not a clear trend on the hemispheric dominance of the discrimination of movements. Hemispheric dominance in these patients may be influenced by the residual limb sensation, phantom limb pain, and time after amputation. Moreover, patients may inadvertently project the actions of the phantom limb to the intact one, which might explain the topographical distributions of subjects 2, 3 and 6 in which the focal regions of low misclassification rates are at the left side (Figure 2, arrow markers), i. e. ipsilaterally to the amputated limb.

An interesting finding was that best classification performances were obtained from patients with the most recent amputations. Figure 3 shows that there may be a correlation trend between classification performance and time after amputation, which is probably related to processes of cortical reorganization that follows the amputation [1, 2].

## 5 Conclusion

A recently proposed pattern recognition method, based on adaptive wavelets, has been used to discriminate cortical activity related to variation of "speed" (RTD) in movements of phantom limbs in amputees. Excellent classification performance (error $< 5\,\%$) could be achieved in two subjects at scalp sites overlying sensorimotor brain regions. The best results, however, were obtained in recently amputated subjects, suggesting that the ability of cortically expressing movements of phantom limbs depends on the time from the amputation.

**Acknowledgments:** The Danish Research Agency (Contract 2117-05-0083) and The Obel Family Foundation supported this study.

## References

[1] D. Borsook, L. Becerra, S. Fishman, A. Edwards, C. L. Jennings, M. Stojanovic, L. Papinicolas, V. S. Ramachandran, R. G. Gonzalez, and H. Breiter. Acute plasticity in the human somatosensory cortex following amputation. *Neuroreport*, 9:1013–1017, 1998.

[2] H. Flor, C. Denke, M. Schaefer, and S. Grusser. Effect of sensory discrimination training on cortical reorganisation and phantom limb pain. *Lancet*, 257:1763–1764, 2001.

[3] R. Kurth A. Karl, W. Muhlnickel and H. Flor. Neuroelectric source imaging of steady-state movement-related cortical potentials in human upper extremity amputees with and without phantom limb pain. *Pain*, 110:90–102, 2004.

[4] S. Slobounov, M. Hallett, and K. M. Newell. Perceived effort in force production as reflected in motor-related cortical potentials. *Clin. Neurophysiol.*, 115:2391–2402, 2004.

[5] O. F. Nascimento, K. D. Nielsen, and M. Voigt. Movement-related parameters modulate cortical activity during imaginary isometric plantar-flexions. *Exp. Brain Res.*, 171:78–90, 2006.

[6] D. Farina, O. F. do Nascimento, M. F. Lucas, and C. Doncarli. Optimization of wavelets for classification of movement-related cortical potentials generated by variation of force-related parameters. *J. Neurosci. Methods*, 162:357–363, 2007.

[7] G. H. Klem, H. O. Luders, H. H. Jasper, and C. Elger. The ten-twenty electrode system of the international federation. the international federation of clinical neurophysiology. *Electroencephalogr. Clin. Neurophysiol. Suppl.*, 52:3–6, 1999.

[8] A. Maitrot, M. F. Lucas, C. Doncarli, and D. Farina. Signal-dependent wavelets for electromyogram classification. *Med. Biol. Eng. Comput.*, 43:487–492, 2005.

[9] C. Saunders, M. O. Stitson, J. Weston, L. Bottou, B. Schlkopf, and A. Smola. Support vector machine reference manual. Royal Holloway, Univ. of London, Egham, UK, Tech. Rep. CSD-TR-98-03, 1998.

[10] O. F. do Nascimento, K. D. Nielsen, and M. Voigt. Relationship between plantar-flexor torque generation and the magnitude of the movement-related potentials. *Exp. Brain Res.*, 160:154–165, 2005.

[11] L. Ersland, G. Rosen, A. Lundervold, A. I. Smievoll, T. Tillung, H. Sundberg, and K. Hugdahl. Phantom limb imaginary fingertapping causes primary motor cortex activation: an fMRI study. *Neuroreport*, 8:207–210, 1996.

[12] N. Maruno, T. Kaminaga, M. Mikami, and S. Furui. Activation of supplementary motor area during imaginary movement of phantom toes. *Neurorehabil. Neural Repair*, 14:345–349, 2000.

# Using individual auto-regression models in an SSVEP-based brain-computer interface

T. Lüth, A. Moltsaar, A. Teymourian, A. Gräser

Institute of Automation, IAT, University of Bremen, Bremen, Germany

lueth@iat.uni-bremen.de

**Abstract**

Brain-Computer interface (BCI) systems can provide an alternative communication channel for severely disabled people. Rapid recognition of user intent is important for many BCI applications, such as navigating a wheelchair, controlling a complex robotic system, online games or chatting, or military applications, and is especially important if the user must communicate during an emergency. Classification can occur more rapidly if a shorter segment of EEG data is used, but this typically impairs accuracy. Changing the model order number of an autoregression (AR) approach may make it possible to reduce segment length while maintaining good accuracy. This paper shows that the optimal model order varies across subjects. Thus, individual model orders should be developed for each user.

## 1 Introduction

Brain-Computer Interface (BCI) systems detect specific patterns in brain activity and translate them into control commands for soft- or hardware devices [1]. The principal goal of BCI research is to provide a communication system for severely disabled people. These communication systems vary from simple spelling applications to complex control of robotic systems [2], prostheses [3] or a wheelchair [4]. Yet the main problem with BCIs remains low transfer rates, which results partly from the fact that a few seconds of EEG data are typically needed to infer user intent. Reducing the amount of data needed for a BCI to attain accurate performance could reduce the latency between forming an intention and executing a command. This could increase the number of commands per minute, improve information throughput, and make BCIs more practical for applications and situations that require rapid communication from the user [5].

The brain signal is quite unstable and varies between different users and different sessions. Therefore, the BCI must be adapted to every user. These adaptations consider many variables, e. g., the proper electrode positions for acquiring EEG data, the segment length of the data to be analyzed during one signal processing step [6], the threshold for the classifier or even the classifier itself [7], the optimal SSVEP frequency, etc. Common for all these adaptations is that there is often a constant feature extraction method for the brain activity patterns, whereas the preprocessing or the classification can be individual to each subject. To quickly respond to each user's intention, all parts of the system should be as fast and reliable as possible. Therefore, the analyzed data should be as short as possible and other adaptation methods should be used.

Some BCIs use, for example, auto-regression (AR) to model the user's intention or noise during the signal processing [8, 9, 10]. The order of the AR model stays constant over all subjects and varies only between the BCIs themselves, whereas the order of the AR model is mainly chosen between 5 and 20 [9, 11, 12]. Liavas et al. mentioned also higher AR orders for modelling EEG data [13].

This paper suggests adapting the order of the auto-regressive model for noise estimation in a BCI based on steady-state visual evoked potentials (SSVEP) and validates a positive effect on the classification of the user's intention for individual AR-orders.

# 2 Methods

## 2.1 Subjects and procedure

Six healthy subjects (5 male, 1 female), between 25 and 31 years old, participated in this study. All of them took part in several earlier BCI studies and needed no vision correction.

The subject's task was to consecutively focus attention on one of 4 LEDs blinking with different frequencies. The used frequencies (13 Hz, 14 Hz, 15 Hz and 16 Hz) were chosen according to prior work [14]. The overall run lasted 55 seconds. During the first 10 seconds, the subject had to relax and not focus on any of the LEDs. After that and every 10 seconds, the subject heard a sound signal indicating to switch attention immediately to the next LED (starting from 13 Hz). After focussing on the last LED (16 Hz), another sound signal instructs the subject to relax again. The run ends 5 seconds after focussing on the last LED. After every run (2 or 3 total, depending on the user), the subject got a short break (30 s) before the next run started.

The data were recorded non invasively with an EEG-cap. The electrodes for measuring the SSVEP response were placed at sites $PO_3$, $PO_4$, $O_9$, $O_{10}$, $O_z$ and $P_z$ using the extended 10-20 system of electrode placement [15]. The reference electrode was placed at $C_z$ and the ground electrode at $AF_z$. The data acquisition was done at a sampling frequency $F_s = 512\,\text{Hz}$.

## 2.2 Signal processing

Because of environmental noise and artifacts, the frequency the subject is focussing on during an SSVEP experiment can not be clearly identified in the acquired EEG data. To magnify the SSVEP response and to decrease the noise, one possibility is to combine the electrode signals into new channel signals. For the creation of one or several channel signals, Friman et al. considered the minimum energy combination as the best [11]. Due to good results for that method verified in other applications [14], the minimum energy combination is also used in this paper.

### 2.2.1 Feature extraction

The extraction of stimuli frequencies in the recorded data is done by calculating their signal-to-noise ratios (SNR):

$$\text{SNR} = \frac{\hat{P}}{\hat{\delta}}$$

where $\hat{P}$ is the estimated total power at the SSVEP frequency, and $\hat{\delta}$ is the estimated noise power in the same frequency.

For estimating the noise power, auto-regressive AR($p$) models of order $p$ are fitted to the channel signals by solving the Yule-Walker equations using a Levinson-Durbin recursion [16]. With the resulting AR($p$) model parameters $\alpha_1, \ldots, \alpha_p$, the variance $\hat{\sigma}^2$ of the white noise driving the AR($p$) process, the number of considered samples $N_t$ and the sampling frequency $F_s$, the following equation estimates the noise power of the $k$th SSVEP harmonic of stimulus frequency $f$ in the $l$th channel signal $s_l$:

$$\hat{\delta}_{k,l} = \frac{\pi N_t}{4} \cdot \frac{\hat{\sigma}^2}{|1 + \sum_{j=1}^{p} \alpha_j \exp(-2\pi i j k f / F_s)|^2}$$

where $i$ is the complex $\sqrt{-1}$.

### 2.2.2 Classification

A threshold based linear classifier is used to classify the frequency the subject is focussing on. The SNR of a frequency has to exceed a threshold to be considered as the desired frequency. If more than one SNRs exceeds the threshold the frequency with the highest SNR is classified.

| Number of classifications | | | | | |
|---|---|---|---|---|---|
| AR order | 13 Hz | 14 Hz | 15 Hz | 16 Hz | Threshold |
| 6 | 13 | 9 | 0 | 1 | 2.06 |
| 20 | 18 | 10 | 0 | 1 | 2.24 |
| 40 | 17 | 17 | 1 | 7 | 2.51 |
| 60 | 12 | 10 | 1 | 9 | 3.12 |
| First correct classification (in seconds) | | | | | |
| AR order | 13 Hz | 14 Hz | 15 Hz | 16 Hz | Threshold |
| 6 | 11.9 | 23.8 | – | 50.2 | 2.06 |
| 20 | 11.8 | 21.4 | – | 50.2 | 2.24 |
| 40 | 12.0 | 20.7 | 30.1 | 40.7 | 2.51 |
| 60 | 11.9 | 23.9 | 30.1 | 40.7 | 3.12 |

Table 1: Results of different auto-regressive (AR) orders for noise estimation for one subject and one run. The upper part of the table shows the number of correct classifications during each period of focussing on that specific frequency. A frequency is classified if the SNR of that frequency exceeds a threshold. The threshold is the same for each frequency in each AR order calculation, and is determined as the minimal threshold (considering two decimal places) for which the accuracy reaches 100 % correct classifications. The lower part shows the timepoint of the first correct classification (according to the protocol) of each frequency in that run.

### 2.3 Offline analysis

To compare the noise estimation with different AR-orders, an offline analysis of the data was done. Every 0.1 s of the recorded data, a classification was made. The window length of the data that has to be analyzed during each feature extraction step was set to 0.5 s to guarantee fast classifications. The noise estimation was calculated using 4 different AR-orders (6, 20, 40 and 60). For every AR-order, the threshold was set to a common threshold over the 4 frequencies according to the classification output, i. e., the minimal possible threshold that guarantees only true positive classifications with the recorded data was chosen.

## 3 Results

Table 1 shows the result of the offline analysis for subject 3 and one run (run 2). The numbers of classifications for all frequencies and all 4 analyzed AR orders are given as well as the timepoint (according to the protocol) in the data, when a frequency was classified the first time. From that timepoint the time that is necessary to classify a frequency when a person starts to focussing on that frequency can be derived.

Table 2 shows the average results of all runs for each of the 6 subjects. The first classification of a frequency is the average from the values of the 4 frequencies and is therefore not given as specific timepoints as in Table 1. Table 2 also shows the classification accuracy. Though the determined threshold allows only true positive classifications, the accuracy is lowered if a specific frequency could not be classified at least once during the 10 s period the subject was supposed to focus on that frequency. 100 % accuracy means that all frequencies could be classified during each run.

## 4 Discussion

The results in Table 1 were calculated for different noise estimation AR orders for the data recorded with one subject. As it is shown, with an AR order $p = 6$ or even $p = 20$, which is the common range of AR orders for Brain-Computer Interfaces, the BCI was able to detect and classify 3 frequencies (13 Hz, 14 Hz and 16 Hz). The 15 Hz frequency was not classified at all. These quite bad results can be explained with the short time-segment (0.5 s) of data used for one classification and

| Subject 1 | | | |
|---|---|---|---|
| AR order | Classifications | Accuracy (in %) | Time (in s) |
| 6 | 45.5 | 100 | 2.64 |
| 20 | 59 | 87.5 | 2.56 |
| 40 | 62 | 100 | 2.43 |
| 60 | 50.5 | 87.5 | 1.75 |
| Subject 2 | | | |
| AR order | Classifications | Accuracy (in %) | Time (in s) |
| 6 | 10.5 | 87.5 | 2.23 |
| 20 | 5.5 | 50 | 1.23 |
| 40 | 9.5 | 87.5 | 2.18 |
| 60 | 7.5 | 87.5 | 3.16 |
| Subject 3 | | | |
| AR order | Classifications | Accuracy (in %) | Time (in s) |
| 6 | 10.7 | 75 | 3.82 |
| 20 | 19 | 75 | 2.83 |
| 40 | 23.3 | 91.7 | 1.66 |
| 60 | 20 | 75 | 1.60 |
| Subject 4 | | | |
| AR order | Classifications | Accuracy (in %) | Time (in s) |
| 6 | 111 | 100 | 0.96 |
| 20 | 139 | 100 | 0.71 |
| 40 | 106 | 100 | 1.07 |
| 60 | 103 | 100 | 0.79 |
| Subject 5 | | | |
| AR order | Classifications | Accuracy (in %) | Time (in s) |
| 6 | 10 | 66.7 | 3.03 |
| 20 | 12.3 | 91.7 | 3.88 |
| 40 | 14.3 | 91.7 | 2.63 |
| 60 | 9.67 | 83.3 | 2.89 |
| Subject 6 | | | |
| AR order | Classifications | Accuracy (in %) | Time (in s) |
| 6 | 25.3 | 83.3 | 1.93 |
| 20 | 21.3 | 83.3 | 3.31 |
| 40 | 15.3 | 75 | 2.40 |
| 60 | 12 | 66.7 | 1.76 |

Table 2: Average results of all runs for each subject. For different AR orders the average number of classifications (i. e., SNR exceeds the threshold), the accuracy of all classifications (in %) and the time (in s) for the first classification of a frequency after the subject was supposed to focus on that frequency, is given. The threshold for the classification was set to the minimal threshold (considering two decimal places) according to the request that only true positive classifications are allowed. Therefore, if all frequencies could be classified at least once during a run, the accuracy will be 100 %.

with the used threshold. These analyses only considered the minimal threshold where the accuracy reaches 100 % true positive classifications for each frequency. With a higher segment length, a lower threshold or individual thresholds for each frequency, the results should be much better. But, as mentioned before, the goal is to lower the segment length to get a faster classification when the subject starts to focus on another LED. As seen in Table 1, the classification rate increased with the order of the auto-regression model for the noise estimation. With an AR order $p = 40$ or $p = 60$, the BCI could classify all 4 frequencies in the recorded data. After the subject started to focus on the 16 Hz LED, the BCI classified that frequency 9.5 s faster, when the AR order was set to 40. The 15 Hz frequency was correctly classified after 0.1 s after the subject was supposed to focus at that frequency. This effect seems to be a limitation of the used protocol. In the present study, subjects knew which stimulus would next be designated as the target. This is realistic in some BCIs, such as if the subject is moving a cursor in one direction and intends to move it in a known direction at the next opportunity. Obviously, the subject focussed on the 15 Hz frequency earlier than instructed. But, the analyze is done on exactly the same data for all different AR orders. Therefore, if an AR order gives better results than another one, this statement is independent of the protocol.

Table 2 proves that increasing the AR order of the noise estimation does not always lead to better classification results. The average result for subject 3 is quite similar to Table 1, because that table shows the results of one run of subject 3. In Table 1 one frequency could not be detected for that subject in that run. Therefore, the average accuracy over all runs for that subject is not 100 %. Similar results to subject 3 could be obtained for subject 1, subject 2 and subject 5. For all these subjects, the noise estimation with an AR order of $p = 40$ led to the best classification results regarding accuracy and speed. Contrary to those results, the offline analysis has shown the worst results for an AR order of $p = 40$ for that subject with perfect classification (100 %) of each frequency during all runs and all different AR orders (subject 4). The BCI needed on average 1.07 s to classify a frequency after subject 4 got the task to focus on that frequency if the noise estimation uses an auto-regression order of $p = 40$. However, the time was lowered to 0.71 s if the AR order was set to $p = 20$. The results for subject 6 also prove that the AR order should not be set to a common value for all subjects, because the best accuracy and especially the best speed was obtained for an AR order of $p = 6$ for that subject. The results for accuracy and speed correlate with the overall number of true positive classifications during the 10 s period and lead therefore to the same conclusion: the order of the auto-regressive model for the noise estimation should be adjusted for each subject to increase the classification rate and speed.

# 5 Conclusion

Assume that the segment length of the analyzed data is increased due to misclassifications of the BCI. But, rapid recognition and classification of user intent is not possible anymore, when the segment length is increased, because a certain time is necessary after the user starts to produce the desired brain activity pattern to acquire enough data for the feature extraction step. For an SSVEP-based BCI that can react quickly to changes in user intent, the length of the window of the analyzed data should be as short as possible. This paper suggests a possible alternative to keep good classification results with a shorter segment length: an individual AR order of the noise estimation for each user. Some users show better results with higher AR orders and some with lower ones. Therefore, it is necessary to determine the best AR order for each user in individual calibration steps. Future work should address several topics: verifying the results with different protocols (e. g., using randomized classes); analyzing the cost and benefits of additional calibration routines in detail; automating the calibration steps so that the optimal model order can be determined for each user without expert help; exploring different thresholds for different frequencies, rather than using the same threshold for all frequencies as in this work; extending present results to other BCI approaches that use autoregression, such as ERD [10]; and validating the adaptation of the AR model order with online experiments.

# References


[1] J. Wolpaw, N. Birbaumer, D. McFarland, G. Pfurtscheller, and T. Vaughan. Brain-computer interfaces for communication and control. *Clin. Neurophys.*, 113(6):767–791, 2002.

[2] T. Lüth, D. Ojdanic, O. Friman, O. Prenzel, and A. Gräser. Low level control in a semi-autonomous rehabilitation robotic system via a Brain-Computer Interface. *10th Int. Conf. Rehab. Robotics (ICORR)*, pages 721–728, 2007.

[3] G. R. Müller-Putz and G. Pfurtscheller. Control of an electrical prosthesis with an SSVEP-based BCI. *IEEE Trans. Biomed. Eng.*, 55(1):361–364, 2008.

[4] E. Lew, M. Nuttin, P. Ferrez, A. Degeest, A. Buttfield, G. Vanacker, and J. del R. Millan. Non-invasive brain computer interface for mental control of a simulated wheelchair. *Proc. 3rd International BCI Workshop and Training Course*, 2006.

[5] A. Nijholt, D. Tan, G. Pfurtscheller, C. Brunner, J. del R. Millan, B. Allison, B. Graimann, F. Popescu, B. Blankertz, and K.-R. Müller. Brain-computer interfacing for intelligent systems. *IEEE Intell. Syst.*, in press.

[6] Y. Wang, R. Wang, X. Gao, B. Hong, and S. Gao. A practical VEP-based brain-computer interface. *IEEE Trans. Neural Syst. Rehab. Eng.*, 14(2):234–239, 2006.

[7] B. Blankertz, G. Dornhege, M. Krauledat, K. R. Müller, V. Kunzmann, F. Losch, and G. Curio. The Berlin brain-computer interface: EEG-based communication without subject training. *IEEE Trans. Neural Syst. Rehab. Eng.*, 14(2):147–152, 2006.

[8] C. W. Anderson, E. A. Stolz, and S. Shamsunder. Multivariate autoregressive models for classification of spontaneous electroencephalographic signals during mental tasks. *IEEE Trans. Biomed. Eng.*, 45(3):277–286, 1998.

[9] D. P. Burke, S. P. Kelly, P. de Chazal, R. B. Reilly, and C. Finucane. A parametric feature extraction and classification strategy for braincomputer interfacing. *IEEE Trans. Neural Syst. Rehab. Eng.*, 13(1):12–17, 2005.

[10] D. J. McFarland and J. R. Wolpaw. Sensorimotor rhythm-based brain-computer interface (BCI): feature selection by regression improves performance. *IEEE Trans. Neural Syst. Rehab. Eng.*, 13(3):372–379, 2005.

[11] O. Friman, I. Volosyak, and A. Gräser. Multiple channel detection of steady-state visual evoked potentials for brain-computer interfaces. *IEEE Trans. Biomed. Eng.*, 54(4):742–750, 2007.

[12] C. E. Davila, R. Srebro, and I. A. Ghaleb. Optimal detection of visual evoked potentials. *IEEE Trans. Biomed. Eng.*, 45(6):800–803, 1998.

[13] A. P. Liavas, G. V. Moustakides, G. Henning, E. Z. Psarakis, and P. Husar. A periodogram-based method for the detection of steady-state visually evoked potentials. *IEEE Trans. Biomed. Eng.*, 45(2):242–248, 1998.

[14] O. Friman, T. Lüth, I. Volosyak, and A. Gräser. Spelling with steady-state visual evoked potentials. *3rd International IEEE/EMBS Conf. Neural Eng.*, pages 354–357, 2007.

[15] G. E. Chatrian, E. Lettich, and P. L. Nelson. Ten percent electrode system for topographic studies of spontaneous and evoked EEG activity. *Am. J. EEG Tech.*, 25:83–92, 1985.

[16] S. Kay. *Modern spectral estimation: theory and application.* Prentice-Hall, Upper Saddle River, NJ, 1988.

# Designing P300-based brain-computer interface for Chinese typewriter

B. Wu[1,2], Y. Su[1,3], W. Chen[1,3], J. Zhang[1,3], J. Zhang[1,3], X. Li[1,3], Y. Zhuang[1,3], X. Zheng[1,2]

[1] Qiushi Academy for Advanced Studies, Zhejiang University, Hangzhou 310027, China
[2]Dept of Biomedical Engineering, Zhejiang University, Hangzhou 310027, China
[3]College of Computer Science, Zhejiang University, Hangzhou 310027, China

zxx@mail.bme.zju.edu.cn

**Abstract**

Brain Computer Interface (BCI) enables locked-in patients to communicate with other people or control environmental devices. Different components of electroencephalogram (EEG) signal recorded from the scalp can serve as the input of a BCI system, and P300 potential is one of them. This paper describes a P300-based BCI: a Chinese typewriter, which utilizes the Chinese phrasal strokes to type Chinese characters. To achieve this, its user interface uses seven intensifications in total to elicit user's P300 potentials. Signal processing module detects P300 potentials and sends the corresponding output back to the user interface. By selecting targets through stroke mode and character mode, one can type Chinese characters in real time, and thus communicate with other people. System design, experimental methods as well as results are presented in this paper. Experimental results show the user can actually type Chinese characters via this typewriter.

## 1 Introduction

Brain-computer interface (BCI) systems aim to provide severely disabled patients with a new communication or control channel that does not depend on the brain's neural output pathways of peripheral nerves and muscles [1]. BCIs utilize signals recorded from the brain as system input and convert the signals into machine commands by recognizing different signal patterns. For human-computer interaction, BCIs have shown a new way of communication between the human and the machine. Invasive BCIs use brain signals recorded below the scalp for pattern recognition while non-invasive BCIs utilize a variety of neural features extracted from the scalp electroencephalograph (EEG) [2, 3, 3]. P300 is one component of event-related potentials in EEG that appears as a positive peak at around 300 ms after the target stimulus onset [3]. The Oddball Paradigm (OP) is used to elicit P300 potential, in which less frequent target stimuli interspersed with more frequent non-target stimuli are presented. P300-based BCIs require less operant training than most other non-invasive BCIs, but averaging over trials is necessary in order to extract P300 from the background EEG [4]. In recent years, several P300-based BCIs differing from the $6 \times 6$ letter matrix speller developed by Farwell and Donchin [5] were designed. Sellers and Donchin [6], Piccione et al. [7], and Citi et al. [8] all tried four-choice paradigms, while Hoffmann et al. [9] developed an electrical appliance controller with a six-choice paradigm in 2007.
In this paper, a P300-based Chinese typewriter is presented. Although most people type Chinese characters using the input method based on phrasal Pinyin (an input method using 26 English letters to spell Chinese characters according to their pronunciations), the use of 26 letters on the user interface is complicated and time-consuming for intensifications. Comparably, input method based on phrasal stroke (Chinese characters are made of strokes) requires only 5 strokes to form Chinese characters, which results in a much simplified user interface. Utilizing this input method

plus 2 functional buttons ("enter" and "back"), our system is able to elicit P300 potential with a seven-choice oddball paradigm.

# 2 Methods

A BCI system consists of the brain signal (input), an amplifier, a signal processing module and an application (output) [1]. In our system, we used P300 potentials as the input and Chinese typewriter as the output. A 32-channel NuAmps (NeuroScan Inc.) served as the amplifier and two computers running Windows XP were for user interface (UI) and signal processing. All programs relative to visualization were implemented in C# while codes related to data were written in C++, and communication between modules was by Windows Socket.

## 2.1 Data acquisition

Four electrode channels Fz, Cz, Pz and Oz according to the standard 10–20 system of the International Federation were selected to record scalp EEG. They were all referenced to the nose, grounded to the forehead and digitized at 250 Hz by the amplifier, followed by a low-pass filter at 70 Hz. Vertical and horizontal EOGs were also recorded for artifact removal. Participants were asked to count in their minds silently every time the target stimulus flashed during the experiments. Experiment procedures are is as follows:

1. Testing: One testing session was conducted for each participant at the first time. A two-choice visual oddball paradigm, followed by a two-choice audio oddball paradigm was tested. During these runs, participants were asked to click the mouse when the target stimulus flashed. In the following runs, same paradigms were presented except that no mouse clicking was required.

2. Training: 2 sessions – 1 session a day and each containing 10 runs – constitute the training period. The UI was activated as training mode, where no feedback was available from the signal processing module. EEG signal was recorded during these runs and subsequently analyzed offline to generate a template of P300 waveform for each participant. The template would be later used for signal processing during typing.

3. Copy typing: In the next 4 sessions, participants were instructed to practise typing strokes or characters in the copy typing way. This time, targets as well as feedbacks were presented on the UI.

4. Free Typing: In these 2 sessions, we tested participant performances of free typing, where they could type characters as they wanted. Before free typing in each session, 2 warm-up runs were conducted since we found that subjects performed better after warm-up.

## 2.2 User interface (UI)

Chinese and English differ in that Chinese characters are hieroglyphic while English words are alphabetic. Chinese characters are made of strokes and different sequences of strokes form different characters. One widely used Chinese input method on the mobile phone roughly classifies strokes into 5 categories: horizontal stroke ("—"), vertical stroke ("|"), left-falling stroke ("/"), right-falling stroke ("\") and turning stroke ("¬"). Our P300-based typewriter utilizes this input method, where the five strokes together with two functional buttons ("enter" and "back") are presented on the user interface constituting a 7-choice oddball paradigm.

When the typewriter is turned on, it is first in the stroke mode (Figure 1, left) where five strokes with functional buttons "back", "enter" are laid out in the bottom part of the UI, and they are intensified one by one in a random sequence as the stimuli. The top-left part of the UI lists stroke and character outputs from the signal processing module. Corresponding characters made of the strokes are updated within the top-right part of the UI in response to the ongoing

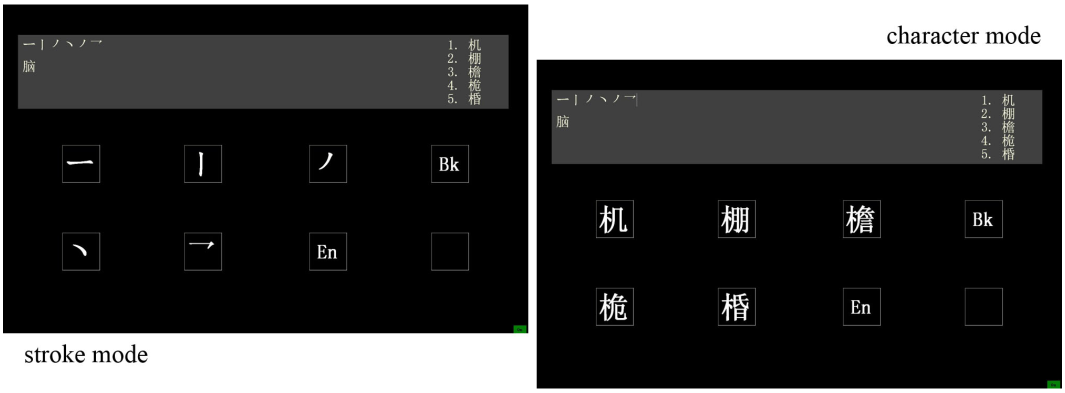


Figure 1: User interface of the Chinese typewriter.

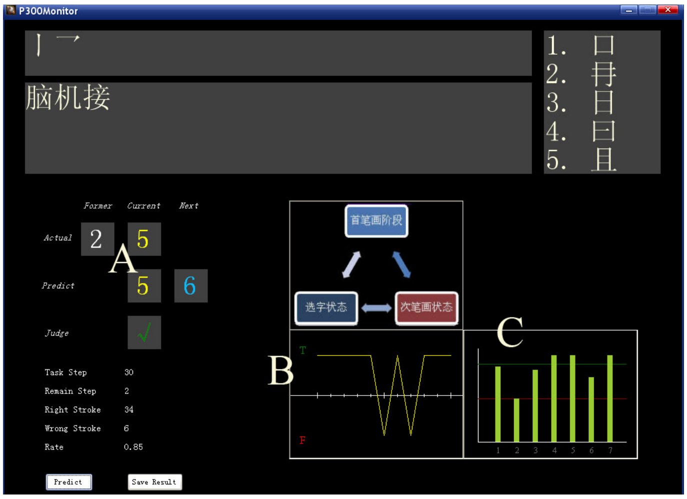


Figure 2: Operator interface on the signal processing PC.

outputs and if the target character appears in this area, the user stops "typing" strokes. Then he will select "enter" to turn the typewriter into character mode (Figure 1, right). In this mode, characters previously shown in the top-right part of the UI will substitute strokes as stimuli, and the user selects a character in the same way as he selects a stroke. All characters that the user "types" are listed below the outputted strokes. After the selection of a character, the UI automatically turns back into stroke mode. To customize layouts of the stimuli for different users, the UI provides a stimuli layout dialogue to coordinate positions of each stimulus. In addition, there are also dialogues to set up experiment parameters such as intensification time of a stimulus, ISI (inter-stimulus interval), interval between trials as well as the number of trials for averaging.

## 2.3 Operator interface

Working simultaneously with the online data analysis, an operator interface is presented on the signal processing computer. The top part (see Figure 2) is a mirror of the user interface presented to the participants and the bottom part provides the operator with some real-time information of the ongoing experiments during copy typing. In Figure 2, area A prompts the current, the previous and next selections in their intensification codes; area B draws correctness of the last 10 selections, true above the line and false below the line; area C shows the accuracies of intensification separately so that the operator can check the user's performance on every single intensification.

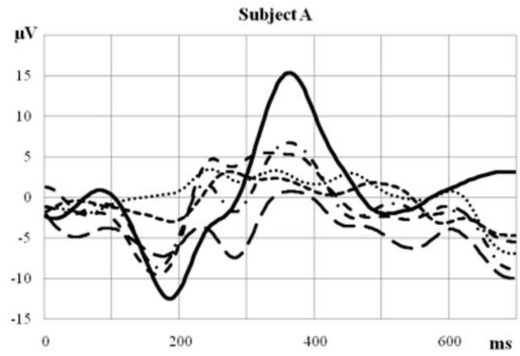


Figure 3: Target and non-target EEG waves.

### 2.4 Data analysis

Data analysis of the feature extraction and pattern translation followed procedures below:

1. Artifact reduction: First, a correction based on "least squares" regression was applied to eliminate effects of the EOGs [10]. Then DC components were removed from the recorded EEG signals, followed by a drifting correction step.
2. Filter and down-sampling: data from the last steps went through a band-pass filter (0.1 Hz 25 Hz) to remove both high and low frequency signals. Then we used the average value of every three points to reduce dimensionality of the EEG signals.
3. Segmentation and average: Since single trial P300 was generally Submerged within the background EEG signals, averaging EEG over trials was necessary to enhance P300. This step segmented continuous data into epochs. Each epoch contained signal data of 800 ms duration, starting 100 ms before the stimulus onset and ending 700 ms afterwards. Then epochs from 10 trials were averaged to get an enhanced epoch for each stimulus.
4. Translation: practically, everyone has his/her own waveform of P300 potential, and this led us to a simple but reasonable method for translation – template matching. It was a straightforward method for finding the best fitted test pattern with the template pattern [11]. The correlation between test patterns and the template pattern was computed as measurement of "similarity". And if ratio of the largest and second largest similarity values surpassed the threshold we pre-set in the configuration, the epoch with the biggest similarity would be selected as the target.
5. Feedback: stimulus code corresponding to the selected epoch data was returned to the user interface. If no stimulus code was selected, 0 was sent back.

## 3 Results

Four healthy subjects (males aged 23, 23, 24 and 26) from our lab took part in the preliminary experiments and none of them had BCI experience before. They all went through the experiment procedure described in Section 2.1 in 6 weeks' time. ISI in the experiments was 100 ms and data from every 10 trials was averaged for P300 detection. Figure 3 shows P300 and non-P300 waveforms of subject A averaged over 20 trials at PZ, the solid line is the target P300 wave and all the other are non-target waves.

All the four could "type" Chinese characters with our system in both the copy typing and free typing sessions. The time for one selection was $100 \cdot 7 \cdot 10 + 3000 = 10000$ ms (ISI: 100 ms, Interval

| | Subject A | Subject B | Subject C | Subject D |
|---|---|---|---|---|
| Average of copy typing | 47.97 % | 70.54 % | 65.79 % | 67.42 % |
| Average of free typing | 67.20 % | 84.91 % | 72.32 % | 75.42 % |

Table 1: Performances for each subject.

Table 2: bit rates per minute in free typing for each subject

| | Subject A | Subject B | Subject C | Subject D |
|---|---|---|---|---|
| Bit rate per minute | 5.15 | 10.62 | 6.67 | 7.61 |

between selections: 3000 ms) and the participants could make 6 selections per minute. Table 1 lists accuracies for each subject in different sessions during copy typing and free typing.

Measurement of bit rate first mentioned by Shannon and Weaver [12] is generally used to compare performances of different BCIs. The formula below calculates the bit rate per selection:

$$B = \log_2 N + P \log_2 P + (1 - P) \log_2[(1 - P)/(N - 1)]$$

Where $N$ is the possible choices and $P$ is the accuracy. Then bit rate per minute can be obtained from $B$ multiplied by the number of selections in a minute. Wolpaw et al. suggested number of choices and accuracy contributed to bit rate equally [3], which means functional design of a BCI system should also be taken into account. In our system, the user could make 6 selections every minute, with accuracies between 67.20 % and 84.91 % in free typing, so we got bit rates ranging from 5.15 to 10.62 bits/minute (see Table 2). All the results were obtained under the condition of real time experiments.

# 4 Discussion

Factors like inter stimulus intervals (ISI), size of the stimuli may affect P300 induction. In our experiments, we found that layout of stimuli may also have great influence in eliciting P300. The layout was asymmetrical due to the number of stimuli, which made the effects of the seven stimuli not completely identical. We tried to identify the seven stimuli by coordinating the layout but ended without any good solution. Neither ring nor symmetrical layouts made the user feel better. This led to interesting consequences that subject B showed a high accuracy on button “back”, which gave him ease at correcting mistaken selections. Nevertheless, subject A did better on selecting the “turning stroke”. On the contrary, subject D felt hard at typing “horizontal stroke”. All these observations were reported by the participants and confirmed by the operator through the operator interface during the copy typing experiments. This indicated that different stimulus positions might cause variations in eliciting P300 potentials and further investigation is necessary to prove this issue.

Besides, experimental results showed that participants performed better in free typing than copy typing. The main reason for this might be that warm-up runs were absent in copy typing sessions and the participants usually performed not well in the first several runs. This gave us the idea to add 2 warm-up runs at the beginning of free typing sessions. Typing Chinese requires more user concentration than English typing, since the user has to synchronize his mind with the updated character candidates after every feedback. So besides checking the feedback stroke, the user should also check updated character candidates. Before the next selection occurs, enough duration should be granted on the UI for the user to transfer his focus from update area to stimulus area.

“Back” button plays an important role in our typewriter, since it provides a mechanism for the user to correct his mistake in typing. Due to this correcting mechanism, the same task for different participants may cause distinctive experimental times and correct selections of “back” button should also be taken into account during accuracy calculation.

## 5 Conclusion

The aim of this preliminary study was to investigate the usability of a P300-based Chinese typewriter. The typewriter utilized a 7-choice oddball paradigm, with an ISI of 100 ms and averaging number of 10. The results revealed that participants could freely type Chinese characters in an online context by our typewriter with bit rates up to 10.62 bits/minute and accuracies up to 84.91 %. "Back" button appeared to be an important element during free typing and this indicated that functional design of a BCI would be a key in real world applications. However, much more work is required to improve the performance of the typewriter. System robustness and adaption ability should be further improved so that bit rates would remain relatively constant over subjects. And more functions could be integrated into the UI so that the user can do things like turning on/off the system on their own. Finally, tests with disabled patients are also important and necessary.

## References

[1] J. R. Wolpaw, N. Birbaumer, W. J. Heetderks, D. J. McFarland, P. Hunter Peckham, G. Schalk, E. Donchin, L. A. Quatrano, C. J. Robinson, and T. M. Vaughan. Brain-computer interface technology: a review of the first international meeting. *IEEE Trans. Rehabil. Eng.*, 8:164–173, 2000.

[2] M. A. Lebedev and M. A. L. Nicolelis. Brain-machine interfaces: past, present and future. *Trends Neurosci.*, 29:536–546, 2006.

[3] J. R. Wolpaw, N. Birbaumer, D. J. McFarland, G. Pfurtscheller, and T. M. Vaughan. Brain-computer interfaces for communication and control. *Clin. Neurophysiol.*, 113:767–791, 2002.

[4] N. Birbaumer. Brain-computer interface research: coming of age. *Clin. Neurophysiol.*, 117:479–483, 2006.

[5] L. A. Farwell and E. Donchin. Talking off the top of your head: toward a mental prosthesis utilizing event-related brain potentials. *Electroencephalogr. Clin. Neurophysiol.*, 70:510–523, 1988.

[6] E. W. Sellers and E. Donchin. A P300-based brain-computer interface: Initial tests by ALS patients. *Clin. Neurophysiol.*, 117:538–548, 2006.

[7] F. Piccione, F. Giorgi, P. Tonin, K. Priftis, S. Giove, S. Silvoni, G. Palmas, and F. Beverina. P300-based brain computer interface: Reliability and performance in healthy and paralysed participants. *Clin. Neurophysiol.*, 117:531–537, 2006.

[8] L. Citi, R. Poli, C. Cinel, and F. Sepulveda. P300-based BCI mouse with genetically-optimized analogue control. *IEEE Trans. Neural Syst. Rehabil. Eng.*, 16:51–61, 2008.

[9] U. Hoffmann, J.-M. Vesin, T. Ebrahimi, and K. Diserens. An efficient P300-based brain-computer interface for disabled subjects. *J. Neurosci. Methods*, 2007.

[10] R. J. Croft and R. J. Barry. Removal of ocular artifact from the EEG: a review. *Neurophysiol. Clin.*, 30:5–19, 2000.

[11] T. S. A. K. Koutroumbas. *Pattern recognition.* Boston: Elsevier/Academic Press, 2006.

[12] C. E. Shannon and W. Weaver. *The mathematical theory of communication.* Urbana, Illinois: Univ. Illinois Press, 1963.

# Assessing the performance of a BCI: a task-oriented approach

B. Dal Seno[1], L. Mainardi[2], M. Matteucci[1]

[1]Department of Electronics and Information, IIT-Unit, Politecnico di Milano, Italy
[2]Department of Bioengineering, IIT-Unit, Politecnico di Milano, Italy

bernardo.dalseno@polimi.it

**Abstract**

An accurate way to measure the performance of a brain-computer interface (BCI) is important to compare different analysis methods and different protocols. The decision of which BCI and what parameters to use should take into consideration the expected performance. Information transfer rate has been proposed as a benchmark, but existing information-based metrics measure the channel capacity of the BCI classifier, which may be much higher than what a BCI achieves in practice. Therefore, we introduce a novel task-oriented approach to the measuring of BCI performances, which takes into account how all the components of the BCI and the user interact. We apply it to the case of a P300 speller and show how the information transfer rate may be misleading. Moreover, we determine when the introduction of an automatic error-correction method is advantageous for a given user. This shows that our approach can be used to compare BCI variants.

## 1 Introduction

A brain-computer interface (BCI) [1] is an interface that does not entail muscle movements, but it bypasses any muscle or nerve mediation and connects a computer directly with the brain by picking up the brain activity signals. This simple definition hides two relevant issues: how fast it is possible to communicate with such an interface, and how often errors are made. These issues are obviously related since the communication speed highly depends on the error rate of the BCI.

An accurate way to measure a BCI performance is important to compare different analysis methods and different protocols. If many BCIs or many variants are available to a user, the decision of which one to use should take into consideration the expected performance for that user (other aspects, which are important, are not the focus of this work). To this aim, the measurement of the performance should be tailored to each specific BCI. For example, there are ongoing studies to introduce automatic correction systems in BCIs [2] based on error potentials (ErrPs), which are specific variations in the EEG induced by the subjective recognition of a committed mistake [3]. Such systems may have false positives, and hence introduce new errors; so, the evaluation of the opportunity of their introduction in a BCI requires the estimation of the potential improvement in the performance of the particular BCI. Intuitively, if the reliability of the ErrP detector is poor, the introduction of ErrP-based corrections will cause more damages than benefits.

In the literature, the performance of a BCI has been quantified by using different metrics, such as classification accuracy, information transfer rate, letters or words per minute, kappa statistic, and others. Among them, the information transfer rate (sometimes simply called bit rate) has been proposed as a benchmark for the evaluation of BCI performances because it does not depend on any particular protocol, it takes into account both the number of choices and time needed, and it could be applied also to continuous ranges of choices [4]. A formula for the information transfer rate is derived in [5] to compute the (mean) number of bits transferred per trial:

$$B = \log_2 N + p \log_2 p + (1-p) \log_2 \frac{1-p}{N-1}\,, \tag{1}$$

where $N$ is the number of possible choices per trial, and $p$ is the accuracy of the BCI, i. e., the probability that the BCI selects what the user intends. Equation (1) divided by the trial duration gives the mean number of bits transferred per time unit. This formula is derived from Shannon's theory [6], and it represents a measure of the mutual information between the user's choice and the BCI selection, under the assumption that all choices convey the same amount of information (i. e., they are chosen by the user with equal probability), $p$ is the same for all the possible choices, and that all the wrong choices have the same probability in case of error. In other words, a BCI system is seen as a noisy channel, in which the selection of a wrong option is the noise.

According to Shannon's noisy channel coding theorem [6], it is possible to achieve an arbitrarily small error probability in a communication on a noisy channel as long as the information transfer rate does not go beyond a certain limit (the channel capacity). The channel capacity is given by the mutual information, and this seems to justify the use of mutual information in Equation (1). The only problem is that Shannon proved his famous theorem by transferring information embedded in ever increasing blocks of bits, and in telecommunication practice only very complex error correction schemes have permitted to get near Shannon's limit. For a BCI, where a human subject sits at one end of the noisy channel, it is not possible to implement such complex error correction schemes, and thus the limit given by the mutual information, as in Equation (1), represents a theoretical figure, unreachable by any real BCI whose error rate is significantly different from zero.

To better understand how far from practice can be the performance measure of Equation (1), let us focus on a simple example with a standard P300 speller [7], where the P300 is used to select letters in matrix of 36 symbols. Let us suppose that the speller speed is 4 letters per minute, and that a user achieves a performance of 45 % in accuracy, which is low, but still far better than random-level accuracy (2.7 %). By substituting $p = 45\,\%$ and $N = 36$ in Equation (1), we get $B = 1.36$ bits, and the information transfer rate for this user would be $4 \cdot B = 5.4$ bits/min; this is not very fast, but, still, communication should be possible. Now let us look at the practical use of such a BCI: the most natural way would be to move on to the next letter when the speller gets one right, and to "hit" backspace every time the speller is wrong. What is the real transfer rate for this speller? Since every letter is more likely to be wrong than not, and this happens to backspace as well, the expected time to spell a letter correctly is infinite, and thus the answer is, on average, exactly 0 bits/min (see also the derivation of Equation (7) in the next section). While it could be still possible to raise $p$ above. 5 by increasing the number of stimulations per letter and render the P300 speller of the example usable, the channel capacity measured by Equation (1) promises a performance far beyond what is attainable once the details of the BCI are taken into account. For this reason, we propose that the measure of the performance of a BCI, e. g., the information transfer rate, takes into account not only the behavior of the classifier contained in the BCI, but how all the components of the BCI and the user interact to perform the task the BCI is designed for.

There exists a generalization of formula (1) that makes use of the confusion matrix and allows each letter to have a different probability of occurrence and a different accuracy [8], but such formula has the same shortcoming of (1), i. e., it treats the BCI as a communication channel with no reference to the way the channel is actually used, and it has a huge number of parameters. In order to keep the exposition simpler, we have chosen to limit the discussion to the simplified formula. All our considerations can be easily extended to the general formula as well.

In the next section we show how the idea of a task-oriented approach to performance measurement can be applied to a P300 speller, and we compare it to Equation (1). In Section 3 we show how our approach can be used to evaluate the opportunity of introducing ErrP detection in the P300 speller. Some concluding remarks follow in Section 4.

# 2 Task-related performance measurement

We give an example of a task-related performance measurement by deriving the performance of a P300 speller, based on the computation of the expected time $t_{\mathrm{L}}$ required to spell a letter correctly.

As explained above, we use the assumptions of Equation (1) to keep the exposition simpler;

moreover, we assume that the accuracy of the speller $p$ is constant and the system has no memory, i. e., each trial is not influenced by the result of the previous one. If $c$ is the time duration of every single trial, the expected time to correctly spell a letter is

$$t_{\mathrm{L}} = p \cdot c + (1-p) \cdot (c + t_{\mathrm{B}} + t_{\mathrm{L}}^{(1)}) = c + (1-p) \cdot (t_{\mathrm{B}} + t_{\mathrm{L}}^{(1)}) \,, \tag{2}$$

where the term $p \cdot c$ is the contribution of the case where the letter is correctly spelled at the first attempt, while the second term represents the case where the letter is wrong, so a backspace must be entered (which takes $t_{\mathrm{B}}$ time) and the letter respelled ($t_{\mathrm{L}}^{(1)}$ time). As the system is stationary, we obviously have $t_{\mathrm{L}}^{(1)} = t_{\mathrm{L}}$. In addition, as the backspace should be treated as any other symbol, $t_{\mathrm{B}} = t_{\mathrm{L}}$ (this can be derived formally). We can rewrite Equation (2) in an iterative formulation

$$t_{\mathrm{L}} = c + 2 \cdot (1-p) \cdot t_{\mathrm{L}} \,, \tag{3}$$

which leads to

$$t_{\mathrm{L}} = \frac{c}{2p-1} \,. \tag{4}$$

This relationship is valid only when $2p - 1 > 0$, i. e., $p > 0.5$; when $p \leq 0.5$, it should be apparent from the expanding of (2) or (3) that the expected time to correctly spell a letter goes to infinite.

Using Equation (4), we can compute the information transfer rate for our P300 speller. This can be obtained as the ratio between the information contained in an ever growing number of symbols spelled and the time taken to spell them:

$$I_{\mathrm{R}} = \mathrm{E}\left[\lim_{K\to\infty} \frac{b \cdot K}{\sum_{i=1}^{K} c \cdot n_i}\right] \,, \tag{5}$$

where $b$ is the information content (in bits) of one spelled symbol, and $n_i$ is the number of trials needed to spell correctly the $i$-th symbol. Since

$$\lim_{K\to\infty} \frac{\sum_{i=1}^{K} c \cdot n_i}{K} = \mathrm{E}[c \cdot n] = t_{\mathrm{L}} \,, \tag{6}$$

and it holds $b = log_2(N-1)$ bits, Equation (5) can be rewritten as

$$I_{\mathrm{R}} = \frac{b}{t_{\mathrm{L}}} = \frac{(2p-1) \cdot \log_2(N-1)}{c} \,. \tag{7}$$

Only $N - 1$ symbols can appear in real words (the backspace cannot), and we are measuring the information contained in the spelled text, therefore the assumption of equal probability leads to the value of $log_2(N-1)$ bits.

This expression represents the expected performance of our speller, and we can compare it with the theoretical limit derived from Equation (1):

$$I_{\mathrm{T}} = \frac{B}{c} = \frac{\log_2 N + p \log_2 p + (1-p) \log_2 \frac{1-p}{N-1}}{c} \,. \tag{8}$$

Figure 1 compares the two measures of information transfer rates and shows how the effective performances can be far from the theory. In fact, while the (8) measures the capacity of a channel, i. e., the maximum performance obtainable by a noisy channel, the (7) measures the expected performance of the same channel when information is conveyed in a specific way; in our case, this is the natural way of using a P300 speller. As expected, the latter curve lies always below the theoretical limit, and it is equal to zero when the accuracy is too low. For high accuracy values, the two curves almost coincide.

It is worth noting that the graph may evidence regions in where the channel cannot work (when $p \leq 0.5$, in our case) and also areas where differences are very far from the theoretical limit.

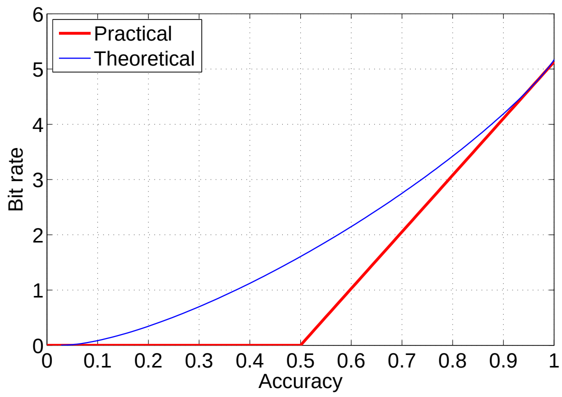


Figure 1: Comparison between theoretical and practical information transfer rate for a P300 speller with 36 symbols.

# 3 Performance measurement with error detection

We now make use of the previous result to measure the improvement of the performance gained when an error-correction capability (based on ErrP detection) is added to our P300 speller. With the new feature added, the speller works as follows: it selects a letter by means of P300 detection and displays it on the screen; if an error is recognized, the latest letter is canceled, while if no error is detected, the latest letter is kept.

To derive the performance of this new system, we need to define the performance of the error-correction system. We characterized it with two parameters: 1. the recall for errors ($r_{\mathrm{E}}$, the fraction of times that an actual error is recognized by the error classifier), and 2. the recall for correct trials ($r_{\mathrm{C}}$, the fraction of times that a correctly spelled letter is recognized by the error classifier). We assume that $r_{\mathrm{E}}$ and $r_{\mathrm{C}}$ are constant and do not depend on the actual letter.

For each trial, four possible cases can happen, which are listed in Table 1. Each case occurs with a certain probability, and the expected time to correctly spell a letter obviously varies case by case. Both the probability and the expected time are reported in the table. The expected time to spell a letter correctly can be computed as in Equation (2) by summing the time required by each case weighted by their respective probabilities:

$$\begin{aligned} t_{\mathrm{L}} &= p_1 \cdot c + p_2 \cdot (c + t_{\mathrm{B}} + t_{\mathrm{L}}) + p_3 \cdot (c + t_{\mathrm{L}}) + p_4 \cdot (c + t_{\mathrm{L}}) \\ &= p \cdot r_{\mathrm{C}} \cdot c + (1-p) \cdot (1-r_{\mathrm{E}}) \cdot (c + t_{\mathrm{B}} + t_{\mathrm{L}}) + p \cdot (1-r_{\mathrm{C}}) \cdot (c + t_{\mathrm{L}}) + (1-p) \cdot r_{\mathrm{E}} \cdot (c + t_{\mathrm{L}}) \,, \end{aligned} \tag{9}$$

where $c$ is the constant duration of a trial, as before. Reasoning as in the previous section, we obtain

$$t_{\mathrm{L}} = t_{\mathrm{B}} = \frac{c}{p \cdot r_{\mathrm{C}} + (1-p) \cdot r_{\mathrm{E}} + p - 1} \,, \tag{10}$$

| Event | Probability | Expected time |
|---|---|---|
| The P300 speller selects the correct letter, and the ErrP classifier correctly recognizes it. | $p_1 = p \cdot r_{\mathrm{C}}$ | $c$ |
| The P300 speller selects the wrong letter, and the ErrP classifier does not recognizes the error. | $p_2 = (1-p) \cdot (1-r_{\mathrm{E}})$ | $c + t_{\mathrm{B}} + t_{\mathrm{L}}$ |
| The P300 speller selects the correct letter, and the ErrP classifier wrongly detects an error. | $p_3 = p \cdot (1-r_{\mathrm{C}})$ | $c + t_{\mathrm{L}}$ |
| The P300 speller selects a wrong letter, and the ErrP classifier recognizes the error. | $p_4 = (1-p) \cdot r_{\mathrm{E}}$ | $c + t_{\mathrm{L}}$ |

Table 1: Probabilities and expected times for the four possible outcomes of a trial.

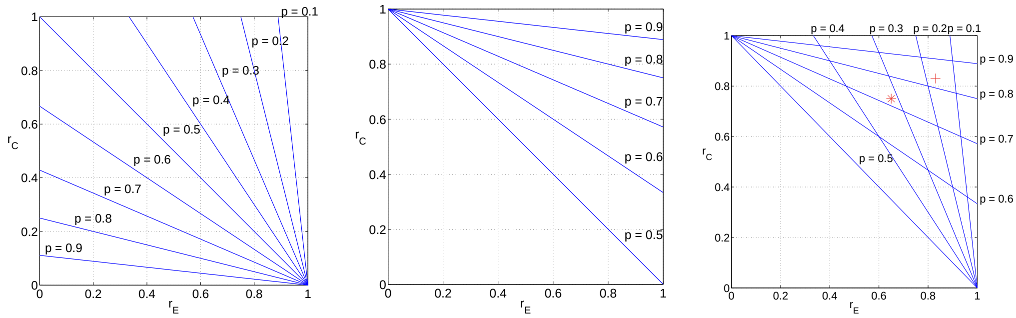


(a) (b) (c)

Figure 2: (a) Condition for the usability of a P300 speller with ErrP detection. (b) Comparison between two P300 speller with and without ErrP detection. (c) When ErrP detection improves the performance of a P300 speller.

where the result is valid only if the denominator is positive, i.e., when

$$r_{\mathrm{C}} > \frac{1-p}{p}\left(1 - r_{\mathrm{E}}\right). \tag{11}$$

Figure 2. a shows the boundaries defined by Inequality (11) for different values of $p$; the inequality is satisfied for the points lying above the lines, and only in these cases the time for spelling a letter is finite (i. e., the P300 speller can be useful). It can be noticed that the constraint becomes tighter as $p$ diminishes, with recall of errors becoming more and more important.

If we now compare Equation (4) with (10), we can evaluate when the error-detection system gives any improvement to the P300 speller. In order to have an improvement, the expected time, $t_{\mathrm{L}}$, should be lower when error detection is used; this leads to the inequality

$$r_{\mathrm{C}} > \frac{p-1}{p}\, r_{\mathrm{E}} + 1\,. \tag{12}$$

Figure 2. b shows the boundaries defined by Inequality (12) for different values of $p$ (for $p < 0.5$ the comparison has no sense); points above the lines represent values of $r_{\mathrm{C}}$ and $r_{\mathrm{E}}$ for which ErrP detection is advantageous. In this case, as $p$ grows the area defined by Inequality (12) shrinks; this happens, because as $p$ grows the performance of the P300 speller gets better and better, and it becomes harder and harder for the ErrP classifier to improve the speller performance.

Figure 2. c summarizes the first two graphs in Figure 2, and shows the values of $r_{\mathrm{C}}$ and $r_{\mathrm{E}}$ for which ErrP detection is advantageous for the whole range of $p$. As before, the part of the plane above the lines is the useful part; values below the lines are either useless or counterproductive. Figure 2. c can be used as a guide to decide to bias the ErrP classifier either toward correct or erroneous epochs, depending on the value of $p$.

Some practical examples may help to better understand the above ideas. Let say that for a particular user the P300 speller reaches 90 % accuracy without error correction, and the error detection reaches $r_{\mathrm{C}} = r_{\mathrm{E}} = 83\%$. This situation corresponds to the cross in Figure 2.c, and the cross lies below the line $p = 90\,\%$. So, for this particular user the automatic error correction system is counterproductive. Another user's performance may be expressed by $p = 70\,\%$, $r_{\mathrm{E}} = 65\,\%$, $r_{\mathrm{C}} = 75\,\%$ (the asterisk in Figure 2.c); the asterisk lies above the line $p = 70\,\%$, and therefore the automatic error correction system should help this user.

# 4 Conclusions

We have shown that the measure of the information transfer rate of a BCI, intended as the channel capacity of the BCI classifier, can be highly misleading. We have proposed a task-oriented approach that takes into account how all the components of the BCI and the user interact, and we have applied it to a P300-based speller. We have compared the measure obtained with our approach to a formula for the information transfer rate that relies on a few simplifying assumptions; it is been possible to use a more general formula with less assumptions and reach the same conclusions, because the main shortcoming lies in the measuring of the channel capacity of the BCI classifier and not in the simplifying assumptions used.

The results for the P300 speller have been extended to derive a formula for a speller with an ErrP-based correction system added, and the formula has been used to assess the utility of the correction system. The use of a task-oriented model permits to make firm observations about the usefulness of ErrPs in a P300 speller, and to identify operating regions/settings in which a real improvement can be obtained. Using a model strictly related to the task performed by the BCI under study is fundamental to understand and quantify the real impact of variations of a BCI protocol, like the introduction of ErrP-based corrections. While we have applied the proposed approach to two specific cases, it is possible to use the same approach to study other kinds of BCIs and the impact of the modification of other parameters, and we think this should lead to a better comparison between different protocols.

**Acknowledgments:** This work has been partially supported by the Italian Institute of Technology (IIT), and by the grant "Brain-Computer Interfaces in Everyday Applications" from Politecnico di Milano and Regione Lombardia.

## References

[1] J. R. Wolpaw, N. Birbaumer, D. J. McFarland, G. Pfurtscheller, and T. M. Vaughan. Brain-computer interfaces for communication and control. *Clin. Neurophysiol.*, 113:767–791, 2002.

[2] P. W. Ferrez and J. del R. Millán. Error-related EEG potentials generated during simulated brain-computer interaction. *IEEE Trans. Biomed. Eng.*, 55(3):923–929, March 2008.

[3] M. Falkenstein, J. Hohnsbein, J. Hoormann, and L. Blanke. Effects of crossmodal divided attention on late ERP components. II. Error processing in choice reaction tasks. *Electroencephalogr. Clin. Neurophysiol.*, 78(6):447–455, June 1991.

[4] A. Schlögl, C. Keinrath, R. Scherer, and G. Pfurtscheller. Information transfer of an EEG-based brain computer interface. In *Proc. 1st Int. IEEE EMBS Conf. Neural Eng.*, pages 641–644, 2003.

[5] J. R. Wolpaw, N. Birbaumer, W. J. Heetderks, D. J. McFarland, P. H. Peckham, G. Schalk, E. Donchin, L. A. Quatrano, C. J. Robinson, and T. M. Vaughan. Brain-computer interface technology: A review of the first international meeting. *IEEE Trans. Rehabil. Eng.*, 8(2):164–173, June 2000.

[6] C. E. Shannon and W. Weaver. *The Mathematical Theory of Communication*. The University of Illinois Press, 1949.

[7] Lawrence A. Farwell and Emanuel Donchin. Talking off the top of your head: toward a mental prosthesis utilizing event-related brain potentials. *Electroencephalogr. Clin. Neurophysiol.*, 6(70):510–523, December 1988.

[8] A. Schlögl, J. Kronegg, J. E. Huggins, and S. G. Mason. *Towards Brain-Computer Interfacing*, chapter Evaluation Criteria for BCI Research, pages 327–342. MIT Press, 2007.

# A tactile P300 BCI and the optimal number of tactors: effects of target probability and discriminability

A.-M. Brouwer, J. van Erp

TNO Human Factors, Soesterberg, The Netherlands

anne-marie.brouwer@tno.nl

**Abstract**

For P300 based BCIs, tactile stimuli are potentially more suitable than visual or auditory ones, since they do not occupy the visual or auditory channel and they can be delivered to the user without being noticed by others. In this study, we investigate whether a BCI controlled by EEG responses to vibro-tactile stimuli around the waist is feasible. In addition, we explore the effect of varying the number of (equally spaced) tactors: whereas a large number of tactors is expected to enhance the P300 amplitude since the target will be less frequent, it could negatively affect the P300 since it will be difficult to identify the target when the distance between target and distracters is smaller. Participants were asked to attend to the vibrations of a (varying) target tactor, embedded within distracters. The number of tactors could be two, four or six. We demonstrated a functioning tactile P300 BCI. Although the P300 in the condition with two tactors (where target and distracter were equally often presented) was smaller compared to the other conditions, we did not find a difference in SWLDA classification performance between the different numbers of tactors.

## 1 Introduction

The P300 event-related potential is a positive deflection in EEG that occurs 300 ms (or somewhat later) after a target stimulus has been presented. In most studies investigating the P300, the target stimulus is presented within a series of distracter stimuli. Participants are asked to attend to the target by mentally counting the number of times it is presented, or by pressing a button each time it occurs. Participants can determine themselves which of the presented stimuli is a target and which are distracters, but when a target stimulus physically stands out from the distracters, it can elicit a P300 "by itself" (e. g. [1]), probably because it automatically draws attention.

Because participants can choose for themselves which of the presented stimuli to attend to, and because the P300 can relatively easily be detected, this ERP is a likely candidate for driving brain-machine interfaces (BMIs or brain-computer interfaces – BCIs). A well-known example is the P300 speller in which rows and columns of a matrix consisting of letters are sequentially flashed in random order [2]. Every time the row or column is flashed that contains the symbol that the user wants to spell, a P300 occurs. In this way, users can communicate with their environment. Other P300 based BCIs have been designed to control a robot wheelchair, to switch devices on or off in a virtual room and to stop a virtual car.

The P300 based BCIs mentioned so far all use visual stimuli to elicit P300s. The fundamental research on P300s focuses on visual and auditory stimulation. However, for BCI purposes tactile stimuli can be an interesting alternative. Tactile stimuli can be delivered by tactors that can be hidden under the user's clothes, making the device invisible to others. Using tactile stimuli will also keep the eyes and ears of the user free. Recently, tactors applied around the waist have proven to be successful as navigation display [3], and may therefore be a natural choice for designing BCIs for navigation. Users can focus their attention on the tactile stimulus that corresponds to the direction in which they want to move, possibly eliciting a useful P300 signal.

Tactile stimuli can elicit P300s [4]. In these studies, electrical and mechanical stimuli were delivered to the hands and wrists and relatively long inter stimulus intervals were used (around 2 seconds in [4]). Obviously, for brain-machine interface purposes, short stimulus durations and inter stimulus intervals are required. The finding that P300s can be elicited by tactile stimulation of the hands does not guarantee that tactile stimulation of the torso easily elicits P300s as well because the haptic sensitivity and spatial resolution of the torso is lower than that of the hands.
Recently, we investigated whether quickly presented vibro-tactile stimuli at different locations around the waist can elicit robust P300s. We presented participants with bursts of vibration delivered by one of eight tactors around the participants' waist. In other conditions, we presented analogous visual stimuli consisting of flashed circles on a monitor in a schematic drawing of the tactor layout. Participants attended to the vibrations and/or flashes of the target tactor presented in a rapid stream of stimuli that also contained the seven distracters. The target was always the front tactor. In addition, this tactor physically stood out from the distracter: the distance to the distracters was larger than the distance between the distracters themselves, and the stimulus intensity of the target was stronger than of the distracters (in the tactile condition, a tactor above and below the target tactor vibrated simultaneously with the target, whereas in the visual condition the target circle was enlarged when flashed). The experiment demonstrated that the amplitudes of P300s elicited by tactile and visual stimuli depended on electrode site, but on the whole, they were equally high. Whereas other results could probably be obtained when different experimental parameters are used, we can conclude that it is possible to elicit reliable P300s with quickly presented vibro-tactile stimuli around the waist.
The present study aims at extending these findings to a more realistic BCI setting. Whereas the oddball task as used in the previous experiment more or less guarantees the attention of the participant to the target, it can not be generalized to a BCI where the user should be able to choose the target her- or himself, and where it should be possible for different tactors to function as targets. Furthermore, for a BCI classification accuracy (how well an online algorithm can identify the target stimulus) is more important than the size of the P300 amplitude.
Besides tackling the issues mentioned above, we also want to explore the effect of varying the number of stimuli (i. e. the number of tactors around the waist). With a large number of tactors, it will be difficult to identify the individual targets because they will be close to the distracters. It has been shown that a low discriminability reduces the P300 amplitude [5]. On the other hand, with a large number of tactors, the target is presented relatively infrequent, which positively affects the P300 [6], possibly via a longer target-to-target interval: [7]. In case of few tactors, the discriminability is high but the probability of target presentation is also high. In order to guide the development of a tactile BCI for navigation, we are interested in the relative importance or tradeoff of these potential effects within the context of our vibro-tactile stimuli around the waist.

# 2 Methods

## 2.1 Participants and stimuli

Six female and five male participants volunteered to participate in the experiment. They were between 20 to 27 years old. None of the participants had participated in BCI experiments before.

Participants wore an adjustable vest over their clothes lined with 5 rows of 12 equally spaced tactors spanning the whole trunk circumference. For this study, we only used one row of tactors around the participant's waist, approximately at the height of the navel. Different tactors were activated in different conditions. Tactors vibrated successively with a vibrating time of 188 ms and breaks in between vibrations of 438 ms. The tactors were custom built. They consisted of plastic cases with a contact area of $1 \times 2$ cm, containing 160 Hz vibrating motors. (TNO, The Netherlands, model JHJ-3). During the experiment, participants viewed a dimmed LCD (20 inch, refresh rate 75 Hz) displaying instructions and a fixation cross.

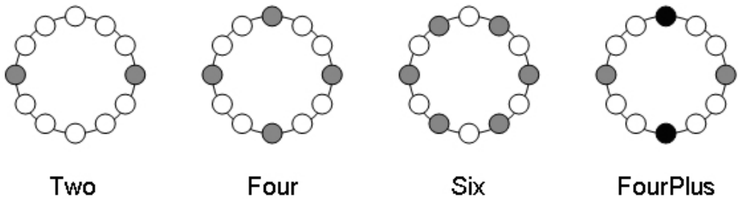


Figure 1: Schematic overview of the tactor layout (top view) in the different conditions. The tactors being used are colored gray whereas the inactive tactors are white. In the FourPlus condition, only the gray tactors could be targets. The black tactors vibrated twice as often as the gray tactors.

## 2.2 Recording materials

EEG activity was recorded at the Fz, Cz, Pz, Oz, P3, P4, PO7 and PO8 electrode sites of the 10–20 system using electrodes mounted in an EEG cap (g.tec medical engineering GmbH). A ground electrode was attached to the forehead. The EEG electrodes were referenced to linked mastoid electrodes. The impedances of all electrodes were below 5 kΩ. Data were sampled with a frequency of 256 Hz and filtered before storage by a 0.1 Hz high pass-, a 60 Hz low pass- and a 50 Hz notch filter (USB Biosignal Amplifier,g.tec medical engineering GmbH). The experiment (stimulus presentation and data recording) was controlled by custom built software and BCI2000 [8].

## 2.3 Conditions and design

We used four conditions: Two, Four, Six and FourPlus. Conditions Two, Four and Six refer to the number of equally distributed tactors used (see Figure 1 for a schematic indication of their location). In these conditions, the number of distracters was respectively one, three and five. The probability of target presentation decreases over these conditions (expected to enhance the P300), whereas the distance between the tactors and therewith the discriminability between target and distracters decreases (expected to reduce the P300). The FourPlus condition served as a comparison for condition Four and Six. In this condition, the same tactors are used as in condition Four (see Figure 1), that is, the discriminability in Four and FourPlus is the same. However, by having the front and back tactor vibrate twice as often as the other tactors and by only designating the left and right tactors as targets, we made the target probability equal to that in condition Six. This will allow us to directly evaluate the relative importance of the factors discriminability and target probability: when discriminability plays a more important role, condition Four and FourPlus will produce similar results; when target probability is more important, condition Six and FourPlus will produce similar results.

The order of conditions was randomized for each participant. For every condition, there were three blocks: two training blocks followed by one test block. After the training blocks, a classification algorithm was applied to the collected data. The resulting model was used in the test block to give participants feedback about the tactor that the algorithm classified as the target. Aside from this feedback, the training and test blocks were the same (please note that training refers to training the classifier, not training the participant).

A block consisted of six sequences of stimuli. Each sequence started with one of the tactors being designated as the target. In condition Six, each of the tactors served as a target once in one block, starting with the front-left tactor and every time going to the next tactor counter-clockwise. In condition Four, the front target and the one counter clockwise served as targets again after the others had been a target. In condition Two and FourPlus, the left and right tactor were designated as a target three times each, alternating and starting with the tactor at the left.

Each of the six sequences consisted of activating each tactor in that condition (the target and the one, three or five distracters) 10 times, in random order. With a stimulus presentation time of 188 ms and an inter-stimulus interval of 438 ms this results in average target-to-target intervals of

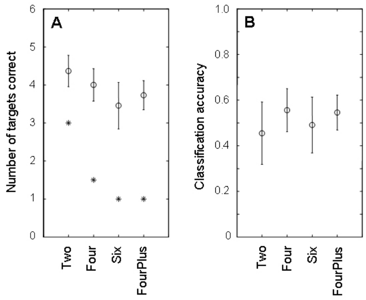


Figure 2: Average performance of the classification model in the four conditions as expressed in the number of targets correct (A) and classification performance (B). The stars in (A) indicate chance performance. In panel B, we corrected for chance by subtracting change performance from the observed number correct and normalizing the results. Error bars represent standard errors of the mean.

1252 ms (condition Two), 2504 ms (condition Four) and 3756 ms (conditions Six and FourPlus).

## 2.4 Task and procedure

Before the experiment started, the complete procedure was explained to the participants, with their task being to concentrate on the target by counting the number of times it occurred, and to ignore the distracters. They were further asked to fixate the fixation cross displayed on the screen, to blink as little as possible and to limit any other movements during tactile stimulation.
Participants were seated comfortably in front of a monitor in a dimly lit, shielded room, wearing the tactile vest and an EEG electrode cap. During the recording, an analog noise generator produced pink noise in order to mask the sound of the tactors. The monitor always displayed a fixation cross. A sequence of stimuli started by the appearance of the word “focus” on the monitor. Simultaneously, one of the tactors vibrated for 750 ms. This indicated the target for the upcoming sequence. Then, each of the tactors used in that condition vibrated 10 times in random order. The appearance of a dashed line (in the case of a training block) or the word “result” (in the case of a test block) indicated the end of a sequence. In the latter case, one of the tactors vibrated for 750 ms simultaneously with the word “result”, to indicate to the participant which tactor the algorithm designated as being the target. Participants took 1 to 5 minute breaks in between blocks.

## 2.5 Classification algorithm and analysis

Classification models were built during the experiment for each participant and each of the four conditions after two training blocks. Using step-wise linear discriminate analysis (SWLDA) a maximum of 60 features were extracted from the EEG data. The epochs used in the analysis started at stimulus onset and ended 797 ms afterwards. The data was down sampled with a factor of four.
For each participant and each condition, we determined the number of targets that was correctly identified by the algorithm. For all conditions, the maximal number correct is six. However, the conditions differ with respect to chance level, so we also present the results after correcting for chance. We used one sample $t$-tests and a repeated measures ANOVA to evaluate classification accuracy.

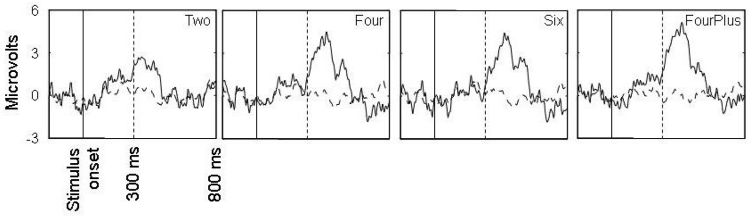


Figure 3: EEG averaged across participants and presented separately for targets (solid lines) and distracters (dashed lines) in the four conditions. Only data from electrode Pz is presented here.

# 3 Results

Figure 2 shows the classification performance. In Figure 2A the number correctly identified targets is presented for each condition, together with an indication of chance performance. Figure 2B presents the classification accuracy, corrected for chance. The one sample $t$-tests show that classification accuracy is well above chance for all conditions ($t_{10} = 3.32$ or higher, all $p$-values $< 0.01$). A repeated measures ANOVA on classification accuracy with condition as independent variable shows no effect of condition ($F_{(3,30)} = 0.19$, $p = 0.90$).

Figure 3 depicts the average Pz EEG samples from 200 ms before stimulus onset until 800 ms after, for each condition, and separately for target and standard presentations (solid and dashed curves respectively). Pz is a location where the P300 is usually strongly displayed (e. g. [9]). Clearly, a P300 is present in all conditions, even in condition Two, although the amplitude seems to be smaller. The P300 occurs later than 300 ms after the start of the stimulus. This corresponds to many P300 studies that report this as well (e. g. [9, 10]).

# 4 Discussion

We demonstrated that a BCI based on P300s elicited by tactile stimuli around the waist is feasible. Using different tactors as targets, classification performance was always well above chance for all conditions; for FourPlus it was approximately 62 % correct with 17 % guessing chance. Note that in this experiment, we did not specifically try to optimize classification performance. Each model was trained on all data acquired in the 4 to 10 minutes before. Acquiring more training data and leaving out less representative blocks (e. g., at the start of the experiment) could increase the model's performance.

Surprisingly, we did not find significant differences in classification performance between the conditions that varied in target-distracter discriminability and target probability. We expected at least to find a difference between the FourPlus condition and either the Four or the Six condition, or both. The FourPlus condition was expected to produce clearer P300s than the Four condition because of a more favourable target probability, and than the Six condition because of a more favourable discriminability. An explanation could be that in all conditions, target probability was low enough (or target-to-target interval long enough [6, 7]) and that the distinction between target and distracter was clear enough (even though some participants remarked that in the Six condition they experienced difficulties in distinguishing the target from adjacent distracters).

The average EEG signals showed a slightly different picture than the classification results. The amplitude of FourPlus seems a bit larger than Six and Four, but the clear difference is between condition Two and the other three conditions. In Two the amplitude is considerably smaller. The fact that this is not reflected in the classification accuracy could be because even though the amplitude was smaller, it was sufficiently different from that of the distracters. When fewer trials would have been used to train the classification algorithm, there may have been a difference. Another reason for the discrepancy between classification results and P300 amplitudes could be that the classification model used different features than P300 amplitude only. From classification results obtained in experiments that are supposed to manipulate the P300, one cannot directly conclude anything about P300s without further looking at the signals and the features that a model uses. We varied the number of tactors across conditions in order to get an idea of a suitable tactor configuration for a tactile BCI. Since the results pointed out that the number of tactors does not affect classification accuracy (at least for the specific configurations we tested) the choice can be guided by the specific application that one has in mind. One could for example have the number of tactors depend on the number of choices that one wants to give the user.

# 5 Conclusion

This study demonstrated a BCI controlled by EEG responses, elicited by attending to specific vibro-tactile stimuli around the waist. Tactile stimuli are particularly useful in BCIs since they allow users to look and listen to their environment rather than to stimuli necessary for controlling the BCI, and tactile stimuli can easily go unnoticed by others. A BCI based on tactile stimuli around the waist could be a natural choice for navigation BCIs. We tested stimulus configurations consisting of two, four and six equally distributed tactors and did not find a difference in classification performance. This suggests that all of these tactors could be used in a BCI.

**Acknowledgments:** Thanks to Fabio Aloise, Antoon Wennemers, Febo Cincotti and Marieke Thurlings. This work was supported by the Dutch Smartmix project BrainGain.

# References

[1] B. H. Jansen, A. Allam, P. Kota, K. Lachance, A. Osho, and K. Sundaresan. An exploratory study of factors affecting single trial P3 detection. *IEEE Trans. Biomed. Eng.*, 51:975–978, 2004.

[2] L. A. Farwell and E. Donchin. Talking off the top of your head: A mental prosthesis utilizing event-related brain potentials. *Electroencephalogr. Clin. Neurophysiol.*, 70:510–523, 1988.

[3] J. B. F. van Erp. Presenting directions with a vibro-tactile torso display. *Ergon.*, 48:302–313, 2005.

[4] Y. Nakajima and N. Imamura. Relationships between attention effects and intensity effects on the cognitive N140 and P3 components of somatosensory ERPs. *Clin. Neurophyiol.*, 111:1711–1718, 2000.

[5] M. D. Comercho and J. Polich. P3a and P3b from typical auditory and visual stimuli. *Clin. Neurophysiol.*, 110:24–30, 1999.

[6] J. Polich, T. Brock, and M. W. Geisler. P300 from auditory and somatosensory stimuli: Probability and inter stimulus interval. *Int. J. Psychophysiol.*, 11:219–223, 1991.

[7] R. J. Croft, C. J. Gonsalvez, C. Gabriel, and R. J. Barry. Target-to-target intervals versus probability effects on P300 in one- and two-tone taks. *Psychophysiol.*, 40:322–328, 2003.

[8] G. Schalk, D. J. McFarland, T. Hinterberger, N. Birbaumer, and J. R. Wolpaw. BCI2000: a general purpose brain-computer interface (BCI) system. *IEEE Trans. Biomed. Eng.*, 51:1034–1043, 2004.

[9] D. Ravden and J. Polich. On P300 measurement stability: habituation, intra-trial block variation, and ultradian rhythms. *Biol. Psychol.*, 51:59–76, 1999.

[10] A. D. Gerson, L. C. Parra, and P. Sajda. Cortically coupled computer vision for rapid image search. *IEEE Trans. Neural Syst. Rehabil. Eng.*, 14:174–179, 2006.

# A home automation interface for BCI application validated with SSVEP protocol

P. Perego[1], L. Maggi[1], S. Parini[2] and G. Andreoni[1]

[1]Indaco Dept., Politecnico di Milano, Italy
[2]Bioengineering Dept., Politecnico di Milano, Italy

paolo4.perego@mail.polimi.it

**Abstract**

This work aimed at developing a BCI driven application for the control of a commercial home automation system. The application was developed using the BCI framework proposed by the SensibiLab Laboratories (Politecnico di Milano) and interfaced with a four command SSVEP based system.

A specific software module was implemented in order to provide an interaction layer with an home automation system. A MyHome gateway was provided by BTicino spa (Erba, Italy) and a basic demonstrator was set-up in our laboratory. The standard physical communication layer of the adopted gateway is RS-232 and, in order to maximize the ease of installation, a specific RS-232 to Bluetooth module was designed. The Application layer was implemented using the OpenWebNet language proposed by BTicino. Although the current demonstrator supports only a few light-point and some auxiliary devices, the software module supports all the options provided by the home automation system. Six healthy subjects, whose ability to use the SSVEP system was already assessed, were able to control the demonstrator.

## 1 Introduction

Home automation (or domotics) is a field of building automation aimed at the development of specific technical solutions for private homes and dedicated to the application of technologies for the comfort and security of its residents.

Many technological fields are involved in the realization of an home automation system ranging from electronics and computer science, to communication networks and the internet. From the technological research point of view, the main focus is the creation of a smart system able to efficiently control and integrate all the typical home installations, such as:

- Heating, ventilating, and air conditioning (HVAC)
- Lighting
- Water delivery
- Access control
- Audio and video switching and distribution
- Intercommunication
- Remote process monitoring and control

thus optimizing power consumption, comfort and safety [1]. While generally conceived as a commercial technology for comfort and luxury in high-end buildings, this technology adds alternative and flexible pathways to the typical interaction paradigm of the user with his domestic environment, thus representing an accessible and efficient solution aimed at providing disabled people with direct environmental interaction and significantly increasing the quality of life [2].

# 2 Materials

The home automation interface control application is part of the BCI framework developed by the Sensibilab. The framework is composed of several hardware and software tools which were used in the development and testing of the system, even if the most part of the adopted libraries are cross platform, the current available version is for Windows only. A brief description of the framework architecture is here proposed using a signal-path based approach:

- The hardware acquisition unit (Kimera II) is an improvement of our previous system [3] and it consists in an eight channel battery powered EEG featuring a wireless Bluetooth communication protocol
- A Hardware Interface Module (HIM) is the gateway between KimeraII and the controlled application. This module receives the EEG data from the device, processes it and sends the estimated classification to the AEnima module using a TCP/IP connection
- The AEnima module is based on an Open Source graphical engine (IrrLicht) used to manage the Graphical User Interface guaranteeing flexible and versatile 2D/3D applications design tools. Communication with external control/stimulation devices and HIM timing and triggering issues are managed by a dedicated Protocol class
- The signal processing Module consists of a spatial filtering block (SFB), a raw band pass filter between 5–40 Hz, a features extraction block and a supervised classifier. The features are the result of a ratio between the amplitude of a stimuli time-synchronous averaging of the signal, compared to the estimation of the amplitude of the raw signal. The classifier consists of a Multiclass (LEFT, RIGHT, UP; DOWN and NULL) regularized linear discriminant analysis (RLDA) based on the modified samples covariance matrix method. The RLDA includes a boosting algorithm based on a cyclic minimization of the classification error on the training set and an algorithm for outliers rejection

The home automation application was developed using the commercial MyHome system developed by BTicino (Erba, Italy). MyHome system is based on a proprietary SCS bus technology (patented by Bticino) which guarantees the minimization of cabling requirements and a flexible modular system for easy upgrades and future system extensions. MyHome domotics system was interfaced with a personal computer using a specific RS-232 to SCS gateway: a specific communication protocol called OpenWebNet was also adopted.

## 2.1 MyHome library and configuration software

The Home Automation Interface software is based on a communication library which was developed in order to assure a certain independence of the software from the physical connection medium and to guarantee, through modularity, ease of inclusion in any software.

The library has been built, using native C, with two different layers: the Serial layer and the OpenWebNet layer. The Serial layer takes care of the communication between the residential gateway and the PC: it provides communication with the home automation control device using a standard RS232 port. The OpenWebNet layer implements the basic commands of the OpenWebNet communication protocol for the control of the home automation system. The two-layer structure of the library allows the use of different type of connection only by adjusting the Serial Layer.

The application is able to support different installations of MyHome system and, according to this purpose, three different configuration software were created:

- MyHome Config
- Scenarios Config
- MyHome Test


Figure 1: Main menu of MyHome protocol.

The three configuration software were designed in order to guarantee efficiency and ease of use for the end-user: an intuitive graphics interface allows the setting up of the system in a few mouse clicks. MyHome Test software also features a specific Preview Mode which allows the testing of the entire installed system directly from the PC.

## 2.2 User interface and testing procedure

MyHome protocol was used in order to demonstrate the flexibility of the proposed BCI system interfacing with external components. Using the libraries illustrated in the previous chapter it was possible to create a button based menu application for the control of the home automation system. The first menu (Figure 1) allows the selection between six submenus of commands:

- Lighting controls
- Environments
- Automations
- Shutdown all
- Exit – return to main menu
- Scenarios

By selecting one among the different submenus, the user gains access to the corresponding GUI with the related buttons and controls: when the user selects an operation in the submenu, the protocol forces the system to return to the main menu. In order to simplify and optimize user control, the cursor movement was constrained by the grid shown in Figure 2.

As shown in Figure 2, a simple example of home automation system was set-up in the room where the BCI sessions took place. The user could activate two devices and two independent lights behind the user's seat. Since the SSVEP protocol is based on external optical stimulation and on the related evoked cerebral response, the activation of light-points and the consequent environmental lighting variation could have a potential effect on the SSVEP potential. During the experimental protocol it was decided to verbally guide the user in the use of the application, thus it was also possible to verify the effect of an uncontrolled environment on system usability. Ten healthy subjects between 22 and 50 years old took part to the study. The subjects were sitting on a standard office chair in front of a 19 inch LCD screen at a distance of about one meter. Each subject performed a 5 steps protocol consisting in:

- A screening phase that lasted 190 seconds performed in order to identify the four best stimulation frequencies

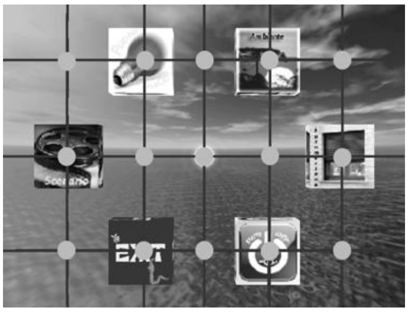

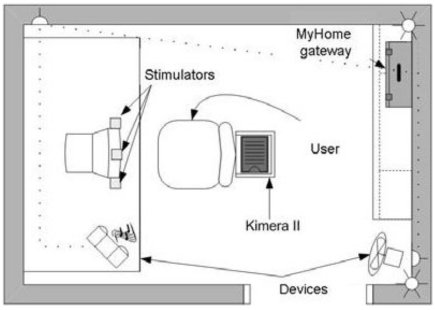


Figure 2: On the Left: Cursor movement grid. On the right: Planimetry of the acquisition room.

- A calibration phase that lasted 160 seconds for the registration of a training set for the classifier
- A testing phase involving the selection of 8 different symbols that was used in order to verify the performances of the classifier
- A gaming protocol which consisted of a 15 trials target reaching session
- A home automation session which consisted of a free will use of the automation system

Only the subjects that were able to successfully complete the testing phase proceeded to the gaming and to the home automation protocol.

# 3 Results

Six subjects out of ten were able to generate an SSVEP response suitable to robustly train the classifier and to complete the testing phase with 100 % accuracy and an average elapsing time of approximately $68.2 \pm 8.3$ seconds. All the six subjects were consequently able to easily drive the Home-Automation system demonstrating high robustness to false positives: in order to simplify the interaction with the graphical user interface, a researcher was near the subject and helped him/her in the navigation of the menu by verbal instructions during the session itself. Since a key point in the SSVEP protocol is the visual stimulation, a change in the environmental lighting could compromise the functioning of the system. In order to verify the robustness of the system against this specific aspect, the first operation the user was asked to perform was to switch on the lights of the room (Two standard 60 W bulb light placed approximately at 2.5 meters from the floor, see Figure 2 for details). All users were able to operate the system even during increased environmental lighting conditions.

# 4 Discussion and conclusion

In this work a four command based graphical user interface (UI) and a communication layer with the domotics system were developed. By interfacing the system with an SSVEP-Based Brain-Computer Interface it was possible to demonstrate the usability and the reliability of the application; the test with other BCI paradigms is mandatory; from this point of view many current BCI systems [4] may be compatible with the developed application while other may require the adaptation of the UI layer without changing the communication layer.

# References

[1] G. Andreoni, L. Piccini, and L. Maggi. Active customized control of thermal comfort. In *International Encyclopedia of Ergonomics and Human Factors, 2nd edition*, 2006.

[2] A. Kübler, T. Kotchoubey, J. Kaiser, J. R. Wolpaw, and N. Birbaumer. Brain-computer communication: Unlocking the locked in. *Psychol. Bull.*, 127:358–375, 2001.

[3] L. Maggi, S. Parini, L. Piccini, and G. Andreoni. A four-class BCI system based on the SSVEP protocol. In *Proc. IEEE EMBC 2006*, 2006.

[4] F. Beverina, G. Palmas, S. Silvoni, F. Piccione, and S. Giove. User adaptive BCIs: SSVEP and P300 based interfaces. *Psychnol. J.*, 1:331–354, 2003.

# Spelling with the Bremen brain-computer interface and the integrated SSVEP stimulator

D. Valbuena, I. Sugiarto, A. Gräser

Institute of Automation, IAT, University of Bremen, Bremen, Germany

valbuena@iat.uni-bremen.de

**Abstract**

In this work, the performance of a visual stimulator displayed on a computer screen was evaluated in a brain-computer interface (BCI) spelling task. The stimulator and spelling program were tested in a group of 106 subjects at the CeBIT 2008. The task was to spell words with the Bremen Brain-computer interface based on steady-state visual evoked potentials. Subjects navigated a cursor through a matrix of 32 characters by selective attention to one of five flickering lights. Each light encoded cursor movement commands (up, down, right, left) or select. A mean accuracy of 92 % was achieved.

## 1 Introduction

Brain-computer Interfaces (BCIs) are systems that can detect and classify patterns in ongoing brain signals that are associated with specific intentions, tasks or events [1]. A commonly used brain pattern for BCIs and focus of this work is the SSVEP (steady-state visual evoked potential) [2], which depends on an external source to generate the brain activity that carries the information. SSVEP patterns are the result of a visual selective attention task in which users focus their attention on light sources that flicker with particular frequencies. The frequency of the evoked SSVEP matches the frequency of the flickering stimulus or one of its harmonics [3]. The characteristic of the SSVEP response differs from the spontaneous activity of the brain and it can be therefore robustly detected. In a BCI, each flickering light and its corresponding SSVEP are associated with a certain control command [4, 5, 6, 7, 8]. The task of the BCI system is to reliably detect SSVEPs in the ongoing brain signals and also to determine its frequency in order to identify which command the user wants to convey. A robust BCI based on SSVEP is the Bremen BCI. The brain signal is modeled as a composite of SSVEP response, background brain activity, and noise. At the core of this method is a spatial filtering algorithm for extracting SSVEP responses. This algorithm gives reliable and robust results [9].

In this work, the Bremen BCI was used in a spelling task to test the integrated speller and visual stimulator, which consist of a matrix of 32 characters, a cursor and five virtual LEDs (VLEDs) flickering at different frequencies and encoding five different commands. The VLEDs are located on the screen depending on the command they encode, for example, the upper VLED corresponds to the up command and the bottom VLED corresponds to the down command. The select VLED was positioned on the top-left of the screen. With this integrated system, the stimulus and the visual feedback are provided on the same screen and therefore the user's attention is kept on the same place, making the execution of tasks faster and avoiding error-classifications. The user does not need to switch his attention between the stimulus and the feedback provided by the speller application to see if the output corresponds to what he wanted to spell. An earlier version of our system [10] had an array of LEDs (light emitting diodes), but subjects had to shift attention from the monitor to one of five LEDs to effect control. Subjects complained that switching attention from the monitor to another target, often located outside the fovea, impaired performance and ease of use.

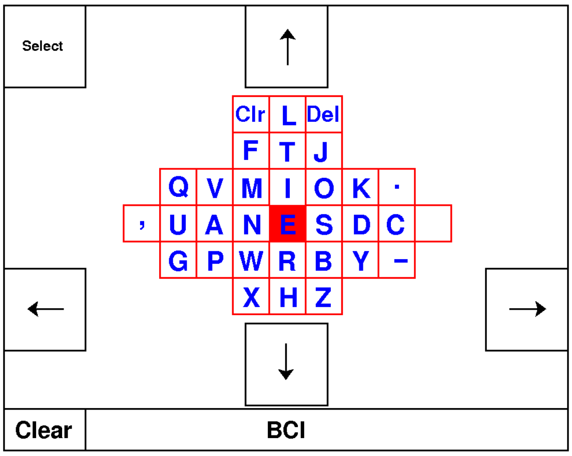


Figure 1: Rhombus layout with 32 characters, in which the cursor is navigated right, left, up and down to reach a character by focusing on the flickering boxes. Each box contains an arrow (up, down, right, left) or the word select indicating the command it encodes. After selection, the cursor starts over at the center position E. The bottom of the screen presents the characters that the subject has selected.

## 2 Methods

In this section, the method used to develop a visual stimulator integrated to a spelling layout is presented. This application was implemented in C++ and the Qt4 [11] software framework for developing high-quality 2D applications was used.

### 2.1 Spelling layout

The strategy for spelling was chosen depending of the number of commands that the BCI can detect. In the current work, 5 different commands were used, requiring five light sources that flicker with 13, 14, 15, 16 and 17 Hz. In prior work [12], two different spelling layouts and selection schemes were compared and evaluated to be controlled with five commands. The Row-Column layout, similar to the design commonly used in P300 spelling programs [13], where letters are chosen by first selecting the row containing the desired letter and then the column. The Rhombus layout, in which a cursor is navigated right, left, up and down to reach the desired letter. Because with the Rhombus layout is easier to keep a constant visual attention and accidental commands or error-classifications can easily be corrected by the user, this layout was selected as spelling layout for this application. Some modifications to the Rhombus layout were done. Delete and clear functions were implemented as additional characters and some other characters were added as shown in Figure 1. This layout contains 32 characters including delete and clear options. Letters were ordered depending on their occurrence in the English language. The selection of a letter requires navigating the cursor right, left, up and/or down until the desired letter is reached. This letter is then selected using the select command and presented at the bottom of the screen. Once a letter has been selected, the cursor starts over at the center position.

### 2.2 Visual stimulator

In a typical SSVEP-based BCI application, a custom made array with light emitting diodes (LEDs) flickering with different frequencies is normally used as stimuli [12]. The flickering frequencies are generated using a microcontroller. In this case, the user should switch his attention between looking at the lights and receiving the visual feedback provided on the screen. Therefore, a visual stimulator integrated to the speller application was needed. The stimulator consists of 5 objects called VLEDs (virtual LEDs) that flicker to a desired frequency on the computer screen. The state of the VLED is changed in constant intervals. VLED properties like color, text, and frequency can be changed in a configuration file before starting the application. The flickering frequency is produced by software based on timers; one timer is needed for each VLED. Timer intervals are calculated in seconds as follows:

$$\text{Interval} = \frac{1}{2 \times f_{\text{LED}}} \tag{1}$$

Where $f_{\text{LED}}$ is the flickering frequency of the VLED.

### 2.3 Software architecture

The software framework Qt was used for developing the spelling program and the integrated visual stimulator. Qt supports 2D graphics applications by incorporating a broad set of rendering, texture mapping, animations, special effects, and other powerful visualization functions. For a better understanding of this software, an UML (Unified modelling language) [14] class diagram is shown in Figure 2. This model follows an object oriented design and its implementation is in C++. The spelling program consist of the following classes:

- CMainApplication: Main window widget class. It inherits from the QWidget class. A widget is the base element in Qt and the base class of all user interface objects. CMainApplication receives the commands sent by the BCI via TCP/IP. It contains a CTCPServer and a CSpeller object.

- CSpeller: This class is responsible for displaying the spelling layout and five flickering boxes. It is based on the graphics view framework of Qt. Graphics view provides a surface for managing a large number of 2D graphical items. The spelling layout consist of a matrix of QGraphicsTextItems with 32 characters and a matrix of QGraphicsRectItems that represents the cursor. The matrix of QGraphicsTextItems and QGraphicsRectItems are created and added to a QGraphicsScene, that serves as a container for QGraphicsItems. QGraphicsScene is used together with QGraphicsView for visualizing the items. The cursor highlights the character at the current position and responds to four commands, left, right, up and down. When the command “select” is sent, the current character is written on the QLineEdit at the bottom of the screen. The cursor is moved or a letter is selected at the current cursor position depending of the received command. The speller class also provides acoustic feedback when a character is selected and when the cursor is moved. A QTimer is needed to update the state of the VLEDs; this timer is set with a timeout of 0. It means that it will time out as soon as all events in the window system’s event queue have been processed. VLEDs are QGraphicsRectItems and inherit from the QGraphicsItem class; the member function setVisible() was used to perform the flickering action.

- CTCPServer: TCP/IP server class. This class receives the commands sent by the Bremen BCI. The protocol of communication is TCP/IP (Transmission Control Protocol/Internet Protocol). The spelling program is started as server and waits until the BCI connects to start flickering the VLEDs objects. Commands are strings. As soon as a command is received, the speller class maps this command into a cursor movement or character selection.

- CLed: This class holds all VLED properties like flickering frequency, position on the screen, shape, color, text and size. An object of the class CTimer is needed for changing the current visible state of the VLED.

- CTimer: Timer class. It is used to change the state of a VLED. If the state member variable is true the VLED is shown, otherwise it is hidden. In this way the flickering frequency is generated. Timers are started with specific intervals depending of the desired flickering frequency. An event is sent each time the timer finishes counting.

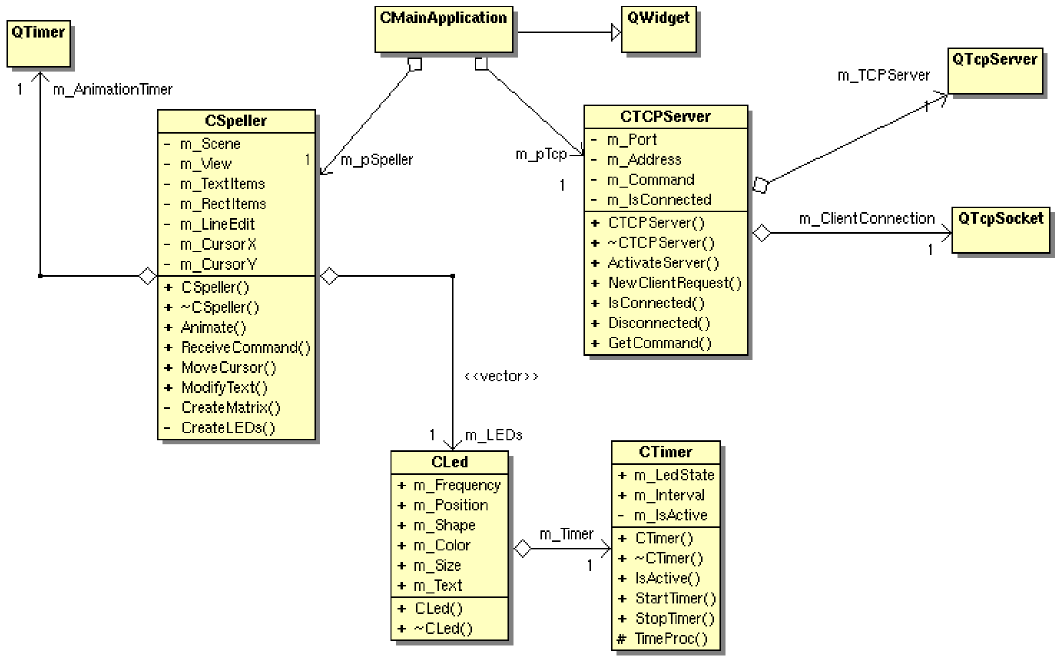


Figure 2: UML class diagram of the integrated spelling program and visual stimulator. This application was implemented in C++ and based on the Qt4 software framework.

# 3 Results

The result of this work is a spelling program with an integrated visual stimulator presented on the screen. The frequency of each flickering box was measured with a standard analog oscilloscope. The voltage was measured on a phototransistor, which is a device that reacts to light changes. The frequency was then calculated as the number of oscillations per second. The goal of the study was to test the performance of the system across a large number of subjects and in non-laboratory conditions. To accomplish that, the integrated speller was used during the CeBIT 2008 in Hanover. A total of 106 healthy subjects in the ages 18–79 years were recruited from our booth visitors. All data were recorded from sites $PO_3$, $PO_4$, $O_9$, $O_{10}$, $O_z$ and $P_z$ aligned with the standard 10–20 system of electrode placement. Data were referenced to site $FC_z$ with a ground at site $AF_z$. They were given the task to write 4 phrases chosen by the experimenter and one free spelling phrase chosen by the subject. The order in which these phrases were spelled was determined randomly. The accuracy and time needed to spell the 5 phrases are reported in Table 1. The response column shows the number of subjects who could perform the task. The accuracy was calculated only for the subjects who spelled the desired phrase, or the desired phrase with some errors. Studying the remaining subjects, the average accuracy was calculated as the number of spelled letters divided by the number of errors. In some cases, subjects made used of the delete and clear functions but it did not affect the accuracy. It was looked at their skill at spelling the whole message. Thus, backspaces were ignored. These results show that the most spelled word was BCI. In contrast, only 34 subjects spelled BRAIN COMPUTER INTERFACE. Results showed a main spelling accuracy of 92.2 % and main response of 53 participants. It means that at least 50 % of the participants could spell effectively. 65 % of the participants could at least write one of the phrases while 35 % of the participant could not spell at all. The reason for this is that some subjects had weak SSVEP responses and therefore signals could not be well detected by the BCI. Another reason could be that the stimulus was not strong enough because of bad lighting conditions to produce SSVEP responses.

| Task | Response | Accuracy (%) | Time (s) |
|---|---|---|---|
| BCI | 69 | 88.5 | 122.1 |
| BRAIN COMPUTER INTERFACE | 34 | 92.5 | 460.7 |
| SIREN | 53 | 92.5 | 111.1 |
| CHUG | 49 | 93 | 139.3 |
| FREE SPELLING | 62 | 94.3 | 204.2 |
| AVERAGE | 53 | 92.2 | 208.5 |

Table 1: BCI spelling performance.

## 4 Discussion

The integrated speller program was evaluated across a large number of subjects who had no prior experience with BCI control. Results showed that most of the subjects could spell effectively with the system. It is known that there is considerable inter-subject variability across different BCI approaches [5]. But this topic was not the goal of this study. In this work, the software used to produce a visual stimulator on a computer screen integrated with a spelling application was evaluated. Therefore problems related with the software are stated here. For example, problems with the real-time accuracy of the timers used to generated the stimulation frequencies were experimented. As explained before, the stimulator works showing and hiding VLEDs objects on the screen at certain intervals. Qt provides the QTimer class for high-level programming interface for timers. Unfortunately, under Windows environment QTimer can not provide a very high resolution with high accuracy since QTimer depends on the underlying operating system and hardware. Windows 98 has 55 millisecond accuracy; other systems can handle 1 millisecond intervals [11]. If Qt is unable to deliver the requested number of timer clicks, it will silently discard some, making the flickering process slow. In order to get the desired flickering frequency, the Multimedia Timer from Windows API was chosen, because of its high accuracy while maintains its resolution. But in any case, timers depend on the operating system and hardware. Windows or Linux are not, in their native form, real-time operating systems. For either of these operating systems, it is not possible to get a reliable timer interval. Setting thread priorities only minimizes this effect.

In order to get smooth animation, i. e. avoiding nuisance lines on the flickering animation, all graphical objects on the screen must be rendered in regards to the vertical synchronization of the screen monitor. Fortunately, desktop windows manager of Windows Vista (by which the Aero effect of Windows Vista relies on) provides convenient way to handle this matter. The integrated spelling program was running on a PC compatible laptop with a 15.4" TFT ($1280 \times 800$) monitor display and Intel Core 2 Duo ($2 \times 1.50$ GHz) processor running Windows Vista. For our system the maximum synthesizable frequency is 30 Hz. Beyond this limit, the frequencies are unstable. The drawbacks using the computer to produce an SSVEP stimulator are low luminance, light reflection on the screen from other light sources and unstable frequencies. Since light intensity will affect subject's SSVEP response, it is preferable to create virtual LED animation which is big enough covering the screen without overlapping the Rhombus layout.

## 5 Conclusion

The software architecture of a visual stimulator integrated to a spelling application has been presented and the robustness of the system has been evaluated. It was found that an integrated stimulator captures constant attention of the user and produces fewer spelling errors than a custom array of LEDs. The location of the virtual LEDs was an important aspect, because it made easier for the user to encode the commands and control the system. It was found that a population of 65 % could spell effectively, subjects achieved a mean spelling accuracy of 92.2 %.

## References

[1] J. R. Wolpaw, N. Birbaumer, D. J-McFarland, G. Pfurtscheller, and T. M. Vaughan. Brain-computer interfaces for communication and control. *Clin. Neurophysiol.*, 113(6):767–791, 2002.

[2] D. Regan. *Human Brain Electrophysiology: evoked Potentials and Evoked Magnetic Fields in Science and Medicine.* Elsevier, New York, 1989.

[3] C. Herrmann. Human EEG responses to 1–100 hz flicker: resonance phenomena in visual cortex and their potential correlation to cognitive phenomena. *Exp. Brain Res.*, 137(3-4):346–353, 2001.

[4] M. Middendorf, G. McMillan, G. Calhoun, and K. Jones. Brain-computer interfaces based on the steady-state visual-evoked response. *IEEE Trans. Rehabil. Eng.*, 8(2):211–214, 2000.

[5] M. Cheng, X. Gao, S. Gao, and D. Xu. Design and implementation of a brain-computer interface with high transfer rates. *IEEE Trans. Biomed. Eng.*, 49(10):1181–1186, 2002.

[6] G. R. Müller-Putz, R. Scherer, C. Brauneis, and G. Pfurtscheller. Steady-state visual evoked potential (SSVEP)-based communication: impact of harmonic frequency components. *J. Neural Eng.*, 2(4):123–130, 2005.

[7] S. P. Kelly, E. C. Lalor, C. Finucane, G. McDarby, and R. Reilly. Visual spatial attention control in an independent brain-computer interface. *IEEE Trans. Biomed. Eng.*, 52(9):1588–1596, 2005.

[8] Y. Wang, R. Wang, X. Gao, B. Hong, and S. Gao. A practical VEP-based brain-computer interface. *IEEE Trans. Neural Syst. Rehabil. Eng.*, 14(2):234–239, 2006.

[9] O. Friman, I. Volosyak, and A. Gräser. Multiple channel detection of steady-state visual evoked potentials for brain-computer interfaces. *IEEE Trans. Biomed. Eng.*, 54(4):742–750, 2007.

[10] D. Valbuena, M. Cyriacks, O. Friman, I. Volosyak, and A. Gräser. Brain-computer interface for high-level control of rehabilitation robotic systems. *10th Int. Conf. Rehabil. Robotics – ICORR*, pages 619–625, 2007.

[11] Trolltech. Qt: Cross-platform rich client development framework. `www.trolltech.com/products/qt`, 2008.

[12] O. Friman, T. Lueth, I. Volosyak, and A. Gräser. Spelling with steady-state visual evoked potentials. *3rd Int. IEEE/EMBS Conf. Neural Eng.g*, pages 354–357, 2007.

[13] E. Donchin, K. M Spencer, and R. Wijesinghe. The mental prosthesis: assessing the speed of a P300-based brain-computer interface. *IEEE Trans. Rehabil. Eng.*, 8(2):174–179, 2000.

[14] Object Management Group. UML Unified Modeling Language. `www.uml.org`, 2008.

# Benchmarking common BCI algorithms for fast-paced applications

C. Kothe, T. O. Zander

Department of Psychology and Ergonomics, Chair for Human-Machine Systems, Team PhyPA, Berlin Institute of Technology, Berlin, Germany

{cko,tza}@mms.tu-berlin.de

**Abstract**

A core subject in contemporary brain-computer interface (BCI) research is the discrimination of electroencephalogram (EEG) patterns correlated to hand movements, both executed and imagined. In this context, methods of statistical machine learning have recently proven to be very successful. Yet, the field is still lacking a large-scale objective comparison of these methods. Thus, the heart of this study is the objective evaluation and comparison of several of the most important methods for BCI. We have split this task into two parts: The first one, which is presented here, focuses on executed hand movements in a context chosen for its applicability with respect to BCI usage in human-machine systems (HMS), giving upper performance bounds for these applications. The second one focuses on control via imagined movements. We have realized a homogeneous experimental design and used a representative sample of people, in order to give consideration to the inter-individual and inter-experimental variability of the EEG data. The data basis consists of 32 channel EEG, electrooculogram, electromyogram, noise level and ambient temperature data, measured under highly controlled conditions for 43 naive and healthy subjects. We compared feature extraction methods for event-related (de)synchronization (ERD/ERS) – logarithmic Band-power, Common Spatial Patterns (CSP), Spectrally Weighted CSP, and for Contingent negative variation – SCP Pattern Matching and CSP for SCP. Also, some of the most prevalent statistical classifiers – Support Vector Machines, Gaussian Mixture Models, (regularized) Linear Discriminant Analysis and (regularized) Quadratic Discriminant Analysis (QDA) have been compared against each other based on these EEG features. The primary evaluation measure was (nested) cross-validation error rate. The results show that SCP Pattern Matching outperforms ERD/ERS-based methods by a significant margin. Differences among classifiers were surprisingly insignificant, apart from plain QDA, whose bad performance could be attributed to overfitting.

## 1 Introduction

In this study, we investigated the performance of a selection of state-of-the-art BCI algorithms in an executed-movement scenario, chosen to allow for HMS-related predictions. Thus, we are giving upper bounds that can be used to generalize BCI performance to similar use cases. Machine learning methods were used exclusively, mostly because they are are suited for naive subjects and because they are nowadays widely used.

Due to the significant inter- and intra-individual variability in observed EEG patterns, this benchmarking survey was conducted on a large number of subjects. To date, few methods have been tested with data from more than a dozen subjects, so many of them have yet to become supported by statistically significant and representative results. Also, there is still a lack of publicly available EEG data sets that are applicable for method comparisons [1]. Therefore, one major contribution of this study is the acquisition and publication of EEG data from 43 naive subjects. To ensure internal consistency and quality of the data, all experiments have been conducted under highly controlled conditions. In addition to 32 channel EEG, electromyogram (EMG) and electrooculogram (EOG) data, as well as ambient temperature and noise level have been recorded, to provide fine-grained information over external effects. However, no data in the subsequent results had to be discarded due to artifacts. All data sets and results are available for open access on the website `www.phypa.org`, which will also serve as a hub for the publication of data by other researchers.

# 2 Experimental design

We followed an approach widely known as offline analysis [2]. This was done because it lends itself well to method comparisons, since the subject's behavior is not influenced by the performance of a particular algorithm, and multiple methods can later be compared based on identical data. Also, chaotic effects like the Loss of Controllability (LoC) [3] are avoided.

An experimental session consisted of 650 trials. During each trial, a black letter, randomly chosen from the set {L,R}, was displayed in front of a grey background for 700 ms, followed by a 300 ms pause showing just the background. The subjects were textually instructed to press the left (or right) Ctrl key, when an L (or R) was presented, and to react as quickly and accurately as possible. The inter-trial interval of 1000 ms was chosen to make the results applicable to more general HMS-like scenarios. For some of the investiaged methods, such as the CSP variants, this relatively fast-paced operation is a mostly unexplored territory.

# 3 Analysis

The offline evaluation followed a method known from machine learning as cross-validation (CV) [4], in which a classifier is repeatedly trained and tested on disjoint trial sets. Out of the several data partitioning variants, such as randomized CV, blockwise or chronological CV, we chose randomized $10 \times 10$-fold CV as it is the most widely used method in the current BCI field. For the estimation of meta-parameters, e. g. for regularization, we performed a $10\times$ repeated $10 \times 10$-fold nested CV.

Common to all examined BCI algorithms are the following steps: First, the raw EEG data for a trial is preprocessed in a strictly causal way. Then, a short feature vector is extracted from the preprocessed data. Finally, a classifier is employed to map from the feature vector to a binary decision value. Implementations closely correspond to their cited reference descriptions. The CSP and SpecCSP methods were successfully applied in several online control sessions in our lab e. g. via the well-known basket paradigm (see video on `www.phypa.org`). The SCP algorithm implementation was also validated in an upcoming online study.

The EEG features that enable the discrimination of left and right hand movements fall into two categories: Slow Cortical Potentials (SCPs) features, in our case the Contingent Negative Variation (CNV) [5], and Event-Related (De)Synchronization [6] (ERD/ERS, henceforth called ERD for brevity) features.

## 3.1 ERD feature extraction

It is well known from neuroscience that idle (sensori-) motor neurons tend to exhibit locally synchronous polarity oscillations which can be observed in the EEG channels above the motor cortex. Performance of motor actions causes this synchrony to break down and as a result, the measured amplitudes in the affected EEG channels drop accordingly. This can be used to infer the laterality of the ongoing motion. [6] In Figure 3 it can be seen that the measured ERD effects are in fact emitted from the motor cortex, and take place within some subband of 7–30 Hz, as is predicted by neurobiology.

**The log-BP algorithm** In this ERD-based feature extractor [7], the EEG data is first laplacian-transfomed, and then the logarithmic power spectral density (or band-power/BP) in some frequency sub range within [7–30 Hz] is calculated for each channel. The time is determined by the

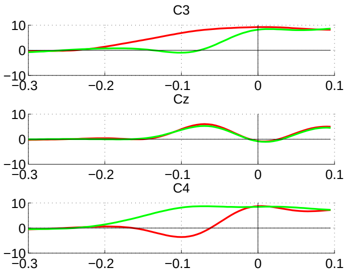


Figure 1: Event-related potentials (here: CNV) for both classes (red: left, green: right) over channels C3, Cz and C4. $y$-axis is in microvolts. Time is relative to the keypress.

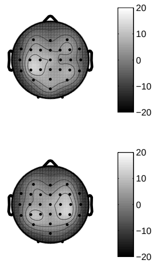


Figure 2: Cortical Topography of the SCP data for Left (top) and Right (bottom) class at $-0.08\,$s relative to keypress.

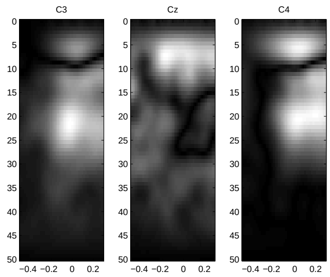


Figure 3: Spectral difference between left/right movements over time for channels C3, Cz and C4. The $y$-axis goes from 0 Hz (top) to 50 Hz (bottom). Brighter means more pronounced.

application of some appropriate window (in our case [-175 to 0 ms] prior to the key press). This gives a feature space of 32 dimensions.

**The CSP algorithm** A more complex feature extractor for ERDs is the Common Spatial Patterns (CSP) algorithm [8]. The idea of CSP is to find few, e. g. 4 to 6, linear combinations (patterns) of EEG channels such that the variance in each trial projected according to these patterns is most discriminative (i. e. differs maximally between the two classes). Subsequently, the EEG data for each trial is projected according to each of these patterns and then the log-PSD is calculated similarly to the logBP method, yielding 4 to 6 features.

**The SpecCSP algorithm** Unlike CSP, the variant Spectrally Weighted CSP (SpecCSP) [2] not only learns spatial patterns, but also frequency filters for each pattern, with bands weighted according to how much each band contributes to the discrimination of the classes.

Other common spectral variants of CSP, like CSSP and CSSSP were not investigated here, since they are by now basically superseded by SpecCSP, as was shown in [2].

## 3.2 SCP feature extraction

The SCPs, local low-frequency polarity changes (1–5 Hz) in the EEG, that we are interested in are typically located above the motor cortex. In these channels, a slow negativity (the CNV) can be observed prior to a movement. From the spatial distribution of this negativity the laterality of the upcoming movement can be inferred. [9] Figure 1 shows that the measured SCP features are in fact mainly driven by the CNV. Its location (Figure 2) is also consistent with neurobiologic predictions [5].

**The SCP algorithm** SCP features are the basis of the SCP feature extractor as proposed in [9]. Each channel is preprocessed by a short raised-cosine windowed FFT filter and then the average potentiation within four subsequent non-overlapping windows of 50 ms length each is retained prior to the key press. In total, the features extracted by this method are represented in a $4 \times 32 = 128$ dimensional space.

**The CSP for SCP algorithm** This algorithm attempts to reduce the complexity of the SCP feature space by first projecting the EEG channels down to a small set of meta-channels. This is done by a modified CSP algorithm, which optimizes for maximum discriminability according to deflection from zero, instead of variance [10].

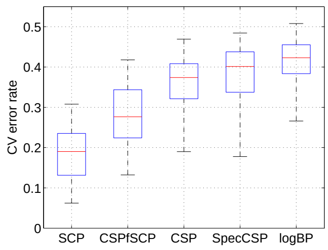


Figure 4: Performance of feature extraction methods with their respective best classifier.

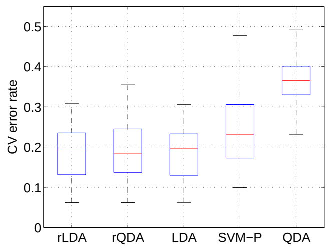


Figure 5: Performance of classifiers on SCP features.

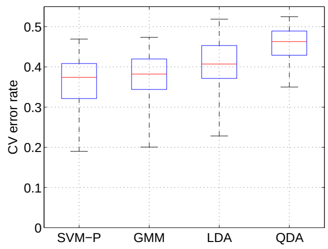


Figure 6: Performance of classifiers on CSP features.

### 3.3 Classifiers

Given a feature space, classifiers are required to perform the final inferential step from feature vectors to the binary decision values. Several classifiers were compared for this task.
Linear Discriminant Analysis (LDA) [11] is the simplest model, which is optimal as long as two requirements are met: First, the noise that gets projected into the feature space must be gaussian and uncorrelated to the class membership of each trial. And second, there must be a sufficient number of data points, which is dependent on the feature space dimension, because LDA relies on the estimation of covariance matrices for the feature distributions.
Quadratic Discriminant Analysis (QDA) [12] separates the data by a quadratic hyper surface and can be used if noise is class-correlated. Its downside is that it requires at least twice as many trials as LDA to work properly.
Regularized LDA or QDA (rLDA, rQDA) is often used when the number of trials is critically low [13], since here, the chance of overfitting is minimized.
Gaussian Mixture Models (GMMs) [4] model each class by a weighted mixture of different gaussians. Therefore, they require an even higher number of trials than QDA. The implementation is based on GMMBAYES.
Support Vector Machines (SVMs) [14] do not estimate the full covariance matrices for both classes. Therefore, they are relatively robust in the presence of few training trials. Also, they can be used in combination with the kernel trick. The polynomial kernel, specifically, is referred to as SVM-P in the following. The SVM implementation is based on LibSVM.

## 4 Results

Most noticable is that the ERD-based algorithms generally performed significantly worse than the SCP-based ones (Figures 4 and 7). Still, logarithmic band-power features (logBP) were outperformed by the more complex CSP and SpecCSP methods, as was expected. For SCP feature extractors, the faster variant of the SCP algorithm, CSP for SCP, performed slightly worse than the pure SCP algorithm. Figure 5, which compares different classifiers on SCP features, shows that the simplest classifier model, LDA, was not significantly worse than any other tested classifier, which is highly interesting. On the other hand, there are commonly used classifiers which failed hard on SCP features, especially plain QDA. Also, GMM failed to converge for too many subjects, so it could not be presented here.

## 5 Discussion

According to Figure 9, CSP significantly outperformed logBP. The former learns the subject-specific spatial projection of the signal, while the latter only has a static mapping between channels and features. This shows that there is critical inter-individual (and inter-experimental) variability

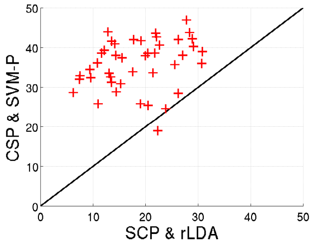


Figure 7: SCP versus ERD feature extractions, with their respective best classifier.

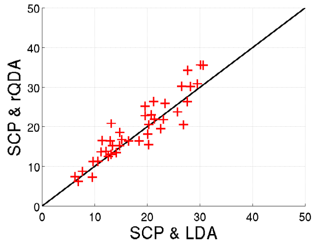


Figure 8: LDA versus the best non-linear classifier, on SCP features.

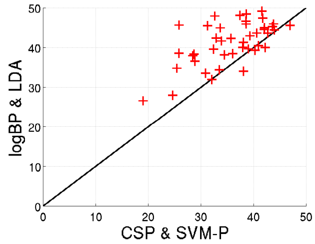


Figure 9: The benefit of adaptive versus static spatial filtering. CSP with its best classifier versus logBP with its best classifier.

in how the motor brain rhythms are projected across the cortex and onto features. Interestingly, the benefit of SpecCSP with respect to CSP, namely that it learns the frequency spectrum of the relevant brain rhythms, is hardly reflected in the results (Figure 4). This can be deduced to the difficulty of measuring the frequency spectra precisely, when the number of oscillations is small, as is the case here.

From the comparison of classifiers on SCP features, two important observations can be made. First, that none of the non-linear classifiers could outperform linear discriminant analysis, which is strong evidence that the data is in fact linearly separable (Figure 8). And second, that the danger of overfitting is high with these features, as was proven by the failure of QDA (Figure 5), and GMM, which was unable to build models on SCP, but worked comparatively well on ERD (Figure 6). Some regularized non-linear methods, such as SVMs with polynomial kernel and rQDA, however, handle the features expectedly well.

Concerning the ERD case (Figure 6), it can be seen that non-linear models did in fact perform better than linear models on CSP features. Also, since the feature space dimensionality is much lower at 4–6 dimensions, no method overfitted as dramatically as in the SCP case.

Figures 7, 8 and 9: One-vs-one comparisons. The position of each dot is determined by the average error rate of a single subject (the first method's error rate maps to vertical position, the second method's error rate maps to horizontal position; bottom left is best.)

# 6 Conclusion

The ERD-specific results (Figure 7) suggest that for the majority of subjects, the speed of the key-pressing movements is too high to allow for discriminative ERD. A recent offline study [15] comparing multiple tap rates (0.5 s, 1 s, 2 s) over six subjects shows similar results for self-paced executed movements. Thus, they are not yet ready for everyday motoric BCI control; neither offline, as shown here, nor online. On the other hand, we provide evidence that the sometimes neglected SCP-based algorithms are interesting for active control scenarios in which highly competitive information transfer rates and response latencies are demanded. Another important result of this study is that linear classifications models are among the best choices for some highly relevant motor BCI features.

# References

[1] B. Blankertz, K.-R. Müller, G. Curio, T. M. Vaughan, G. Schalk, J. R. Wolpaw, and et al. The BCI competition 2003: Progress and perspectives in detection and discrimination of EEG single trials.

[2] R. Tomioka, G. Dornhege, K. Aihara, and K.-R. Müller. An iterative algorithm for spatio-temporal filter optimization. In *3rd International BCI Workshop and Training Course*. Verlag der Technischen Universitaet Graz, 2006.

[3] S. Jatzev, T. O. Zander, M. De Filippis, C. Kothe, S. Welke, T. Fowinkel, and M. Roetting. Examining causes for non-stationarities 2: The loss of controllability is a factor which induces non-stationarities. In *Neuroscience*, San Diego, 2007.

[4] R. O. Duda, P. E. Hart, and D. G. Stork. *Pattern Classification (2nd Edition)*. Wiley-Interscience, November 2000.

[5] W. G. Walter, R. Cooper, V. J. Aldridge, W. C. Mccallum, and A. L. Winter. Contingent negative variation: An electric sign of sensorimotor association and expectancy in the human brain. *Nature*, 203:380–384, 1964.

[6] G. Pfurtscheller and Lopes. Event-related eeg/meg synchronization and desynchronization: basic principles. *Clin. Neurophysiol.*, 110(11):1842–1857, November 1999.

[7] G. Townsend, B. Graimann, and G. Pfurtscheller. A comparison of common spatial patterns with complex band power features in a four-class bci experiment. *IEEE Trans. Biomed. Eng.*, 53(4):642–651, April 2006.

[8] J. Müller-Gerking, G. Pfurtscheller, and H. Flyvbjerg. Designing optimal spatial filters for single-trial EEG classification in a movement task. *Clin. Neurophysiol.*, 110(5):787–798, 1998.

[9] B. Blankertz, G. Curio, and K.-R. Müller. Classifying single trial eeg: Towards brain computer interfacing. In *Advances in Neural Inf. Proc. Systems (NIPS 01)*, volume 14, pages 157–164, Jan 2002.

[10] G. Dornhege, B. Blankertz, and G. Curio. Speeding up classification of multi-channel brain-computer interfaces: Common spatial patterns for slow cortical potentials. In *Proceedings of the 1st International IEEE EMBS Conference on Neural Engineering. Capri 2003*, pages 591–594, January 2003.

[11] R. A. Fisher. The use of multiple measurements in taxonomic problems. *Annals Eugen.*, 7:179–188, 1936.

[12] C. Vidaurre, A. Schloegl, R. Cabeza, R. Scherer, and G. Pfurtscheller. Adaptive on-line classification for eeg-based brain computer interfaces with aar parameters and band power estimates. *Biomed. Tech.*, 50(11):350–354, 2005.

[13] J. H. Friedman. Regularized discriminant analysis. *J. Am. Stat. Assoc.*, 84(405):165–175, 1989.

[14] V. N. Vapnik. *Statistical Learning Theory*. Wiley-Interscience, September 1998.

[15] B. Blankertz, G. Dornhege, M. Krauledat, K.-R. Müller, V. Kunzmann, F. Losch, and G. Curio. The Berlin brain-computer interface: EEG-based communication without subject training. *IEEE Trans. Neural Syst. Rehabil. Eng.*, 14:147–152, 2006.

# Implementation of a realtime feedback system based on multichannel near-infrared spectroscopy

J. Kurzmann, S. C. Wriessnegger, C. Neuper

Department of Psychology, University of Graz, Austria

kurzmann@uni-graz.at

**Abstract**

In present neuroscience research there is an ongoing focus on feedback systems and their applications. Most of these feedback systems are based on the EEG. The alternative measurement method of brain activity via near-infrared spectroscopy (NIRS) provides the possibility of feedback research with this new imaging technology. In this paper we present the realization of a realtime feedback system based on a commercial multichannel recording hardware. The software was implemented with Simulink, providing the facility of an easy and flexible creation of feedback scenarios. For evaluation of the feedback system we collected exemplary data with a simple motor imagery paradigm. In three sessions nine participants were presented a sliding time bar with 40 alternating marked epochs of activation and rest, each lasting 20 s. Simultaneously to the presented cues, they could visually track their oxyhemoglobin concentration changes over the corresponding motor cortical areas online on the screen. The participants were instructed to enhance the feedback signal (i. e. the oxygenated hemoglobin level) through motor imagery during the activation, and to decrease it during rest epochs. Offline data analysis shows significant differences between the two conditions, supporting the supposition that individuals can bring the blood oxygenation levels of their cortex under voluntary control.

## 1 Introduction

In the past 35 years numerous studies have demonstrated that various parameters linked to human brain activity can be brought under voluntary control by means of operant conditioning. Neurofeedback, as this sophisticated form of biofeedback technique is often referred to, has meanwhile emerged to an established research field in neuroscience. Findings demonstrate the feasibility of learned self-regulation of EEG characteristic, such as evoked potentials [1], event-related potentials [2], slow cortical potentials [3], and EEG frequency components [4].
Besides EEG, neurofeedback systems have been also realized with functional magnetic resonance imaging (fMRI) [5]. Since temporal dynamics of the hemodynamic responses recorded with fMRI and near-infrared spectroscopy (NIRS) are highly correlated, as combined measurements have shown [6], the implementation of a NIRS feedback system appears very promising. Recent work has introduced developments for motor imagery based brain-computer interfaces (BCIs) with NIRS [7, 8], but up to the present there exists only one published realization of a NIRS BCI [9].
This paper presents the implementation of a realtime feedback system, based on a commercial NIRS system, which should give the opportunity to explore the potential and limits of NIRS neurofeedback in the context of feasibility and possible future clinical studies based on multichannel measurements. The article also includes a first evaluation of the feedback system in practice. The simple design was aimed to obtain exemplary data, that revealed promising results for further research, as well as demands for future improvements.

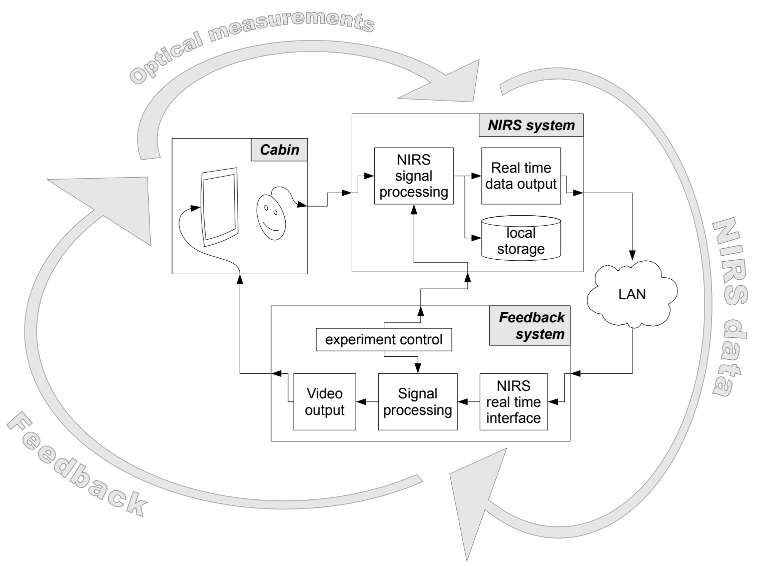


Figure 1: Flow chart of the implemented NIRS feedback system.

# 2 NIRS realtime feedback system

## 2.1 System design and data flow

The NIRS realtime feedback system (Figure 1) is based on a commercial 52 channel NIRS system (ETG-4000, Hitachi Medical Co., Japan) working in continuous wave mode at wavelengths 695 nm and 830 nm. Change in oxyhemoglobin (oxyHb) and deoxyhemoglobin (deoxyHb) concentrations are provided through the implemented algorithms and stored on the system. Over the provided "real time data output" module, data is simultaneously sent over the local area network (LAN) to the feedback system.

The feedback system itself is based on a standard PC (Intel Pentium 4 2.4 GHz, 1 GB RAM) as hardware, whereas data acquisition, signal processing, data output and control of the NIRS system are implemented in MathWorks Simulink on the software side. Its core component consists of the developed data acquisition extension (NIRETI "NIRS realtime interface"), which receives the data packages from the LAN and decodes them for further processing in Simulink. The feedback loop is closed by the generated visual output, which is displayed on the monitor. Optionally, the NIRS system can be controlled via serial connection with start, stop and trigger commands.

## 2.2 NIRS realtime interface (NIRETI)

The NIRS realtime interface is a Simulink data acquisition extension block for Hitachi's "real time data output" module. It converts the received TCP/IP packages to Matlab-native data types, providing the obtained data as Simulink output ports. The block provides soft realtime capabilities based on the RT-blockset [10]. Since the feedback system is running asynchronously on its own clock cycle, immediate signal propagation is not possible if TCP/IP data packages are delayed, and would result in a bucking feedback. To avoid this effect, the feedback system operates with an predefined offset of 200 ms behind the NIRS system, buffering the meantime received data package(s). This time delay assures that the buffer always holds at least one package, that can be decoded and allocated by the feedback system without idle time.

# 3 Materials and methods

## 3.1 Subjects

Nine healthy volunteers, 4 male and 5 female, participated in the study (mean age: 22±1.55). After a detailed description of the study, the subjects gave their informed consent to their participation. All participants had normal or corrected-to-normal vision and were right-handed.

## 3.2 Procedure

The experimental sequence can be subdivided into sessions, runs and trials. All subjects participated in 3 sessions, each taking place on a different day and lasting about 45 minutes. Within one session, they performed 3 runs. One run consisted of 20 trials, split into an activation and a rest period. Hence the experimental cue information presented on the monitor per run consisted of a sliding time bar with 40 alternating color coded epochs of activation (green) and rest (gray). The task of the subject was to increase the feedback signal during green marked epochs by a right hand motor imagery, and to decrease the signal during gray marked epochs by relaxation. In detail the experimental sequence of one run was as follows: After a baseline period of 30 seconds, a green bar appeared on the screen indicating an activation period. This period lasted 20 seconds and was followed by a rest period of also 20 seconds length which was indicated by a gray bar. This sequence was iterated 20 times. Altogether each subject performed three sessions (3 runs each) on three different days, resulting in overall 9 runs.
Additionally to the cue information (color coded bar), the subjects received feedback of their oxygenation levels of the corresponding motor cortical areas, so that they could simultaneously track the time course of their hemoglobin oxygenation above the bar. Data from the selected channels #4 and #9 (Figure 2B) was averaged, smoothed with a moving average (window length: 10 samples) and fed back to the subject. The feedback channels were chosen according to results of several pilot studies on motor imagery, showing the highest activation (oxyHb increase) over these channels (#4, #9) representative for hand areas of the contra lateral primary motor cortex (left hemisphere).
Figure 3 shows a condensed illustration of the described setting for a length of 5 minutes. During actual feedback, the participants could only track a time window of 120 seconds, being presented the oxyHb time course of the last minute, as well as a preview of the following cues of the next minute.

## 3.3 Measurements

Changes in optical density in the near-infrared range (700–1100 nm) at different wavelength are converted into changes in concentration of oxyHb and deoxyHb, respectively. A more detailed description of the NIRS technology can be found elsewhere [11, 12]. In the present study measurements were performed on a continuous wave system (ETG-4000, Hitachi Medical Co., Japan) using two $3 \times 3$ optode probe sets (consisting of 8 photo-detectors and 10 light emitters) resulting in a total number of 24 channels (Figure 2A). Sampling rate was set to 10 Hz.

The NIRS probe set of 24 channels was positioned over the right and left sensorimotor cortex. According to the international 10–20 system we used Cz position as a marker for ensuring replicable placements of the optodes. The middle detectors (#16 and #12) of the probe sets were placed symmetrically beside Cz, covering representative hand areas of the primary motor cortex of both hemispheres (EEG positions C3 and C4).

## 3.4 Offline data analysis

The offline processing of the NIRS data can be subdivided into the following steps: drift correction, averaging of channels 4 and 9 and segmentation of activation and rest sections. Drift correction of the recorded signal was accessed by subtraction of a forward and reverse filtered moving average

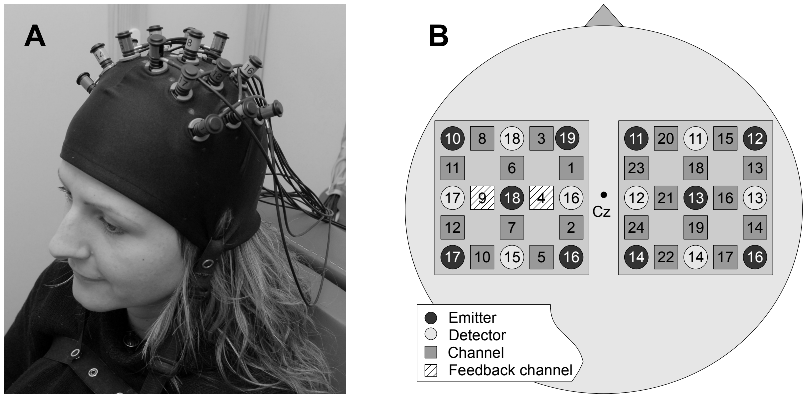


Figure 2: A: Illustration of the optode montage of one subject. B: Channel configuration of the optode probe set ($3 \times 3$).

(window length: 400 samples) . The resulting continuous data was averaged over channels #4 and #9, divided into activation and rest periods and $z$-transformed for intersession comparisons. For the plotted illustrations, the grand averages over different sets of sessions was built and smoothed by a moving average window of 5 samples length.
To compare activation periods with rest periods two $2 \times 3 \times 3$ analysis of variance (ANOVAs) for repeated measures were performed on the variables oxyHb and deoxyHb separately. The ANOVA design included the within subject factors CONDITION (activation, rest), SESSION (1, 2, 3) and RUN (1, 2, 3).

# 4 Results

Figure 3 shows a condensed illustration of the online feedback time course exemplary for the first 5 minutes of one run (of one participant). Noticeable in this illustration are higher oxyHb levels at activation than at rest periods, as well as a superposed signal drift.

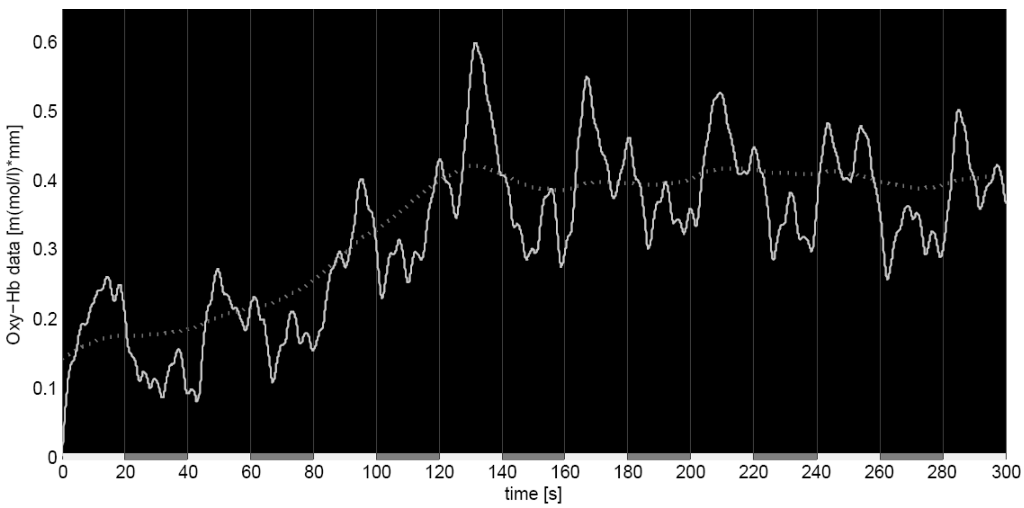


Figure 3: Continuous oxyHb raw data of the first 5 minutes of one run. Activation periods (light) and rest periods (dark) are marked in the time bar. The dotted line visualizes the signal drift detected and removed in offline analysis.

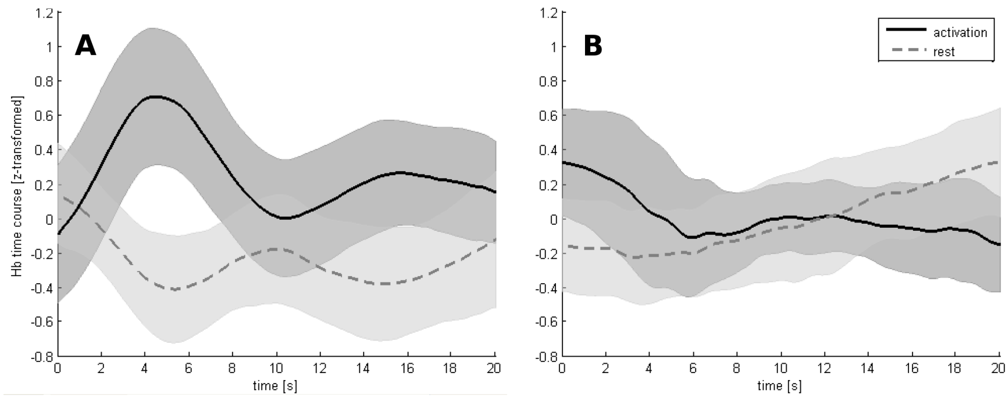


Figure 4: Mean oxyHb (A) and deoxyHb (B) concentration changes and standard deviation bands during activation (solid lines) and rest period (dotted lines), grand averaged over all sessions of all participants.

For offline analysis the repeated measurements ANOVA of oxyHb concentration means revealed one significant main effect CONDITION ($F(1,9) = 31.831$; $p < 0.001$). The main effect represents the highly significant increased oxyHb concentration during activation period (mean = $0.265 \pm 0.125$ (normalized), $0.01269 \pm 0.00778$ mmol·mm/l) compared to rest period (mean = $-0.251 \pm 0.117$ (normalized), $-0.01240 \pm 0.00725$ mmol·mm/l). The response pattern is predominantly consistent for all participants, showing an oxyHb response of 10 seconds length with a clear peak at second 5 during activation period and inverted characteristics with lower amplitude for the rest condition (Figure 4A). Only two subjects were able to hold the oxyHb concentration at a high level during the entire interval of 20 s. DeoxyHb concentration, which was not presented during feedback is only marginally modulated (Figure 4B) and provides no significant results.

# 5 Discussion

In this paper we presented a realization of a NIRS realtime feedback system based on a commercial recording hardware. Key features of this system are its multichannel functionality (24 channels), a minimal feedback signal delay of 200 ms, and the possibility of an easy customization through the chosen implementation platform Simulink.

The system has been proven to work well with the presented implementation of a simple motor imagery paradigm with realtime feedback of oxyHb concentrations of the motor cortical areas. Results of the present study show that with the aid of this feedback oxyHb concentrations could be significantly increased over rest levels. In this context it is remarkable that all subjects show a very consistent and clear pattern for oxyHb concentrations in either activation and rest period, while in contrast deoxyHb levels, which have not been fed back, are only marginally, not significantly modulated. Oxygenation onset latencies of about 2 seconds that can be observed in motor imaginary compared to motor execution [13], vanish in our experimental setup with feedback. This difference can also be seen, when comparing our results to typical peak location of motor imagery response [9, 7] and gives further evidence for the feedback's influence.

However this study remains preliminary and was mainly intended for just a functional evaluation of the feedback system. For follow-up studies pertaining to NIRS feedback itself, some important enhancements are necessary, such as simultaneous recording of electromyogram (in context of motor imagery), as well as electrocardiogram and respiration measurements to control their influence on the NIRS signal. Larger numbers of sessions are essential to address the issue of training effects. Further enhancements include a larger number of participants, as well as the use of a non-contingent control group, especially for specifying the role of feedback. For clarifying the individual feedback performance, one could further introduce a sequence of activation and rest periods of randomized lengths. We expect that feedback responders could adapt to the changing time conditions, while non-responders show a constant response pattern to the varying stimuli. Special focus for future applications will also state the development of methods for online artifact correction. As a simple approach for online elimination we suggest the use of differential signals for feedback, e. g. region of interest against rest of channels, which is planned for follow-up studies.

# 6 Conclusion

This work has successfully demonstrated the feasibility of a multichannel NIRS realtime feedback system, but further research is needed to investigate the potentials of NIRS feedback and its application.

# References

[1] J. P. Rosenfeld, A. P. Rudell, and S. S. Fox. Operant control of neural events in humans. *Science*, 165(895):821–3, 1969.

[2] N. Birbaumer, T. Elbert, B. Rockstroh, and W. Lutzenberger. Biofeedback on event-related potentials of the brain. *Int. J. Psychol.*, 16:359–415, 1981.

[3] T. Elbert, B. Rockstroh, W. Lutzenberger, and N. Birbaumer. Biofeedback of slow cortical potentials. *Electroencephalogr. Clin. Neurophysiol.*, 48(3):293–301, 1980.

[4] A. Y. Kaplan, J. J. Lim, K. S. Jin, B. W. Park, J. G. Byeon, and S. U. Tarasova. Unconscious operant conditioning in the paradigm of brain-computer interface based on color perception. *Int. J. Neurosci.*, 115(6):781–802, 2005.

[5] N. Weiskopf, R. Veit, M. Erb, K. Mathiak, W. Grodd, R. Goebel, and N. Birbaumer. Physiological self-regulation of regional brain activity using real-time functional magnetic resonance imaging (fMRI): methodology and exemplary data. *Neuroimage*, 19(3):577–86, 2003.

[6] T. J. Huppert, R. D. Hoge, S. G. Diamond, M. A. Franceschini, and D. A. Boas. A temporal comparison of BOLD, ASL, and NIRS hemodynamic responses to motor stimuli in adult humans. *Neuroimage*, 29(2):368–82, 2006.

[7] R. Sitaram, H. Zhang, C. Guan, M. Thulasidas, Y. Hoshi, A. Ishikawa, K. Shimizu, and N. Birbaumer. Temporal classification of multichannel near-infrared spectroscopy signals of motor imagery for developing a brain-computer interface. *Neuroimage*, 34(4):1416–27, 2007.

[8] H. Zhang and C. Guan. A kernel-based signal localization method for NIRS brain-computer interfaces. In *18th Int. Conf. Patt. Recogn.*, pages 1158–1161, Hong Kong, 2006.

[9] S. M. Coyle, T. E. Ward, and C. M. Markham. Brain computer-interface using a simplified functional near-infrared spectroscopy system. *J. Neural Eng.*, 4(3):219–226, 2007.

[10] L. Daga. Rt blockset, `http://digilander.libero.it/LeoDaga/Simulink/RTBlockset.htm`, 2007.

[11] Y. Hoshi. Functional near-infrared optical imaging: utility and limitations in human brain mapping. *Psychophysiol.*, 40(4):511–20, 2003.

[12] H. Obrig and A. Villringer. Beyond the visible – imaging the human brain with light. *J. Cereb. Blood Flow Metab.*, 23(1):1–18, 2003.

[13] S. Wriessnegger, J. Kurzmann, and C. Neuper. Spatio-temporal differences in brain oxygenation between movement execution and imagery: A multichannel near-infrared-spectroscopy study. *Int. J. Psychophysiol.*, 67(1):54–63, 2008.

# Reducing the blood pressure influence on characteristic hemodynamic responses: a preliminary NIRS study

G. Bauernfeind[1], R. Leeb[1], C. Neuper[1,2], G. Pfurtscheller[1]

[1]Institute for Knowledge Discovery, BCI Lab, Graz University of Technology, Graz, Austria
[2]Institute of Psychology, University of Graz, Graz, Austria

g.bauernfeind@tugraz.at

**Abstract**

Near-infrared spectroscopy (NIRS) is a non-invasive optical technique for the assessment of functional activity in the human brain. With NIRS characteristic hemodynamic responses (changes in oxy- and deoxyhemoglobin concentration) during cognitive, visual, or motor tasks can be measured. In order to determine whether the recorded signal is due to a local cortical activation or to a global response of the cardiovascular system, it is essential to identify systemic influences. In the present study we report on heart rate and blood pressure (BP) changes of two subjects during periodic, cue-paced brisk finger movements performed in 10 s and 13 s intervals and investigate the influence of these changes on simultaneously recorded brain oxygenation changes. Furthermore, we present signal processing approaches to reduce systemic influences in the recorded NIRS signals. The results show a strong influence of the BP on the hemodynamic response. In the uncorrected data, the hemodynamic response shows unexpected differences for 10 s and 13 s intervals, respectively. After removing the BP influence, the responses result in similar time courses for both intervals. The proposed method to eliminate slow BP oscillations (around 10 s) from the NIRS signal may be very useful to increase the signal to noise ratio in optical Brain-Computer interface and other applications.

## 1 Introduction

The near-infrared spectroscopy (NIRS) is a non-invasive optical technique for the assessment of functional activity in the human brain and allows the measurement of characteristic hemodynamic responses during cognitive, visual or motor tasks. These characteristic responses can be detected and used to control e. g. an external device. A strong limitation of the use of hemodynamic responses for an optical Brain-Computer interface (BCI) is, however, the nature of the response, which is in the range of some seconds. A further challenge is the classification of single trial data. For this it is essential to improve the signal to noise ratio (SNR) and to decrement false classifications which occur primarily due to misclassification of physiological noise. A spectral analysis of the optical signal reveals various quasi-periodic physiological rhythms, such as cardiovascular, vascular, respiratory and blood pressure (BP) rhythms [1], which may influence the recorded signals [2, 3, 4]. These rhythms cause additional changes in the hemodynamic signal and may superimpose the changes caused by cerebral activation. The frequency of the pulse waves is in the range between 1 Hz (60 bpm) and 2 Hz (120 bpm). The respiration frequency lies around 0.25 Hz (15 breaths per minute) and the Mayer-Traube-Hering waves (MTH) [5], which are 3$^{rd}$ order BP waves, occur with a frequency around 0.1 Hz [3, 4]. The goal of this paper is to investigate the influence of these rhythms on recorded changes in oxy- ($HbO_2$) and deoxyhemoglobin (Hb) during periodic brisk finger movement execution. Another aim is to propose appropriate signal processing approaches to reduce the systemic influences in the recorded NIRS signals.

# 2 Methods

## 2.1 Subjects and experiment

The investigations were carried out on two 28 year old right-handed subjects (S01, S02). The subjects were seated in a comfortable arm-chair. The right index finger of the subjects was wrapped in aluminum foil, resting on an inductive sensor to detect the required finger movements.
The experiment consisted of the following task: The participants had to execute a brisk finger extension/flexion each time a cue stimulus (red arrow) appeared on screen (distance between the subjects and the screen was approximately 130 cm). In one session the cue was presented periodically in 10 s intervals, in a second session in 13 s intervals. Both sessions comprised 60 repetitions.

## 2.2 Recording

All signals described later were recorded with a sampling frequency of 500 Hz and downsampled to 10 Hz after the following preparation steps.

### 2.2.1 Systolic and diastolic blood pressure

For BP recording a continuous non-invasive BP monitoring system (CNAP$^{TM}$ Monitor 500, CN-Systems Medizintechnik AG, Austria) was used. The BP was measured on the proximal limp of the left index or middle finger (automatic alternating). The measuring method is based on the vascular unloading technique (for a detailed description of the method see [6]) and delivers a BP signal without interruptions. From the BP recording the systolic and diastolic BP signals were extracted, linearly interpolated and resampled to the recording frequency to obtain equidistant signals (Figure 1A). Subsequently the relative event-related systolic and diastolic BP changes (in %) were calculated by averaging the changes across all trials of each task (referenced to the mean systolic or diastolic BP).

### 2.2.2 Instantaneous heart rate

For the data recording a commercial biosignal amplifier (g.tec, Guger Technology OEG, Graz, Austria) was used. The electrocardiogram (ECG) was recorded bipolar from electrodes placed on the thorax (sensitivity 2 mV) and filtered between 0.5 and 100 Hz. From the ECG the beat-to-beat intervals (RR intervals in ms) were calculated. Afterwards the RR intervals time series was transformed into the heart rate (HR) (in bpm), linearly interpolated, resampled to the recording frequency and displayed as instantaneous HR (IHR) (Figure 1B). The relative event-related HR change (in %) was then calculated by averaging the IHR across all trials of each task (referenced to the mean HR).

### 2.2.3 Respiration

The respiration patterns (Figure 1C) of the subjects were obtained by using a piezo respiratory effort sensor (Pro-Tech Inc., Mukiteo, USA). The sensor was fitted individually; for data recording the biosignal amplifier (sensitivity 2 mV, high pass 0.01 Hz, low pass 100 Hz) was used.

### 2.2.4 Brain oxygenation (NIRS recording)

For recording the brain oxygenation a custom made one-channel near infrared spectroscopy system was used [4]. The sources and the detector were placed on the frontal cortex 1.5 cm to the left and right of position FP1 according to the international 10/20 system for EEG recording. Unfortunately with the custom made system only measurements over the frontal region are practicable. The system measures hemodynamic concentration changes in $HbO_2$ and Hb (Figure 1D) during mental tasks (details see [4]). After calculating Hb and $HbO_2$ a digital 3 Hz low pass Butterworth filter of order 5 with an attenuation of 30 dB in the stop band was used. Afterwards a 0.01 Hz high pass filter was used to remove baseline drifts.

### 2.3 Removing the pulse, the respiratory and the blood pressure related influences

The pulse can be removed from the hemodynamic concentration changes by using a cardiac pulse removal algorithm [3] or, as implemented in this work, by low pass filtering (a 0.6 Hz low pass Butterworth filter of order 4 with 60 dB in the stop band was used). By using the signals obtained by the respiratory effort sensor and the diastolic blood pressure ($\mathrm{BP_{dia}}$), transfer function models [7] were applied to remove the BP- and respiratory-related influence. These models are of the form

$$\mathrm{X}\left[n\right] = \sum_{u=0}^{m} g_u \mathrm{Y}\left[n-u\right] + \mathrm{N}\left[n\right] \tag{1}$$

where X refers to the time series of the signal and Y to the respiration or blood pressure rhythms. The term

$$\sum_{u=0}^{m} g_u \mathrm{Y}\left[n-u\right] \tag{2}$$

stands for the influence and N is the signal without the influence. By minimizing the mean squared error $\mathrm{E}\left(\mathrm{N}^2\left[n\right]\right)$ the parameters $g_u$ of the transfer function where estimated

$$\gamma_{xy}\left(-j\right) = \sum_{u=0}^{m} g_u \gamma_{yy}\left(u-j\right) \tag{3}$$

with $j = 0, 1, 2, ..., m$ where $\gamma_{xy}$ is the autocovariance function of $\mathrm{Y}\left[n\right]$ and $\gamma_{xy}$ is the cross-covariance function between $\mathrm{X}\left[n\right]$ and $\mathrm{Y}\left[n\right]$.
At least one needs to find the optimal value of $m$ in equation (2). According to [8] the values for $m$ were chosen between 5 and 15. With the calculated parameters of $g_u$ it was now possible to compute the signal without influence

$$\mathrm{N}\left[n\right] = \mathrm{X}\left[n\right] - \sum_{u=0}^{m} g_u \mathrm{Y}\left[n-u\right] \tag{4}$$

For further information on this algorithm see [8].

### 2.4 Correlation of blood pressure and brain oxygenation

The cross-correlation between the brain oxygenation, the $\mathrm{BP_{dia}}$ and the HR was calculated after HP-filtering (0.01 Hz, to remove baseline drifts) of the $\mathrm{BP_{dia}}$ and HR signal. After searching for the maximal correlation and the corresponding time shift the cross-correlation coefficient, also known as the "product-moment coefficient of correlation", (time shift considered) between the signals was calculated using the "Pearson's correlation". The significance of the correlation was calculated by testing the null hypothesis that the "product-moment correlation coefficient" is zero using Student's t-test on the statistic $t = r \cdot \frac{\sqrt{N-2}}{\sqrt{1-r^2}}$ where $N$ is the number of samples [9].

## 3 Results

In Figure 2B the corrected (elimination of respiratory related influence [8]) movement related HR changes for the 10 s and 13 s datasets show an initial deceleration followed by an acceleration. The thick line represents the mean HR and the thin lines the mean HR $\pm$ standard error (SE). The vertical line at second three indicates the time point of the cue. Figure 2C shows the averaged relative $\mathrm{BP_{dia}}$ changes (in %) of each subject. The mean task related concentration changes of $\mathrm{HbO_2}$ and Hb (in mmol $\cdot$ mm) after removing the respiratory influence are displayed in Figure 2A. The two concentrations display nearly the same time shifted changes as found in the $\mathrm{BP_{dia}}$. Table 1 shows the result of correlation analysis (maximal correlation and corresponding time shift) between

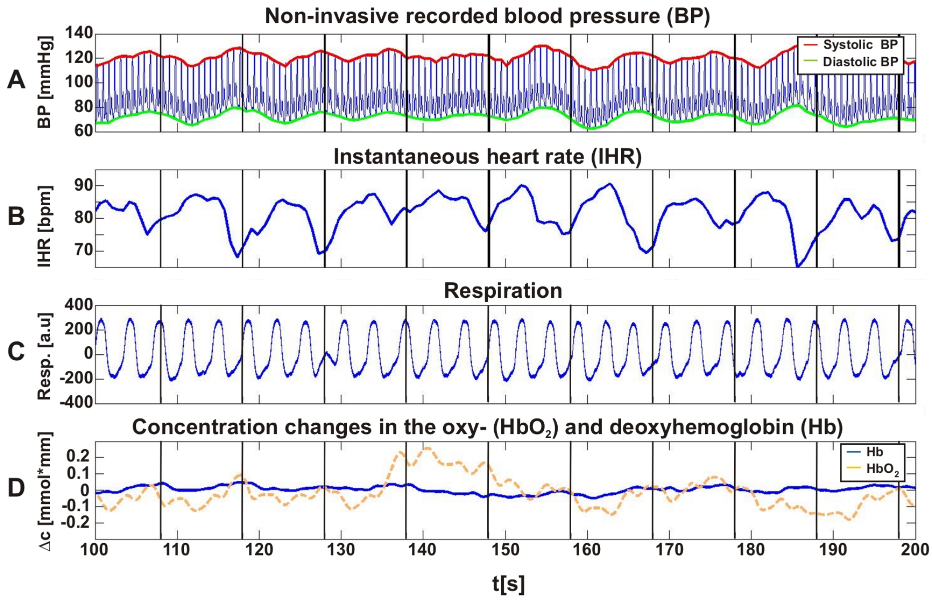


Figure 1: Examples of recorded signals: (A) Noninvasively recorded continuous BP signal with calculated systolic (red line) and diastolic (green line) BP course. (B) Linear interpolated IHR. (C) Recorded respiration pattern. (D) Concentration changes of $HbO_2$ and Hb. The black vertical lines indicate the onset of the cues.

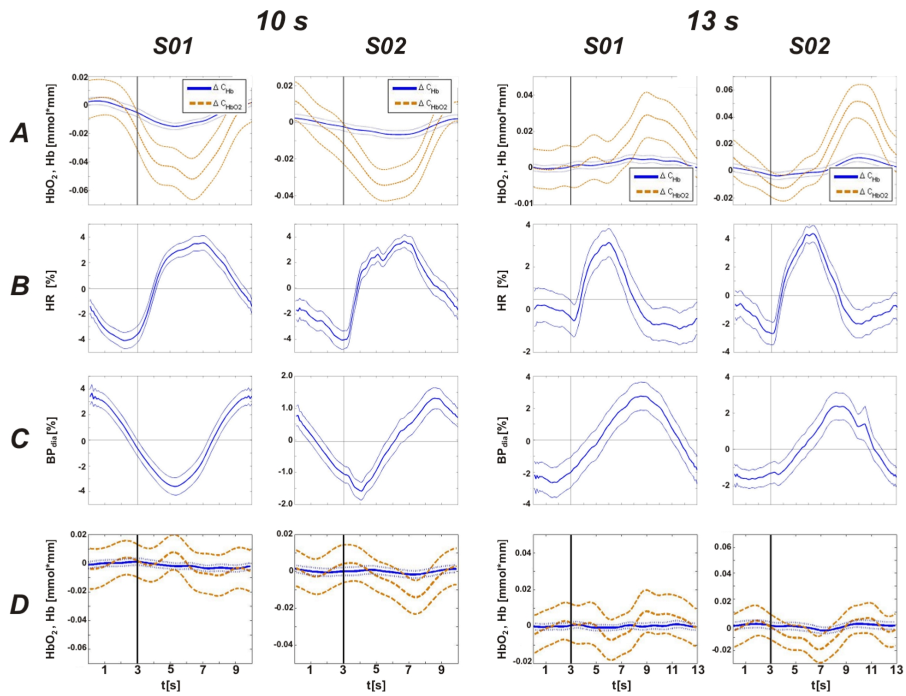


Figure 2: Task-related changes (mean ± SE) (A) $HbO_2$ and Hb (mmol · mm), (B) HR (%) and (C) $BP_{dia}$ (%) of subject S01 and S02. (D) Task-related concentration changes of $HbO_2$ and Hb after removing the BP influence. The line at second three indicates the onset of the cue stimulus.

the whole time series of concentration changes ($HbO_2$ and Hb) and $BP_{dia}$. In Figure 2D one can see the mean task related changes of $HbO_2$ and Hb (in mmol · mm) of the two subjects after eliminating the $BP_{dia}$ influence.

| subjects | | S01 | | S02 | |
|---|---|---|---|---|---|
| task | | 13 | 10 | 13 | 10 |
| $HbO_2$ | $r$ | $0.27^{**}$ | $0.38^{**}$ | $0.53^{**}$ | $0.40^{**}$ |
| | $\Delta t$ | 0.7 s | 0.7 s | 1.5 s | 1.4 s |
| Hb | $r$ | $0.60^{**}$ | $0.41^{**}$ | $0.56^{**}$ | $0.35^{**}$ |
| | $\Delta t$ | 0.1 s | 0.2 s | 1.5 s | 1.5 s |
| HR | $r$ | $0.64^{**}$ | $0.59^{**}$ | $0.29^{**}$ | $0.36^{**}$ |
| | $\Delta t$ | 4.0 s | 3.9 s | 2.5 s | 2.5 s |

Table 1: Maximal cross-correlations and time shifts between $BP_{dia}$ and $HbO_2$, Hb or HR, respectively. All correlations marked with ** are significant on the level of $p < 0.001$.

# 4 Discussion

In the present study the influence of BP rhythms on changes in $HbO_2$ and Hb during periodic brisk finger movement is investigated and a method to reduce these systemic influences is shown. The analysis of the task-related $HbO_2$ and Hb shows a strong correlation ($p < 0.001$) with the BP signal (Table 1). Visual inspection of Figure 2A reveals that this influence obviously causes different $HbO_2$ and Hb changes, a decrease of both concentrations in the case of 10 s and an increase of both in the case of 13 s periodic finger movement. The HR (Figure 2B) displays an anticipatory deceleration with an acceleration during the motor action in the case of 10 s and 13 s finger movement. In contrast to the HR, the motor actions are associated with a decrease of the BP during 10 s, but with an increase during 13 s periodic finger movement (Figure 2C). Depending on the stimulation frequency the BP oscillations display a maximum up to 4.0 seconds after the HR oscillation. Additionally a further delay up to 1.5 seconds between BP wave (diastolic pressure) and the $HbO_2$ and Hb oscillations was found. Similar periodic responses (oscillations) were found in the HR, BP and concentration changes of $HbO_2$ and Hb during 10 s and 13 s finger movement. This is not surprising, because "central commands" result in a strong drive into the brain stem (for review see [10]). In the brain stem not only the cardiovascular nuclei and the respiratory center but also the blood pressure control loops are affected. The central commands, the cardiac efferents in the brain stem [1], the modulation of arterial baroreflex sensitivity, the reflex responses to mechanically induced changes in arterial BP, the chemoreceptor influences and others are responsible for the BP and NIRS oscillations with periods of 10 and 13 seconds, respectively. An explanation of the different phases of HR, BP and NIRS oscillations may be the "relative coordination" of different oscillation systems as described by von Holst [11]. After eliminating the $BP_{dia}$ influence from the $HbO_2$ and Hb concentration changes, by using the described method, both datasets display similar changes during the motor action (a slight decrease of the $HbO_2$ concentration). Inspection of Figure 2 reveals that the oscillations deviate from the sinusoidal form; therefore, the elimination of the BP oscillation out of the NIRS signal results in an periodic residual signal (Figure 2D). Whether this reflects the task-related response in the NIRS signal can only be speculated. A reason could be that the cue was presented periodically in 10 s and 13 s intervals, thus overlaps with MTH wave frequency and $3^{rd}$ order BP waves. So it can not be ruled out that maybe some parts of the hemodynamic responses are eliminated by the method as well. To clarify this issue, further research with continuous BP recording on a larger group using different tasks is necessary. Further a rest time should be included for better comparison. For an optical BCI it is important that the elimination of slow BP oscillations around 10 s in the NIRS signal is principally possible.

Additional it is of interest to explore whether self-paced movement at free will may be triggered by the oscillations. It is also relevant to investigate ultra slow changes in the alpha band [12] and the cortical excitability cycle, respectively.

**Acknowledgments:** This work was funded by the NeuroCenter Styria, the EU Project PRESENCCIA IST- 2006-27731 and the EU Cost BM0601 action. The authors also would like to thank CNSystems Medizintechnik AG, Austria for providing the non-invasive blood pressure monitoring system, R. Ortner for implementing the elimination method and P. Linortner for data recording.

# References

[1] H. P. Koepchen. Physiology of rhythms and control systems: an integrative approach. In H. Haken and H. P. Koepchen, editors, *Rhythms in physiological systems: an integrative approach*, pages 3–20. Springer, 1991.

[2] C. E. Elwell, R. Springett, and E. Hillman. Oscillations in cerebral haemodynamics – implications for functional activation studies. *Adv. Exp. Med. Biol.*, 471:57–65, 1999.

[3] S. Coyle, T. Ward, and C. Markham. Physiological noise in near-infrared spectroscopy: implications for optical brain computer interfacing. *Engineering in Medicine and Biology Society, 2004. IEMBS '04. 26th Annual International Conference of the IEEE*, 6:4540–4543, 2004.

[4] G. Bauernfeind, R. Leeb, S. Wriessnegger, and G. Pfurtscheller. Development, set-up and first results of a one-channel near-infrared spectroscopy system. *Biomed. Tech.*, 53:36–43, 2008.

[5] R. W. De Boer, J. M. Karemaker, and J. Strackee. On the spectral analysis of blood pressure variability. *Am. J. Physiol. Heart Circul. Physiol.*, 251:H685–H687, 1986.

[6] J. Fortin, W. Marte, R. Grüllenberger, A. Hacker, W. Habenbacher, A. Heller, C. Wagner, P. Wach, and F. Skrabal. Continuous non-invasive blood pressure monitoring using concentrically interlocking control loops. *Comp. Biol. Med.*, 36(9):941–957, 2006.

[7] M. B. Priestley. *Spectral Analysis and Time Series; Volumes 1 and 2.* Academic Press, 1981.

[8] G. Florian, A. Stancák, and G. Pfurtscheller. Cardiac response induced by voluntary selfpaced finger movement. *Int. J. Psychophysiol.*, 28:273–283, 1998.

[9] M. R. Spiegel and L. J. Stephens. *Schaum's Outline of Statistics, Fourth Edition.* McGraw-Hill, 2007.

[10] A. J. M. Verberne and N. C. Owens. Cortical modulation of the cardiovascular system. *Prog. Neurobiol.*, 54:149–168, 1998.

[11] E. von Holst. Die relative Koordination als Phaenomenon und als Methode zentralnervöser Funktionsanalyse. *Ergebnisse der Physiologie, biologischen Chemie und experimentellen Pharmakologie*, 42:228–306, 1939.

[12] G. Pfurtscheller. Ultralangsame Schwankungen innerhalb der rhythmischen Aktivität im Alpha-Band und deren mögliche Ursachen. *Pflügers Archiv*, 367:55–66, 1976.

# Continuous brain-actuated control of an intelligent wheelchair by human EEG

F. Galán[1,2], M. Nuttin[3], D. Vanhooydonck[3], E. Lew[1,4], P. W. Ferrez[1], J. Philips[3], J. del R. Millán[1,4]

[1]IDIAP Research Institute, Martigny, Switzerland
[2]University of Barcelona (UB), Spain
[3]Katholieke Universiteit Leuven (KUL), Belgium
[4]Swiss Federal Institute of Technology Lausanne (EPFL), Switzerland

jose.millan@idiap.ch

**Abstract**

The objective of this study is to assess the feasibility of controlling an asynchronous and non-invasive brain-actuated wheelchair by human EEG. Three subjects were asked to mentally drive the wheelchair to 3 target locations using 3 mental commands. These mental commands were respectively associated with the three wheelchair steering behaviors: turn left, turn right, and move forward. The subjects participated in 30 randomized trials (10 trials per target). The performance was assessed in terms of percentage of reached targets calculated in function of the distance between the final wheelchair position and the target at each trial. To assess the brain-actuated control achieved by the subjects, their performances were compared with the performance achieved by a random BCI. The subjects drove the wheelchair closer than 1 meter from the target in 20 %, 37 %, and 7 % of the trials, and closer than 2 meters in 37 %, 53 %, and 27 % of the trials, respectively. The random BCI drove it closer than 1 and 2 meters in 0 % and 13 % of the trials, respectively. The results show that the subjects could achieve a significant level of mental control, even if far from optimal, to drive an intelligent wheelchair, thus demonstrating the feasibility of continuously controlling complex robotics devices using an asynchronous and non-invasive BCI.

## 1 Introduction

Brain-computer interfaces (BCI) research aims at operating mentally a variety of devices [1, 2, 3, 4, 5, 6, 7]. Our work is focused on developing asynchronous and non-invasive EEG-based brain-computer interfaces for continuous control of robots and wheelchairs [6, 8]. These BCI systems allow users to control such robotics devices spontaneously, at their own pace without needing any external cue that drives the interaction. To do so the users learn to voluntary modulate EEG oscillatory rhythms by executing different mental tasks (i. e., mental imagery) that are associated to different steering commands. We facilitate this learning process selecting those stable user-specific EEG features that maximize the separability between the EEG patterns associated to each mental task. Furthermore, we implement shared control techniques between the BCI and the intelligent wheelchair to assist the subject in the driving task [9, 10]. This paper describes one experiment that shows the feasibility of mentally controlling an intelligent wheelchair.

## 2 Methods

### 2.1 EEG data acquisition

Data was recorded with a portable Biosemi acquisition system using 64 channels sampled at 512 Hz and high-pass filtered at 1 Hz. Then, the signal was spatially filtered using a common

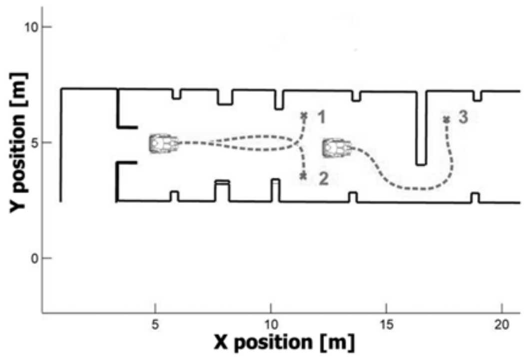


Figure 1: Indoor environment utilized in the experimental task. The subjects were asked to drive the wheelchair to targets 1, 2 and 3. The figure also depicts the initial positions and ideal trajectories for each target. $x$- and $y$-axis in meters.

average reference (CAR) before estimating the power spectral density (PSD) in the band 8–46 Hz with 2 Hz resolution over the last 1 second. The PSD was estimated every 62.5 ms (i. e., 16 times per second) using the Welch method with 5 overlapped (25 %) Hanning windows of 500 ms. Thus, an EEG sample was a 1344-dimensional vector (64 channels times 21 frequency components).

Obviously, not all these 1344 features are used as control signals. Section 2.3 describes the algorithms to estimate the relevance of the features for discriminating the mental commands and the procedure to select the most stable discriminant features that are fed to the classifier embedded in the BCI. This classifier processes each of the EEG samples and the BCI combines 8 consecutive responses to deliver a mental command every 0.5 seconds.

## 2.2 Experimental task and analysis

Three subjects were asked to mentally drive the wheelchair to reach 3 target locations while avoiding obstacles (see Figure 1). Reaching a target is a more complex task than simply navigating. This experiment is more challenging in a second respect, namely subjects cannot manoeuver back the wheelchair if they overshot the target by more than 2 meters, thus missing the correct turn. If this is the case, the trial was considered a failure. The motivation for this experiment is to assess how well naive (or almost naive) subjects can mentally drive the wheelchair along "almost" optimal trajectories. To measure the performance of our brain-actuated wheelchair we have compared the final position of the wheelchair with the end point of the desired trajectory. In particular, we have calculated the percentage of reached targets as a function of the distance between the final wheelchair position and the target at each trial. Furthermore, to assess the degree of mental control achieved by the subjects, their performances were compared with that of a random BCI utilized as a baseline – i. e., the wheelchair was driven by such a random BCI.

Subject 1 had previous experience in mentally driving in simulated environments but no experience driving the wheelchair, subject 2 had previous experience in mentally driving the simulated and real wheelchair (3 days). Subject 3 did not have any previous driving experience. Each subject, and the random BCI, participated in 30 randomized trials (10 trials per target). To drive the wheelchair, subjects 1 and 2 utilized the following three mental commands: imagination of a left hand movement, words associations and rest. These mental commands were respectively associated with the three wheelchair steering behaviors: turn left, turn right and move forward. Subject 3 utilized different mental commands: words associations, arithmetic operations and rest, associated with the aforementioned steering behaviors, respectively.

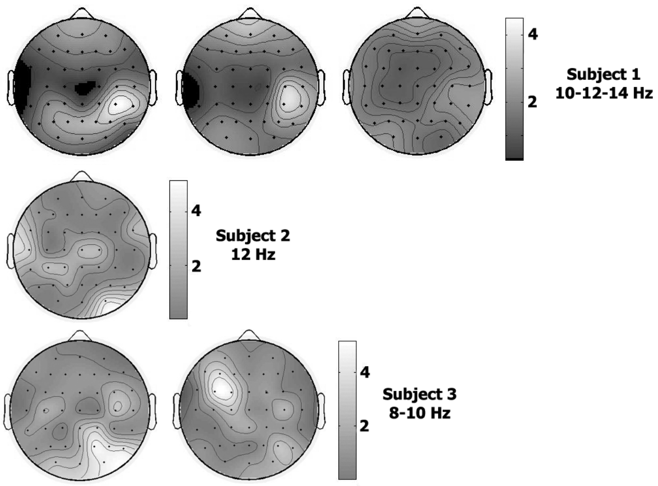


Figure 2: Electrode contribution in % for each selected frequency component for each subject.

## 2.3 Calibration sessions and EEG feature extraction

The three subjects participated in 20 calibration sessions utilized to extract subject specific stable discriminant EEG features and build a BCI classifier (statistical Gaussian classifier, see [6] for details) for each subject. In these sessions, the subjects sat in a chair looking at a fixation point placed in the center of a monitor. The subjects were asked to execute the three mental tasks in a counterbalanced order informing the operator when they started executing the task. Each calibration session was integrated by 6 trials each, 2 trials per class. Each trial lasted for 7 seconds but only the last 6 were utilized in the analysis to avoid preparation periods where the subjects were not yet engaged in the execution of the mental task. During these sessions the subjects did not received any feedback.

The feature extraction procedure was the same than that utilized in other experiments involving a simulated wheelchair [8]. The data from the 20 calibration sessions were grouped in 4 blocks (B1, B2, B3 and B4) of 5 consecutive sessions. Taking into account the recordings timing, we built different configurations of training and testing sets (train-test): B1–B2, B1–B3, B1–B4, B2–B3, B2–B4, B3–B4, (B1+B2)–B3, (B1+B2)–B4, (B1+B2+B3)–B4. Feature extraction was done in a sequential way, where we first pick stable frequency components and then chose the best electrodes. To assess the stability of the frequency components we applied 21 canonical variates analysis (CVA) [11], one per frequency component, on the training set of each configuration. For each canonical space we ranked the electrodes according to their contribution to this space. Then, we built up to 15 LDA classifiers, each using those electrodes that contributed more than $c\,\%$, with $c \in \{1.0, 2.0, \ldots, 15.0\}$ (see [11] for more details). We used the stability of the classifier accuracy over the different configurations to select the frequency components. In particular, we selected those frequencies that performed systematically among the top 5. Afterwards, for each selected frequency, we took the configuration of electrodes (out of the 15 possible ones) that yielded the highest classification accuracy on the configuration (B1+B2+B3)–B4. Finally, we tested the different combinations of selected frequencies (with their associated electrodes) on the configuration (B1+B2+B3)–B4 and chose the best one. At the end of this sequential process the selected frequencies were $\{10, 12, 14\}$ Hz for subject 1, $\{12\}$ Hz for subject 2, and $\{8, 10\}$ Hz for subject 3. Figure 2 depicts the electrodes contribution, for each selected frequency component for each subject. Finally, we built the statistical Gaussian classifier for each subject using their individual selected features from all the data of the calibration sessions. The reasons for using a LDA classifier for feature extraction rather than the final Gaussian classifier were the simplicity and speed of training of the former. Furthermore, LDA is a special case of our Gaussian classifier.

### 2.4 EEG features and EOG/EMG offline analysis

To assess whether the experimental subjects were using eye movements or muscular activity components embedded in the EEG as control signals, electromyogram (EMG) was recorded from subjects 1 and 2 (subjects that executed imagination of left hand movement to turn left). Bipolar EMG was recorded using 2 surface electrodes placed on the forearm muscle Extensor Digitorum. Bipolar electrooculogram (EOG) was measured from the three subjects using 2 surface electrodes placed below and laterally to the left eye respectively. The PSD was estimated for EMG and EOG using the same procedure as for EEG (see Section 2.1).

If there were EMG and EOG components embedded in the EEG utilized as control signals, these components would not be equiprobably distributed over the mental commands recognized by the BCI (i. e., the embedded statistical Gaussian classifier). To visually explore how they were distributed, the 21 frequency components estimated from EMG and EOG of each subject (only EOG in the case of subject 3) were utilized to built a canonical space (utilizing all samples from the 30 trials) according to the mental commands recognized by the BCI. Then all the samples were projected in the canonical space. Finally, an LDA classifier was applied to assess the separability of the mental commands. Figure 3 shows the canonical space for each subject built using both the EEG features utilized as control signals (left column) as well as the EOG and EMG frequency components (right column). As expected, the mental commands distributions recognized by the statistical Gaussian classifier are highly separable in the canonical space when it is built with the EEG features (see Figure 3, Left). This is reflected by the LDA classification accuracies: 76.34 %, 71.81 % and 76.50 % for subjects 1, 2 and 3, respectively. However, the mental commands distributions are not separable when the canonical space is built with the EOG and EMG frequency components (see Figure 3, Right), what means that they are uniformly distributed among the mental commands. In this case, the LDA classification accuracies are close to chance level: 41.08 %, 38.04 % and 35.75 %, for subjects 1, 2 and 3, respectively. All together, these results show that the experimental subjects did not utilize eye movements or muscular activity components embedded in the EEG as control signals.

## 3 Results

Figure 4 shows the percentage of targets reached by each subject and the random BCI as a function of the distance between the final wheelchair position and the target at each trial. The results reflect the importance of previous experience in order to successfully drive the wheelchair. Subject 2, who had previous driving experience with both the simulated and the real wheelchair, brought it closer to the targets. On the contrary, subject 3, who did not have any previous driving experience, had more difficulties to place the wheelchair close to the targets. Subject 1, who had only previous experience in simulation, achieved an intermediate performance.

Despite the different driving performances among subjects, the three of them showed a significant degree of mental control of the wheelchair, which requires rather fast and accurate decisions. For instance, to drive the wheelchair to target 3, the most difficult one, the subject needs to pass through of the narrow passage in the opposite direction, right, and then immediately make a sharp turn to the left. It's also worth noting that the subjects missed quite a few times targets 1 and 2 because they tried to reach them following a straight line and the collision avoidance behavior of the wheelchair (for details see [9, 10]) pushed the wheelchair away from the target. As shown in Figure 1, the optimal trajectory is not straight, but the subjects needed some time to learn appropriate driving strategies compatible with the behavior of the intelligent wheelchair.

To measure the degree of mental control exhibited by the subjects, and to show the complexity of the task, we run an experiment where the wheelchair was driven by a random BCI (i. e., the mental steering command – left, right, or forward – was selected randomly every 0.5 seconds). The performance of such a random BCI was such that it never brought the wheelchair closer than 1 meter from the target whereas subjects 1, 2 and 3 did it in 20 %, 37 % and 7 % of the trials, respectively. The subjects' level of mental control is even higher when we consider the percentage

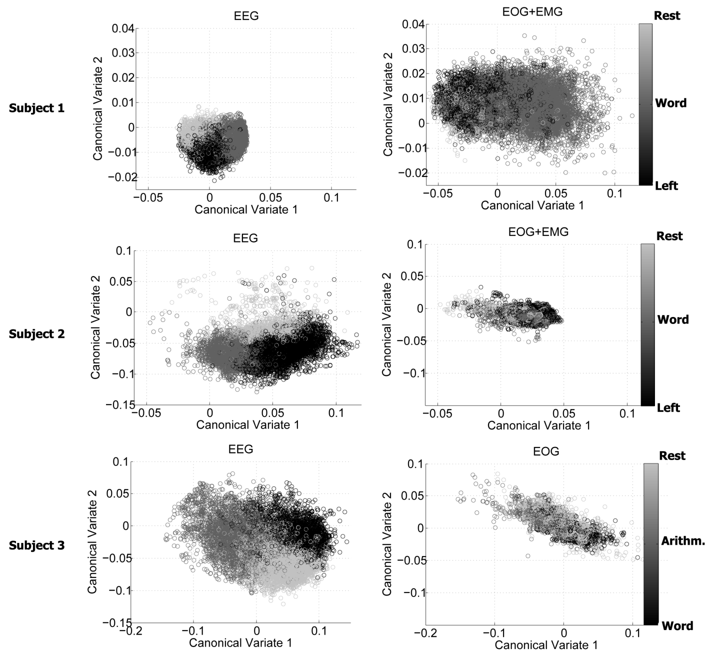


Figure 3: Left: canonical spaces built using the EEG features utilized as control signals. Right: canonical spaces built using the EOG+EMG (subjects 1 and 2) or EOG (subject 3) frequency components. All canonical spaces built according to the mental commands recognized by the BCI (statistical Gaussian) classifier.

of trials where the wheelchair was driven closer than 2 meters from the target. In this case, subjects 1, 2 and 3 achieved the task in 37 %, 53 % and 27 % of the trials, whereas the random BCI did it only in 13 % of the trials.

# 4 Conclusions

The results of this experiment show that subjects can operate our asynchronous EEG-based BCI to control a wheelchair, task that requires rather fast and accurate decisions. Also, they can autonomously operate the BCI without the need for adaptive algorithms externally tuned by a human operator to minimize the impact of EEG non-stationarities. However, the performances seem to be lower than the obtained with the simulated version of the wheelchair [8]. Moreover, subjects 1 and 2, who had previous experience with the simulated wheelchair, report that it is

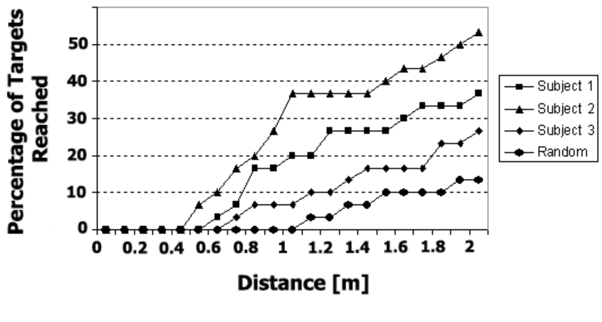


Figure 4: Percentage of reached targets by each subject and the random BCI as a function of the distance between the final wheelchair position and the target (distance in meters).

more difficult to drive the real wheelchair because of its more complex behavior. Nevertheless, it is worth noting that the performance of the subjects, even the naive subject, is significantly better than a random BCI. This proves that the intelligent wheelchair cannot achieve the task by itself, but requires appropriate mental commands delivered by the subject at the right times.

In summary, these results show that subjects can rapidly achieve a significant level of mental control, even if far from optimal, to drive an intelligent wheelchair, thus demonstrating the feasibility of continuously controlling complex robotics devices using an asynchronous and non-invasive EEG-based BCI.

**Acknowledgments:** This work was supported in part by the European IST Programme FET Project FP6-003758 (MAIA) and by the Swiss National Science Foundation through the NCCR "IM2".

## References

[1] N. Birbaumer, N. Ghanayim, T. Hinterberger, I. Iversen, B. Kotchoubey, A. Kübler, J. Perelmouter, E. Taub, and H. Flor. A spelling device for the paralysed. *Nature*, 398:297–298, 1999.

[2] B. Obermaier, G. R. Müller, and G. Pfurtscheller. Virtual keyboard controlled by spontaneous EEG activity. *IEEE Trans. Neural Syst. Rehabil. Eng.*, 11:422–426, 2003.

[3] J. D. Bayliss. Use of the evoked potential P300 component for control in a virtual apartment. *IEEE Trans. Neural Syst. Rehabil. Eng.*, 11:113–116, 2003.

[4] J. del R. Millán. Adaptive brain interfaces. *Comm. ACM*, 46:75–80, 2003.

[5] M. A. Nicolelis, and J. K. Chapin. Controlling robots with the mind. *Sci. Am.*, 287:46–53, 2002.

[6] J. del R. Millán, F. Renkens, J. Mouriño, and W. Gerstner. Noninvasive brain-actuated control of a mobile robot by human EEG. *IEEE Trans. Biomed. Eng.*, 51:1026–1033, 2004.

[7] J. M. Carmena, M. A. Lebedev, R. E. Crist, J. E. Doherty, D. M. Santucci, D. F. Dimitrov, P. G. Patil, C. S. Henriquez, and M. A. L. Nicolelis. Learning to control a brain-machine interface for reaching and grasping by primates. *PLoS Biol.*, 1:193–208, 2003.

[8] F. Galán, M. Nuttin, E. Lew, P. W. Ferrez, G. Vanacker, J. Philips, and J. del R. Millán. A brain-actuated wheelchair: Asynchronous and non-invasive brain-computer interfaces for continuous control of robots. *Clin. Neurophysiol.*, to appear.

[9] J. Philips, J. del R. Millán, G. Vanacker, E. Lew, F. Galán, P. W. Ferrez, H. Van Brussel, and M. Nuttin. Adaptive shared control of a brain-actuated simulated wheelchair. In *Proc. 10th Int. Conf. Rehabil. Robotics*, 2007.

[10] G. Vanacker, J. del R. Millán, E. Lew, P. W. Ferrez, F. Galán, J. Philips, H. Van Brussel, and M. Nuttin. Context-based filtering for assisted brain-actuated wheelchair driving. *Comp. Intell. Neurosci.*, 2007, Article ID 25130, 2007.

[11] F. Galán, P. W. Ferrez, F. Oliva, J. Guàrdia, and J. del R. Millán. Feature Extraction for Multi-class BCI using canonical variates analysis. In *Proc. 2007 IEEE Intl. Symp. Intell. Signal Process.*, 2007.

# Brain-computer communication: navigating freely through a virtual environment using two mental tasks

R. Ron-Angevin, F. J. Liebana-Castellano, A. Diaz-Estrella

Dpto. Tecnología Electrónica, University of Málaga, Málaga, Spain

rra@dte.uma.es

**Abstract**

One of the main applications of a Brain-Computer Interface (BCI) is for the control of a wheelchair. To this end, it is very important to guarantee a high level of classification accuracy. The choice of a wrong command due to a classification error can have important consequences, inducing to very dangerous situations. The main purpose of this paper is to introduce a new type of BCI, based on virtual reality techniques, that enable to navigate through a VE using four different navigation commands: turn right, turn left, move forward and move back. To reduce the probability of misclassification, the BCI is controlled by only two mental tasks. Three untrained subjects participated in the experiments following an initial training based on 3 sessions. Two of them were able to navigate through the VE discriminating between imagination of right hand movements and relaxed state, improving their performance over the runs.

## 1 Introduction

A Brain-Computer Interface (BCI) translate the intent of a subject measured directly from brain signals into control commands. Recently, BCI research is targeted for motion disabled people's rehabilitation, existing many BCI applications to control a virtual environment (VE). The goal of this research is to have a BCI as a real world application for the control of a wheelchair. However, to get this objective it is necessary to train subjects to get a good control of the BCI, being necessary to provide safe environments to learn how to operate a wheelchair. Motor imagery has been used successfully to navigate within different VEs. Some of the most significant works reported in this field allow navigating through a VE only in two directions. Since only two classes are discriminated (e. g. left hand versus right hand movement imagery task [1], right hand versus foot movement imagery task [2, 3, 4], foot imagery task versus rest period [5]), only two navigation commands are possible (e. g. turn right or left, move forward or stop). To explore an environment or to navigate through a virtual world, at least 3 different commands are necessary: turn right, turn left and move forward. In [6], a BCI system is proposed to navigate freely through a virtual apartment using only two motor imagery tasks. The system automatically guided the subject to each junction and then, the subject could only select between two possible directions: right–straight, left–straight or right–left.

A possible way to increase the number of navigation commands allowing to explore a virtual world is by moving from a binary decision to a more diverse decision, giving a choice between more options [7], for example, increasing the number of mental tasks. Very recently, the Graz group has reported on a BCI system which was able to discriminate between three brain states to navigate through a VE [8]. Many studies have reported that an increasing number of classes resulted in a decrease of the classification accuracy [7, 9]. These studies suggest that the highest classification accuracy is achieved by classifying only two classes.

One of the BCI applications to navigate through a VE is focused on the possibility of controlling an external device as a wheelchair. To this end, it is very important to guarantee a high level of classification accuracy, because the choice of a wrong command due to a classification error can have important consequences, inducing to very dangerous situations.

The main purpose of this paper is to introduce a new type of BCI, based on virtual reality techniques, that enables to navigate through a VE using four different navigation commands: turn right, turn left, move forward and move back. As proposed in [7] and [9], to reduce the probability of misclassification, the BCI is controlled by only two mental tasks. The used paradigm to select a specific command is based on the methodology used in the design of the typewriter Hex-o-spell developed within the BBCI project [10]. In this paradigm, the different navigation commands are surrounding a circle. A bar in the center of the circle is continuously rotating. The subject controls the bar extension to reach the chosen command.

# 2 Methods

## 2.1 Subjects and data acquisition

Three subjects, named S1, S2 and S3 (2 male, 1 female, right handed, age $24.6 \pm 1.43$), participated in this study. None of them had any previous experience in BCI, and all were selected independently of their initial ability to control EEG signals. The EEG was recorded from two bipolar channels with electrodes placed over the right and left hand sensorimotor area. Active electrodes were placed 2.5 cm anterior and posterior to electrode position C3 and C4 according to the 10/20 international system. The reference electrode was placed at FPz position. Signals were amplified by a 4 channel Coulborn V75-08 amplifier and then digitalized at 128 Hz by a 12 bit resolution data acquisition card DAQCard-6025E (National Instruments).

## 2.2 Initial training

Before using the BCI system to explore the VE, subjects had to follow an initial training based on the training paradigm proposed by Graz group [11]. The training protocol consisted of 3 sessions: a first one without feedback and other two providing continuous feedback. The different sessions were carried out on separate days within a week. The session without feedback was used to set up classifier parameters for the next feedback sessions. Data of the third session were used to set up classifier parameters for the session of VE exploration.

During each session, subjects were looking at a computer screen placed at a distance of 100 cm and were instructed to carry out 4 experimental runs, consisting of 40 trials (20 on the left and 20 on the right randomly distributed). The training was carried out discriminating between two mental tasks: a relaxed state and imagined right hand movements. The duration of each trial was 8 seconds. The trial began with the presentation of a red cross in the centre of the screen, indicating that subjects should stay as relaxed as possible. At 2 s, a short beep signalled the beginning of the mental task to be carried out. The appearance, during 2.25 s, of a green arrow on top of the cross pointing to the right, was the cue for subjects to imagine continuous movements of the right hand. Otherwise, subjects should stay in a relaxed state. In the case of a feedback session, at 4.25 s the feedback stimulus was presented for 3.75 s. This one consisted of a blue horizontal bar which extended further to the right or left according to the classification result. At 8 s, the trial finished returning to a black screen, and started again after a pause, ranging from 0.5 s to 3 s (randomly distributed). The developed BCI system for subject training was done in MATLAB.

## 2.3 Signal processing

The signal processing included EEG feature extraction and classification. The scheme used was the one proposed by Guger et al. in [12]. The feature extraction consisted of estimating the average band power of each channel in predefined, subject specific reactive frequency bands at intervals of 500 ms. The classification was based on linear discriminant analysis (LDA) [13]. Signal processing was done in MATLAB.

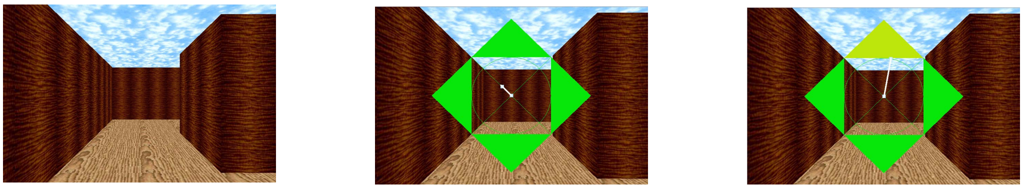

(a) (b) (c)

Figure 1: Exploration sequence.

For each session, an error time course was computed with a ten times 10-fold cross validation of a linear discriminant [11, 12] , for each time point $t = 500$ ms. In the session without feedback, the extracted feature parameters of the classification time points with the lowest classification error, were used to set up the LDA classifier parameters (weight vector) for the following sessions with feedback [11]. In the feedback sessions, the LDA classification result was converted on line to the length L of a feedback bar, which was updated on the screen every 4 samples (31.25 ms), to make feedback as continuous as possible. A negative/positive value of L was translated into a left/right extension of the feedback bar, indicating that trial was classified as a left/right trial.

## 2.4 Exploration of the VE using the BCI system

The VE consisted of a group of corridors with different junctions among them, setting a kind of labyrinth. The subject started to navigate from a specific position (Figure 1(a)) and his point of view changed continuously until reaching the first junction. At this moment, the subject stopped and the decision period started, showing a graphical interface as shown in Figure 1(b). This interface consisted on a circle divided into four quadrants (indicated by four green triangles), one for each navigation command: move forward (upper quadrant), turn right (right quadrant), move back (lower quadrant) and turn left (left quadrant). For the selection of a quadrant, there is a bar in the center of the circle. At the moment this graphical interface appeared, the subject had two seconds to prepare himself before starting the decision period. During this period, the bar was pointing to the beginning of the upper quadrant with its minimal length (Figure 1(b)). Then the bar started to turn clockwise automatically at a specific speed (several grades with each acquisition process, that is, 31.25 ms) and to extend according to the mental task carried out by the subject. Just like the BCI system used for initial training, the LDA classification result was converted on line to the length L of the feedback bar, which was updated each 31.25 ms. However, in that case, a negative value of L (relaxed state) kept the bar in its minimal length and a positive value of L (by imagining continuous right hand movements) was translated into an extension of the feedback bar. If the bar attained the limit circle of a specific quadrant, this one stopped the rotation and the triangle changed to yellow indicating that the movement option according to this region had been pre-selected (Figure 1(c)). To actually take the decision, the pre-selected movement option had to be pre-selected during a specific decision period before applying the necessary command to render the VE. However, if the right hand imagination movement was not performed for this necessary time, the movement option did not keep selected, so the bar became shorter and continued turning clockwise without selecting any option. Once the decision was made, the graphical interface disappeared and the subject continued walking through the corridor to the next junction following the decided movement option. The duration of the decision period and the rotating speed of the bar were configurable for each subject, depending on his ability to focus on one particular mental state. The whole application was made by Visual C++ and OpenGL (integrated in Microsoft Foundation Class with Measurement Studio) was used for the creation, visualization and animation of the VE.

To increase the degree of immersion, the VE was projected on a large front-projected screen

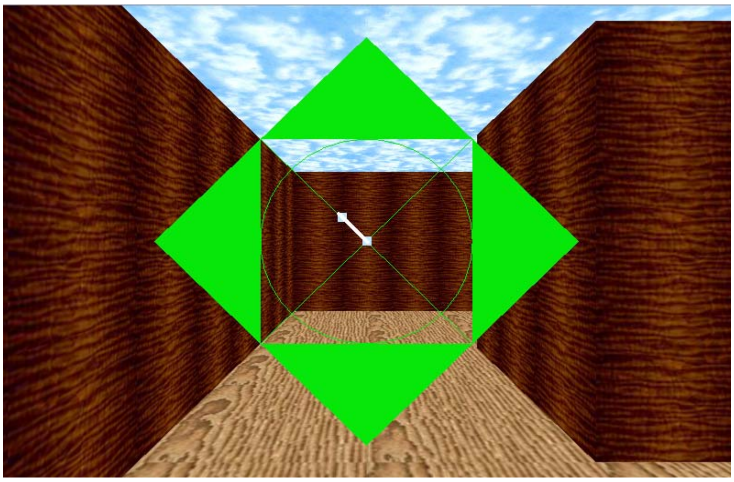

Figure 2: Error rates over the trial time for each subject and each session.

($2.5 \cdot 1.8$ m) and subjects were placed at a distance of 3 m. Each subject participated in one session with 4 experimental runs with variable duration. The first run was 10 minutes long and its aim was that subjects become familiar with the VE, navigating freely through the labyrinth. In the other three runs, the subjects were instructed to navigate until reaching 20 junctions. At each junction, an operator proposed a specific navigation command, and this one had to be chosen by the subject. The rotating speed of the bar was selected to turn at one grade each 31.25 ms, needing 2.81 s to cross a quadrant and 11.25 s to complete a turn. As proposed by [6], the performance error can be calculated by dividing the number of wrong decisions by the total number of junctions. The required time to select a specific command is also an interesting parameter.

# 3 Results

The error time courses obtained for each experimental training session of each subject are graphically presented in Figure 2. Continuous and dash lines represent error curves for feedback sessions (F) and non-feedback sessions (NF) respectively. Thick marks represent minimum error rate obtained for each experimental session of each subject(squares for S1, circles for S2 and diamonds for S3). Subject S2 and S3 increased their performance during training sessions. However, subject S1 did not have a good performance and did not participate to explore the VE.

Regarding the results obtained during the exploration of the VE, the number of wrong decision (WD) and the performance error (PEr) for subject S2 and S3 of each experimental run is shown in Table 1. Both subjects improved their performance in each run, being the mean error rates between 60 % and 10 %, with a mean $\pm$ SD of $25 \pm 19.3$ %. However, the high number of wrong decisions for subject S3 in run 1 (12) was due to a parameter related to the bar extension and no well regulated. Because of this, the obtained mean result (MEr) got considerably worse. The duration of the decision period was 0.75 s for subject S2 and 0.5 s for subject S3. In the 4 last columns, the number of correct decisions for each navigation command is showed (move forward (F), turn right (R), move back (B) and turn left (L)). The numbers in brackets indicate the number of correct decisions that needed an additional round of the bar to make the choice. For subject S2, from 51 correct decisions, 47 were reached during the first turn. For subject S3, the rate was

| Subject | Run | WD | PEr(%) | F | R | B | L |
|---|---|---|---|---|---|---|---|
| S2 | 1 | 5 | 25 | 4 | 4 | 4 | 3(1) |
| | 2 | 2 | 10 | 4(1) | 5(1) | 5 | 4(1) |
| | 3 | 2 | 10 | 0 | 6 | 6 | 6 |
| MEr (S2) | | $3 \pm 4.3$ | $15 \pm 21.5$ | | | | |
| Mt (s) (S2) | | | | $1.8 \pm 0.56$ ($3.13 \pm 3.17$) | $5.8 \pm 0.56$ ($6.7 \pm 2.09$) | $9.21 \pm 0.23$ ($9.21 \pm 0.23$) | $11.59 \pm 0.68$ ($14.9 \pm 5.35$) |
| S3 | 1 | 12 | 60 | 3 | 2(1) | 2 | 1 |
| | 2 | 5 | 25 | 4(2) | 5 | 2(1) | 4 |
| | 3 | 4 | 20 | 5(1) | 4(1) | 3 | 4(1) |
| MEr (S3) | | $7 \pm 10.8$ | $35 \pm 54.1$ | | | | |
| Mt (s) (S3) | | | | $2.15 \pm 0.5$ ($4.9 \pm 3.2$) | $5.53 \pm 0.82$ ($8.61 \pm 4.8$) | $8.65 \pm 0.97$ ($10.1 \pm 3.63$) | $11.66 \pm 0.5$ ($12.82 \pm 2.71$)) |
| MEr | | $5 \pm 3.8$ | $25 \pm 19.3$ | | | | |
| Mt (s) | | | | $1.97 \pm 0.34$ ($4.2 \pm 2.13$) | $5.7 \pm 0.44$ ($7.6 \pm 2.38$) | $9.02 \pm 0.32$ ($9.53 \pm 1.12$) | $11.62 \pm 0.38$ ($13.92 \pm 2.83$) |

Table 1: Performance of each experimental run (WD: wrong decision; PEr: performance error; MEr: average of wrong decision; Mt: average time to choose a command; F, R, B, L: commands).

32 of 39. The required average time to choose a specific command is also showed (Mt). These temporal parameters include the decision period required for each subject. The given parameters in brackets have been obtained including all the correct decisions and the ones without brackets represent this average time excluding the correct decisions that needed an additional turn. Finally, taking into account only these last correct decisions, the mean time for each navigation commands (in bold face) do not differ very much from the theoretical temporal limits, which are (excluding the decision period): 0–2.81 s, 2.84–5.62 s, 5.65–8.43 s and 8.46–11.25 s to select (F), (R), (B) and (L) respectively.

# 4 Discussion and conclusion

The results of this study suggest that it is possible to navigate freely through a VE controlling only two mental tasks. Three untrained subjects participated in the experiments following an initial training based on 3 sessions. Two of them were able to navigate trough the labyrinth discriminating between imagination of right hand movements and relaxed state, improving their performance over the runs. The used training paradigm was based on the bar extension because it was the same principle used to select the different navigation commands. It is important to adjust all the parameters and adapt them to the subjects to guarantee a good performance. The two most important parameters are: the duration of the decision period and the rotating speed of the bar. In this experiment, the speed of the bar rotation was selected so that the bar needed 11.25 s to complete a turn. It could be interesting to test the system increasing this parameter, for example, doubling the speed. Sometimes, subjects reached to extend the bar until the limit circle. However, due to a short lack of control of the EEG signals, the bar went back inside the circle for an instant, resetting the accumulated time for the decision period. Therefore, it would be desirable to include a new temporal parameter that would be the time that the bar must be inside the circle to reset this accumulated time. The bar turned clockwise automatically while it did not attain the limit circle. On several occasions, the subjects carried out the mental task to extend the bar without reaching the limit circle, causing that the bar exceeded the limit of a specific quadrant, and forcing to wait for an additional round. It would be interesting to test the system stopping the rotation once the bar starts extending, providing more time to select the quadrant.

The system presented in this study is in the development phase and many options can be added to improve its performance. However, the preliminary results obtained show that this BCI system provides an effective method to increase the navigation commands without a decrease of the classification accuracy. This is very important in some applications, for example to control a real wheelchair, being essential to guarantee a high level of classification accuracy. Actually, this

BCI is designed for synchronized operation. In the near future, we are planning on modifying the presented system to get an asynchronous BCI. In this way, the users control the BCI output whenever they want by intentionally performing a specific mental/cognitive task.

**Acknowledgments:** This work was partially supported by Excellence Project P07-TIC-03310 of Junta de Andalucia.

## References

[1] R. Leeb, R. Scherer, C. Keinrath, C. Guger, and G. Pfurtscheller. Exploring virtual environments with an eeg-based bci through motor imagery. *Biomed. Tech.*, 52:86–91, 2005.

[2] G. Pfurtscheller, R. Leeb, C. Keinrath, D. Friedman, C. Neuper, C. Guger, and M. Slater. Walking from thought. *Brain Res.*, 107:145–152, 2006.

[3] R. Leeb, C. Keinrath, D. Friedman, C. Guger, R. Scherer, C. Neuper, M. Garau, A. Antley, A. Steed, M. Slater, and G. Pfurtscheller. Walking by thinking: The brainwaves are crucial, not the muscles! *Presence*, 15:500–514, 2006.

[4] D. Friedman, R. Leeb, C. Guger, A. Steed, G. Pfurtscheller, and M. Slater. Navigating virtual reality by thought: What is it like? *Presence*, 16:100–110, 2007.

[5] R. Leeb, D. Friedman, G. R. Müller-Putz, R. Scherer, M. Slater, and G. Pfurtscheller. Self-paced (asynchronous) BCI control af a wheelchair in virtual environments: a case study with a tetraplegic. *Comput. Intell. Neurosci.*, 79642:1–8, 2007.

[6] R. Leeb, F. Lee, C. Keinrath, R. Scherer, H. Bischof, and G. Pfurtscheller. Brain-computer communication: Motivation, aim and impact of exploring a virtual apartment. *IEEE Trans. Neural Syst. Rehabil. Eng.*, 15:473–482, 2007.

[7] B. Obermaier, C. Neuper, C. Guger, and G. Pfurtscheller. Information transfer rate in a five-classes brain-computer interface. *IEEE Trans. Neural Syst. Rehabil. Eng.*, 9:283–289, 2001.

[8] R. Scherer, F. Lee, A. Schlögl, R. Leeb, H. Bischof, and G. Pfurtscheller. Toward self-paced brain-computer communication: Navigation through virtual worlds. *IEEE Trans. Biomed. Eng.*, 55:675–682, 2008.

[9] J. Kronegg, G. Chanel, S. Voloshynovskiy, and T. Pun. EEG-based synchronized brain-computer interfaces: A model for optimizing the number of mental tasks. *IEEE Trans. Neural Syst. Rehabil. Eng.*, 15:50–58, 2007.

[10] B. Blankertz, G. Dornhege, M. Krauledat, M. Schröder, R. Murray-Smith, and K.-R. Müller. The Berlin brain-computer interface presents the novel mental typewriter Hex-o-Spell. *3rd International BCI Workshop and Training Course*, Graz (Austria):108–109, 2006.

[11] C. Guger, A. Schlögl, C. Neuper, D. Walterspacher, T. Strein, and G. Pfurtscheller. Rapid prototyping of an EEG-based brain-computer interface (BCI). *IEEE Trans. Neural Syst. Rehabil. Eng.*, 9:49–58, 2001.

[12] C. Guger, G. Edlinger, W. Harkam, I. Niedermayer, and G. Pfurtscheller. How many people are able to operate an eeg-based brain-computer interface (BCI)? *IEEE Trans. Neural Syst. Rehabil. Eng.*, 11:145–147, 2003.

[13] C. M. Bishop. *Neural Networks for Pattern Recognition.* Oxford University Press, 1995.

# Amyotrophic lateral sclerosis patients are able to direct a computer screen cursor using a P300-based BCI

F. Piccione[1], C. Volpato[1], M. Marchetti[2], K. Priftis[1,2], A. Merico[1], M. Cavinato[1], G. Soraru[3], A. Palmieri[3], L. Tonin[4], S. Silvoni[1]

[1]IRCCS San Camillo Hospital, Venice, Italy
[2]Dept. of General Psychology, University of Padua, Italy
[3]Dept. of Neurosciences, University of Padua, Italy
[4]Dept. of Information Engineering, University of Padua, Italy

francopiccione@alice.it

**Abstract**

The aim of the present study was to propose the use of P300 event-related potentials (ERPs) as control signals for amyotrophic lateral sclerosis (ALS) patients. Fourteen patients with ALS took part in the study to test a new graphical interface, which can control the motion of a cursor using ERPs [1]. Visual stimuli, consisting of four arrows (upward, rightward, downward, leftward), were randomly presented in peripheral positions of a screen. ALS patients were instructed to pay attention only to the stimulus related to the preferred cursor movement direction. We reported that ALS patients were able to learn how to direct a computer screen cursor through the use of a brain-computer interface (BCI). In addition, ALS patients were assessed with a battery of clinical and neuropsychological tests. Data analysis revealed that ALS patients can reach good communication abilities using the BCI system, independently from their motor disability and cognitive status.

## 1 Introduction

Amyotrophic lateral sclerosis (ALS) is a neurodegenerative disease caused by the degeneration of motor neurons and it is characterised by progressive muscle weakness and atrophy. After a mean time of 3–5 years, patients ultimately lose the ability to initiate and control all voluntary movements, except those of the eyes, becoming tetraplegic and anarthric. Recent studies have been focused on the usefulness of the BCI technology as a communication tool for patients affected by ALS. To prevent the failure of completely paralysed patients to achieve BCI communication, some authors have suggested that ALS patients should begin the BCI training before becoming locked-in [2]. The present study describes the use of the P300 as a control signal for a four-option BCI [1, 3] by ALS patients. Furthermore, the study aimed to assess whether the P300 BCI system may be affected by the clinical and cognitive status of patients.

## 2 Methods

### 2.1 Participants

A group of 14 patients with ALS diagnosis based on the El Escorial criteria (admitted to the San Camillo Hospital for rehabilitative treatment) participated in the study. The research was approved by the Ethical Committee of the San Camillo Hospital. Informed consent was obtained according to the Declaration of Helsinki. Disability level of patients was assessed using the Revised ALS Functional Rating Scale (ALSFR-R [4]) which is characterised by the inclusion of autonomic,

| Demographic and clinical data of ALS patients | |
|---|---|
| Age (years) | 54 (15) |
| Gender (m/f) | 9/5 |
| Education (years) | 10.5 (4.3) |
| Disease duration (months) | 47 (30) |
| ALSFR-R (scores) | 29.9 (6.4) |
| MMSE (scores) | 27.7 (2.4) |

Table 1: Means (standard deviations) of demographic and clinical data in ALS.

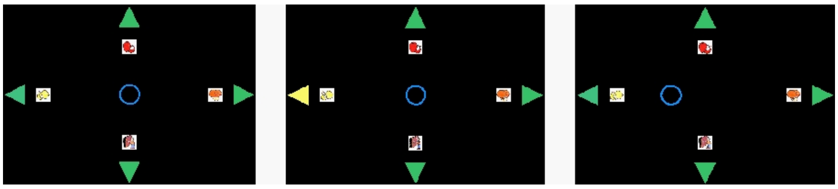

Figure 1: Representation of a trial. (a) The cursor, the target images and the four arrows; (b) the flashed arrow; (c) the movement of the cursor after P300 recognition.

respiratory, and motor items. Global cognitive impairment was assessed by using the Mini Mental State Examination (MMSE [5], Table 1). A further battery of psychometric tests [6] was administered to evaluate non-verbal intelligence (Raven's Coloured Matrices [7]), attention (Attentive Matrices [8]), executive functions (Modified Wisconsin Card Sorting Test [9], Phonemic Verbal Fluency [8], Digit Span Backward [10], Trail Making Test A and B [11]), short-term memory (Verbal Digit Span Forward [10], Corsi Blocks tapping test [8]), long-term memory (Prose Memory, [8]), and language (Semantic Verbal Fluency [8]). All patients had preserved speech, reading and writing abilities to perform all neuropsychological tests. ERP recordings were performed using an active auditory odd-ball paradigm in which frequent tones (1000 Hz, occurrence 0.8) were coupled to rare tones (2000 Hz, occurrence 0.2). The stimuli were presented randomly with an inter-stimulus interval (ISI) of 2 s. P300 latencies and peak-to-peak amplitudes (N2–P3) were measured. To analyse the P300 parameters we used normative data of the International Federation of Clinical Neurophysiology [12] replicated with 50 healthy participants grouped by age in our laboratory. P300 amplitudes and latencies of each participant were manually peak-picked from average data by two expert electrophysiologists.

## 2.2 BCI system

The visual interface was presented on a computer screen. Participants were asked to control the movement of a cursor (blue ball) from the centre of the monitor to one out of four peripheral target images representing a basic need (i. e. "I'm hungry", "I'm sleepy", "I would like to eat an apple"). The initial distance between the cursor and the target image was of four discrete steps.

Four arrows (i. e., upward, rightward, downward, and leftward) were randomly flashed in peripheral positions of the monitor (Figure 1a). Each arrow indicated one out of four possible directions concerning the movement of the cursor. Participants had to pay attention to the arrow indicating the direction of the target image (i. e. target arrow; probability of occurrence: 25 %) and to ignore the arrows indicating the wrong directions (i. e. distracting arrows: overall probability of occurrence 75 %). Participants had to move the cursor along only one direction, according to the target image specified by the examiner, until the target was reached. Each trial consisted of the flashing of an arrow for 150 ms (Figure 1b), followed by data processing necessary for P300 recognition, and by the generation of feedback concerning the movement of the cursor (Figure 1c). The time interval between two flashed arrows (inter-trial interval: ITI) was 2.5 s, in order to achieve optimal on-line data processing. A session was defined as the complete sequence of trials sufficient to reach the target image (range: 13–92 trials).

We hypothesised that every target arrow should elicit the P300 wave. Every time the P300 was detected during the trial, the cursor moved on the graphical interface according to the direction of the flashed arrow. Each participant performed eight learning sessions (LS) in the first day, and sixteen testing sessions (TS) spread over the following 11 days (i. e., first day 8 LS → second day 4 TS → two days interval → fifth day 4 TS → two days interval → eighth day 4 TS → two days interval → eleventh day 4 TS).

The learning sessions were characterised by an "ideal feedback", provided to the participant by a correct movement of the cursor: every time the target arrow flashed, the cursor made one step toward the target image (i. e., the "ideal feedback" represents what should have been the consequence of a correct P300 classification following participant's concentration on the target image). In contrast, during the testing sessions the cursor moved toward the target image only as a response to a brain wave classified as P300 (i. e.,"real feedback" based on participant's concentration on the target image).

### 2.3 BCI data acquisition

Registration electrodes were placed according to the international 10–20 system at Fz, Cz, Pz and Oz; the Electrooculogram (EOG) was recorded from a pair of electrodes below and laterally to the right eye; all electrodes were referenced to the left earlobe. The five channels were amplified, band-pass filtered between 0.15 Hz and 30 Hz, and digitized (with a 16 bit resolution) at 200 Hz sampling rate. Every ERP epoch, synchronized with the stimulus, began 500 ms before the stimulus onset, up to 1000 ms after stimulus trigger signal (total 1500 ms). Thus, after each stimulus (trial) presentation the system recorded a matrix of 300 samples per 5 channels, available for on-line and off-line data processing.

### 2.4 Data analysis

A modified version of the classification algorithm reported in a previous study [1] was used to test the BCI system. Before each testing day, a classifier (adapted ad personam) was trained with a three-step procedure: Independent Component Analysis (ICA) decomposition, features extraction, and Support Vector Machine (SVM) classification. All ERP epochs, with at least one channel's activity greater than 100 µV (including EOG), were excluded from each training set, while all available ERPs epochs were analysed for each testing set. During on-line operations, the classification procedure was applied to every single sweep synchronised with the stimulus, while the output of the SVM classifier was converted to a binary value (1: P300 detected; 0: P300 absent) to control the discrete movements of the cursor.

To define a complementary performance index, we grouped all testing sessions in two class: "successfully completed sessions" and "unsuccessful sessions". The first were characterised by the reaching of the target image. This implied that at least four epochs related to the target direction were correctly classified. Conversely, in an "unsuccessful session" the cursor reached a non-target image, or the number of presented stimuli reached the maximum number decided by the authors (92) without reaching any image. We also defined the "learning period" as the number of stimuli received by the participants before reaching the first successful session (i. e., number of stimuli needed to reach the first time a target image), who refers to the whole system which comprised both the participant and the classifier.

Participants mean (standard deviation) neurophysiological, neuropsychological, and BCI-skills are reported in Tables 2, 3 and 4. To examine the possible relations among clinical, neurophysiological, neuropsychological, and BCI data, the Spearman's rank correlation test was used.

## 3 Results

Participants' BCI skills were described by the indexes shown in Table 2: classification performance (accuracy %), transfer bit rate (bit/min), percentage of successfully sessions (target image reached

| BCI parameters of ALS patients | |
|---|---|
| Performance (%) | 77.8 (5.2) |
| Transfer bit rate (bit/min) | 6.76 (2.03) |
| Percentage of sessions successfully completed (%) | 77.7 (15.8) |
| Learning Number of Stimuli (LNS) | 253 (152) |
| Performance trend (%/session) | 0.43 (0.65) |
| Artefact index (%) | 7.7 (6.9) |

Table 2: Means (standard deviations) of BCI measures.

| Neuropsychological performance of ALS patients | |
|---|---|
| Raven's Coloured Matrices (scores) | 28.4 (4.8) |
| Semantic Verbal Fluency (scores) | 40.2 (7.2) |
| Phonemic Verbal Fluency (scores) | 27.3 (8.9) |
| Trail Making Test A (seconds) | 46.2 (12.3) |
| Trail Making Test B (seconds) | 159.8 (81.5) |
| Trail Making Test A-B (seconds) | 113.6 (110.5) |
| Digit Span Forward (scores) | 5.4 (4.8) |
| Digit Span Backward (scores) | 3.3 (0.9) |
| Corsi Blocks tapping test (scores) | 5.2 (0.9) |
| Prose Memory (scores) | 13.1 (3.2) |

Table 3: Means (standard deviations) of neuropsychological scores in ALS patients.

by the blue cursor, Figure 1), "learning period" (Learning Number of Stimuli, LNS), and the classification performance trend among all 16 testing sessions. A further index was evaluated to monitor the influence of on-line artefacts on participants' performance: the percentage of the target epochs with at least one channel's activity greater than 100 µV, and classified as true positives, with respect to all target epochs.

ALS patients performed within normal ranges in all neuropsychological tests. Mean performance (standard deviation) of ALS patients in neuropsychological measures is reported in Table 3.

Neurophysiological data are reported in Table 4. P300 waves parameters (amplitude and latency) resulted within normative values collected in our laboratory.

Moreover, the statistical analysis revealed a significant correlation between ALS patients' age and some BCI parameters: performance ($\rho = 0.75$, $p < 0.01$), transfer bit rate ($\rho = 0.66$, $p < 0.01$), and percentage of successfully sessions ($\rho = 0.67$, $p < 0.01$). No other significant correlations were found between BCI skills and demographic, clinical, neurophysiological and neuropsychological data.

# 4 Discussion

In this study ALS patients reached good BCI skills (Table 2): the average of successfully completed sessions was about 75 %; the mean "learning period" was 253 stimuli; the communication speed was low compared to others works [13], but there is also a slightly positive trend on classification performance, denoting the existence of a mutual learning mechanism [14] between the participant and the BCI system.

| Neurophysiological data of ALS patients | |
|---|---|
| Auditory odd-ball P300 latency (ch. PZ) (ms) | 389 (65) |
| Auditory odd-ball P300 amplitude (ch. PZ) (µV) | 10.8 (5.2) |

Table 4: Means (standard deviations) of neurophysiological indexes in ALS.

Our ALS patients performed within normal ranges in all neuropsychological tests suggesting preserved cognitive functions. Moreover, they obtained good results in BCI skills comparable to those of healthy participants [1]. The absence of correlation between neuropsychological tests and BCI parameters suggests that the preserved cognitive status of our ALS patients did not affect BCI skills. A positive correlation was found between age and some BCI parameters. This finding may be interpreted as an effect of the small number of participants or a consequence of the greater compliance of older participants with the slow speed and high error rate of the present BCI system.

Enabling these patients to control a computer cursor may allow them, in the late stage of disease, to communicate by moving the cursor to a specific word or icon on a computer screen. This interface could be adapted to allow patients to perform other actions besides communicating, such as controlling a domotic house or even using a thought-controlled wheelchair. Longitudinal research is required to test this hypothesis and the present study constitutes the first step toward this direction.

## 5 Conclusion

The present study confirms the possibility to use P300 as a control signal for a BCI in ALS patients before the disease becomes advanced, suggesting a possible application of the BCI training in other clinical populations.

## References

[1] F. Piccione, F. Giorgi, P. Tonin, K. Priftis, S. Giove, S. Silvoni, G. Palmas, and F. Beverina. P300-based brain computer interface: Reliability and performance in healthy and paralised participants. *Clin. Neurophysiol.*, 117:531–537, 2006.

[2] N. Birbaumer. Brain-computer interface research: coming of age. *Clin. Neurophysiol.*, 117:479–483, 2006.

[3] E. W. Sellers and E. Donchin. A p300-based brain–computer interface: Initial tests by als patients. *Clin. Neurophysiol.*, 117:538–548, 2006.

[4] M. Cedarbaum, N. Stambler, E. Malta, C. Fuller, D. Hilt, B. Thurmond, and A. Nakanishi. The ALSFRS-R: a revised ALS functional rating scale that incorporates assessments of respiratory function. *J. Neurol. Sci.*, 169:13–21, 1999.

[5] M. F. Folstein, S. E. Folstein, and P. R. McHugh. A practical method for grading the cognitive state of patients for the clinician. *J. Psychiatric Res.*, 12:189–19, 1975.

[6] J. Phukan, N. Pender, and O. Hardiman. Cognitive impairment in amyotrophic lateral sclerosis. *Lancet Neurol.*, 6:994–1003, 2007.

[7] J. C. Raven. RCPM: guide to using the colored progressive matrices. *New York: Psychol. Corp.*, 1965.

[8] H. Spinnler and G. Tognoni. Standardizzazione taratura italiana dei test neuropsicologici. *Ital. J. Neurol. Sci.*, 8:1–120, 1987.

[9] H. E. Nelson. Modified card sorting test (1976). *Firenze, Italy: O.S.,Firenze*, 2003.

[10] D. Wechsler. *Wechsler Adult Intelligence Scale Revised (WAIS-R)*. Italy: O.S., Firenze, 1998.

[11] R. M. Reitan. Validity of the trail making test as an indicator of organic brain damage. *Percept. Mot. Skills*, 8:271–276, 1958.

[12] H. J. Heinze, T. F. Münte, M. Kutas, S. R. Butler, R. Näätänen, M. R. Nuwer, and D. S. Goodin. Cognitive event-related potentials. *Electroencephalogr. Clin. Neurophysiol.*, 52:91–95, 1999.

[13] U. Hoffmann, J. M. Vesin, T. Ebrahimi, and K. Diserens. An efficient P300-based brain-computer interface for disabled subjects. *J. Neurosci. Methods*, 167:115–125, 2008.

[14] J. del R. Millán. Adaptive brain interfaces. *Commun. ACM*, 46:74–80, 2003.

# BCI demographics: how many (and what kinds of) people can use an SSVEP BCI?

B. Allison, I. Volosyak, T. Lüth, D. Valbuena, I. Sugiarto, M. A. Spiegel, A. Teymourian, I. S. Condro, A. Brindusescu, K. Stenzel, H. Cecotti, A. Gräser

Institute of Automation, IAT, University of Bremen, Bremen, Germany

allison@iat.uni-bremen.de

**Abstract**

Brain-computer interface (BCI) systems enable communication without movement. It is unclear why some BCI approaches or parameters are less effective with some users. This study elucidates BCI demographics by exploring correlations among BCI performance, personal preferences, and different subject factors such as age or gender. Results showed that most people, despite having no prior BCI experience, could use the Bremen SSVEP BCI system in a very noisy field setting. Performance was best in both young and female subjects. Most subjects, especially younger subjects, stated that they did not consider the flickering stimuli annoying and would use or recommend this BCI system. These and other demographic analyses may help identify the best BCI for each user.

## 1 Introduction

Brain-computer interface (BCI) systems are devices that allow people to communicate without moving. Instead, direct measures of brain activity are translated into messages or commands. The classic goal of BCI research has been to provide severely disabled users with communication and control [1]. This remains a principal focus of most research groups. However, there has been increasing attention recently to using BCIs to provide communication for new user groups, such as healthy users or persons with less severe disabilities. Similarly, BCIs have recently been validated as advanced neurofeedback tools for stroke, autism, attention disorders, and other disorders, in which the principal goal of the BCI is not communication but rehabilitation [2–5].

BCI demographics should be better explored and addressed before BCIs can become practical tools – for existing or new user groups. Such research could help identify the best BCI for each user. One of the most consistent observations in the BCI literature is considerable inter-subject variability, and thus the need to customize various parameters according to each user [1, 6–10]. Inter-subject variability often leads to the well-documented "BCI illiteracy" phenomenon; across different BCI approaches (SSVEP, P300, ERD/ERS), about 20 % of users are unable to attain effective control, while about another 30 % attain only poor control [4,6,9,11]. While many authors have noted the problems of inter-subject variability and BCI illiteracy, and speculated about it, there has been amazingly little applied research to study why this occurs.

One of the greatest oversights in BCI research is negligence of BCI demographics. Why are some users better at BCI use than others? How do genetic, background, and lifestyle differences affect performance and preferences with different BCI systems? Could the best BCI approach and parameters be anticipated without extensive testing and modification? Can BCI illiteracy be predicted? How could demographic information help to provide the best BCI for each user, ideally with little or no expert help to configure and adapt key parameters?

The present project is the first BCI effort to address these questions through applied research with a sufficient number of subjects. Some prior articles have used questionnaires to assay individual differences (e. g., [7, 9, 10]), but often did not use enough subjects for reliable conclusions.

For example, recent work suggested that female subjects, and subjects with a gaming background, performed better with SSVEP BCIs, but these results did not attain statistical significance [9]. Only one BCI article has used several dozen subjects, and it did not use questionnaires nor any means of evaluating correlations between BCI performance and individual characteristics. This important paper, titled "How many people can use a BCI?" provided an excellent overview of how 99 different subjects performed with an EEG-based BCI, but no insight as to why some subjects were better than others [12].

The principal goal of the present study was to assess SSVEP BCI performance across a large number of subjects and evaluate correlations between performance, preferences, and individual characteristics assessed with brief questionnaires both before and after BCI use. Performance was compared across different message lengths, number of cursor movements needed to select each letter, and copy vs. free spelling tasks. In addition to evaluating objective dependent variables such as EEG measures, spelling speed, and accuracy, we also assessed subjective information such as whether subjects found SSVEP BCI use fatiguing or unpleasant.

# 2 Methods and materials

## 2.1 Subjects

106 subjects participated in the study. Additional information about subject demographics is available in Table 1. All subjects were recruited from visitors to our booth at CeBIT 2008. All subjects were healthy and had no prior experience with BCIs. Potential subjects were asked if they were at least 18 years old or ever had a seizure, epilepsy, mental or physical disorders, or skin contact allergies. Subjects would have been rejected had they answered yes to any of these screening questions, but none of them did. All subjects completed a consent form and questionnaires that were all approved by the ethic commission of the University of Bremen.

## 2.2 Procedure

After completing the consent form, each subject was asked to complete a brief electronic questionnaire (called the pre-questionnaire) and was prepared for EEG recording. Next, each subject used the SSVEP BCI system described below to spell five messages. Four of these messages were chosen by the experimenter (copy spelling), and the fifth was chosen by the subject (free spelling). The four copy spelling phrases were BCI, SIREN, CHUG, and BRAIN COMPUTER INTERFACE. These four messages were chosen because they represent a range of message lengths (short vs. long) and the letters' distances from the center (short vs. long; see Figure 1). Before the free spelling run, each subject verbally told the experimenter of the message that s/he intended to spell so spelling efficacy could be assessed. The order in which these five phrases were presented was determined randomly. After the phrases were spelled, subjects completed a second electronic questionnaire (called the post-questionnaire) and the procedure was complete.

Figure 1 presents the display used in this study. The center of the display contained 32 letters and other characters that the subject could communicate. At the beginning of each run, a cursor was present over the "E" character. Subjects spelled by focusing on one of five boxes presented on a laptop monitor. Each box contained either an arrow (up, right, down, or left) or the word "Select". Each box oscillated at a different constant frequency: 13, 14, 15, 16, or 17 Hz (respectively). These frequencies were determined through prior work [13] and pilot work. If the SNR at a specific frequency exceeded a predetermined threshold, the corresponding command was executed. For example, if activity at 14 Hz exceeded a preset threshold, the cursor moved to the right. There was no "wraparound" feature; if the cursor could not move further to the left, then the cursor did not move if 16 Hz activity exceeded the threshold. If activity at 17 Hz exceeded the threshold, the character highlit by the cursor was selected.

The bottom of the screen presented the message that the subject already selected. Thus, the bottom of the screen contained no characters at the beginning of each run. Figure 1 below shows

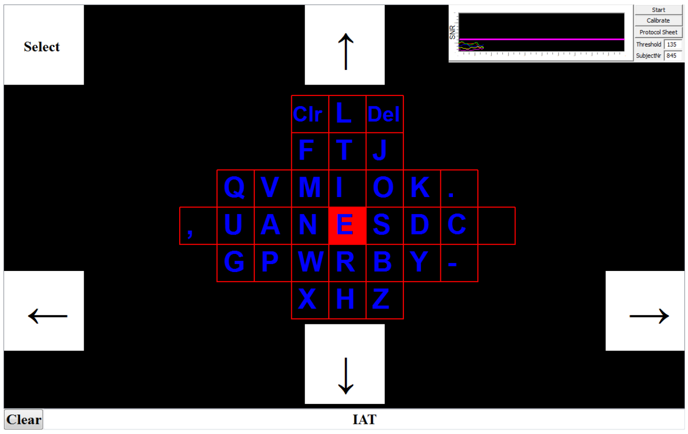


Figure 1: The display used in this study. The bottom of the screen presents the text that the subject already spelled. The five white boxes contain the commands that can be sent: up, down, left, right, and select.

an example of a screenshot when the subject successfully spelled the word “IAT”. Each run ended when the subject spelled the desired phrase, or a similar phrase with some errors. At the end of each run except the last run, each subject had a short break lasting about 30 seconds, then was reminded of the next phrase.

### 2.3 Hardware and software

All data were recorded from sites $PO_3$, $PO_4$, $O_9$, $O_{10}$, $O_z$ and $P_z$ aligned with the standard 10–20 system of electrode placement. Data were referenced to site $FC_z$ with a ground at site $AF_z$. Electrodes and caps were provided by Electro-cap, International. These electrodes required electrode gel, as is typical of conventional EEG recording systems. Data were digitized and amplifier through a g.USBamp (Guger Technologies), which included a bandpass filter of 2–50 Hz. Data were collected and stored anonymously on a PC compatible laptop with a TFT monitor display running Windows Vista.

## 3 Results

Tables 1 and 2, and Figures 2 and 3, present results from subjects’ BCI performance and questionnaire replies. All 106 subjects completed the consent form and answered at least the questions about age and gender, were prepared for EEG recording, and began using the BCI. About 22 subjects did not complete some or all questionnaire items. Some subjects did not complete the study for various reasons. For example, some subjects’ recording sessions ended because the subject asked to use the bathroom, wanted to see a specific CeBIT event, decided to stop because of poor performance, or had to meet a friend. Other subjects chose to spell phrases of their choosing rather than the “copy spelling” phrases suggested in the protocol, and thus some subjects’ data are incomplete. No subjects stopped participating because they reported any pain, discomfort, fatigue, annoyance, or similar problems.

The results show that a wide variety of people can effectively use a BCI. Table 2 shows that letters closer to the center, such as SIREN, can be spelled more quickly than letters near the periphery. The long phrase, BRAIN COMPUTER INTERFACE, was spelled with a higher bitrate than shorter phrases (except SIREN). There was no strong difference between free spelling and copy spelling. The average word length during free spelling was 6.6 characters. Performance was best for subjects who were female and relatively young. Men averaged 10.7 bits/min, while women averaged 14.9 bits/min. The youngest 10 subjects averaged almost 15 bits/min, while the oldest

| Question | | Number of Respondents | Average Response | SD | Range |
|---|---|---|---|---|---|
| **PRE-Questionnaire** | | | | | |
| Age(years) | | 106 | 30.6 | 11.9 | 18–79 |
| Gender | Male | 106 | 81 (76.4 %) | | |
| | Female | 106 | 25 (23.6 %) | | |
| Need for vision correction | Yes | 88 | 46 | | |
| | No | 88 | 42 | | |
| Education | Junior high school=1 | 88 | 10 | | 1–4 |
| | High school=2 | 88 | 37 | | 1–4 |
| | College or university=3 | 88 | 31 | | 1–4 |
| | PhD=4 | 88 | 10 | | 1–4 |
| Computer work (h/week) | | 88 | 33.1 | 16.9 | 2–80 |
| Computer games (h/week) | | 88 | 3.3 | 9.3 | 0–60 |
| Hours of sleep last night | | 88 | 6.2 | 2.3 | 0–13 |
| Substances | Alcohol | 88 | 23 | | |
| | Caffeine | 88 | 21 | | |
| | Cigarretes | 88 | 16 | | |
| Are you tired? | (1–5 scale) | 88 | 2.09 | 1.03 | 1–5 |
| **POST-Questionnaire** | | | | | |
| Did system work? | (1–5 scale) | 84 | 3.39 | 1.33 | 1–5 |
| Recommend system? | (1–5 scale) | 84 | 3.82 | 1.2 | 1–5 |
| Easier | to concentrate on LED | 84 | 54 | | |
| | to gaze at LED | 84 | 30 | | |
| Easy to switch? | (1–5 scale) | 84 | 3.6 | 1.28 | 1–5 |
| Were stimuli annoying? | (1–5 scale) | 84 | 2.54 | 1.27 | 1–5 |
| Are you tired? | (1–5 scale) | 84 | 2.30 | 1.24 | 1–5 |

Table 1: Questionnaire answers. This table presents the answers collected from pre- and post-questionnaires. In questions that could be answered in a 1–5 scale, 1 means no and 5 means yes.

10 subjects averaged almost 10 bits/min. Figure 3 shows the three post-questionnaire items that differed significantly with age. Older subjects were more likely to find flickering stimuli annoying and less positive about their BCI use.

# 4 Discussion

The performance data show that this SSVEP BCI system could provide effective communication for most subjects. The ITR and illiteracy rate reported here are good compared to other BCI field studies with unscreened novice subjects (e. g., [12]). Longer phrases might exhibit higher ITR since subjects get absorbed in the task of using a BCI. The questionnaires showed that the SSVEP BCI system used here was generally not perceived as annoying or difficult to use, and did not produce significant fatigue.

# 5 Conclusion

These results could help identify the best BCI for each user. For example, this system might be best suited to women and younger users, although subjects younger than 18 were not tested. Further demographic research should identify how individual subject factors relate to performance with other BCIs, and with other parameters such as the best frequencies, thresholds, tasks, mental imagery, training regimens, feedback, or other adjustable parameters. This research should facilitate BCIs that can adapt to each user, ideally with little or no expert help.

| Goal text | Number of respondents | Mean accuracy (%) | SD accuracy (%) | Range accuracy (%) | Mean Time (s) | SD Time (s) | Range Time (s) | ITR (bits/ min) |
|---|---|---|---|---|---|---|---|---|
| BCI | 69 | 88.5 | 21.1 | 75–100 | 122.1 | 98.9 | 21.5–463.6 | 10.1 |
| SIREN | 53 | 92.5 | 13.2 | 57–100 | 111.1 | 86.4 | 27.4–431.6 | 18.3 |
| CHUG | 49 | 93 | 15.7 | 25–100 | 139.3 | 103.3 | 43.6–450.6 | 11.6 |
| BRAIN COMPUTER INTERFACE | 34 | 92.5 | 12.8 | 50–100 | 460.7 | 190.8 | 185.7–1029.5 | 16.1 |
| Free spelling | 62 | 94.3 | 11.1 | 57–100 | 204.2 | 167.9 | 29.7–911.7 | 13.1 |
| AVERAGE | 53.4 | 92.2 | 14.0 | 56.2–100 | 208.5 | 130.8 | 72.6–657.4 | 13.9 |

Table 2: BCI spelling performance. This table presents performance results from subjects at CeBIT 2008.

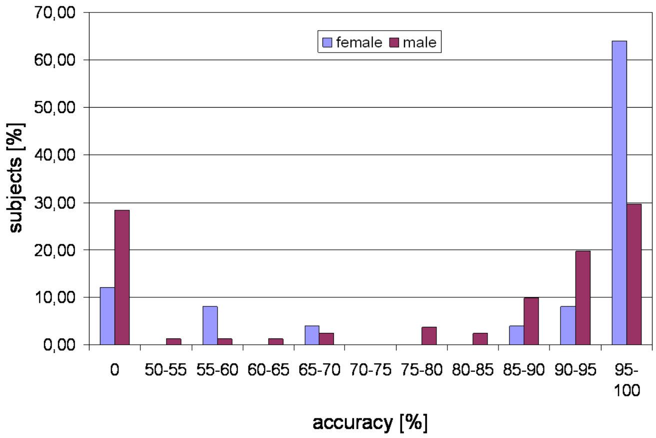


Figure 2: Gender and accuracy histogram. This figure shows the relationship between gender and performance.

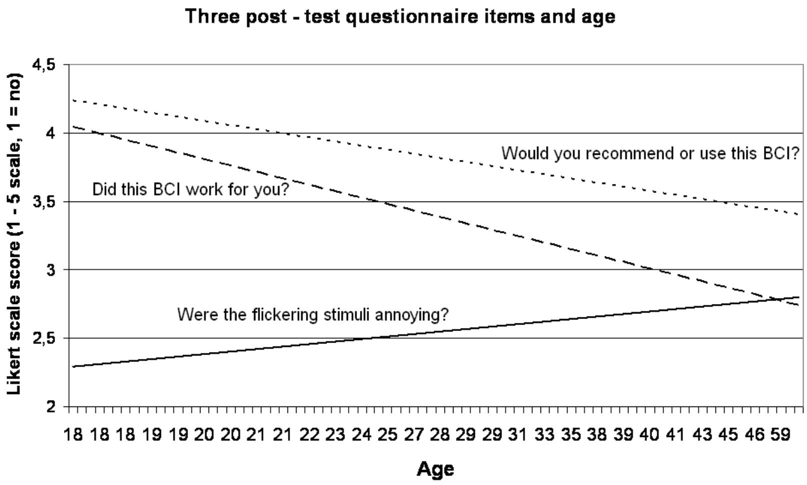


Figure 3: Age and subjective report. This figure shows the relationship between age and the replies given to three questions presented in the post-test questionnaire. Note that the $x$-axis does not increase linearly because most subjects were younger than the median age.

# References


[1] J. R. Wolpaw, N. Birbaumer, D. J. McFarland, G. Pfurtscheller, and T. M. Vaughan. Brain-computer interfaces for communication and control. *Clin. Neurophysiol.*, 113(6):767–791, 2002.

[2] G. Pfurtscheller and C. Neuper. Future prospects of ERD/ERS in the context of brain-computer interface (BCI) developments. *Prog. Brain Res.*, 159:433–437, 2006.

[3] N. Birbaumer and L. G. Cohen. Brain–computer interfaces: communication and restoration of movement in paralysis. *J. Physiol.*, 579(3):621–636, 2007.

[4] A. Nijholt, D. Tan, G. Pfurtscheller, C. Brunner, J. del R. Millán, B. Z. Allison, B. Graimann, F. Popescu, B. Blankertz, and K.-R. Müller. Brain-computer interfacing for intelligent systems. *IEEE Intell. Syst.*, in press.

[5] J. A. Pineda, D. Brang, E. Hecht, L. Edwards, S. Carey, M. Bacon, C. Futagaki, D. Suk, J. Tom, C. Birnbaum, and A. Rork. Positive behavioral and electrophysiological changes following neurofeedback training in children with autism. *Res. in Autism Spectr. Disord.*, in press, 2008.

[6] M. Cheng, X. Gao, S. Gao, and D. Xu. Design and implementation of a brain-computer interface with high transfer rates. *IEEE Trans. Biomed. Eng.*, 49(10):1181–1186, 2002.

[7] B. Z. Allison and J. A. Pineda. ERPs evoked by different matrix sizes: implications for a brain computer interface (BCI) system. *IEEE Trans. Neural Syst. Rehabil. Eng.*, 11(2):110–113, 2003.

[8] D. J. McFarland, W. A. Sarnacki, and J. R. Wolpaw. Brain-computer interface (BCI) operation: optimizing information transfer rates. *Biol. Psychol.*, 63(3):237–251, 2003.

[9] B. Z. Allison, D. J McFarland, G. Shalk, S. D. Zheng, M. M. Jackson, and J. R. Wolpaw. Towards an independent brain-computer interface using steady state visual evoked potentials. *Clin. Neurophysiol.*, 119(2):399–408, 2008.

[10] B. Z. Allison and J. A. Pineda. Effects of SOA and flash pattern manipulations on ERPs, performance, and preference: Implications for a BCI system. *Int. J. Psychophysiol.*, 59(2):127–140, 2006.

[11] A. Kübler, V. K. Mushahwar, L. R. Hochberg, and J. P. Donoghue. BCI meeting 2005 – workshop on clinical issues and applications. *IEEE Trans. Neural Syst. Rehabil. Eng.*, 14(2):131–134, 2006.

[12] C. Guger, G. Edlinger, W. Harkam, I. Niedermayer, and G. Pfurtscheller. How many people are able to operate an EEG-based brain-computer interface (BCI)? *IEEE Trans. Neural Syst. Rehabil. Eng.*, 11(2):145–147, 2003.

[13] O. Friman, I. Volosyak, and A. Gräser. Multiple channel detection of steady-state visual evoked potentials for brain-computer interfaces. *IEEE Trans. Biomed. Eng.*, 54(4):742–750, 2007.

# Control of a smart home with a brain-computer interface

C. Guger[1], C. Holzner[1], C. Grönegress[2], G. Edlinger[1], M. Slater[2]

[1]g.tec medical engineering GmbH, Guger Technologies OEG, Graz, Austria
[2]Centre de Realitat Virtual, Universitat Politècnia de Catalunya, Barcelona, Spain

guger@gtec.at

**Abstract**

An electroencephalogram (EEG) based brain-computer interface (BCI) was connected with a Virtual Reality system in order to control a smart home application. Therefore special control masks were developed which allowed using the P300 component of the EEG as input signal for the BCI system. Control commands for switching TV channels, for opening and closing doors and windows, for navigation and conversation were realized. Experiments with 3 subjects yielded accuracies of the BCI system between 83 and 100 % and showed that such a BCI system can be used for smart home control. The Virtual Reality approach is a very cost effective way for testing the smart home environment together with the BCI system.

## 1 Introduction

An EEG based brain-computer interface (BCI) measures and analyzes the electrical brain activity (EEG) in order to control external devices. BCIs are based on slow cortical potentials [1], EEG oscillations in the alpha and beta band [2, 3], the P300 response [4] or steady-state visual evoked potentials (SSVEP) [5]. BCI systems are used mainly for moving a cursor on a computer screen, controlling external devices or for spelling purposes [2, 3, 4].
BCI systems based on slow cortical potentials or oscillatory EEG components with 1–5 degrees of freedom were realized up to now. However, high information transfer rates were reached based on 2 degrees of freedom as otherwise the accuracy of the BCI systems dropped down. SSVEP based systems allow selecting up to 48 different targets and are limited by the number of distinct frequency responses that can be analyzed in the EEG. P300 response based BCIs typically used a matrix of 36 characters for spelling applications [4].

## 2 Methods

Three subjects participated in the experiments and were trained firstly in spelling characters and numbers based on their P300 EEG response. Therefore, the characters of the English alphabet (A, B, . . . , Z) and Arabic numbers (1, 2, . . . , 9) were arranged in a $6 \times 6$ matrix on a computer screen. Then the characters were highlighted in a random order and the subject had the task to concentrate on the specific character he/she wanted to spell. All experiments were undertaken in 2 modes: (i) the row/column speller – all items of one row or column are highlighted at the same time, (ii) the single character speller – only one character is highlighted. For the single character speller each character was highlighted 15 times. For the row/column speller each row and each column was also highlighted 15 times. This results in a speed up of 3 for the row/column speller. Another important parameter in the P300 experiment is the flash time (character is highlighted) and the dark time (time between 2 highlights). Both times should be as short as possible to reach a high communication speed, but must be long enough so that the subject can detect the flash and that the single P300 responses are not overlapping.

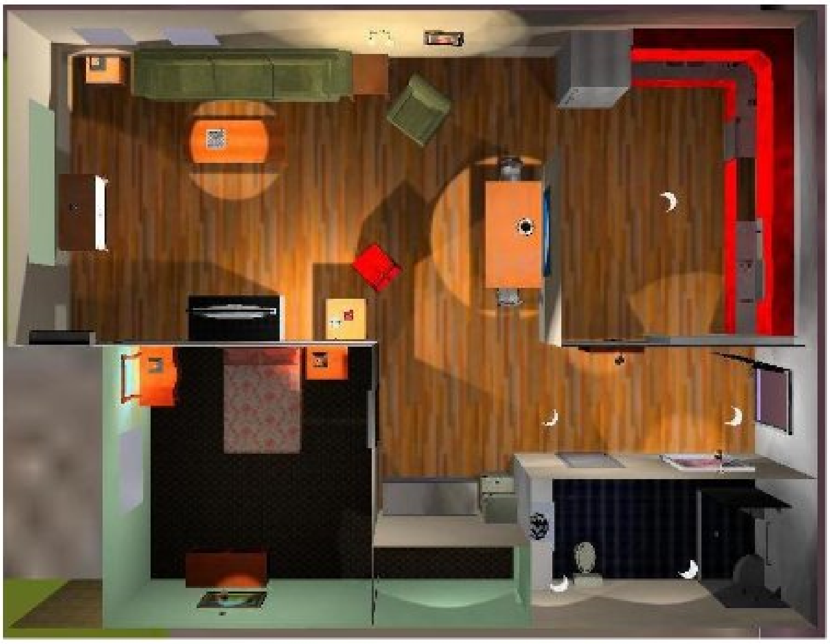

Figure 1: Virtual representation of a smart home

At the beginning of the experiment the BCI system was trained based on the P300 response of 42 characters of each subject with 15 flashes per character (about 40 minutes training time). All 3 subjects needed between 3 and 10 flashes (mean 5.2) per character to reach an accuracy of 95 % for the single character speller and between 4 and 11 flashes (mean 5.4) for the Row/Column speller. This resulted in a maximum information transfer rate of 84 bits/s (60 ms per character flash time) for the single character speller and 65 bits/s (100 ms per character flash time) for the row column speller.

Then the P300 based BCI system was connected to a Virtual Reality (VR) system. A virtual 3D representation of a smart home with different control elements was developed as shown in Figure 1.

In the experiment it should be possible for a subject to switch on and off the light, to open and close the doors and windows, to control the TV set, to use the phone, to play music, to operate a video camera at the entrance, to walk around in the house and to move him/herself to a specific location in the smart home. Therefore special control masks for the BCI system were developed containing all the different necessary commands. In total 7 control masks were created: a light mask, a music mask, a phone mask, a temperature mask, a TV mask (see Figure 2, left), a move mask and a go to mask (see Figure 2, right).

The experiment for the P300 smart home control was divided into 3 parts with 15, 11 and 16 decisions respectively. One task was e. g. to go to the living room, to switch on the TV and to select a specific channel, . . .

## 3 Results

Table 1 shows the results of the 3 subjects for the 3 parts of the experiment and for the 7 control masks. Interestingly, the light, the phone and the temperature mask were controlled by 100 % accuracy. The Go to mask was controlled with 94.4 % accuracy. The worst results were achieved for the TV mask with only 83.3 % accuracy.

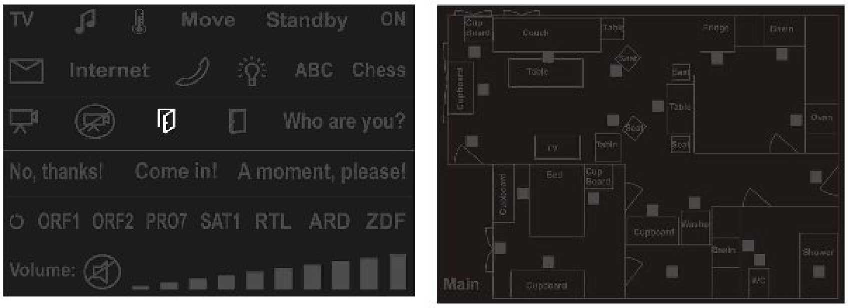


Figure 2: Left: Control mask with the main menu in the first 2 rows, the icons for the camera, door control and questions in the 3rd and 4th row and the TV control in the last 2 rows. Right: Control mask for going to a specific position in the smart home.

| Mask | Part1 | Part2 | Part3 | Total |
|---|---|---|---|---|
| Light | 100 % | 100 % | 100 % | 100 % |
| Music | – | 89.6 % | – | 89.6 % |
| Phone | – | 100 % | – | 100 % |
| Temperature | 100 % | – | – | 100 % |
| TV | 83.3 % | – | – | 83.3 % |
| Move | 88.9 % | – | 93.3 % | 91.1 % |
| Go to | 100 % | – | 88.9 % | 94.4 % |

Table 1: Accuracy of the BCI system for each part and control mask of the experiment for all subjects.

Table 2 shows the number of symbols for each mask and the resulting probability that a specific symbol flashes up. If more symbols are displayed on one mask then the probability of occurrence is smaller and this results in a higher P300 response which should be easier to detect. The flashes column shows the total number of flashes per mask until a decision is made. The translation time per character that is longer if more symbols are on the mask.

# 4 Discussion

The P300 based BCI system was successfully used to control a smart home environment with an accuracy between 83 and 100 % depending on the mask type. The difference in accuracy can be explained by the arrangement of the icons.

| Mask | Symbols | Probability (%) | Flashes | Time per character (s) |
|---|---|---|---|---|
| Light | 25 | 4 | 375 | 33.75 |
| Music | 50 | 2 | 750 | 67.50 |
| Phone | 30 | 3.3 | 450 | 40.50 |
| Temperature | 38 | 2.6 | 570 | 51.30 |
| TV | 40 | 2.5 | 600 | 54.00 |
| Move | 13 | 7.7 | 195 | 17.55 |
| Go to | 22 | 4.5 | 330 | 29.70 |

Table 2: Number of symbols, occurrence probability per symbol, number of flashes per mask (e. g. $25 \times 15 = 375$) and conversion time per character for each mask.

However, the experiment yielded 2 important new facts: (i) instead of displaying characters and numbers to the subject also different icons can be used, (ii) the BCI system must not be trained on each individual character. The BCI system was trained with EEG data of the spelling experiment and the subject specific information was used also for the smart home control. This allows using icons for many different tasks without prior time consuming and boring training of the subject on each individual icon. This reduces the training time in contrast to other BCI implementations were hours or even weeks of training are needed [1, 2, 3]. This reduction in training time might be important for locked-in and ALS patients who have problems with the concentration over longer time periods. The P300 concept works also better if more items are presented in the control mask as the P300 response is more pronounced if the likelihood that the target character is highlighted drops down [4]. This results of course in a lower information transfer rate, but enables control of almost any device with such a BCI system. Especially applications which require reliable decisions are highly supported. Therefore the P300 based BCI system is an optimal tool for the smart home control. The virtual smart home acts in such experiments as a testing installation for real smart homes. Also wheelchair control, which many authors identify as their target application, can be realized with this type of BCI system in a goal oriented way. In a goal oriented BCI approach it is then not necessary e. g. to move a robotic hand by thinking about hand or foot movements and controlling right, left, up, down commands. Humans just think “I want to grasp the glass” and the real command is initiated by this type of BCI implementation.

## 5 Conclusions

A P300 based BCI system is optimally suited to control smart home applications with high accuracy and high reliability. Such a system can serve as an easily reconfigurable and therefore cheap testing environment for real smart homes for handicapped people.

**Acknowledgments:** The work was funded by the EU project PRESENCCIA.

## References

[1] N. Birbaumer, N. Ghanayim, T. Hinterberger, I. Iversen, B. Kotchoubey, A. Kübler, J. Perelmouter, E. Taub, and H. Flor. A spelling device for the paralysed. *Nat.*, 398:297–298, 1999.

[2] C. Guger, A. Schlögl, C. Neuper, D. Walterspacher, T. Strein, and G. Pfurtscheller. Rapid prototyping of an EEG-based brain-computer interface (BCI). *IEEE Trans. Rehabil. Eng.*, 9:49–58, 2001.

[3] T. M. Vaughan, J. R. Wolpaw, and E. Donchin. EEG-based communication: prospects and problems. *IEEE Trans. Rehabil. Eng.*, 4:425–430, 1996.

[4] D. Krusienski, E. Sellers, F. Cabestaing, S. Bayoudh, D. McFarland, T. Vaughan, and J. R. Wolpaw. A comparison of classification techniques for the P300 speller. *J. Neural Eng.*, 6:299–305, 2006.

[5] G. R. McMillan and G. L. Calhoun. Direct brain interface utilizing self-regulation of steady-state visual evoked response. *Proc. RESNA*, June 9–14:693–695, 1995.

# Brain computer interface applications for a cybernetic prosthetic hand control

F. Aloise[1,2], A. Accardo[1,3], M. L. Blefari[4], D. Mattia[1], F. Babiloni[1,5], S. Salinari[3], M. G. Marciani[6], C. Cipriani[4], F. Vecchi[4], M. C. Carrozza[4], F. Cincotti[1]

[1]NEILab,Fondazione Santa Lucia IRCCS , Rome, Italy
[2]Dipartimento di Ingegneria Elettronica, Università "Tor Vergata", Rome, Italy
[3]Dipartimento di Informatica e Sistemistica (DIS), Università di Roma "Sapienza", Italy
[4]ARTSLab, Scuola Superiore S.Anna, Pisa, Italy
[5]Dipartimento Fisiologia Umana e Farmacologia, La Sapienza Università di Rome, Italy
[6]Dipartimento di Neuroscienze, Università "Tor Vergata", Rome, Italy

f.cincotti@hsantalucia.it

**Abstract**

Abstract The EEG based Brain Computer Interfaces (BCIs) have been eliciting an enormous interest in the field of neuroprosthetic device control. In this pilot study, we explore the opportunity to interface an EEG based BCI system with a cybernetic prosthetic hand (Cyberhand). Two BCI control signals, P300 and sensorimotor rhythm modulation, have been considered to operate a control of the Cyberhand. A P300-based BCI system was used to select different hand grasps between a set of eight global grasps of the Cyberhand and the preliminary findings indicated that a "gross" Cyberhand control can be achieved. As for the sensorimotor rhythm based BCI control, a twofold approach has been followed: a) the investigation of the EEG sensorimotor rhythm responsiveness to motor imagery of a set of simple movements to increase the number of recognizable "mental states" and b) the implementation of a software platform able to translate these mental states into direct motor commands for the prosthetic hand fingers. Altghough, this latter approach still needs validation, the results are promising for its future application.

## 1 Introduction

Over the last decade, an enormous interest has been elicited by the use of EEG signals in brain-controlled devices [1, 2, 3]. The Brain Computer Interface (BCI) paradigm bypasses the normal biological pathways mediating volitional movements and employing upstream neural activity that may have a complex relationship to motor or cognitive behavior. The transformation between this neural activity and the required control parameters can be facilitated by the BCI simply communicating the user's goal to devices that can handle some of the high-degrees of motor control [4].

This "shared approach" appears particularly relevant when BCIs are designed to operate prosthetic arm device, since it may compensate for the distributed interactions between the different central and peripheral neuromuscular elements underlying physiological motor control. This prompted us to follow a similar approach to implement a BCI operated a prosthetic robotic hand, represented by the Cyberhand which is a multifingered underactuated limb based on tendon transmission [5]. In the present pilot study, we implement a paradigm in which two BCI control signals will be employed to either select a global grasp of the prosthetic hand or to control directly the motors of CyberHand fingers. In this experimental context, we also explore the benefits of extra-vision somatosensory modality of feedback, namely tactile stimulation, for user training and control of the BCI system. The exploitation of different modalities of feedback is relevant for

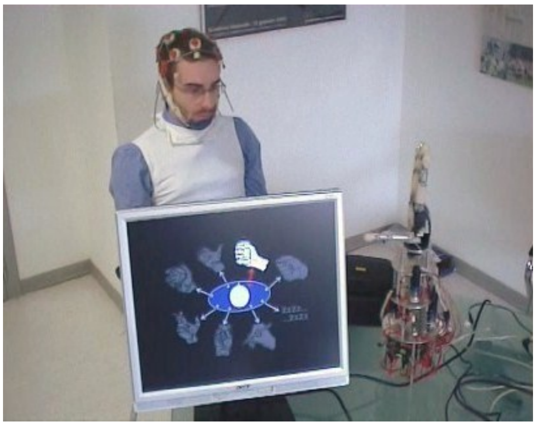

Figure 1: The experimental set-up of P300 prosthetic hand control.

the development of more efficient brain-computer communication, since the components of the visual system such as vision, visual attention, focusing gaze are physiologically engaged during the dynamic contact between the body and environment.

# 2 Methods

## 2.1 P300 BCI control signal

First, we allowed 4 subjects (1 female; 3 male; mean age 25) to control the CyberHand by means of P300 [6] evoked potentials induced by external stimulation (visual or tactile). Scalp activity was collected with a 12 electrode position cap and an EEG system (Brain Amp, Brain Products GmbH, Germany). EEG data sampling frequency was 250 Hz). The experimental setup also comprised: a tablet PC containing the BCI software platform [7], a set of vibro-tactile devices (tactors) and the CyberHand (Figure 1). The visual feedback was composed by a train of flashing stimuli representing eight actions: seven types of grasp (including cylindrical, lateral and tri-digital grasps) plus a "DoNothing" action to maintain the actual grasp (illustrated on the video-screen in Figure 1). In order to select an action, the subject was required to focus her/his attention on the stimulus related to the grasp, (e. g. counting the number of a given grasp appearance). Is in the case of Figure 1, when tactile feedback modality was used, every action was linked to the vibration of an electromechanical device (for a total number of eight devices) placed on the subject back or chest (Figure 1, the subject received tactile stimuli by the tactors mounted on a t-shirt) and the vibrotactile feedback was given for 200–360 ms at 250 Hz. The tactile feedback modality was meant to replace the ash of the visual stimuli, so to implement the entire platform as more portable. In both cases the application configuration could be modified acting on three fundamental parameters: Sequences (number of stimuli); Inter-Stimulus-Interval; Stimulus-Duration (visual/tactile stimulus). Once the subject made her/his selection, the Cyberhand performed the selected grasp or maintained the previous. Each experimental session consisted of 8 runs, either with visual and tactile feedback modality; each run consisted of 8 trials corresponding to the number of the actions, 7 hand grasps and 1 "DoNothing" actions. Each trial consisted of 16 to 32 stimuli (visual or tactile) according to the number of target presenting sequences (from 2 to 4 sequences). Each run lasted from 1 to 2 min, for a total of 10–15 min each experimental session. The subjects underwent 2 experimental sessions, for a total of 16 runs .

## 2.2 Sensorimotor rhythm BCI control signal

In the second part of the study, 3 subjects underwent several EEG recording sessions with a BCI system based on detection of simple motor imagery mediated by modulation of sensorimo-

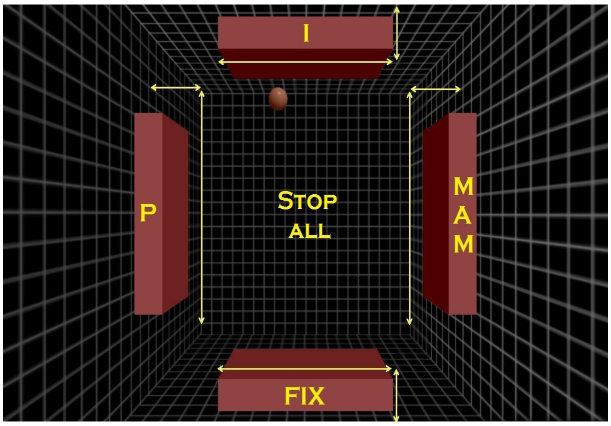


Figure 2: The user-interface of sensorimotor-based prosthetic hand control.

tor rhythms [7]. The detailed procedures for subject training are described elsewhere [8]. In brief, subjects needed to learn to modulate their sensorimotor rhythms (8–12 Hz and 14–30 Hz) to achieve more robust control (training) than the simple imagination of limb movements can produce (screening). In this set of experiments, a 61-channel electrocap was used to acquire the EEG signals and a subset of 1–3 channels (among C3, C4, Cz, CP3, CP4, CPz), re-referenced to the common average reference (CAR; the spatial filter used for training), was used to control horizontal or vertical cursor movement.

An initial screening session was meant to defined the EEG frequency peaks and scalp locations of each subject's spontaneous $\mu$- and $\beta$-rhythm activity during execution and imagination of simple movements. In coupled runs, the subject was asked to execute (first run) or to image (second run) movements of her/his hands, feet and tongue upon the appearance of different target positions. This sequence was repeated three times for a total of 12 trials. During following training sessions, the task consisted in moving the cursor toward a target, as soon as the latter appeared on any of the four sides of the screen (Figure 2). Appearance of each target was equally probable. The cursor movement was controlled by the subject, either by modulating amplitude of her/his mu rhythm bilaterally (vertical movement), or by lateralizing the rhythm (horizontal movement). To facilitate subject's training, she/he was suggested to concentrate on kinaesthetic imagination of movement [9] of her/his hands (HND, cursor up), his feet (FT, cursor down), his right or left hand (RH, LH, cursor right or left, respectively). EEG spectral features were extracted online using an autoregressive estimator running on overlapped, sliding epoch of 300 ms. Band power in the band 10–12 Hz from channels C3 and C4 was used to detect lateralization of $\mu$-rhythm (horizontal movement); an average of the same spectral features, contrasted with spectral power in the band 24–26 Hz from channel Cz, was used to detect bilateral (de)synchronization (vertical movement). Each training session lasted about 40 minutes and consisted of eight 3-minute runs of 30 trials each. We collected a total of 5 training sessions for each subject; training ended when performance was stabilized.

User performances was assessed by accuracy, namely the percentage of trials in which the target was hit and by the variable named $R^2$, a parameter used to characterize BCI performance [2]. This variable is computed as the correlation between the amplitude of the signal used to control cursor movement and the target position (top or bottom/right or left). Finally, in order to increase the number of possible contrasts (namely HND vs FT, RH vs LH), one more "mental task" was evaluated during the screening session, namely the imagination of tongue movements (TNG).

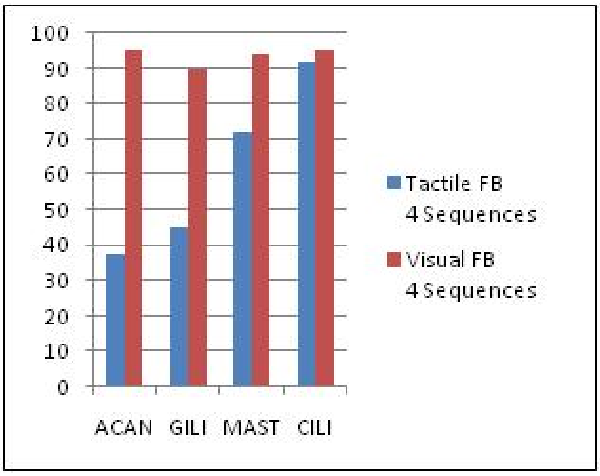


Figure 3: P300 control for the prosthetic hand, subjects performance.

# 3 Results

## 3.1 P300 BCI control signal

Figure 3 shows that all subjects ($n = 4$ subjects) were able to select different hand grasp types, which in turn imposed the movements of the Cyberhand, by means of the P300 based BCI paradigm, with performance percentage ranging from 72 % and 100 % when visual feedback modalities was utilized. On the contrary, level of performance decreased when all subjects (particularly for subject ACAN and GILI, in Figure 3) were provided with the tactile feedback modality (Figure 3; level of performance between 37 % and 92 %). Moreover, the tactile feedback was associated with a longer time of grasp classification, with the best subject CILI: 3.2 s for visual feedback versus 9.6 s for tactile feedback.

## 3.2 Sensorimotor rhythm BCI control signal

As for the mono- and bi- dimensional tasks, 2 subjects were able to control the both horizontal and vertical cursor movements with a high level of performance (100 %) within the first 2 sessions of BCI training (Figure 4, top panels). Similar level of performance were achieved by both subjects during the bi-dimensional task with a gradual increase of performance within the 4 BCI training sessions. (Figure 4, bottom panel).

We also investigated the EEG sensorimotor rhythm responsiveness to motor imagery of simple movements, including the imagery of tongue movements, during the screening phase. As shown in Figure 5, three distinct patterns of EEG sensorimotor reactivity could be found in association with the 3 different contrasts (Right-Hand vs. Left-Hand, Hands vs Feet and Tongue vs Foot), in all subjects. The level of r2 was higher for the Hands vs Feet contrast (Figure 5, HND vs FT, 0.5 in all subjects) with respect to both Right Hand vs. Left Hand (Figure 5, RH vs. LH; 0.2, first subject, 0.3 second and third subject) and Tongue vs. Feet (Figure 5, TNG vs FT, 0.2 in all subjects) contrasts.

Finally, we implemented the sensorimotor rhythm based BCI system to operate the Cyberhand. The implementation consisted in allowing the cursor to reach “areas” defined within a bidimesional space nearby the target (“target areas”) to control the Cyberhand flexion and extension movements, rather than the cursor hitting the target to achieve the Cyberhand movement control. As represented in Figure 2, the presence of the cursor within 5 defined “target areas” will allow for 3 global degree of freedom (gDoF). Three “target areas” correspond to: thumb (“P”), index (“I”) and the last three fingers (“MAM”) flexion whereas the remaining 2 areas are devoted to the extension of movements (“FIX”), and to the finger movement stop (“StopALL”). As regards the

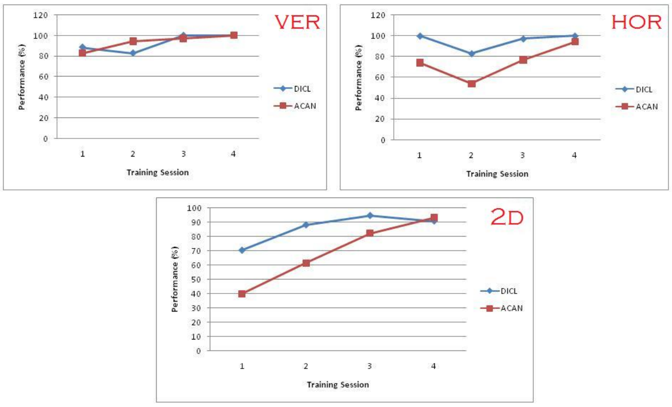


Figure 4: Sensorimotor control for the prosthetic hand, subjects performance.

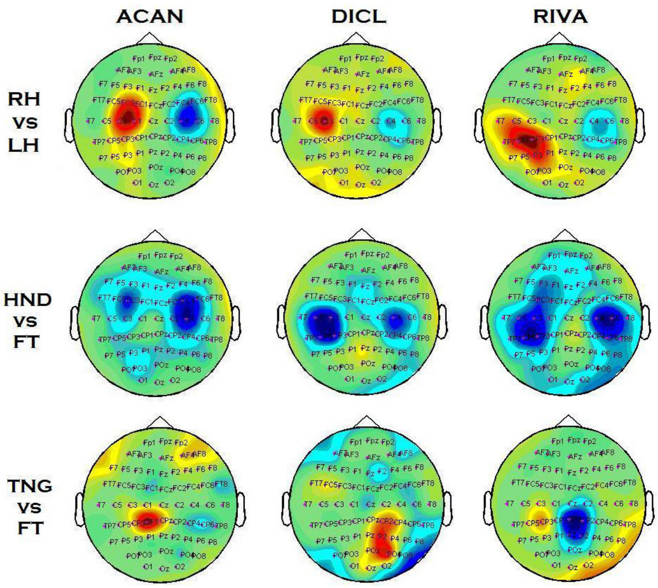


Figure 5: Sensorimotor Rhythm Patterns (3 subjects, 3 couple-tasks).

"FIX- target area", it also provides for a way to correct undesired (wrong) finger flexion, during the prosthetic hand control.

# 4 Discussion

This pilot study provide for a promising exploitation of two BCI control signals, P300 and sensorimotor rhythm modulation, to actuate a cybernetic prosthetic hand. Indeed, our findings indicated that P300 based BCI system can efficiently operate a "gross" control of the Cyberhand by selecting a desired grasp among a set of eight grasps. Although, the validity of the second BCI control signal considered has to be demonstrated, the opportunity to increase the number of distinguishable "mental states" together with the implementation of appropriate interface may represent a potential strategy for a successful "fine" EEG based BCI control of the Cyberhand.

## 5 Conclusion

In conclusion, this pilot study provides for promising findings for future BCI applications in cybernetic prosthetic hand control.

## References

[1] J. R. Wolpaw, N. Birbaumer, D. J. McFarland, G. Pfurtscheller, and T. Vaughan. Brain-computer interfaces for communication and control. *Clin. Neurophysiol.*, 113:767–791, 2002.

[2] J. del R. Millán, F. Renkens, J. Mourino, and W. Gerstner. Noninvasive brain-actuated control of a mobile robot by human EEG. *IEEE Trans. Biomed. Eng.*, 51:1026–1033, 2004.

[3] G. R. Müller-Putz, R. Scherer, G. Pfurtscheller, and R. Rupp. EEG-based neuroprosthesis control: a step towards clinical practice. *Neurosci. Lett.*, 10:1767–1771, 2005.

[4] J. R. Wolpaw. Brain-computer interfaces as new brain output pathways. *J. Physiol.*, 579:613–619, 2007.

[5] M. C. Carrozza, G. Cappiello, S. Micera, B. B. Edin, L. Beccai, and C. Cipriani. Design of a cybernetic hand for perception and action. *Biol. Cybern.*, 95:629–644, 2006.

[6] E. W. Sellers, D. J. Krusienski, D. J. McFarland, T. M. Vaughan, and J. R. Wolpaw. A P300 event-related potential brain-computer interface (BCI): the effects of matrix size and inter stimulus interval on performance. *Biol. Psychol.*, 73:242–252, 2006.

[7] G. Schalk, D. J. McFarland, T. Hinterberger, N. Birbaumer, and J. R. Wolpaw. BCI2000: A general-purpose brain-computer interface (BCI) system. *IEEE Trans. Biomed. Eng.*, 51:1034–1043, 2004.

[8] F. Cincotti, D. Mattia, F. Aloise, S. Bufalari, G. Schalk, G. Oriolo, A. Cherubini, M. G. Marciani, and F. Babiloni. Non-invasive brain-computer interface system: Towards its application as assisitive technology. *Brain Res. Bull.*, 75:796–803, 2008.

[9] C. Neuper, R. Scherer, M. Reiner, and G. Pfurtscheller. Imagery of motor actions: Differential effects of kinesthetic and visual motor mode of imagery in single-trial EEG. *Cogn. Brain Res.*, 25:668–677, 2005.

# Using a brain-computer interface for rehabilitation: a case study on a patient with implanted electrodes

A. Van Langhenhove[1], M.-H. Bekaert[1], J.-P. N'Guyen[2]

[1]LAGIS, CNRS UMR-8146, University of Lille, Villeneuve d'Ascq, France
[2]Laënnec Hospital, Service of neurosurgery, Nantes, France

a.van-langhenhove@ed.univ-lille1.fr

**Abstract**

Brain-computer interfaces (BCIs) allow direct communication between men and computers thanks to the analysis of brain activity. Current applications of BCIs in assistive technologies are: palliative communication systems for patients with complete muscular paralysis and restoration of movement for people with a motor infirmity (orthetic or prosthetic devices controlled by the thought). It appears today that brain-computer interfaces can also be used in therapeutic approaches to rehabilitation or functional recovery through neurofeedback. In this paper we briefly review several therapeutic uses of brain-computer interfaces and present a clinical experiment with an hemiparetic patient who has used a BCI as a motor rehabilitation tool.

## 1 Introduction

### 1.1 BCIs and therapeutic approach

Brain-computer interfaces open a new pathway between the human brain and machines [1]. By analyzing his cerebral activity, a BCI gives an additional communication channel to its user, to restore motor functions (orthesis or prosthesis control), to drive machines (a robotic arm, a wheelchair) or to communicate with his environment [2, 3, 4]. A recent field of BCI application is the study of brain mechanisms, dysfunction and functional recovery. Another one is the assistance to diagnosis and functional rehabilitation [5]. In synchronous BCIs, event related potentials allow studying the recovery of neuronal mechanisms related with language amongst aphasic patients with brainstem strokes [6]. Control of slow cortical potentials in asynchronous BCIs allow the reduction of epileptic attacks in some cases [7]. Brain-computer interfaces can also be useful in neural rehabilitation of patients with severe impairments while reinforcing the use of damaged neuronal paths using their plasticity [8]. Finally, the use of BCIs for motor rehabilitation must not be disregarded [9]. This article presents a clinical experience with a patient who is suffering from hemiparesis. Here the BCI is used as an assistive tool for motor recovery (hand re-education).

### 1.2 The BCI structure

BCIs can be non-invasive (the cerebral activity is recorded from the scalp) or invasive. In the latter case, cerebral activity is recorded by tiny multielectrode arrays or by isolated electrodes, either implanted in the cortex, or laid out over the cortex epi- or sub-durally. We present in this article a case study on a patient with an electrode array placed over the dura mater, above the sensory-motor area.

In many applications, BCIs give the user a feedback that is often visual, and sometimes auditory or tactile. This feedback informs the user about the state of the application and/or about his own mental state. The therapeutic use of biofeedback appeared in the USA in the early 1970s [10]. The neurofeedback (biofeedback from EEG oscillations or ERPs) consists in recovering and presenting to the patient some of the characteristic cerebral signals of his mental state. With specific training the patient learns how to increase the signal power in a chosen frequency band (for example the signals of the sensorimotor rhythm, 8 to 12 Hz) and how to decrease the activity of other signals. Thus he/she succeeds in modulating his/her own physiological reactions. The studies carried out on the regulation of the slow cortical potentials, the sensorimotor rhythms and the BOLD response (Blood Oxygen Level Dependent response measured with functional magnetic resonance imaging) showed various effects on behavior. The regulation of slow cortical potentials enables us, for example: to decrease the reaction time in motor tasks; to accelerate the lexical decisions; to increase memory performance.

In the clinical experiment described below the neurofeedback is displayed as a simple cursor. The cursor movement is associated with the movement of the patient's paretic hand. There is a correlation between event-related desynchronization of mu rhythm and shift in the cursor. In our interface, the feedback does not inform the patient about the application state nor about his mental state, but only about the efficiency of command signals appearing in his motor cortex.

# 2 Experimentation

## 2.1 Context

The subject is a 39 year old right-handed man. He suffers from hemiparesis and neuropathic pains on the right side of his body due to deep contusions of his brainstem. When neuropathic pains are resistant to drug treatments, a therapeutic alternative is motor cortex stimulation [11]. In this particular case, the surgical operation was performed at Nantes hospital. The surgery consisted in placing eight electrodes over the dura mater, above sensorimotor cortex areas that correspond to the painful limbs, in order to stimulate electrically these cortical areas. A partial reduction of pains resulted from this chronic electrical stimulation. In compliance with the patient, we diverted the normal use of electrodes to measure his brain activity in order to control a BCI. Since the subject keeps partial control of his right side limbs, more especially of his hand, we wanted to verify if a BCI could be used as a rehabilitation tool. We had access to electrodes during only three days. After this short period, a stimulator was connected to the electrodes which were then only used for cortical stimulation.

## 2.2 Neurophysiologic phenomenon

The neurophysiologic phenomenon used to drive the interface is the mu rhythm desynchronization in motor cortex area which corresponds to the deficient hand.

In Figure 1, we show the power spectrum of two signals recorded on the scalp at location C3 (according to the 10–20 international system of electrodes placement). This location is above the cortical area controlling the right hand. The solid curve corresponds to a measurement while the person moves his right hand (e. g. alternately opens and closes the hand). The dotted curve corresponds to a resting situation. We observe that there is a significant decrease of the signal power in the 8 to 12 Hz frequency range, when the person is moving his hand. Experiments show that the desynchronization of the mu rhythm usually starts two seconds before the actual movement.

## 2.3 Signal acquisition

During the experiment, two electrodes of EMG (Electromyography) were placed on the patient's right forearm above the muscles that control the opening and the closing of the hand. Moreover, as we explained earlier (see 2.1), stimulation electrodes were implanted over the patient's dura mater, above the sensorimotor areas corresponding to his deficient limbs. Two flat, four-pole inline electrode strips were positioned over the sensorimotor area perpendicular to the central sulcus.

One grid on foot areas and one on hand areas. For both grids, two electrodes cover the primary motor cortex and the others cover the primary sensory cortex.

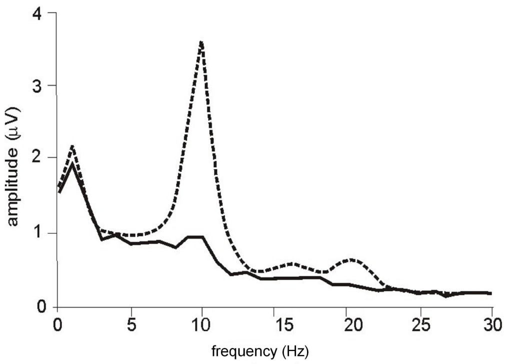


Figure 1: Two signals measured on a patient's scalp at location C3.

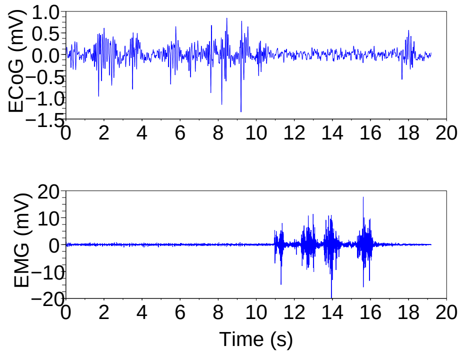


Figure 2: ECoG band-pass filtered between 0.5–20 Hz and EMG band-pass filtered between 3–256 Hz.

All electrodes were connected to a biosignal amplifier. It measures the voltage difference between each electrode relatively and a reference electrode placed on the patient's right mastoid. The ground electrode was placed on the patient's healthy forearm (left hand side). Signals were recorded using a 512 Hz sampling-rate, filtered by a eigth order band-pass filter [0.1 Hz; 200 Hz] and by a fourth order notch filter [48 Hz, 52 Hz].

## 2.4 Brain-computer interfacing

We used a portable BCI system assembled in our laboratory [12]. The system is composed of a biosignal amplifier (g.USBamp by Guger Technologies), a laptop, BCI2000 software, and of an extra LCD screen. The interface measures and records brain signals, and performs signal processing in order to transform them into commands. In this experiment, we only used a basic visual feedback, i. e. a small red square moving up and down on the computer screen.

The interface isolates the mu rhythm in the signal corresponding to the motor area of the hand. The value of the signal power, in the 8–12 Hz frequency band, is subtracted from a threshold corresponding to the half of its maximal power. The maximal power is determined when the patient is resting. The difference is multiplied by a coefficient that allows us to correlate the strength of the movement with the speed at which the cursor moves. When the patient keeps his impaired hand motionless, the cursor drops. As soon as the patient moves the hand, the cursor goes up. If the patient maintains the movement, the cursor reaches the top of the screen. The more effective the force and the speed of the movement are, the more the power of the mu rhythm decreases, which accelerates the rise of the cursor toward the top of the screen. We can adjust two values: the threshold value and the correlation coefficient. By decreasing the threshold, the difficulty of the exercise is increased (the cursor appears "heavier" to raise). By altering the correlation coefficient, the movement of the cursor is slower (the cursor appears "help up").

## 2.5 Experiment chronology

The experiment unfolded in two steps. The first one consisted in measuring the patient's brain activity during a motor task, i. e. when he alternately closed and opened his deficient hand, without using the feedback from the brain-computer interface. This measurement was composed of two episodes of ten seconds each. During the first ten seconds, the patient had to remain motionless and relaxed. Then, the investigator asked him to open and close his hand alternately during the next ten seconds. This task was carried out a significant number of times (ten to fifteen times) in order to collect enough data. Using these data, we first determined what pair of ECoG electrodes

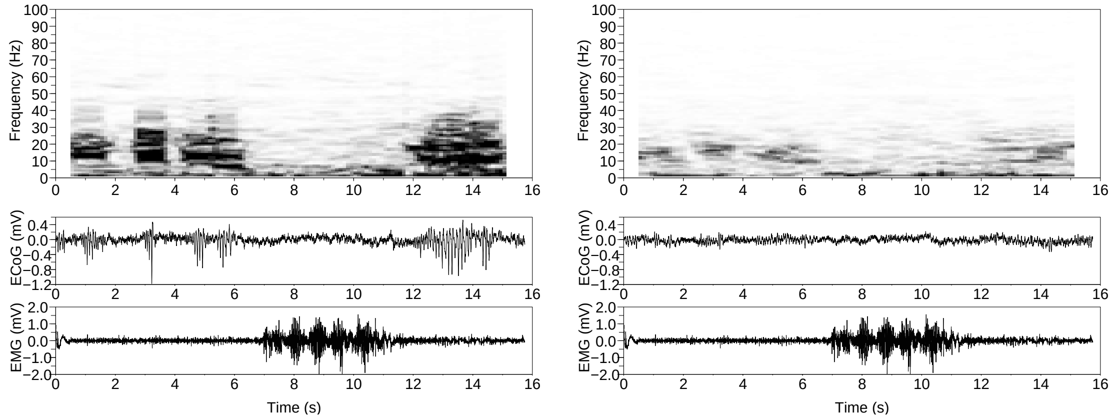


(a) 6-1

(b) 8-1

Figure 3: Signal spectrograms by bipolar measure between two channels.

should be chosen in order to identify optimally the patient's brain activity in the hand motor area. Secondly, we determined what configuration parameters should be used for the BCI to respond properly to the orders given by the patient when moving his hand.

The second step included several sessions. During these sessions, the patient tried several times to open and close his paretic hand. Each attempt lasted about twenty seconds. During the first five seconds, the patient had to keep still and relaxed. Then, after an instruction from the investigator, the subject started opening and closing his deficient hand alternately. He had to open and close his hand as fast as possible. After ten seconds, the investigator asked him to stop moving and to remain still and relaxed. The recording continued for five seconds after the movements had stopped. Every other attempt was performed without feedback. When the feedback was used, the patient's goal became lifting up the cursor as fast as possible in order to reach the top of the screen. In fact, to succeed, he also had to open and close his paretic hand as fast as possible, but without looking at the latter.

# 3 Results

## 3.1 Choice of electrodes and parameters

Among the implanted electrodes, four electrodes are above the foot area (channels 1 to 4) and four are above the hand area (channels 5 to 8). We have chosen the most appropriate pair of electrodes (one above the foot area and one above the hand area). In order do so we have compared the signal spectrograms obtained by bipolar measurements. The selected pair corresponds to channels 6 and 1. We have verified afterwards that this corresponds exactly to the somatotopy, since electrode 6 was just above the hand region in the motor cortex and electrode 1 above the foot region in the sensory cortex, i. e. in a region with an activity as different as possible from the activity recorded by electrode 1. The spectrogram computed with signals from this electrode pair clearly shows a decrease in the signal power (in the spectrogram, the darker the gray level, the more powerful the signal). This decrease shows desynchronizations of mu and beta rhythms that occur during movements. Figure 3(a) and 3(b) illustrate our choice.

For this experiment, signal processing parameters and classifier parameters were manually identified by simulation. We generated offline signals with characteristics similar to those of the recorded brain signals (amplitude and frequency) and used them to adjust the parameters of the classifier.

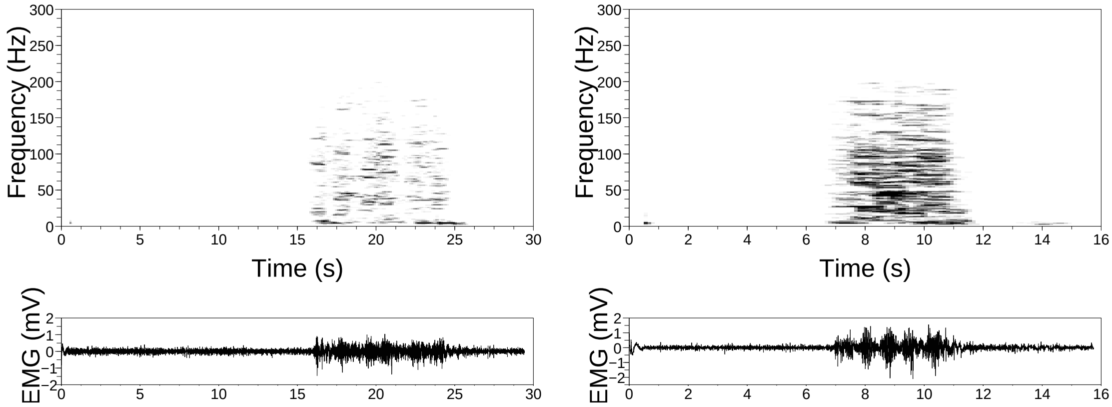


(a) Without feedback. (b) With feedback.

Figure 4: EMG of attempt with and without feedback.

### 3.2 Results interpretation on an sample session

During a single session, the subject tried to move his paretic hand several times, sometimes with feedback and sometimes without. Each attempt lasted twenty seconds (five seconds of rest, ten seconds of movement, five seconds of rest). Figure 4 shows the EMG signal for the first two attempts during the same session. We can observe a high power spectrum in the high-frequencies during the attempts with feedback (Figure 4(b)). This power is correlated with the intensity of the clamping force of the hand. In addition bursts appear more distinctly in attempts with feedback and each one corresponds to a complete closing movement of the hand. In Figure 4(a), no burst is visible and the spectrogram clearly shows less power.

Eventually, the visual observation of the patient during attempts showed that with feedback his movements seemed complete and fast, whereas without feedback they seemed more painstaking and less powerful.

## 4 Conclusion

Publications don't relate any experience using a BCI in the context of functional rehabilitation. There are mainly examples in which a BCI is used to restore the movement of a completely paralyzed limb, but using an orthetic device. The experiment that we carried out in Nantes seems to show that motor rehabilitation could be a new field of BCI application in the clinical environment.

The electrodes implanted over the dura mater allowed us to get signals of very good quality, which probably explains the success of this short-duration experiment. The results presented only use informations extracted from the low frequency bands similar to those extracted from surface signals in most other studies. However, since intracranial signals carry higher frequencies components (for example the $\gamma$ rhythm in the frequency band 50–200 Hz), these can probably be used to improve system performance. Discrimination between various movements of the hand is likely to be made easier with those signals.

As we could only use the electrodes for three days, the results must now be verified under a more precise and longer experimental protocol and on a larger population. We still have to compare these results with those provided by signals recorded on the patients scalp.

## References

[1] G. Dornhege, J. del R. Millán, T. Hinterberger, D. J. McFarland, and K.-R. Müller. *Toward Brain-Computer Interfacing*. MIT Press, 2007.

[2] G. Pfurtscheller, G. R. Müller-Putz, J. Pfurtscheller, and R. Rupp. EEG-based asynchronous BCI control functional electrical stimulation in a tetraplegic patient. *EURASIP J. Appl. Signal Proc.*, 19:3152–3155, 2005.

[3] J. Philips, J. del R. Millán, G. Vanacker, E. Lew, G. Ferran, P. W. Ferrez, H. Van Brussel, and M. Nuttin. Adaptive shared control of a brain actuated simulated wheelchair. *IEEE 10th Int. Conf. Rehabil. Robotics*, pages 408–414, 2007.

[4] J. R. Wolpaw, N. Birbaumer, D. J. McFarland, G. Pfurtscheller, and M. Vaughan. Brain-computer interfaces for communication and control. *Clin. Neurophysiol.*, 113(6):767–791, 2002.

[5] M. Stokes and C. J. James. W9 brain-computer interfacing (BCI) in rehabilitation. *Workshops/Clin. Neurophysiol.*, 117:S25–S31, 2006.

[6] F. Pulvermüller, B. Mohr, and W. Lutzenbergers. Neurophysiological correlates of word and pseudo-word processing in well-recovered aphasics and patients with right-hemispheric stroke. *Psychophysiol.*, 41(4):584–591, 2004.

[7] B. Kotchoubey, U. Strehl, C. Uhlmann, S. Holzapfel, M. Koenig, W. Frescher, V. Blankenhorn, and N. Birbaumer. Modification of slow cortical potentials in patients with refractory epilepsy: a controlled outcome study. *Epilepsia*, 42(3):406–416, 2001.

[8] B. H. Dobkin. Brain-computer interface technology as a tool to augment plasticity and outcomes for neurological rehabilitation. *J. Physiol.*, 579(3):637–642, 2007.

[9] N. Birbaumer and L. G. Cohen. Brain-computer interfaces: communication and restoration of movement in paralysis. *J. Physiol.*, 579(3):621–636, 2007.

[10] J. Stoyva, T. Barber, L. V. DiCara, J. Kamiya, N. E. Miller, and D. Shapiro. *Biofeedback and Self-Control*. Aldine-Atherton, 1970.

[11] J. P. Nguyen, J. P. Lefaucheur, C. Le Guerinel, J. F. Eizenbaum, N. Nakano, A. Carpentier, P. Brugières, B. Pollin, S. Rostaing, and Y. Keravel. Motor cortex stimulation in the treatment of central and neuropathic pain. *Med. Res.*, 31:263–265, 2000.

[12] A. Van Langhenhove, M. H. Bekaert, and F. Cabestaing. Vers une BCI utilisable en dehors du milieu clinique. *1ère Conférence Internationale sur l'Accessibilité et les Systèmes de Suppléance aux personnes en situations de Handicaps, ASSISTH'2007*, pages 369–375, 2007.

# Brain2Robot: a grasping robot arm controlled by gaze and asynchronous EEG BCI

M. Danóczy[1], S. Fazli[1], C. Grozea[1], K.-R. Müller[1,2], F. Popescu[1]

[1]Fraunhofer Institute FIRST, IDA Laboratory, Berlin, Germany
[2]Berlin Institute of Technology, Berlin, Germany

florin.popescu@first.fraunhofer.de

**Abstract**

The Brain2Robot system is described and basic functionality is presented as tested on healthy users. A 6 degree of freedom robot arm with a gripper, of similar size to a human arm and designed to be mounted on a wheelchair, is controlled by a combination of signals obtained by gaze tracking and motor imagination detected via EEG BCI. Design aspects are described, including 3D gaze tracking and requirements of self-paced BCI control for sending reliable commands to the robot arm. Results are presented in which healthy subjects grab objects arbitrarily placed on the table by fixating at them and imagining a movement of the arm.

## 1 Introduction

Although detection of mental activity appears to be a singularly convenient channel of communication in cases of severe paralysis, and is the only option in the rare cases for locked-in state, serious challenges remain before BCI technology can be used in the everyday life of patients. In the case of non-invasive BCI, EEG being most common as sensor technology, much progress has been made in the last few years: the users no longer need lengthy training and mental imagination detection can be highly accurate in some users. Nevertheless, the information transmission rate (ITR) achievable is modest, at less than 50 bits per minute (bpm). Even for the best performers, this communication speed is insufficient for practical 3D control of a robot which can grab objects and manipulate them, being less than that seen in a single 1D human arm joint control. Some EEG-BCI designs, however, have achieved 2D cursor control, though it requires extensive user training [1]. Since information can be used (decoded) in a variety of ways, and can benefit from innovative control paradigms for controlling objects such as wheelchairs [2] the 'conservation' law of information means that the control of 3 or more joints is possible with EEG-BCI at the cost of time: a well coordinated grasping movement would require an impractical amount of time to complete.

The other issue, besides speed, is the concentration level (mental effort) required on the part of the user, who must master BCI as well as a possibly complex control paradigm. In order for BCI control of prosthetics to be practical – that is, be accepted by the disabled user population – it must be easy and intuitive enough to be 'worth the effort'. As such, invasive BCI designs over an ITR speed increase of a factor of 2 to 4 over EEG BCI: the costs here would be the risk of surgical intervention and the degradation and variation of signal quality with time, for an ITR level which is still much below that needed for grasping. In the Brain2Robot project, a possible solution is presented which preserves intuitiveness of use and leaves much of the joint coordination and control to the computer rather than relying on brain signals. The target position is indicated by tracking the 3D point of gaze of the user, which is normally coordinated with a grasping movement in healthy users.

# 2 Methods

## 2.1 BCI calibration trials

2 healthy volunteer subjects (both male) participated in this study. A 70-channel DC amplifier set-up (BrainAmp128DC, Munich, Germany) was used (64 EEG channels and 4 bipolar EMG/EOG channels). In the first part of the experiment ("calibration session"), 2 sequences of 70 left/right/foot cues was presented visually by means of a letter which appears in the middle of the computer screen. The subject was asked to imagine the cued class without moving either limbs or the eye. Apart from offline checks, electromyograms and electro-oculograms were monitored. During this part the 2 active classes are chosen (most discriminative of three movement imagination trials: of left hand, right hand, or foot). Another class we refer to is the "rest class", which is sometimes called an "idle class".

In a second part of the experiment subjects were asked to move a cross displayed on the screen to a target represented by a bar on either the right or left side of the screen by imagining the corresponding class ("1D feedback trials"). The cross movement provided continuous performance feedback to the subjects. After training, 70 trials of normal, synchronous left/right target feedback trials were performed (no rest state, cursor moved as soon as the target was presented): this was done to ensure quality of common spatial patterns as well as to compare "usual" BCI performance to asynchronous performance. Cross-validation with LDA classifiers was used on the resulting CSPs only on training trials.

The subject then performed 80 idle-to-active feedback trial attempts, in 2 blocks of 40 trials each with cued rest periods ("rest class training"). The cues are given to imagine the one of the two active classes (Left Hand, Right Hand, or Foot, as is best for that subject) or to relax, for 15 seconds. Afterward the rest class training session the asynchronous control is ready for use, using control law parameters which are optimized over the data collected during block 1. For further reference the active classes will be designated as "L" and "R" (left and right movement of the cursor used in training) and the "rest" class (otherwise known as an idle class) as "X".

## 2.2 BCI classification and data processing

In controlling a grasping robot, it is essential that the control be self-paced (the robot move when intended) and have an idle or rest class (the robot moves only when intended). This is for reasons of usability as well as safety. For this reason, we have implemented a self-paced idle state paradigm whose further details can be found in [3]. It introduces adaptive covariance estimation and a control law to a Mahalanobis distance approach first introduced in [4]. The basic algorithm depends on the CSP algorithm and semi-automatic frequency filter of the Berlin Brain Computer Interface described introduced in [5]. The raw EEG is filtered by a spatial (CSP) and temporal filter combination:

$$y(z) = W \cdot h(z) \cdot \epsilon(z) \tag{1}$$

Where $\epsilon(z)$ is the $z$-transform of the raw EEG signal. The features used for classification are the first 2 and last 2 elements of $y$, (corresponding to the 2 most discriminative components for each class), fed through a moving window of size $w$ (800 ms) upon which the log of the variance is calculated.

The feature vectors are either passed through a linear discriminant analysis, as is customarily done (LDA classifier), or an adaptive covariance and mean estimation of the feature vectors is performed according to an update calculated at the end of each new trial (adaptive Gaussian classifier). Assuming a labeling function $l(k,T)$ which assigns every recorded time point to a desired class $k$ and trial number within that class $T$, we can define an adaptive estimator containing an adaptation coefficient $\alpha$ which is adjustable.

$$\begin{aligned}
\hat{\mu}_{l(k,T+1)} &= (1-\boldsymbol{\alpha})\hat{\mu}_{l(k,T)} + \boldsymbol{\alpha}\mu(\mathbf{x}(l(k,T+1))) \\
\hat{\Sigma}_{l(k,T+1)} &= (1-\boldsymbol{\alpha})\hat{\Sigma}_{l(k,T)} + \boldsymbol{\alpha}\mathbf{x}(l(k,T+1))^{2\otimes} - \boldsymbol{\alpha}(1-\boldsymbol{\alpha})\left(\hat{\mu}_{l(k,T)} - \hat{\mu}_{l(k,T+1)}\right)^{2\otimes}
\end{aligned} \tag{2}$$

The adaptation parameter is optimized on the rest-class training data and involves the minimization of the average Mahalonobis distance between the data in each new trial to the distribution estimated on the previous trial, $x(l(k, T+1))$. Once the controller operates on unlabeled data (self-paced) the adaptation ceases. Furthermore in the adaptive Gaussian classifier the mean and covariance estimates for each of the classes (rest, left, right) are used to transform the feature vectors into normalized probabilities of class membership:

$$p(\mathbf{x}(t)|\text{class} = k) = N(\mathbf{x}(t), \hat{\mu}_{l(k,T)}, \hat{\Sigma}_{l(k,T)}) \tag{3}$$

$$P_k(t) = \frac{p(\mathbf{x}(t)|\text{class} = k)\mathbf{p}_k}{\sum_j p(\mathbf{x}(t)|\text{class} = k)\mathbf{p}_j} \tag{4}$$

Finally these class probabilities are fed into a "control law" which moves the cursor (not necessarily seen) and has an adjustable parameter $z$:

$$c_{k+1} = c_k + dt((P_L - P_R)(1 - P_0) - \mathbf{z}P_0 c_k) \tag{5}$$

Finally, the classes L and R are "activated" when the cursor reaches the adjustable thresholds $q_L$ and $q_R$. The cursor begins at zero after every activation of a class or after initialization of the idle-class classifier. Finally, the ITR is calculated, either from actual trials or through simulation from recorded data from the confusion matrix of the 3 classes (the probability of activation $A$ given intended class $K$) and their respective average (optimal) activation times and optimal prior class distribution :

$$\begin{aligned} \mathbf{p}_A &= P_{A|K}\mathbf{p}_K, \mathbf{h}_{A|K} = P_{A|K}\mathbf{p}_K \\ \text{ITR}(A|K) &= \frac{\sum -h(\mathbf{p}_A) - \mathbf{h}_{A|K}}{\mathbf{t}_K^T \mathbf{p}_K} \end{aligned} \tag{6}$$

Where $h(x) = -x\log_2(x)$. This ITR value can be calculated either for the actual indexing function used in the rest-classtraining session of on a class of indexing functions which provide the optimal (in terms of maximally achievable ITR) random sequence of classes and desired message durations (determining the probabilities $\mathbf{p}_k$ and durations $\mathbf{t}_k$ which are called source code parameters). Adaptation and control law parameter were optimized for the maximal ITR.

## 2.3 Eye tracking

In contrast to common applications such as tracking the user's gaze trajectory over a computer screen or an image, which requires 2D gaze tracking, identifying the target position in 3D space requires 3D (stereo) gaze tracking. For this purpose we use two of goggle-mounted cameras which track both left and right pupil (ViewPoint Eye Tracker, Arrington Research, Scottsdale, AZ). The three spatial coordinates of the gaze point are parametrized in spherical coordinates as azimuth, elevation and distance, relative to the origin of the head reference frame. A schematic is shown in Figure 1. The position and rotation of the head reference frame, as well as other tracked objects described in this paper were located and tracked in 6 degrees of freedom using an OptiTrack system with Rigid Body Software (Natural Point, Inc., Cornvallis, OR).

The 3D gaze tracking problem is to map pupil coordinates for left and right eye, which are the outputs of the eye-tracking cameras, to a 3D point in head space. To learn this mapping, we train a linear basis function model, $y = w^T\ f(x)$, where the four-dimensional input vector $x$ comprises the pupil coordinates, $x = [x_L, x_R, y_L, y_R]$, $y$ is any of the outputs $\phi$, $\theta$ or $r$, and the basis functions $f(x)$ of all polynomials up to 2$^{\text{nd}}$ order, i. e. $f(x) = \{1, x_L, x_L^2, x_L y_L, \ldots, x_R, x_R^2\}$. To prevent overfitting, we assume a Gaussian prior over the weights, leading to quadratic regularization term. The covariance of the prior is chosen by maximizing model evidence [6]. For parameter learning, 30 gaze points are collected using a target, the position of which is given by the 3D tracking system. Since in our experience the estimation of target distance $r$ tends to be imprecise, we intersect the gaze line $w$.

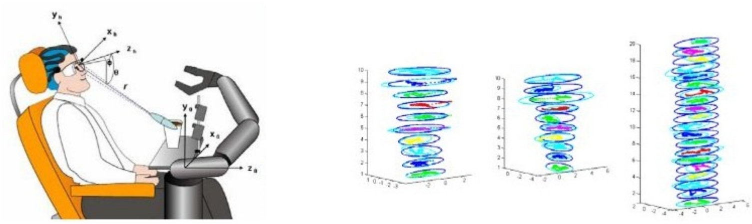

Figure 1: Left: Schematic of coordinate systems and position variables. The base coordinate system ($x_0$, $y_0$, $z_0$) is centered at the base of the robot arm's shoulder joint. The head tracking cameras provide acurrent estimate of the head-centered coordinates ($x_h$, $y_h$, $z_h$), while eye tracking cameras provide gaze azimuth and elevation angles ($\phi$ and $\theta$) and gaze distance $r$, in head coordinates. The final gaze position, and its 1 standard deviation estimate, is shown graphically by the ellipsoid at the end of the gaze vector. Right: Adaptation of covariance and mean estimates (optimal) for L class (leftmost), R class (middle) and X (right panel). The 1$^{\text{st}}$ and 4$^{\text{th}}$ components of the feature vector trajectories are shown. The thin ellipse is the covariance, mean estimation within the trial, and the thick ellipses are the optimally adapted estimates.

### 2.4 Robot control

The subjects manipulated objects (standard drinking cups randomly placed on the table) using a robot arm (Assistive Robotic Manipulator, Exact Dynamics, NL) mounted on a facing table. The "grab" command is given when the robot is in "home" position, the head position and gaze vector are stable (within 2 degrees for over 2 s), the gaze distance is less than 1 m, the target point was within the robot's workspace and an activation threshold was hit by the BCI command. The target point was the intersection of the gaze vector with the table ($z_0 = 0$ in Figure 1). We implemented the action of grabbing a cup standing sitting on the table by moving the robot with an open gripper 10 cm closer to the subject in the $z_0$ direction than the target point and moving forward 20 cm while closing the gripper. The cup was brought by the robot to "drinking position" (near the subject's mouth) and then placed back upon the table ("place") upon BCI activation, with the robot returning to "home" position. The sequence was repeated 20 times. The position of the mouth is known relative to the glasses (it does not vary considerably from subject to subject).

## 3 Results

The two subjects had 1D feedback performance of 90 and 68 % respectively. The optimal ITR for the first subject (49.53) is found in Figure 2. For the second subject it was 6.29 with $t_k$ (optimal) of 2.23, 2.14 and 3.08 – significantly poorer. A graphic representation of the class covariance and mean estimates and their evolution is found in Figure 1 (right) and further details of idle-state control design are shown in Figure 2.

The idle-state controller was able to activate the cup grabbing, and the eye tracking was accurate enough such that the cup was not knocked over in any trial for either subject. Traces of a sample cup grabbing sequence is shown in Figure 3. Gaze tracking errors (test set validation) were ($\phi$, $\theta$, $r$) 0.19°, 0.74°, 5.18 cm in Subject 1 and 0.84°, 0.68°, 7.46 cm in Subject 2.

## 4 Discussion

The results shown represent a moderately complex system of interacting components representing a serious engineering challenge, which can be separated into three components: robot control, eye tracking and self-paced BCI. The robot control part was the least challenging, at this stage, since the sequence of commands depends mostly on the detected position of an object on a table, which was accurate enough.

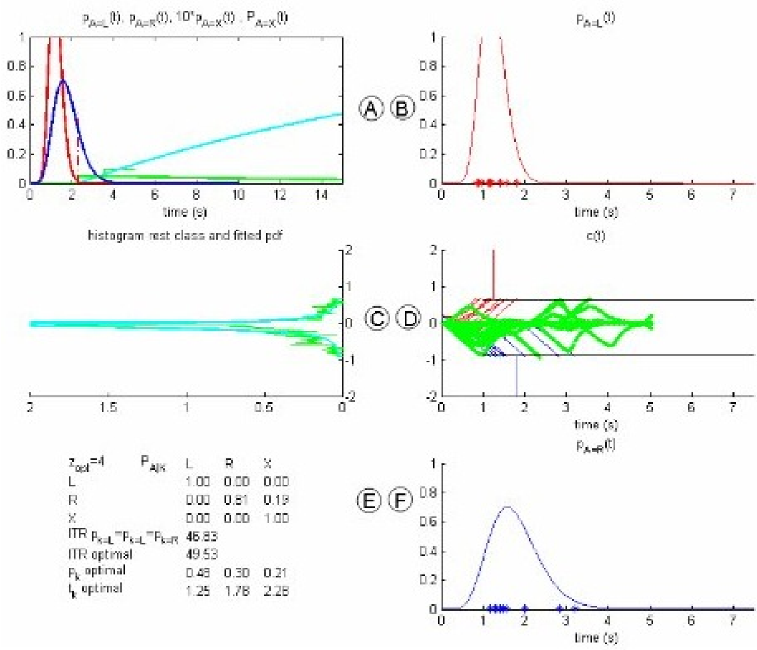

Figure 2: Idle-state control. Data is from subject 1. Panels: D) cursor trajectories for each cued class. Active class cursor trajectories intercept optimized thresholds $q_L$ and $q_R$ (horizontal lines) with average intercept times depending on these thresholds (vertical lines). Rest class – thick lines – trajectories stay within the thresholds. B) and F). Intercept times (* on $x$-axis) and their fitted probability distribution (gamma) for the L and R classes. C) Rest class trajectory histogram and fitted probability distribution function (pdf). A) same probability distribution functions as in B) and F) the probability distribution function of rest class intercept of threshold $p(A = L, R|K = X) = \beta \exp(-\alpha t), t > t_0$ fitted from histogram of rest class intercept (false positive rate). Respective cumulative distribution is also shown. E) optimized control law parameter $z$, confusion matrix, ITR with equal message probability, optimal message probabilities and activation times for each class. The rest class activation time is an optimized time-out parameter.

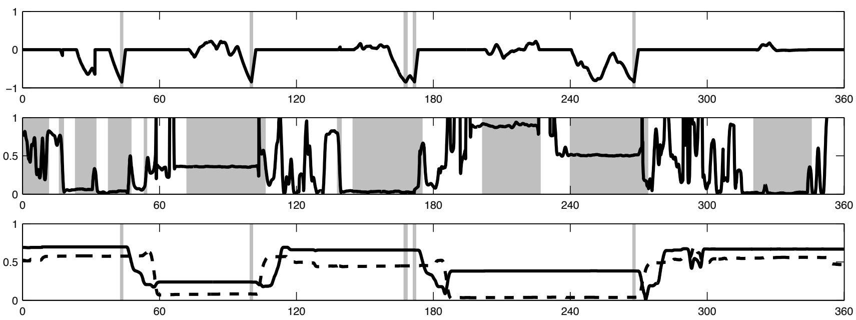

Figure 3: Time courses (s) of cup grabbing. Top: BCI cursor $c$. Highlighted: states above activation threshold. Middle: Distance of the gaze point from the cup ($m$). Highlighted: stable gaze state. Bottom: Distances robot to cup (solid) and cup to head (dashed). Highlighted: simultaneous activation of BCI and stable gaze.

The 3D eye tracking problem was most difficult, technically since it requires work with very noisy and sometimes faulty sensors (outliers are common). The direction of gaze is fairly accurate, distance is less accurate. However, intercepting gaze at table height is realistic since a single "workbench" is most likely to be primarily used by a disabled user. It is also equally useful to reach first to the closest (1 s.d.) point of the "uncertainty" ellipse when sensors are optimally functional. The asynchronous BCI design is adjustable: moving the cursor thresholds in/out can make activation faster at the cost of increased false positives. When the subject is BCI proficient (such as Subject 1) then the control is easy, fast, and failsafe (the same subject has performed this task in public for several hours). In cases of limited proficiency BCI subjects (Subject 2) the control becomes more laborious. Brain2Robot itself contains further safeguards against involuntary activation: the robot will only move when the gaze point is stable (during fixations) and will not move towards targets outside its workspace (for which the gaze distance estimation is accurate enough). For BCI illiterate subjects, another input modality can substitute for BCI. Tetraplegic persons who are not locked in retain residual communication channels (such as neck, tongue, eye movements, speech, limited, residual control of fingers) by means of which ITR and ease of use is usually higher than BCI.

This study demonstrates that useful prosthetic control is possible using EEG-BCI. One may reasonably ask why BCI is necessary when other control modalities may compete in speed and convenience, depending on the degree of disability. The basic advantage of BCI is that it can offer a sensation of control over the body which these other information channels cannot, while not interfering with these residual functions. Of further importance to eventual increase of quality of life via BCI use in disabled users is reliability and how practical and aesthetic EEG is to set-up and use daily [7]. For this purpose we have developed a dry-electrode cap which can be set up and used in a matter of minutes, and found it to function suitably for BCI purposes [8]. Therefore eventual acceptance of BCI depends on a delicate balance between cost, risk and benefit. We believe that we have proven the feasibility of striking that balance favorably.

**Acknowledgments:** This work was supported by the European Commission's Marie Curie Excellence Team grant MEXT-CT-2004-014194 "Brain2Robot"

## References


[1] J. R. Wolpaw and D. J. McFarland. Control of a two-dimensional movement signal by a noninvasive brain-computer interface in humans. *Proc. Nat. Ac. Sci.*, 101:17849–17854, 2004.

[2] J. del R. Millán, P. W. Ferrez, F. Galán, E. Lew, and R. Chavarriaga. Non-invasive brain-actuated interaction. *Adv. Brain, Vision, and Artificial Intell.*, 4729:438–447, 2007.

[3] S. Fazli, M. Danóczy, M. Kawanabe, and F. Popescu. Asynchronous, adaptive BCI using movement imagination training and rest-state inference. *Proc. Artificial Intell. Applications (AIA) 2008 Calgary*, ACTA press:85–90, 2008.

[4] J. del R. Millán, F. Renkens, J. Mouriño, and W. Gerstner. Brain-actuated interaction. *Artif. Intell.*, 151:241–259, 2004.

[5] B. Blankertz, G. Curio, and K.-R. Müller. Classifying single trial EEG: Toward brain computer interfacing. *Adv. Neural Inf. Process. Syst. (NIPS 01)*, 14:157–164, 2002.

[6] D. J. C. MacKay. Bayesian interpolation. *Neural Comput.*, 4:415–447, 1992.

[7] B. H. Dobkin. Brain-computer interface technology as a tool to augment plasticity and outcomes for neurological rehabilitation. *J. Physiol.*, 579:637–642, 2007.

[8] F. Popescu, S. Fazli, Y. Badower, B. Blankertz, and K.-R. Müller. Single trial classification of motor imagination using 6 dry EEG electrodes. *PLoS ONE*, 2:e637, 2007.

# Brain painting – BCI meets art

A. Kübler[1,2], S. Halder[2], A. Furdea[2], A. Hösle[3]

[1]Clinical and Heatlh Psychology Research Centre, School of Human and Life Sciences, Roehampton University, London, UK
[2]Institute of Medical Psychology and Behavioural Neurobiology, University of Tübingen, Germany
[3]Babenhausen, Germany

a.kuebler@roehampton.ac.uk

**Abstract**

In collaboration with an artist (AH), who created an oeuvre with the brain as central topic (www.retrogradist.de), we developed a novel application for a brain-computer interface (BCI) controlled by the P300 event-related potential: instead of letters, numbers, icons, or internet links, we assigned shape, colour, intensity and other commands to each cell of the matrix. With arrows a cursor could be moved on the canvas to the desired position. The artist and a locked-in patient (LEK) with amyotrophic lateral sclerosis (ALS) were able to produce paintings in the laboratory as well as during an exhibition of the Künstlerbund Tübingen (artist association). To ensure that the resulting pictures were not just random selection of figures and shapes, the artist reproduced one of his previously produced paintings. A development from simplistic to more sophisticated work has already been visible in the artist's paintings. As both the artist and the patient performed during an exhibition, a high number of stimulus repetitions was chosen to guarantee high accuracy, albeit at the cost of speed. Thus, AH painted at a rate of 2 and LEK of 1.15 selections per minute. The patient was enthusiastic about the program as it enabled her to communicate creatively and not just with words. The caveat of the current Brain Painting is the restriction to the matrix allowing the user cursor positions at predefined positions only. Future development will employ sensorimotor rhythm based asynchronous BCI for painting. Brain Painting will also be further tested with patients to assess whether it may constitute a useful application for entertainment.

## 1 Introduction

Brain-computer interfaces have extensively demonstrated their potential of providing a means for communication and control for people with severe motor impairment, such as patients with amyotrophic lateral sclerosis (ALS), high spinal cord injury, or brain stem stroke [1, 2]. ALS is a progressive neurodegenerative disease of the central nervous system which mainly, but not exclusively, affects the 1. and 2. motoneurons leading to severe motor paralysis which also affects speech. With the progressive loss of the ability to speak, devices for assistant communication become more and more important for quality of life (QoL). When patients at the beginning of the disease are asked for their most important domains for QoL, communication is hardly ever mentioned. However, as the disease progresses, patients start to list communication as an important factor contributing to QoL – a phenomenon known as response shifts [3]. On average, patients die 3 to 5 years after diagnosis from respiratory failure unless they chose artificial ventilation. If artificial ventilation is provided, the disease may progress to the locked-in state (LIS) in which only residual muscular movement is possible.

Several components of the electroencephalogram (EEG) such as slow cortical potentials, sensorimotor rhythms, or event-related potentials (e.g., P300) were used for brain-computer interface (BCI) control. By means of regulation of slow cortical potentials, patients with ALS in almost all stages of the disease could communicate messages of considerable length using a language support program [4, 5]. The P300-BCI takes advantage of the brain's reaction to visual, auditory, or tactile presentation of rare (target) stimuli in a stream of standard stimuli [6], and is typically recorded over central-parietal scalp locations [7]. Already in 1988 Farwell and Donchin showed that the P300 could be used to select letters from a matrix with a BCI [8]. The advantages of the P300-BCI are (1) that no feedback learning is required (as with BCI depending on the regulation of a specific component of the EEG) and (2) that it has already been shown that people with ALS can operate the P300-BCI with high an accuracy. A disadvantage is that it requires a component of the EEG that is elicited by external stimulation and if no classifiable response to stimulation is detected, the potential BCI user cannot be trained to produce this response and thus, is excluded from using the P300-BCI. ALS-patients, some of them in the locked-in state, were able to communicate with the P300-BCI and up to 10 letters per minute could be selected [9]. Recently, an internet browser was realized for the P300-BCI and is currently under investigation for its feasibility in locked-in patients ([10] and unpublished data). In an effort to go further beyond plain communication with a BCI, to offer users a greater variety of options, and inspired by AH, we developed a P300 matrix suitable for painting; we refer to this endeavour as Brain Painting. The aims of the current study were to assess (1) the general feasibility of Brain Painting, (2) a patient's satisfaction with the application (important for BCI users), and (3) whether Brain Painting would be suitable and manageable at art exhibitions (important for the artist).

# 2 Methods

## 2.1 Hardware, software and participants

The EEG of the user was recorded with a g.USBamp amplifier (g.tec, Graz, Austria) sampled at 256 Hz using a 16 channel subset of the 10–20 system (Highpass: 0.1 Hz, Lowpass: 60 Hz, Notchfilter: 50 Hz). The left mastoid (A1) electrode served as ground and the right mastoid (A2) as reference. BCI2000 was used to present the stimuli, record, and classify the signals [11].

Two users participated in this pilot study. (1) The artist (AH), male, 59 and (2) a woman (LEK), 51, diagnosed with the sporadic and spinal form of ALS in 2004. At the time LEK was provided with Brain Painting, toward the end of 2007, she was artificially ventilated and fed. With residual hand movement she controlled a device for assistant communication and she had control over facial muscles, but no speech.

## 2.2 The Brain Painting matrix

Painting commands were presented to the user in an $8 \times 6$ matrix (Figure 1). Commands comprised colours, colour intensities, figures, shapes, brush size, "canvas" resolution, zooming function, undo-redo, cursor directions, unsharp masking filter and stop function (Figure 1). The commands associated with each symbol in the matrix were sent to the painting application via an UDP socket connection. Each row and column was intensified in random order. Throughout one trial the participant had to focus attention on one of the 48 cells of the matrix. The random sequence of six row and eight column flashes constitutes an oddball paradigm. The rare target, i. e. the intensification of the row and column containing the desired command, elicits the P300 component of the ERP. Each flashing of row or column lasted 62.5 ms and the interstimulus interval (ISI) was 125 ms for LEK and 62.5 ms for AH (he wished to have such short an ISI). One sequence consisting of 6 row and 8 column flashes with ISI lasted 39.38 s for LEK and 17.5 s for AH. One trial (i. e., one selection of the matrix) consisted of 15 sequences for LEK and of 10 for AH. The inter trial interval was 12.5 s to allow both users enough time to regard the selection and to decide what to select next. Thus, time for selection of a command was 51.87 s for LEK and 30 s for AH.

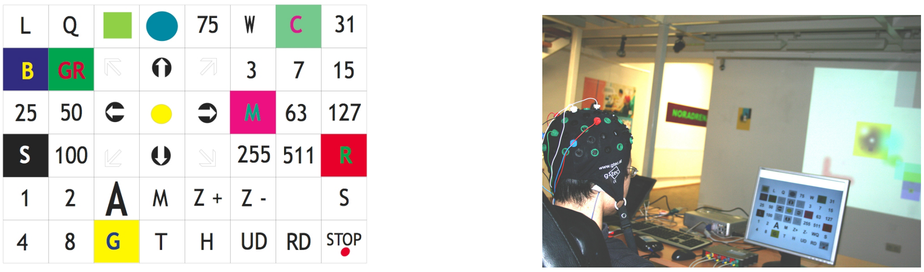


Figure 1: Left: The 8 × 6 Brain Painting matrix. The parameters of the brush such as form, size and opacity have to be chosen, and thereafter, an arbitrary number of these shapes can be placed on the canvas by selecting the desired colour (cells with gray background correspond to red, magenta, blue, green, yellow and black). Thus the colour is the function which places the desired element on the "canvas". Right: A visitor hooked up to the Brain Painting BCI during the exhibition (right) in the gallery of the Künstlerbund Tübingen (artist association).

### 2.3 Data analysis

We used the stepwise linear discriminant analysis method (SWLDA) for classification and weight generation [8]. The method, an extension of the Fisher's Linear Discriminant (FLD), is well established as a successful classification method for EEG data in general, and more recently for BCI data, for which rapid classification is essential. Previous studies of classification methods have demonstrated that SWLDA provides good overall performance in classifying the visually evoked P300 [9, 12]. The algorithm seeks an optimal discriminant function by adding spatiotemporal features (amplitude values from particular channel locations and time samples) to a linear equation. A combination of forward and backward stepwise analysis was used [13].

The input features were weighted using least-squares regression to predict the stimulus type (target or standard). Initially the discriminant function does not contain any features. In each following step, the algorithm evaluates every input feature, determines the statistically most significant single feature having a $p$-value $< 0.1$ and adds it to the discriminant function. Each new entry is then followed by a backward stepwise analysis to remove any features that no longer meet the predetermined criterion to remain in the discriminant function (a $p$-value $> 0.15$ was used in this study). This procedure eliminates features which no longer account for a significant amount of unique variance after additional features have entered the model. The process is repeated until no features satisfy the criteria for entering in or being removed from the model, or both, or until the discriminant function contains a pre-defined number of features, 60 in the present study [14].

For each of the recorded channels, 800 ms data segments were extracted and averaged after each presentation of stimuli. A moving average filter was then applied to the segments which were further decimated with a factor of 20. The feature vector which resulted from concatenating the data segments was then used to train the classifier. The classification coefficients, derived using the stepwise discriminant function, were then applied to the averaged values of the data at critical time points as selected by the algorithm [14].

## 3 Results

Both users were able to select commands from the matrix and to produce paintings (Figure 2). AH selected 2 and LEK 1.15 commands per minute. To ensure that the produced paintings were not just the result of random selection, the artist exactly reproduced one of his paintings. Additionally, the manner of how the "objects" are shaped and placed on the canvas is clearly not random (Figures 2 and 3).

As AH continued painting during the exhibition and at home, a development toward more ambitious and sophisticated paintings could be seen in his work and he made use of the "zooming

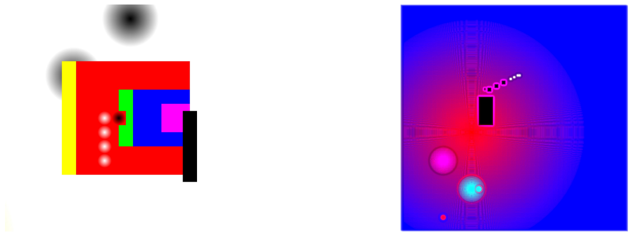

Figure 2: Left: One of the early paintings produced by AH during the exhibition in the gallery of the Künstlerbund Tübingen. Right: Painting produced by LEK (blue and violett are her favourite colours).

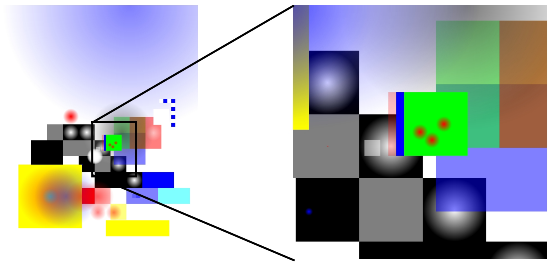

Figure 3: Left: a Brain Painting from AH several months later. Right: by using the "zooming in" option, the user is able to paint details within a cell of the matrix.

in" option (Figure 3).

Peak amplitudes, yielding highest $r^2$, and latencies were 2.6 µV and 207.03 ms (AH) and 2.7 µV and 500 ms (LEK) (Figure 3). The $r^2$ is the proportion of the total variance of the amplitude of the event-related potential that was accounted for by the targeted matrix cell. These data were derived from a pre-painting screening session.

## 4 Discussion

The Brain Painting matrix reliably elicited the P300 of the ERP albeit earlier as typically seen in simple oddball paradigms. A selection rate of 2 options per minute may appear rather low. However, we chose such high a number of stimulations, because we wished to ensure high accuracy, albeit at the cost of speed. Selection accuracies of more than 90 % can be achieved in healthy users and in some patients with 5 to 7 sequences only ([9] and unpublished data). However, it has to be taken into account, that usually BCI sessions are conducted in an EEG laboratory shielded from noise or at the patients' home. Although at a patient's home there are sources of distraction, such as the phone or caregivers, this environment is not comparable to a public location such as an art gallery with people watching the performance while talking. For this reason we chose a high repetition of sequences and both users agreed to give accuracy priority over speed.

Both, the artist and the ALS-patient expressed their satisfaction with the new application. LEK reported that she tremendously enjoyed the opportunity to express herself, albeit with restraints imposed by the matrix, over and beyond pure verbal communication. During the 6 weeks of the exhibition, she came to the gallery every Thursday afternoon to work on her painting. This implied a high level of compliance as organising trips to downtown Tübingen constituted a major effort for LEK in the locked-in state.

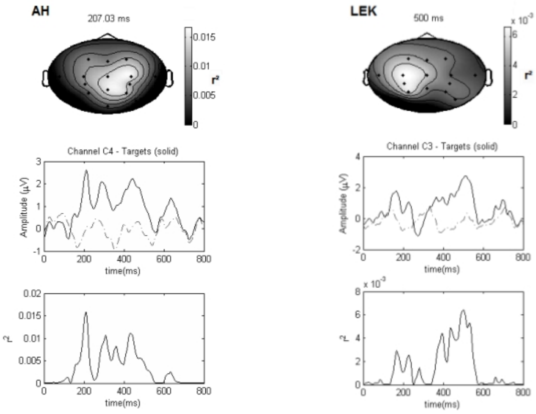

Figure 4: Left column AH, right column LEK. Top: $r^2$ topographies at 207 ms for AH and 500 ms for LEK. Both users showed highest $r^2$ in central-parietal areas which is in line with the expected location of the P300. Middle: Average across target (solid line; 7.560 for AH and 13.500 for LEK) and non-target (dashed line; 1260 for AH and 2250 for LEK) stimuli. In AH the stimulation frequency of around 6 Hz can be clearly seen in the average across non-target stimuli. Bottom: $r^2$ as a function of time.

# 5 Conclusion

With Brain Painting we successfully introduced a new application for BCI. The caveat of the current version of Brain Painting is the restriction to the $8 \times 6$ matrix for positioning of the cursor. To overcome these restrictions, Brain Painting will be further developed to be used with BCI allowing the user asynchronous and rapid cursor control [15, 16]. In further studies it has to be investigated whether Brain Painting constitutes an application for entertainment in patients with motor paralysis.

**Acknowledgments:** The contribution of Dirk Franz to programming of the painting matrix is gratefully acknowledged. This work was supported by g-tec, Graz, Austria.

# References

[1] A. Kübler, F. Nijboer, and N. Birbaumer. Brain-computer interfaces for communication and motor control-perspectives on clinical application. In G. Dornhege, J. del R. Millán, T. Hinterberger, D. J. McFarland, and K.-R. Müller, editors, *Toward brain-computer interfacing*, pages 373–391. MIT Press, 2007.

[2] A. Kübler and K.-R. Müller. An introduction to brain-computer interfacing. In G. Dornhege, J. del R. Millán, T. Hinterberger, D. J. McFarland, and K.-R. Müller, editors, *Toward brain-computer interfacing*, pages 1–25. MIT Press, 2007.

[3] M. A. Sprangers and C. E. Schwartz. Integrating response shift into health-related quality of life research: a theoretical model. *Soc. Sci. Med.*, 48:1507–1515, 1999.

[4] J. Perelmouter, B. Kotchoubey, A. Kübler, E. Taub, T. Hinterberger, and N. Birbaumer. Language support program for thought-transalation-devices. *Automedica*, 18:67–84, 1999.

[5] N. Neumann, A. Kübler, J. Kaiser, T. Hinterberger, and N. Birbaumer. Conscious perception of brain states: mental strategies for brain-computer communication. *Neuropsychologia*, 41:1028–1036, 2003.

[6] J. Polich. Comparison of P300 from a passive tone sequence paradigm and an active discrimination task. *Psychophysiol.*, 2:41–46, 1987.

[7] M. Fabiani, G. Gratton, D. Karis, and E. Donchin. Definition, identification and reliability of measurement of the P300 component of the event-related brain potential. *Psychophysiol.*, 2:1–78, 1987.

[8] L. A. Farwell and E. Donchin. Talking off the top of your head: toward a mental prosthesis utilizing event-related brain potentials. *Electroencephalogr. Clin. Neurophysiol.*, 70:510–523, 1988.

[9] F. Nijboer, E. Sellers, J. Mellinger, T. Matuz, U. Mochty, M. Jordan, D. Krusienski, T. M. Vaughan, J. R. Wolpaw, and A. Kübler. A brain-computer interface (BCI) for people with amyotrophic lateral sclerosis(ALS). *Clin. Neurophysiol.*, In Press.

[10] E. Mugler, M. Bensch, S. Hadler, W. Rosentiel, M. Bogdan, N. Birbaumer, and A. Kübler. Control of an internet browser using the P300 event-related potential. *Int. J. Bioelectromagnetism*, 10:56–63, 2008.

[11] G. Schalk, D. J. McFarland, T. Hinterberger, N. Birbaumer, and J. R. Wolpaw. BCI2000: a general-porpouse brain-computer interface (BCI) system. *IEEE Trans. Biomed. Eng.*, 51:1034–1043, 2004.

[12] E. W. Sellers and E. Donchin. A P300-based brain-computer interface: initial tests by ALS patients. *Clin. Neurophysiol.*, 117:538–548, 2006.

[13] D. J. Krusienski, E. W. Sellers, F. Cabestaing, S. Bayoudh, D. J. McFarland, T. M. Vaughan, and J. R. Wolpaw. A comparison of classification techniques for the P300 speller. *J. Neural Eng.*, 3:299–305, 2006.

[14] A. Furdea, S. Hadles, D. Bross, F. Nijboer, N. Birbaumer, and A. Kübler. An auditory oddball (P300) spelling system for brain-computer interfaces (BCI). *Psychophysiol.*, Submitted.

[15] B. Blankertz, G. Dornhege, M. Krauledat, K.-R. Müller, and G. Curio. The non-invasive Berlin brain-computer interface: fast acquisition of effective performance in untrained subjects. *Neuroimage*, 37:539–550, 2007.

[16] G. R. Müller-Putz, R. Scherer, G. Pfurtscheller, and R. Rupp. Brain-computer interfaces for control of neuroprostheses: from synchronous to asynchronous mode of operation. *Biomed. Tech.*, 51:57–63, 2006.

# P300-based brain computer interface: to operate domotic appliance

F. Aloise[1,2], S. Marchionni[3], G. Romito[3], A.-M. Brouwer[4], J. B. F. van Erp[4], D. Mattia[1], F. Babiloni[1,5], S. Salinari[3], M. G. Marciani[6], F. Cincotti[1]

[1]Neurofisiopatologia Clinica, Fondazione Santa Lucia, IRCCS, Rome, Italy
[2]Dipartimento di Ingegneria Elettronica, Università "Tor Vergata", Rome, Italy
[3]Dipartimento di Informatica e Sistemistica, La Sapienza Università di Rome, Italy
[4]TNO Human Factors, The Netherlands
[5]Dipartimento Fisiologia Umana e Farmacologia, La Sapienza Università di Rome, Italy
[6]Dipartimento di Neuroscienze, Università "Tor Vergata", Rome, Italy

f.aloise@hsantalucia.it

**Abstract**

Present-day non-invasive Brain Computer Interfaces (BCI) determine the intent of the user from a variety of different electrophysiological signals. P300 potentials recorded from the scalp are one example of signals can be used to determine the subject's intent. In the present study, we investigate the influence of different stimulus modalities (visual, tactile, and auditory) during sessions of P300-based BCI. In all the subjects ($n = 8$), on-line classification displayed the highest accuracy of target selection (93 %) using visual stimulus modality when compared to the audio (70 %) and tactile (68 %) stimulus modalities . When observed under different modalities of stimulation, the elicitation of P300 was found to be affected by the type of stimulus modality used. This suggests that it is not possible to generalize the feature classification of a single subject for various stimulation modalities using a single set of parameters. Identifying the elements necessary for the successful implementation of various P300 stimulation modalities will facilitate the integration of P300-based BCI with domotic appliances, and will offer the opportunity to boost the translation of BCI research from the laboratory to a clinical context.

## 1 Introduction

The P300 event-related brain potential is a positive endogenous potential which occurs over the parietal scalp region when infrequent or particularly significant stimuli are interspersed with frequent or routine stimuli [1]. Because of its stability and reproducibility, the P300 has been proposed as a control signal for brain computer interface (BCI) systems [2].

Indeed, P300-based BCIs have the apparent advantage of requiring no initial user training. P300 is a typical, or naive, response to the presentation of a desired choice. However, P300 potential can vary according to the type of stimulation utilized to evoke it [Fabiani1987]. In this study, different modalities of stimulation were used to elicit the P300 response. These modalities were then further explored within a P300-based BCI system, and their impact on the on-line classification of performance was estimated. The ultimate goal will be to exploit this experimental paradigm tocontrol domotic appliances via BCIs [3].

## 2 Material and methods

Eight subjects (23–37 years, 3 males, 5 female) with no previous experience controlling BCIs, participated in the study. Visual acuity was normal or corrected to normal in all subjects. One subject was color blind. Scalp EEG data (61 channel EEG system; Brain Products, Germany; sampling rate 250 Hz) was acquired from each subject during BCI sessions operated by the BCI2000 software [4]. Data was stored for offline analysis. An external program was implemented to integrate the BCI2000 framework with a tactor hardware system (C-2 Tactors; Engineering Acoustics, Inc, WinterPark, USA) to deliver vibrotactile stimuli to the subject. Each participant underwent five 30 minute recording sessions. Each session consisted of four runs of 6 minutes each, during which a given stimulation modality was used. Runs consisted of 8 trials. Trials were separated into three phases, presentation of target phase, stimulation phase, and presentation of result phase. During the presentation phase, the target was presented to the subject. During the stimulation phase, the subject was required to mentally count the occurance of the target stimuli (target stimuli were, interspersed with nontarget stimuli and each stimulus occurred 15 times). The stimulation duration (192 ms), interstimulus interval (ISI, 160 ms) and number of stimulations were constant across stimulation modalities. The presentation of result phase reported the subject's selection to the subject. Performance accuracy was assessed by calculating the percent of trials in which the target presented to the subject during the presentation of target phase corresponded with the subject's selection. Experimentation progressed in four sessions, one for each modality: classic oddball[1], visual, auditory,tactile stimuli. A fifth session consisted of 4 runs, one for each stimulus modality during which the best extracted control features found in the previous four sessions were used asses performance with each modality

The modalities were implemented in the following ways, During the visual stimulus modality, subjects were provided with 8 different images showing one black circle surrounded by one small red circle. The red circle could occupy 8 different target positions. The auditory stimulation was delivered by using 8 different stimuli, ('do', 're', 'mi', 'fa', 'sol', 'la', 'si' and 'ut'; pronounced at the same tone height). The tactile stimulation was provided by means of eight tactors positioned on different sites of the hands and wrists (frequency of stimulation was tuned on a narrow carrier band of about 250 Hz). As a control condition, a "classic oddball" task was designed in which a commonly occurring, non-target stimulus (the presentation of a red circle) was interspersed with an uncommon target stimulus,a(the presentation of a blue square) . The best control features for each modality were extracted from the EEG data acquired during the first 4 sessions by using off-line step-wise linear discriminate analysis (SWLDA). The control feature is modeled using half of the data set (2 runs) to create a model of the control feature. This model is cross-validated by comparison to the remaining two runs. The resulting model is composed of 60 different features. Each feature is composed of one channel, its latency and its weight.

## 3 Results

As shown in Figure 1, the performance of the online classification reached the highest accuracy in all subjects when using the visual modality (93 % on average) when compared to the auditory and tactile stimulation modalities (which yielded correct classification percentages of 70 % and 68 % respectively). Similarly, the $r^2$ computed for the 3 types of stimulation (visual, auditory and tactile) yielded higher values for the visual modality than those observed for the auditory and tactile modalities (Figure 2). The analysis of the characteristics of the P300 elicited under the 3 different stimulus conditions revealed that the latency of the principal P300 (P3a subcomponent) component was increased (600ms peak after stimulus, Figure 3) with auditory and tactile stimuli when compared to the visual stimulation (400 ms peak after stimulus). No evident changes were observed in the topography of the P300 principal component evoked with different stimulus modalities Figure 4.

[1]The classic oddball task described refers to the definition presented in the literature where only two different stimuli are presented. While all stimulation elicited P300 due to the presence of oddball events, in the case of the classic oddball trial, the novelty of the stimuli was imposed by the presentation system and not on the users decision to focus on a particular target.

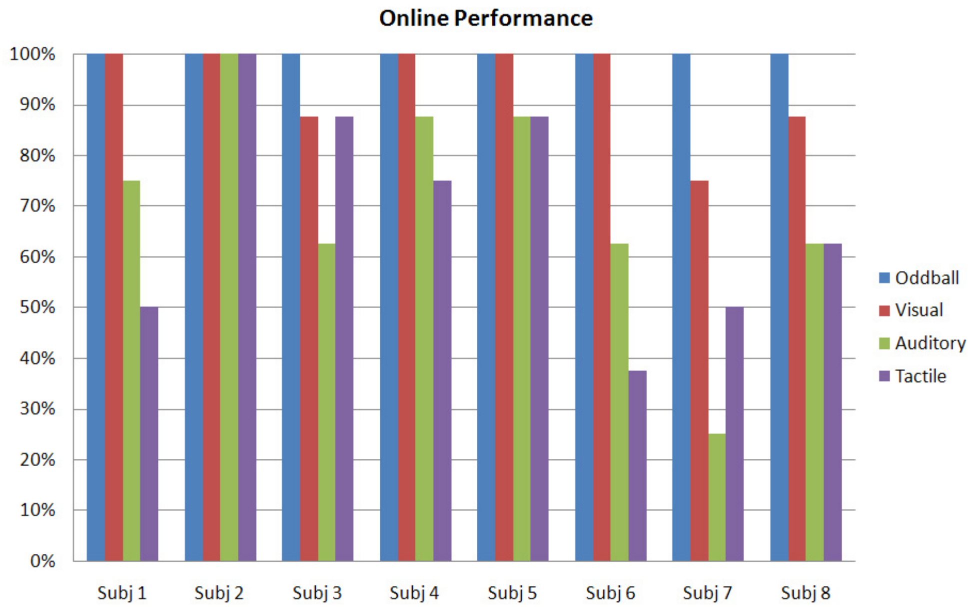


Figure 1: Histogram showing the averaged values from $n = 15$ trials of on-line classification performance (in percentage) obtained for each stimulus modality (fifth session).

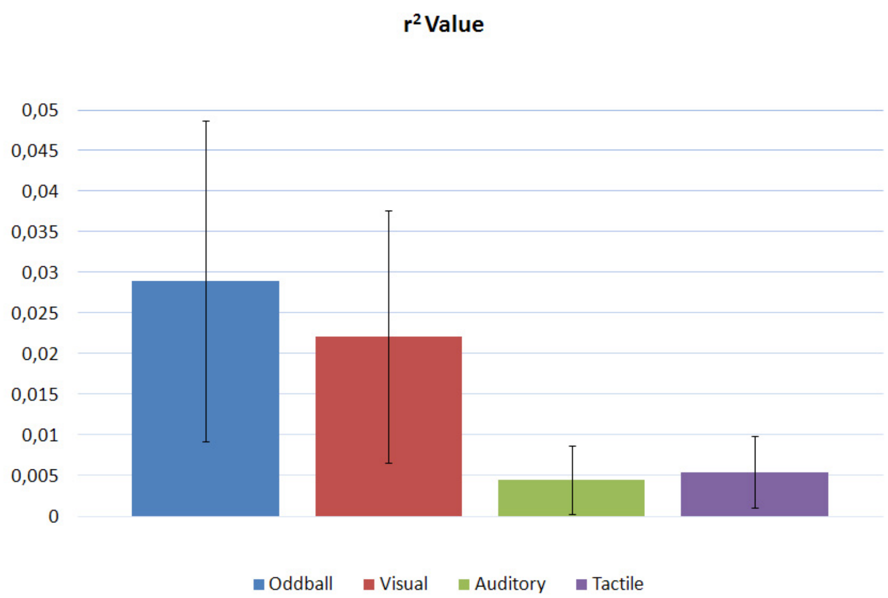


Figure 2: Histogram of the $r^2$ mean values obtained for all subjects during each stimulus modality.

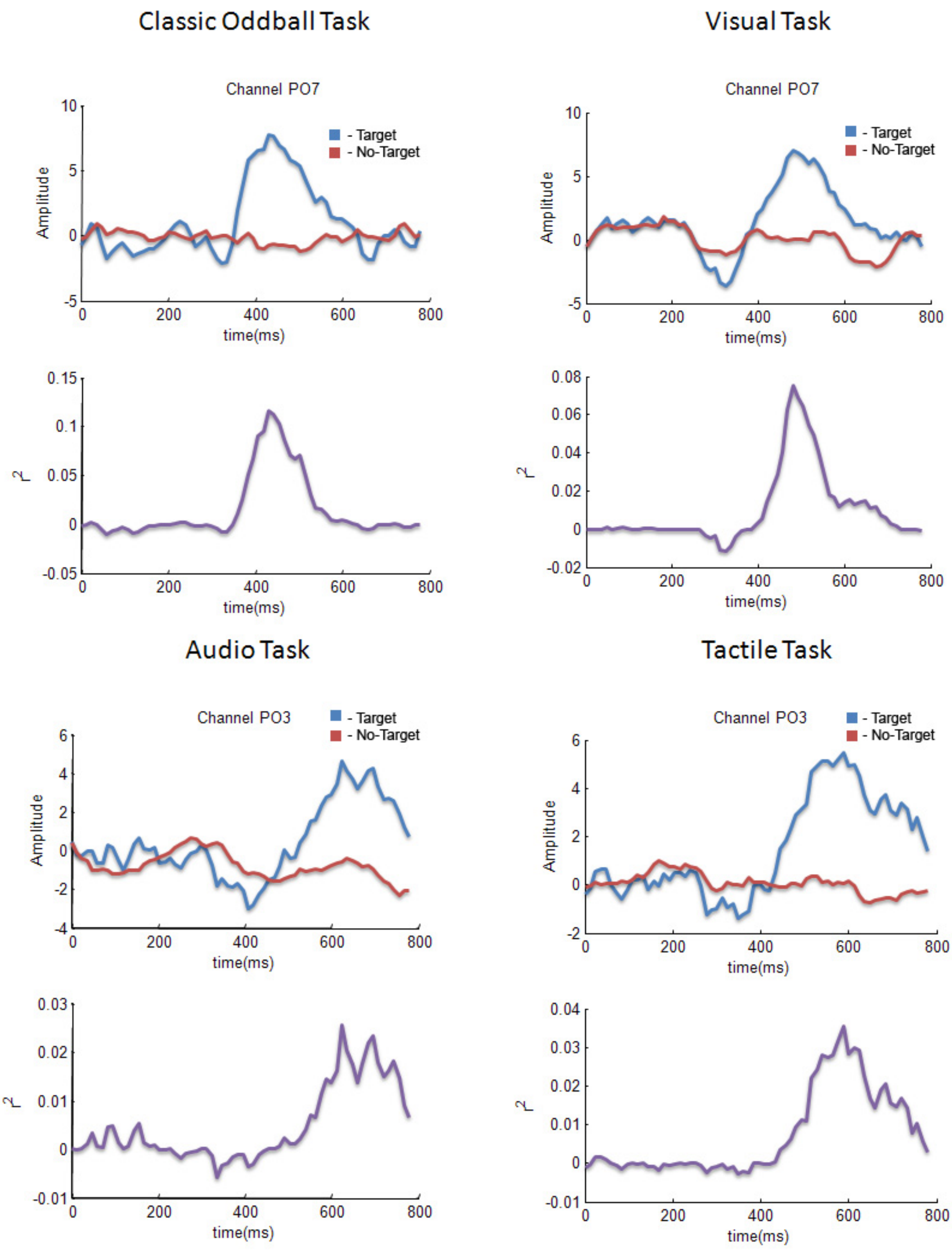


Figure 3: Plots of the time courses of P300 amplitude and $r^2$ values for different modalities in a representative subject. In this figure the channel with the maximum $r^2$ value in each modality is plotted.

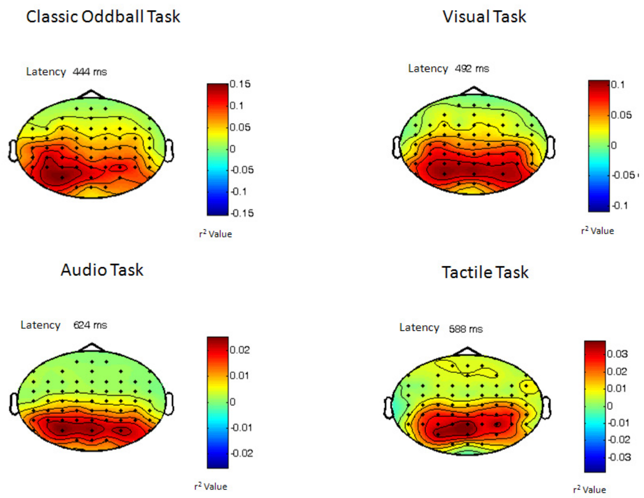


Figure 4: Topographical distributions of max $r^2$ values in a representative subject for each modality.

Figure 5: Prototype setup in which a P300-BCI control signal is utilized to control domotic appliances

# 4 Discussion

These preliminary findings suggest that different types of stimulation can be of effectively utilizedin a P300-based BCI application. The increase in P300 latency observed with auditory and tactile stimulation can presumably be related to the less intuitive nature of these modalities (ease of target recognition) when compared to what occurs during visual presentation of the target. The identification of P300 characteristic modification as function of the stimulus modality indicates that tuning of the control parameters is required for a P300-based BCI application to employ diverse modalities effectively. Future lines of research will be directed towards the exploitation of this BCI control signal in a prototype of BCI controlled domotic appliances (Figure 5). At first, we will consider the P300 classical paradigm based on visual feedback modalities (Figure 5) in order to take advantage of the reliability of the visual feedback that favors large scale experimentation. Subsequently, the opportunity to train subjects in a "real" domotic environment controlled by the BCI system prototype will better determine if and how different stimulation modalities can be implemented to elicit P300 (feedback) that will positively affect subject training and performance.

## 5 Conclusion

The P300 can function as an efficient BCI control signal. The integration of P300-based BCIs with domotic appliances will offer the opportunity to boost the translation of BCI research from the laboratory to a clinical context.

## References

[1] E. Donchin, K. M. Spencer, and R. Wijesinghe. The mental prosthesis: assessing the speed of a P300-based brain-computer interface. *IEEE Trans. Neural Syst. Rehabil. Eng.*, 8:174–179, 2000.

[2] S. Sutton, M. Braren, J. Zubin, and E. R. John. Evoked correlates of stimulus uncertainty. *Sci.*, 150:1187–1188, 1965.

[3] F. Cincotti, D. Mattia, F. Aloise, S. Bufalari, G. Schalk, G. Oriolo, A. Cherubini, M. G. Marciani, and F. Babiloni. Non-invasive brain-computer interface system: Towards its application as assisitive technology. *Brain Res. Bull.*, 75:796–803, 2008.

[4] G. Schalk, D. J. McFarland, T. Hinterberger, N. Birbaumer, and J. R. Wolpaw. BCI2000: a general purpose brain-computer interface (BCI) system. *IEEE Trans. Biomed. Eng.*, 51:1034–1043, 2004.

# Self-paced brain-computer interaction with virtual worlds: a quantitative and qualitative study "out of the lab"

F. Lotte[1,2,3], Y. Renard[1,3], A. Lécuyer[1,3]

[1]Research Institute for Computer Science and Random Systems (IRISA), Rennes, France
[2]National Institute for Applied Sciences (INSA), Rennes, France
[3]National Institute for Research in Computer Science and Control (INRIA), Rennes, France

fabien.lotte@irisa.fr; anatole.lecuyer@irisa.fr

**Abstract**

This paper describes the results of an evaluation of a self-paced brain-computer interface (BCI) application conducted with 21 naïve subjects. We studied both performances and preferences of subjects placed voluntarily in a challenging situation: first-time session, no human learning, no machine learning of the mental state to be detected, "out of the lab", use of a single EEG channel. The application consisted of an entertaining interaction with a virtual world inspired by the famous "Star Wars" movie. Subjects were asked to control the take-off and height of a virtual spaceship by using their motor-related brain activity. Results showed that, without training, roughly half of the subjects were able to control the application by using real foot movements and a quarter were able to control it by using imagined foot movements. Taken together, the results of subjective questionnaires stressed the importance of mental strategies and the need to provide subjects with a continuous and complete visual feedback, even when the non-control state is detected. In addition, the whole application appeared as enjoyable and motivating for the subjects.

## 1 Introduction

A lot of brain-computer interfaces (BCI) studies are conducted inside laboratories, in highly controlled conditions, and with a relatively small number of subjects trained over a number of sessions which may be large. Furthermore, most current studies are focused on the BCI performances and not on the subjects' preferences. A notable exception is the work of Guger et al. which has evaluated a BCI with 99 naïve subjects during an exposition [1]. This work focused on the performances of subjects who had to control a synchronous, 2-class BCI based on 2 bipolar EEG channels and a trained classifier. Subjects were asked to imagine movements of their right-hand or their feet and were provided with a simple 2D visual feedback. Their results showed that 93 % of the subjects were able to reach an accuracy equal or greater than 60 %.

In this paper, we study both the performances and the preferences of 21 naïve subjects during an exhibition. These subjects used a self-paced (asynchronous) BCI, based on a single EEG channel, which does not use machine learning of the mental state to be detected. The subjects could interact with an entertaining virtual reality application inspired from the Star Wars movie.

## 2 Method

### 2.1 The BCI system

We have designed a simple self-paced BCI system based on real or imagined foot movements. This BCI is based on a single EEG channel, located at position Cz and aims at detecting a beta event-related synchronisation (ERS), appearing posterior to the real or imagined foot movement [2]. To this end, the EEG signal is first band-pass filtered in the 3–45 Hz band. Then, a band power (BP) feature [2] is extracted in the Beta band (16–24 Hz) for the last second of data. This feature is extracted every 100 ms and the last four consecutive features are averaged (with a moving average) in order to produce a smooth control signal (CS).

To detect the beta ERS, and hence, the foot movement, we used a simple threshold Th. If the computed CS was higher than this threshold Th, a foot movement was detected (intentional control state) and a command was sent to the application. If the CS was lower than the threshold Th, the non-control state was detected and no command was sent to the application. The value of Th was simply determined according to the mean $\mu$ and standard deviation $\sigma$ of a CS epoch obtained while the subject was relaxed, according to Equation 1.

$$\mathrm{Th} = \mu + 3\sigma \tag{1}$$

## 2.2 The Virtual Reality application: "Use the force!"

We have developed an entertaining Virtual Reality (VR) application, as Leeb et al. have shown that VR can increase the motivation and interest of subjects during BCI experiments [3]. Our virtual environment corresponds to a "Star Wars" space vessel, in which the subject could see a virtual spaceship (a Tie-Fighter) and a static character (Darth Vader) (see Figure 1). The purpose of the application was to lift the Tie-Fighter up by using the BCI. This task established an analogy between the use of the BCI and the use of "the force" in the Star Wars movie. As such, the application was named "Use the force!". More precisely, the Tie-Fighter was lifted up when the VR application received the corresponding command from the BCI. The Tie-Fighter was lifted up at a speed proportional to the value of the CS. When no command was received, the Tie-Fighter went down.

The VR application was developed with the OpenMASK VR platform [4] and the BCI was developed with the OpenViBE BCI platform[1]. The VR application and the BCI system were easily connected using the VRPN protocol, thanks to the dedicated modules of OpenViBE.

## 2.3 The experiment

Subjects participated in an experiment which lasted about 45 minutes. This experiment was divided into seven succesive steps:

**Electrode montage:** Only three electrodes were used: a ground electrode (located on the forehead), a reference electrode (located on the nose) and the Cz electrode. Electrode Cz was fixed using an adhesive paste instead of a cap, for a faster setup.

**Signal visualization:** Subjects were shown their EEG signal recorded at Cz (band-pass filtered in 3–45 Hz) while they were clenching their teeth or blinking. This aimed at showing them the need to be as relaxed as possible during the experiment and the need to avoid blinking. During the next steps, subjects were regularly reminded to stay as relaxed as possible.

**Baseline:** During this step, subjects were asked to stay relaxed. Once they were relaxed, 20 seconds of EEG signal were recorded and converted into a CS which was used to compute Th using Equation 1.

**Free time:** During this step, the subject could interact freely with the VR application by using real foot movements. When the BCI detected a beta ERS, the Tie-Fighter was lifted up. Alternatively, the CS was shown to the subject so that he could see the impacts of real foot movements on the beta power. This step aimed at making the subject familiar with the application and with the task. If the user seemed unable to lift the spaceship, the baseline step was performed again, in order to obtain a new Threshold Th. Then, the next steps followed.

**Real movement game:** During this game, subjects had to lift the Tie-Fighter up, by performing real foot movements during specific periods instructed by the application. These instructions

[1] www.irisa.fr/bunraku/OpenViBE

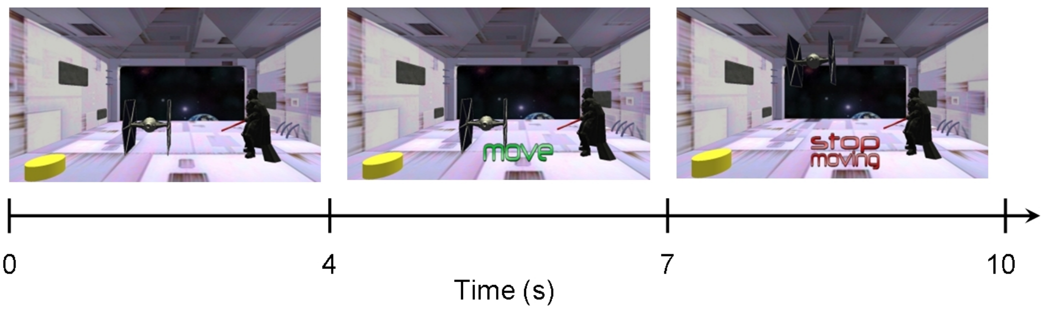


Figure 1: Temporal structure of a trial of the VR game.

are used to evaluate the system but are not used by the BCI for classifying the input data. Actually, the user can lift the Tie-Fighter up at any time and all the game long, independantly from the instructions. In other words, we used a "paced test environment" to evaluate this self-paced BCI [5]. The game was composed of 10 trials. Each trial lasted 10 s, and was divided in three phases (see Figure 1): 1) A resting phase lasting 4 seconds during which no specific task was given to the subject. 2) A "move" phase, lasting 3 seconds, during which the subject was instructed to perform real foot movements. The instruction was given using a green text "move" appearing on the screen. 3) A "stop" phase lasting 3 seconds, during which the subject was instructed to stop performing the movement in order to lift the Tie-Fighter up. The instruction was given using a red text "stop moving" appearing on the screen. If the subject managed to lift the Tie-Fighter up during this third phase, his score was increased and displayed using a yellow gauge located on the left corner down the screen.

**Imagined movement game:** This game was identical to the previous one except that subjects were instructed to perform imagined foot movements instead of real foot movements. We instructed subjects to perform kinaesthetic motor imagery rather than visual motor imagery.

**Questionnaire:** After the experiment, subjects were asked to fill out a questionnaire.

# 3 Results

The experiments took place during the Laval Virtual 2008 VR exhibition, on a booth. As such, the environment was a noisy environment with persons moving and talking around. 21 naïve subjects (mean age: $33.48 \pm 9.14$), 18 males and 3 females, participated voluntarily to the experiment. No selection was performed and all volunteers were accepted. All subjects gave their written informed consent before the experiment.

## 3.1 Subjects' performances

We assessed the subjects' performances by computing the number of True Positives (TP) and False Positives (FP) they obtained during the games [5]. We counted a single TP when the CS value became higher than the threshold Th once or more times during the "stop moving" phase (see section 2.3). We counted a single FP when the CS value became higher than the threshold Th once or more times during the "move" phase, during which a beta event-related desynchronisation (ERD) should be observed and not a beta ERS. What happened during the resting phase was not taken into account in the performance analysis. From the FP and TP, we computed the Hit-False (HF) difference, which corresponds to the number of TP minus the number of FP [5]. Performances obtained by subjects are summarized in Figure 2, under the form of absolute frequency diagrams for TP and HF difference. They show the number of subjects who obtained a given performance, for real and imagined movement games separately.

These diagrams shows that about half of the subjects (12 subjects out of 21) reached an HF difference $\geq 3$ using real movements, and that about a quarter (5 subjects out of 21) reached an

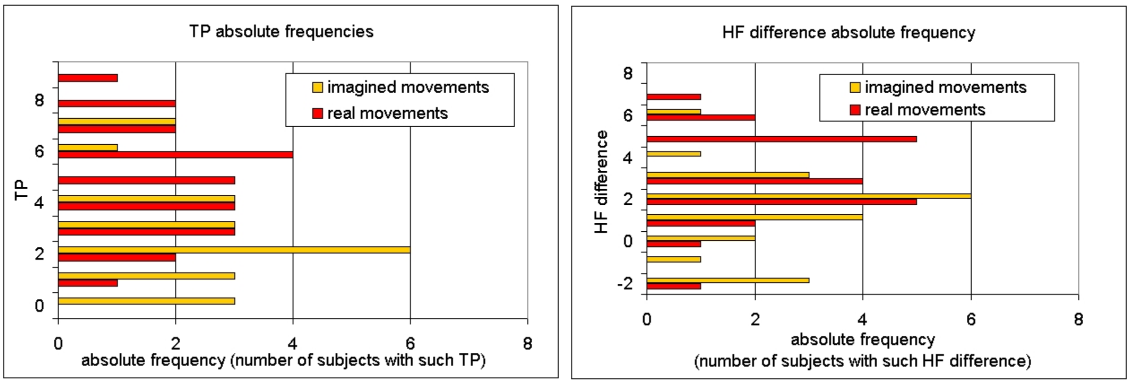


Figure 2: Absolute frequency diagrams for TP and HF difference, for real or imagined movements.

| Question | Answer for real movements | Answer for imagined movements |
|---|---|---|
| 1 – Did you get tired because of the experiment? (1: not tired at all, 7: very tired) | $1.76 \pm 1.04$ | $2.05 \pm 1.40$ |
| 2 – Did you find the experiment comfortable? (1: not comfortable at all, 7: very comfortable) | $5.10 \pm 1.26$ | $5.29 \pm 1.23$ |
| 3 – Did you feel that you could control the spaceship (that is that you could lift it voluntarily?) (1: you didn't feel you could control it at all, 7: you controlled it perfectly) | $3.95 \pm 1.80$ | $2.81 \pm 1.86$ |
| 4 – Did you feel frustration or annoyance during the experiment? (1: no frustration or annoyance, 7: a lot of frustration and annoyance) | $2.33 \pm 1.56$ | $3.29 \pm 1.65$ |

Table 1: Average marks given by the subjects in the questionnaire, for the two conditions.

HF difference $\geq 3$ using imagined movements. According to simulations performed as described in [6], a system which reached an HF difference $\geq 3$ with 10 trials per class, is better than a randomly performing system (one-tailed test) with a probability of type I error $\leq 0.054$. This suggests that, roughly half of the subjects had at least a small control over the Tie-Fighter using real movements and that a quarter had at least a small control using imagined movements. The mean HF difference was $3.14 \pm 2.24$ for real movements and $1.33 \pm 2.03$ for imagined movements while the mean TP was $4.95 \pm 2.18$ for real movements and $2.67 \pm 2.08$ for imagined movements. These results may appear as modest but one should consider the fact that subjects were naive and untrained and that a very simple BCI design was used. Actually, we used a single EEG channel, placed at a standard location (i. e., a non-optimized location) and we used a single feature, based on a standard frequency band (i. e., a non-optimized frequency band), with a simple threshold. In future works, it would be interesting to study subjects' performances while using different frequency bands and electrode locations.

## 3.2 Subjective questionnaires

### 3.2.1 Quantitative data

Subjects were asked to grade questions by giving a mark between 1 and 7. Table 1 displays the average marks given by the subjects for the two conditions (real movement game and imagined movement game) according to various criteria.

Our results first showed that the experiments did not seem tiring for the subjects. The experiments with imagined movements seemed however more tiring than that with real movements. However, this difference is not statistically significant (Wilcoxon test $W = -28$, $p > 0.1$). Despite the use of pastes to fix the electrodes, subjects found the experiment comfortable (global mean for question 2: $5.19 \pm 1.23$). According to oral discussions with subjects, it seemed that their curiosity and will to test a BCI was stronger than their apprehension to have gel in their hair.

Concerning the control, it seems that subjects felt to have an average control over the spaceship using real movements whereas they felt to have a lower control using imagined movements. As expected, subjects had significantly more trouble controlling the spaceship using imagined movement than using real movements ($W = 79$, $p < 0.01$). Globally, subjects were able to assess properly their performances, as the marks they gave for question 3, related to their feeling of control, are significantly correlated with the HF differences obtained (Spearman correlation $r_s = 0.63$, $p < 0.00001$). Concerning only imagined movement games, the marks given by subjects to question 3 are significantly correlated with both the HF difference and the TP rate they obtained ($p < 0.05$). Interestingly enough, this correlation is slightly higher between the marks and the TP rate ($r_s = 0.56$, $p < 0.01$) than between the marks and the HF difference ($r_s = 0.51$, $p < 0.05$). This is not the case for real movement games for which there is no correlation between the marks and the TP obtained ($r_s = 0.31$, $p > 0.05$). This might suggest that for a difficult task such as lifting the spaceship using imagined movements, subjects paid more attention to the fact that the spaceship went up when it should have (TP) than when it should not have (FP).

Finally, questionnaire answers showed that subjects found real movement games not really frustrating or annoying whereas imagined movement games where more frustrating and annoying. The difference between the two conditions is significant ($W = -64$, $p < 0.05$). This frustration might be due to the inscreased difficulty to lift the spaceship with imagined movement. However and surprisingly, there is no correlation between the frustration felt by subjects during the imagined movement games and their performance, i. e., the HF difference they obtained, ($r_s = -0.11$, $p > 0.05$) nor between the frustration felt and the subject impression of control ($r_s = 0.26$, $p > 0.05$). One explanation could be related to the absence or lack of visual feedback. Indeed, during imagined movement games, subjects had generally fewer feedback as the spaceship was lifted up less often or it was lifted up less high and stayed in the air a shorter time. This may suggest that less feedback leads to more frustration, whatever the performance. This seemed to be confirmed by oral discussions with subjects.

#### 3.2.2 Qualitative data

Thanks to the use of open questions, the questionnaire enabled us to investigate which kinds of imagined movements the subjects performed, as well as to obtain their remarks and comments concerning the application itself.

Regarding the kinds of movement imagined by the subjects, it is interesting to note that a large variety of strategies where employed. For instance, subjects reported that they imagined themselves swimming, running, taping their feet, braking and accelerating, walking or using stairs. 7 subjects reported they imagined the same foot movement that the one they did in the real movement game, whereas 10 reported they imagined a different movement. On average, subjects for whom the real and imagined movements were the same obtained better results (mean HF = $3 \pm 2.67$) than the others (mean HF = $0.8 \pm 1.75$). However, this difference is not statistically significant (Mann-Whitney test $U_{7,10} = 20$, $p = 0.16$), but it would be interesting to study this point further in the future, by using a dedicated experiment. Interestingly, 13 subjects reported they used a single strategy during the experiments whereas 7 reported they used several strategies. However, there is no difference between these two groups in terms of performances ($U_{13,7} = 41$, $p = 0.75$).

Concerning the free remarks of subjects, it is interesting to note that 3 subjects complained about the difficulty to concentrate considering the environment they were in, i. e., an exhibition. They would have prefered to be in a more isolated place. Most subjects reported that they found the application and the interface well designed, enjoyable and motivating. These remarks are in line with previous studies that showed that VR could increase the motivation of subjects for BCI [3]. Finally, another valuable comment made by 2 subjects concerned the frustration they felt due to the absence or lack of feedback when they did not succeed to lift the spaceship. They suggested that an additional or more complete feedback could be used in order to give them more information and, possibly, improve their learning.

## 4 Discussion and conclusion

This paper described the results of an evaluation of a self-paced BCI application conducted with 21 naïve subjects. We studied both performances and preferences of subjects placed voluntarily in a challenging situation: first-time session, no human learning, no machine learning of the mental state to be detected, "out of the lab", use of a single EEG channel. Subjects interacted with an entertaining Virtual Reality application and were asked to control the take-off and height of a virtual spaceship by using real or imagined movements. Results showed that, without training, roughly half of the subjects were able to control the application by using real foot movements, and a quarter were able to control it by using imagined foot movements.

Taken together, the results of the subjective questionnaire stressed the importance of the mental strategies and the visual feedback. More precisely, results suggested that a lack or an absence of feedback during the detection of the non-control state could lead to an increased frustration for the subjects. Thus, when designing a self-paced BCI, we recommend to provide subjects with a continuous feedback, and to provide feedback (possibly a different one) even when the non-control state is detected. For instance, we could imagine a feedback indicating the subject how close he is from the intentional control state. This may be likely to reduce the subject frustration, to improve his motivation and possibly accelerate his learning.

**Acknowledgments:** This work was supported by the French National Research Agency within the Open-ViBE project and grant ANR05RNTL01601. Authors also thank Dr. Virginie Attina, Dr. Guillaume Gibert, Dr. Emmanuel Maby and Bruno Renier for their help and support related to this work.

## References

[1] C. Guger, G. Edlinger, W. Harkam, I. Niedermayer, and G. Pfurtscheller. How many people are able to operate an EEG-based brain-computer interface (BCI)? *IEEE Trans. Neural Syst. Rehabil. Eng.*, 11(2):145–147, 2003.

[2] G. Pfurtscheller and F. H. Lopes da Silva. Event-related EEG/MEG synchronization and desynchronization: basic principles. *Clin. Neurophysiol.*, 110(11):1842–1857, 1999.

[3] R. Leeb, R. Scherer, D. Friedman, F. Lee, C. Keinrath, H. Bischof, M. Slater, and G. Pfurtscheller. *Toward brain-computer interfacing*, chapter Combining BCI and Virtual Reality: Scouting Virtual Worlds. MIT Press, 2007.

[4] D. Margery, B. Arnaldi, A. Chauffaut, S. Donikian, and T. Duval. Openmask: Multi-threaded or modular animation and simulation kernel or kit: a general introduction. In *VRIC*, 2002.

[5] S. Mason, J. Kronegg, J. Huggins, M. Fatourechi, and A. Schlögl. Evaluating the performance of self-paced BCI technology. Technical report, Neil Squire Society, 2006.

[6] G. Müller-Putz, R. Scherer, C. Brunner, R. Leeb, and G. Pfurtscheller. Better than random: a closer look on BCI results. *Int. J. Bioelectromagn.*, 10(1):52–55, 2008.

# BCI++: an object-oriented BCI prototyping framework

L. Maggi[1], S. Parini[2], P. Perego[1], G. Andreoni[1]

[1]Indaco Dept., Politecnico di Milano, Italy
[2]Bioengineering Dept., Politecnico di Milano, Italy

luca.maggi@polimi.it

**Abstract**

This work aimed at providing a set of tools for the development of home Brain Computer Interfaces based on a low cost acquisition and processing device which could be used by both the end-user in their domestic activities and by the researcher in order to develop new protocols and algorithms and all the software modules necessary to ease the interfacing of the system to external devices (e. g. Home automation systems). The framework was validated by setting up a BCI system based on the SSVEP protocol. Six subjects out of ten healthy users were able to use the system in a home automation and in a gaming application.

## 1 Introduction

A Brain Computer Interface (BCI) is a man machine interface which allows to establish a new communication channel between the brain and the computer. This technology could be used in order to restore or to supersede lost body functions and it could potentially represent a substantial improvement to the quality of life of disabled people. In the last years many efforts were produced in order to demonstrated the applicability of the brain computer interface to daily life by moving the BCI systems from a controlled laboratory environment to a more complex context like a domestic one. During this "out-of-lab transfer" procedure many technological, man machine interaction, signal modification and financial problems must be faced; the aim of this work is that of contributing at reducing the burden of those activity by providing a set of tools studied to ease the development of novel BCI systems or the porting of existing systems. When compared to other existing tools, the main difference in our approach is the final goal of considering the acquisition device like a common personal computer peripheral thus the device should perform both signal acquisition and signal processing.

## 2 Materials and methods

The proposed methodological approach for the development of a domestic BCI is here presented step by step:

- Data-set recording
- Offline algorithm prototyping in Matlab
- Online test
- Identification of the possible user-specific customization
- High level profiling of the most important blocks (memory, execution time)
- Optimization of the algorithm and the protocol

- Porting into a lower level language
- Execution by the ARM7 CPU of the EEG device
- User interface customization

The framework provides both the final device and all the intermediate tools necessary for the setup of the protocol and the algorithms following the depicted development approach. The framework is composed of:

- A low cost acquisition unit
- A mathematical C library (C4M)
- A dynamic mathematical engine (C4MEngine)
- An hardware interface module
- A graphic user interface (AEnima)
- A home automation system interface

The signal acquisition is performed using Kimera II, a low cost Bluetooth EEG unit composed of an EEG amplifier and a digital acquisition and elaboration unit. The EEG amplifier was developed in the laboratory implementing a patented topology for the signal conditioning. Thought being 3.3 V battery powered, the device is robust against artefacts and out-of-band noise thanks to the adopted novel circuitry which provides a fast recovery from saturation and enhanced dynamic reserve [1]. The signal acquisition module was specifically designed and produced by SxT – Sistemi per Telemedicina s.r.l. (Lecco, Italy), it features a real time operating system (RTOS) and a specifically designed firmware. The system was controlled by an ARM7 32 bit microcontroller which accomplishes the following tasks:

- Analog to digital conversion using an external 8-channel ADC
- Local data storage on a micro-SD card in a PC compatible format (FAT16)
- Communication with the PC or a PDA by an onboard Bluetooth module (SPP profile)
- Onboard data processing using a specifically designed mathematical library written in C language

The connection with the acquisition unit and, in the early stages of the development, the signal processing is performed by the Hardware Interface Module (HIM): a software designed in order to assist the researcher during the prototyping of a new BCI system. It provides a solid structure for the acquisition, storage and visualization of the signal, for the communication with the BCI user interface and for the real-time execution of algorithm both in C and Matlab environment. This software was written in C++ language using the cross-platform wxWidgets library. The source code was structured in order to promote application specific customization using hereditary and polymorphism techniques. The basic version supports several kind of instruments; some are real, other are virtual and are useful for debug and simulation purposes. They are:

- Kimera version II and I
- g.tec g.Mobilab;
- An ideal signal generator
- An instrument simulator which load previously recorded signal from a file and play it ad the same sample frequency
- An interactive file player which can load pieces of dataset depending on the operator's needs

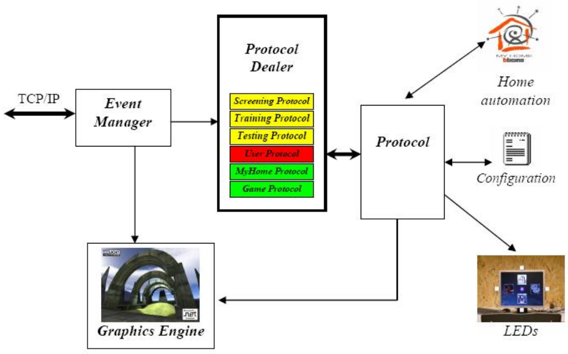


Figure 1: Structure of the AEnima module.

It is possible to add a new instrument by deriving a specific class from the basic Instrument class: for example, in four hours it was possible to enable the HIM with the g.Mobilab instrument (g.tec, Graz, Austria). The HIM also provides a basic algorithm class which handles all the operation related to data buffer management, performance monitoring and, if necessary, the communication with Matlab. In order to test a new algorithm the researcher only have to focus on writing the specific code, in C or Matlab language according to his need and the HIM will manage all the other issues. In order to simplify the problem of porting BCI algorithms to different platforms, especially those not supporting Matlab based development, the C4M Mathematical library was developed. The C4M library is a powerful tool for the efficient porting of generic algorithms on single chip embedded system, which have limited performances in terms of speed and memory resources, when compared with those available in a standard PC. This library was already described in other works [2]. A mathematical engine provides a command line high level language which allow the test of new functions directly on the final hardware device: using a terminal software and a serial port it is possible to use the a standard personal computer in order to interact with the mathematical engine running on the device in a manner which is similar to a simplified Matlab version.

The graphical user interface module, AEnima is an independent application and was written using a multi-platform and multi-API based graphical engine in order to provide a more realistic and challenging experience to the user. A TCP/IP socket based layer managed the communication with the hardware interface module which can be executed by both the same personal computer which executes the HIM and by another one. The following figure shows the structure of application:

- The core of the system: it is an open source high performance realtime 3D engine written and usable in C++. It is cross-platform, using D3D, OpenGL and its own software renderer
- The protocol class implements the user application and the stimulation protocol
- The protocol dealer is a coordination object used for messages dispatch to handle the interaction between different user applications

A specific software module was implemented in order to provide an interaction layer with an home automation system. A MyHome gateway was provided by BTicino spa (Erba, Italy) and a basic demonstrator was set-up in our laboratory. The standard physical communication layer of the used gateway is RS-232; in order to maximize the ease of installation a specific RS-232 to Bluetooth module was designed.

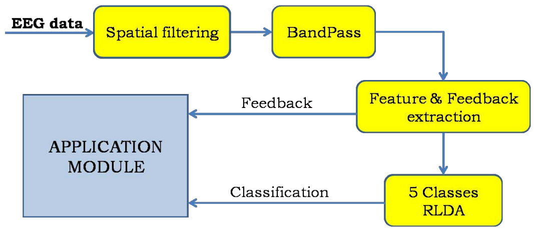


Figure 2: Structure of the algorithm

# 3 Results

The consistency of this tool chain was verified by using BCI++ to implement an SSVEP based BCI system. In the next paragraph a detailed description of the system will be given in order to demonstrate that all the specific modules were used in implementing a real-time working system. The framework proved a good flexibility and the wide set of debugging instruments dramatically simplified the debug and the test of a new system. Starting from a previous experience and a set of algorithms for the SSVEP protocol it was possible to set-up a complete BCI system in the Sensibilab laboratory in CampusPoint@Lecco (Lecco, Italy) in a few weeks. The visual stimulation system consisted of four cubic spotlights with high efficiency LED, the cubes were fixed to the edge of the screen ideally associating each light to a direction: up, down, left or right. The stimulation device autonomously generated and was controlled by the AEnima module. The following figure shows the structure of the SSVEP classification algorithm.

A spatial filtering block (SFB) was used in order to reduce the dimensionality of the eight acquired monopolar leads. The SFB computes a custom derivation on the basis of the analysis of the calibration data-set. The spatial filtering is computed performing a linear combination of the acquired channel. A band pass filter between 5 and 40 Hz eliminated the out of band noise.

The features were the result of a ratio between the amplitude of a stimuli time-synchronous averaging of the signal, compared to the estimation of the amplitude of the raw signal. For each frequency the algorithm extract one feature. The resulting estimation is a numerical value which theoretically ranges from 0, in case of total disruptive interference within the main window, to 1, when the signal has only one periodic component at the same period of the stimulation. The classifier consisted of a regularized linear discriminant analysis (RLDA) based on the modified samples covariance matrix method. The RLDA included a boosting algorithm based on a cyclic minimization of the classification error on the training set and an algorithm for outliers rejection. The classification algorithm was conceived for use in an asynchronous protocol, thus the system was trained in order to identify five different classes referred to as LEFT, RIGHT, UP; DOWN and NULL for the non-stimulus or non-command class. The both a Matlab and a C language versions of the algorithm were developed and were activated by the HIM, with the same results. A classification post processing was inserted in the user interfaces in order to achieve a better usability.

The adopted SSVEP protocol was composed of the following phases each one corresponding to a specific user interface implemented with AEnima: the first three are needed for the set-up and for the validation of the classifier, the second group are for “free will” use and can be considered as real applications.

The screening phase was studied in order to understand the best user specific stimulation frequencies. One LED flashed a increasing frequencies between 6 and 17 Hz and an off-line analysis GUI allowed the identification of the four best stimulation frequencies. The training or calibration phase guided the user in a four direction sequence studied in order to record a dataset for the calibration of the classifier. The test was an eight symbols sequence for online evaluation of the classifier performances. BCI-User is a main menu for application selection: the user can control a cursor in order to select one of the four applications (AstroBrainFight, Home automation, communication and media player) which are graphically represented by a 3D box with and appropriate


Figure 3: AstroBrainFight game. The used drives the ship in order to reach the other one.

texture. The AstroBrainFight (Figure 3) game was studied to test a cursor like control: the user can control a spaceship in order to collide with another one put in a semi-random position of the screen. The task for the user was to reach 15 collision in the minimum time. The Home automation protocol was implemented to demonstrate the usability of the home automation system, set-up in the laboratory. An interface similar to the one described for BCI-user, allowed the user to activate some devices like light and a fan.

The system was tested on ten healthy subjects between 22 and 55 years old, 9 of them were males. The standard testing procedure was composed of:

- One screening session
- One calibration session without feedback
- One testing session with feedback

If the testing was successfully carried out:

- One AstroBrainGame with feedback session
- One home automation usability test

During the first part of the testing procedure the subject was verbally instructed about the structure of the graphic interface. In order to increase users participation and the interest in the protocol, they were informed that a "hall of fame" of the best AstroBrainGame players was being formed. Some subject enjoyed the system and asked for other BCI sessions after the standard one: in those cases the database was updated, but the score was not recorded in the results table.
Seven subjects out of ten generated an SSVEP and six of them were able to train a classifier and use the system (subject HE, showed an SSVEP response, but had problems with electrodes). Subject HL was able to use the system, but the test times were not considered in the statistics because he did not completely understand the instruction. The average time to complete the eight symbols test was: 68.2 seconds (std 8.2 s). The best performance was 59 seconds. We have to point out that this speed test was not a measurement of the maximum performance reached by a skilled user with an user optimized classifier, but the transfer rate obtained by a first time BCI user. All the six subject that acceded to the second part of the protocol were able to control the home automation system even after having switched the lights on, thus the system results strong to environmental light variation.

| Subject | SSVEP | Frequencies (Hz) | | | | Test time | Game time | MyHome |
|---|---|---|---|---|---|---|---|---|
| | | L | R | U | D | | | |
| HA | Yes | 9.14 | 6.9 | 5.9 | 8 | 73 | 265 | Used with lights |
| HB | Yes | 8 | 9.10 | 9.8 | 11.1 | 59 | 206 | Used with lights |
| HC | No | | | | | | | |
| HD | No | | | | | | | |
| HE | Yes | X | X | X | X | | | Only screening |
| HF | Yes | 8 | 11.1 | 12.2 | 14.2 | 80 | 205 | Used with lights |
| HG | No | | | | | | | |
| HI | Yes | 9.14 | 9.8 | 11.13 | 16 | 65 | 210 | Used with lights |
| HL | Yes | 9.8 | 11.1 | 12.8 | 15.1 | 170* | 461* | Used with lights |
| HM | Yes | 8 | 9.8 | 11.1 | 12.2 | 64 | 295 | Used with lights |

Table 1: Subject performances using the SSVEP based BCI-

# 4 Discussion and conclusions

The most relevant aspect of the developed framework is the possibility for unskilled developers (e g. Master thesis students) to develop and test their own work and to actively help increasing the number of available instruments in the framework. The usability of the framework was demonstrated in the implementation of the SSVEP based system: during the development of the system a Bioengineering master thesis student without previous C++ programming experience, was successfully involved in the development two new BCI-driven applications (Home automation and AstroBrainFight). When Matlab algorithms are provided, the implementation of a new testing protocol usually takes a few hours for the user interface customization and a few hours for testing purposes; thus evaluation of a new operative protocol isn't constrained by technical issues. The final goal is to make this fascinating technology available at home by any potential user with the help of their family members. The next steps planned in order to reach this objective are in the following directions:

- software platform distribution
- application to disabled people
- usability enhancement for people without technological background
- availability of low cost acquisition devices

In the immediate future all the software platform will be available free-of-charge to other research group and further efforts will be done in documenting and disseminating the obtained results in order to give a better visibility to this project, in the hope that the community will help to complete the framework in all the specific aspects.

# References

[1] L. Maggi, L. Piccini, S. Parini, G. Andreoni, and G. Panfili. Biosignal acquisition device: A novel topology for wearable signal acquisition devices. In *Proc. Biosignal*, 2008.

[2] L. Mazzucco, S. Parini, L. Maggi, L. Piccini, G. Andreoni, and L. Arnone. A platform independent framework for the development of real-time algorithms: application to the SSVEP BCI protocol. In *Proc. Int. BCI Workshop*, 2006.

# A platform-independent open-source feedback framework for BCI systems

B. Venthur, B. Blankertz

Machine Learning Laboratory, Berlin Institute of Technology, Berlin, Germany

venthur@cs.tu-berlin.de

**Abstract**

This paper introduces the Pythonic Feedback Framework which provides a platform independent framework to develop BCI feedback applications in Python. It was designed to make the development of feedback applications as easy as possible. Existing solutions have either been implemented in C++, which makes the programming task rather tedious, especially for non-computer-scientists, or in Matlab, which is not well suited for more advanced visual (flickering is inavoidable which is unconfortable for the user and has side effects in the EEG) or auditory feedback applications.

This framework solves this problem by moving the feedback implementations to a general purpose, and easy to learn language like Python. Python provides many so called bindings to other libraries, which allow it to develop high quality multimedia feedback applications, with little effort.

The framework communicates with the rest of the BCI system via a standardized communication protocol using UDP and XML and is therefore suitable to be used with any BCI system that may be adapted to send its control signal via UDP in the specified format.

Having such a general feedback framework will also foster a vivid exchange of feedback applications between BCI groups, even if individual system for processing and classification are used.

## 1 Motivation

The motivation for the development of the presented feedback framework was to facilitate the implmentation of high quality BCI feedback applications and to allow the interchange of such applications between BCI groups. Accordingly, the feedback framework was designed as a standalone program which may receive the control signal from a BCI system via a standardized protocol. In order to make the implementation of new applications easy, many of the basic tasks common to most feedback applications are accomplished in the framework and have not to be re-implemented in the individual feedback applications. As programming language Python was chosen, because it is easy to learn (interpreted language) and recognized as a very mature and stable language which runs platform independent and already includes a very comprehensive class library. If Python is too slow for certain time critical methods, it is possible to write those parts in C/C++ and call them within Python. Most interesting about Python are the so called bindings. Bindings are Python libraries which make other libraries, written in other languages than Python, available to Python. We found Pygame (`http://www.pygame.org/`), a set of Python modules designed for writing games a very useful resource for writing feedback applications. Pygame allows to create high quality games and multimedia applications in Python. Since Python offers countless other bindings like bindings to OpenGL, it is even possible to create feedbacks with complex 3D graphics and special effects.

In contrast to compiled languages like C++, Python is also known to be very easy to learn. Users with Matlab experience will find the syntax of Python familiar.

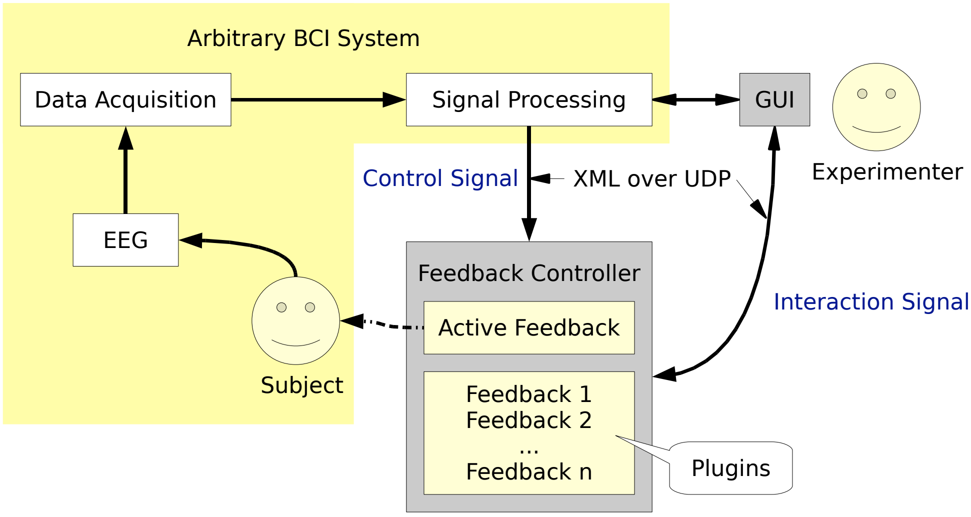


Figure 1: Setup of an BCI experiment using the Pythonic Feedback Framework. The Feedback Controller receives the control- and interaction signlas via UDP and XML.

## 2 Overview of the framework

Figure 1 shows the setup of a generic BCI system using our Feedback Framework. The subject is wearing a EEG cap and sitting in front of a computer which runs a feedback application. Brain signals are collected and submitted to the data acquisition and signal processing units. The signal is processed and the result (control signal) is sent to the Feedback Controller which processes the incoming signal and forwards it to the feedback. The feedback application translates the control signal into a visual, audible and/or tactile output.

The experimenter can remote-control the feedback and manipulate its variables via the GUI, which also sends singals to the Feedback Controller. Those signals are called interaction signals.

The framework communicates with the rest of the BCI system via a standardized communication protocol using User Datagram Protocol (UDP) and Extensible Markup Language (XML) and is therefore not bound to a single BCI system, but should be usable with any BCI system providing control signals of some kind.

The feedbacks are realized as plugins of the Feedback Controller.

## 3 Components of the framework

The feedback controller (Section 3.1) and the feedback base classes (Section 3.2) are components that are general and take over the much of the programming load for the implementation of new feedback applications by providing much of the general functionality.

### 3.1 Feedback controller

The Feedback Controller manages the communication between the feedback and the rest of the BCI system. It acts like a server, collecting control- and interaction signals over the network. Once the Feedback Controller ist started, it is fully remotely controllable from the GUI: it is possible to load feedbacks, manipulate their variables, start, pause and stop them. The data is sent in XML format and must be therefore translated into Python compatible data structures and commands. The Feedback Controller takes care of this. It sets feedback variables if necessary and calls the appropriate event methods of the feedback.

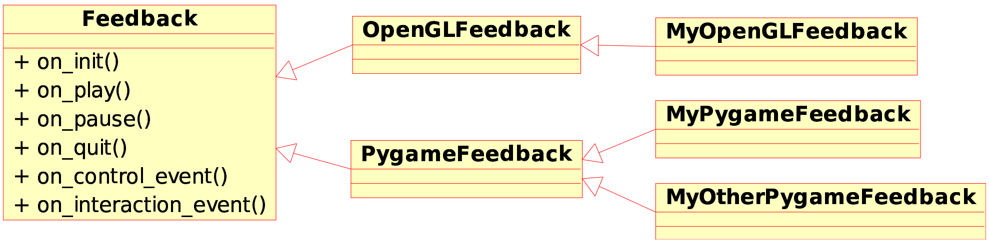


Figure 2: Possible classdiagram: OpenGLFeedback and PygameFeedback are derived from the Feedback base class and implement common functionality needed in all OpenGL- and Pygame feedbacks.

Feedbacks are realized as plugins of the the Feedback Controller. Since the Feedback Controller takes care about the whole communication between the feedback and the rest of the BCI system, implementing feedbacks is straight forward. Furthermore, since there is a uniform interface between the feedback and the Feedback Controller, it is even possible, to exchange feedbacks between various BCI systems of different BCI groups when using this framework.

## 3.2 Feedback base class

The Feedback base class is the interface to the Feedback Controller's plugin system. The base class provides methods, the Feedback Controller needs to communicate with the feedback. By subclassing the Feedback base class, the derived class becomes a valid and ready-to-use feedback, available to the Feedback Controller.

Feedbacks are event driven. Whenever the Feedback Controller receives a signal, it calls the appropriate methods of the feedback to notify it: an incoming control signal causes an `on_control_event` on the feedback, an incoming interaction signal with the play command an `on_play`, and so on. To react on such events, only the respective `on_`-method of the feedback has to be implemented. It is not necessary to implement all available events of the Feedback base class, if the Feedback Controller triggers an event which was not implemented in the feedback, nothing happens.

The object oriented approach of this framework makes it possible to further simplify the development of feedbacks: If it becomes obvious that for example feedbacks using Pygame often share the same blocks of code, it is possible to derive a PygameFeedback baseclass from the Feedback base class, which already implements the shared functionality. Actual feedbacks using Pygame can be derived from the PygameFeedback baseclass which can reduce the amount of code per feedback drastically. Figure 2 illustrates the example.

## 3.3 GUI

The GUI is responsible for sending interaction signals to the Feedback Controller. It acts like a remote control for the Feedback Controller and the running feedback: it allows to load, un-load feedbacks, modify their variables, start, stop and pause them.

Once the GUI is connected to the Feedback Controller, the Feedback Controller publishes all available feedbacks to the GUI. The experimenter can now select the desired feedback in the GUI and tell the Feedback Controller to load it. Once the Feedback Controller has loaded the feedback, the feedback's variables are automaticly published to the GUI. The GUI presents those variables and their values in tabular form, allowing to modify their values or create new ones and send them back to the Feedback Controller where they are directly applied to the running feedback.

The GUI is written in Python and QT and runs – like the rest of the framework – platform independently.

### 3.4 Documentation and examples

Part of the framework is also a complete documentation of the system and its interfaces. The documentation also provides a guide how to write own feedback applications using this framework. Several well documented examples, explaining every major aspect of the feedback implementation, are included.

## 4 A simple feedback example

The following listing shows a trivial feedback written with the framework. Although it does nothing but printing the current control signal two times per second, it already shows the basic structure of every feedback.

```
from Feedback import Feedback
import time

class ExampleFeedback(Feedback):

    def on_init(self):
        print "Feedback successfully loaded."
        self.quitting, self.quit, self.pause = False, False, False

    def on_quit(self):
        self.quitting = True
        print "Waiting for main loop to quit."
        while not self.quit:
            pass

    def on_play(self):
        self.quitting, self.quit = False, False
        self.main_loop()

    def on_pause(self):
        self.pause = not self.pause

    def main_loop(self):
        while 1:
            time.sleep(0.5)
            if self.pause:
                continue
            elif self.quitting:
                break
            print self._data
        print "Left main loop."
        self.quit = True
```

There are three variables which control the behavior of the feedback: `pause` tells the feedback to pause it's action, `quitting` tells the feedback to quit it's main loop and `quit` is set when the main loop has quit.

The heard of the feedback is the `main_loop` method. As the name suggests, it contains an infinite loop where each iteration represents a tick (a very short amount of time) of the running feedback. Each tick, the feedback checks the aforementioned variables `pause` and `quitting` and decides what to do. If `pause` is set, the feedback just skips this tick, if `quitting` is set, it leaves the loop and sets the `quit` method. If none of the two variables is set, it just executes the tick, in this case by printing the content of the control signal.

The event `on_play` starts the main loop, `pause` and `on_quit` control the main loop's behavior by setting the `pause` and `quitting` variables. `on_quit` does a bit more than just setting the `quitting` variable: after the variable has been set, it waits until the main loop has quit by repeatingly checking the `quit` variable. Only after `quit` has been set, the `on_quit` method returns, which tells the Feedback Controller that the feedback has successfully terminated.

## 5 Communication with the rest of the BCI system

In order to couple the Framework as loosely as possible with the rest of the BCI system and thus allowing to support many different BCI systems, the Feedback Controller receives the control- and interaction signals via User Datagram Protocol (UDP), a very lightweight network protocol supported by all major operating systems and programming languages. UDP servers and -clients are trivial to implement and allow the communication between programs on different machines in the network or on the same machine.

The the content of the signals is send via Extensible Markup Language (XML) which is a well known standard for exchanging information especially over internet. Libraries to parse XML files or creating new ones are available for most modern programming languages.

The utilization of UDP and XML as a standardized interface to communicate with the framework, should make it very easy to adapt most existing BCI systems to use this framework to develop Feedbacks in Python.

## 6 Requirements

The framework itself has very few dependencies. It needs Python 2.4 or higher and optionally pyParallel (`http://pyserial.sourceforge.net`) to utilize the parallel port to send markers to the EEG acquisition system. No requirements are imposed regarding the operating system. The framework will run on every platform which is supported by Python.

To use the GUI which uses Python's QT bindings, PyQT (`http://www.riverbankcomputing.com/software/pyqt/`) is needed. PyQT also runs on every major platform.

To use this framework in a specific BCI system, the BCI system should be able to send the control signal via XML and UDP. Modifying existing BCI systems to create valid XML files containing the control signal and sending them over UDP, should be fairly easy regardless of the programming language being used.

## 7 Conclusion

The Pythonic Feedback Framework provides a solution for writing high quality BCI feedback applications with minimal effort. Through the use of a standardized interface using a standard protocol for the communication with the BCI system, this framework is very generic and it should be easily adaptable to most existing BCI systems.

Moreover such a unified feedback framework creates the unique opportunity of exchanging BCI feedback applications between BCI groups, even if individual systems are used for processing and classification.

The presented framework runs on every major platform (Linux, Mac and Windows), is Free Software and licensed under the terms of the GNU General Public License (GPL) for non-commercial purposes. The homepage of the project is `http://www.bbci.de/pyff`.

# Defining and using standards in brain-computer interface research

L. R. Quitadamo[1], M. Abbafati[1], G. C. Cardarilli[2], M. G. Marciani[1,3], L. Bianchi[1,3,4]

[1]Department of Neuroscience, University of Tor Vergata, Rome, Italy
[2]Department of Electronic Engineering, University of Tor Vergata, Rome, Italy
[3]Fondazione Santa Lucia IRCCS, Rome, Italy
[4]Centro di Biomedicina Spaziale, University of Tor Vergata, Rome, Italy

luigi.bianchi@uniroma2.it

**Abstract**

Brain-Computer Interface (BCI) systems have caught the attention and the interest of a lot of research labs all around the world in the last years, as they represent a novel method of communication for severely disabled people and appear to be a feasible application in a lot of others fields, such as games or virtual reality. Also a lot of disciplines became involved in this fascinating research field, such as neurology, mathematics, engineering, psychology, rehabilitations, etc., since BCIs are very complex systems which require manifold contributions to reach the final goal of communication. However, the fact that there are different research units which work on BCI, everyone with an own system and own protocols, represents an obstacle when different systems have to be compared and evaluated, as a common language for talking about BCI entities, a standard model for describing BCI systems, a common metric for evaluating systems and common file formats to share data, partially lack to date.

In this regard in this paper we want to show the importance of defining and using standards for BCI systems and to offer a view on the UML-based BCI model we implemented, on the metric we use for evaluating systems, on the XML-based file format we use for physiological data and other BCI entities and on the tools we implemented for the optimization of BCI systems; all these latter can represent a milestone in the attempt of standardizing and optimizing BCI systems.

## 1 Introduction

Severely disabled people, affected for example by ALS, degenerative muscular pathologies, strokes, etc., lose the ability to move their body and so the possibility to satisfy most of their basilar needs and to communicate with the external world. These people can find a valid solution to some of their problems thanks to BCI systems, which try to translate some changes in their cerebral signals into commands towards an output peripheral (a robotic arm, a cursor on a screen, a speller), without passing through the normal physiological paths (nerves and muscles) [1].

A functional model that has gained a wide acceptance in BCI research field was proposed by Mason et al. [2]. In this model a BCI systems is divided into two main functional blocks, the Transducer and the Control Interface (Figure 1). The Transducer is the only module which deals with physiological signals: it acquires signals by means of the Acquisition block and then processes them by means of the Classifier. The Classifier, on its turn, is constituted by the Feature Extractor, which extracts some features of interest from the signals and the Features Translator which translates these features into some logical symbols (LSs), belonging to a logical alphabet (LA), which are the input to the Control Interface. This module translates LSs into semantic symbols (SSs), belonging to a semantic alphabet (SA), which constitute the input to an output device controller.

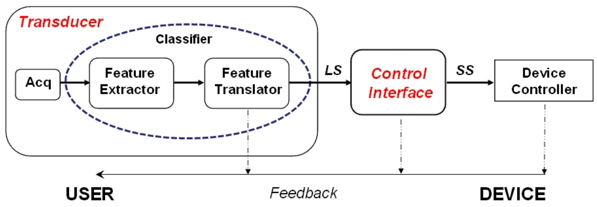


Figure 1: Functional model of a BCI system.

The Control Interface holds some encoding strategies for the translation of LSs into SSs: for example with a LA of three symbols ($\alpha$, $\beta$, $\gamma$), the entire English alphabet plus the space character (SA) can be encoded by means of all the possible permutations on sequences of three LSs.

It is important to note that the Control Interface manages only alphabets and encoders and does not deal with physiological signals at all. Vice versa the Transducer deals with cerebral signals and does not need to know which is the actual encoding strategy to work well. This means that the Transducer and the Control Interface are separate modules and that for the optimization of a BCI system both of them must be considered; in other words, the best BCI system can be obtained from the best combination of Transducer and Control Interface.

Moreover SSs have their own probabilities of occurrence and so the implemented encoding strategy determines the number of times a LS occurs; then since each LS is correctly classified with a different probability, the choice of the most adequate encoding (the best Control Interface) and of the classifier which properly recognizes the current LS (the best Transducer), reflects in the choice of the best BCI system so that only the best combination of transducers and control interfaces can be used for the purpose of optimizing BCI systems [3].

A model for BCI systems is the starting point for the process of their standardization; however, there are other different levels of standardization which span from methods for the evaluation of systems to format file and tools and must be considered equally important: in fact, in order to a have a common language for BCI systems, a standard model and standard definitions are important; to evaluate which is the best system to adapt to the user, among a set of different systems, a common metric to evaluate them is necessary; to share data among laboratories, a standard file format is needed and finally tools are required to simulate systems, even if this represents the less important aspect to consider as everyone can use his own tools, still adopting a standard model and a standard metric. In the following section an overview of these different levels will be presented. Our solutions to the standardization problem will be also shown.

# 2 Methods

## 2.1 A model for the description of BCI systems

A functional model for BCI systems represents the first stage for standardization; the one described in [2] is fundamental for this process as it identifies two main functional blocks, the Transducer and the Control Interface, with their own specific functionalities.

However this model is static, as it does not consider the temporal aspects of BCI systems, that is which is the flux of operations which lead to the classification of a symbol. A successful attempt to supply this model with the timing information was made in [4]; we identified a set of actors which control the execution of an experimental BCI session and a set of operations which lead from the starting of a trial to the classification of a symbol. This temporal schema can be applied to the most diffused BCI protocols implemented to date: P300, slow cortical potentials, $\mu$-rhythms, steady-state evoked potentials, fMRI-based, etc. With this model it has been demonstrated that a unique temporal structure can be used to describe different BCI systems; we think that this fact is very important for the purpose of unification and standardization of BCI systems.

The model implemented in [3] has been documented with the Unified Modeling Language, that is a wide-spread standard visual language for the design and the documentation of systems, software and processes and is managed by the Object Management Group (OMG). UML is based on the object-oriented paradigm and so it allows the design of a system by means of objects which have some particular features and operations and which interact among each other to define the different behaviors of the system itself. Being a very simple to use and well-established standard, it was natural to believe that it would be suitable for describing complex systems and for allowing their standardization.

## 2.2 A new metric for evaluating the efficiency of a BCI system

Classical metrics such as Mutual Information [5], Bit Rate, Entropy, etc. fail in the purpose of evaluating the performances of BCI systems as a whole, as they do not take into account how transducers and control interfaces adapt each other or how the system behaves when errors occur.

The question is: how can one determine if the performances of a system are mostly determined by the transducer, which deals with cerebral signals, or by the control interface that in general does not deal with brain signals?

The answer has been found in the proposal of a new metric [3], which evaluates the performances of a system, in a copy-spelling task, as a function of the performances of both the Transducer and the Control Interface. This metric adheres to the functional model described in the previous section.

### 2.2.1 Describing the transducer

The starting point of the proposed metric is the Extended Confusion Matrix (ECM), which evaluates the performances of a TR and which represents on the rows the LSs to be classified and on the columns the LSs actually classified; the last column of the matrix represents the cases in which the transducer was not able to classify and so abstained from decisions [6]. An example of ECM is now reported:

$$\mathrm{ECM} = \begin{array}{c|c|c|c|c} & \alpha & \beta & \gamma & ? \\ \hline \alpha & 56 & 24 & 0 & 0 \\ \hline \beta & 0 & 64 & 13 & 3 \\ \hline \gamma & 8 & 8 & 62 & 2 \end{array} \tag{1}$$

As you can see from the matrix in (1), most of the classification errors are associated to the generation of the first symbol $\alpha$; this is of great importance in the choice of the encoding strategy to implement, as selecting an encoding which minimizes the occurrence of the $\alpha$ symbol will result in the minimization of the errors and in the optimization of the system. Note that describing transducers with classical metrics, instead of ECM, makes impossible to use this simple optimization strategy.

With an ECM and some relations (reported below) one can calculate a Misclassification Probability Matrix (MPM):

$$\mathrm{MPM}[i,j] = \begin{cases} \frac{\mathrm{ECM}[i,j]}{n_i},\ i \neq j \\ \mathrm{MPM} = 0,\ i = j \end{cases} \tag{2}$$

$$\mathrm{MPM} = \begin{array}{c|c|c|c|c} & \alpha & \beta & \gamma & ? \\ \hline \alpha & 0 & 0.3 & 0 & 0 \\ \hline \beta & 0 & 0 & 0.1625 & 0.0375 \\ \hline \gamma & 0.1 & 0.1 & 0 & 0.025 \end{array} \tag{3}$$

where $n_i$ represents the number of total cases associated to a LS, and an Extended Overtime Matrix (EOM):

$$\text{EOM} = \begin{array}{c|c|c|c|c} & \alpha & \beta & \gamma & ? \\ \hline \alpha & 0 & 2 & 2 & 1 \\ \hline \beta & 2 & 0 & 2 & 1 \\ \hline \gamma & 2 & 2 & 0 & 1 \end{array} \tag{4}$$

The MPM represents the probabilities concerning incorrect classifications and EOM represents the "costs" associated to error and indeterminateness cases and which depend on CI error correction strategy [3]. In the example in (4), a cost of "0" means that no error was done during the selection of the LS (principal diagonal of the matrix); a cost of "1" is associated to indeterminate cases (last column of the matrix) and means that only a reselection of the correct LS is needed; finally a cost of "2" means that, after an error, one has to perform two additional steps to correct the error, that is, one to delete the wrong LS and one to reselect the right one.

## 2.3 Measuring error consequences: Super Tax Vector

When a misclassification or an abstention occur the information rate of the system will be reduced; this loss of information can be quantified with the Super Tax Vector, whose $i$-th element is given by:

$$\text{ST}(i) = \sum_{j=1}^{N_{LA}+1} \text{MPM}[i,j] \cdot \text{EOM}[i,j] \tag{5}$$

where each element of ST represents the fraction of additional selections that are necessary to correct a mistake. For the above-mentioned example we have:

$$\text{ST} = \begin{bmatrix} 0.6 \\ 0.3625 \\ 0.425 \end{bmatrix} \tag{6}$$

One can easily see that the generation of the first symbol appears to be the most difficult, as already illustrated. Finally, the Expected mean Selection Cost (ESC), that is the number of classifications required to generate a correct logical symbol, is defined as:

$$\overline{\text{ESC}} = \sum_{i=1}^{N_{LA}} \frac{\hat{p}_{occ}(i)}{1 - \text{ST}_i} \tag{7}$$

where $p_{occ}(i)$ is the probability of the $i$-th logical symbol to occur.

If $N_{SA}$ is the length of the SA, $p_{SS}(n)$ is the probability on the $n$-th SS to occur and $l(n)$ is the number of LSs used for the encoding, then the mean codeword length can be defined as:

$$\overline{\text{L}_{CW}} = \sum_{n=1}^{N_{SA}} p_{SS}(n) \cdot l(n) \tag{8}$$

Finally the efficiency $\text{Eff}_{\text{SYS}}$ of a system can be defined as:

$$\text{Eff}_{\text{SYS}} = \frac{1}{\overline{\text{L}_{CW}} \cdot \overline{\text{ESC}}} \tag{9}$$

It has been demonstrated in [3] that this index is a better indicator of the performances of a BCI system than Mutual Information in a copy-spelling task.

It is easy to see that the Efficiency of a system depends on both the Transducer, by means of LCW, ECM and MPM, and the Control Interface, by means of EOM, even if they have been separately implemented; so the choice of the best BCI system to adapt to the user requirements can be performed only after the evaluation of the performances of the best Transducer-Control Interface combination.

### 2.4 An XML-based file format for BCI

Once a model and a metric have been implemented, there is the need to create a file format for the dissemination of data. An optimal technology for implementing file formats in a flexible way that allows the sharing of data among different research groups is the Extensible Markup Language (XML). By following some simple strict syntactic rules everyone can define the structure of a document: XML tags are unspecific, easy to understand and can be extended without breaking the compatibility with preexistent data or tools. This technology is supported by a lot of platforms and operative systems so that data can be exchanged without errors and with no need of special software conversion tools. In our research we used XML for storing all the data used for the description of the entities above mentioned: LSs, SSs, ECMs and Encoders, etc. Also we used XML for storing data regarding the simulation performed with BF++ Toys [7], a set of C++ routines implemented for the evaluation of the performances of BCI systems and which will adequately be described in the next paragraph.

In order to support all the aspects of BCI systems (performances, protocols information, experimental setup, information about feedback), also an XML-based file format for representing electrophysiological data has been defined and called NPX (NeuroPhysiological data in Xml) [8]. It supports a virtually unlimited number of sensors and events. Data can be stored in various ways with respect to the accuracy (8, 16, 32, 64 bits), the internal representation (integer, floating point), and where the data are stored: because XML files are not as efficient as binary ones, if the amount of sampled data is huge (e.g., an EEG recording) they can be stored in an additional distinct binary file, otherwise (e.g., ERP, spectral data) they can be stored in the XML file itself. In both cases the XML file will contain a complete description of the sensors (dynamics, number of bits, gain, coordinates, etc. ), events (type, occurrence, etc. ), processing, etc. Source code to read and write a NPX file is available and written in ANSI C++ to allow an easy porting under virtually any platform.

### 2.5 Tools for the optimization of BCI systems: BF++Toys

BF++ Toys are a set of software tools aimed at evaluating and optimizing the performances of a system. They implement the metric previously described and are formed by four main tools which simulate or define the behavior of complete systems or part of them [7]. They are:

1. The ECM generator, which simulates the characteristics of a transducer on the basis of several different strategies.
2. The Encoder generator, which generates the encoding of sequences of LSs into semantic ones.
3. The Simulators, which simulate the behavior of complete systems virtually built by assembling transducers and control interfaces.
4. The Optimizers, which determine among a collection of transducers and control interfaces which combination will result in the most performing system.

## 3 Discussion

The model, the metric, the file format and tools described in this paper constitute the core of the new incoming version of the Body Language Framework (BF++) [10], a C++ set of routines for the implementation and optimization of BCI systems. As described in this paper, the model used is UML documented, so it represents a valid standard that anyone can adopt according to his needs; the implemented metric optimizes a BCI system by selecting the best combination of Transducer and Control Interface and so represents a way to tune systems; the file format is based on the XML standard, so it is compatible with a lot of platforms, easily extensible and so suitable for the sharing of information; finally, the C++ based Toys, even if less important than the previous features, represent a valid mean for systems simulation and optimization. More importantly all of them adhere to the same unique model.

## 4 Conclusion

Standards are very important in all research fields as they allow the unification of the resources and so their dissemination. BCI research needs some standards to which anyone interested in BCI can adhere, in order to improve the communication among labs, the sharing of tools and researches and finally the optimization of BCI systems. In this paper we presented our vision about the problem of standardization of BCI and the solutions we adopted in terms of a UML model, a metric for evaluating systems, a XML-based file format and tools which make use of the previous resources to simulate BCI systems and find the best one. We hope that they can represent an important step toward the unification of resources in BCI field.

Most of the tools and resources described here can be found at `www.brainterface.com`. Everyone can download them, modify them and use them for his own needs and even suggest us adjustments and improvements.

**Acknowledgments:** This work was partially supported by the DCMC (Disorders of Motor and Cardio-respiratory Control) Project of the Italian Space Agency and dedicated to the memory of Renato Grasso and Aleksandar Kostov.

## References

[1] J. R. Wolpaw, N. Birbaumer, D. J. McFarland, G. Pfurtscheller, and T. M. Vaughan. Brain-computer interfaces for communication and control. *Clin. Neurophysiol.*, 113:767–791, 2002.

[2] S. G. Mason, M. M. Moore Jackson, and G. E. Birch. A general framework for characterizing studies of brain interface technology. *Ann. Biomed. Eng.*, 33:1653–1670, 2005.

[3] L. Bianchi, L. R. Quitadamo, G. Garreffa, G. C. Cardarilli, and M. G. Marciani. Performances evaluation and oprimization of brain-computer interface systems in a copy spelling task. *IEEE Trans. Neural Sys. Rehab. Eng.*, 15:207–216, 2007.

[4] L. R. Quitadamo, M. G. Marciani, G. C. Cardarilli, and L. Bianchi. Describing different brain-computer interface systems through a unique model: a UML implementation. *Neuroinformatics*, to be published.

[5] A. Schlögl, C. Keinrath, R. Scherer, and G. Pfurtscheller. Information transfer of an EEG-based brain-computer interface. Mar. 2003.

[6] T. Pietraszek. Optimizing abstaining classifiers using ROC analysis. Jun 2005.

[7] L. R. Quitadamo, M. G. Marciani, and L. Bianchi. Optimization of brain-computer interface system by means of XML and BF++Toys. *Int. J. Bioelectromagnetism*, 9:172–184, 2007.

[8] L. Bianchi, L. R. Quitadamo, M. G. Marciani, B. Maraviglia, M. Abbafatu, and G. Garreffa. How the NPX data format handles EEG data acquired simultaneously with fMRI. *Magn. Reson. Imaging*, 25:1011–1014, 2007.

[9] E. W. Sellers, D. J. Krusienski, D. J. McFarland, T. M. Vaughan, and J. R. Wolpaw. A P300 event-related potential brain-computer interface (bci): the effects of matrix size and inter stimulus interval on performance. *Biol. Psychol.*, 73:242–252, 2006.

[10] L. Bianchi, F. Babiloni, F. Cincotti, S. Salinari, and M. G. Marciani. Introducing BF++: a C++ framework for cognitive bio-feedback systems design. *Methods Inform. Med.*, 42:104–110, 2003.

# SigViewer – an open source viewing and scoring program for biomedical signals

C. Brunner[1], A. Schlögl[2], G. Pfurtscheller[1]

[1]Institute for Knowledge Discovery, BCI Lab, Graz University of Technology, Graz, Austria
[2]Institute for Human-Computer Interfaces, Graz University of Technology, Graz, Austria

clemens.brunner@tugraz.at

**Abstract**

This paper presents a feature-rich application called SigViewer to display biosignals such as the electroencephalogram, the electrooculogram and others. SigViewer is part of the BioSig project and aims to be a universal program to open many different biosignal file formats (at the moment more than 15 formats are supported) and display the contained signals. Moreover, it is possible to create annotations in the data and mark artifacts for example. The application is open source and does not depend on any proprietary or closed source software. It is also a cross-platform program that runs under many different operating systems such as Microsoft Windows, Mac OS X and Linux/X11 (and other Unix-based systems with X11 such as OpenSolaris, but the three mentioned platforms are officially supported and tested). SigViewer is a valuable tool for brain-computer interface research since it displays the raw EEG data (together with suitable highlighting of trials or events) and supports an easy and straightforward artifact rejection procedure.

## 1 Introduction

Biosignals such as the electroencephalogram (EEG), electromyogram (EMG), electrooculogram (EOG) or the electrocardiogram (ECG) are stored in suitable file formats. Unfortunately, there is no standardized way of saving these data streams – as a consequence, many different rivaling file formats are available on the market. Some specifications and implementations are open source whereas others were developed by companies with no interest in disclosing the specifications or even the source code of their proprietary file formats. To date, no single application is available that reads all those formats and displays the contained signals.

The BioSig project [1, 2] in general and SigViewer as part of the project in particular aim to fill this spot by providing import filters for as many file formats as possible. Moreover, the application itself is open source as well as completely free, not only as in free beer (free of charge) but also as in free speech (having freedom). It does not depend on any proprietary closed-source software and is distributed under the GNU General Public License (GPL)[1].

In addition to viewing the biosignals contained in the various file formats, SigViewer is also able to create annotations (or events), a process often referred to as scoring. That way, users can mark specific data segments continuously in time, for example to tag a certain time segment in a specific EEG channel as an artifact. Last but not least, the program is cross-platform, meaning that it runs on many different operating systems such as Windows, Linux/X11, and Mac OS X (and other Unix-based systems with X11 such as OpenSolaris, but these three mentioned platforms are officially supported and tested). All properties mentioned above make SigViewer a valuable tool for brain-computer interface research.

[1]`http://www.gnu.org/licenses/gpl.html`

## 2 Methods

SigViewer is written in standard ANSI/ISO C++ and compiles with any standard-compliant compiler. Due to the nature of the BioSig project, the open source compiler g++ (part of the GNU compiler collection GCC) is used to build the official binaries. In addition, the Qt 4 framework by the Norwegian company Trolltech[2] is used, also in its open source incarnation. This library was specifically designed to make the development of powerful graphical user interfaces (GUIs) as simple as possible. That way, SigViewer adopts the platform-specific look and feel without having to change a single line in the source code.

Recently, SigViewer was extended and incorporates now the library biosig4c (also part of the BioSig project). This library is written in standard ANSI/ISO C and implements reading and writing routines for many different biosignal file formats. At the moment, over 15 different formats are supported including GDF [3], EDF [4], BDF, BCI2000 [5], CNT, BrainVision, SCP-ECG (EN 1064) [6], HL7aECG [7] and several others[3]. When a new file format is added to this library, the source code of SigViewer does not have to be modified; it must only be recompiled with the new version of the library. Moreover, the same library can also be used from within Octave or MATLAB[4] using tools from the BioSig toolbox.

## 3 Results

An example screenshot of SigViewer (Version 0.2.1) running on Mac OS X 10.5.2 is shown in Figure 1. As can readily be seen, GUI elements such as the horizontal and vertical scrollbars adopt the native look of the operating system, and the menu bar (not visible in the screenshot) is at the top of the screen, just like any other native Mac OS X application. Below the window title (showing also the current file name) some toolbars are displayed. At the bottom of the window, a status bar shows the total length, the number of channels and the number of trials of the signal. Most of the space inside the window is dedicated to the signal visualization – in the example, five EEG channels are shown within a time range of 50 seconds. The scale of the $y$-axis is shown on the left, whereas the channel labels are displayed on the right. The user can scroll horizontally through time as well as vertically through channels.

Besides basic viewing functionality to zoom in and out (autozoom is also available), to scroll through the signals and to choose specific channels to display, an important feature of SigViewer is to display, create and modify annotations. Figure 1 shows such annotations over the actual signals as colored blocks. An annotation has a starting and an end point as well as a type which is reflected in a (customizable) color. The blocks are transparent so that more than one type can be visualized simultaneously. If the mouse cursor is placed over events, a tool tip will pop up showing information (name, type, position, and duration) about the annotations below the mouse cursor (see Figure 2).

Naturally, new events can be created and existing annotations can be edited or deleted graphically by selecting the corresponding mode and dragging with the mouse cursor. It is possible to quickly switch between all available types, to create long events that exceed the time period displayed in the window (then the signals will automatically scroll) and to create annotations for specific channels or for all channels. In addition to the graphical display, a table widget is available that lists all events contained in the data file. This list can be sorted with respect to the position, duration, channel or event type. Events can also be deleted with the help of this list widget.

The events can be exported into a separate EVT file (which is basically a GDF file without signal data). To that end, the desired event types can be selected and only those annotations are stored in the new EVT file. Similarly, events can also be imported from EVT files. Using this strategy, even file formats without native support for annotations (unlike GDF for example) can benefit from additional event information.

[2] `http://trolltech.com/`

[3] the complete list is available at `http://hci.tugraz.at/schloegl/biosig/TESTED`

[4] `http://www.mathworks.com/`

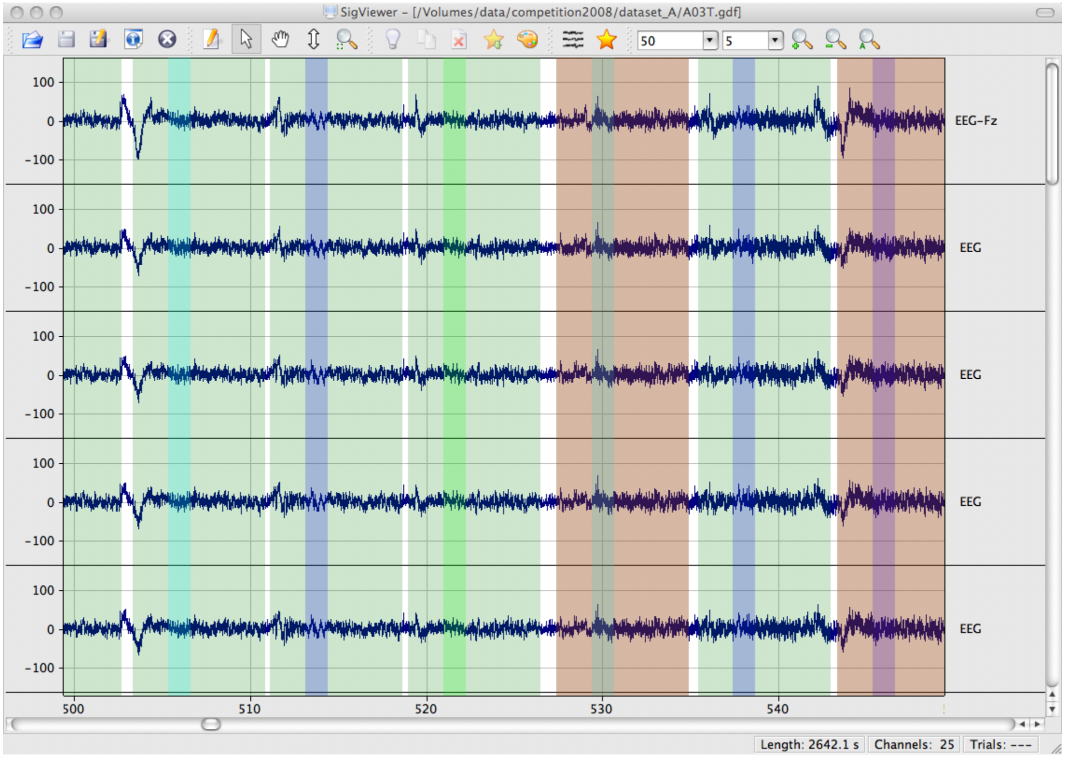


Figure 1: Main window of SigViewer running on Mac OS X displaying five EEG channels on a time scale of 50 seconds.

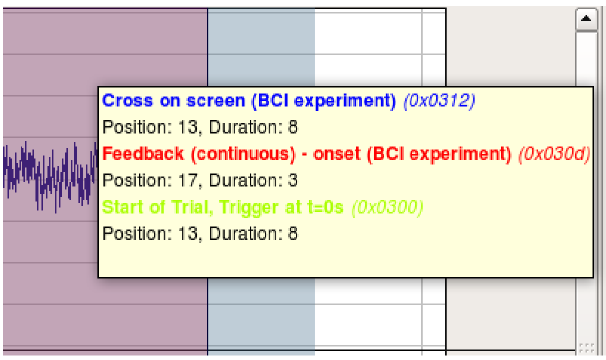


Figure 2: Popup window showing information about the annotations below the mouse cursor (SigViewer running on Ubuntu 8.04).

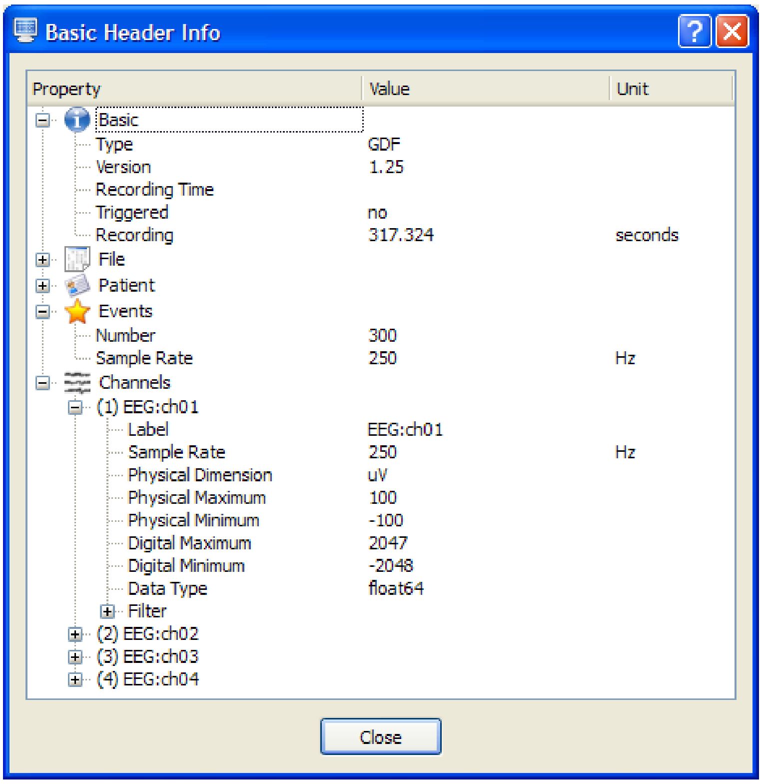


Figure 3: Basic header information window (SigViewer running on Windows XP).

At the moment, over 15 different file formats for storing biosignals are supported in biosig4c and thus also in SigViewer. Support for new data formats is planned and will be continuously added to the underlying library biosig4c.

Binary versions of the program are available at `http://biosig.sourceforge.net/` for Windows XP or Vista (an installation package), for Mac OS X 10.5 (universal binary for both x86 and PPC architectures), and for Linux/X11 (Ubuntu 8.04 was used to build the package). Due to the open source license GPL, the source code can also be obtained (and modified, adapted, . . . ).

## 4 Discussion

The viewing and scoring program SigViewer presented in this paper is unique in several aspects. First, it is completely free due to its open source license. Second, it is not restricted to a certain operating system and there is only one source code for all supported platforms. Third, it supports many biosignal file formats on the market with the help of the biosig4c library, where new formats are constantly added.

The development of SigViewer is continuing and many useful features will be added in future (besides removing bugs). One important step will be to get rid of all old Qt 3 classed and port the program to Qt 4 (at the moment, some important classes are still used from version 3). Undo and redo functions are also planned as well as an option to convert any arbitrary file format to GDF. The usability of the program will also constantly be improved and feedback is highly welcome; bug reports and feature requests can be deposited at the project's website, and the authors can always be contacted if there are any problems with the application. On the other hand, interested developers can join the project and help to improve SigViewer.

## References


[1] BioSig – an open source software library for BCI research. http://biosig.sourceforge.net/.

[2] A. Schlögl, C. Brunner, R. Scherer, and A. Glatz. BioSig: an open-source software library for BCI research. In G. Dornhege, J. del R. Millán, T. Hinterberger, D. J. McFarland, and K.-R. Müller, editors, *Toward brain-computer interfacing*, chapter 20, pages 347–358. MIT Press, 2007.

[3] GDF – a general dataformat for biosignals. http://arxiv.org/abs/cs.DB/0608052, 2006.

[4] B. Kemp, A. Värri, A. C. Rosa, K. D. Nielsen, and J. Gade. A simple format for exchange of digitized polygraphic recordings. *Electroencephalogr. Clin. Neurophysiol.*, 82:391–393, 1992.

[5] J. Mellinger and G. Schalk. BCI2000: a general-purpose software platform for BCI. In G. Dornhege, J. del R. Millán, T. Hinterberger, D. J. McFarland, and K.-R. Müller, editors, *Toward brain-computer interfacing*, chapter 20, pages 359–368. MIT Press, 2007.

[6] Standard communication protocol – computer-assisted electrocardiography (EN 1064).

[7] Annotated ECG. http://www.hl7.org/V3AnnECG/sectioncontent/ZI/HMPOZI_SB_RM.htm#POZI_RM020001-rmi.

# INDEX